ISSN 0386－5878
土木研究所資料第3086号

土 木 研 究 所 資 料

第７回日米橋梁ワークショップ論文集

平成４年３月

建設省土木研究所

Copyright © (1992) by P.W.R.I.

All rights reserved. No part of this book may be reproduced by any means, nor transmitted, nor translated into a machine language without the written permission of the Director General of P.W.R.I.

この報告書は，土木研究所長の承認を得て刊行したものである。したがって，本報告書の全部又は一部の転載，複製は，土木研究所長の文書による承認を得ずしてこれを行ってはならない。

土木研究所資料
第3086号1992年3月

第7回日米橋梁ワークショップ論文集

構造橋梁部長 藤原　稔

要　旨

1991年5月8日，9日の2日間にわたって，建設省土木研究所において第7回日米橋梁ワークショップが開催された。本資料は，同ワークショップに提出された論文および会議プログラム，討議内容，ワークショップ後に行われた視察旅行の内容をとりまとめたものである。

キーワード：橋梁工学，日米技術協力，耐風工学，耐震工学

まえがき

第７回日米橋梁ワークッショップが平成３年５月８日，９日の２日間にわたり、建設省土木研究所において開催された。

会議には米国側より13名、日本側から68名が参加し、橋梁の耐風設計や耐震設計、既設橋梁の維持管理や補修などの橋梁工学に関する課題について提出された32編の論文発表とこれらに関する討議が行われた。

日米橋梁ワークッショップは、天然資源の開発利用に関する日米会議（ＵＪＮＲ）の耐風耐震構造専門部会における作業部会Ｊ（ＴＣ－Ｊ）「交通システムの耐風耐震技術」において橋梁に関連した課題をより深く論議することを目的に、昭和58年５月に筑波の建設省土木研究所において第１回が開催されたのが最初であり、その後米国と日本の交互で開催されている。昨年の第６回までに、延べ日本側148名、米国側102名、計250名の参加を得ている。

本報告書は、このように本ワークッショップが継続的に開催されている状況を考慮し、今後の参考に資するとともに、会議の成果を記録に残して有効に活用したいとの願いのもとにとりまとめたものである。

本ワークッショップが日米両国のこの分野における研究活動の推進に役立つとともに、関係者の理解と協力を得て今後ますます発展していくことを期待している。

最後に、本ワークッショップに参加された各位ならびに現地視察旅行を含め、会議開催にあたり数々の御支援を頂いた関係各機関の皆様に厚く御礼申し上げます。

平成４年３月

藤　原　　稔
ＵＪＮＲ耐風耐震構造専門部会
作業部会(Ｊ)日本側部会長
土木研究所 構造橋梁部長

目　　次

1．日米橋梁ワークショップの概要 …… 1

1．1　背景と過去の経緯 …… 3

1．2　目的 …… 3

1．3　全体計画 …… 3

参考資料　ＵＪＮＲ耐風耐震構造専門部会の概要 …… 5

2．会議プログラム …… 9

3．会議参加者 …… 17

4．論文および討議 …… 29

（1） Session 1 …… 31

（2） Session 2 …… 33

（3） Session 3 …… 93

（4） Session 4 ……155

（5） Session 5 ……205

（6） Session 6 ……253

（7） Session 7 ……281

（8） Session 8 ……349

（9） Session 9 ……387

(10) Session 10 ……419

(11) Session 11 ……459

(12) Session 12 ……501

(13) 討議録 ……503

5．視察旅行記 ……511

あとがき ……519

付属資料

（1） ＵＪＮＲ耐風耐震構造専門部会
第23回合同部会におけるワークショップ報告（英文） ……523

（2） ＵＪＮＲ耐風耐震構造専門部会
第23回合同部会におけるＪ部会 部会報告（英文） ……527

（3） ＵＪＮＲ耐風耐震構造専門部会
第23回合同部会におけるＪ部会 部会報告（和文） ……533

1．日米橋梁ワークショップの概要

1．日米橋梁ワークショップの概要

1.1 背景と過去の経緯

我国とアメリカ合衆国との間には、政府間ベースの技術協力プログラムを有しており、活発な活動が種々の分野で行われている。ＵＪＮＲ耐風耐震構造専門部会の活動はその一つであり、建設省土木研究所と米国商務省国立標準技術研究所を中心として、20年以上にわたる会議や共同研究の実績がある。ＵＪＮＲ耐風耐震構造専門部会の詳しい説明は本章末の参考資料に譲ることとするが、同部会は10の作業部会を有しており、その一つが作業部会(Ｊ)「交通システムの耐風耐震技術」であり、作業部会長は日本側が建設省土木研究所の藤原稔構造橋梁部長、米国側が連邦道路局研究開発技術部門のJ.D.Cooper次長が務めている。

作業部会(Ｊ)は主として道路橋の耐風耐震技術に関する研究をテーマにしており、昭和58年５月に土木研究所で開催されたＵＪＮＲ耐風耐震構造専門部会の第15回合同部会において、作業部会(Ｊ)は道路橋の耐風耐震技術に関する研究協力を推進するために、日米橋梁ワークショップの実施を提案し、同専門部会で承認された。これを受けて第一回のワークショップが筑波で昭和59年２月に開催され、以降表－１に示すように日米交互で開催されている。

1．2 目　的

第７回橋梁ワークショップは、前回までのワークショップの成果を踏まえ、道路橋の耐風耐震技術に加えて設計・施工一般および既設橋梁の維持管理に関する研究にまで幅広く範囲を広げ、これらの課題について日米両国間でより深く論議することを目的に実施されたものである。具体的な課題としては以下のとおりである。

（１）橋梁の耐震設計と耐震補強
（２）長大橋の耐風設計
（３）橋梁の維持管理・補修補強（橋梁維持管理システムなど）
（４）新しい設計・施工技術（超長大橋，施工新技術など）
（５）新しい設計基準の開発（限界状態設計法など）
（６）新しい要素技術（新材料，動的制御）

1．3 全体計画

全体計画は、今回米国側の窓口となったネバダ大学 B.M.Douglas 教授，E.A.Maragakis 教授と連絡をとりながら、土木研究所構造橋梁部基礎研究室が事務局となって検討された。

全体日程を表－２に示す。ワークショップには２日間があてられ、その後、阪神高速道路，関西国際空港，本州四国連絡橋への視察旅行に２日間があてられた。

ワークショップの参加者は、米国側から13名，日本側から68名（内土木研究所38名，自治体・公団22名，民間８名），計81名であった。

発表論文については、日本側から19編，米国側から13編，計32編であった。これらの論文は、3ないし4編ごとにグループ分けし、それぞれセッションを構成することとし、各論文発表を15分、セッション全体での討議を15分とした。会議は英語によることとし、通訳を付けずに行った。各セッションは、日米両国双方から各1名、計2名の議長の進行のもとに行われた。

表－1　日米橋梁ワークショップの活動経緯

場所，日時	参加者，論文	内　　容
第1回　筑 波 (1984.2.20～22)	日：31名,20編 米：14名,19編	設計基準 地震力および橋の応答を含む地震問題
第2回　SanFrancisco (1985.8.19～20)	日：12名，9編 米：13名,12編	吊橋および斜張橋の耐風安定性 コンクリート充填鋼管を含むRC橋脚の地震時挙動 地震被災橋梁の復旧技術，耐震設計・施工の実態 耐震補強技術，強震観測データ分析 橋梁振動の現場測定試験
第3回　筑 波 (1987.5.8～9)	日：33名,15編 米：14名,12編	斜張橋の動的解析，設計上の信頼性 耐震設計と地震動，既設橋の補修・補強 吊橋及び斜張橋の耐風安定性，免震設計 RC橋脚の耐震設計，地中連壁基礎の設計
第4回　San Diego (1988.5.11～12)	日：13名,13編 米：20名,19編	橋梁の空力特性，風工学と現場試験 耐震評価・耐震補強および免震 橋梁の維持・点検・補強 耐震およびその他の解析と設計 橋梁および部材に関する実験
第5回　つくば (1989.5.8～9)	日：38名,13編 米：11名,10編	耐震設計，耐風設計，設計・施工一般 既設橋梁の維持管理・補修補強 計測・監視，非破壊検査
第6回　Lake Tohoe (1990.5.7～8)	日：18名,14編 米：31名,29編	耐風工学，耐震評価・補強，吊橋・斜張橋 橋梁点検・補修試験と評価，実験・数解析 構造物の監視・診断システム，振動制御

表－2　第７回日米橋梁ワークショップ全体日程

月　日	行　　程	宿　泊
5/8（水）	ワークショップ（土木研究所）	つくば （建設省研修会館）
9（木）	ワークショップ（土木研究所）	つくば （建設省研修会館）
１０（金）	視察旅行　　つくば→ 大阪 阪神高速道路	大　阪 （大阪後楽園ホテル）
１１（土）	視察旅行関西国際空港 明石海峡大橋 → 東京	東　京 （ 新橋第一ホテル ）

参考資料　ＵＪＮＲ耐風耐震構造専門部会の概要

１．ＵＪＮＲ

天然資源の開発利用に関する日米会議（U.S.-Japan Conference on Development and Utilization of Natural Resources＝U．J．N．R．）の設立については、昭和39年１月27日東京で開催された第３回日米貿易経済合同委員会第１回全体会議の席上米国側から提案され、日米科学委員会および日米貿易経済合同委員会のいずれにも属さないものとして、同年から発足しました。そのとき提案された主旨は、「日米が両国の利益のために人的および天然資源の分野で技術要員と調査結果の交換を、新たに政府レベルで行いたい。また、本計画を実現するために日米両国の政府職員による会議を早い機会に開催してはどうか。」というもので、日本側もこの旨を了解し、科学技術庁を中心として活動が開始されました。

この会議の目標は、世界の天然資源の有効利用と保全および人間の居住環境問題の解決のために日米両国が互いの協力を通じて、可能な限り学びとることにあります。

昭和39年5月に、日米両国の最高責任者が会合する本会議の第１回が開催されて以来、既に20年以上を経過し、その間「試行と組織化」の段階から「実施と拡充」の段階へと発展したこの会議は、技術研究情報の交換，研究の交流だけでなく、共同研究も実施され、ますます重要性を増しつつあります。

この会議の運営組織は、本会議、事務担当官会議並びに日米両国におかれた16の専門部会、その内の海洋に関する７つの専門部会を調整する海洋資源工学調査委員会から成り立っています。本会議は、両国の担当行政部局の最高責任者が会合するものであり、適宜、東京またはワシントンで交互に開催されています。事務担当官会議は本会議の円滑な運営を図るため両国の事務担当官が会合するものであり、本会議の間に開催

されています。また、両国の専門部会が合同して行う合同部会はおよそ１年に１回開催され、情報交換，成果の検討，意見交換等を行っています。

なお、専門部会の組織図を参考として以下に示します。

天然資源の開発利用に関する日米会議（ＵＪＮＲ）
専　門　部　会　の　組　織

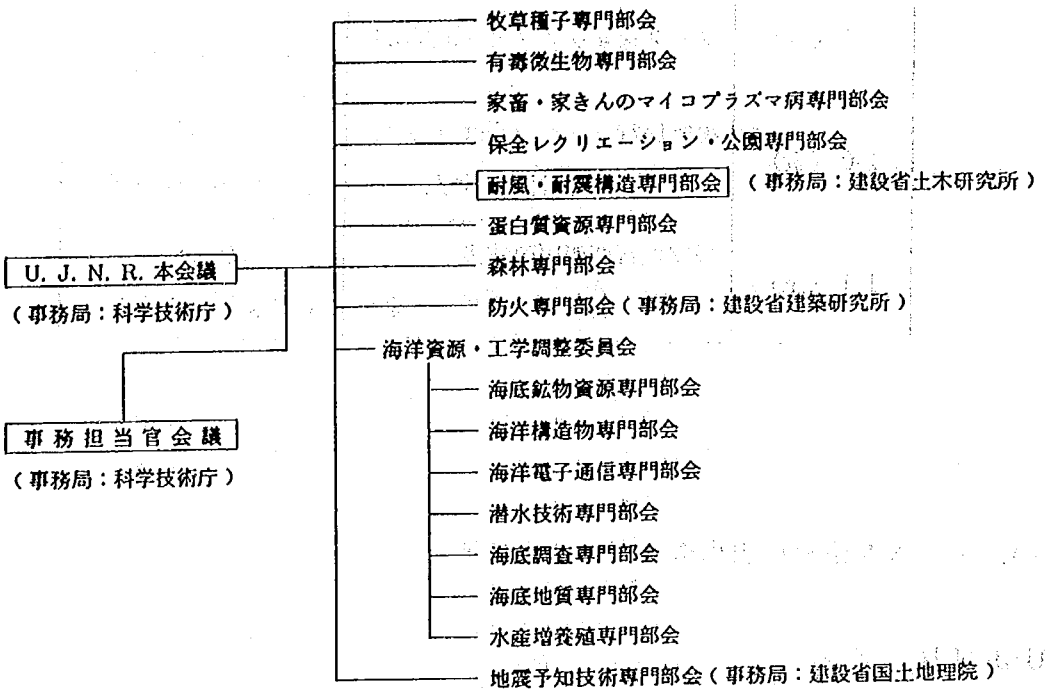

２．耐風・耐震構造専門部会

○ 目的と主な活動

耐風・耐震構造専門部会は、昭和42年東京で開かれた第３回本会議の席上で新しい協力活動として取り上げられました。このプログラムは、日米両国が互いに地震、強風、高潮、津波の被害国である実状に鑑み、従来別々に行われたきた構造物の耐風・耐震設計法などの開発研究の成果を持ち寄り、意見交換する機会をもたらすことに主眼がおかれています。その後活動範囲は拡大され、設計基準の改正上の問題点に関連して実施された調査研究の成果の交換、さらには強風、地震、高潮、津波により生ずる災害から人命および財産の損失を防止するための総合的対策、技術分野の開拓を目標としています。具体的には、毎年１回日米両国で交互に合同部会を開催する外に、共同研究の実施、研究者の交流、ワークショップの開催などの活動を続けています。昭和63年には合同部会の開催も20回となり、20年の活動を振り返り、「耐風耐震構造専門部会20年の歩と将来展望」を両国でとりまとめ報告しました。また、米国国立標準技術研究所から友好の記念に

「ニュートンのりんごの木」が日本側に贈られました。

○ 組　織

日本と米国の双方に設置され、日本側の部会は、建設省土木研究所長を部会長として、同土木研究所，同建築研究所，同国土地理院，運輸省港湾技術研究所，同気象研究所，科学技術庁防災科学研究所から選ばれた計28名の委員で構成され、部会事務局は土木研究所企画部企画課に置かれています。

米国側の部会は、国立標準技術研究所建築技術センター所長のR.N.ライト博士を部会長として、国立標準技術研究所，地質調査所，住宅都市開発省，連邦道路局，国立海洋気象庁，内務省開拓局，陸軍工兵隊，海軍土木工学研究所等の機関より選出された計34名の委員で構成されています。

○ 現在の活動方針

1．災害防除を考慮した構造物や地域社会の設計・計画に関連する研究協力および技術情報や研究資料の交換

2．実施した最近の調査研究の相互検討

3．都市の再開発に関連する災害の防除対策の調査研究の成果

4．開発途上国に対する技術援助の現況紹介

5．科学者・技術者の人材交流の促進

6．両国保有の大型実験施設を使用する日米共同研究の実施の促進

7．両国保有の実験施設の利用を含む共同研究計画の推進

○ 作業部会

耐風・耐震構造専門部会の活動をより緊密にするため下記の作業部会を設け、研究情報の交換、作業部会ごとのワークショップなどを実施しています。

作業部会名	作業部会長（日本）	作業部会長（米国）
A．強震計配置計画と強震記録	野田節男（港湾研）	A.G.Brady(USGS)
B．大型実験計画	大谷圭一（防災研）	H.S.Lew(NIST)
C．既存構造物の補修および補強	広沢雅也（建　研）	K.P.Chong(NSF)
D．構造物の性能評価	岡本　伸（建　研）	G.R.Fuller(HUD)
E．地震動および設計地震力	川島一彦（土　研）	S.T.Algermissen(USGS)
F．ライフライン施設の災害防止	佐々木康（土　研）	R.Dikkers(NIST)
G．パッシブ・アクティブおよびハイブリッドコントロール	北川良和（建　研）	S.C.Liu(NSF)
H．地震時における地盤の挙動と安定	常田賢一（土　研）	A.G.Franklin(WES)
I．高潮および津波	宇多高明（土　研）	H.Meyers(NOAA)
J．交通システムの耐風耐震技術	藤原　稔（土　研）	J.D.Cooper(FHWA)

○ 将来の計画

耐風・耐震構造専門部会は、強風，強震，高潮，津波による災害を防ぐための技術的諸問題の解決を図るものであり、そのためには従来から実施してきたこれらの自然現象を的確に把握することの外に、さらにそれらに対する構造物の挙動を明確に把握すること、人命や財産の損失を最小限にするための総合的対策を追求することが必要となります。これらの目的を達成するためには、従来の活動に加えて以下の諸事項について、より具体的な計画の立案および実施の強化が緊要とされています。

1．試験機・実験装置の共同利用，資料，模型の相互交換を含む共同研究計画を推進すること。

2．上記目的のための科学者・技術者の相互交換を推進すること。

3．関連分野からのより広汎な協力を求め活動分野を拡大すること。

4．作業部会において各分野の研究ニーズを明確にし、各作業部会間で連絡・調整を図り、今後の研究計画を作成すること。

5．国際防災の10年の計画に注意し、専門部会の活動がより有意義なものとなる方向を模索すること。

2．会議プログラム

WORKSHOP PROGRAM

7th U.S.-JAPAN BRIDGE ENGINEERING WORKSHOP

May 8 and 9, 1991

Tsukuba City, Japan

Wednesday, May 8, 1991 — Place: Conference Room (8F) PWRI

SESSION 1: OPENING SESSION
(Chairman: M. Fujiwara) 9:00am～9:15am

Welcome Remarks: Toshio Iwasaki (Director General, PWRI)

Remarks: James D. Cooper(Chairman for the U.S. side)

SESSION 2: SEISMIC DESIGN(1) 9:15am～10:35am
(Co-Chairmen: Y. Sasaki, B. M. Douglas)

(1) T. Kazama, S. Kurasawa, T. Nakamura* and Y. Yukawa: The Seismic Design of Usui Bridge
(9:15am～9:30am)

(2) H. Eddin and A. M. A. Ghaffar* : Seismic Performance of Cable-Stayed Bridges with Elastmetric and Lead-Rubber Bearings
(9:30am～9:45am)

(3) A. Nanjo* and S. Kayano: Aseismic Design of the Umemachi Bridge
—A Continuous Five-Span Rigid-Frame Bridge with V-Shaped Legs—
(9:45am～10:00am)

(4) K. Kawashima* , S. Unjoh and M. Tsunomoto: Estimation of Damping Characteristics of Cable Stayed Bridge for Seismic Design
(10:00am～10:15am)

DISCUSSION
(10:15am～10:35am)

COFFEE BREAK
(10:35am～10:50am)

SESSION 3: SEISMIC DESIGN(2) 10:50am～0:10pm
(Co-Chairmen: K. Kawashima, J. Gates)

(5) O. Nakano, H. Konno, H. Taniguchi* and Y. Ono: On the Behavior of Base-Isolated Bearings at Low Temperatures
(10:50pm～11:05pm)

(6) I. G. Buckle: Code Developments and Current Applications of Seismic Isolation to Bridges in the United States
(11:05am～11:20am)

(7) K. Kawashima and K. Hasegawa* : Evaluation of Lateral Inertia Force of Bridges for Seismic Design
(11:20am～11:35am)

(8) J. B. Mander: Damage Assessment of Existing Bridges in Low to Medium Seismic Risk Zones
(11:35am～11:50am)

DISCUSSION
(11:50am～0:10pm)

LUNCH (Conference Room, 1F)
(0:10pm～1:30pm)

PHOTOGRAPH (Entrance of PWRI Main Building)
(1:30pm～1:45pm)

SESSION 4: SEISMIC DESIGN(3) 1:45pm～3:05pm
(Co-Chairmen: K. Tokida, I. Buckle)

(9) G. A. MacRae* , K. Kawashima, K. Hasegawa, T. Ikeuchi and K. Ohshima: Behaviour of Stiffened Box-Section Steel Bridge Piers in Seismic Regions from Model Tests
(1:45pm～2:00pm)

(10) J. H. Gates* and M. Yashinsky: Performance of Retrofit Bridges in California
(2:00pm～2:15pm)

(11) K. Tokida, K. Tamura* and K. Aizawa: Experimental Study of Phase-Different Ground Motion Effects on the Response of a Suspension Bridge
(2:15pm～2:30pm)

(12) A. F. Goldschmidt: Foundation Considerations for the Seismic Retrofit of CALTRANS Bridges
(2:30pm～2:45pm)

DISCUSSION
(2:45pm～3:05pm)

COFFEE BREAK
(3:05pm～3:20pm)

SESSION 5: WIND RESISTANT DESIGN(1) 3:20pm～4:20pm
(Co-Chairmen: K. Yokoyama, Abdel-Ghaffar)

(13) E. Sato, H. Tominaga* , K. Namikawa, R. Kiyota, K. Tanida and T. Nose : A Damping Device on Main Tower Erection (The Suspension Bridge in Metroporitan Expressway Route No. 12)
(3:20pm～3:35pm)

(14) N. P. Jones , R. H. Scanlan and F. Ehsan : Effect of Sidewalk Vents on Bridge Response to Wind
(3:35pm～3:50pm)

(15) M. Niiyama, H. Kawasaki and Y. Saito* : Resistance/Stability to the Wind of Hakucho-Ohhashi
(3:50pm～4:05pm)

DISCUSSION
(4:05pm～4:20pm)

COFFEE BREAK
(4:20pm～4:35pm)

SESSION 6: WIND RESISTANT DESIGN(2) 4:35pm～5:20pm
(Co-Chairmen: K. Yokoyama, N. P. Jones)

(16) Y. Fuse, N. Takahashi and T. Kobayashi* , T. Ujihara and K. Tamura: Measurement of Antivibration Effects by TMD Used in Steel-Decked Box-Girder
(4:35pm～4:50pm)

(17) K. Yokoyama and T. Kusakabe* : Preliminary Study on Active Control for Wind-Induced Oscillation of Long Span Bridges
(4:50pm～5:05pm)

DISCUSSION
(5:05pm～5:20pm)

RECEPTION BY DIRECTOR GENERAL OF PWRI
Place: Akatsuki no Ma of GRAND SHINONOME (TEL: 0298-56-2211)
Time : 6:30pm-8:30pm
Transportation: Bus of GRAND SHINONOME leaves from Entrance of Main Building

Thursday, May 9, 1991 Place: Conference Room (8F) PWRI

SESSION 7: DESIGN METHOD(1) 9:15am～10:35am
(Co-Chairmen: H. Kawano, J. Clark)

(18) M. Okahara, S. Takagi and Y. Kimura* : Non-Linear Horizontal Bearing Characteristics of Column Type Foundation
(9:15am～9:30am)

(19) C. W. Roeder: Accommodation of Movements in Bridge Design
(9:30am～9:45am)

(20) H. Watanabe* and H. Kawano: Estimation of Ultimate Deformation of Column-Footing Joint
(9:45am～10:00am)

(21) T. Hashimoto, A. Makita* and K. Kobayashi:Design, Construction and Model Experiments on Corner Parts of Y-Shape Steel Bridge Piers
(10:00am～10:15am)

DISCUSSION
(10:15am～10:35am)

COFFEE BREAK
(10:35am～10:50am)

SESSION 8: DESIGN METHOD(2) 10:50am～11:50am

(Co-Chairmen: M. Fujiwara, J. Kulicki)

(22) E. Maragakis* , M. Saiidi, B. M. Douglas, G. Norris, R. Siddharthan and D. Sanders:Bridge Engineering Research In Progress at The University of Nevada, Reno
(10:50am～11:05am)

(23) M. Fujiwara, K. Nishikawa* , K. Minosaku, J. Murakoshi, S. Yamamoto: Current Condition on Introduction of Limit State Design Method to Highway Bridge Design in Japan
(11:05am～11:20am)

(24) J. M. Kulicki* and D. R. Mertz: United States LRFD Bridge Specification
(11:20am～11:35am)

DISCUSSION
(11:35am～11:50am)

LUNCH (Conference Room, 1F)
(11:50am～1:10pm)

SESSION 9: BRIDGE CONSTRUCTION(1) 1:10pm～1:55pm
(Co-Chairmen: K. Nishikawa, E. Maragakis)

(25) T. Maruyama* , M. Kamei and H. Tanaka: Design and Erection of Mono-Cable and Self-Anchored Suspension Bridge
(1:10pm～1:25pm)

(26) J. H. Clark: West Seattle Swing Bridge
(1:25pm～1:40pm)

DISCUSSION
(1:40pm～1:55pm)

COFFEE BREAK
(1:55pm～2:10pm)

SESSION 10: BRIDGE CONSTRUCTION(2) 2:10pm～3:10pm
(Co-Chairmen: M. Okahara, C. Roeder)

(27) N. Nomura and Y. Yoshida* : Foundation Design and Construction for the Akashi Kaikyo Bridge
(2:10pm～2:25pm)

(28) B. M. Douglas* , M. Blakely, M. Saiidi and E. A. Maragakis: Construction of the New Bridge Engineering Laboratory Facility at the University of Nevada, Reno
(2:25pm～2:40pm)

(29) Y. Kagawa, T. Meta, S. Nakamura and H. Kato* : Planning and Design of Multi-Span Continuous Bridges
(2:40pm～2:55pm)

DISCUSSION
(2:55pm～3:10pm)

COFFEE BREAK
(1:55pm～2:10pm)

SESSION 11: BRIDGE MAINTENANCE 3:25pm～4:25pm
(Co-Chairmen: M. Fujiwara, J. Mander)

(30) C. H. McGogeney and J. D. Cooper* : Magnetic Perturbation for Cable Inspection of Suspension Bridges
(3:25pm～3:40pm)

(31) T. Shiozaki and K. Takizawa* : Maintenance and Repair of Bridges in Tokyo
(3:40pm～3:55pm)

(32) G.L.Hoffman: Emphasis Areas in PennDOT'S Bridge Inspection and Repair Program
(3:55pm～4:10pm)

DISCUSSION
(4:10pm～4:25pm)

SESSION 12: CLOSING SESSION 4:25pm～4:40pm
(Co-Chairmen: M. Fujiwara, James D. Cooper)

Settlement of Resolution

Remarks: James D. Cooper (Chairman for the U.S. side)

Closing Remarks: Minoru Fujiwara (Chairman for the Japan side)

3. 会議参加者

7th U.S.-JAPAN BRIDGE WORKSHOP

LISTS OF PARTICIPANTS

May 8 and 9, 1991

Tsukuba City, Japan

—U.S. SIDE—

(1) Dr. Ahmed Abdel-Ghaffar

Position: Professor, Civil Engineering Department, Kaprielian Hall
University of Southern California
Address: Los Angeles, California 90089-2531
Tel: (213)743-6915

(2) Dr. Ian G. Buckle

Position: Deputy Director
National Center for Earthquake Engineering Research, SUNY
Address: Red Jacket Quadrangle, Buffalo, New York 14261
Tel: (716)636-3391

(3) Dr. John H. Clark

Position: Chief Bridge Engineer
Anderson Bjornstad Kane Jacobs
Address: 220 West Harrison Street, Seattle, Washington 98119-4108
Tel: (206)285-1185

(4) James D. Cooper

Position: Deputy Chief, Structures Division
Federal Highway Administration (HNR-10)
Address: 6300 Georgetown Pike, Nclean, Virginia 22101
Tel: (703)285-2447

(5) Dr. Bruce M. Douglas

Position: Director, Center for Civil Engineering Earthquake Research
University of Nevada, Reno
Address: Reno, Nevada 89557
Tel: (702)784-1519

(6) James H. Gates

Position: Structural Mechanics Engineer
CALTRANS, Division of Structures
Address: P.O. Box 942874, Sacramento, Calif. 94274
Tel: (916)445-1439

(7) Adlai F. Goldschmidt

Position: Senior Engineering Geologist
CALTRANS
Address: P.O. Box 942874, Sacramento, Calif. 94274
Tel: (916)327-3481

(8) Gary L. Hoffman

Position: Director, Bureau of Bridge and Roadway Technology
Pennsylvania Dept. of Transportation
Address: Commonwealth Ave. and Forster St., Trans, and Safety Building (Room 1009)
Harrisbulg, Pennsylvania 17120
Tel: (717)783-6182

(9) Dr. Nicholas P. Jones

Position: Assistant Professor, Department of Civil Engineering
The Johns Hopkins University
Address: Baltimore, Maryland 21218-2699
Tel: (301)338-7874

(10) Dr. John M. Kulicki

Position: Partner
Modjeski and Masters
Address: P.O. Box 2345
Harrisburg, PA 17105
Tel: (717)790-9565

(11) Dr. John B. Mander

Position: Assistant Professor
230 Ketter Hall, SUNY at Buffalo
Address: Buffalo, New York 14260
Tel: (716)636-2263

(12) Dr. Emmanuel A. Maragakis

Position: Associate Professor, Civil Engineering Department
University of Nevada, Reno
Address: Reno, Nevada 89557
Tel: (702)784-4839

(13) Dr. Charles W. Roeder

Position: Professor, Civil Engineering Department
University of Washington
Address: 233 B More Hall FX-10, Seattle, Washington 98195
Tel: (206)543-6199

-JAPAN SIDE-

(Public Works Research Institute)
Address: 305, 1-chome, Asahi-machi, Tsukuba-shi, Ibaraki-ken
Tel: (0298)64-2211

(1) Toshio Iwasaki

Position: Director General

(2) Yukihiko Sumiyoshi

Position: Deputy Director General

(3) Hiroshi Kohno

Position: Assistant Director General

(4) Takashi Iijima

Position: Director, Plannning and Research Administration Dep.

(5) Shigetoshi Kobayashi

Position: Director, Geology and Chemistry Dep.

(6) Masao Shibata

Position: Director, Road Dep.

(7) Minoru Fujiwara

Position: Director, Structure and Bridge Dep.
※Chairman of Japanese-side of J task committee

(8) Yasushi Sasaki

Position: Director, Earthquake Disaster Prevention Dep.

(9) Masashi Ikemura

Position: Research Coordinator for Advanced Technology,
Plannning and Research Administration Dep.

(10) Akira Fujimoto

Position: Coordinator for International Research Cooperation
Planning and Research Adiministration Dep.

(11) Junzo Inoue

Position: Bridge Instructor, Planning and Research Adiministration Dep.

(12) Hirotaka Kawano

Position: Head, Concrete Div., Geology and Chemistry Dep.

(13) Michio Okahara

Position: Head, Foundation Engineering Div., Structure and Bridge Dep.

(14) Koichi Yokoyama

Position: Head, Structure Div., Structure and Bridge Dep.

(15) Kazuhiro Nishikawa

Position: Head, Bridge Div., Structure and Bridge Dep.

(16) Ken-ichi Tokida

Position: Head, Ground Vibration Div., Earthquake Disaster Prevention Dep.

(17) Kazuhiko Kawashima

Position: Head, Earthquake Engineering Div., Earthquake Disaster Prevention Dep.

(18) Kazumasa Morihama

Position: Research Engineer, Concrete Div., Geology and Chemistry Dep.

(19) Hiroshi Watanabe

Position: Research Engineer, Concrete Div., Geology and Chemistry Dep.

(20) Jiro Fukui

Position: Senior Research Engineer, Foundation Engineering Div.
Structure and Bridge Dep.

(21) Yoshitomi Kimura

Position: Research Engineer, Foundation Engineering Div., Structure and Bridge Dep.

(22) Ken-ichi Asai

Position: Research Engineer, Foundation Engineering Div., Structure and Bridge Dep.

(23) Tomoki Kanazaki

Position: Senior Research Engineer, Structure Div., Structure and Bridge Dep.

(24) Norihumi Sawada

Position: Research Engineer, Structure Div., Structure and Bridge Dep.

(25) Takaaki Kusakabe

Position: Research Engineer, Structure Div., Structure and Bridge Dep.

(26) Koichi Minosaku

Position: Research Engineer, Bridge Div., Structure and Bridge Dep.

(27) Jun Murakoshi

Position: Research Engineer, Bridge Div., Structure and Bridge Dep.

(28) Satoshi Yamamoto

Position: Research Engineer, Bridge Div., Structure and Bridge Dep.

(29) Keiichi Tamura

Position: Senior Research Engineer, Ground Vibration Div.
Earthquake Disaster Prevention Dep.

(30) Yoshio Ninomiya

Position: Research Engineer, Ground Vibration Div., Earthquake Disaster Prevention Dep.

(31) Hideo Matsumoto

Position: Research Engineer, Ground Vibration Div., Earthquake Disaster Prevention Dep.

(32) Seitaro Yoshimi

Position: Research Engineer, Ground Vibration Div., Earthquake Disaster Prevention Dep.

(33) Kinji Hasegawa

Position: Senior Research Engineer, Earthquake Engineering Div.
Earthquake Disaster Prevention Dep.

(34) Shigeki Unjoh

Position: Research Engineer, Earthquake Engineering Div.
Earthquake Disaster Prevention Dep.

(35) Hideki Sugita

Position: Research Engineer, Earthquake Engineering Div.
Earthquake Disaster Prevention Dep.

(36) Hiroyuki Nagashima

Position: Research Engineer, Earthquake Engineering Div.
Earthquake Disaster Prevention Dep.

(37) Gregory Anthony MacRae

Position: Ocerseas Researcher, Earthquake Engineering Div.
Earthquake Disaster Prevention Dep.

(38) Mohsen Sultan

Position: Project Manager, California Department of Transportation,
Division of Structures, Office of Structure Design
(Visiting Researcher, Earthquake Engineering Div.
Earthquake Disaster Prevention Dep.)

(Highway Pub. Corp. etc.)

(1) Takeo Nakamura

Position: Structural Engineer Section
Tokyo Second Construction Bureau, Japan Highway Public Corporation (JH)
Address: 160, 1-21-1 Nishishinjuku, Shinjuku-ku, Tokyo-to
Tel: 03-3343-0451

(2) Yasuyuki Yukawa

Position: Tomioka Construction Office
Tokyo Second Construction Bureau, JH
Address: 370-24, 118-6 Ichinomiya, Tomioka-shi, Gunma-ken
Tel: 0274-64-0981

(3) Teruyou Hashimoto

Position: Senior Engineer, Design Div. First Construction Department,
Metropolitan Expressway Public Corporation (MEPC)
Address: 101, Iwamoto-Chou 3-2-4, Chiyoda-ku, Tokyo-to
Tel: 03-3861-8171

(4) Atuhiro Makita

Position: Design & Survey Div. Kanagawa Management Department, MEPC
Address: 221, Higashikanagawa 1-3-4, Kanagawa-ku, Yokohama-shi, Kanagawa-ken
Tel: 045-461-2021

(5) Toru Terayama

Position: Design & Research Div. Engineering Department, MEPC
Address: 100, Kasumigaseki 1-4-1, Chiyoda-ku, Tokyo-to
Tel: 03-3502-7311

(6) Eisaku Sato

Position: Assistant Section Manager, Design Div. Third Construction Department, MEPC
Address: 104, Hacchobori 2-14-4, Cyuoh-ku, Tokyo-to
Tel: 03-3553-1231

(7) Hiroo Tominaga

Position: Group Leader, Design Div. Third Construction Department, MEPC
Address: 104, Hacchobori 2-14-4, Cyuoh-ku, Tokyo-to
Tel: 03-3553-1231

(8) Yorimichi Maekawa

Position: Advisory Officer, Engineering Department,
Hanshin Expressway Public Corporation (HEPC)
Address: 541, OSAKA CENTER BLDG, Kyutaro-machi 4-1-3, Chuoh-ku, Osaka
Tel: 06-252-8121

(9) Atsushi Nanjo

Position: Chief Engineer, Design Div. Engineering Department, HEPC
Address: 541, OSAKA CENTER BLDG, Kyutaro-machi 4-1-3, Chuoh-ku, Osaka
Tel: 06-252-8121

(10) Toshihiko Naganuma

Position: Chief Engineer, Maintenance Engineering Section,
Maintenance & Facility Design Div. HEPC
Address: 541, OSAKA CENTER BLDG, Kyutaro-machi 4-1-3, Chuou-ku, Osaka
Tel: 06-252-8121

(11) Naoshige Nomura

Position: Manager, Third Design Div. Design Dep.,
Honshu-Shikoku Bridge Authority
Address: 105, Toranomon 45 Mori Bld., Toranomon 5-1-5, Minato-ku, Tokyo-to
Tel: 03-3434-7281

(12) Kazuhiko Yamagishi

Position: Deputy Manager, Third Design Div. Design Dep.,
Honshu-Shikoku Bridge Authority
Address: 105, Toranomon 45 Mori Bld., Toranomon 5-1-5, Minato-ku, Tokyo-to
Tel: 03-3434-7281

(13) Yoshitaka Yoshida

Position: Manager, Design Div. First Construction Bureau,
Honshu-Shikoku Bridge Authority
Address: 653, Hamabedori 5-1-14, Chuoh-ku, Kobe-shi, Hyougo-ken
Tel: 078-251-6622

(14) Osamu Nakano

Position: Head, Structure Div. Civil Engineering Research Institute,
Hokkaido Development Bureau
Address: 064, 1-20-902, Minami6, Nishi17, Chuoh-ku, Sapporo-shi, Hokkaido
Tel: 011-551-7604

(15) Hideyuki Taniguchi

Position: Research Engineer, Structure Div. Civil Engineering Research Institute,
Hokkaido Development Bureau
Address: 062, 3-chome, 1-jyo, Hiragishi-cho, Toyohira-ku, Sapporo-shi, Hokkaido
Tel: 011-841-1111

(16) Yoshiyuki Saito

Position: Member of Design Group, 2nd Construction Section, Muroran Road Office,
Muroran Development & Construction Department, Hokkaido Development Bureau
Address: 051, Shukuzu 1, Muroran-shi, Hokkaido
Tel: 0143-27-2211

(17) Takeyoshi Shiozaki

Position: Director, Road & Street Administruction, Divion, Bureau of Construction, Tokyo Metropolitan Government
Address: 362, Kasuga 2-15-6, Ageo-shi, Saitama-ken
Tel: 0487-75-6497

(18) Kazuo Takizawa

Position: Chief, Construction Section, Monorail Construction Office, Bureau of Construction, Tokyo Metropolitan Government
Address: 350-13, Irumagawa 3161, Sayama-shi, Saitama-ken
Tel: 0429-59-7735

(19) Katsuhiko Maruyama

Position: Chief, Construction Section, First Construction Office, Bureau of Construction, Tokyo Metropolitan Government
Address: 356, Namiki 13-41, Kawagoe-shi, Saitama-ken
Tel: 0492-35-3145

(20) Isao Hirahara

Position: Assistant Director, Road & Bridge Construction Section, Bureau of Construction, Tokyo Metropolitan Government
Address: 260, Masago 2-2-5, Chiba-shi, Chiba-ken
Tel: 0472-77-4673

(21) Tadaaki Maruyama

Position: Chief of Bridge Dept, Public Works Bureau, Osaka Municipal Government
Address: 530, Umeda 1-2-2-500, Kita-ku, Osaka
Tel: 06-208-9521

(22) Masahiro Kamei

Position: Staff Officer, Elevated Crossing Dept. Road & Street Div. Public Works Bureau, Osaka Municipal Government
Address: 530, Umeda 1-2-2-500, Kita-ku, Osaka
Tel: 06-208-9484

(23) Toshihiro Meta

Position: Deputy Section Manager, The 3rd Section of Design Department, Trans-Tokyo Bay Highway Co, Ltd.
Address: 154, Kamiuma 5-16-23, Setagaya-ku, Tokyo-to
Tel: 03-3487-3813

(24) Hisato Kato

Position: The 3rd Section of Design Department, Trans-Tokyo Bay Highway Co, Ltd.
Address: 245, Gumisawa 4-26-25, Totsuka-ku, Yokohama-shi, Kanagawa-Ken
Tel: 045-871-2789

(25) Noboru Takahashi

Position: Special Assistant to General Manager, Engineering Department 2
Kansai International Airport Company Ltd.
Address: 542, Minamisenba 3-11-10, Chuoh-ku, Osaka
Tel: 06-282-2272

(26) Tetsuhisa Kobayashi

Position: Section Chief, Engineering Department 2,
Kansai International Airport Company Ltd.
Address: 542, Minamisenba 3-11-10, Chuoh-ku, Osaka
Tel: 06-282-2274

(27) Kiyoshi Kobayashi

Position: Manager, Engineering Department, Steel Structure & Civil Engineering Div.
Mitsui Engineering & Shipbuilding Co.,Ltd. (MES)
Address: 290, Yawata Kaigandouri 1, Ichihara-shi, Chiba-ken,
Tel: 0436-43-2877

(28) Ken-ichi Kano

Position: Manager, Refreshment Engineering Department,
Steel Structure & Civil Engineering Div. MES
Address: 104, Tsukiji 5-6-4, Chuoh-ku, Tokyo-to
Tel: 03-3544-3076

(29) Kouji Tanida

Position: Section Manager, Machinery & Vibration Dept. Research Institute
Ishikawajima-Harima Heavy, Industries Co.,Ltd.
Address: 235, Shin-Nakahara 1, Isogo-ku, Yokohama-shi, Kanagawa-ken
Tel: 045-759-2061

(30) Hiroshi Tanaka

Position: Assistant Manager, Bridge Design Section, Steel Structures Design Dept.
Hitachi Zosen Corporation Industries Co.,Ltd.
Address: 864, Sakurajima 1-3-40, Konohana-ku, Osaka-shi, Kanagawa-ken
Tel: 06546593071

4．論文および討議

(1) Session 1

Wednesday, May 8, 1991 Place: Conference Room (8F) PWRI

SESSION 1: OPENING SESSION
(Chairman: M. Fujiwara) 9:00am～9:15am

Welcome Remarks: Toshio Iwasaki (Director General, PWRI)

Remarks: James D. Cooper(Chairman for the U.S. side)

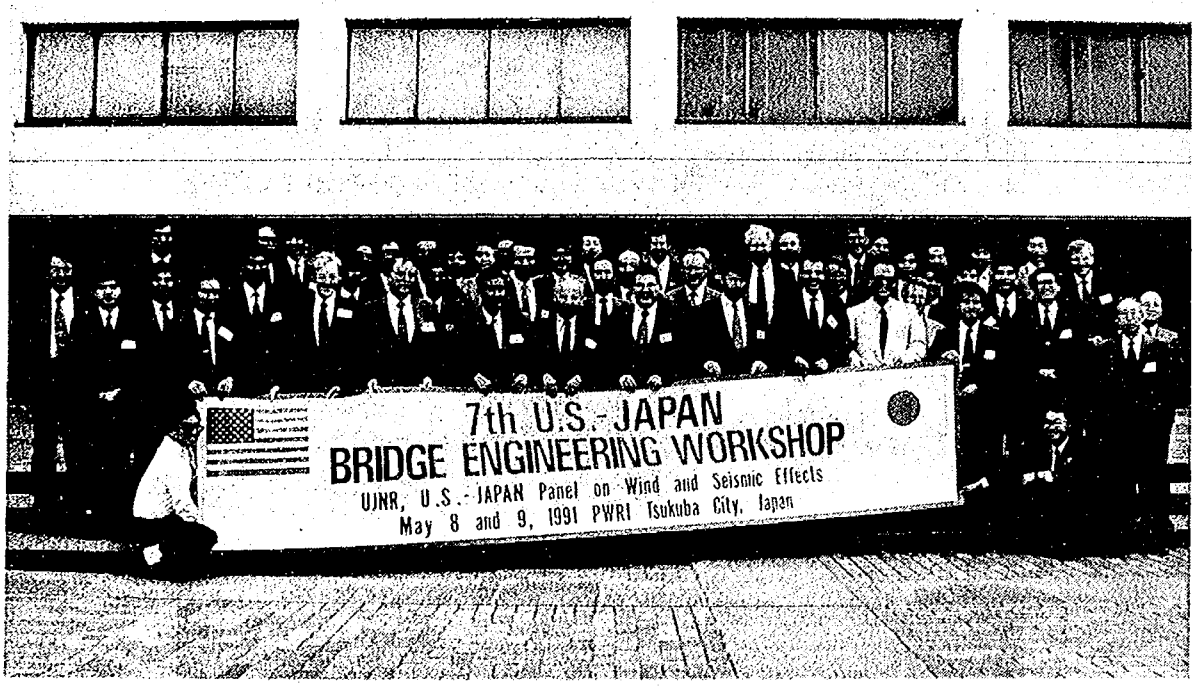

BRIDG
UJNR, U
May

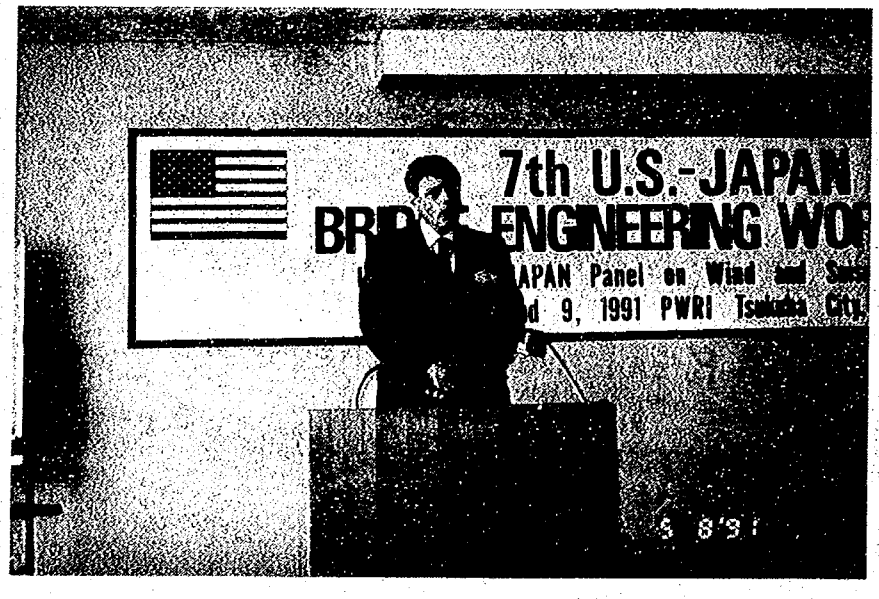
7th U.S.-JAPAN
ENGINEERING WO
APAN Panel on Wind and
d 9, 1991 PWRI Tsukuba City

(2) Session 2

SESSION 2: SEISMIC DESIGN(1) 9:15am～10:35am
(Co-Chairmen: Y. Sasaki, B. M. Douglas)

(1) T. Kazama, S. Kurasawa, T. Nakamura* and Y. Yukawa: The Seismic Design of Usui Bridge
(9:15am～9:30am)

(2) H. Eddin and A. M. A. Ghaffar* : Seismic Performance of Cable-Stayed Bridges with Elastmetric and Lead-Rubber Bearings
(9:30am～9:45am)

(3) A. Nanjo* and S. Kayano: Aseismic Design of the Umemachi Bridge
—A Continuous Five-Span Rigid-Frame Bridge with V-Shaped Legs—
(9:45am～10:00am)

(4) K. Kawashima* , S. Unjoh and M. Tsunomoto: Estimation of Damping Characteristics of Cable Stayed Bridge for Seismic Design
(10:00am～10:15am)

DISCUSSION
(10:15am～10:35am)

THE SEISMIC DESIGN OF USUI BRIDGE

by
Tohru Kazama[1], Sadao Kurasawa[2], Takeo Nakamura[3] and Yasuyuki Yukawa[4]

ABSTRACT

This paper presents a seismic design of a two-span continuous prestressed concrete cable stayed bridge named "Usui Bridge" which is currently under construction. First of all, this paper shows the position of the seismic design among other design works. As seismic design, dynamic analysis was made by response spectrum method as well as static analysis by seismic coefficient method which is popular in Japan. This paper introduces these analysis methods and the results of the analyses. As the tower stands 113 meters tall, a slender column stability analysis, in which nonlinear analysis under earthquake was considered, was also carried out. The data on the processes leading to failure of concrete column were obtained, and comparison of the load level in ultimate state was made with the results of linear analysis.

INTRODUCTION

Usui Bridge is located in Gunma-Prefecture, Japan. The bridge is under construction as a part of Joshin-Etsu Expressway by NIHON DORO KODAN. It is a 222-meter long, 21.4-meter wide two-span continuous prestressed concrete cable-stayed bridge. The bridge has a tower of inverse Y-shape, and stay cables arranged on 1 vertical plane in fan shape. It is currently under construction above the Shin-Etsu Line of JR and the Kirizumi River. The girder has a 3-cell box cross section. Fig. 1 shows the general view of Usui Bridge. The support condition of the girder is rigid type instead of continuous type which needs large bearings and floating type for which the amount of stay cables becomes great and the pier section becomes large. There was little problem concerning the behavior under earthquake as natural period was relatively long even for the rigid structure.

Basically, seismic design was required to be made in accordance with seismic coefficient method. But dynamic analysis was also made as it might be unreasonable for the structure with a high tower to be modeled as single mass system, and as this bridge is a highway bridge which will play an importnat role in Japan's policy for roads and crosses the major JR trunk, Shin-Etsu line. As the tower is subjected to high compression and the

1 Manager, Structural Engineering Division, Engineering Department, Nihon Doro Kodan, 3-3-2, Kasumigaseki, Chiyoda-ku Tokyo 100, JAPAN
2 Head, Tomioka Construction Office, Tokyo Second Construction Bureau, Nihon Doro Kodan, 118-6 Ichinomiya, Tomioka City Gunma Pref. 370-24, JAPAN
3 Engineer, Structural Engineering Section, Tokyo Second Construction Bureau, Nihon Doro Kodan, 1-21-1, Nishishinjuku, Shinjuku-ku Tokyo 160, JAPAN
4 Engineer, Tomioka Construction Office, Tokyo Second Construction Bureau, Nihon Doro Kodan, 118-6 Ichinomiya, Tomioka City Gunma Pref. 370-24, JAPAN

maxium displacement at the tower top is 152mm by the dynamic analysis, slender column stability analysis was made in consideration of material nonlinearity and geometric nolinearity of the concrete members.

In this paper, a focus will be placed on seismic design applied to Usui Bridge.

General description of the bridge

(1) Highway condition

Number of lanes	:	2 lanes for each line
Effective width	:	8.5 m x 2 (entire width 21.4 m)
Design speed	:	80 km/h
Longitudinal gradient	:	2.039%
Crossfall	:	2.0%
Radius of curvature	:	R = 1,600 m

(2) Structural Type

Bridge type	:	Two-span continuous prestressed concrete cable-stayed bridge
Bridge length	:	222 m = 2 x 111 m
Girder	:	3-cell box girder cross section (prestressed concrete structure)
Tower	:	Inverse Y-shape (steel framed reinforced concrete structure)
Arrangement of stay cables	:	fan-shaped arrangement on 1 vertical plane
Pier	:	2-cell cross section
Foundation	:	Intermediate support; pneumatic caisson foundation End supports; spread foundation, pile foundation
Girder support condition	:	Intermediate support; Main girder, pier and corbel are to be fixed together End supports; Movable

General Description of the Design

This bridge was designed basically by the allowable stress method.

The each structural member of the bridge was designed in consideration of dead load, live load, thermal load, wind load, earthquake load, and erection load, according to SPECIFICATIONS FOR HIGHWAY BRIDGES, PART III CONCRETE BRIDGE (1978). Each member section was checked for its safety in design load acting state and in ultimate load acting state.

The member force under earthquake load was obtained in static analysis by "modified seismic coefficient method" in accordance with SPECIFICATIONS FOR HIGHWAY BRIDGES, PART V SEISMIC DESIGN (1980). The member section and the quantity of reinforcement steel were basically determined by static analysis.

However, for the reason mentioned in the introduction, dynamic analysis was carried out by response spectrum method. Comparing the results of the analysis with that of a static analysis, the quantity of additional reinforcement steel was calculated when needed.

The flow of overall design works on Usui Bridge and the role of the seismic design among other design works are shown in Fig. 2.

Seismic Design

1. Static analysis

As the first stage of seismic design applied to Usui Bridge, the cross sections of members were checked by seismic coefficient method. In that method, earthquake load was statically applied to the structure and member force was calculated. The design horizontal seismic coefficient Kh used in the calculation was obtained by the following formula:

$$Kh = \nu_1 \cdot \nu_2 \cdot \nu_3 \cdot \beta \cdot kho$$

where

Kho: Basic design horizontal seismic coefficient (Kho=0.2). The basic design seismic coefficient applies to important bridges with short natural period, which are built on diluvium or ordinary alluvium where possibilities for strong earthquake are high.

ν_1 : Correction coefficient by region. It is not reasonable to apply to areas where earthquakes occurr less frequently the same design horizontal seismic coefficient as is applied to areas with frequent earthquakes occurring. For this reason, correction of the seismic coefficient is made by region.

ν_2 : Correction coefficient by ground. Seismic coefficient is corrected by considering the differences in the degrees of seismic damages to be inflicted on the bridge depending on the type of ground at the site.

ν_3 : Correction coefficient by degree of importance. Design horizontal seismic coefficient is corrected according to the degree of importance of the bridge so that the entire construction cost will be effectively used.

β : Correction coefficient by natural period. The characteristic of seismic response differs greatly depending upon the bridge structural characteristics. Factors connected with the bridge structural characteristics are natural period, damping characteristic, and vibration mode, etc. As there is a certain relationship between damping characteristic and natural period, and vibration mode and natural period are mutually dependent, the natural period is used for correcting the seismic coefficient. Correction coefficient by natural period β is determined as listed in Table 1 on the basis of an acceleration response spectrum for each type of ground, which is obtained through analyzing the records of strong earthquakes comprising 44

constituents that have been observed in Japan, characteristics of damages inflicted on bridges by earthquakes in recent years, and the facts obtained through observation and experiments. Fig. 3 shows this correction coefficient in a diagram.
The type of ground is provided in detail in SPECIFICATIONS FOR HIGHWAY BRIDGES, PART V SEISMIC DESIGN (1980). Type 1, 2, 3 and 4 correspond roughly to rock, diluvium, alluvium, and weak alluvium, respectively.

As the natural period in the longitudinal direction of this bridge was 2.3 seconds and the ground is Type 1, β turned out to be 0.64. However, we adopted $\beta=1.0$ because of the importance of this bridge and of considering that the earthquake load was supported by only one pier. The natural period in the transverse direction was found to be 0.84 second, and $\beta=1.25$.

Accordingly, design horizontal seismic coefficient with responses taken into consideration turned out to be 0.18 in the longitudinal direction and 0.23 in the transverse direction.

Member force under earthquake was obtained by loading a frame analysis model with load obtained from dead load multiplied by design horizontal seismic coefficient. The member force is shown in the next section together with the results of dynamic analysis.

2. Dynamic analysis

In dynamic analysis of this bridge, eigenvalue analysis was carried out on completed structure and on the last stage of cantilever erection. Using response spectrum method, response value was calculated, with which study of earthquake resistance after completion and during catilever erection of the bridge was carried out. The acceleration response spectrum used in dynamic analysis was the one obtained in Kaihoku Bridge, which was the recorded data of the 1978 earthquake which occurred in an offshore area of Miyagi Prefecture (Refer to Fig. 4), as the ground condition is similar to that of Usui Bridge (type 1) and the peak of response spectrum occurs around 2 and 3 seconds (the natural period of the first mode is 2.3 seconds for Usui bridge). Since the bridge is an important concrete bridge and it is necessary to obtain response value on the safety, the damping constant h was conservatively set to be 3% for the superstructure, 5% for the substructure, and 10% for the foundation.

The structure model was a three-dimensional frame structure model as shown in Fig. 5. The influence of deformation taking place in foundation ground under earthquake was taken into consideration by applying an appraisal of the spring value of the foundation.

The results of eigenvalue analysis are shown in Fig. 6 (completed structure) and Fig. 7 (structure under construction). In the figures, F, T and P.F denote natural frequency, natural peirod and participation factor, respectively. X shows the longitudinal direction, Y shows the transversal direction and Z shows the vertical direction.

Fig. 8 and Fig. 9 show the major maximal response member forces in longitudinal direction and transverse direction of the completed bridge, together with member forces calculated by static analysis. The following are observed by comparing member forces by static analysis with the maximal

response member forces by dynamic analysis:

1) The Bending moment of the girder in the longitudinal direction obtained by dynamic analysis was larger than that obtained by static analysis. Compressive stress of concrete was 159 kgf/cm^2 (allowable stress is 210 kgf/cm^2) at the pier head. The quantity of reinforcement steel on the tension side was sufficient, which determined under live load acting state. Transversal bending moment obtained by dynamic analysis was considerably larger. However, the girder's maximum compressive stress remains 126 kgf/cm^2, since this bridge is wide and the transverse rigidity is large.

2) Stay cable tensile force calculated by dynamic analysis was partially larger. However, it does not pose any problem, because stay cable capacity was determined under construction.

3) The Bending moment of the tower calculated by dynamic analysis was considerably larger in transverse direction. The maximum tensile stress of reinforcement was around 1100 kgf/cm^2, and compressive stress in concrete remained within allowable stress. The quantity of reinforcement steel was determined under live load acting state for the tower as well.

4) Regarding the torsional moment of the girder, reinforcement determined under live load acting state was enough for the results of dynamic analysis.

In short, sectional forces obtained by dynamic analysis were generally greater than those by static analysis. However the steel reinforcement was determined in live load acting state was sufficient for earthquake load acting state since the allowable stresses were increased by 1.5 times under earthquake load.

The input accelation for the dynamic analysis in the construction stage was set as half of that for the completed structure, 287 gal. Bending moments of the girder in transversal direction were fairly great comparing with the completed structure. However the maximum compressive stress was 171 kgf/cm^2 (allowable stress is 210 kgf/cm^2) and the steel reinforcement required for the completed structure was enough for the structure under construction.

3. Slender column stability analysis

Towers and piers of prestressed concrete cable stayed bridges are always under high axial compression. When the towers and piers under high axial compression receive a horizontal force by earthquake, it is considered that the effect of additional member force caused by horizontal displacement cannot be ignored. Horizontal displacements of slender concrete column increase by decrease of rigidity due to cracks in concrete and by yielding of reinforcement. Consequently, the bearing force of the structural system was checked out by using a nonlinear structure analysis computer program, which enabled us to consider simultaneously material nonlinearity characterized by decrease of rigidity of concrete members due to cracks and yielding of reinforcement, and geometric nonlinearity in which additional member force caused by displacements was taken into account.

As shown in the work flow in Fig. 10, member force generated by permanent load such as dead load was set as initial condition. Next, member force, displacement, stress and strain caused by earthquake load was calculated one after another by incremental approach until part of the structure was failed. Analysis was made by using plane frame structural analysis model and checks were made on two cases where earthquake load acted in longitudinal direction and in the transverse direction. Failure was defined as a state of a section where the compressive strain in concrete reached the ultimate strain (0.35%).

The analysis model is as shown in Fig. 12. In this model, material nonlineality is considered for the tower, and the pier, but it is not considered for the girder and stay cables.

In the cases of earthquakes oscillating in the longitudinal direction and in the transverse direction, failure occurred at the bottom of the pier. Seismic coefficient at failure kHV exceeded design seismic coefficient kh, and their ratio exceeded the load factor 1.3 in ultimate load acting state against earthquake load, which is provided in SPECIFICATIONS FOR HIGHWAY BRIDGES. Subsequently we concluded that the bearing capacity of the bridge tower was sufficient. (Refer to Table 2).

Fig. 13 shows tower displacement in the longitudianl direction. Slender concrete column begined to show nonlinear behaviors from around Kh = 0.05. Fig. 14 shows the equivalent flexural rigidity EI at the bottom of the pier. When kh = 0.025, it was observed that the rigidity decreased sharply due to cracks. The processes taking place at the bottom of the pier leading to its failure, in the longitudinal direction, were as follows:

kH = 0.025 cracks were generated.
kH = 0.06 further cracks occured.
kH = 0.21 reinforcing steel at the outmost tension side yielded.
kH = 0.245 concrete was failed with compressive stress.

CLOSING REMARKS

This paper provided a general description of seismic design applied to the Usui Bridge. By means of dynamic analysis by response spectrum method and slender column stability analysis considering the material and geometrical nonlinearity, we verified the safty of Usui bridge against earthquake, which has an important function as highway bridge and crosses JR's Shin-Etsu line. And we confirmed the validity of "seismic coefficient method" for this bridge as the dynamic analysis didn't required any additional steel reinforcement. We would be very happy if this paper could be of any help in the future when constructing prestressed concrete cable stayed bridges.

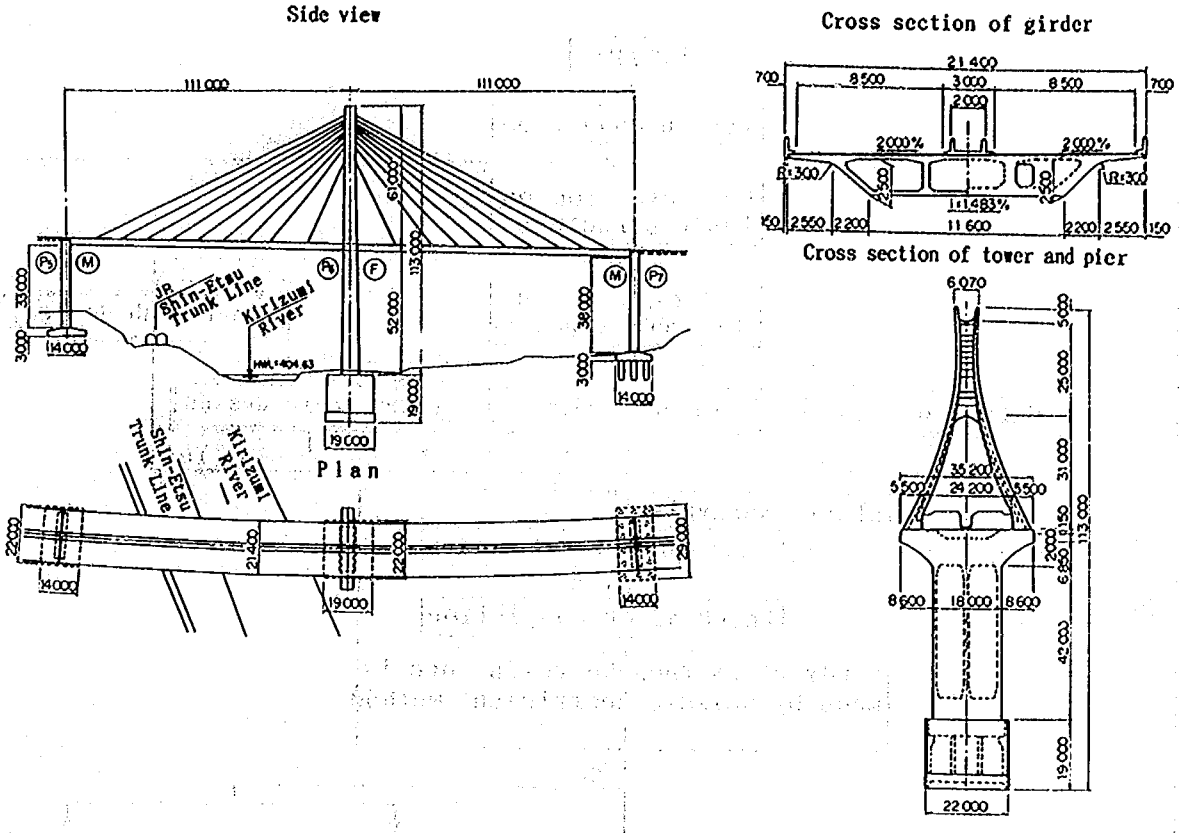

Fig.1 General view of Usui Bridge

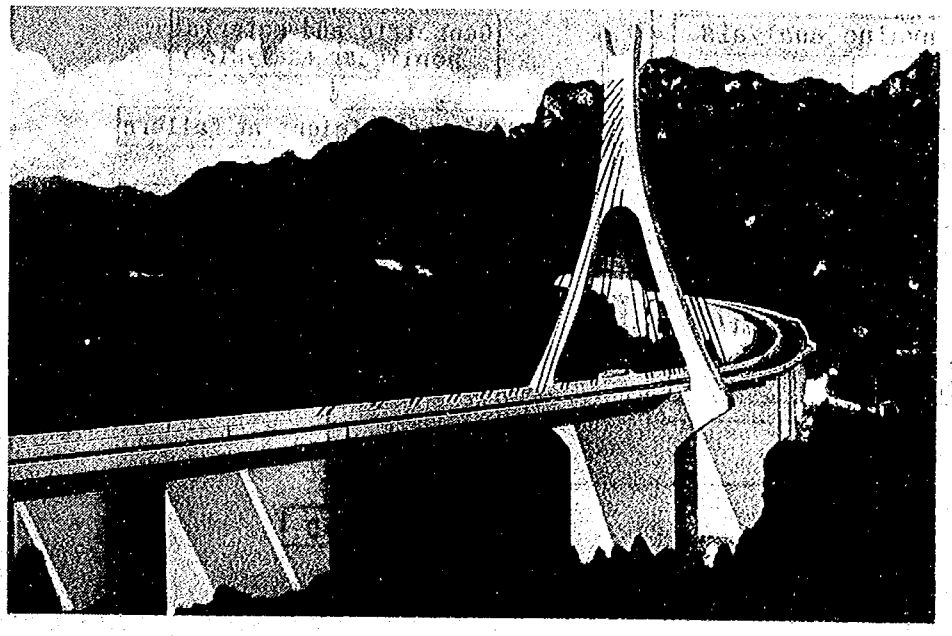

Photo 1 Photomontage

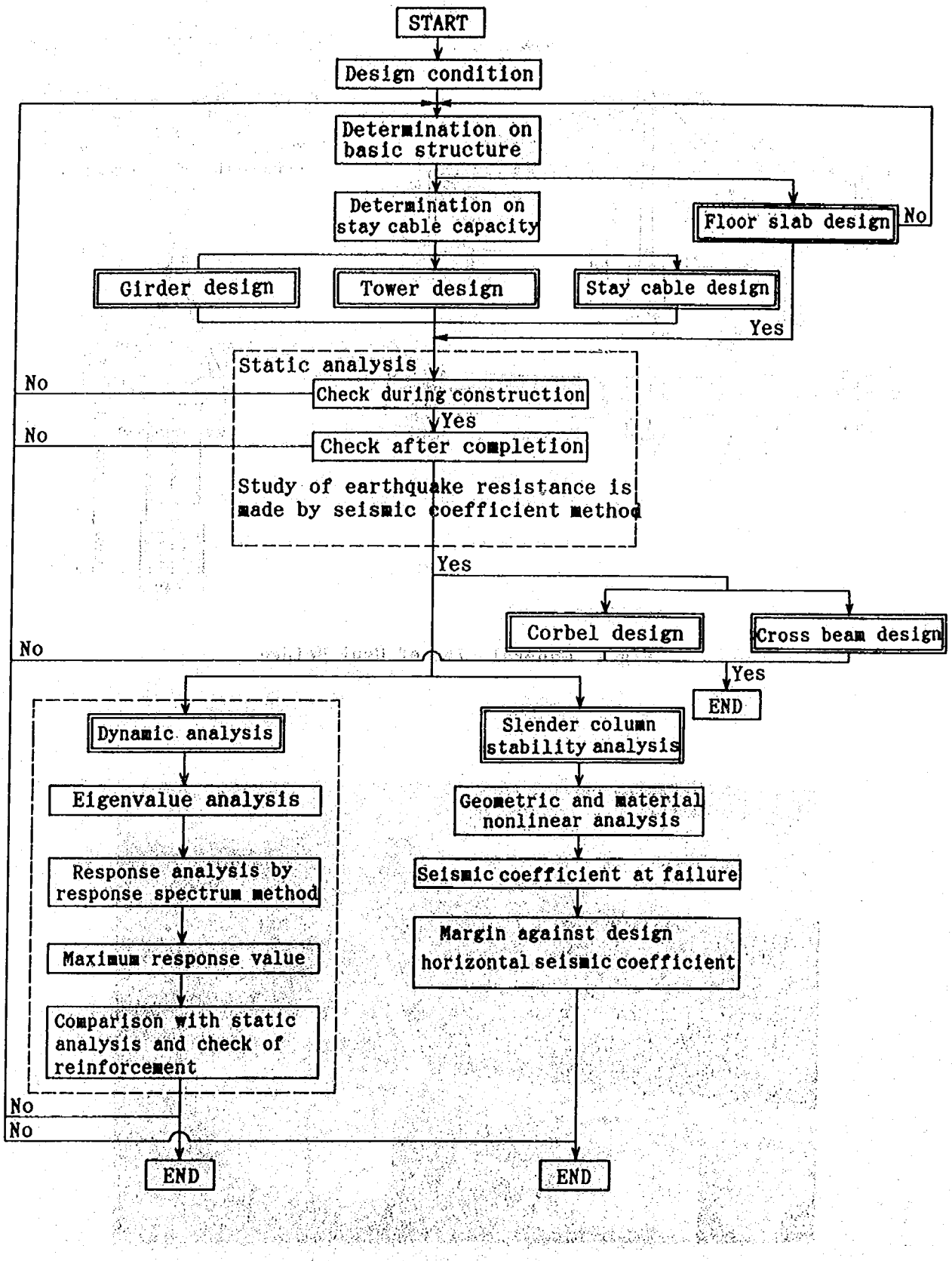

Fig. 2 Design work flow

Table-1 Correction coefficient by natural period β

Type of ground	β valuefor natural period t(s)				
Type I	T≦0.5 β=1.0	0.5<T≦0.625 β=2T	0.625<T≦1.12 β=1.25	1.12<T≦2.8 β=1.40/T	2.8<T β=0.50
Type II	T≦0.5 β=1.0	0.5<T≦0.625 β=2T	0.625<T≦1.4 β=1.25	1.4<T≦3.5 β=1.75/T	3.5<T β=0.50
Type III	T≦0.5 β=1.0	0.5<T≦0.625 β=2T	0.625<T≦1.68 β=1.25	1.68<T≦4.2 β=2.10/T	4.2<T β=0.50
Type IV	T≦0.5 β=1.0	0.5<T≦0.625 β=2T	0.625<T≦2.0 β=1.25	2.0<T≦5.0 β=2.50/T	5.0<T β=0.50

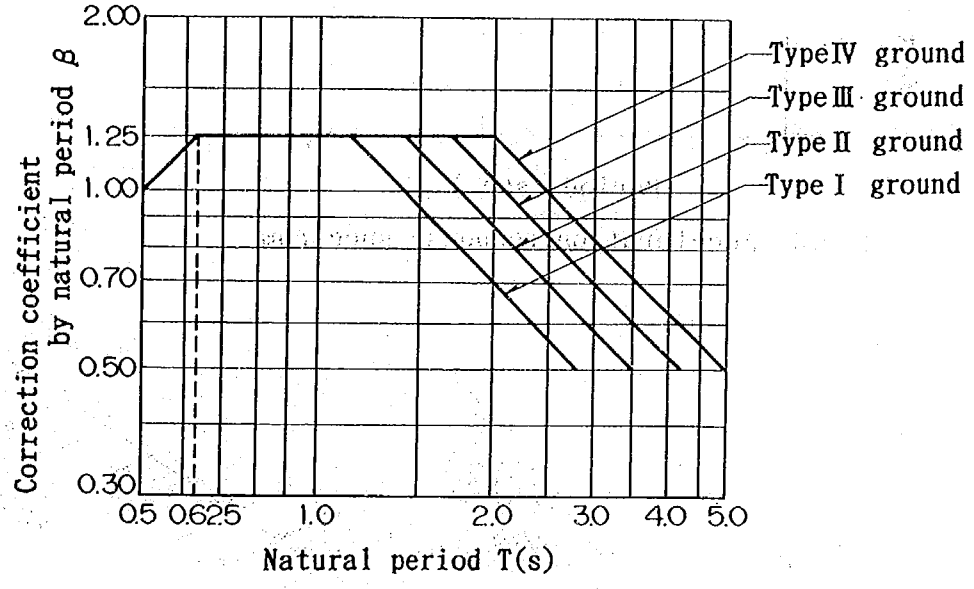

Fig. 3 Correction coefficient by natural period

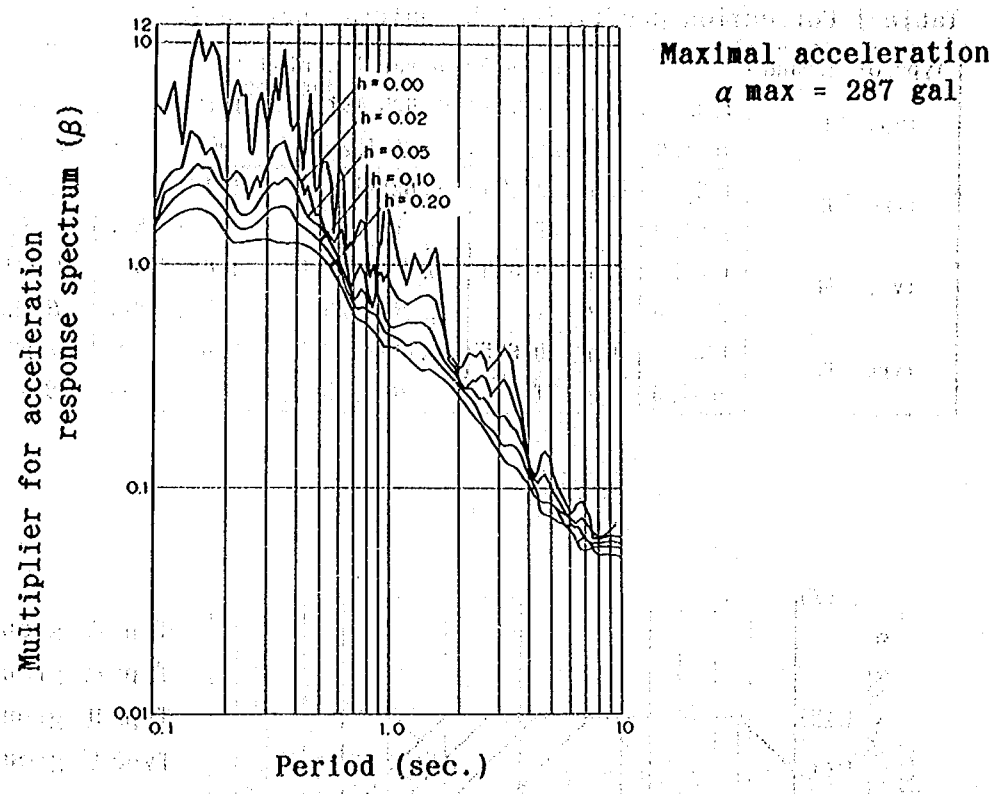

Fig.4 Acceleration response spectrum

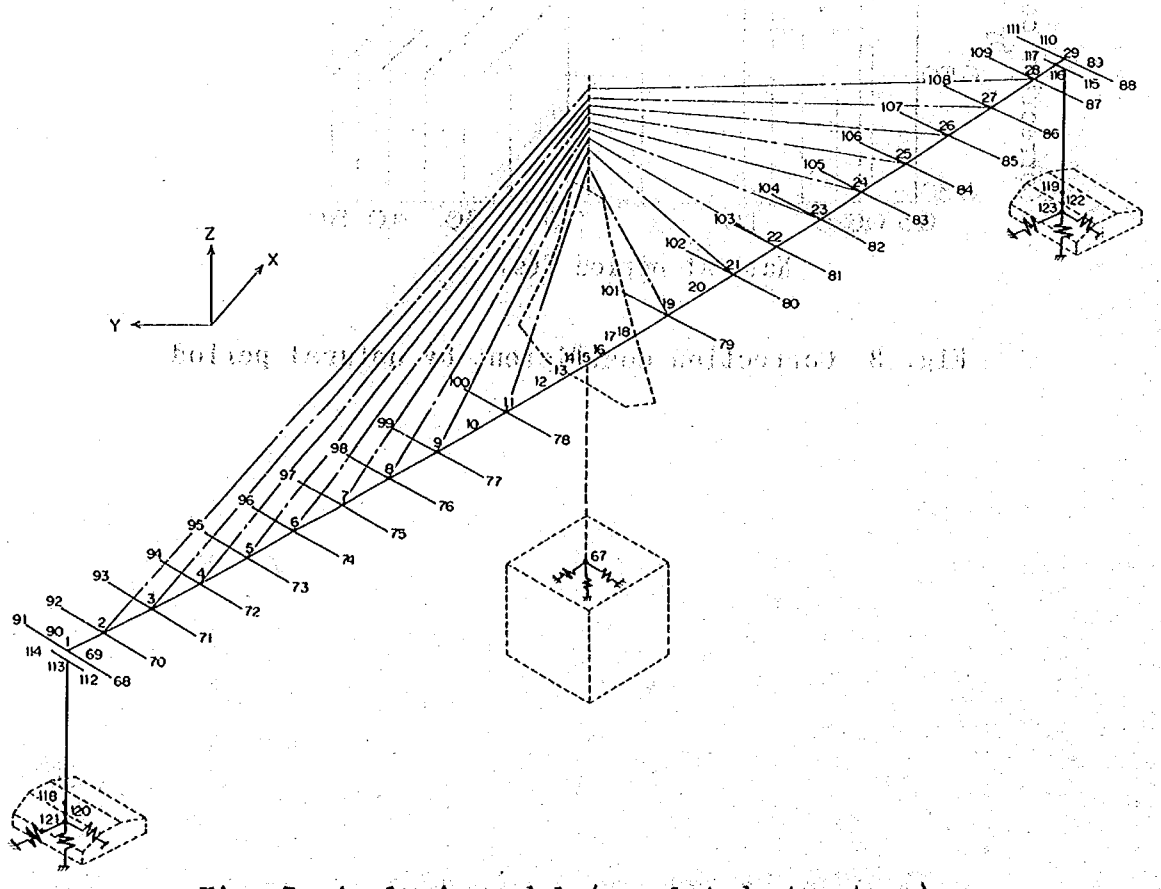

Fig. 5 Analysis model (completed structure)

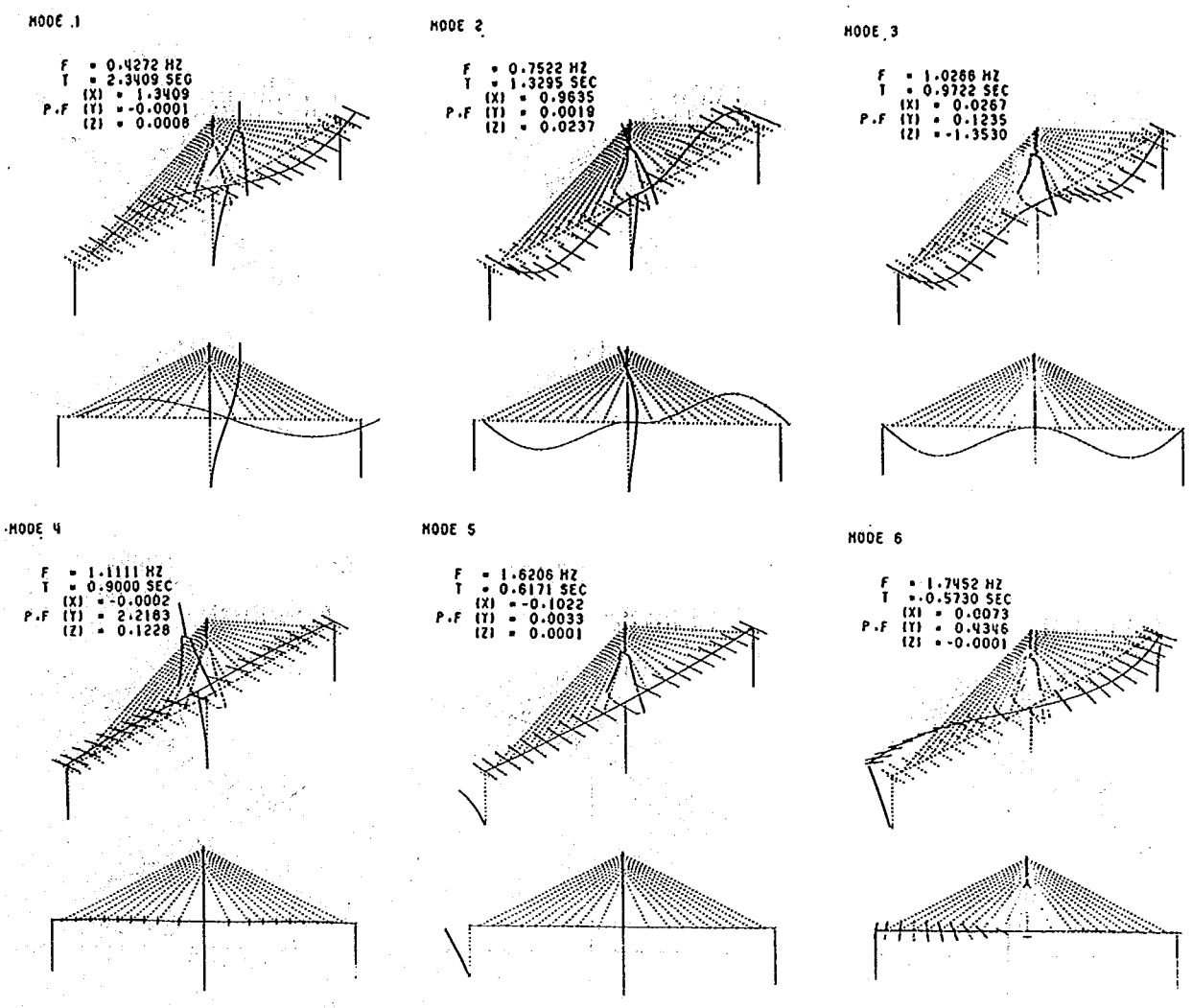

Fig. 6 Natural vibration mode diagrams (completed structure)

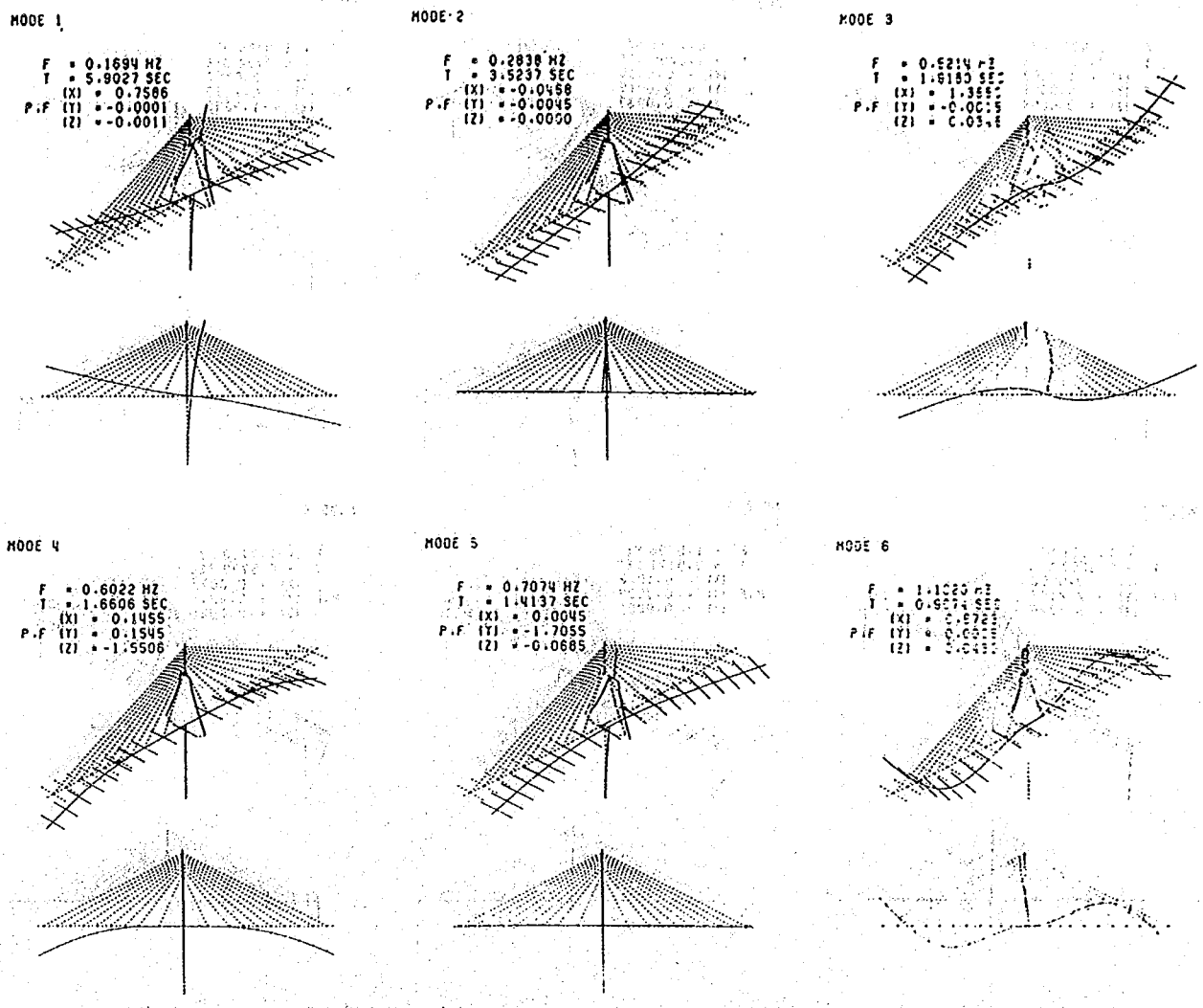

Fig. 7 Natural vibration mode diagrams (structure under construction)

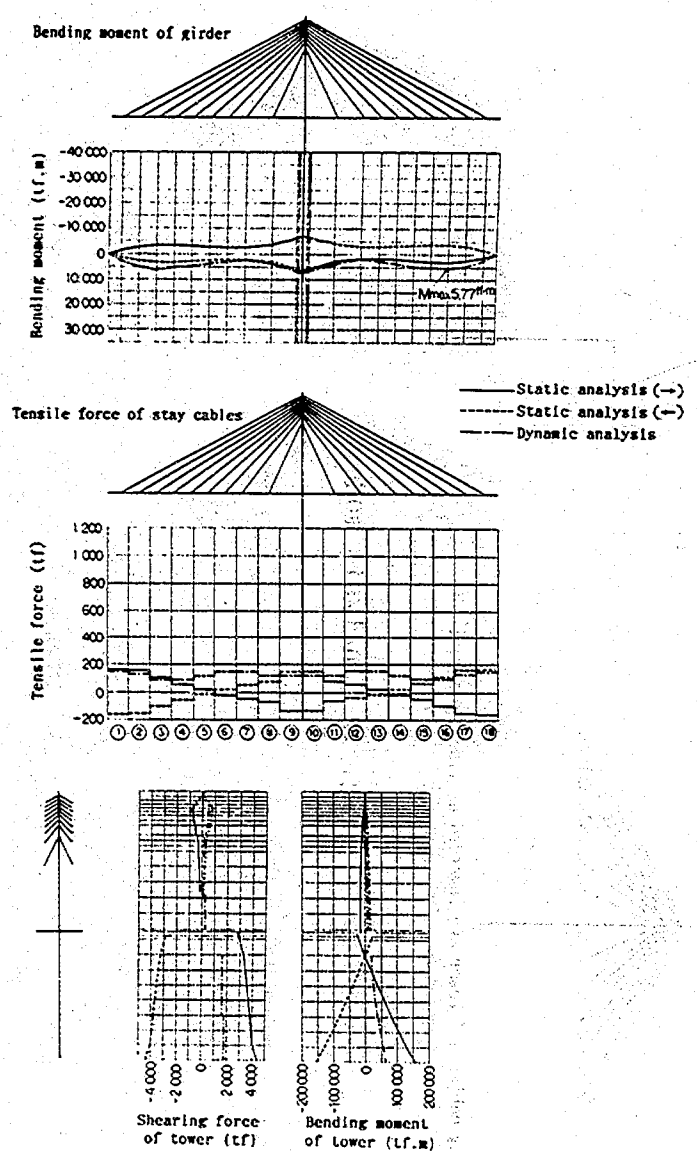

Fig. 8 Maximal response member force (longitudinal direction)

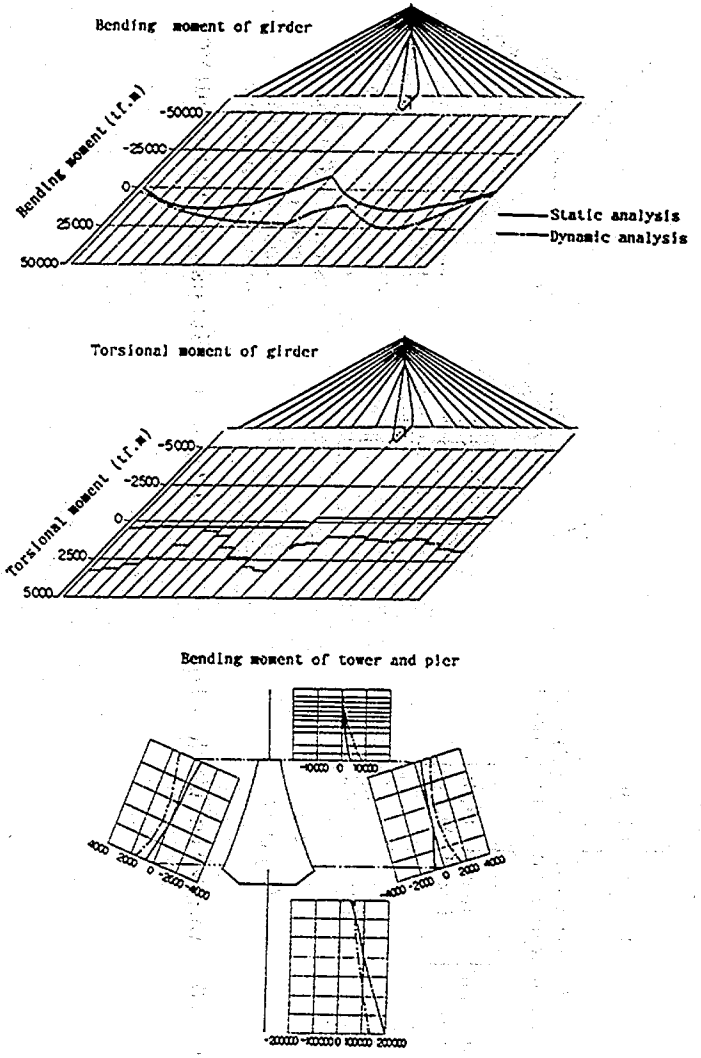

Fig. 9 Maximal response member force (transverse directiton)

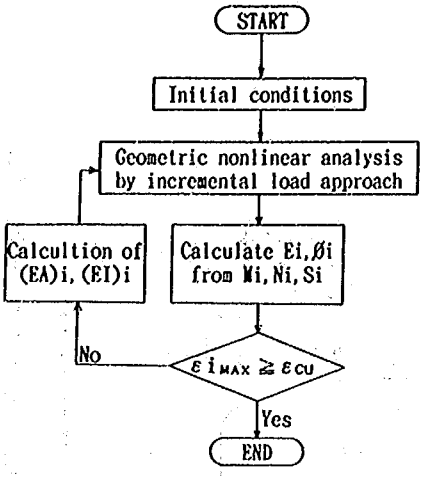

Fig. 10 Analysis work flow

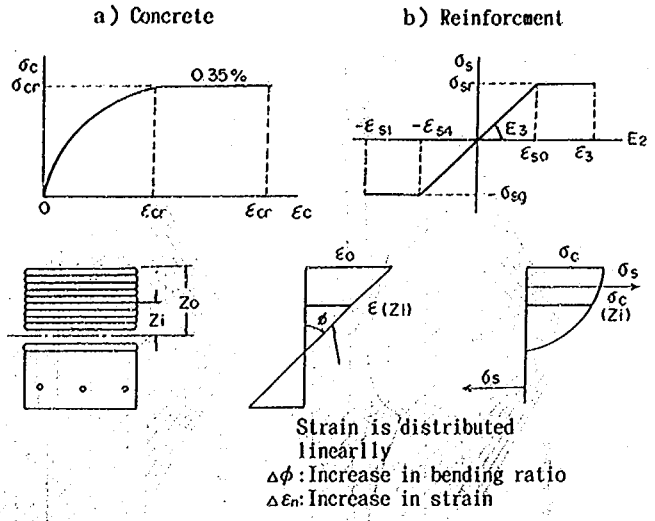

Fig. 11 Stress-strain curves

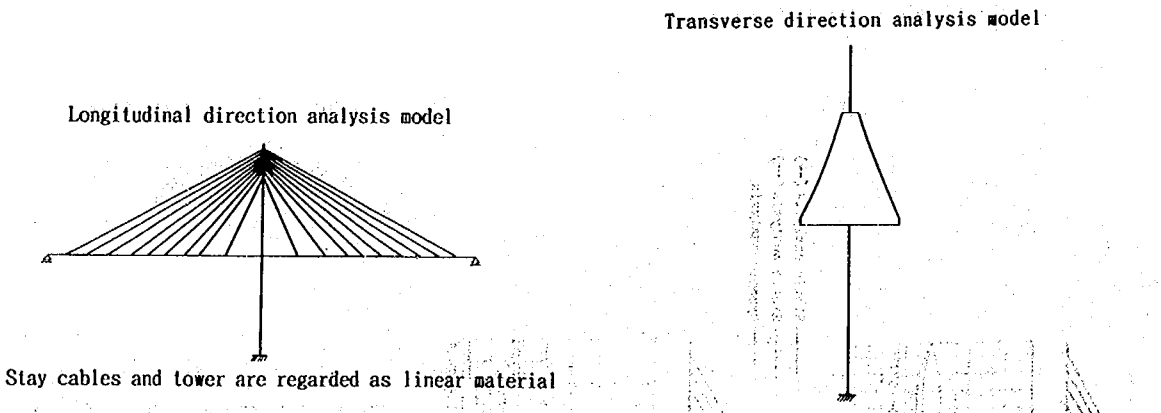

Fig. 12 Analysis model

Table-2 Seismic Coefficient at Failure

Seismic direction	Seismic coefficient at failure kHV	Design seismic coefficient kH	β=KHV/KH
Longitudinal	0.245	0.18	1.36 > 1.3
Transverse	0.633	0.23	2.75 > 1.3

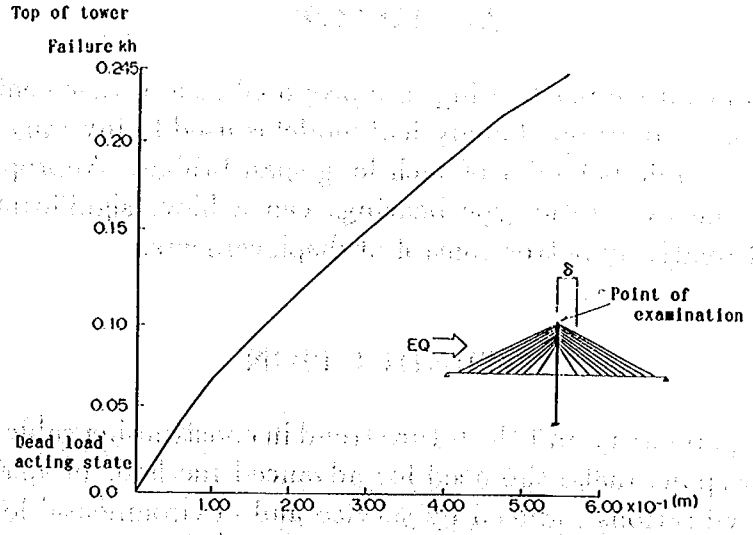

Fig. 13 Changes in displacement (longitudinal direction)

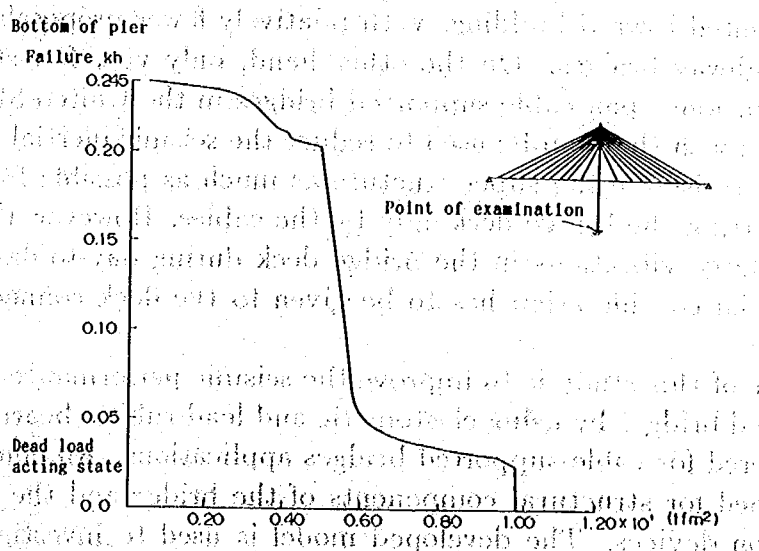

Fig. 14 Change in equivalent flexural rigidity (longitudinal direction)

SEISMIC PERFORMANCE OF CABLE-STAYED BRIDGES WITH ELASTOMERIC AND LEAD-RUBBER BEARINGS

Hosam-Eddin M. Ali and Ahmed M. Abdel-Ghaffar

Civil Engineering Department, University of Southern California,
Los Angeles, CA 90089-2531,
U.S.A.

ABSTRACT

Elastomeric and lead-rubber bearings are proposed as a passive control system for cable-stayed bridges. A developed analytical model is used to investigate the effect of the devices on the seismic behavior of such long span bridges. Appropriate locations and properties of the hysteretic-type bearings can achieve significant reduction in seismic forces and relatively better control of displacements.

INTRODUCTION

The increasing popularity and the future trend in constructing cable-stayed bridges with longer center spans make the need for advanced methods of analysis and techniques to supress vibrations induced by service and environmental loads inevitable. Moreover, the fact that very few bridges have been subjected to strong earthquake shaking makes such need even urgent. Most of the applications in the energy dissipation field are oriented toward buildings with relatively fewer proposals for short and medium span highway bridges. On the other hand, only very few studies [1] have been presented for long span cable-supported bridges in the United States.

The main approach that can be used to reduce the seismic inertial forces of cable-stayed bridges is to isolate the superstructure as much as possible from the ground motion by supporting the bridge deck only by the cables. However, this kind of isolation produces large vibrations in the bridge deck during day-to-day performance. Accordingly special consideration has to be given to the deck connections at abutments and towers.

The objective of this study is to improve the seismic performance of new and existing cable-stayed bridges by using elastomeric and lead-rubber bearings which have not been considered for cable-supported bridges applications. An efficient analytical model is developed for structural components of the bridge and the hysteretic-type energy dissipation devices. The developed model is used to investigate the important parameters that affect the efficiency of lead-rubber bearings as a passive control system.

MODELING OF CABLE-STAYED BRIDGES

The behavior of cable-stayed bridges can be placed in the context of large displacements but small strains. Geometrical nonlinearity originates from: (1) the cables sag which governs the elongation of cables and the corresponding axial tension, (2) the action of compressive loads, due to the inclination of cables, on the bridge deck and towers in terms of their interaction with bending moments, and (3) the effect of the relatively large deflection of the structure on stresses and forces. The material nonlinearity depends on the type of materials (steel or concrete) used in construction. However, it is usually attempted not to allow plastic deformations for such structures for economical and structural stability reasons. In this study, the geometrical nonlinear behavior is considered using the Total Lagrangian approach of three-dimensional beam elements for deck and tower modeling and a truss element for cables idealization. By adopting a continuum approach and employing four-node isoparametric elements, the formulation is applicable to structures consisting of straight or curved members.

In order to accurately model the deck, the main girders and the towers of the bridge to obtain the response of each part and section of the structure, very large number of finite elements are required including plate and beam elements. The problem becomes unsolvable within the today-computer capabilities. Instead, the global behavior of different sections along the structure will be dealt with. The details of the local parts of the bridge can then be estimated out of the global behavior. The approach is practically adequate and can provide a reasonable alternative to predict the dynamic properties of cable-supported bridges. Beam elements can therefore be used to idealize the deck and towers without great loss of accuracy.

The formulation of a typical beam element stiffness matrix and load vectors is general and includes the possibility of modeling sections with different cross section shapes as shown in Fig. 1-c. Among the cross sections that can be dealt with are the box sections with multiple vents and cut-off corner sections as well as different combinations of rectangular shape parts such as I-beams and plate sections. It should be mentioned that the cut-off corner sections can be used for towers for wind resistance reasons while the box sections may be used for main girders and towers as well.

The analysis of cables under different configurations and loading conditions is extremely complex. These structures are generally elastic in nature but are highly nonlinear in the geometric sense. Fortunately, in cable-stayed bridges, vibrations of cables are not very large (compared to the size of the structure) and the geometry of the cables is somewhat well defined before the analysis. The use of the general and complicated algorithms will always be correct; however, the use of a more restrictive formulation can be more effective and may also provide more insight into the response prediction. A four-node isoparametric cable element, as shown in Fig. 1-b, is proposed for cables idealization. The element can predict both in plane and out of plane responses. In addition, the cable element takes into consideration the effect of pretension which is one of the features of cable-stayed bridges.

In modeling cable-stayed bridges, cables are connected to the tower beam elements and deck beam elements at an eccentricity from the middle plane of the beam as schematically shown in Fig. 1-a. Accordingly, end nodes of the cable don't coincide with nodes of beams. The problem becomes more pronounced if one beam is used to model the whole deck where consideration of offset becomes inevitable. In this analysis, the cable nodes are treated as slave nodes where degrees of freedom can be expressed in terms of those at the corresponding master nodes of the beam elements by means of transformation.

During the solution process of equilibrium equations, the internal nodes of both beam and cable elements can be eliminated using a condensation technique. However, the response can be retrieved at their locations without approximations or loss of accuracy [2].

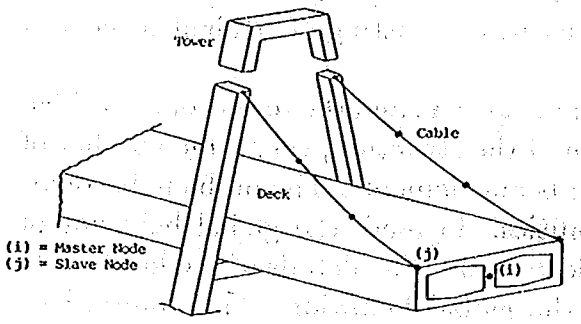

(a) Offset at cable-deck connection

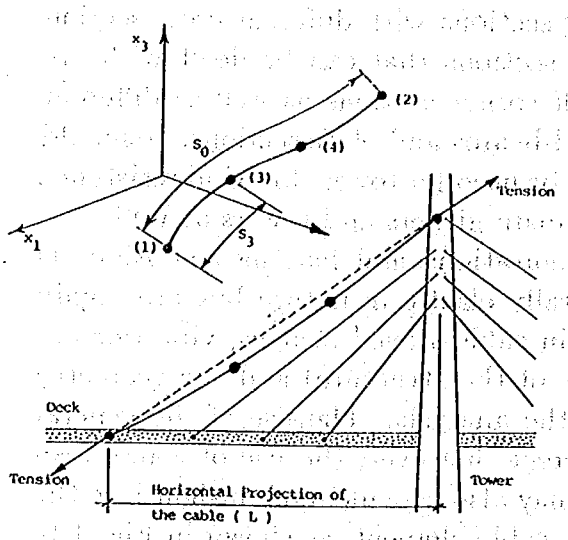

(b) Four-node cable element

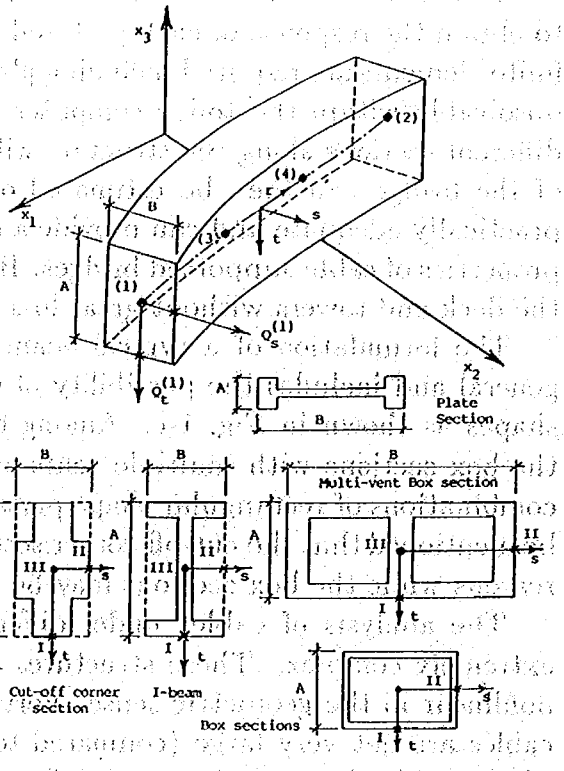

(c) Four-node beam element

Figure 1: Modeling of cable-stayed bridges

MODELING OF ELASTOMERIC AND LEAD-RUBBER BEARINGS

Elastomeric bearings are widely used as supports for bridge girders of many types. They are also increasingly used as seismic isolation devices. There are quite a few techniques that are used for base-isolation. However, the case of lead-rubber bearings, in which a laminated elastomeric bearing is modified by placing a lead plug down its center, provides a relatively inexpensive and reasonable solution. The bearing carries, in part, the weight of the structure and supplies a horizontal restoring force. The plastic deformation of the lead produces hysteretic damping. Thus, one component provides the stiffness under day-to-day loadings, flexibility under severe earthquake excitations, and damping which are the basic elements required in most base-isolation systems.

Analytical modeling and formulation of the bearing behavior is not an easy task. The device is composed of steel sheets, rubber layers, and the lead plug. Most of the difficulties encountered in modeling the behavior, result from the material nonlinearity of lead and the material, geometric and boundary nonlinearities associated with the rubber parts. In addition, rubber is virtually incompressible during the deformation process which leads to numerical instability in standard linear elastic analysis [3]. Practically, the force-displacement hysteresis loop of elastomeric bearings without a lead plug was broadly assumed elastic with a constant shear stiffness and a small amount of hysteresis. These hysteretic properties provide useful damping for seismic applications, but they are not so well defined as to justify their inclusion in the analysis. Thus, linear elastic analysis is widely acceptable for most bridge elastomeric bearing applications.

In this study, both geometrical and material nonlinearities are considered to model rubber, steel and lead which are the three basic materials in passive devices. For rubber materials, large displacement/large strain finite element model is proposed based on the Total Lagrangian formulation and different strain energy functions that cover wide spectrum of assumptions from restrictive to complicated representation of stress-strain relationship. The incompressibility is handled by using a consistent penalty method in which a solution is efficiently reached by approaching the equilibrium state through a series of decreased compressibility. For steel and lead materials, a loading-bounding stress point plasticity model is developed. Moreover, a multi-yield surface model can be optionally used dependent upon the experimental results of stress-strain relationship. The analytical model is checked against experimental results for lead-rubber bearings where satisfactory agreement is generally obtained [2].

The control and improvement of the vibrations of cable-stayed bridges necessitates the inclusion of energy dissipation devices at certain locations as shown in Fig. 2-b. The problem becomes difficult to solve with the very large number of degrees of freedom associated with accurate modeling for both bearings and bridge components. A simplified model is accordingly proposed for the dissipation devices in which a two-node element is introduced for a stiffness-type approach, as shown in Fig. 2-a. The element is capable of withstanding axial and shear forces. The parameters

that control the hysteretic behavior of the element can be estimated out of analytical and/or experimental results. The model has the capability of considering an eccentric installation with regard to the beam nodes. In order to check the analytical model, the responses of different bearings are compared to experimental results. One of these results is shown in Fig. 3-b.

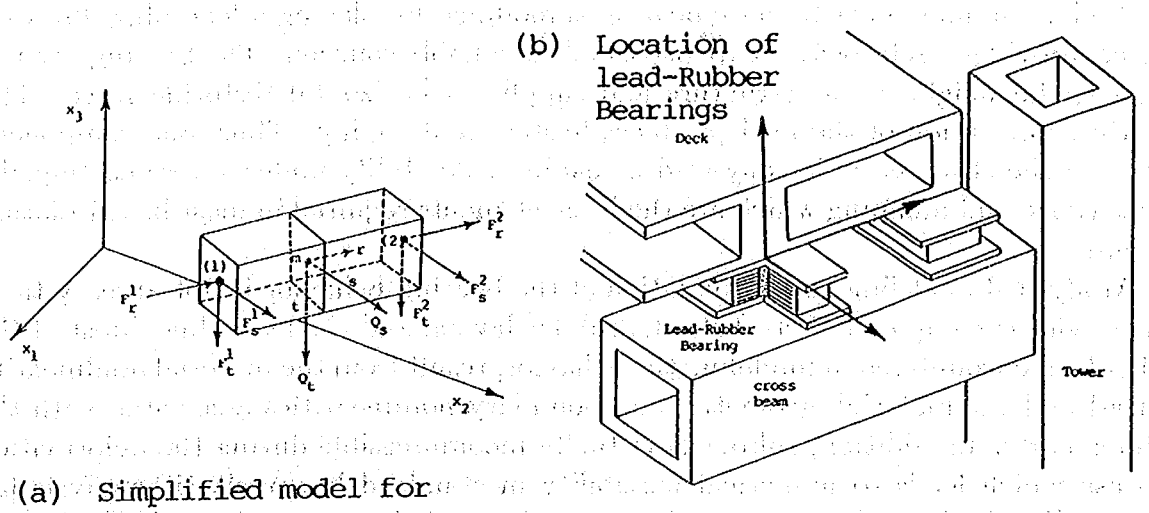

Figure 2: Location and practical model for bearings

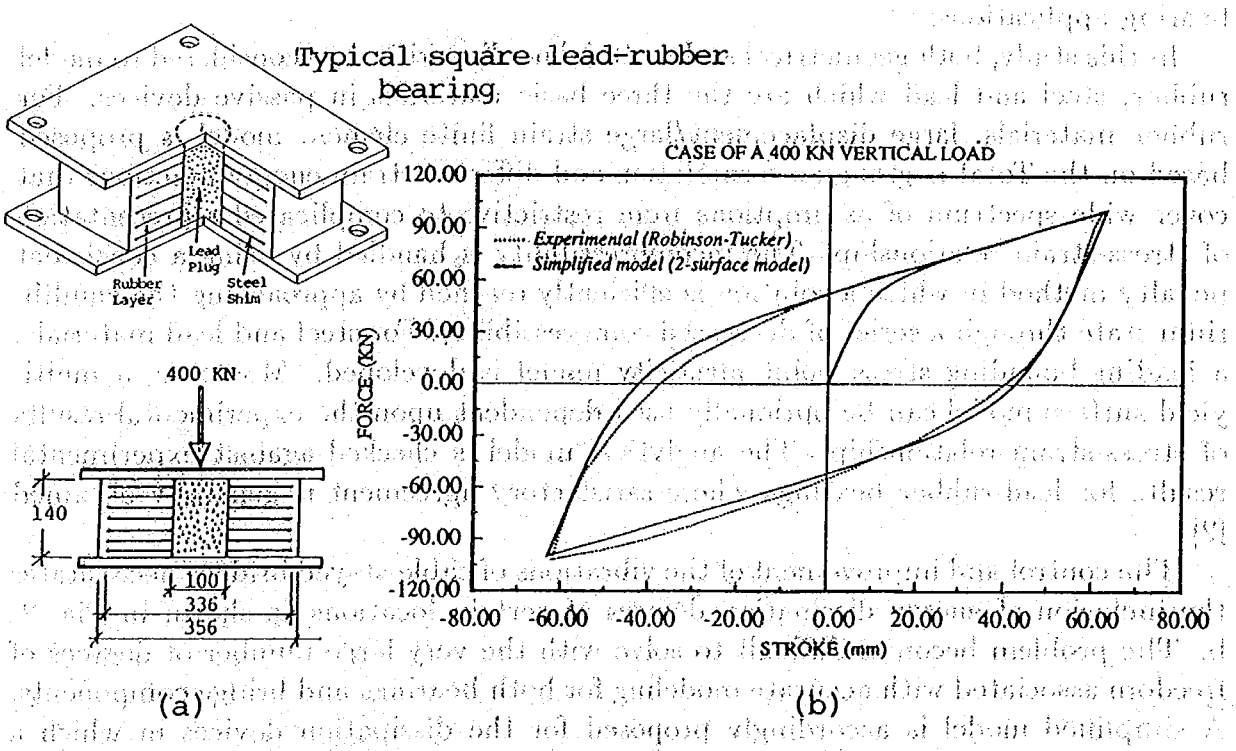

Figure 3: Hysteretic behavior of a lead-rubber bearing

BRIDGE MODEL AND ANALYTICAL PROCEDURE

In order to investigate the sensitivity of cable-stayed bridges response to different parameters of passive control systems, a bridge model is proposed to represent most of the bridge systems and the effective spans. The three-dimensional view of the model is shown in Fig. 4-a. The bridge has a center span length of 1100 ft (330 m), and two side spans of 450 ft (135 m) each. A double plane multi-cable harp system is chosen for the bridge. The finite element nodes and different elements along with the cross sections are shown in the same figure. In the models, cables are anchored to concrete pylons and steel box section-type deck. It can be noticed that one beam element is used to idealize the deck accompanied with different slave nodes at various locations along the bridge to take care of the offset associated with cable-deck connections and the eccentric installation of devices with respect to nodes of beams as shown in Fig. 4-b.

In the seismic analyses presented in this study, it is assumed that the bridge starts motion at rest in the dead load deformation position. It is therefore necessary to perform a nonlinear static analysis to compute the tangent stiffness matrix, mass matrix, internal forces, displacements and rotations, and the stress distribution of the bridge structural components. The rationale for the nonlinear static analysis is the fact that cables are pre-taut which significantly affect deflections of the structure and accordingly its dynamic characteristics. In case of lead-rubber bearings, the bearings may undergo considerable shear and compression deformations under the bridge own weight as shown in Fig. 4-c. Excessive deformations of the bearings due to creep, specially in shear, can jeopardize their performance. It is proposed that the bridge be constructed and consequently analyzed with rollers provided at the deck-abutment connections. Once the bridge settles in its dead load deformed shape, bearings can be installed and rollers may then be removed. Some simple construction details have to be provided in order to achieve this task. It may be argued that the structure may suffer more deformations, with the rollers, than elastomeric bearings had they been mounted from the beginning. However, the magnitude and distribution of deformations can be controlled by changing magnitude and distribution of initial tensions in cables.

In the dynamic analysis, the Newmark's constant average acceleration method is used for a 0.01 sec time step. Damping matrix is evaluated considering the Rayleigh approach utilizing the first two eigenvalues with 2% damping ratio. Array no. 6 of Imperial Valley earthquake is used for the ground motion input [2]. Components $S40°E$, $S50°W$ and $DOWN$ are used for longitudinal, lateral and vertical directions respectively. This array is the strongest among the other recorded arrays. Ideally, a number of earthquake records, which cover the range of frequencies and peak values of interest, should be chosen as input. The choice of these records must be based on geological and local soil conditions of different seismic zones and the expected ground motion characteristics. Based on only one earthquake, the results can nevertheless explain the physics of the problem and evaluate the different parameters that are still applicable to different excitations as well.

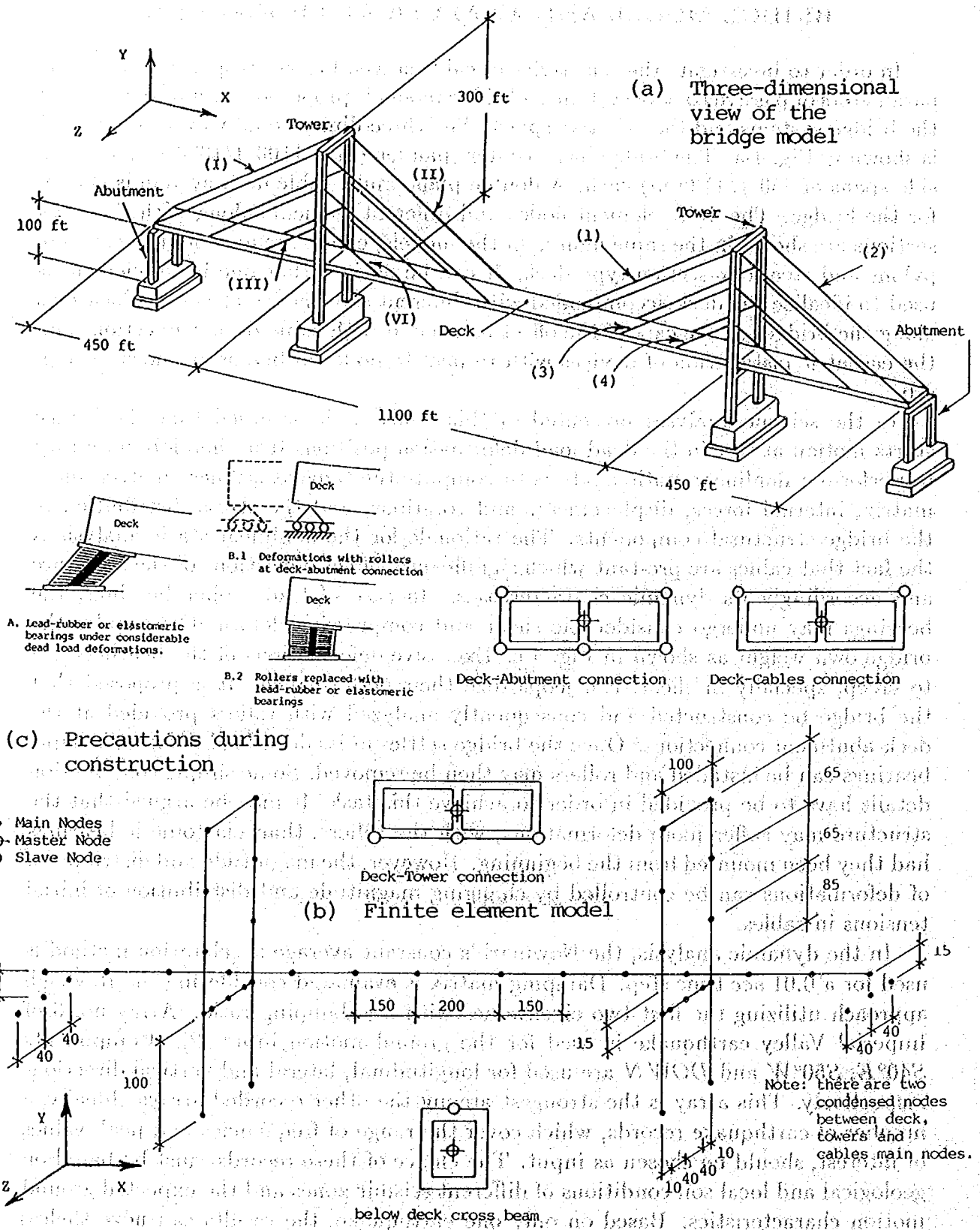

Figure 4: Bridge model and suggested construction procedure for bearings

LOCATION OF LEAD-RUBBER BEARINGS

The structural synthesis of cable-supported bridges provides few options for mounting the passive control devices. The deck-abutment and deck-tower connections are among the few practical locations for such installation. The option becomes however whether to have all the devices at one connection-type location or to rather distribute them. One more possibility of installing the devices would be at tower-pier connection. However, the construction pattern, stability behavior and bearings performance at this location are practically questionable. This case is therefore not considered in this study.

The seismic energy dissipation capability of an isolation unit depends on the force required to have the device behave in the plastic range. In case of lead-rubber bearings, the process becomes related to the yielding of the lead plugs. Accordingly and in a very simplified way, given the total shear force required to yield all lead plugs at the abutment and the tower combined, V_{all}, and the lead yield stress ($10 - 10.5\ MPa$), the total area of the lead plugs can be obtained. The shear force required to yield the lead plugs located in bearings at the deck-tower is termed V_{dt}. The ratio of the area of the lead plugs located at the deck-tower connection to the total lead area, (V_{dt}/V_{all}) may vary between zero and one. A ratio of zero represents the case when all the lead plugs are located at the deck-abutment connection only, while a ratio of one represents the case when all the lead plugs are located at the tower-deck connection only. By varying the ratio (V_{dt}/V_{all}) between zero and one, the effect of the location of the lead-rubber bearings on the response of cable-stayed bridges can be investigated in order to identify the most suitable location of the hysteretic-type units.

In order to have a clear picture of the location parameter, different structural properties and non-related parameters of bearings should be kept unchanged. In the analysis, the yield strength of all isolation units is taken equal to 5% of the deck weight, W. For each lead-rubber bearing, the ratio of the initial stiffness to the plastic stiffness is taken equal to ten. For each case of the location parameter, the response of different quantities is normalized to the corresponding response for the non-isolated bridge as shown in Fig. 5. Another parameter of interest is the idealization of the hysteretic loop. Shown in the same figures are the results for two different idealization cases. In the first case, the force-displacement curve for each device element is represented by a two surface (loading-bounding) model. For the second idealization, a bi-linear force-displacement curve is adopted.

The introduction of energy dissipators significantly reduces the earthquake induced forces as compared to the non-isolated bridge case. However, displacements generally increase but with slower rates. Installing lead-rubber bearings only at the abutments reduces dramatically the forces in towers compared with the case of introducing all lead plugs at the towers only associated with relatively slight increase in the displacements of the towers. The deck displacements are least if all hysteretic-type devices are not concentrated at the towers only. More forces are noticed at the abutment side of the deck as well when all lead plugs are placed at the abutments while forces in sections of the deck near the mid-span decrease.

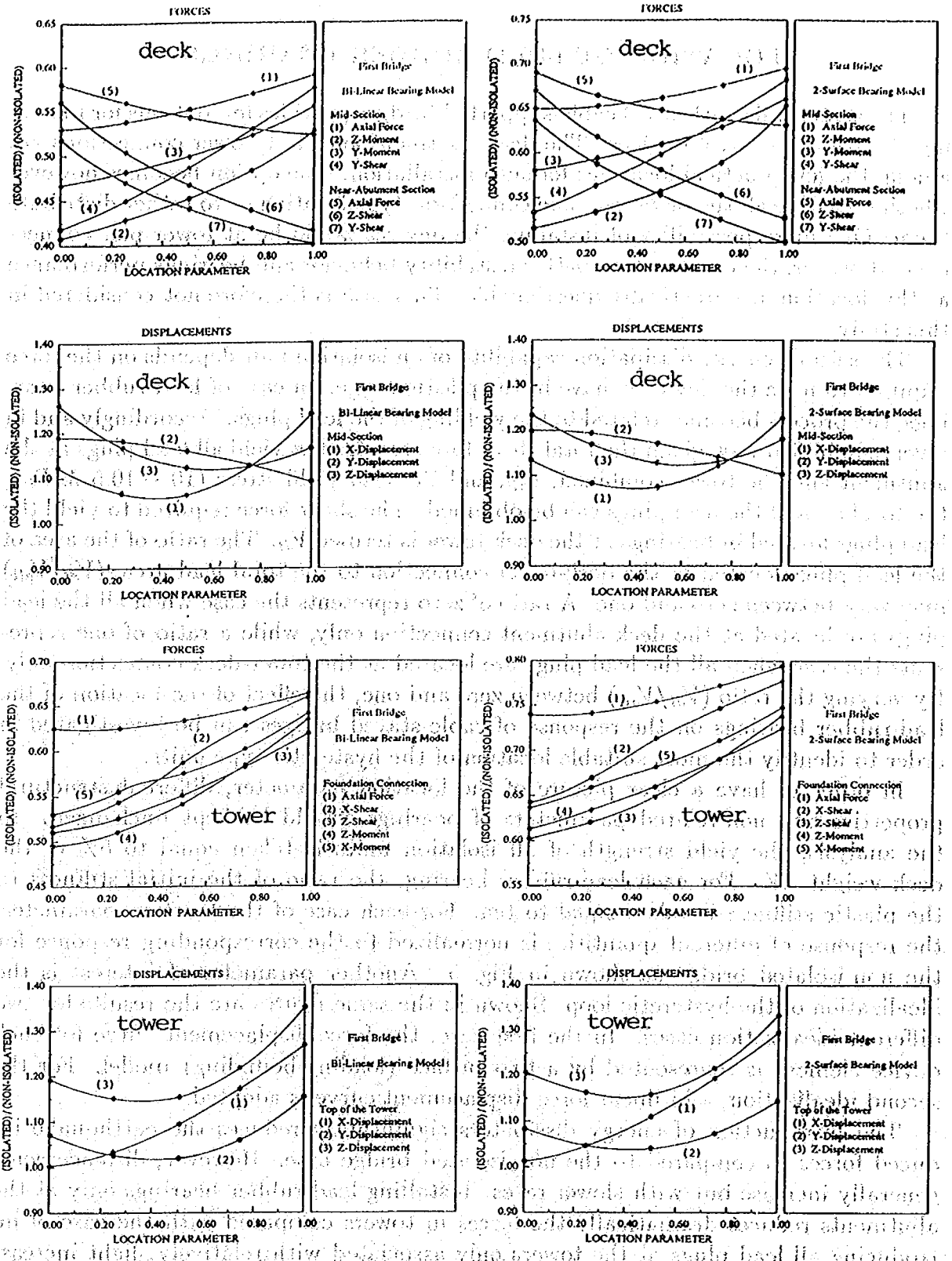

Figure 5: Effect of location of lead-rubber bearings on deck and towers

The difference in the bridge performance for different idealizations of the bearing hysteretic response, as shown in Fig. 5, illustrates the importance of the careful and accurate prediction and representation of the bearings behavior. The results obtained in this section can provide a solution for existing towers, piers and abutments with inadequate strength. Installing energy dissipators at the abutment, for instance, attracts more forces to the abutment rather than to the towers and piers which provides an alternative way to strengthening towers and their foundation. The supporting structures along with the approach spans (which is referred to as abutment side) may be, for some existing bridges, among areas most vulnerable to earthquake induced damage. Appropriate choice of location of hysteretic-type devices can create new avenues for seismic response control of these parts.

SHEAR STRENGTH OF LEAD PLUGS

The shear force at which plastic behavior of hysteretic-type units becomes predominant is an important parameter in the design philosophy of energy dissipators. In the case of lead-rubber bearings, given the shear force level and the lead yielding strength, the number and cross sectional area of the lead plugs can be approximately designed. The level of the devices shear strength depends on the mechanism by which all lateral loads, including those arising from sources other than earthquakes, are resisted [5]. Such shear force level should be selected to achieve two objectives. First, the device is required to be stiff under the action of wind, traffic forces, and small earthquakes. Second, during severe seismic events where forces exceed the design shear strength, the level of forces and displacements of the structure are required to remain within acceptable limits to ensure that the bridge continues to function satisfactorly.

The response for different cases with varying yield shear force of lead dissipators are investigated. Various ratios of shear strength of combined devices at the abutment and the tower, V_{all}, to the weight of deck, W, up to 15% were considered in the numerical analysis. The results are normalized to those of the non-isolated bridge. One case of the energy dissipation devices locations are attempted where all lead plugs are inserted in the bearings located at the abutment. The different bridge response quantities are shown in Fig. 6.

The main advantage of lead plugs, as devices that provide a force limiting mechanism for the supporting structure, is quite clear in Fig. 6. The effect of dissipators may be regarded as similar to that of extra equivalent viscous damping. It can be seen that incorporating higher ratios of yield strength at the abutments reduces significantly the forces in the tower and the displacements of the deck and towers but increase the forces on the abutment (for the considered location parameter).

The choice of the shear strength of the isolation system should achieve relatively a good balance between magnitude of forces along the bridge and control of deck and tower vibrations. In small to medium span highway bridges, a lead yield force of about 5% of the superstructure weight, seems to be an optimum value for bridge design applications [4]. In long-span cable-stayed bridges, a comprehensive statistical

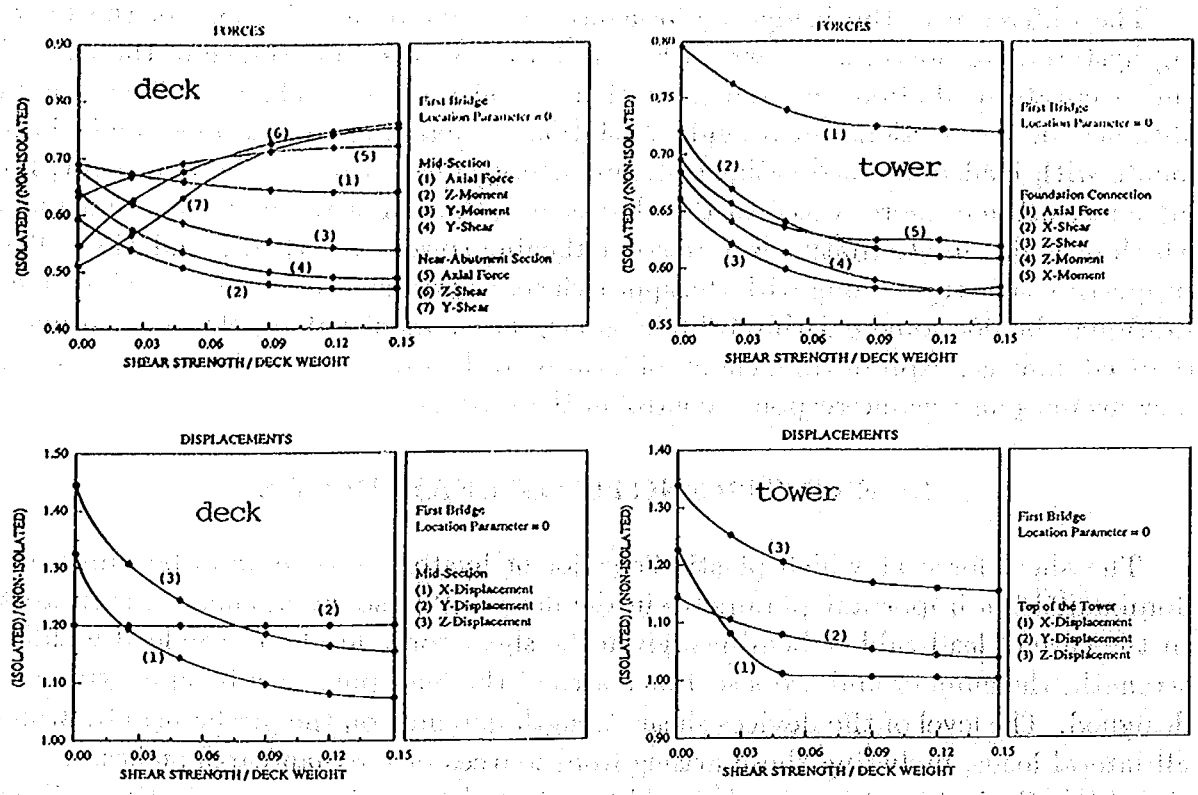

Figure 6: Effect of shear strength of lead plugs on deck and towers

study is needed for analytical and experimental results using different ground motion time histories. The analysis presented herein suggests a ratio of $8-9\%$. Insignificant change in response quantities can be noticed for higher ratios. Moreover, higher ratios may create problems for the required sizes of lead plugs that can be accommodated in elastomeric bearings.

CONCLUSIONS

The use of passive energy dissipation devices offers a potential advantage for the design of earthquake resistant bridges. Generally, the magnitude and distribution of forces for the bridge structural components can be controlled by proper choice of properties and locations of the devices. However, an increase in displacements is to be expected.

The effect of lead inserts in lead-rubber bearings can be regarded as similar to providing extra equivalent viscous damping. A bi-linear representation of the lead-rubber hysteretic loop may overestimate the effectiveness of the bearing. An accurate modeling of the force-displacement relationship based on either experimental or analytical procedure is therefore essential for reliable prediction of the structural performance.

The yield strength of the hysteretic-type devices can be conveniently expressed as a ratio of the superstructure's weight. A ratio of 8 – 9% can be recommended as a practical value. Higher percentages don't help improve the performance significantly.

The distribution of forces transmitted to the towers, deck girders and cables depends on the location of hysteretic-type devices. Incorporation of lead plugs, as energy dissipating devices in the lead-rubber bearings, at the abutments rather than at the towers, for instance, reduces the seismic forces generated in the towers and consequently on the foundations. Displacements can be controlled if hysteretic-type devices are not fully concentrated at the deck-tower connections. The appropriate choice of the location of energy dissipation devices can create new avenues for retrofitting inadequate supporting parts of the bridge.

ACKNOWLEDGEMENTS

This study is supported in part by the National Science Foundation through Grants No. CES-8717252 and CES-8819548 with Dr. S.C. Lin as the Program Director, and partly by the department of civil engineering at University of Southern California.

REFERENCES

1. Abdel-Ghaffar, A.M. and Ali, H.M. (1991), *Energy Dissipation Devices for Cable-Stayed Bridges*, Proceedings of the second Workshop on Bridge Engineering Research in Progress, pp. 221-224, Reno, Nevada.
2. Ali, H.M. (1991), *Nonlinear Seismic Analysis of Cable-Stayed Bridges with Passive Energy Dissipation Devices*, Ph.D. Dissertation, Department of Civil Engineering, University of Southern California, Los Angeles.
3. Chang, H. (1988), *Nonlinear Elastomer Analysis - Survey of Computer Codes and Case Study for Caliper Seal*, Computers and Structures, Vol. 30, No. 5, pp. 1165-1173.
4. Ghobarah, A., and Ali, H.M. (1990), *Seismic Design of Base-Isolated Bridges Utilizing Lead-Rubber Bearings*, Canadian Journal of Civil Engineering, Vol. 17, No. 3, pp. 413-422.
5. Mayes, R.L., Jones, L.R., Kelly, T.E., and Button, M.R. (1984), *Base Isolation Concepts for Seismic Bridge Retrofit*, Proceeding of a symposium sponsored by the Technical Council of Lifeline Earthquake Engineering of the ASCE, San Francisco, California.
6. Robinson, W.H. and Tucker, A.G. (1981), *The Results of Lead-Rubber Bearings for W.M. Clayton Building, Toe Toe Bridge and Waiotukupuna Bridge*, Bulletin of the New Zealand National Society for Earthquake Engineering, Vol. 14, No. 1, pp. 21-33.

ASEISMIC DESIGN OF THE UMEMACHI BRIDGE —A CONTINUOUS FIVE-SPAN RIGID-FRAME BRIDGE WITH V-SHAPED LEGS—

Atsushi NANJO
Chief Engineer,
Design Division,
Engineering Department,
Hanshin Expressway Public Corp.

Shigeru KAYANO
Chief Official,
Toll Road Division,
Road Bureau,
Ministry of Construction

Abstract

The Umemachi Bridge is a continuous five-span rigid-frame bridge with V-shaped legs. In view of the fact that the bridge has a very complicated configuration (a curved alignment and greatly varying width along the roadway), space-frame modeling was used in the structural analysis. Aseismic design of the members was chosen based on dynamic response analysis, as well as on the modified seismic coefficient method. Furthermore, on-line hybrid loading tests (pseudo-dynamic tests) were carried out in order to investigate the deformability and ductility of the V legs and the ultimate safety of the structure during strong earthquakes.

1. Introduction

The Umemachi Bridge, one of the world's largest continuous five-span rigid-frame bridge with V-shaped legs, is part of the Wangan (Bay) Route of the Hanshin Expressway which crosses the Umemachi waterway on the north side of Osaka Port. There are various types of long-span bridges (existing or under construction) near the Umemachi Bridge, namely: the Minato Bridge (a truss bridge), the Tenpozan Bridge (a cable-stayed bridge), the Shorenji-gawa Bridge (a box-girder bridge), the Kanzaki-gawa Bridge (a Nielsen arch bridge), the Konohana Bridge (a monocable-suspended bridge) and others.

In order to maintain a well-balanced view with this group of bridges, a V-leg configuration was employed. This ensures the necessary canal width and sufficient space under the bridge girder for navigation of boats. Using V-shaped configuration also enables the reduction of the effective center span of the main girder to 160m as compared to the center-to-center spacing of 215m between the two V legs. Furthermore, effective cross sections could be achieved by utilizing the arch action generated monolithically by the main girder and the V legs. This consequently led to accomplishment of a relatively economical bridge design.

The Umemachi Bridge was erected over a busy waterway, and hence various considerations in design and execution of work on the bridge had to be done. In addition to axial compressive and in-plane bending loads, the V legs are also expected to be subjected to out-of-plane bending moments leading to a very complex dynamic behavior during earthquakes. This paper will discuss the characteristics of the adopted aseismic design of the Umemachi Bridge with particular emphasis on the bridge superstructure.

2. Structural Overview

The main elements of the superstructure of the bridge consist of the main frame (the main girder and the V legs) with connecting cross beams and girders. Fig. 1 shows a general plan of the Umemachi Bridge, and some general specifications for the construction of this bridge is given in Table 1.

Each segment of the main girder consists of two curved box girders running side-by-side and rigidly connected to the V legs. There is no other girder in the space between the two main members.

The length of the deck overhang is allowed to vary to meet the changes in the width of the bridge; and whenever such variation is in excess of 7m, a parallel longitudinal girder and supporting braces have been provided. In addition, transverse girders are located at intervals of approximately 20m.

Each of the V legs has a box cross section varying along the member length. As the main girder is curved, the member axes of the legs are not on the same plane, but are arranged so that they are meet at certain angles at the bases. All cross beams also have a box cross section. These are provided at the top, intermediate and base levels of all end supports and V legs.

The foundation of the substructure was constructed using cast-in-place concrete piling for economic considerations and ease of work execution. The intermediate piers which are subjected to horizontal loads from the bases of the V legs were constructed using reinforced concrete. The end piers were constructed of steel materials fabricated to form the shape of a portal.

3. Erection Method

Due to topographical factors at the project site and the restriction on the time for completion, a method in which the center span segment and each of the V legs could be erected independently of each other was adopted. Fig. 2 illustrates the erection procedure.

First, the main frames for the V-leg segments were fabricated and assembled in the shops, and then welded at the yard. These are then transported to an intermediate yard where these were subsequently raised upright. The cross beams, steel deck, and other parts were attached to completely assemble each V leg. Next, each V leg was suspended and towed by a 3500tf class floating crane up to its final position. The V legs were then installed on the intermediate supports.

In the second stage, the side spans were erected using the "crane bent" method. The entire center span segment was assembled on the ground at the intermediate yard, and towed to the site by a floating crane. Lastly, the gaps between the connecting members were joined. As it had been foreseen that the joints would have to accommodate various errors, an adjustable allowance of 200mm was specified and connecting plates were fabricated based on the measured values.

4. Structural Analysis

4.1 Modeling of Structure

The Umemachi Bridge is a rigid-frame bridge composed of a wide steel deck curved box girder supported by V-shaped legs. As it has curves and altitude, the deck surface will be deformed horizontally not only due to the horizontal loads lateral to the bridge axis but also to the vertical loads such as dead and live loads. In order to accurately calculate the internal forces of the V legs and the end piers generated as an effect of horizontal deformation, it is necessary to assess the overall behavior of the steel deck. As illustrated in Fig. 3, the bridge is modeled by a lattice composed of two main girders, the V legs, cross girders, and a truss modeling the steel deck.

4.2 Design Loads

Table 2 specifies the typical design loads of the superstructure. The design loads were compiled basically from the Hanshin Expressway Public Corporation design criteria, but accounted for some particular loads supported by this bridge. For instance, the vehicle inspection rail load (300kgf/m) specified for Umemachi Bridge is normally not included in the appurtenant loads in the usual design criteria. Considering the large horizontal reactions on the intermediate supports and soft ground conditions, it is required that the structure be designed to withstand support movement of 25mm toward either direction of the side spans due to earthquakes.

5. Aseismic Design

5.1 Aseismic Design Procedure

With the effect of an earthquake on the V legs expected to be great, space-frame analysis using the model described in the previous section was conducted for the aseismic design of the bridge. Also, along with static analysis based on the modified seismic coefficient method, dynamic analysis based on the average response spectral method was conducted using the same model. Larger of the two obtained results was used in the design of members.

5.2 Dynamic Response Analysis

The data for analysis consisted of input from two directions — one along the bridge longitudinal axis and the other from the direction lateral to the bridge longitudinal axis. The input spectra were based on the Specifications for Highway Bridges (simply SHB spectrum, hereafter) [Ref. 2] and the draft Design Guidelines for the Design of the Ajigawa Bridge, which are shown in Fig. 4. It is important to note that the SHB spectrum was applied to a dynamic model of the Umemachi Bridge with soil-foundation interaction spring elements. On the other hand, a dynamic model of the Umemachi Bridge with fixed base was used in applying the Ajigawa spectrum since this spectrum already included soil-foundation interaction.

5.3 Analytical results

Fig. 5 shows the results of the dynamic response analysis using the SHB spectrum which gave the larger sectional forces. The results can be summarized as follows:

- various internal forces act simultaneously in the V legs;
- a moment can generate deformation in a direction different from each input direction even in the case when a seismic force is caused in the axial direction of the bridge or in the direction lateral to it;
- the axial forces in the V legs are greater depending on the deformation of the entire bridge.

5.4 Comparison Between Static Analysis and Dynamic Analysis

Before carrying out the design of the cross sections, a comparison of the internal forces between dynamic response analysis and static analysis was made. With the seismic force assumed to occur from an arbitrary direction, the internal force from dynamic response analysis was computed by adding the components of the internal forces in the direction of the longitudinal and lateral axes from either of the input direction according to the following expression:

$$[F] = \sqrt{[F_1]^2 + \frac{[F_2]^2}{2}}$$

where $[F_1]$, $[F_2]$ are internal forces parallel or lateral to the bridge longitudinal axis with the larger of the two forces taken as $[F_1]$.

The V leg cross beam had its cross section determined by the seismic bending moment in the direction lateral to the bridge axis. However, some parts of the bridge (e.g., the cross sections of the top cross beams and the bases of the V legs) were determined based on the results of the dynamic response analysis as indicated in Fig. 6.

6. On-line Hybrid Loading Tests of the Bridge Pier Specimens

6.1 Objective of Tests

The Umemachi Bridge is a curved bridge with the main girder rigidly connected to the V legs creating a rigid frame. Due to the asymmetrical nature of the frame, three-dimensional dynamic behavior of the structure will be considerably complicated during an earthquake. Hence, a detailed verification of the behavior was carried out through the dynamic response analysis while proceeding with the design of the cross sections. In order to assess the behavior of the structure in the plastic region when damaged and in order to evaluate the ultimate safety of the structure, the V legs are regarded as the most critical and experimental tests were conducted on specimens of a reduced scale prototype considering varying axial forces and lateral forces.

6.2 Testing Method

A cross section near the base of the V legs (P52) shown in Fig. 7 was modelled. This specimen had cross section of 300mm × 270mm which corresponds to a scale of 1:10.5 in relation to the real member. The length of the specimens used was 1800mm (Fig.8). The stiffeners met the requirements stipulated in the Specifications for Highway Bridges. Specimens included different patterns of stiffener arrangement with their longitudinal to transverse ratio approximately near the value of the real bridge.

On-line hybrid test (better known as pseudo-dynamic test in U.S.) is a computer-controlled experimental technique in which direct numerical time integration is used to solve the equations of motion. The computed displacement at each step is statically imposed on a specimen through a computer-controlled load actuators in order to measure its restoring forces at the current deformation state. The measured restoring forces are then fed into the equations of motion to compute the next set of displacements. Current implementation of this method has been extended to substructured hybrid loading test procedure [Ref. 3] in which the earthquake response of a multidegree-of-freedom system could be simulated by testing only the critical experimental substructure.

The bridge model for the on-line hybrid loading test of the pier specimens was a single-degree-of-freedom system with period of 1.25 seconds. The set-up shown in Fig. 9 was used to impose computed lateral displacements and axial loads on the tip of a specimen. The input seismic wave used was 30 seconds of the strong portion of the 1968 Tokachi Earthquake recorded at Hachinohe (Fig. 10). The spectral characteristics of this earthquake is shown in Fig. 11. The Hachinohe record was obtained on relatively unstable ground giving a low-frequency band at around 0.4Hz. Hence, this earthquake was used as the input record for the hybrid tests simulating the model to long period waves. The input acceleration was γ times the yielding acceleration of the specimen which are 6 and 9 times that of the actual bridge.

6.3 Results of Experiment

Figs. 12 and 13 plot the load-displacement response of the pier specimen. When $\gamma = 6$, the loop is in the plastic zone without large plastic deformation, and the hysteretic loop shows the shape of a stable spindle. When $\gamma = 9$, great deformation occurs on the negative side of the load axis at 9.5 seconds, but after that, the loop is restored to the shape of a stable spindle.

Figs. 14 and 15 plots the time history of energy partitioning for each case. When $\gamma = 6$, the loop enters the plastic zone in about eight seconds resulting in deterioration of the stiffness, but no large change followed.

From the experimental results, it is evident that the deformability of the V legs is great, and they have sufficient aseismicity against any earthquake stronger than those incorporated in the design of this bridge. More detailed results are presented in Ref. 1.

7. Conclusions

Various special considerations had been made in the aseismic design of the Umemachi Bridge, and these can be summarized as follows:

- Because of the complex nature of the earthquake response behavior of the Umemachi Bridge, sophisticated space-frame modeling was used in structural analysis to properly account for in-plane and out-of-plane behavior.
- Results of analysis show that various internal forces act simultaneously in the V legs, and the axial forces greatly vary depending on the deformation of the entire bridge.
- Out-of-plane loads are of important concern, i.e., a moment can generate deformation in a direction different from the input direction.
- Aseismic design of members were made based on larger of the design forces obtained by dynamic response analysis and modified seismic coefficient method.
- On-line hybrid loading tests of box-shaped pier specimens have verified that the V legs have sufficient deformability and ductility to prevent structural collapse even during extremely severe earthquakes.

Acknowledgements

The authors would like to thank Prof. Yoshikazu Yamada and Assoc. Prof. Hirokazu Iemura of the Earthquake Engineering Laboratory, Civil Engineering Dept., Kyoto University for their advice and cooperation in the earthquake response analysis study and the hybrid loading tests on the pier models. Acknowledgements are extended to all who participated in the design and construction of the Umemachi Bridge.

References

1. The Association for Disaster Prevention Research, "Research Study Report on the Deformation Ability of V legs of a Rigid-Frame Bridge," March 1989. (in Japanese)
2. Japan Road Association, *Specifications for Highway Bridges*, Part V — Earthquake Resistant Design, 1980. (in Japanese)
   Also English summary in pp.135–151 of the *Earthquake Resistant Design for Civil Engineering Structures in Japan*, compiled by the Earthquake Engineering Committee, Japan Society of Civil Engineers, 1988.
3. W. Tanzo, Y. Yamada, H. Iemura, and K. Endo, "Substructured Hybrid Loading of Structural Members under Combined Axial, Shear, and Bending Loads," *Proc., 8th Japan Earthquake Engineering Symposium*, December 1990.

Table 1 Umemachi Bridge Characteristics and Parameters

Route Designation	Wangan (Bay) Route
Road Classification	Class 2, Grade 1 with Design Roadway Speed of 80kph
Bridge Classification	Grade 1 (TL-20 and TT-43)
Superstructure	Continuous Five-Span Curved Steel Deck Box Girder Rigid-Frame Bridge with V Legs
Substructure	Two Steel Rigid-Frame End Piers and Two Reinforced Concrete Intermediate Piers
Foundations	Four Cast-in-Place Reinforced Concrete Pile Foundation of length 36.0 ~ 37.5m
Bridge Length	390m
Spacing Between V Legs	90 + 215 + 85m
Effective Span Length	59.35 + 57.50 + 160.00 + 57.50 + 54.25cm
Road Width	27.332 (six lanes) ~ 47.775m (widened area)
Longitudinal Gradient	0.5%
Transverse Gradient	3.07 ~ 5.0% (one-sided gradient)

Table 2 Design Loads for Umemachi Bridge

Live Loads	TL-20 and TT-43
Appurtenant Loads	50kg/m^2 (weight of associated facilities) 300kg/m (vehicle inspection rail)
Supports Estimated to Shift	Uneven settlement L/1000 (L=effective span length) Horizontal displacement of each intermediate support by 25mm toward the side spans
Temperature Loads	Temperature Change: $\pm 35°C$ Temperature Difference (between the deck and the girders): $15°C$
Wind Loads	Design Basic Wind Velocity in the Bay Coast Area: V = 55m/sec
Seismic Loads	Design horizontal Seismic Coefficient in Static Analysis: Basic Intensity: $k_0 = 0.24$ (for Grade 4 ground) Design Intensity: $k = 0.30$ (modified Seismic Coefficient) Acceleration Response Spectrum in Dynamic Analysis: The spectra were adopted from • the Specifications for Highway Bridges • the Ajigawa Bridge Design Guidelines Maximum acceleration response on top of piers $S_A = 400$gal

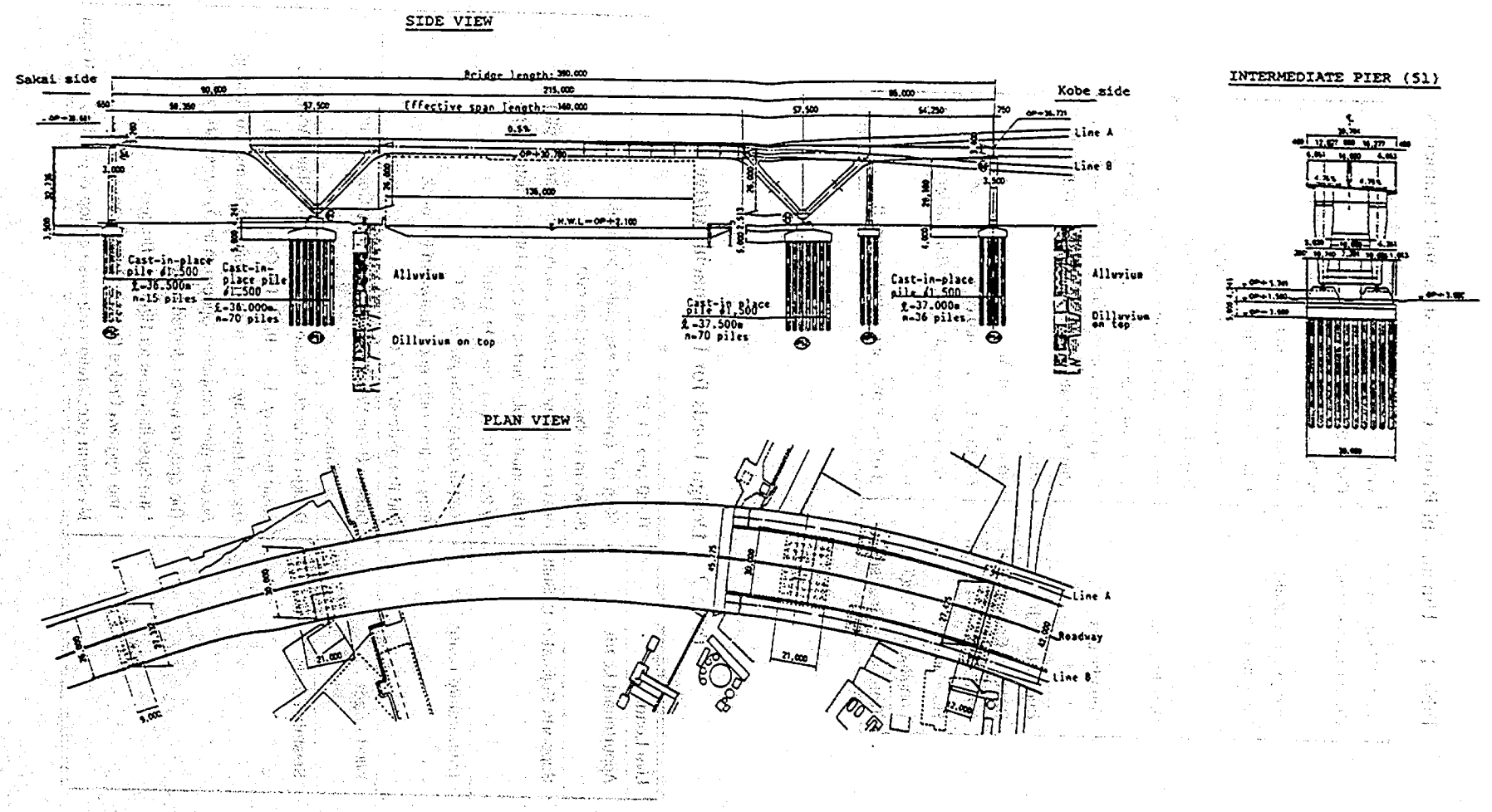

Fig. 1 General Plan of Umemachi Bridge

Step 1: Install bearings for intermediate supports, and install temporary bents

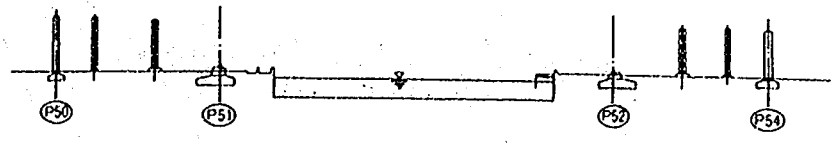

Step 2: Erect the V legs at P52 and P51

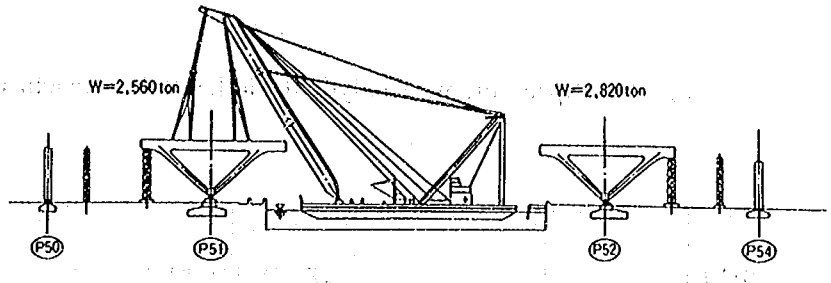

Step 3: Erect the side spans at P50 and P54

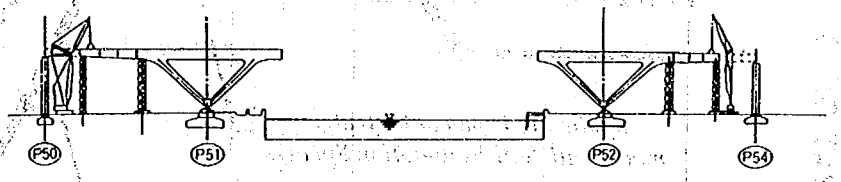

Step 4: Erect the center span

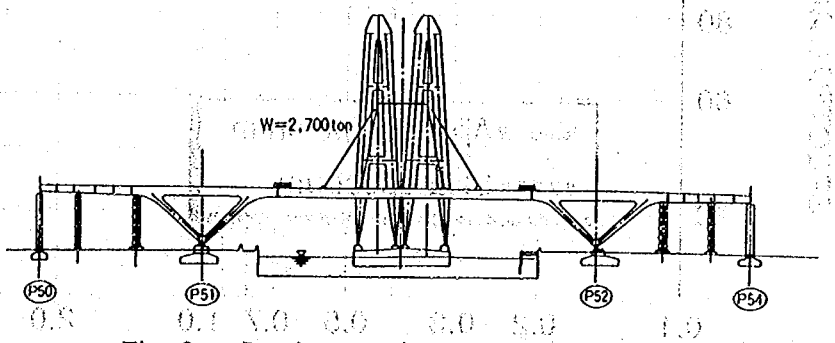

Fig. 2 On-site Erection Procedure for Umemachi Bridge

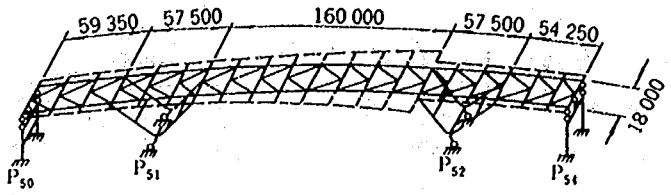

Fig. 3 Space-Frame Analytical Model of Umemachi Bridge

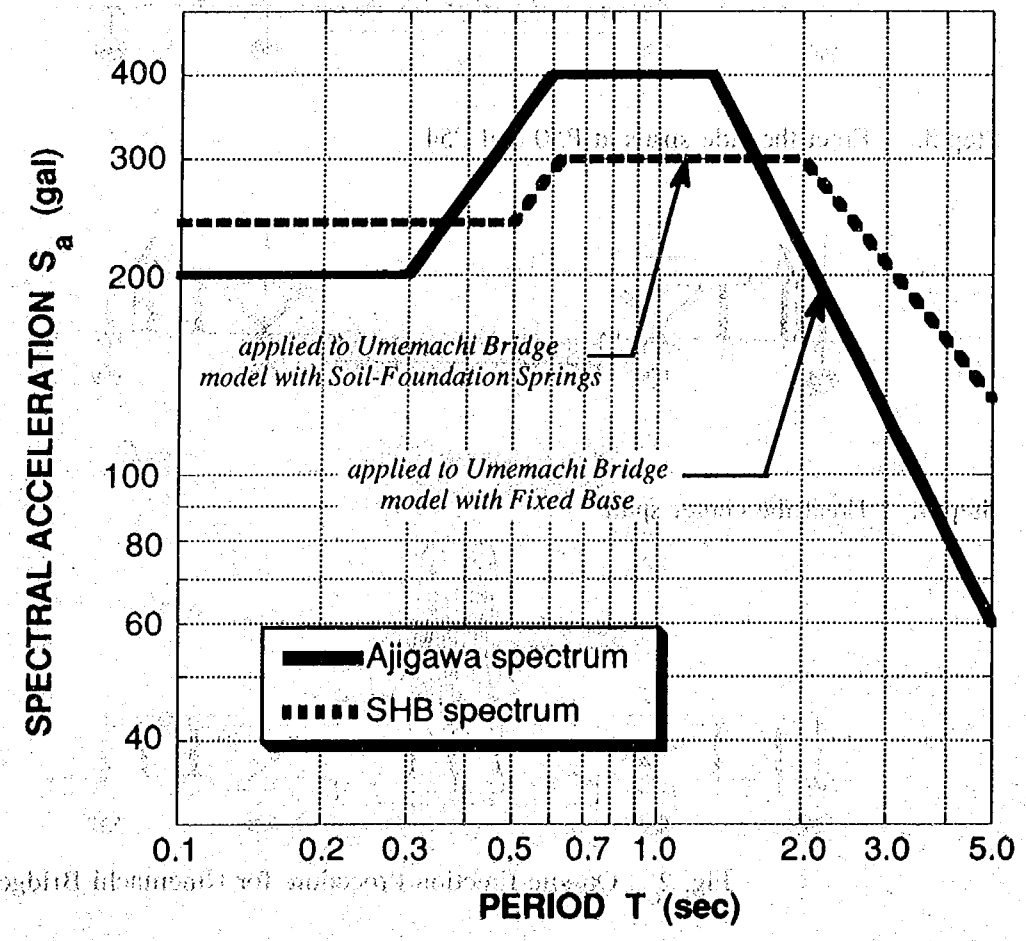

Fig. 4 Design Spectra for Umemachi Bridge

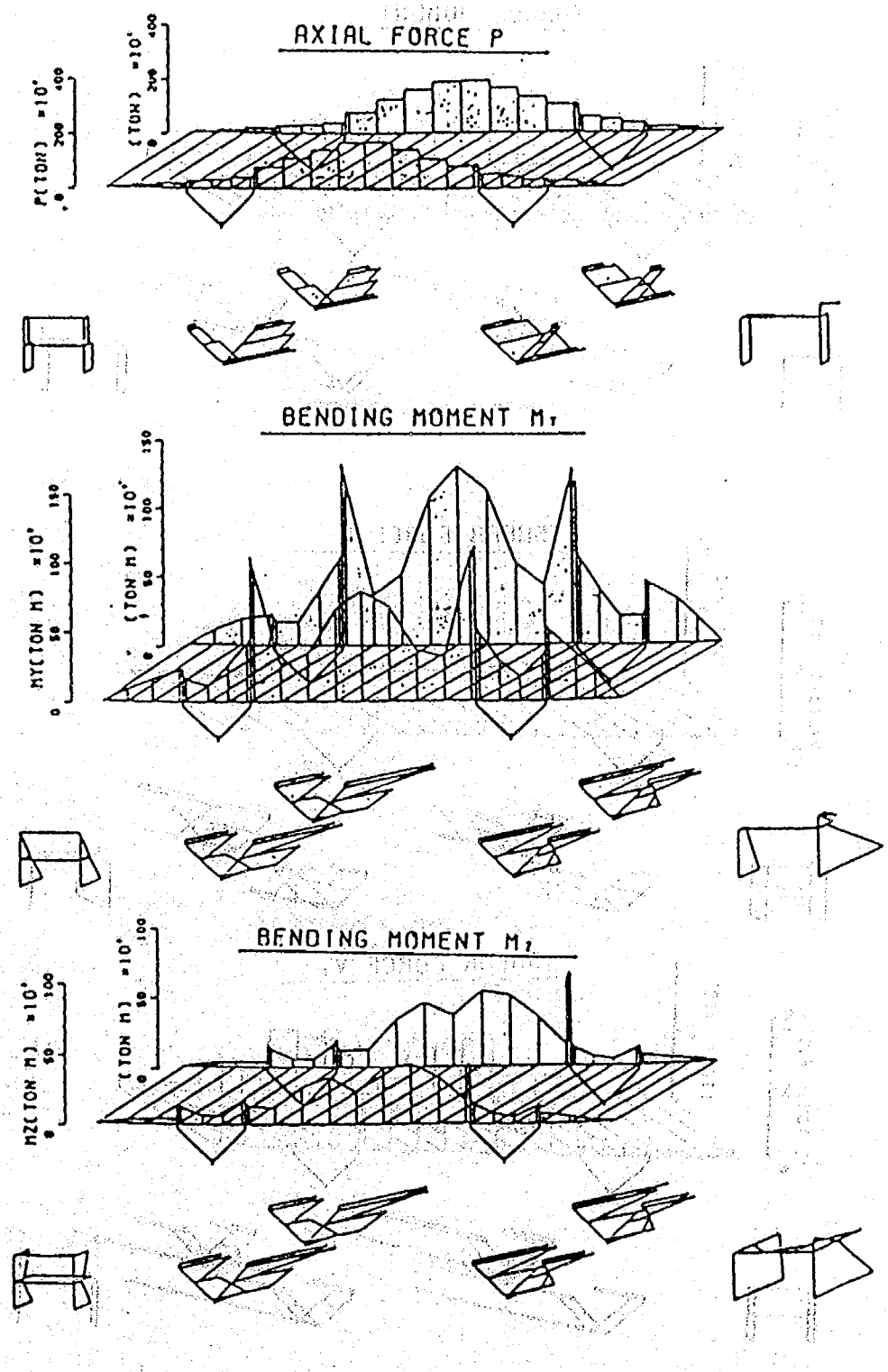

Fig. 5 Analytical Results (spectrum input along longitudinal axis, as per the SHB)

continued on next page

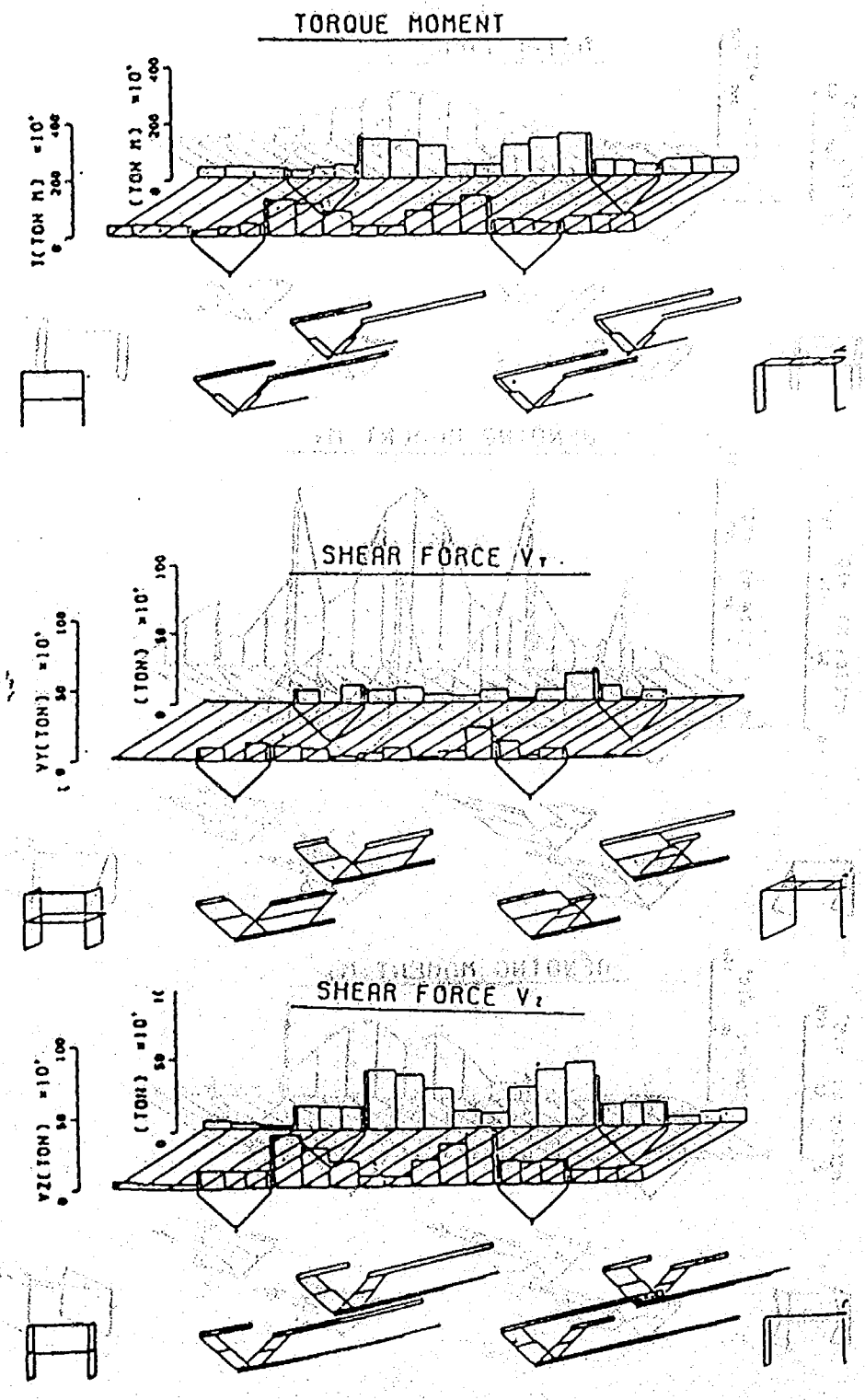

Fig. 5 cont'd Analytical Results (spectrum input along longitudinal axis, as per the SHB)

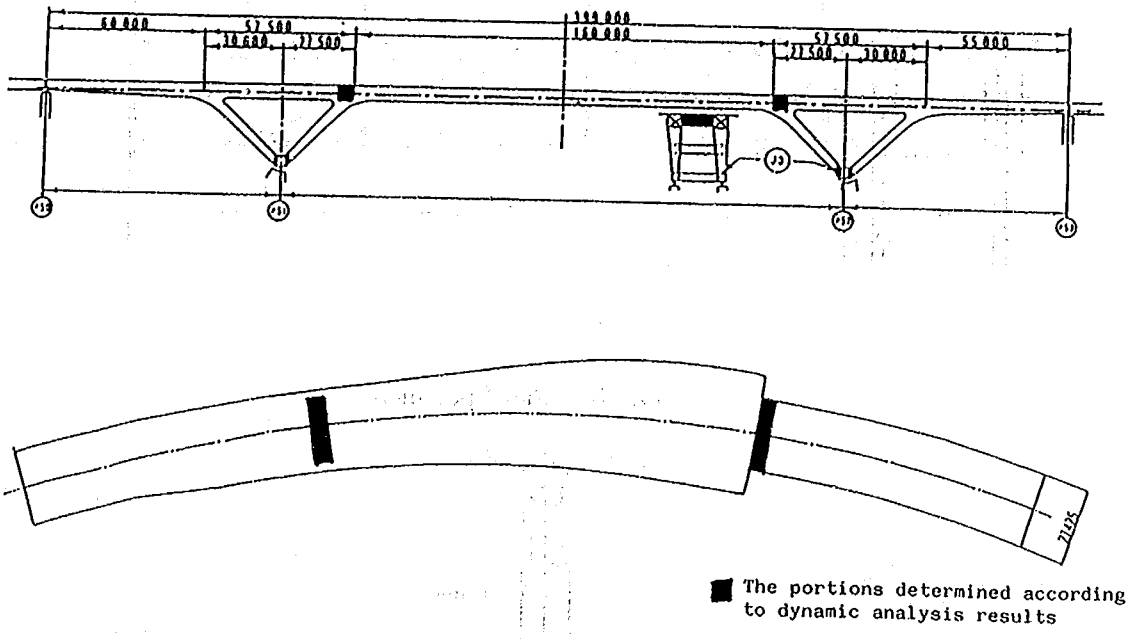

Fig. 6 Design Forces Determined by Dynamic Response Analysis

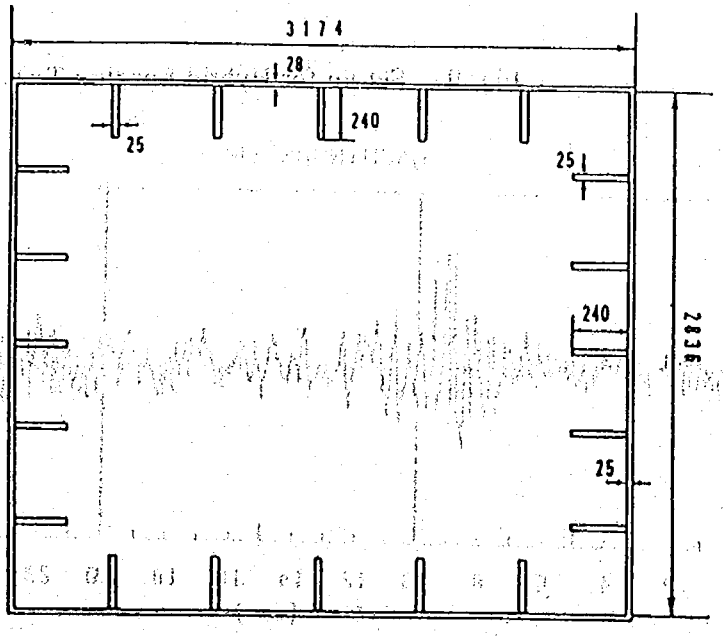

Fig. 7 Section of J3 of the V Leg at P52

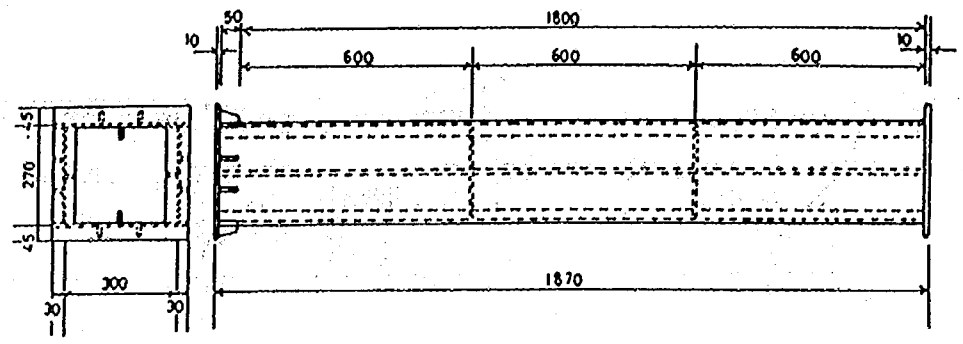

Fig. 8 Pier Specimen

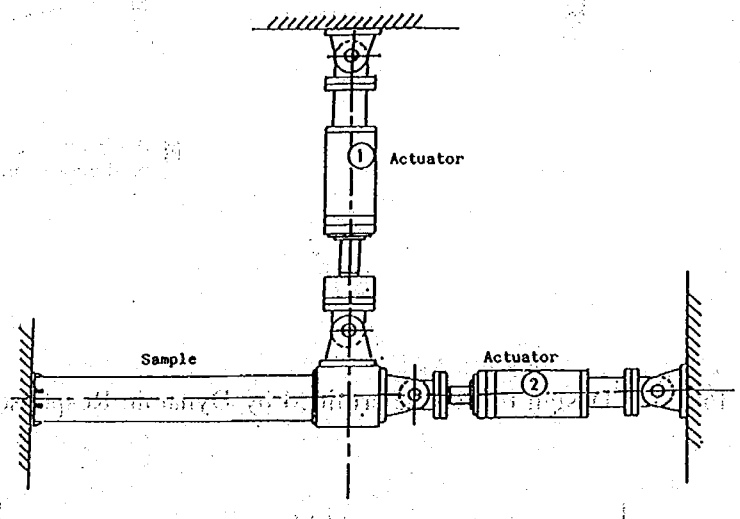

Fig. 9 Set-up for Hybrid Loading Tests

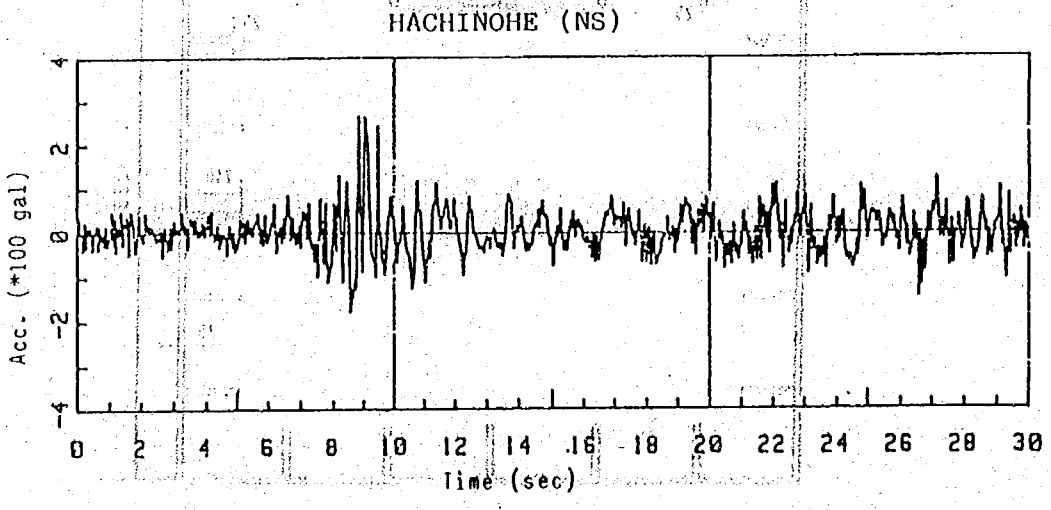

Fig. 10 Hachinohe Record of the 1968 Tokachi-oki Earthquake

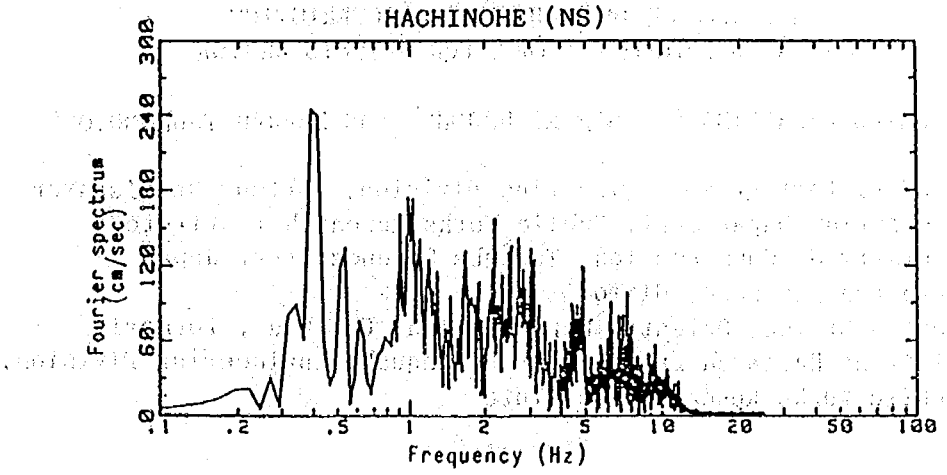

Fig. 11 Spectral Characteristics

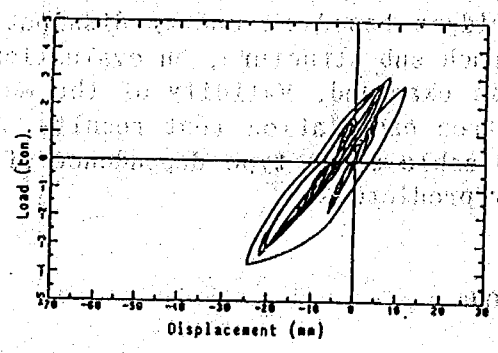

Fig. 12 Load-Deformation Earthquake Response ($\gamma = 6$)

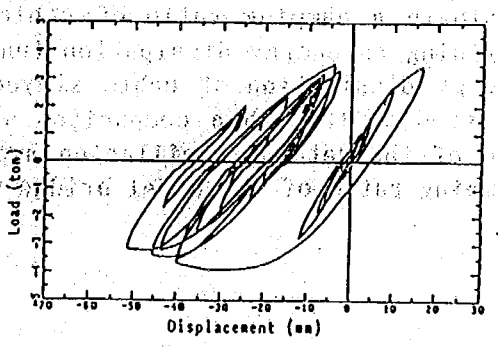

Fig. 13 Load-Deformation Earthquake Response ($\gamma = 9$)

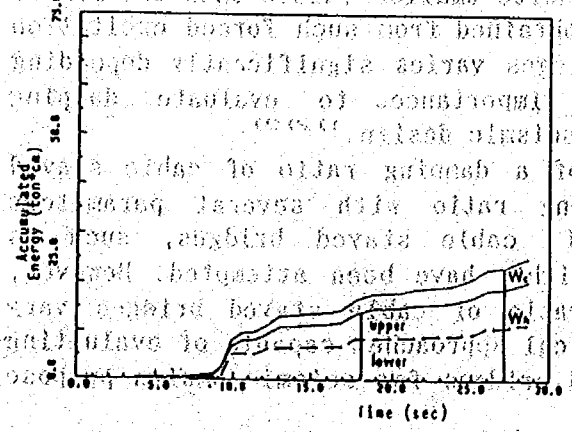

Fig. 14 Time History of Energy Partitioning ($\gamma = 6$)

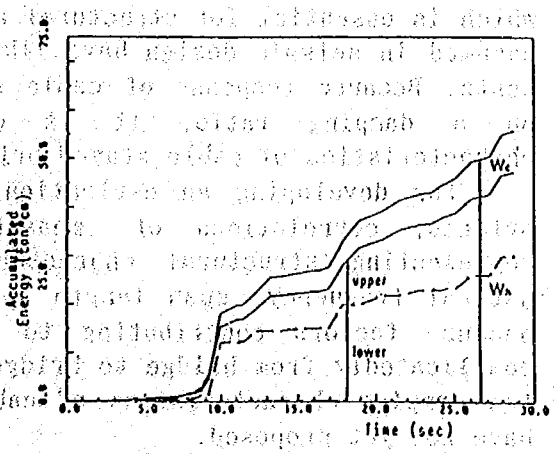

Fig. 15 Time History of Energy Partitioning ($\gamma = 9$)

ESTIMATION OF DAMPING CHARACTERISTICS OF CABLE STAYED BRIDGE FOR SEISMIC DESIGN

Kazuhiko KAWASHIMA[1], Shigeki UNJOH[2] and Meguru TSUNOMOTO[3]

1)Head of Earthquake Engineering Division, Earthquake Disaster Prevention Department, Public Works Research Institute, Ministry of Construction, Tsukuba Science City, Japan
2)Research Engineer, ditto
3)Design Office, Oriental Construction, Co. Ltd., formerly Visiting Research Engineer of Earthquake Engineering Division, Public Works Research Institute

SUMMARY

Although damping characteristics are very important for seismic design of cable stayed bridges, few investigations have been so far made. It is well known from field forced vibration tests conducted for a number of cable stayed bridges that damping ratio estimated from the tests gives much smaller values than the value generally assumed in seismic design. This paper presents a method to evaluate a damping ratio of cable stayed bridges based on energy dissipation. Defining an energy dissipation function for each sub-structure, an evaluation of energy dissipation of cable stayed bridges is examined. Validity of the method is studied through a comparison with model free oscillation test results. With use of the method, oscillation amplitude and cable shape type dependence of the damping ratio of the model bridge was clearly predicted.

INTRODUCTION

According to a number of forced vibration tests conducted for cable stayed bridges at site, it is well known that natural mode as well as natural frequency can be predicted with fairly good accuracy by means of linear analyses which assume appropriate mass and stiffness distribution. However, for a damping ratio which is essential for structural analysis, quite smaller values than the values assumed in seismic design have likely been obtained from such forced excitation tests. Because response of cable stayed bridges varies significantly depending on a damping ratio, it is of great importance to evaluate damping characteristics of cable stayed bridges for seismic design.[1)2)3)]

For developing an estimation method of a damping ratio of cable stayed bridges, correlations of measured damping ratio with several parameters representing structural characteristics of cable stayed bridges, such as natural frequency, span length and pier height, have been attempted. However, because factors contributing to damping ratio of cable stayed bridges vary complicatedly from bridge to bridge, analytical approaches capable of evaluating the damping characteristics of cable stayed bridges for seismic design purpose have not yet proposed.

This paper describes a method of estimating a damping ratio of cable stayed bridges based on energy dissipation, and clarifies its validity through a comparison with free oscillation tests of a scaled model.

EVALUATION METHOD OF DAMPING RATIO

There are various factors causing energy dissipation in cable stayed bridges. Energy dissipation are generally developed by material nonlinearity, structural damping such as friction at movable bearings, radiation of energy from foundations to subground, and friction with air. Predominant factors contributing to damping characteristics of cable stayed bridges varies with structural types. However, an important point to estimate a damping ratio of cable stayed bridges is to evaluate total energy dissipation. Because the energy dissipation capability may not be the same in whole bridge system, it is required to evaluate the energy dissipation in each structural segment depending on type of energy dissipation. Once the energy dissipation in individual structural segments can be determined, the total energy dissipation in a whole structural system can be evaluated by summing up the energy dissipation developed in each structural segment.

Based on such considerations, it is assumed to evaluate energy dissipation in whole bridge as;

1) Divide a cable stayed bridge into several structural segments in which energy dissipation capability can be considered practically the constant. Such a structural segment is referred hereinafter as "a sub-structure". For instance, a cable stayed bridge may be divided into deck(s), tower(s) and cables. Energy dissipation due to material nonlinearity is considered prevailing in such sub-structures. Bearing supports may also be considered as a sub-structure because energy dissipation due to friction occurs at the bearings.[4)]

2) When the i-th sub-structure is idealized by a n-degree of freedom discrete system, the strain energy E_j^i of the i-th sub-structure for j-th mode may be represented as

$$E_j^i = \frac{1}{2} \sum_k (u_j^{ik})^T \cdot k^i \cdot u_j^{ik} \qquad (1)$$

where

u_j^{ik} : amplitude at node k of i-th sub-structure for j-th mode, i.e.,

$$u_j^{ik} = \{ u_j^{i1}, u_j^{i2}, \cdots, u_j^{ik}, \cdots, u_j^{in} \}^T \qquad (2)$$

k^i : stiffness matrix of the i-th sub-structure

Strain energy of the whole structural system for j-th mode can, then, be evaluated as

$$E_j = \sum_i E_j^i \qquad (3)$$

3) For the i-th sub-structure where energy dissipation due to material nonlinearity is predominant, the energy dissipation associated with j-th mode may be represented as

$$\delta E_j^i = f_j^i(E_j^i) \qquad (4)$$

where

δE_j^i : energy dissipation in i-th sub-structure for j-th mode

E_j' : strain energy in i-th sub-structure for j-th mode
f_j' : function relating $\delta E_j'$ with E_j'

The function f_j' represents how the energy dissipation in i-th substructure $\delta E_j'$ be developed in a function of the strain energy in i-th sub-structure E_j', and it would vary depending on type of the structure and material. Therefore, this is referred hereinafter as "an energy dissipation function". Because it is quite difficult in most cases to directly evaluate the energy dissipation function f_j' from analytical studies, it should be determined based on appropriate experiments.

4) For i-th sub-structure where the energy dissipation function f_j' is such a form that it can be represented in terms of a displacement at a specific point $u_j'^k$ within the i-th sub-structure, the energy dissipation function may be represented as

$$\delta E_j' = f_j'(u_j'^k) \tag{5}$$

where
$\delta E_j'$: energy dissipation in i-th sub-structure for j-th mode
$u_j'^k$: displacement at point k in i-th sub-structure for j-th mode
f_j' : energy dissipation function relating $\delta E_j'$ with $u_j'^k$

5) Energy dissipation in the whole structural system can be obtained by summing up the energy dissipation developed in individual sub-structures determined by Eqs.(4) and/or (5) as

$$\delta E_j = \sum_i \delta E_j' \tag{6}$$

where
δE_j : total energy dissipation in whole structure for j-th mode
$\delta E_j'$: energy dissipation in i-th sub-structure for j-th mode

6) Damping ratio of the whole structure for j-th mode may then be obtained from Eq.(4) and Eq.(6) as

$$h_j = \frac{\delta E_j}{4\pi E_j} \tag{7}$$

EVALUATION OF ENERGY DISSIPATION FUNCTION

Cable Stayed Bridge Model Analyzed To show an evaluation of the energy dissipation function, it is appropriate to refer a specific bridge for which actual damping characteristics have been accurately estimated. For such purpose, a model oscillation test with use of a model shown in Fig.1 and Photo 1 was made.[5] The bridge model was made for simulating the Meiko-nishi Bridge[6], with a scale factor of 1/150. Because detailed study on this model bridge was already reported, only outline of the model which is required to understand the analysis presented in this paper will be described here.

Main objectives of the experiments were to study how damping ratio varies in accordance with cable shape type and number of cables. For such purpose, cable shape and number of cables were varied as shown in Fig.2 as parameters to

be studied with main parts of the tower, the deck and the cables being the same. The bridge model was statically displaced either in lateral (longitudinal) direction or in vertical direction, and by smoothly releasing the deck, free oscillation was developed. As will be presented later in Fig.3, the initial deformation is of antisymmetric mode in the free oscillation in longitudinal direction, and is of symmetric mode in the free oscillation in vertical direction. From decay of the free oscillation of the deck, damping ratio of the bridge model was estimated. Although the test was conducted for the connection between the deck and the tower being either free or fixed, only the condition that the deck is free to move from the tower (in this case, the deck is supported only by the cables) is analyzed in this paper for making the experiments to determine the energy dissipation function of sub-structures simple.

Fig.3 shows mode shapes and natural frequencies computed by an elastic analytical model which considers geometrical stiffness to take a compression force induced in the deck and the tower into account. As shown in Table 1 the computed natural frequencies agree well with the experiments.

Figs.4 and 5 show how the damping ratio of the bridge model varies in accordance with the oscillation amplitude and the type of cable shape. It should be noted here that the predicted damping ratio which will be described later is also presented in Figs.4 and 5 for comparison. From Figs.4 and 5, the following characteristics were found on the damping ratio of the bridge model.[5)]

1) The damping ratio of the cable stayed bridge model in longitudinal oscillation increases as the cable shape changes from fan type (type 3A and 2A) to harp type (type 3E and 2C). This tendency is more significant in the model with 3 cables than in the model with 2 cables.

2) On the contrary to 1), the damping ratio of the cable stayed bridge model in vertical flexure oscillation decreases as the cable type changes from the fan type (3A and 2A) to the harp type (3E and 2C). Similar with 1), this tendency is more significant in the model with 3 cables than the model with 2 cables.

3) Based on 1) and 2), when comparing the damping ratio of the cable stayed bridge model in longitudinal oscillation with that in vertical flexural oscillation, the damping ratio in longitudinal oscillation is larger in the harp shape than the damping ratio in vertical flexure oscillation. However, the damping ratio in the longitudinal oscillation and the damping ratio in the vertical flexural oscillation becomes closer to each other as the cable type changes from the harp type to the fan type; and the relation between them is even reversed in the type 3A.

4) The damping ratio increases as the oscillation amplitude increases. Such characteristics are significant in longitudinal oscillation, and, on the contrary, are insignificant in vertical flexure oscillation.

It is the objective of this study to clarify the validity of the evaluation method presented in previous chapter for evaluating the damping ratio through comparisons with the model test results. It is of great interest to know how realistically the above-described damping characteristics of the model bridge can be predicted by the analysis.

For analyzing the damping ratio of the model bridge, the tower, the girder and the anchoring portion of the cables to the tower are considered here as the sub-structure, because these parts contribute to the energy dissipation of the model.

Energy Dissipation Function of Tower For estimating the energy dissipation function of the tower, a simple free oscillation test of the tower was made as shown in Fig.6. Only the tower was taken out from the whole bridge model, and it was supported as a cantilever beam with one of the ends being fixed and the other being free. To avoid energy dissipation at the bottom of the cantilever tower, a special attention was paid to fix it rigidly to a rigid steel member. A weight was placed on the free end of the tower to study the effect of axial force induced in the tower. The weight placed on the free end of the tower was varied from 0.85 kgf to 5.1 kgf. Because the axial force induced at the bottom of the tower due to dead weight of the deck is 6.87 kgf and 6.81 kgf for the model with number of cables of 3 and 2, respectively, the weight of the mass corresponds to 12 % to 74 % of the axial force of the tower. By smoothly releasing the tower top from a displaced position, a free oscillation simulating a first mode was developed. Amplitude of the tower was measured at 33 cm from the bottom by means of an uncontact displacement sensor. From decay of the free oscillation, damping ratio of the tower was estimated.

It should be noted here that the deformation of the isolated tower developed during the free oscillation may not be the same with the deformation of the tower when it is excited as a part of the whole bridge. Although it is the most desirable to evaluate the energy dissipation function for a deformation mode which is actually induced in the tower as a part of the whole bridge, it is quite difficult to displace the isolated tower in such a form. Therefore the difference of the deformed shape of the tower between the actual deformation of the tower as a part of the whole bridge and the cantilever first mode was disregarded here. However, because the relation between $\delta E_j'$ and E_j' given by Eq.(1) may be regarded free from mode shape as will be described later, an energy dissipation function determined for a mode shape would be used for an energy dissipation function for other mode shapes. The validity of this assumption may be verified by comparing the damping ratio estimated by Eq.(7) with the damping ratio obtained experimentally for the whole bridge model.

Fig.7 shows how the damping ratio of the tower varies with the amplitude of the oscillation and the mass of the weight. Predicted damping ratio which will be described later is also presented for comparison. Although there is some scatters at oscillation amplitude smaller than 0.5 mm, this is due to low accuracy of the measurements in such small oscillation amplitude. According to Fig.6, the damping ratio of the tower increases as a whole as the oscillation amplitude as well as the mass of the weight increases.

Why the damping ratio increases as the axial force of the tower increases may require an explanation. The total energy E_j of the structural system oscillating in j-th mode shape comes from two contributions, i.e., energy $E_{\sigma j}$ associated with geometrical stiffness[7] due to compression force induced in the tower and the deck, and strain energy $E_{\varepsilon j}$ associated with the deformation of the structure as

$$E_j = E_{\sigma j} + E_{\varepsilon j} \tag{8}$$

Because the energy dissipation during oscillation is developed only by the strain energy $E_{\varepsilon j}$ and free from the energy $E_{\sigma j}$, the energy dissipating function f_j may be represented as

$$\delta E_j = f_j (E_{\varepsilon j}) \tag{9}$$

in which δE_j represents the energy dissipation during the oscillation. Therefore, damping ratio of the tower may be obtained by substituting Eqs.(8) and (9) into Eq.(7) as

$$h_j = \frac{\delta E_j}{4\pi E_j} = \frac{f_j(E_{sj})}{4\pi (E_{sj} + E_{gj})} \tag{10}$$

Because the energy dissipation E_{sj} associated with the geometrical stiffness takes a negative value if the axial force of the tower is positive (compressive), the damping ratio presented by Eq.(10) increases as the axial force becomes larger.

Because the damping ratio h_j of the tower can be determined through the decay of the free oscillation and the total energy E_j can be computed from Eq.(8), one can determine the energy dissipation δE_j by substituting h_j and E_j into Eq.(10).

Fig.8 shows the relation between δE_1 and E_{s1}. Because the oscillation test was made only for the first mode, Fig.8 represents δE_j vs. E_{sj} relation for $j = 1$. The relation seems almost independent of the weight of the mass placed on the tower top. Then, it is approximated here as

$$\delta E_{s1} = \Sigma \alpha_i E_{s1}^{\beta_i} \tag{11}$$

After determining the coefficients α_i and β_i based on a least square fit, it was obtained as

$$\delta E_{s1} = 0.016 E_{s1} + 0.0021 E_{s1}^{3/2} \tag{12}$$

Based on Eq.(12), the damping ratio vs. the oscillation amplitude of the tower is obtained as shown in Fig.7. It is seen that the predicted damping ratio agrees reasonably well with the experimental result.

Energy Dissipation Function of Deck As was the tower, a part of the deck was taken out from the whole bridge model and was supported as a cantilever beam with a weight being placed as shown in Fig.9. Length of the cantilever deck was varied as 40 cm and 60 cm so that an effect of the deck length on the damping ratio be studied. Because the deck length varies the mode shape, this would show how the energy dissipation function depends on the mode shape.

Fig.10 shows a relation between the damping ratio estimated from the decay of free oscillations and the oscillation amplitude measured at 30 cm from the bottom. Predicted damping ratio which will be described later is also presented for comparison. As is the case for the tower, the damping ratio of the cantilever deck increases as the oscillation amplitude and the weight of the mass increase. It is interesting to note that the damping ratio of the deck is appreciably larger than the damping ratio of the tower. The tower consists of only steel frame, while the deck is fabricated by assembling the main beam, transverse beam and lead weight. The larger damping ratio of the deck may be attributed to an energy dissipation associated with the transverse beam and lead weight attached to the main beam.

Fig.11 shows an relation between δE_{s1} and E_{s1} of the catilever deck. It is interesting to note that the effect of the deck length on δE_{s1} vs. E_{s1} relation is quite small. Therefore, neglecting the effect of the catilever deck length,

the relation between δE_{a1} and E_{a1} may be approximated as

$$\delta E_{a1} = 0.016E_{a1} + 0.083E_{a1}^{1.37} \quad (13)$$

Predicted damping ratio by Eq.(13) agrees fairly well with the experimental result as shown in Fig.10.

Energy Dissipation Function of Anchoring Portion of Cables To simulate an energy dissipation at the cable anchoring portion, where an energy dissipation is developed due to friction between the cables and the anchoring devices as well as deformation of the plate spring (refer to Fig.1), the cable anchoring portion was taken out from the whole bridge model, and a free oscillation test of this sub-structure was made as shown in Fig.11. To isolate the energy dissipation at the cable anchoring portion, both ends of the tower were fixed so that the energy dissipation associated with the tower deformation be as small as possible. Furthermore, the deck was supported by two cables so that flexure deformation of the deck in vertical direction during the free oscillation test be small. To study an effect of the tension force developed in the cables, two masses were placed on the deck. The oscillation amplitude in bridge axis direction was measured at one of the two ends of the deck.

Fig.12 shows a relation between the damping ratio and the oscillation amplitude of the model idealizing the anchoring portion. Being different from the tower and deck, the amplitude dependence of the damping ratio varies in a complicated manner depending on the oscillation amplitude. This seems to be developed probably because the friction between the cables and the anchoring devices delicately changes depending on the oscillation amplitude. Modeling of a cable anchoring portion of the prototype cable stayed bridge is quite complicated and difficult in the scaled model. However, it is considered less important to study such complexity of the amplitude dependence of the damping ratio of the anchoring portion, because the purpose of this study is to clarify the validity for evaluating the total energy dissipation.

Fig.13 shows a relation between the energy dissipation, angular frequency of the free oscillation and the oscillation amplitude at the cable anchoring portion, in which θ and ω represent an angle between the tower and the cable (refer to Fig.11) and angular frequency of the free oscillation. It is interesting to note that the energy dissipation in the sub-structure depends on the angular frequency of the free oscillation. The effect of the tension force induced in the cables by means of two masses placed on the deck seems less significant.

By approximating the relation between δE, θ and ω presented in Fig. 13, the energy dissipation at the cable anchoring portion may be written as

$$\delta E = 0.018\omega^{2.15} \cdot \theta^{2} \quad (14)$$

EVALUATION OF CABLE-STAYED BRIDGE MODEL BASED ON ENERGY DISSIPATION FUNCTIONS OF SUB-STRUCTURES

Damping ratio of the cable stayed bridge model was evaluated based on the energy dissipation functions of the sub-structures determined in the preceding chapter. Predicted damping ratio by Eq.(7) assuming the energy dissipation functions of the sub-structures by Eqs.(12), (13) and (14) is presented in

Figs.4 and 5 in comparison with the experimental results. The predicted damping ratio may be characterized as

1) The predicted damping ratio of the cable stayed bridge model in longitudinal oscillation increases as the cable type changes from the fan type (type 3A and 2A) to the harp type (type 3E and 2C). The dependence of the predicted damping ratio on the oscillation amplitude increases in the same order with the experiments. Such characteristics agree fairly well with the experiments, although the predicted damping ratio is underestimated as the cable type approaches to the harp type.

2) The predicted damping ratio of the cable stayed bridge model in vertical flexure oscillation is almost independent of the cable type. Although the damping ratio estimated from the experiments slightly decreases as the cable type changes from the fan shape to the harp shape when the number of cable is 3, the overall characteristics of the predicted damping ratio seem fairly close with the experimental results.

Through the comparison stated above, it can be said that the estimation method of the damping ratio by Eq.(7) using the energy dissipation functions determined for individual sub-structures is apparently able to realistically simulate the damping characteristics of the bridge model evaluated from the experiments. As a whole, the predicted damping ratio is somewhat smaller than the experimental results probably because of the energy dissipation which are not considered in this analysis would contributed to the total energy dissipation. Therefore, if the energy dissipation at each portion is further evaluated in detail, it may be possible to further enhance the accuracy of the above estimation.

CONCLUSIONS

An evaluation method of the damping ratio of cable stayed bridges by determining an energy dissipation functions for individual sub-structures was presented, and the validity of the method was examined through a comparison with the results of model free oscillation tests.

Through the analysis presented herein, the following conclusions may be deduced:

1) To clarify complicated damping characteristics of cable-stayed bridges, it is important to accurately study energy dissipations in individual sub-structures with a special attention to in what mechanism the energy dissipation is made.

2) Dependence of damping ratio on the cable shape type and oscillation amplitude, which was evaluated through the model free oscillation test of the cable stayed bridge model, can be realistically predicted for longitudinal oscillation and vertical flexural oscillations by the method presented in this paper.

3) It is recommended to clarify the complicated damping characteristics of cable stayed bridges, which have so far been measured based on a number of field forced vibration tests, paying fully attention to the fact that the damping ratio of cable stayed bridges greatly varies depending on the energy dissipation in individual sub-structures. It would be quite important to note that which sub-structure contributed in the field forced vibration tests to the total energy dissipation for mode shapes studied. It is also recommended to conduct careful forced vibration tests for cable stayed bridges using the method

presented in this paper. Tests to determine the energy dissipation functions for sub-structures have to be well implemented for such purpose.

REFERENCES

1) Ito, M. and Katayama, T. : Damping Characteristics of Bridges, Proc. Japan Society of Civil Engineering, Vol.117, 1965 (in Japanese)

2) Kawashima, K., Unjoh, S. and Tsunomoto, M : Damping Characteristics of Cable Stayed Bridges for Seismic Design, Report of the Public Works Research Institute, Ministry of Construction, 1991

3) Kawashima, K., Unjoh, S. and Azuta, Y. : Analysis of Damping Characteristics of A Cable Stayed Bridge Based on Strong Motion Records, Structural Eng./Earthquake Eng., Vol.7, No.1, pp.181-190, 1990

4) Kawashima, K. and Unjoh, S. : Damping Characteristics of Cable Stayed Bridges Associated with Energy Dissipation at Movable Supports, Structural Eng./Earthquake Eng., Vol.6, No.1, pp.145-152, 1989

5) Kato, N., Iioka, Y. and Kawahito, T. : Design of Meiko-nishi Bridge, Bridges and Foundations, 1983(in Japanese)

6) For example, Nishioka, T.: Analysis on Structural Vibration, Bai-hu-kan, 1987 (in Japanese).

Table 1 Comparison of Natural Frequencies between Predicted and Experiments

CABLE TYPE		LONGITUDINAL MODE		VERTICAL MODE	
		EXPERIMENTAL	PREDICTED	EXPERIMENTAL	PREDICTED
THREE CABLES	TYPE 3A	0.54	0.54	0.66	0.68
	TYPE 3B	0.61	0.61	0.65	0.67
	TYPE 3C	0.76	0.76	0.65	0.66
	TYPE 3D	0.96	0.97	0.64	0.65
	TYPE 3E	1.38	1.41	0.65	0.65
TWO CABLES	TYPE 2A	0.48	0.49	0.62	0.63
	TYPE 2B	0.67	0.68	0.61	0.62
	TYPE 2C	0.92	0.95	0.60	0.59

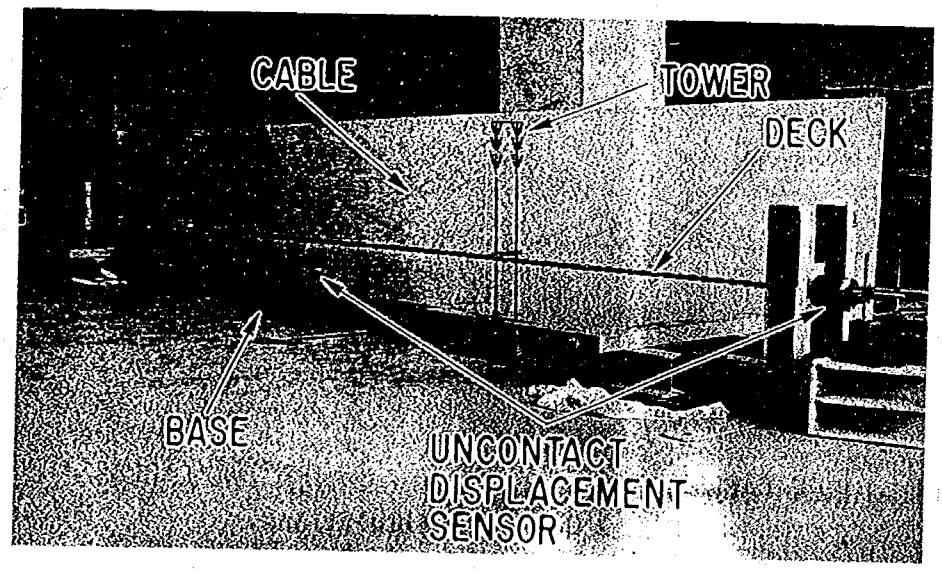

Photo 1 Cable Stayed Bridge Model

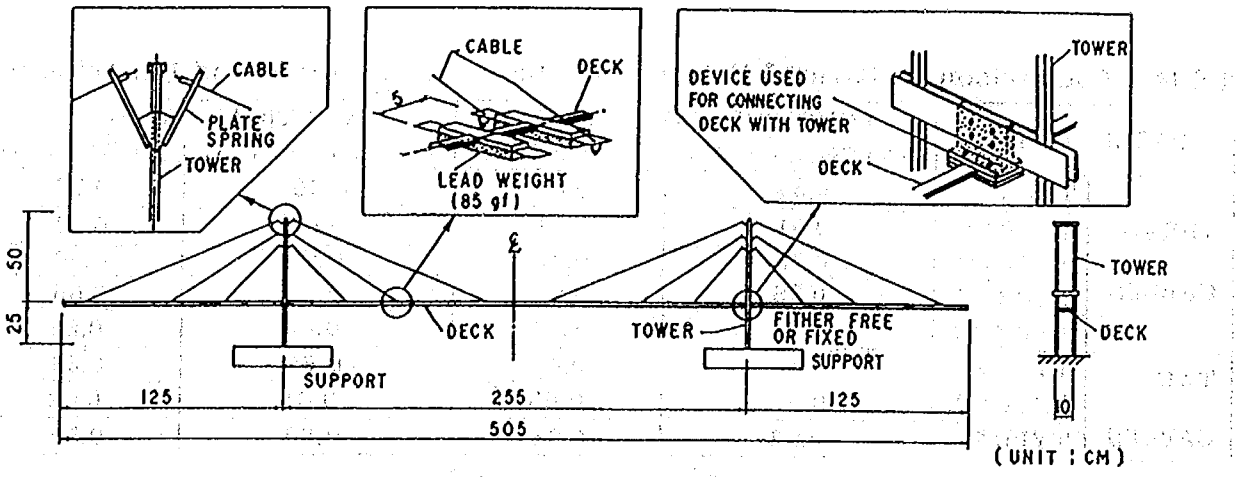

Fig. 1 Cable Stayed Bridge Model

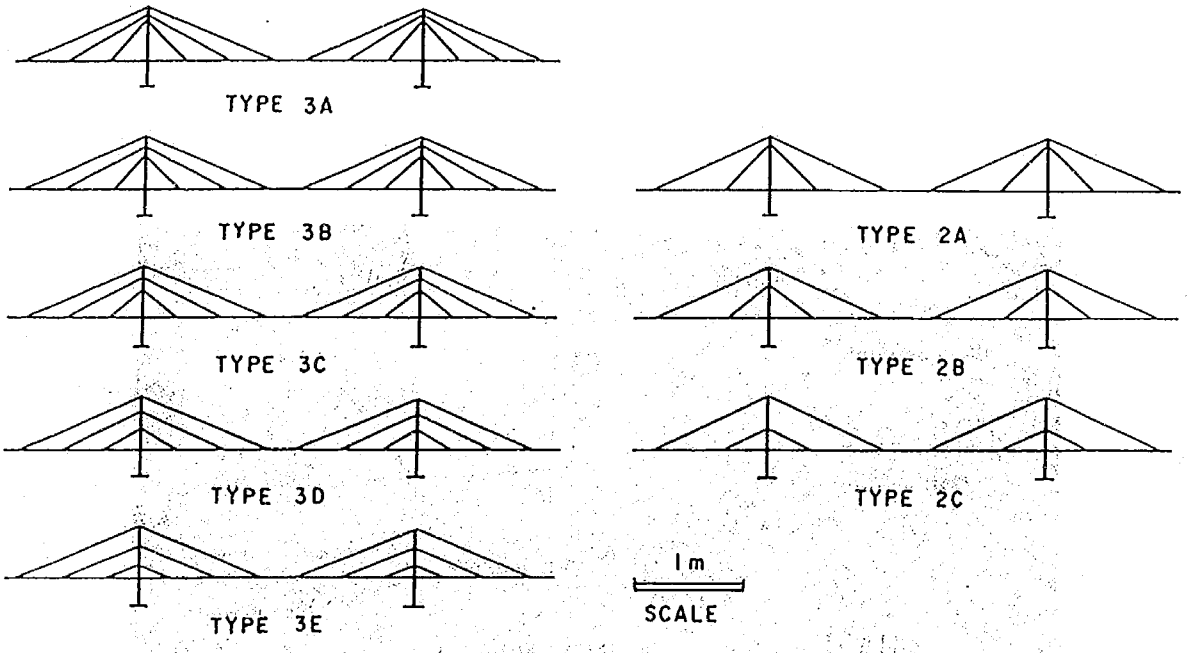

(a) THREE CABLES (b) TWO CABLES

Fig. 2 Cable Configulations

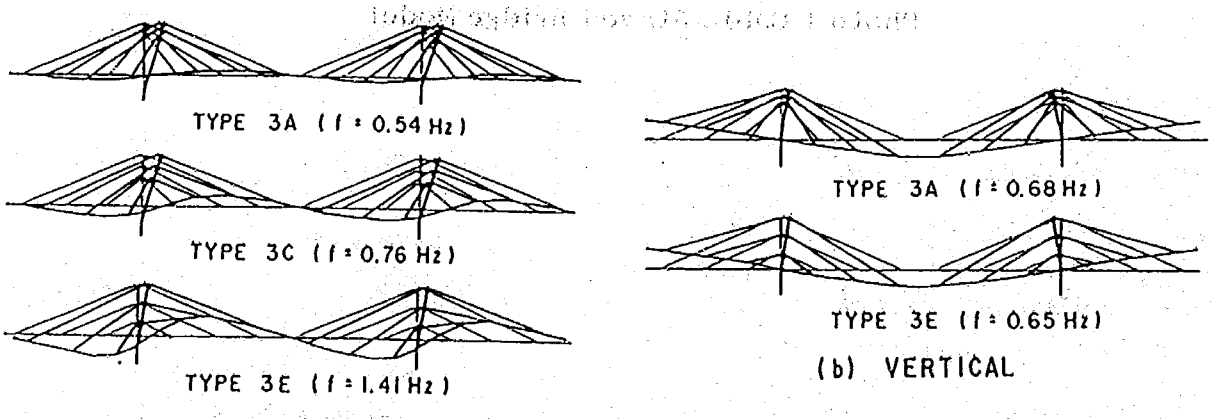

(a) LONGITUDINAL (b) VERTICAL

Fig. 3 Predicted Natural Frequency and Natural Mode Shape

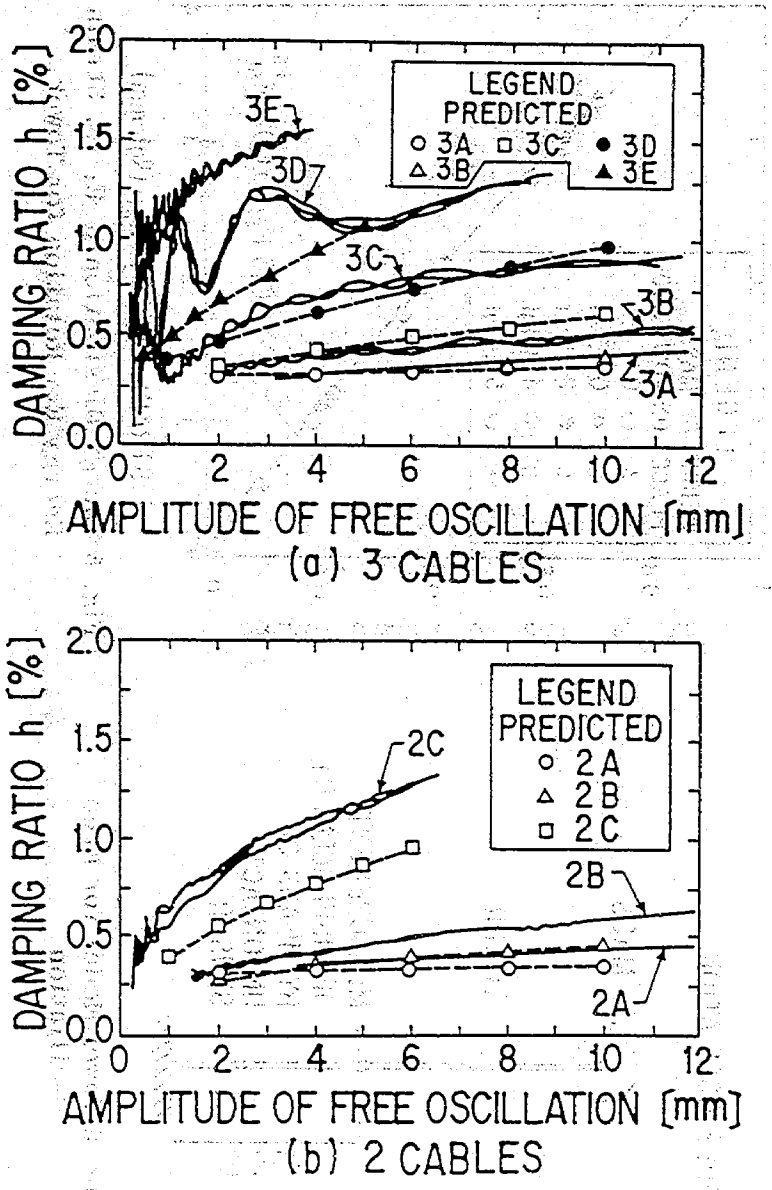

Fig. 4 Damping Ratio for Oscillation in Longitudinal Direction

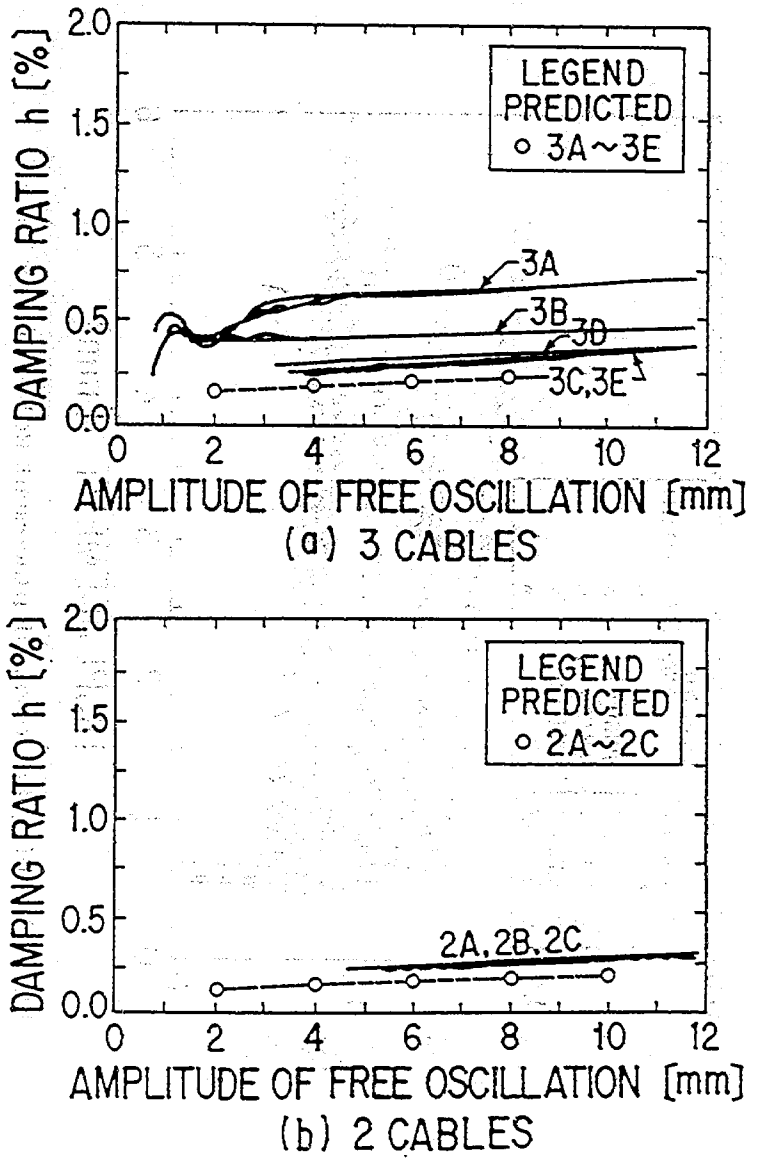

Fig. 5 Damping Ratio for Oscillation in Vertical Direction

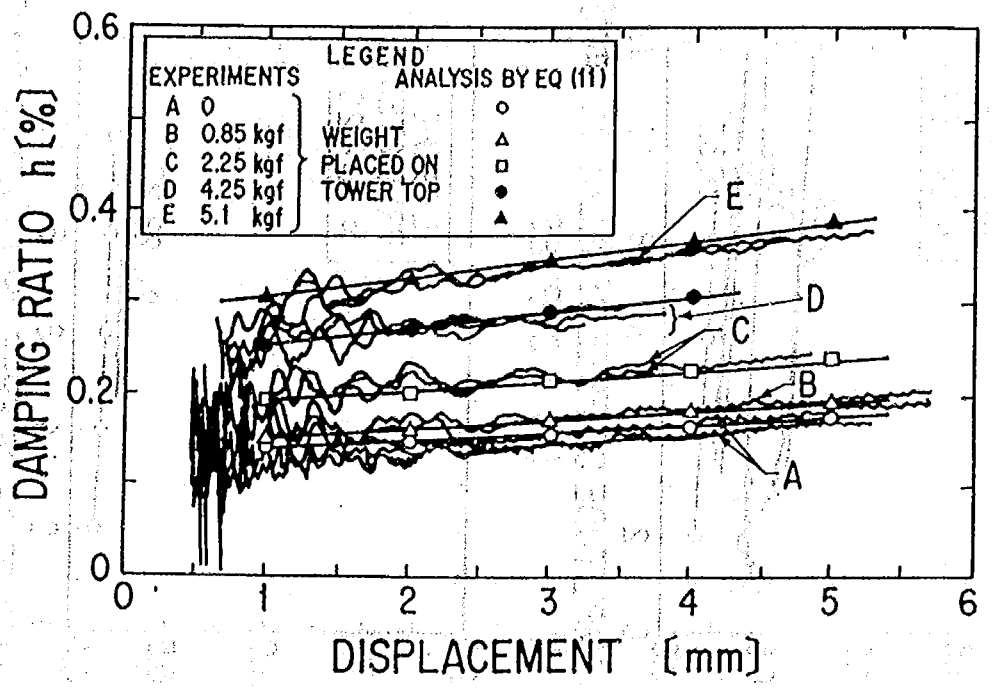

Fig. 7 Damping Ratio vs. Displacement Relation for Tower

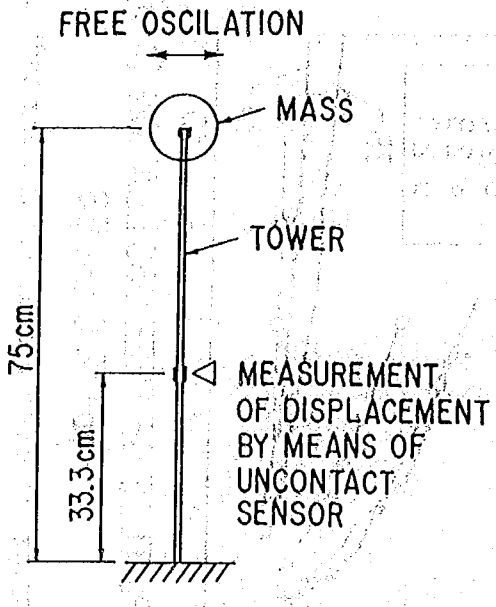

Fig. 6 Tower Model for Free Oscillation

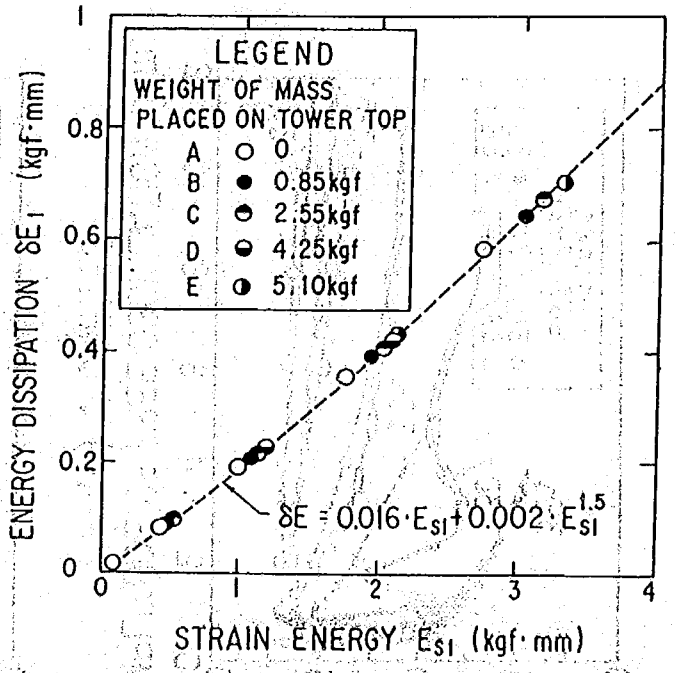

Fig. 8 Energy Dissipation δE_I vs. Strain Energy E_{SI} Relation for Tower

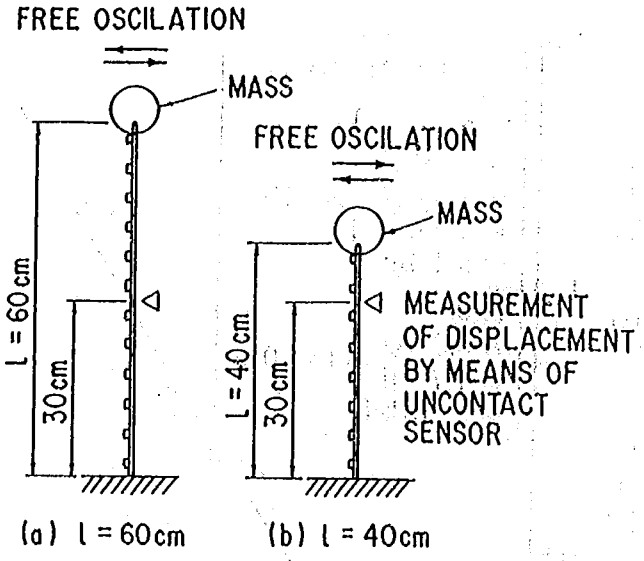

Fig. 9 Deck Model for Free Oscillation

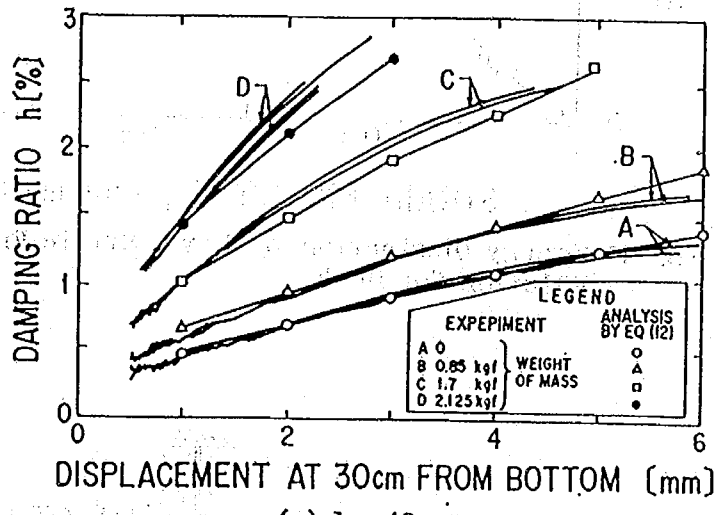

(a) l = 40 cm

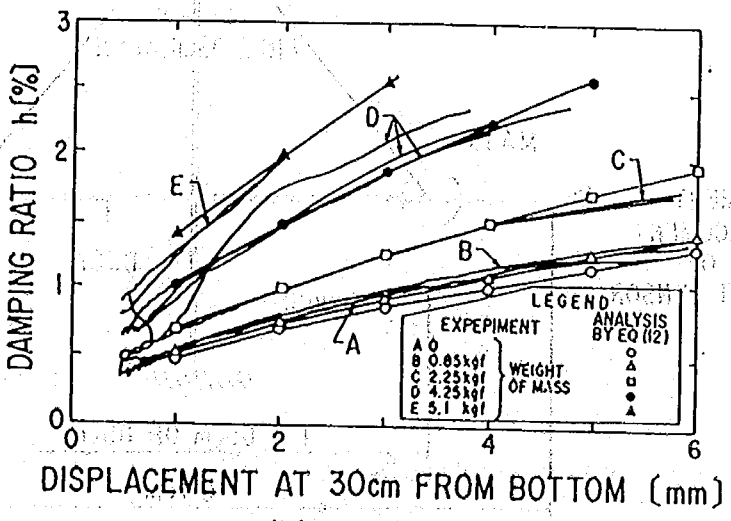

(b) l = 60 cm

Fig. 10 Damping Ratio vs. Displacement Relation for Deck

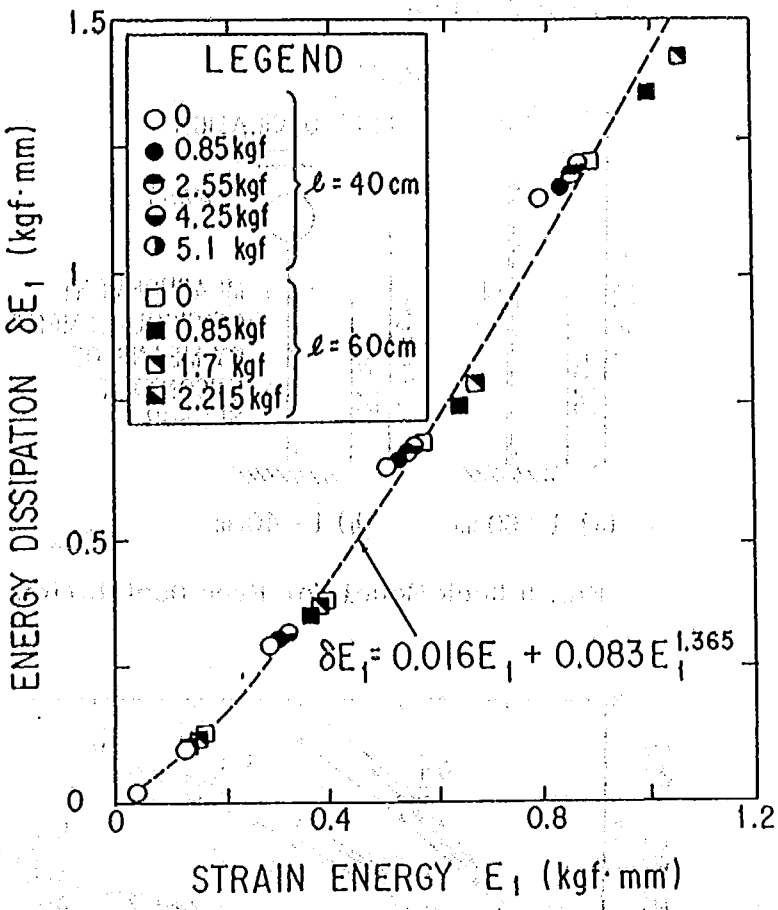

Fig. 11 Energy Dissipation δE_1 vs. Strain Energy E_1 Relation for Deck

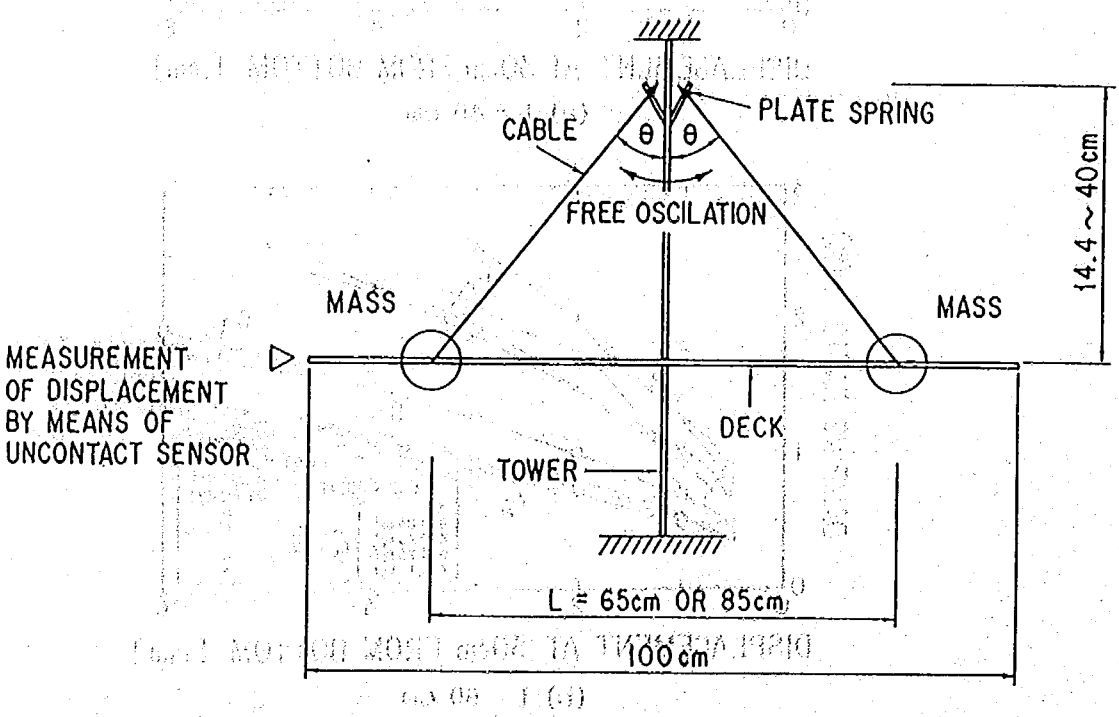

Fig. 12 Anchoring Portion Model for Free Oscillation

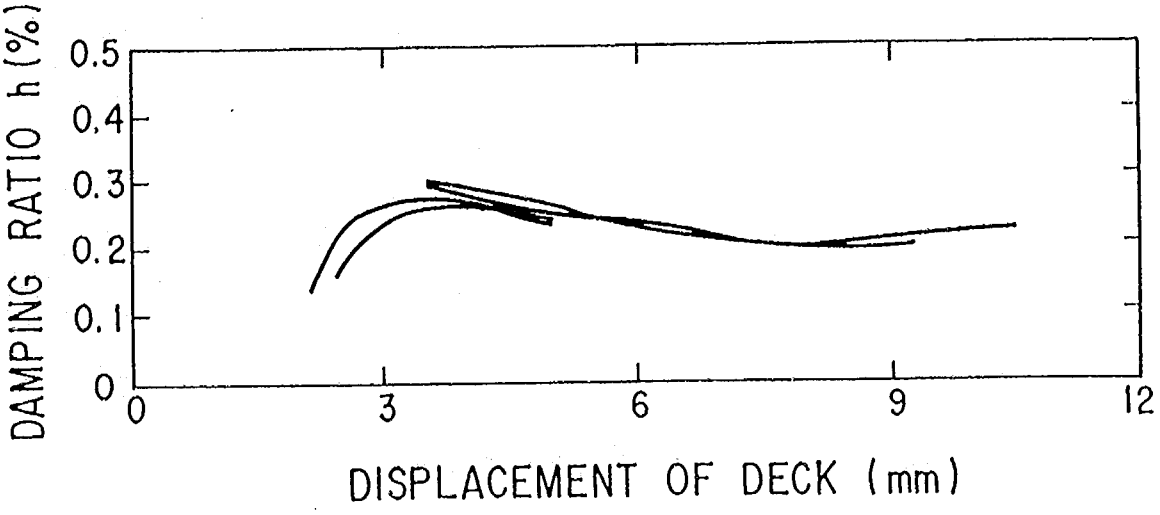

Fig. 13 Damping Ratio vs. Displacement Relation for Anchoring Portion

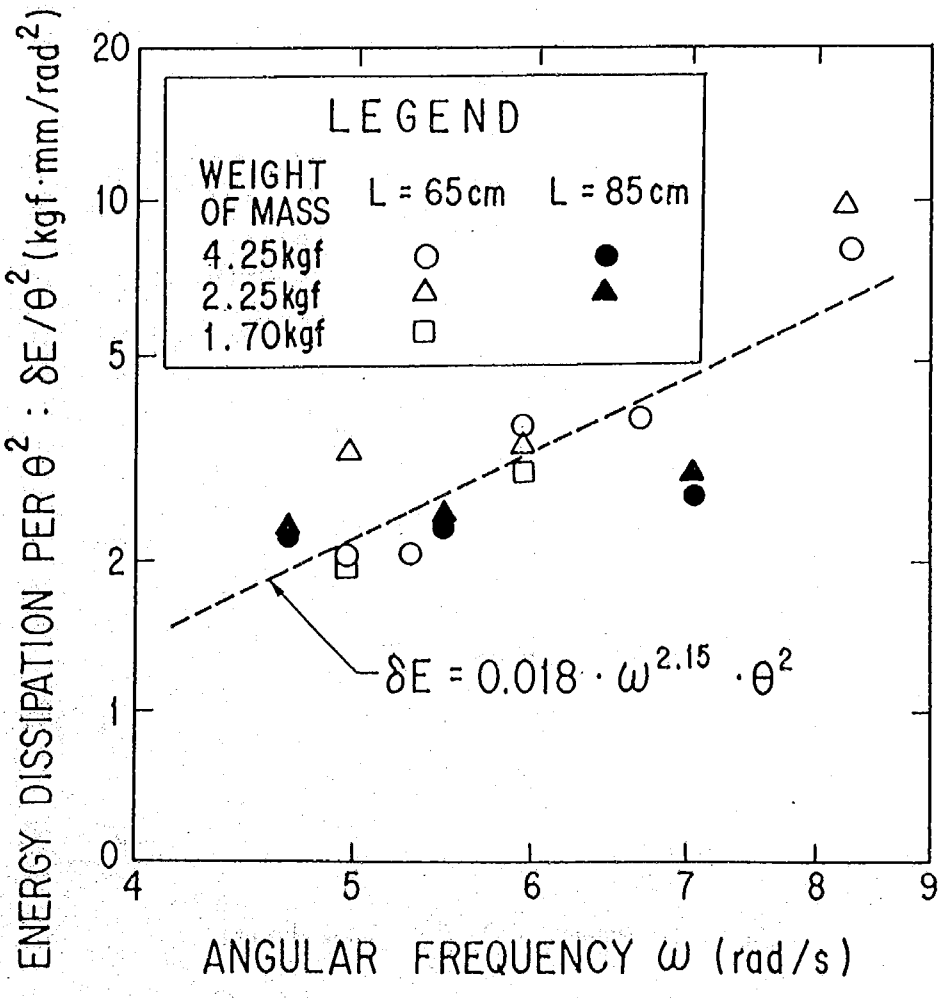

Fig. 14 Energy Dissipation, Angular Frequency and Oscillation Amplitude Relation for Anchoring Portion

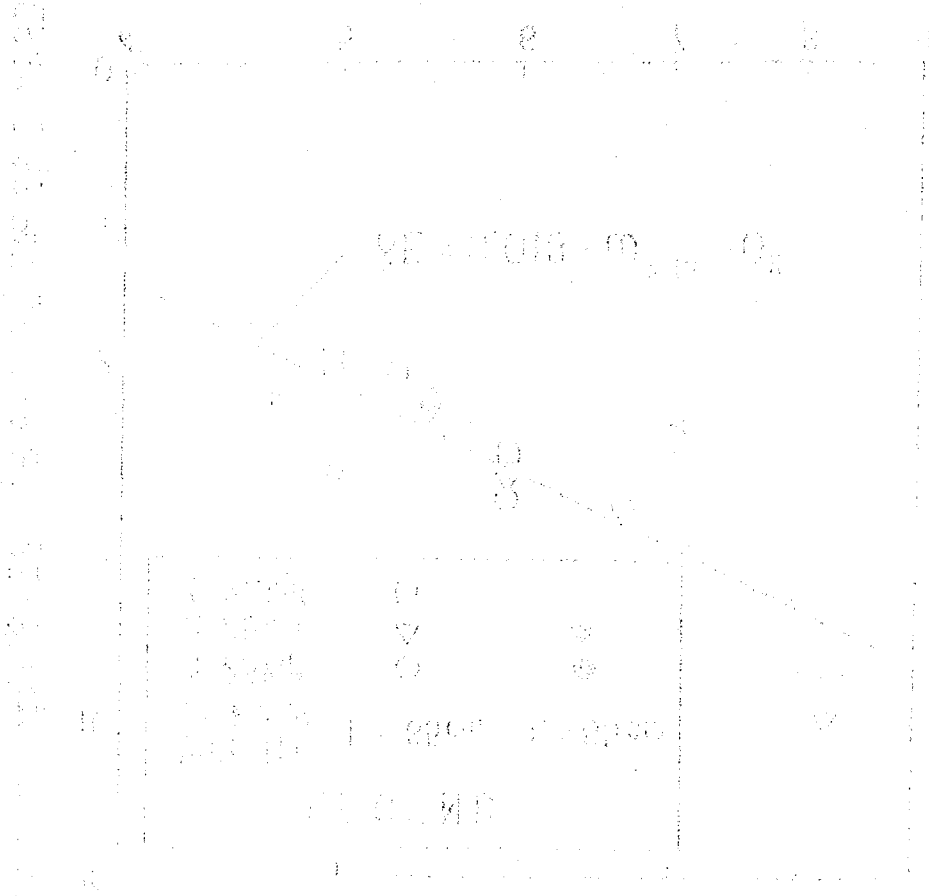

(3) Session 3

SESSION 3: SEISMIC DESIGN(2) 10:50am～0:10pm
(Co-Chairmen: K.Kawashima, J.Gates)

(5) O.Nakano, H.Konno, H.Taniguchi* and Y.Ono: On the Behavior of Base-Isolated Bearings at Low Temperatures
(10:50pm～11:05pm)

(6) I.G.Buckle: Code Developments and Current Applications of Seismic Isolation to Bridges in the United States
(11:05am～11:20am)

(7) K.Kawashima and K.Hasegawa* : Evaluation of Lateral Inertia Force of Bridges for Seismic Design
(11:20am～11:35am)

(8) J.B.Mander: Damage Assessment of Existing Bridges in Low to Medium Seismic Risk Zones
(11:35am～11:50am)

DISCUSSION
(11:50am～0:10pm)

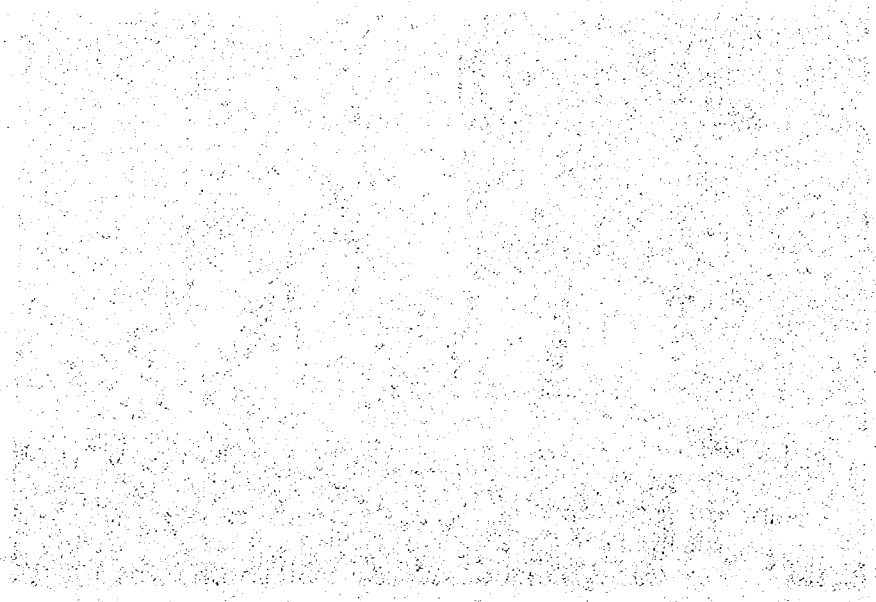

ON THE BEHAVIOR OF BASE-ISOLATED BEARINGS AT LOW TEMPERATURES

Osamu Nakano
Head, Structure Division, Structure Department,
Civil Engineering Research Institute,
Hokkaido Development Bureau

Hisashi Konno, Hideyuki Taniguchi, & Yuji Ono
Research Engineers, Structure Division, Structure Department,
Civil Engineering Research Institute,
Hokkaido Development Bureau

Summary

Our concern is whether the base-isolated bearings, which have recently been introduced to the field of the bridge design in Japan, assure its performance in such cold regions as Hokkaido. For this reason full-size base-isolated bearing models in accordance with an ongoing bridge construction project were prepared in order to pay attention to their behavior at low temperatures through indoor experiments, in which compression and shear tests, etc. were conducted by changing the temperature of the test specimens from 30°C to -20°C. As a result, it was proved that the stiffness of a base-isolated bearing increases with decreasing temperature, which shows the possibility that the base-isolating effect expected at room temperature could not necessarily be obtained at low temperatures.

1 Introduction

Bridge design with base-isolated bearings has begun recently in Japan. At present a total of eight bridges, many of which are located in the eastern part of Japan, are under construction.[1] In Hokkaido the Onnetoh-Oohashi Bridge on National Road 44 in Nemuro (Fig.1) is selected as an experimental bridge by the Hokkaido Development Bureau because the bridge is located at the bottom of the Nemuro Peninsula where many earthquakes took place like the Off Nemuro Peninsula Earthquake (Magnitude=7.4) in 1973.

The base-isolated bearings of these bridges are now being designed according to the "Guidelines for the Design of Base-Isolated Bridges (draft)"[2] (abbreviated to Guidelines hereinafter) which was prepared by the Japan Institute of Construction Engineering in March, 1989. However, the changes in material properties (stiffness,etc.), crystallization of rubber and other unfavorable phenomena will become focal points if the base-isolated bearings are installed in a cold region such as Hokkaido. In this connection,Table 1 represents mean temperature in the past 30 years in some cities of Hokkaido. That is why a series of the tests has been made on the behavior of base-isolated bearings at low temperatures through indoor experiments. This report represents an outline of the experiments and describes how the stiffness of the two base-isolated bearing models used in the tests changes at low temperatures.

2 Outline of the Experiments

2.1 Purpose of the Experiments

In the application of base-isolated bearings in a cold region, the most critical factor is the equivalent shear stiffness. The chapter 3.5 with regard to the "Static Characteristics of Base-Isolated Bearings" in The Guidelines stated that "The ratio of the equivalent stiffness of a base-isolated bearing at -30°C to that at 30°C must be equal to or less than 1.5:1".

Therefore, tests were made to watch the behavior carefully at low temperatures, and particularly to check if the regulation stressed in the Guidelines can be satisfied.

2.2 Specimens used in the Tests

Two full-size models of specimens (Fig.2) were used in the tests ; a lead-rubber bearing (Photo.1) (called LRB hereinafter), and a high damping rubber (Photo.2) (called HDR hereinafter), which were both prepared under the same design conditions of the base-isolated bearings in case of the Onnetoh-Oohashi Bridge.

A total of eight specimens were tested with four for each of the two models, with two specimens for each model having thermistors (T type) inserted in the center (Fig.3), to measure the temperature of a specimen at the beginning of each test, and the change of temperature during the tests.

The design conditions of LRB in the planned bridge were: maximum vertical reaction 135 tons, dead-load reaction 92 tons, design displacement (u_B) approx. 15 cm[3] by the check of ultimate bearing capacity of reinforced concrete piers for lateral force (ground group II). The design conditions of the two kinds of specimens are shown in Table 2, and the test results of material properties of rubber in Table 3.

2.3 Test Method

The instrument used in the tests consists of an actuator (maximum load 50 tons, maximum amplitude ±300 mm) and a hydraulic servo-tester at the vertical-load sustaining part (maximum load 150 tons) (Photo.3), and the temperature of the specimens was controlled by surrounding the instrument with a huge refrigerator. For each specimens, tests were conducted for the items listed in Table 4. The contents of each test are as follows.

1. Compression test

Compressive deformation was measured when the vertical load was varied from 0 to 135 tons (maximum bearing reaction).

2. Shear test

To determine the force-displacement hysteresis loops of each bearings, the experiments on 3-cycle shear test were performed under a vertical load of 92 tons, which is equal to the dead-load reaction, in line with the following procedures.

As the design horizontal displacement u_B is 15 cm, first of all, the test on $1/10*u_B$(1.5cm) was carried out, secondly, the case of $1/5*u_B$(3cm), thirdly, the test on $1/2*u_B$(7.5cm), finally, the specimen was deformed toward u_B.

In this study, data on the third cycle are adopted as representing values in case of no explanation.

After the above-mentioned test using a virgin specimen at room temperature (15-20° C) and the successive shear history test mentioned below, the same procedure has been taken on different temperature levels between -20° C and +30° C.

During the shear tests, the displacement given at a uniform speed due to the characteristics of the actuator was controlled by a personal computer.

3. Shear history test

Immediately after a shear test (Phase 1) at room temperature for collecting basic data, the consecutive shear test (Phase 2) was carried out to observe the influence of the history which means that the equivalent stiffness might depend on an experienced displacement.

4. 50-cycle shear test

The shear test was performed for 50 cycles with horizontal displacement adjusted to the design displacement u_B, and the specimen temperature at -20° C, in order to observe how the number of cycle influences the equivalent shear stiffness and the equivalent viscosity-damping factor, while the change in specimen temperature was recorded.

Also, prior to each test, friction force was measured on the sliding part of the test instrument, confirming that a friction force of approx. 0.48 ton was generated under a vertical load of 92 tons. It is considered, however, that this friction force has little influence on the test results, and therefore the test data are not corrected in terms of friction.

3 Test Results

3.1 Compressive Deformation

Table 5 shows the compressive deformation observed under a vertical load of 92 tons (dead-load reaction) and 135 tons (maximum reaction). The compressive deformation measured at room temperature is slightly smaller in comparison with those of the other four cases. The above reason might be derived from the fact that the specimen at the room-temperature case was virgin of the test. However, the change in temperature causes no significant difference in compressive deformation at temperatures under 30° C. The figures in parentheses in the table represent the rates of compression for the total rubber thickness of the specimens (%). The total rubber thickness of the specimens is 216 mm for LRB and 94.5 mm for HDR, whereas the compressive displacement under a dead-load reaction of 92 tons is approx. 1.3% and 1.0% of the total thickness of LRB and HDR respectively. The mean bearing stress of the rubber part of the specimens is 49.5 kg/cm^2 for LRB, and 32.8 kg/cm^2 for HDR. Concerning the compressive displacement, the Guidelines require that the compressive displacement of the bearings by the dead-load of the superstructure must be within 15% of the total rubber thickness. The above-mentioned requirement, which is related to the static characteristics of a base-isolated device in the Guidelines, is fully satisfied in these cases.

3.2 Change of Equivalent Shear Stiffness at Low Temperatures

Equivalent shear stiffness, equivalent viscosity-damping factor and other values representing the dynamic characteristics of base-isolated bearings may be calculated from its geometric size using the formula for both LRB and HDR given in the Guidelines. These values approximate the relationship between the shear force and the horizontal displacement to a bilinear-type spring model, as shown in Figure 3.

In this study, a comparison between the design value and the equivalent shear stiffness of the base-isolated bearings as well as the equivalent viscosity-damping factor were made, which were obtained by the following method based on the actual shear force - horizontal displacement curve measured in the shear tests. The equivalent shear stiffness, which represent the shear characteristics of a specimen like Fig.4, can be obtained by two different methods.[4)5)] I.C., by taking the inclination of the line connecting the positive maximum horizontal displacement with the negative one, or by taking the shear force into consideration instead of the displacement.

The latter is adopted in this research work, in which the equivalent shear stiffness Ke and the equivalent viscosity-damping factor heq are defined as

$$Ke = AB/CB,\quad heq = 1/\pi \cdot \Delta W/W$$

It is calculated that the equivalent shear stiffness by the latter method was 2 - 8% higher than that by the former one.

Table 6 represents the equivalent shear stiffness (Ke) on the first and the third cycle, and the equivalent viscosity-damping factor (heq) on the third cycle at the horizontal displacement of 15 cm (u_B). The equivalent shear stiffness of LRB and HDR varies only slightly, with an average equivalent stiffness at room temperature of 1,575 kg/cm for LRB, and 2,110 kg/cm for HDR. When the temperature decreases, the equivalent stiffness increases with an equivalent viscosity-damping factor of 0.30 - 0.36 for LRB, and 0.11 - 0.14 for HDR respectively, which implies no significant change in damping factors when temperature changes.

Figure 5 shows the equivalent shear stiffness of LRB1, LRB2, HDR1 and HDR2 at the horizontal displacement 15 cm (u_B) on each temperature level. The design value for the equivalent shear stiffness (Ke) is 2,280 kg/cm for both LRB and HDR. The equivalent shear stiffness (Ke) at room temperature nearly corresponded with the design value for HDR, whereas for LRB it is approx. 30% smaller. The reason why this difference occurred is that the formula given in the Guidelines for calculating the equivalent shear stiffness (Ke) of LRB is based on a shear strain of 50% while the test specimens used here were given a shear strain of approx. 70%.

The ratio of the equivalent shear stiffness (Ke) in the third cycle at -20° C to that at 30° C is 1.63:1 for LRB and 1.59:1 for HDR, where the average of the values of the two specimens were taken for LRB, HDR respectively. These ratios failed to satisfy the requirement stipulated in the Guidelines in 3.5 Item (4), Static Characteristics of Base-Isolated Bearings, that "The ratio for the equivalent shear stiffness of a base-isolated bearing at -20° C to that at 30° C must be equal to or less than 1.5:1." This ratio was determined so that the variation in natural period

of a bridge remains within 20% when the equivalent shear stiffness is varied.

Figure 6 describes the equivalent viscosity-damping factors (heq) of LRB1, LRB2, HDR1 and HDR2 at the specimen displacement of 15 cm (u_B). The design value of the heq is 21% for LRB, and 14% for HDR. While the heq at room temperature is almost the design value for HDR, the factor for LRB is approx. 60% larger than the figure on the design.

Figure 7 represents the shear force - horizontal displacement curves (hysteresis loops) of LRB1 and HDR1, measured at room temperature and at -20° C at the horizontal displacement of 15 cm (u_B). While LRB showed a spindle-shape independent of the horizontal displacement, HDR described a spindle-shape for small horizontal displacements which turned into reversed S-shaped hysteresis loops with increasing the displacement, due to the strain hardening[6] of the rubber material. This figure also gives increments by temperature decrease.

3.3 Relationships Between Ke And Displacement

Figure 8 describes the hysteresis loops on different displacement levels. In which, it is very clear that the Ke becomes smaller with the increase of displacement.(See also Table 7)

3.4 Change in Equivalent Shear Stiffness by Shear History

Table 7 represents the equivalent shear stiffness (Ke) of the new test specimens after the third cycles, measured in the first and the second round of the shear test at room temperature. Both LRB and HDR show a lower stiffness in the second round than in the first, on the other hand, in the case of the maximum horizontal displacement u_B the stiffness is almost the same. This means that the experienced displacement functions as a factor of the Ke.

3.5 50-cycle Shear Test

Figures 9, 10 and 11 show the variation in equivalent shear stiffness(Ke), equivalent viscosity-damping factor (heq) and specimen temperature during the 50-cycle shear test. The results represent decreases in the Ke from the initial stage; LRB by 64% and HDR by 69% respectively. It is noted that for both LRB and HDR the specimen temperature rose by as much as 25° C, but the final temperature of the specimens was approx. 5° C after 50 cycles of the shear test. This gives a lower equivalent shear stiffness than expected from the shear test results at that temperature in Paragraph 3.2, which implies the influence of repeated shear in addition to that of temperature rise. The equivalent viscosity-damping factor, on the other hand, becomes stable after about the 10th cycle, with little influence from repeated shear thereafter. Figure 12 describes the hysteresis loops of LRB and HDR measured at every 10th cycle.

Concerning the 50-cycle shear test, the Guidelines provide in 3.5 Item (1), Dynamic Characteristics of Base-Isolated Bearings, that "The equivalent shear stiffness after the test with a period corresponding to the natural period of the base-isolated bearings must be in the range of 80 - 120% of the initial equivalent shear stiffness. Also, the equivalent

viscosity-damping factor is stipulated not to fall below 80% of the initial value. In our experiments, it should be taken note that the period is approx. 40 seconds, which is not equal to the natural period of the base-isolated bearings.

4 Conclusions

For the purpose of understanding the behavior of base-isolated bearings for bridges, indoor tests were performed with two kinds of full-size laminated rubber bearings, and obtained the following results:

1. The compressive deformation changes only slightly when the temperature changes.

2. As the compressive deformations against dead-load reactions were measured to be approx. 1.3% and 1.0% of the total rubber thickness for LRB and HDR, respectively, it seems that the Guidelines' condition might be slightly stricter.

3. The equivalent shear stiffness (Ke) and the equivalent viscosity-damping factor (heq) were found to take a larger value than the design one for LRB. It is pointed out that the formula in the Guidelines, which assumes the shear strain to be less than 50%, should be improved.

4. The ratios of the equivalent shear stiffness at -20° C to that at 30° C in the shear test with the design displacement uB were 1.63:1 for LRB and 1.59:1 for HDR respectively. As a result it was clarified that the requirement in the Guideline is not satisfied. At the same time it seems that the above condition might be severe.

5. The equivalent viscosity - damping factor changes only slightly when the temperature changes; 0.30 - 0.36 for LRB and 0.11 - 0.14 for HDR respectively.

6. In case of the shear test, both LRB and HDR show a lower stiffness in the second round than in the first. This means that the experienced displacement is a variable in the function of the equivalent shear stiffness. This leads to the idea that the bearing manufacturers should, in order to confirm the design values, carry out shear tests with the maximum possible displacement before delivering their products.

7. As a result of the 50-cycle shear test, the specimen temperature rose by about 25° C from some -20° C level. As the focal points were hardenings of the rubber and recrystallization of the lead cylinders, such phenomenon is not expected before the experiments. Therefore, it is concluded that the base-isolated bearings are applicable to the cold region like Hokkaido as far as the temperature increase is concerned.

8. The equivalent shear stiffness decreased to 64% for LRB and to 69% for HDR during the cyclic test. It is considered that the influences not only of the temperature increase but also of the repeated shear contribute to the decrement because the Ke value is lower than that of the shear test in comparison between Fig.5 and Fig.8 at the same temperature level. This implies also that there are cases in which the stipulations of the Guidelines could not be satisfied.

9. It is difficult to satisfy the condition in the Guidelines regarding the base-isolated bearings related to the natural period.

5 Postscript

The experiments reported in this paper represent that the equivalent shear stiffness of laminated rubber bearings increases at low temperatures and the equivalent shear stiffness decreases by repeated shear. It is necessary, therefore, to confirm by calculation their influences on the natural period of the bridges in question. Based on the result of this calculation, further consideration should be given to judge if the current base-isolated bearings are to be applied without any change for cold regions, or some new base-isolated design method for cold districts is to be proposed with special specifications developed for such regions.

On the other hand, in order to find out to what degree the temperature of bearings decreases, outdoor temperatures are being measured in the vicinity of the Onnetoh-Oohashi bridge, while in our laboratory the correlation is now under study between outdoor temperatures and the specimen temperatures measured.

Bibliography

1) Masataka Koga: The first completed design for base-isolated bearings in the Nagakigawa Bridge construction plan (Akita Prefecture), Nikkei-Construction, March 23, 1990, pp. 6-9 (in Japanese)

2) Japan Institute of Construction Engineering: Guidelines for the base-isolated bearing design method for road bridges (draft), March 14, 1989 (in Japanese)

3) Hokkaido Development Bureau, Kushiro Construction Department: Design Report on base-isolated bearings for the Onnetoh-Oohashi bridge on National Road 44 in Nemuro (laminated rubber bearing), 1988 (in Japanese)

4) Kazuhiko Kawashima, Kinji Hasegawa, Tatsuhiko Koyama, and Takeshi Yoshida: Experiments on dynamic cyclic shear characteristics of rubber bearing for bridges, Civil Engineering Material, 28-8, 1986 (in Japanese)

5) Yoshihide Fukabori: High-Damping Rubber, Journal of the Society of the Rubber Industry, Japan, Vol. 62, No. 5, 1989 (in Japanese)

6) Kazuhiko Kawashima, Kinji Hasegawa, Takeshi Yoshida, Hiroshi Yamauchi, and Hiromi Kosaka: Model vibration experiments concerning the vibration characteristics of base-isolated bridges, Civil Engineering Material 30-10, 1988 (in Japanese)

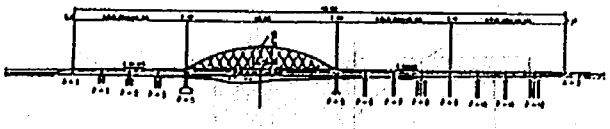

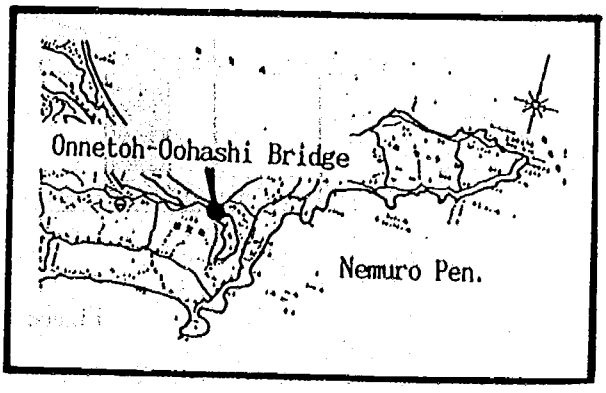

figure 1 Onnetoh-Oohashi Bridge

Table 1 Mean Temperature in past 30 years

Location	Highest(℃)	Lowest (℃)
Sapporo	25.9	-8.9
Asahikawa	25.8	-13.4
Nemuro	20.5	-9.1

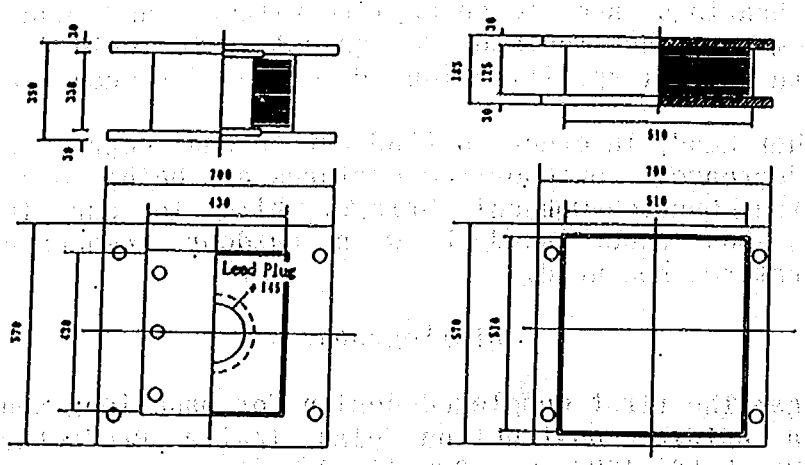

Figure 2 Specimen used in Test

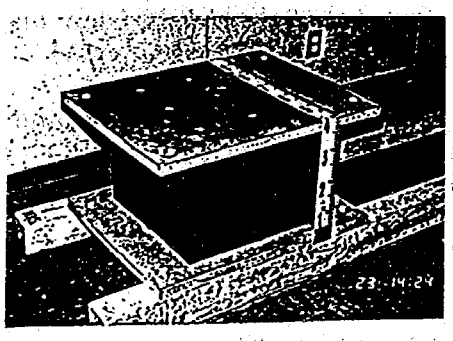

Photo 1 specimen (LRB)

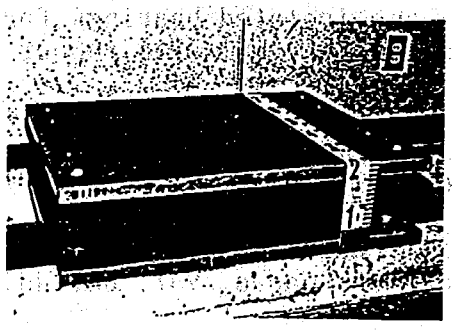

Photo 2 specimen (HDR)

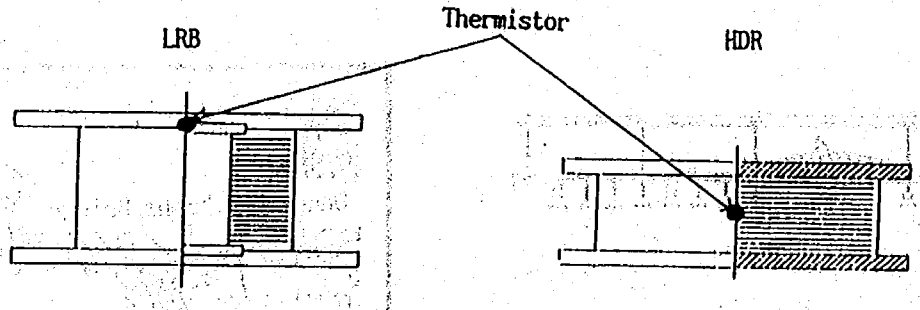

Figure 3 Thermistor

Table 2 Design Condition of Specimen

	LRB	HDR
Maximum Vertical Reaction R (ton)	135	
Dead-Load Reaction W (ton)	92	
Live-Load Reaction W (ton)	43	
Design Displacement u_B (cm)	15	
Equivalent Shear Stiffness K_B (kg/cm)	2280	
Equivalent Viscosity-Damping Factor h_{eq} (%)	21	14

Table 3 Test Result: Rubber Material Properties in Specimen

LRB

Rubber (Natural Rubber) Material Properties			
Test Item		Standard Value	Measured Value
Static Shear Modulus (kgf/cm²)		8 ± 1.0	8.4
Tensile Strength (kgf/cm²)		over 150	229
Elongation (%)		over 450	628
Aging Test	Rate of Stress-Change at 25% Elongation (%)	−10 ~+30	17.1
	Rate of Elongation-Change (%)	over −25	−15.1
Rate of Permanent Compressive Strain (%)		under 25	22
Ozone Resistance		No Cracking	No Cracking
Adhesion Test		Rubber Rupture	18.1 (R100)

·The above result is an average value from 4 specimens
·Test Method by JIS K 6301

HDR

Inner Rubber (KL401) Material Properties		
Test Item	Standard Value at B Company	Measured Value
300% Modulus (kgf/cm²)	37± 6	34
Tensile Strength (kgf/cm²)	over 90	104
Elongation at Rupture (%)	over 650	755

Coating-Rubber (AN920) Material Properties		
Test Item	Standard Value at B Company	Measured Value
Tensile Strength (kgf/cm²)	over 125	147
Elongation at Rupture (%)	over 650	838

·Test Method by JIS K 6301

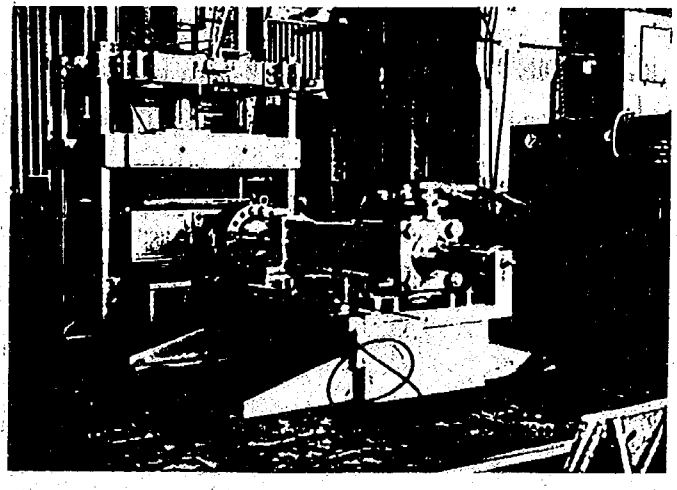

Photo 3 Test Instrument

Table 4 Content of Test for Each Specimen

Specimen	Temperature	Content of Test
LRB1*、HDR1* LRB2*、HDR2*	+30℃	Compression Test、Shear Test
	Room Temperature	Compression Test、Shear Test
	0℃	Compression Test、Shear Test
	−10℃	Compression Test、Shear Test
	−20℃	Compression Test、Shear Test
LRB2*、HDR2*	−20℃	50-Iteration Shear Test
LRB3、HDR3	Room Temperature	Compression Test、Shear History Test
LRB4、HDR4	Room Temperature	Compression Test、Shear Test

* Specimen with Thermistor

Table 5 Compression Test Result

Specimen	Compressive Deformation (mm)									
	+30℃		Room temp.		0℃		−10℃		−20℃	
	92ton	135ton	92ton	135ton	92ton	135ton	92ton	135ton	92ton	135ton
LRB1	4.45 (2.06)	6.18 (2.86)	2.52 (1.17)	4.14 (1.92)	3.20 (1.48)	4.32 (2.00)	2.76 (1.28)	4.28 (1.98)	2.74 (1.27)	4.20 (1.94)
LRB2	3.69 (1.71)	5.37 (2.49)	2.63 (1.22)	4.13 (1.91)	2.78 (1.28)	4.31 (2.00)	2.90 (1.34)	4.30 (1.99)	2.83 (1.31)	4.22 (1.95)
HDR1	1.03 (1.26)	1.36 (1.44)	0.86 (0.91)	1.16 (1.23)	0.95 (1.01)	1.23 (1.29)	0.95 (1.01)	1.22 (1.29)	0.95 (1.01)	1.22 (1.29)
HDR2	1.30 (1.37)	1.58 (1.67)	0.98 (1.03)	1.21 (1.28)	0.98 (1.03)	1.24 (1.31)	0.95 (1.01)	1.19 (1.26)	1.10 (1.16)	1.33 (1.41)

( ):Compressive Deformation/Total Rubber Thickness (%)

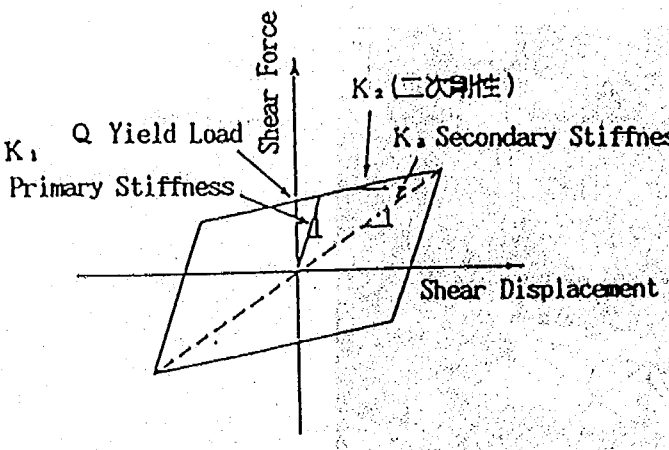

Figure 4 Bilinear-Type Spring

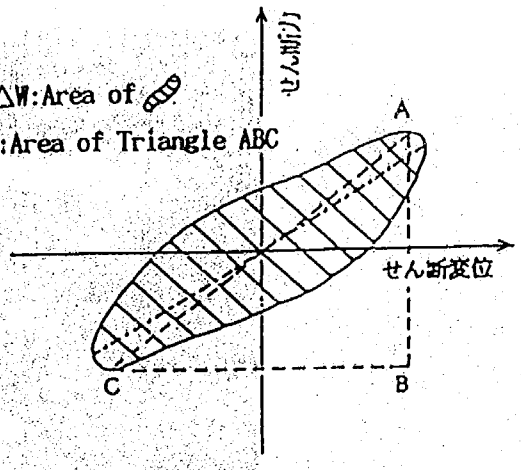

Figure 5 Definition of Dynamic Characteristics

Table 6 Shear Test Result

Specimen	Temperature (℃)	Equivalent Shear Stiffness k_e (kg/cm)		Equivalent Viscosity-Damping Factor h_{eq}
		First Cycle	Third Cycle	
LRB1	+30	1480	1332	0.34
	Room Temp. (14.7)	1843	1645	0.34
	0	2096	1832	0.31
	−10	2309	2072	0.31
	−20	2515	2217	0.31
LRB2	+30	1527	1346	0.34
	Room Temp. (17.4)	1836	1619	0.34
	0	2079	1994	0.33
	−10	2290	2005	0.31
	−20	2437	2155	0.30
LRB3	Room Temperature	1790	1558	0.35
LRB4	Room Temperature	1762	1477	0.36
HDR1	+30	1968	1787	0.13
	Room Temp. (22.7)	2503	2079	0.12
	0	2608	2249	0.12
	−10	2965	2586	0.14
	−20	3353	3044	0.14
HDR2	+30	2193	1944	0.11
	Room Temp. (17.3)	2618	2136	0.12
	0	2682	2340	0.13
	−10	2777	2515	0.13
	−20	3176	2874	0.13
HDR3	Room Temperature	2527	2082	0.12
HDR4	Room Temperature	2613	2143	0.12

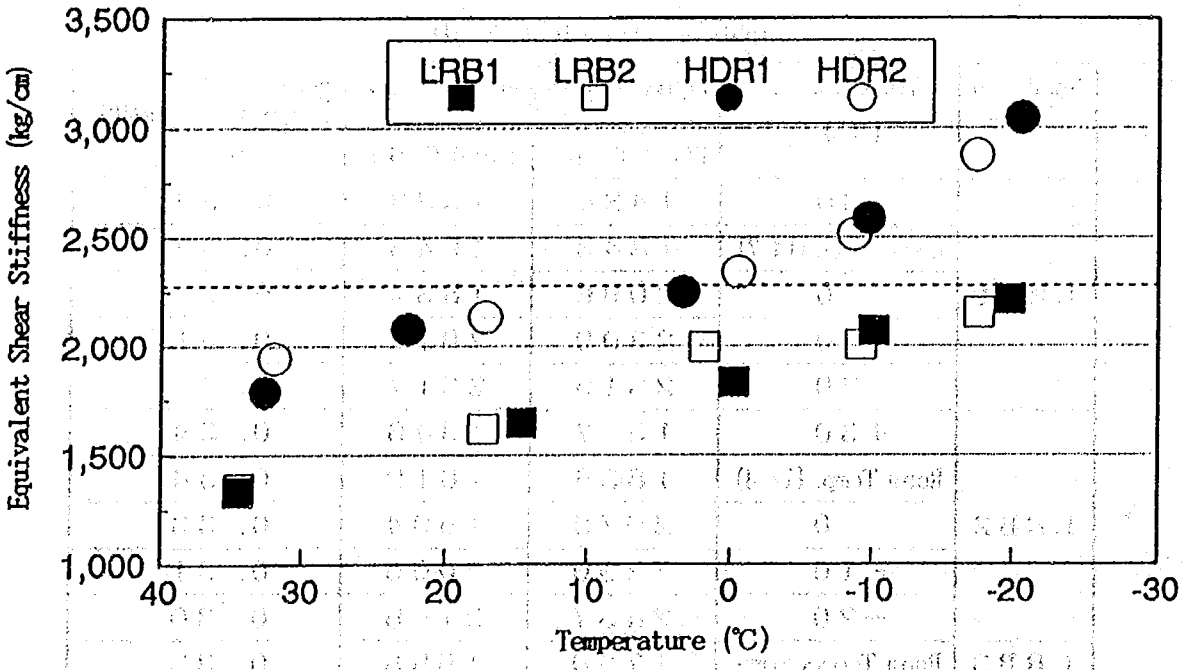

Figure 6 Equivalent Shear Stiffness by Temperature

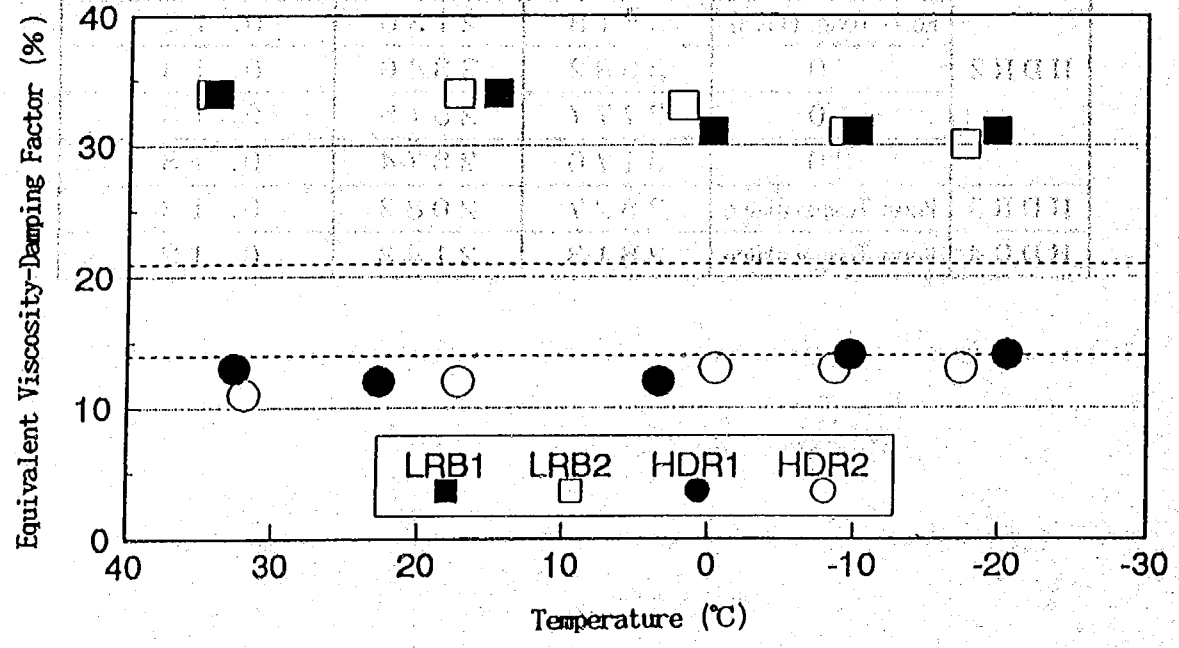

Figure 7 Equivalent Viscosity-Damping Factor by Temperature

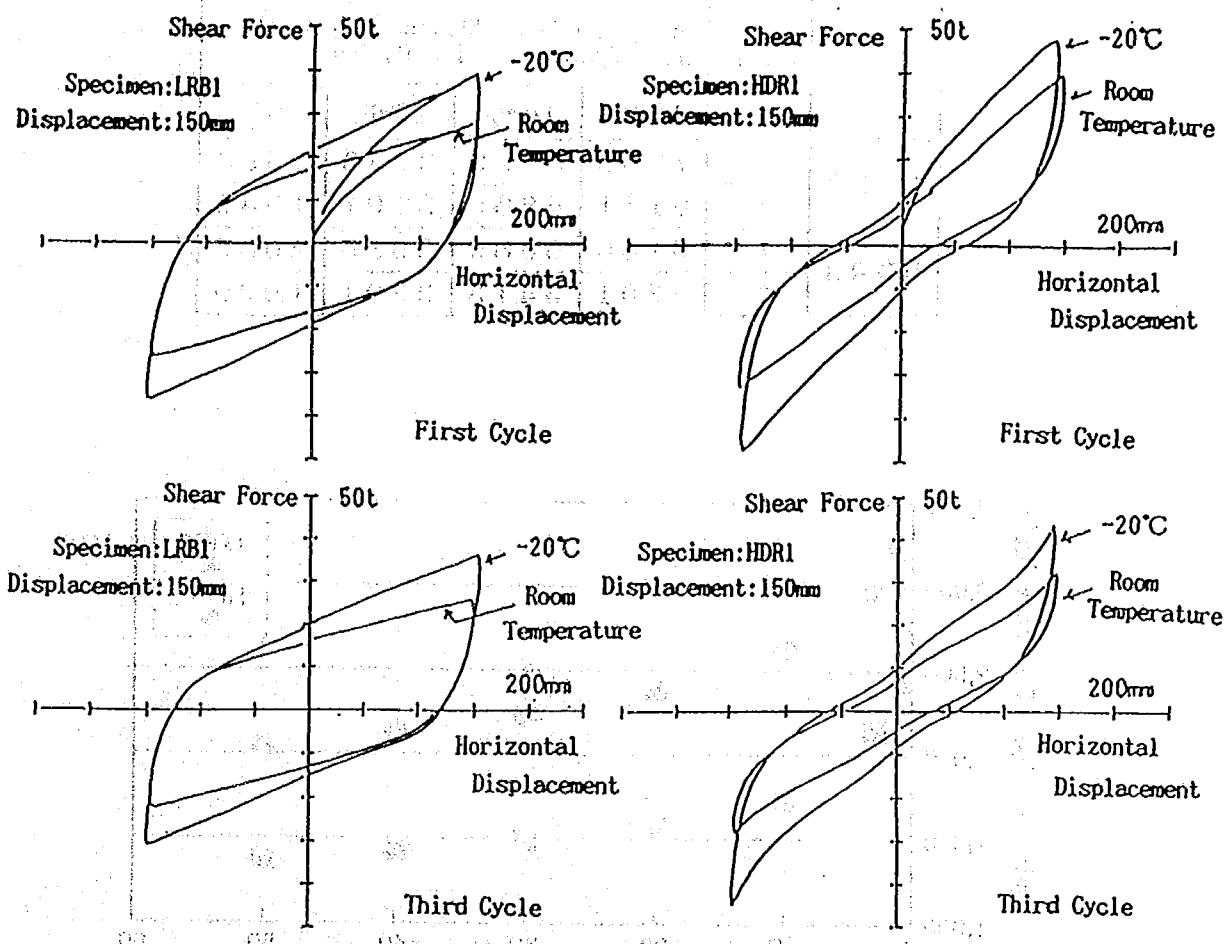

Figure 8 Shear Force-Horizontal Displacement Curve

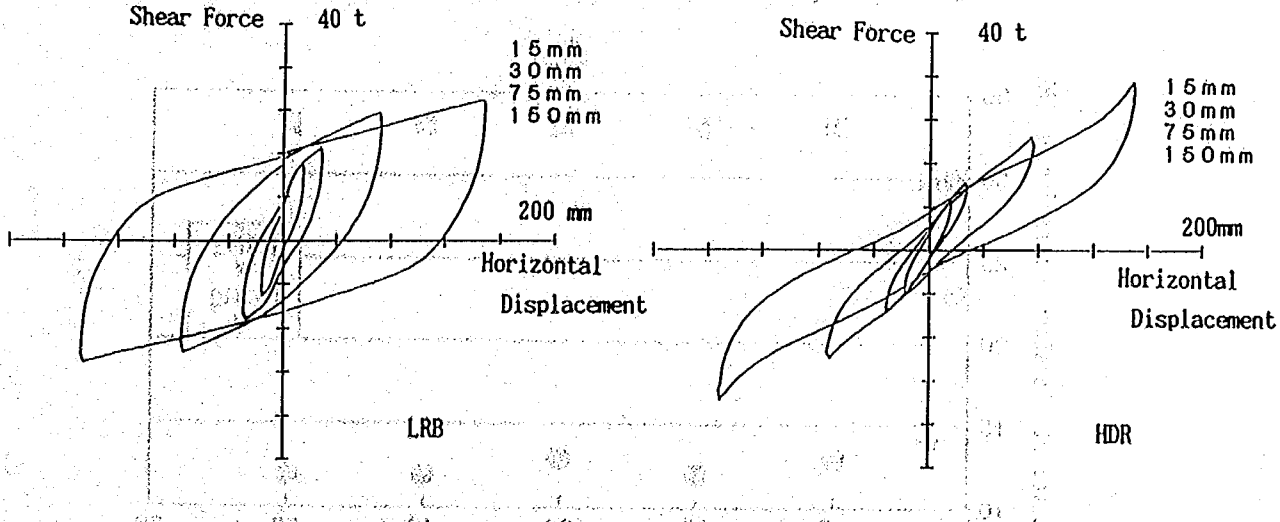

Figure 9 The Histerisis Loops on Different Displacement Levels

Table 7 Shear History Test Result

Specimen	Phase	Equivalent Shear Stiffness after the Third Cycle K_e (kg/cm)			
		1/10*U_B	1/5*U_B	1/2*U_B	U_B
LRB3	1	7753	5429	2943	1558
	2	6151	4689	2701	1543
HDR3	1	9180	5680	2985	2082
	2	4301	3413	2201	1920

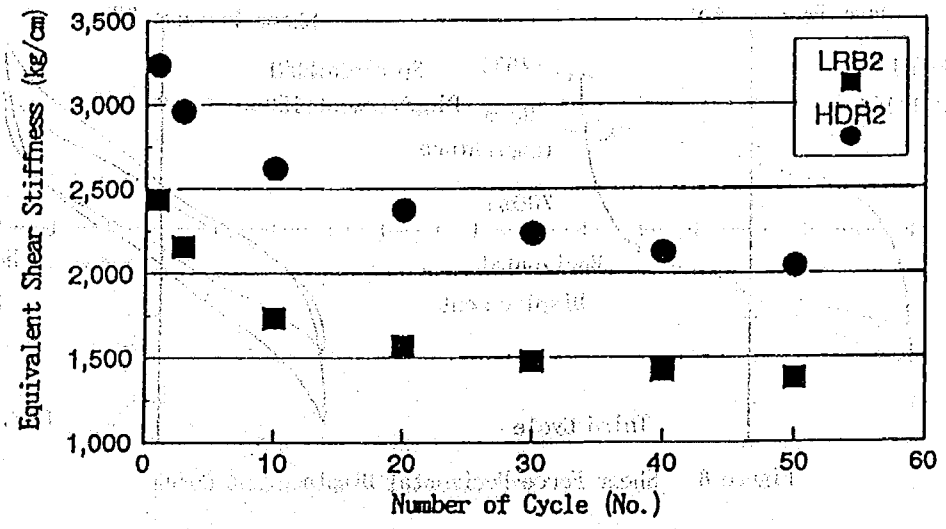

Figure 10 Equivalent Shear Stiffness during 50-Iteration Test

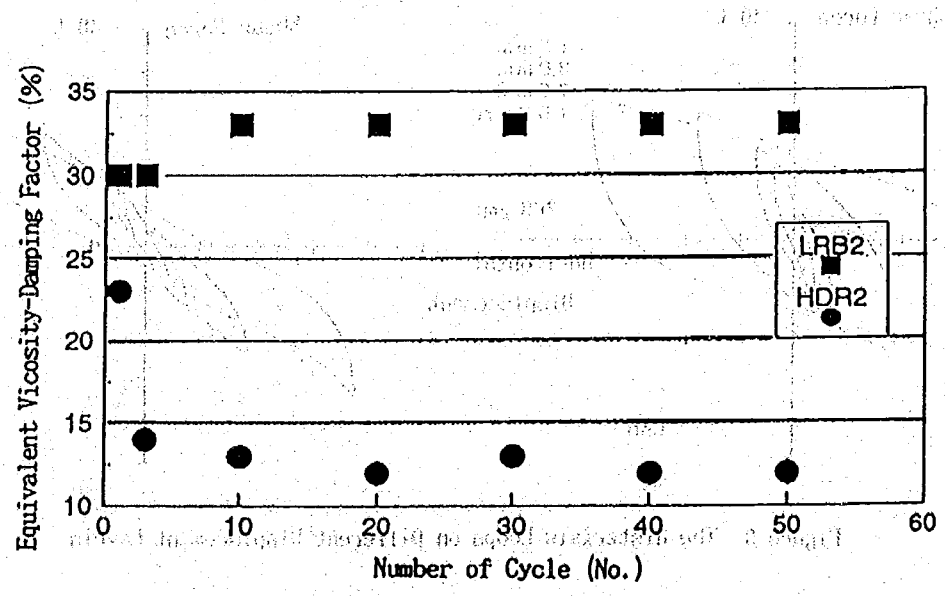

Figure 11 Equivalent Vicosity-Damping Factor during 50-Iteration Test

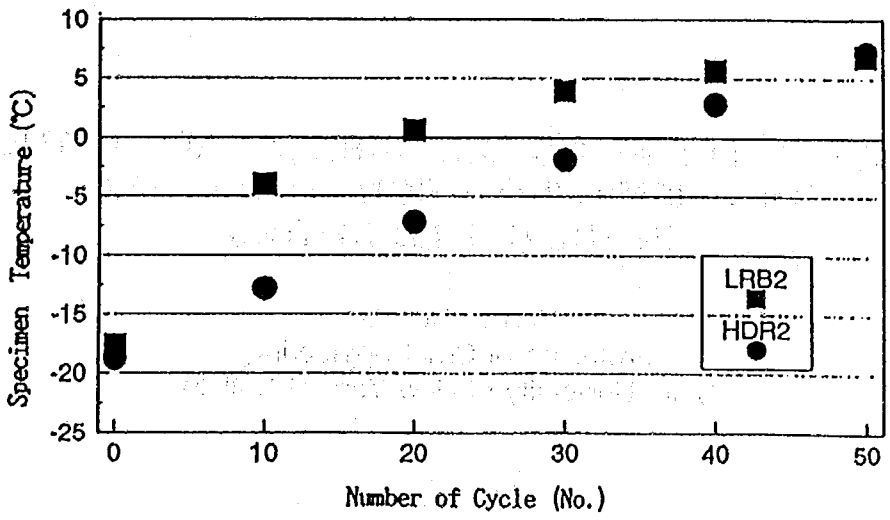

Figure 12 Specimen Temperature during 50-iteration Test

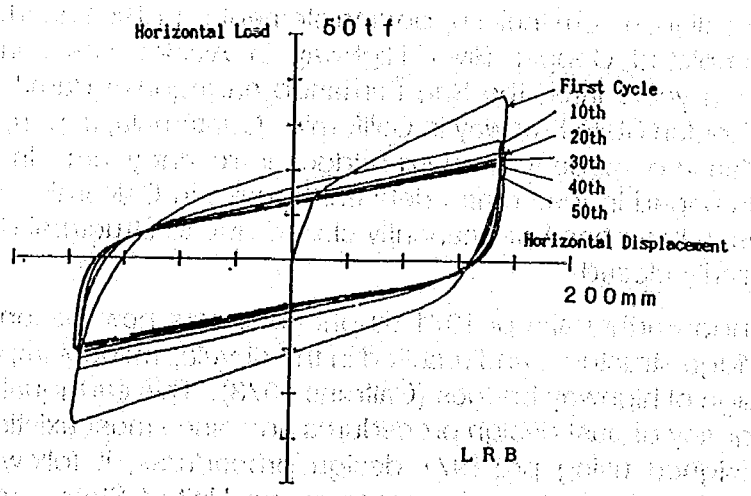

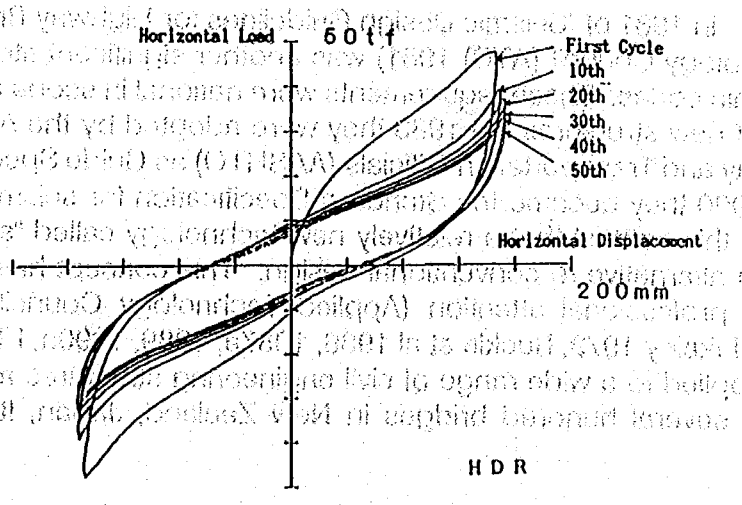

Figure 13 Shear Stress-Shear Displacement Curve during 50-Iteration Test

CODE DEVELOPMENTS AND CURRENT APPLICATIONS OF SEISMIC ISOLATION TO BRIDGES IN THE UNITED STATES

Ian G. Buckle
Professor of Civil Engineering
State University of New York at Buffalo

1. BACKGROUND

Historically, bridges have proved to be vulnerable to earthquakes, sustaining damage to substructures and foundations and in some cases being totally destroyed as superstructures collapse from their supporting elements. In 1964 nearly every bridge along the partially completed Cooper River Highway in Alaska was seriously damaged or destroyed. Seven years later, the San Fernando earthquake damaged more than sixty bridges on the Golden State Freeway in California. Guatemala, Japan, and Chile have also experienced seismic damage to modern bridges in recent years. In 1989, more than 80 bridges were damaged in the Loma Prieta earthquake in California. Of these, 3 suffered collapsed spans, 5 have been permanently closed due to structural damage and another 15 were temporarily closed.

The San Fernando Earthquake of 1971 taught engineers new lessons about the seismic resistance of bridge structures and resulted in the development of improved provisions for the seismic design of highway bridges (Caltrans 1973). This earthquake demonstrated the potential inadequacy of past design procedures and since most existing bridges in service today were designed using pre-1971 design procedures, it follows that many of the highway bridges in seismically active areas in the United States, may have insufficient strength to resist seismic loading.

The publication in 1981 of "Seismic Design Guidelines for Highway Bridges" by the FHWA (Applied Technology Council (ATC) 1981) was another significant step in the evolution of improved seismic codes. These requirements were national in scope and intended for use in the design of new structures. In 1983 they were adopted by the American Association of State Highway and Transportation Officials (AASHTO) as Guide Specifications (AASHTO, 1983) and in 1990 they became the Standard Specification for seismic design (AASHTO, 1990a). It is in this context that a relatively new technology called "seismic isolation" has emerged as an alternative to conventional design. This concept has received increasing academic and professional attention (Applied Technology Council 1986, ASCE 1989, Billings 1985, Blakeley 1979, Buckle et al 1986, 1987a, 1989, 1990a, EERI 1990, Kelly 1986) and is being applied to a wide range of civil engineering structures around the world. To date there are several hundred bridges in New Zealand, Japan, Italy, Iceland and the

United States which use seismic isolation technology for their earthquake protection. The basic purpose of seismic isolation is to increase the fundamental period of vibration such that the structure is subjected to significantly lower earthquake forces.

One of the major impediments to the implementation of seismic isolation in the United States has been the lack of code requirements, (Mayes et. al. 1990). With liability issues being a major concern in the U.S., designers have been slow to use the technology without the protection of professionally acceptable code provisions. Thus the October 1990 adoption of the Seismic Isolation Design Guidelines for Highway Bridges by AASHTO (AASHTO, 1990b) is seen as a major step forward in the implementation of seismic isolation for bridges.

This paper summarizes the AASHTO Guide Specifications for Seismic Isolation Bridge Design (AASHTO, 1990b) and briefly reviews current applications of seismic isolation to bridges. Previous papers (Buckle et al 1987b, 1988, 1990b) have discussed the design and performance of isolated bridges in the U.S. This present paper focuses on code provisions and makes only minor reference to recent applications.

2. OBJECTIVES OF THE PROVISIONS

The underlying objectives when preparing these Guidelines were:

- to be as consistent as possible with the recently adopted AASHTO Standard Specifications for conventional seismic design.
- to be as consistent as possible with the recently adopted Uniform Building Code provisions for seismically isolated buildings.
- to be applicable to a wide range of possible seismic isolation systems.

To satisfy the first objective, the specifications had to be compatible with the seismic performance categories (SPC) framework of the new seismic design provisions. This framework permits a range of design requirements to be specified according to bridge importance and regional differences in seismic risk. For example only nominal default requirements are specified for zones where the acceleration coefficient is less than 0.10 (SPC A). The most stringent requirements are specified for zones where the coefficient is greater than 0.29 (SPC's C and D). The second objective determined the format for the isolation design requirements. Some modifications were necessary due to differences in building and bridge structural form and design loads. Others were required to provide consistency with the first objective.

The third objective necessitated that the requirements be generic and this led to mandatory testing of isolation hardware to confirm the engineering parameters used in design and to verify the overall adequacy of the isolation system. Some systems may not be capable of demonstrating acceptability by test and, consequently, would not be permitted. In general, acceptable systems will:

- remain stable for required design displacements,
- provide increasing resistance with increasing displacement,
- not degrade under repeated cyclic load, and
- have quantifiable engineering parameters (e.g., force-deflection characteristics and damping).

Both static and dynamic analysis procedures are included (depending on the SPC) and are based on the same level of seismic input and require the same level of performance from the bridge. The design earthquake load corresponds to a level of ground motion that has a 10 percent probability of being exceeded in a 50 year time period, i.e. a 475 year return period.

3. PHILOSOPHY OF THE PROVISIONS

Seismic isolation provides a significant reduction in the elastic seismic forces the bridge must resist when compared to conventional fixed base design. As a consequence there are two possible design philosophies that can be used and both are included in the AASHTO Isolation Guide Specifications (AASHTO, 1990b). The first is to take advantage of the reduced forces and provide a more economical bridge design than conventional construction. This option utilizes the same Response Modification Factors (R-Factors) as the recently adopted AASHTO Standard Specifications (AASHTO, 1990a) and thus provides the same level of seismic safety. The advantage of this design option is that if seismic forces are governing the design of the bridge, cost savings up to approximately 10% of the total bridge cost may be realized (Billings 1985).

The second design option is to provide a bridge with improved seismic performance characteristics over that of a conventional design using the AASHTO Standard Specifications. The intent of this design option is to eliminate or significantly reduce damage (inelastic deformation) to the substructure and abutments. In this case an R-Factor of 1.5 will ensure essentially elastic response by eliminating the ductility demand on the substructure. This design option can generally be achieved for similar or less cost than a conventional design. Furthermore, it provides protection against earthquakes that may exceed the 475 year design event. In low-to-moderate seismic zones in the United States the maximum credible earthquake could be 2-3 times the intensity of the design event. In such a case an isolated bridge designed for a R-factor of 1.5, has a considerable reserve capacity to draw upon to survive such an event, especially when compared to a conventional design which uses higher R-factors.

4. METHODS OF ANALYSIS

The basic premise of the seismic isolation design provisions (consistent with those for buildings and hospitals) is twofold. First, the energy dissipation of the isolation system can be expressed in terms of equivalent viscous damping; and second, the stiffness of the nonlinear isolation system can be expressed as an effective linear stiffness (Figure 1). These two basic assumptions permit both the single and multimode methods of analysis to be used for seismic isolation design.

For sliding systems without a self-centering mechanism or for pure elasto-plastic isolation systems the equivalent viscous damping concept is no longer appropriate. The equivalent viscous damping formulation produces a value for the damping ratio that is independent of the coefficient of friction for sliding systems or the yield point for elasto-plastic systems. Furthermore, because these systems lack a restoring force, the total design displacement may be underestimated. Consequently, a non-linear time history analysis is required for all seismic isolation systems that do not have a self-centering mechanism.

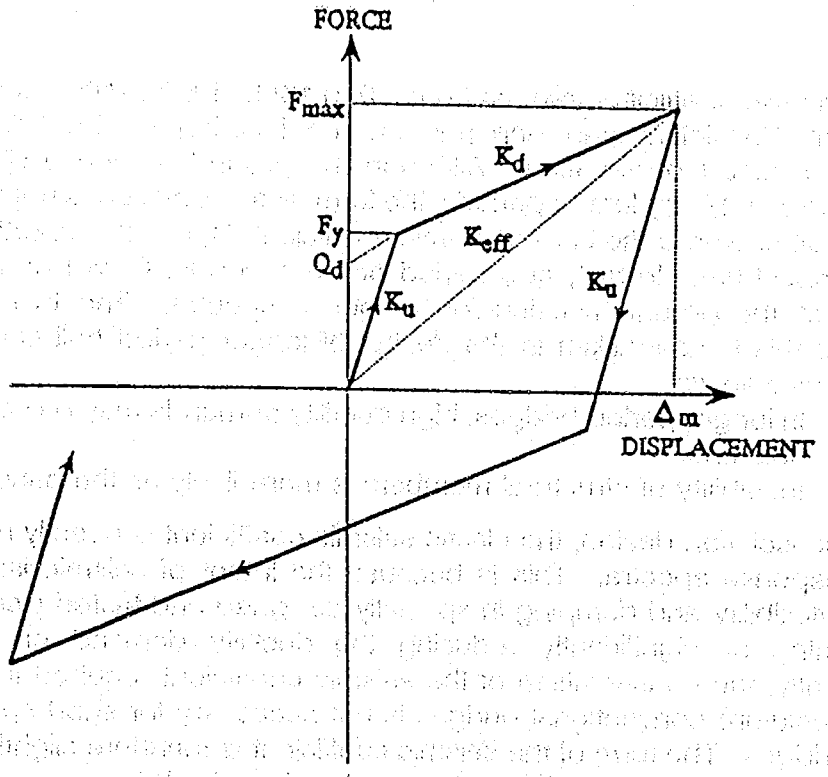

Q_d = Characteristic strength (kips)
F_y = Yield force (kips)
F_{max} = Maximum force (kips)
K_d = Post-elastic stiffness (kip/inch)
K_u = Elastic (unloading) stiffness (kip/inch)
K_{eff} = Effective stiffness
Δ_m = Maximum bearing displacement

Figure 1. Bilinear force-deflection loop for a typical base isolator.

4.1 Statically Equivalent Seismic Force Coefficient

For the design of conventional bridges the form of the elastic seismic coefficient (C_s) is given by

$$C_s = \frac{1.2AS}{T^{2/3}} \qquad (1)$$

where S, the site coefficient, ranges from 1.0 to 1.2 to 1.5 for different soil types. A is the Acceleration Coefficient and depends on the location of the bridge and T is the fundamental period of vibration. Although the ground response spectrum decreases approximately as 1/T for longer periods, the form given above does not decrease as rapidly as 1/T. In other words the elastic seismic coefficient, C_s is not proportional to the ground response spectrum. In fact, at a period of 2.0 seconds, C_s will be approximately 50% greater than the ground acceleration response spectra. The two major reasons for introducing this conservatism in the design of longer period (tall columns, long spans) bridges is as follows:

a. In longer period bridges, high ductility demands may be concentrated in a few columns.
b. Instability of structural members is more likely as the period increases.

For seismic isolation design, the elastic seismic coefficient is directly related to the elastic ground response spectra. This is because the intent of seismic isolation design is to introduce flexibility and damping in specially designed and tested elements with the goal of eliminating or significantly reducing the ductility demand on the substructures. Consequently, the conservatism of the seismic coefficient required for long period (long span, tall column) conventional bridges is not necessary for short span, regular column, isolated bridges. The form of the seismic coefficient is therefore slightly different from that for a conventional design and, for 5% damping, is given by

$$C_s = \frac{AS_i}{T} \qquad (2)$$

As before, A is the acceleration coefficient, S_i is the site coefficient for seismic isolation design and the 1/T factor accounts for the decrease in the response as T increases. The specific S_i values for the isolation requirements reflect the fact that above a period of 1.0 second, there is a 1.0 to 1.5 to 2.0 relationship for the spectral accelerations for Soil Types I, II and III, respectively (Figure 12 of AASHTO, 1990a). Once again, C_s should not exceed a value of 2.5A.

If the effects of damping are included, the elastic seismic coefficient is given by

$$C_s = \frac{AS_i}{TB} \qquad (3)$$

where B is the damping factor for the isolation system. Values for B are given in Table 1; note that for 5% damping, B = 1.0.

The quantity C_s is a dimensionless design coefficient, which when multiplied by the acceleration due to gravity (g) produces the spectral acceleration. This spectral acceleration (S_A) is related to the spectral displacement (S_D) by the relationship

$$S_A = \omega^2 S_D \tag{4}$$

where ω is the circular natural frequency and is given by $2\pi/T$. Therefore, since $S_A = C_s \cdot g$

$$S_A = \frac{AS_1}{TB} g \tag{5}$$

and

$$S_D = \frac{1}{\omega^2} \frac{AS_1}{TB} g = \frac{9.79AS_1T}{B} \text{ inches} \tag{6}$$

Denoting S_D as D, which is the displacement across the elastomeric bearings, the above can be approximated by:

$$D = \frac{10AS_1T}{B} \text{ inches} \tag{7}$$

An alternate form for C_s is possible. The quantity C_s is defined by the relationship

$$F = C_s W \tag{8}$$

where F is the earthquake design force and W is the weight of the structure. Therefore,

$$C_s = \frac{F}{W} = \frac{\sum k_{eff} \times D}{W} \tag{9}$$

where $\sum k_{eff}$ is the sum of the effective stiffnesses of the equivalent linear springs which represent those isolation bearings which are supporting the superstructure segment. The equivalence of this form to the previous form is evident by recalling that $\sum k_{eff} = \omega^2 W/g$, from which

$$C_s = \frac{\omega^2 W}{g} \times \frac{D}{W} = \frac{4\pi^2}{T^2} \times \frac{1}{386.4} \times \frac{9.79AS_1T}{B}$$

$$C_s = \frac{AS_1}{BT} \tag{10}$$

Thus in summary, equations 7 and 9 are used to determine the statically equivalent seismic force. The isolated period of vibration is given by

$$T = 2\pi \sqrt{\frac{W}{\sum K_{eff} \cdot g}} \qquad (11)$$

The base shear (V) (which is equal to the statically equivalent seismic force) is obtained by substituting equations 7 and 9 into equation 8.

$$V = F = \sum K_{eff} \cdot D \qquad (12)$$

$$V = \frac{AS}{TB} \cdot W \qquad (13)$$

Table 1. Damping Factor, B

Equivalent Viscous Damping Ratio	<2%	5%	10%	20%	30%	40%	>50%
B	0.8	1.0	1.2	1.5	1.7	1.9	2.0

4.2 Single Mode Spectral Analysis

The single mode method of analysis, given in Section 5.3 of the AASHTO 1990a, is also appropriate for seismic isolation design. In fact, use of the method is simplified for isolated bridges. Steps 1, 2 and 3 of the procedure are not necessary since the use of an isolation system will ensure a simple rigid body deformation pattern of the superstructure.

In Step 4 of the procedure the value of $p_e(x)$, the intensity of the equivalent static seismic loading, is determined as

$$p_e(x) = w(x) \cdot C_s \qquad (14)$$

where C_s is calculated by equation 9 and w(x) is the dead load per unit length of the bridge superstructure. In Step 5 of the procedure the loading $p_e(x)$ is applied to the superstructure to determine the resulting member forces and displacements.

4.3 Multimode Spectral Analysis

The guidelines given in Section 5.4 of the AASHTO 1990a are also appropriate for the response spectrum analysis of an isolated structure with the following modifications.

a. The isolation bearings are modelled by use of their effective stiffness properties determined at the design displacement D (in Figure 1, D = Δm).
b. The ground response spectrum is modified to incorporate the damping of the isolation system (Figure 2).

The response spectrum required for the analysis needs to be modified to incorporate the higher damping inherent in the isolation system. However this modified response spectrum should only be used for the isolated modes of the bridge and not for the higher modes which do not involve isolator deformations. The spectrum will then have the form shown in Figure 2.

4.4 Time History Analysis

When a time history analysis is required for bridges on isolation systems which do not self center, it is necessary for the time histories to be frequency scaled so they closely match the appropriate ground response spectra for the site. In addition, the analytical model should incorporate the nonlinear deformational characteristics of the isolation system, explicitly.

5. DESIGN DISPLACEMENTS FOR SEISMIC AND OTHER LOADS

Adequate clearance shall be provided at the abutments and elsewhere, for the displacements resulting from the seismic isolation analysis in either of the two orthogonal directions.

The shear deflections in the isolators resulting from braking loads, wind loads and centrifugal forces will be a function of the force-deflection characteristics of the isolators. Adequate clearance at all expansion joints must be provided for these movements.

6. DESIGN FORCES FOR SEISMIC PERFORMANCE CATEGORY A

The AASHTO Standard Specification (AASHTO 1990a) for conventional design has only two requirements for SPC-A. All bearing and column connections are required to be designed for 0.2 times the dead load and minimum support length requirements need to be met. In the isolation design requirements, the isolation bearing connections are required to be designed for

$$F = K_{eff} D$$

where

K_{eff} = Effective linear stiffness of the isolation bearing
D = Displacement of the isolated superstructure using a minimum acceleration coefficient, A, of 0.10.

This permits utilization of the real elastic force reduction provided by seismic isolation and will generally result in a lower connection design force than conventional design. It should be noted that the Acceleration Coefficient for SPC A bridges is specified to have a minimum value of 0.10 if seismic isolation is used. This conservatism will ensure, for most bridges designated as SPC A, that the isolation bearings are capable of resisting force levels associated with twice the design earthquake (most areas within SPC A have Acceleration Coefficients of 0.05).

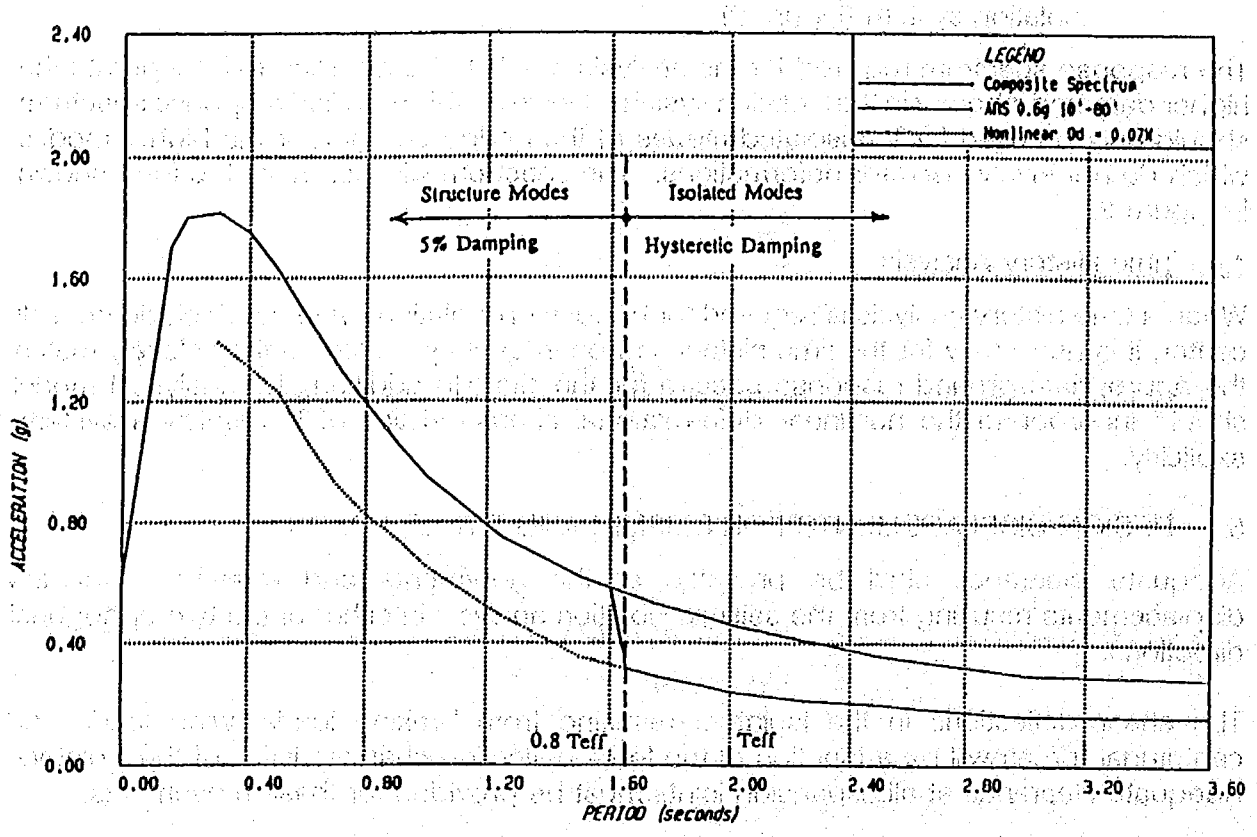

Figure 2. Example of a composite spectrum for use in a multimode analysis (ARS = 0.6g; 10-80 ft. alluvium; Caltrans Spectrum)

7. DESIGN FORCES FOR SPC B, C, AND D

Design forces for seismically isolated bridges in SPC B, C and D are obtained using the same load combinations as for a conventionally designed bridge. The two design philosophies discussed previously are incorporated in the determination of the design forces. The provisions permit the use of the same R-factors as conventional design with a lower limit on the forces being the yield level of the isolation system. This option permits a more economic design with the same performance level as conventional design. If a higher level of performance is desired it is recommended that an R-factor of 1.5 is used to ensure essentially elastic response. For bridges designated SPC B, foundation design forces are determined based on one-half the R value used for column design; they need not be greater than the elastic forces. This is consistent with the foundation design procedure for conventionally designed bridges. For bridges designated SPC C or D, the foundation design forces need not exceed the elastic forces nor the forces resulting from plastic hinging in the columns.

8. OTHER REQUIREMENTS

8.1 Non-Seismic Lateral Forces

Since an element of flexibility is an essential part of an isolation system, it is important that the bridge is not lively under more frequently occurring wind, braking and centrifugal loads. To control service load movements an elastic restraint system may be necessary which has a higher initial stiffness than the element of flexibility (see Figure 1). Limits on displacements resulting from non-seismic loads need to be satisfactory to the design engineer.

8.2 Lateral Restoring Force

The basic premise of the seismic isolation design provisions is that the energy dissipation of the system can be expressed in terms of equivalent viscous damping and the stiffness by an effective linear stiffness. The requirement of this section in the specifications provides the basis for which this criteria is met. Systems that do not meet this requirement are not excluded, provided more stringent analysis requirements and vertical load stability requirements are satisfied.

8.3 Vertical Load Stability

The isolation system shall provide a factor of safety of at least three (3) for vertical loads (dead load plus live load) in its laterally undeformed state. It shall also be designed to be stable under the dead load plus or minus any vertical load resulting from seismic effects at a horizontal displacement of 1.5 times the total design displacement for isolation systems with a lateral restoring force and at 3.0 times the design displacement if there is no lateral restoring force. The detailed design requirements of the system will be dependent on the type of system. The multipliers of 1.5 and 3.0 on the total design displacement are based on a design response spectra corresponding to a 475 year return period event. If a maximum credible response spectra is used for the design, these multipliers are reduced to 1.1 and 2.2 respectively. In some of the low seismic risk areas ($A<0.01$) of the United States a multiplier of 2.0 and 4.0 (instead of 1.5 and 3.0) may be more appropriate since

a longer return period event (2375 years) may be up to 2 times greater than the 475 year design event.

9. REQUIRED TESTS OF ISOLATION SYSTEM

The code requirements are predicated on the fact that the design is based on tested properties of prototype isolators. The testing section of the provisions requires that a comprehensive set of tests be carried out to establish the design properties of the system. Design properties must therefore be based on manufacturers' pre-approved or certified test data. Extrapolation of properties from tests of similar type and size of isolator units is permissible. Systems that have been previously tested to these requirements do not need to have these tests repeated.

10. ELASTOMERIC BEARING DESIGN REQUIREMENTS

Elastomeric bearings which are used for seismic isolation must be designed to carry the vertical loads while simultaneously deformed in shear to accommodate earthquake induced displacements. Since earthquakes are infrequently occurring events, the factors of safety required under these circumstances will be different from those required for more frequently occurring loads.

Since the primary design parameter for earthquake loading is the displacement of the bearing, the design procedures must be capable of incorporating this displacement in a logical consistent manner. The requirements of Section 14.2 of AASHTO 1990a determine the allowable vertical loads through a limiting compressive stress and therefore do not have a mechanism for including the simultaneous effects of seismic displacements. The British Specifications BE 1/76 and BS 5400 recognize that shear strains are induced in reinforced bearings by both compression and shear deformation. In these codes, the sum of these shear strains is limited to a proportion of the elongation-at-break of the rubber (e_u). The proportion (1/2 or 1/3 for service load combinations and 3/4 for seismic load combinations) is a function of the loading type.

Since the approach used in BE 1/76 and BS 5400 incorporates shear deformation as part of the criteria, it can be readily modified for seismic isolation bearings. Therefore the design requirements given in the isolation design guidelines are based on the appropriate sections of BE 1/76 and BS 5400.

The more conservative aspects of BE 1/76 and BS 5400 have been used. For example, BS 5400 requires the summation of compression, thermal and rotational shear strains and requires this to be less than 5.0. BE 1/76 requires the summation of only the compression and thermal shear strains and requires this to be less than $e_u/2$. The Isolation Guide Specification requires the summation of the 3 different shear strains (compression, thermal, rotation) with a limit of $e_u/2$ where $e_u/2$ may not exceed 5.0.

11. DESIGN ISSUES FOR ISOLATION SYSTEMS

The design parameters for any isolation system include the required isolation period, the base shear, the damping of the system and the required margins of safety for the system. There are many interrelated variables involved in such a design and to show how these

variables impact the design process the AASHTO isolation guidelines (AASHTO, 1990b) described above have been used in this section.

The displacement across the isolators (D), the elastic base shear (V) and the isolated period (T) have been derived previously and are given by the following:

$$D = \frac{10AST}{B} \qquad (7)$$

$$T = 2\pi \sqrt{\frac{W}{K \cdot g}} \qquad (11)$$

$$V = KD = \frac{AS}{TB} \cdot W \qquad (12, 13)$$

where

D	=	Isolator displacement, inches
A	=	Acceleration coefficient obtained from a seismic risk map
A_b	=	Bonded area of elastomer
S	=	Site coefficient (1.0 for Soil Type S_1, 1.5 for Soil Type S_2, 2.0 for S_3)
T	=	Isolated period, seconds based on effective stiffness properties
B	=	Damping coefficient (Table 1)
K	=	Isolator stiffness (GA_b/Tr for plain elastomeric isolators)
V	=	Elastic base shear, Kips
W	=	Structure weight, Kips
G	=	Shear modulus of elastomer, Kips/inch
Tr	=	Total thickness of elastomer, inches

The important design variables are affected by the isolation system properties as follows:

Displacement: The isolator displacement is given by equation 7 and it is seen that the two properties that impact isolator displacements, D, are the isolated period T and damping coefficient B. D increases as the isolation period T increases and decreases as the damping coefficient B increases.

Base Shear: The base shear, V, is given by equation 11 and is inversely proportional to the isolation system period T and damping coefficient B. That is, V decreases as both the isolation period T and damping coefficient B increase.

Design of Isolators: The design of an elastomeric isolation system is such that the isolation system period is proportional to the total rubber height (Tr) and inversely proportional to the bonded area (A_b) of the isolator and the elastomer shear modulus (G). Thus the isolated period increases as the total rubber height increases, the plan size decreases and the shear modulus decreases.

Isolator Safety Margins: The margin of safety of an elastomeric isolation system is a function of the plan size, vertical load, the total rubber height, the internal layer thickness and the isolator displacement. The safety margin increases with increased plan size, lower total rubber height, lower vertical load and lower displacement.

12. APPLICATIONS TO U.S. BRIDGES

Tables 1 and 2 list bridges in the United States which have been seismically retrofitted using isolation. Table 1 gives the geometrical details of each bridge and Table 2 gives the details of the isolation hardware used for each bridge. Descriptions of these structures have been previously given by Buckle et al (1987b, 1988, 1990b).

In addition to the nine bridges in Tables 1 and 2 the following new bridges have either recently been completed or are under construction:

Name	Owners
Sexton Creek Bridge	Illinois Department of Transportation
Toll Plaza Road Bridge	Pennsylvania Turnpike Commission
Wabash River bridge (US 40)	Illinois Department of Transportation
Pequannock River Bridge	New Jersey Department of Transportation
St. Louis Light Rail System (several bridges)	Bi-state Development Agency

In all cases the isolation system used is based on lead-filled elastomeric bearings.

13. SUMMARY

Several practical seismic isolation systems have been developed and implemented in recent years as interest in the application of this technique continues to grow. Although seismic isolation offers significant benefits, it is by no means a panacea. Feasibility studies are required early in the design phase of a project to evaluate both the technical and economic issues. If seismic isolation is appropriate from a technical and first-cost perspective, then significant life-cycle cost advantages can be achieved. Thus, seismic isolation represents an important step forward in the continuing search for improved earthquake safety.

Seismic isolation offers particular advantages to bridge structures. Reductions in earthquake loads can be significant and savings can be achieved in the foundations of new designs along with improved seismic performance (elastic response). Isolation also offers an elegant solution to many of the common retrofit problems encountered in existing bridges. Limited experience to date has shown that isolation can be adapted and implemented to meet a wide variety of different site and bridge conditions. The adoption of the seismic isolation guidelines discussed herein should accelerate the implementation of this new technology which in turn will lead to further improvements in the state-of-the-art.

TABLE 1. BRIDGES IN THE UNITED STATES WHICH USE SEISMIC ISOLATION

BRIDGES	GEOMETRY	OWNER	YEAR BUILT	YEAR RETROFIT CONSTRUCTION	DESIGN ENGINEERS	REMARKS
Sierra Point Overhead	S = 616 ft 10 spans 60 skew	Caltrans	1957	1984/5	Caltrans/DIS	Carries US 101 over local access roads and rail tracks, South San Francisco
Santa Ana River	S = 1010 ft 13 spans	Metropolitan Water District of Southern California	1936-8	1986/7	Lindvall Richter & Associates/DIS	Carries 116" diameter steel pipeline for water supply to City of Los Angles, 3 river spans each a 180 ft steel truss.
Eel River	S = 606 ft 2 spans	Caltrans	1940-1	1987	Caltrans/DIS	Carries US 101 over Eel River near Rio Dell. 2 river spans each a 300 ft steel truss.
Main Yard and Shops Access	S = 256 ft 2 spans 58 skew	Los Angeles County Transportation Commission	1952-4	1987	Southern California Rail/Consultants/ Wei Te Koo/ DIS	Conversion of existing rail bridge for vehicle access across Long Beach Freeway; Long Beach-Los Angeles Rail Transit Project.
All American Canal	S = 410 ft 3 spans	Caltrans	1960	1988	Caltrans/DIS	Carries Route 8 over All American Canal, Imperial County. New superstructure on existing concrete pedestals.
Sexton Creek	S = 294 ft 3 spans	Illinois Department of Transportation		1988	Illinois DOT/DIS	Carries Illinois Route 3 over Sexton Creek, Alexander County.
Lacey V. Murrow Bridge	S = 1128 ft 8 spans	Washington State Dept. of Transportation	1940	1990	Arvid Grant & Associates/DIS	Original floating bridge across Lake Washington being upgraded to serve as east bound lanes of I-90. Retrofitted west approach spans and tied arch span of east approach.
Deas Slough Bridge	S = 318 ft 3 spans 38° skew	British Columbia Ministry of Transportation	1958	1990	Phillips Barratt Kaiser Engineering Ltd./DIS	Carries Highway 99 across Deas Slough south of Vancouver, BC.
Cache River Bridge	S = 281 ft 3 spans 21° skew	Illinois Department of Transportation	1946	1990	Illinois Department of Transportation/ DIS	Carries Route 3 over Cache River Diversion Channel in Southern Illinois (Alexander County).

NOTES:

1. S = Total isolated bridge length
2. Caltrans = California Department of Transportation
3. DIS = Dynamic Isolation Systems, Inc.

TABLE 2: ISOLATOR DETAILS AND SEISMIC PERFORMANCE FOR BRIDGES IN THE UNITED STATES

BRIDGE	Isolators			Equivalent Design Spectrum	Effective Period (Seconds)	"Base" Shear	Max. Isolator Displacement (inches)
	No.	Size	Lead Core Dia.				
Sierra Point Overhead	3 13 4 4 5 7	18x18x8 7/8 18x18x8 7/8 18x18x8 7/8 18x18x8 7/8 22dia.x8 7/8 22dia.x9 7/8	0 3 6 3 4 4	Caltrans 0.6g S-I	1.79	0.20W	6.97
Santa Ana River	2 14 4 8	12x12x9 1/8 14x14x10 5/8 20x20x10 1/4 18x18x11 1/2	4 1/2 4 3/4 7 6 1/2	ATC 0.4g S2	1.40	0.20W	3.85
Eel River	8 2 2	22x22x13 1/4 30x30x13 1/4 30x30x18 1/2	5 7 1/2 7 1/2	Caltrans 0.5g S-IV	1.86	0.30W	10.14
Main Yard and Shops Access	4 4	21x21x16 7/8 21x21x16 7/8	3 4 3/4	Caltrans 0.5g S-II	2.44	0.17W	9.95
All American Canal	6 6	19x19x15 1/2 30x30x20 3/4	5 8	Caltrans 0.6g S-IV	2.04	0.32W	12.88
Sexton Creek	10 10	13x13x8 3/8 18x18x8 3/8	4 1/4 0	AASHTO Guide Spec 0.2g, S3	1.48	0.13W	2.80
Lacey V. Murrow Bridge	6 2 4 4 4 8	12x12x7.1 17x17x7.1 19x19x7.1 24x24x7.1 24x24x7.1 24x24x7.1	2 5 5 6 1/4 7 7 1/2	AASHTO Guide Spec A = 0.25 Soil Type I	1.36	0.12W	2.17
Deas Slough Bridge	20 20	10x10x5-1/8 12x17-3/4x 5-1/8	2 1/2 2-3/4	AASHTO Guide Spec A = 0.20 Spll Type II	1.06	0.15W	1.68
Cache River Bridge	10 10	13x13x10.8	3-3/4 0	AASHTO Guide Spec A = 0.2 Soil Type III	1.28	0.15W	2.43

NOTES:

1. Dimensions, in inches, are width x length x height except for circular bearings, as noted.
2. All above isolators used lead cores for hysteretic damping. Diameter of lead core is given in inches.
3. "Base" shear is expressed as a fraction of superstructure weight.

14. ACKNOWLEDGEMENTS

The assistance of Dr. Ronald L. Mayes (President, Dynamic Isolation Systems, Berkeley, California) with the preparation of this paper is gratefully acknowledged. Dr. Mayes was a major contributor to the code provisions described in this paper. The data on new applications of seismic isolation was kindly supplied by Richard Knight of Dynamic Isolation Systems.

REFERENCES

AASHTO (1990a), "Standard Specifications for Highway Bridges", American Association for State Highway and Transportation Officials (AASHTO), 15th Edition, 1989 and Interim Specifications 1990, 1991.

AASHTO (1990b) "Guide Specifications for the Seismic Isolation - Design of Highway Bridges" American Association of State Highway and Transportation Officials, 1990.

AASHTO (1983), "Guide Specifications for Seismic Design of Highway Bridges," American Association of State Highway and Transportation Officials (AASHTO), 1983.

ASCE (1989), "Seismic Engineering: Research and Practice", Proceedings ASCE Structures Congress, May 1989.

APPLIED TECHNOLOGY COUNCIL (1981), "Seismic Design Guidelines for Highway Bridges", Report No. ATC-6, Applied Technology Council, 1981. Also published by Federal Highway Administration as Report FHWA/RD-81-081, 1981.

APPLIED TECHNOLOGY COUNCIL (1986), "Proceedings of a Seminar and Workshop on Base Isolation and Passive Energy Dissipation", ATC Report No. 17, Palo Alto, CA 1986.

BLAKELEY, R.W.G. et al, (1979), "Recommendations for the Design and Construction of Base Isolated Structures" Bulletin of New Zealand National Society for Earthquake Engineering, Vol. 12, No. 2.

BLAKELEY, R.W.G., (1979), "Analysis and Design of a Bridge Incorporating Mechanical Energy Dissipating Devices for Earthquake Resistance", Proceedings of a Workshop on Earthquake Resistance of Highway Bridges, Applied Technology Council, Report No. ATC-6-1, January 1979, pp 313-342.

BILLINGS, I.J. AND KIRKCALDIE, D.K. (1985), "Base Isolation of Bridges in New Zealand" Proceedings US-NZ Workshop on Seismic Resistance of Highway Bridges, Report No. 12-1, Applied Technology Council, May 1985.

BUCKLE, I.G., (1986), "Development and Applications of Base Isolation and Passive Energy Dissipation: A World Overview", Proceedings of a Workshop on Base Isolation and Passive Energy Dissipation, Report No. ATC-17, Applied Technology Council, Palo Alto, CA.

BUCKLE, I.G., MAYES, R.L., AND BUTTON, M.R.(1986), "Seismic Design and Retrofit Manual for Highway Bridges", Computech Engineering Services, Berkeley, CA Also Published by Federal Highway Administration as Report FHWA/RD-86/006, 1987.

BUCKLE, I.G., AND MAYES, R.L. (1987a), "Seismic Isolation of Bridge Structures in the United States of America", Proc. Third U.S.-Japan Workshop on Bridge Engineering, Public Works Research Institute, Ministry of Construction, Tsukuba, Japan, 1987, pp 379-401.

BUCKLE, I.G., AND MAYES, R.L. (1987b), "Seismic Isolation of Bridge Structures in the United States of America," Proc. Third US-Japan Workshop on Bridge Engineering, Public Works Research Institute, Ministry of Construction, Tsukuba, Japan, pp. 379-401.

BUCKLE, I.G., (1988), "Some Innovations in the Seismic Isolation of Bridges," Proc. Fourth US-Japan Workshop on Bridge Engineering Performance, Strengthening and Innovation, San Diego, 1988.

BUCKLE, I.G. AND MAYES, R.L. (1989), "The Application of Seismic Isolation to Bridges", Proceedings ASCE Structures Congress: Seismic Engineering - Research and Practice, May, 1990, pp 633-642.

BUCKLE, I.G. AND MAYES, R.L. (1990a), "Seismic Isolation: History, Application and Performance - A world View", Earthquake Spectra, EERI Vol. 6, No. 2, May 1990.

BUCKLE, I.G. (1990b), "Recent Progress in Base Isolation for Bridges in the United States" Proc. Sixth US-Japan Workshop on Bridge Engineering, Lake Tahoe, Nevada, 1990.

CALTRANS (1973), "Standard Specifications for Highway Bridges Relating to Seismic Design", California Department of Transportation, Division of Structures, 1977.

EARTHQUAKE ENGINEERING RESEARCH INSTITUTE (1990), "Seismic Isolation: From Idea to Reality", Earthquake Spectra Journal, Vol. 6, No. 2, May 1990.

KELLY, J.M. (1986), "Seismic Base Isolation: Review and Bibliography", Soil Dynamic and Earthquake Engineering, Vol. 5, 1986, pp 202-216.

MAYES, R.L., JONES, L.R., AND BUCKLE, I.G. (1990), "Impediments to the Implementation of Seismic Isolation", Earthquake Spectra Journal, Theme Issue: Seismic Isolation, EERI, May 1990.

EVALUATION OF LATERAL INERTIA FORCE OF BRIDGES FOR SEISMIC DESIGN

By Kazuhiko KAWASHIMA[1] and Kinji HASEGAWA[2]

1: Head, Earthquake Engineering Division,
Public Works Research Institute,
Ministry of Construction, Japan
2: Senior Research Engineer, ditto

In the current design practice, for determining a lateral force due to an inertia force developed in a superstructure, which is used for seismic design of substructures, a bridge is generally divided into sub-structures consisting of a substructure and a part of superstructure supported by the substructure. The lateral force considered in seismic design of a substructure in transverse direction is generally computed by multiplying a seismic coefficient with a reaction force developed at the relevant substructure. However as various types of bridge become to be constructed, it became apparent that the lateral force computed by the traditional method is not always adequate. The lateral force at each substructure significantly depends on flexibility of the substructures. This paper proposes a method to evaluate a lateral force of a superstructure for seismic design of substructures based on a static and simple calculations. Validity of the proposed method is also presented through numerical calculations. Application of the method in combination with the traditional method in view of consistency and continuity of the design method is proposed.

1. INTRODUCTION

Because dimensions of bridge substructures are determined in most cases from a requirement of seismic effects, evaluation of a lateral force which is used for seismic design of substructures is of great importance. Seismic design method of highway bridges was firstly introduced in a form of clear stipulations in "Design Specifications of Steel Highway Bridges" issued in 1956 by the Japan Road Association. It was stipulated in the specifications that the lateral force considered in seismic design of a substructure in transverse direction shall be computed by multiplying a seismic coefficient with a reaction force developed at the relevant substructure. This method has been widely adopted for seismic design of highway bridges in Japan.

However as various types of bridge structures become to be constructed, it became apparent that the lateral force computed by the method specified in the specifications is not always adequate[1]. The lateral force at each substructure significantly depends on flexibility and height of the substructures. Therefore, more rational and comprehensive method which can be used to evaluate an inertia force induced in a superstructure for the purpose of seismic design of substructures is required. The same demand also arises in those bridges where a superstructure and substructures are not separated by means of bearing supports. In such bridges, direct application of the stipulations are quite difficult.

This paper proposes a method to evaluate a lateral force of a superstructure for seismic design of substructures based on a static and simple calculation, and also shows its validity through numerical calculations. Application of the method in combination with the traditional

method in view of consistency of the design method is also presented.

2 COMPUTATION OF LATERAL FORCE

For determining a lateral force due to an inertia force developed in a superstructure, which is used for seismic design of substructures, a bridge is generally idealized as shown in Fig. 1. In longitudinal direction, a bridge is generally supported by fixed bearings at least at one support with the others being supported by movable bearings. This is simply to avoid an excessive stress induced in a deck due to variation of temperature.

A lateral force in longitudinal direction at fixed supports is given as[2)]

$$F_d = k_h \times W \qquad (1)$$

in which, F_d : lateral force associated with an inertia force of a superstructure for seismic design of substructures in longitudinal direction, k_h : seismic coefficient, and W : dead weight of a superstructure. An effect of friction force developed due to relative movement of a deck at movable bearings is generally disregarded for evaluating Eq.(1). The friction force is applied to relevant substructures as an external force transferred from the superstructure to the substructures as shown in Fig. 1(a).

A lateral force in transverse direction is more complicated. Because both fixed and movable bearings do not allow relative movement between a deck and substructures in transverse direction, the bridge has to be analyzed as a whole structure to compute lateral forces for use of seismic design of individual substructures. However because this makes the calculation complicated, a bridge is generally divided into several structural segments as shown in Fig. 1(b), which consist of a substructure and a part of superstructure supported by the substructure. Then, a lateral force used for seismic design of a substructure in an i-th structural segment is assumed as

$$F_{di} = k_{hi} \times R_i \qquad (2)$$

in which F_{di} : lateral force associated with an inertia force induced in a superstructure in transverse direction for seismic design of i-th substructure, k_{hi} : seismic coefficient for i-th substructure, and R_i : reaction force developed at i-th substructure due to dead weight of a part of substructure supported by the i-th substructure.

This traditional method, which is referred hereinafter as a reaction force method, assumes that stiffness of a deck is zero. If this assumption is valid, a structural segment can then be taken out for analysis from the bridge without any interaction with remaining parts. Such assumption may only be applied to those bridges which are supported by extremely stiff substructures as compared with the stiffness of the superstructure. Lateral forces are not generally proportional with reaction forces. They vary depending on stiffness of a superstructure and substructures depending on support conditions.

As various types of bridges become to be adopted, more comprehensive and accurate method became required. This requirement is significant for computing a lateral force in transverse direction for a bridge supported with piers with various height. Furthermore, the requirement also arises in bridges which are rigidly or elastically supported by several substructures. In such bridges, the lateral forces in longitudinal direction depend on stiffness of the substructures. For those bridges where a

superstructure is not separated from substructures with use of bearings, lateral force has to be carefully calculated considering whole response of the bridge.

On the other hand from a view point of structural analysis, an effort required for analysis in recent years becomes much less with use of mini- and personal-computers as well as wide spread of software for structural analysis, and it became possible to analyze a whole bridge with various structural and boundary conditions. Therefore, taking the advance of structural analysis into account, it is require to develop a new method which can be used for analyzing bridges for seismic design purpose. This method should be simple and accurate enough to be adopted widely for practical design. Considering that dynamic response analysis is regarded by design engineers as " a special analysis " which is far from the practical design, the method is expected to be based on static calculations avoiding an eigen value analysis.

Based on such requirements, a simple static analysis method, which is referred hereinafter as a static frame method, is proposed for practical and engineering estimation of lateral force for seismic design of bridges.

3 STATIC FRAME METHOD

Because mass distribution of a bridge concentrates at its deck, bridges response in a way of an inverted pendulum. Because first mode is generally predominant in total response, a peak response displacement of the bridge can be approximated as

$$u^{max} \fallingdotseq u_1^{max} = \beta_1 \cdot S_D(T_1, h_1) \cdot \phi_1 \qquad (3)$$

in which, u^{max}: peak response displacement when all modes are considered, u_1^{max} : peak response displacement of first mode, β_1 : mode participation factor for first mode, $S_D(T_1, h_1)$: displacement response spectrum for a natural period T_1 and a damping ratio h_1, and ϕ_1 : first natural mode.

Natural period of bridges can be approximately computed by the Rayleigh method[3]. A first mode shape is generally approximated with a static deformation shape when it is subjected to a static distributed load equivalent with a dead weight. Denoting a displacement of a bridge subjected to a dead weight as $u_d(s)$ at point s, response displacement of the bridge $u(s)$ may be approximated with use of the static displacement $u_d(s)$ as

$$u(s) = u_d(s)\sin(\omega_d t) \qquad (4)$$

in which ω_d represents an angular frequency of the bridge when the static displacement $u_d(s)$ is assumed. It is assumed hereinafter that $u_d(s)$ is non-dimensional.

Assuming the bridge as a one degree of freedom system, the maximum kinetic energy K_{max} of the bridge may be written as

$$K_{max} = (1/2)\omega_d^2 \int_s M(s)\, u_d(s)^2 ds \qquad (5)$$

in which $M(s)$ represents mass at the point s.

On the other hand, the maximum strain energy U_{max} may be written as

$$U_{max} = (1/2) \int_s M(s)\, u_d(s)\, g\, ds \qquad (6)$$

in which g represents an acceleration of gravity.

Because K_{max} and U_{max} should be equal, one obtains from Eqs.(5) and (6)

$$\omega_d^2 \int_s M(s) u_d(s)^2 ds = \int_s M(s) u_d(s) g ds \qquad (7)$$

From Eq.(7), natural period can be obtained as

$$T_d = 2\pi/\omega_d = 2\pi\sqrt{\frac{\int_a M(s)\,u_d(s)^2 ds}{\int_a M(s)\,u_d(s)\,g\,ds}} \quad (8)$$

Defining a coefficient δ as

$$\delta = \frac{\int_a M(s)\,u_d(s)^2 ds}{\int_a M(s)\,u_d(s) ds} \quad (9)$$

, the natural period can be approximated as

$$T_d = 2.01\sqrt{\delta} \quad (10)$$

Eq.(10) may be much better than Eq.(8) because it is the same type of equation which has been used in practical design since the Part V Seismic Design of the Design Specifications of Highway Bridges[2] issued in 1980. Because in design calculation, weight is much more frequently referred to than mass, substituting the weight in stead of the mass, Eq.(9) can be rewritten as

$$\delta = \frac{\int_a W(s)\,u_d(s)^2 ds}{\int_a W(s)\,u_d(s) ds} \quad (11)$$

in which $W(s)$ represents distributed dead weight at point s.

Once first natural period of the bridge can be determined, a seismic coefficient k_h may be assigned. Then, it is required to determine the lateral force transferred from the superstructure to the substructures. When computing the static displacement $u_d(s)$ of the bridge subjected to the dead weight in lateral direction, one can simultaneously compute force $F(s)$ induced at point (section) s in the bridge. Because $F(s)$ represents the force induced in the bridge when it is subjected to the lateral force equivalent with the gravity force in lateral direction, the force induced in the bridge when subjected to the lateral force equivalent with the seismic coefficient k_h can be computed as

$$F_d(s) = F(s) \times k_h \quad (12)$$

It should be noted here that $F_d(s)$ can be treated as either an internal force or an external force. When $F_d(s)$ is considered as an internal force, it represents a sectional force developed at point (section) s as a result of the inertia force. On the other hand, when $F_d(s)$ is considered as an external force, it represents an inertia force to be applied at a section s. Therefore considering consistency with the current design practice, it is appropriate to regard $F_d(s)$ as:

1) For girder bridges, a horizontal force $F_d(s)$ at a gravity center of a superstructure shall be regarded as a lateral force H which represents an inertia force of the superstructure transmitted to the substructure. The lateral force H shall be applied to the substructure as an external force at the gravity center of the superstructure.
2) For those bridges for which a superstructure and substructures are not separated such as an arch bridge, the force $F_d(s)$ given by Eq.(12) shall be used as a sectional force induced in the bridge as a result of the inertia force.

In the static frame method, a bridge can be analyzed as a whole

structure instead of dividing it into several sub-structures consisting of a substructure and a part of superstructure supported by the substructure. However, structural units considered in the analysis should be as simple as possible for seismic design purpose because it makes the calculation simple and easy to check the result. For such purpose, a design structural unit is defined here to identify a structural unit which has to be analyzed as a whole structure.

The design structural unit is proposed to be selected as shown in Table 1. For those bridges in which a superstructure and substructures are not separated by bearing supports, both the superstructure and the substructures shall be considered as the same design structural unit. In girder bridges, the design structural unit has to be changed depending on the direction considered in design.

In longitudinal direction, when a superstructure is supported with fixed bearings by substructure(s) in the direction considered in design, both the superstructure and the substructure(s) shall be included in the same design structural unit. Substructure(s) supporting a superstructure with movable bearings in the direction considered in design may be considered as independent design structural unit(s), because an inertia force exceeding a friction force is not transmitted from the superstructure to the substructures. The friction force developed due to movement of the superstructure relative to the substructures at the movable bearings shall be considered as an external force in that direction for the substructures. It should be noted that even if a superstructure is supported with movable bearings by substructures, the superstructure and the substructures shall be included in the same design structural unit in the direction for which relative movement is not developed at the movable bearings.

In transverse direction, a superstructure and substructures shall be included in the same structural unit. However, because the reaction force method gives a reasonable approximation when the superstructure is supported by the substructures with almost equal stiffness, the substructure and a part of the superstructure supported by the substructure may be considered as the design structural unit.

As a summary, in the static frame method, natural period and the lateral force/sectional force is proposed to evaluate as (refer to Fig. 2)

i) idealize a design structural unit by a linear elastic frame model

ii) apply a distributed lateral force equivalent with dead weight of the superstructure and the substructure in a horizontal direction considered in seismic design, and compute a static displacement $u_d(s)$ and a sectional force $F(s)$.

iii) compute natural period T by Eq.(10).

iv) determine a seismic coefficient k_h depending on the natural period T.

v) compute either an inertia force or sectional force by Eq.(12)

The static frame method assumes that it considers only first mode; it uses a static deformation of a bridge subjected to a dead weight instead of first mode shape; it computes first natural period by the Rayleigh method. Although the static frame method gives more realistic results than the reaction force method, it gives an only approximate result. When the above-described assumptions can not be adopted, structural response has to be computed by a dynamic response analysis.

Finally it should be noted that although the computation process is

different, the static frame method gives the same inertia force/sectional force with a method in which a bridge is directly subjected to a lateral force equivalent with the dead weight multiplied with a seismic coefficient. Even by now when a bridge is complicated, this method has been often used. From such point of view, the static frame method is not necessarily a new method but only one of traditional methods which includes a sub-process to compute a natural period.

4 ACCURACY OF STATIC FRAME METHOD IN COMPARISON WITH DYNAMIC RESPONSE ANALYSIS

For evaluating validity of the static frame method, a comparative study of the static frame method with dynamic response analysis was made for the same highway bridges against the same input ground motions. Analyzed were 36 bridges with varying various conditions as

i) topographical condition
bridges crossing a valley, bridges crossing a river, and overcrossings in urban area

ii) type of superstructure
material(steel and prestressed concrete), shape of cross section (girder bridge and box), number of span, and span length

iii) pier type
wall type piers, single columns, frame piers, steel piers, and flexible piers

iv) pier height

v) type of foundation
spread foundations, caisson foundations and pile foundations

vi) soil condition
ground group I, II and III specified in the Part V Seismic Design of the Design Specifications of Highway Bridges[4]

Analysis was made for bridge responses in transverse direction, because this is a major concern for evaluating an application of the static frame method. Strong motion records measured on ground surface near the Kaihoku Bridge during the 1978 Miyagi-ken-oki Earthquake with an earthquake magnitude of 7.4 and on ground surface near the Tsugaru Bridge during the 1983 Nihon-kai-chubu Earthquake with an earthquake magnitude of 7.7 were used for time history analysis. In the static frame method, a seismic coefficient determined as

$$k_h = S_A(T_1, h_1) / g \qquad (13)$$

was used so that the same input ground motion with the dynamic response analysis be assumed, in which T_1 : first natural period computed by Eq.(10), $S_A(T_1, h_1)$: response acceleration of the input record with the natural period T_1 and damping ratio h_1. Damping ratio was assumed as 5 % for both the dynamic response analysis and the static frame method.

Although the analysis was made for the 36 bridges, results are presented with emphasis on analysis for two bridges as shown in Fig. 3. A-Bridge represents a 3 span continuous steel girder bridge with an equal span length of 30 m over a river. Both ends are supported by abutments. B-Bridge has the same superstructure, but is an overcrossing in urban area. The superstructure is supported by four piers with almost the same stiffness.

Fig. 4 compares the static displacement $u_d(s)$ with exact first mode $\phi_1(s)$. Although $\phi_1(s)$ shows larger deformation of the deck between the

two abutments than $u_d(s)$ in the A-Bridge, overall mode shape $\phi_1(s)$ is well approximated by $u_d(s)$. The eigen value analysis predicts first natural period of 0.41 second for the A-Bridge and 0.3 second for the B-Bridge while the static frame method predicts 0.40 second for the A-Bridge and 0.29 second for the B-Bridge. It is said that the predicted natural period by the static frame method gives a fairly good approximation to the exact natural period. For reference, when the natural period is computed in the reaction force method, it takes a value of 0.21 second for the substructure including the P1 abutment, 0.49 second for the substructure including the P1 pier and for the substructure including the P2 pier, and 0.28 second for the substructure including the A2 abutment. It is apparent that the natural period is considerably underestimated for the two abutments and overestimated for the two piers.

Fig. 5 shows a distribution of the maximum bending moment and shear force when the bridges are subjected to the Kaihoku Record. As well as the results by the static frame method and the dynamic response analysis, results by the reaction force method are also presented in Fig. 5 for comparison. The static frame method gives a realistic approximation for both bridges. This clearly means that the assumptions of the static frame method presented in the preceding chapter are reasonably adopted for engineering analysis of the two bridges.

It is interesting to note here that how the forces predicted by the reaction force method differs with the results predicted by the dynamic response analysis. In the A-Bridge, the reaction force method gives a fairly close result with the dynamic response analysis. However in the B-Bridge, the reaction force method gives considerable underestimation for the sectional force at A1, A2 and P1. This is due to the fact that stiffness of A1, A2 and P1 is significantly larger than the stiffness of P2.

Fig. 6 shows a comparison of natural periods predicted by the static frame method and the eigen value analysis for the 36 bridges. Natural periods predicted by the reaction force method are also presented for comparison. The natural periods predicted by the static frame method give reasonably good approximation to the natural period predicted by the eigen value analysis.

Fig. 7 shows comparisons of the maximum bending moment developed at bottom of the P1 and P2 piers between the static frame method and the dynamic response analysis for the 36 bridges. Results predicted by the reaction force method are also presented for comparison. The static frame method gives a reasonably close agreement for engineering design purpose with the dynamic response analysis. On the other hand, scatter of the bending moment predicted by the reaction force method is considerable.

5 APPLICATION OF STATIC FRAME METHOD FOR EVALUATION OF LATERAL FORCE OF BRIDGES

Although it is apparent that the static frame method gives more rational lateral force for design of substructures, application of the method has to be carefully examined because direct application of the method would result in considerable difference with the current practice in design. To examine the difference in design of substructures by introducing the static frame method, distribution of lateral forces for each substructure was studied for 3 bridges, as shown in Fig. 8. The three bridges have the same superstructures consisting of steel girders with a span length of 30 m.

Difference between the three bridges is only substructure condition, i.e., No.1-Bridge is an overcrossing in urban area with almost the same pier height. No.2-Bridge is a typical 3 span continuous bridge crossing a river. No.3-Bridge is a typical bridge crossing a valley, and has piers with different height. The No.2 and the No.3 Bridges have abutments at both ends.

To compare the three bridges on the same basis, transverse responses of the bridges were computed assuming a seismic coefficient of 0.2 with regardless of natural periods. Dependence of seismic coefficient on the natural periods was disregarded here because the natural period of the three bridges are in the range where the design seismic coefficient takes the same value based on the Part V Seismic Design of the Design Specifications of Highway Bridges[4].

Table 2 shows a comparison of lateral forces (shear forces) which are to be used as inertia forces from the superstructure to the substructures. Because the reaction force method has been widely used by now for seismic design, a special attention was paid how an adoption of the static frame method gives different distributions of lateral forces in design as compared with the reaction force method. Based on Table 2, characteristics of the static frame method in comparison with the reaction force method may be summarized as

1) In the No.1-Bridge, the lateral force predicted by the static framemethod is almost the same with that predicted by the reaction forcemethod. Based on classical elastic theory, reaction force of 3 span continuous beam with an equal span length subjected to uniformly distributed load is 1.0 at both end supports and 2.75 at the two intermediate supports. The lateral force predicted by the reaction force method is, of course, proportional to such reaction force. Because the stiffness of the four piers is almost the same, the static frame method gives a close distribution of the lateral force with the reaction force method.
2) In the No.2-Bridge, the reaction force method predicts the same lateral force distribution with the No.1-Bridge because the superstructure is of the same. On the other hand, the static frame method gives a larger lateral force than the reaction force method by a factor of 2 at the both abutments, and gives almost 40 % lateral force at the two piers. This is simply due to the fact that the stiffness of the abutments are considerably higher than that of the piers.
3) Because in the No.3-Bridge there is a difference in the stiffness between the two piers in addition to the difference of the stiffness between the abutments and the piers, lateral forces predicted by the static frame method are much different with those of the reaction force method. Particular interest is a very small lateral force developed at P2, where the lateral force predicted by the static frame method is only 13 % of the value computed by the reaction force method.

It is apparent from such comparisons that by adopting the static frame method, lateral forces developed at stiff substructure are likely to increase as compared with the current design method, and vice versa for substructures with low stiffness.

Although it is no doubt that the static frame method gives more rational and realistic lateral force than the reaction force method,

considerable changes of the lateral force distribution have to be carefully examined from view point of consistency and continuity of design. When a design of the substructures is made based on the lateral force predicted by the static frame method for the No.2 and No.3-Bridges, sectional dimensions of the piers in transverse direction may be considerably reduced as compared with the current design. Because dimensions of the abutment are selected so that they support an earth pressure of back soils, abutments have generally much redundancy for their bearing capacity in transverse direction. Therefore it is not required to increase the size of the abutments.

Therefore, major change associated with the adoption of the static frame method into the current design practice is that smaller dimensions can be adopted for piers in transverse direction, although an increase of dimensions is required for some piers which have higher stiffness than others. If this is adopted, piers become more flexible, as a whole, than the current design practice. Before adopting the static frame method, the following items have to be considered:

1) Because bridge design is made based on the allowable stress design approach, careful attention has to be paid on what would happen on bridge behavior as a total after parts of the bridge, such as bearing supports and foundations, suffer damage when subjected to larger ground motion than considered as a form of a seismic coefficient. It should be noted that damage of bearing supports occurred as a matter of fact in the past large earthquakes. It is still very difficult to predict bridge response during destructive earthquakes even with sophisticated nonlinear dynamic response analyses.
2) Associated deeply with the reaction force method, it has been the Japanese practice to construct stiff piers, which, in turn, makes seismic force induced in a superstructure limited. Therefore it is very special that the sectional dimensions of the superstructure be determined due to seismic effects. Intention has been paid to construct strong substructures against destructive earthquakes. It should be emphasized that seismic experiences gained in the past are for such bridges. Therefore, sudden decrease of the lateral force for seismic design of piers should be avoided, because it would cause different type of seismic damages never experienced in the past.
3) As is the case of the No.3-Bridge, the lateral force at the flexible pier becomes considerably small. Depending on stiffness of the substructures, the lateral force developed at the flexible pier may take even negative value, which means that the pier can not support even its inertia force but transmits its inertia force to other substructures through the deck.

Based on such considerations, a highly engineering judgement for the minimum lateral force in seismic design seems inevitably important. Therefore it is proposed to use the static frame method as

1) For those bridges with small difference of stiffness between piers, such as the No.1 and No.2-Bridges in Fig. 9, lateral forces shall be computed by the reaction force method.
2) For those bridges with considerable difference of stiffness between piers, such as the No.3-Bridge in Fig. 9, lateral forces shall be computed by the static frame method. However, in girder bridges the lateral forces shall not be smaller that the values computed by the

reaction force method.

It should be noted here that the minimum lateral force was included based on an engineering judgement considering experiences on bridge seismic design and on seismic damages in the past, and consistency and continuity with the current design practice.

6 CONCLUDING REMARKS

The preceding pages presented a new seismic design method referred herein as a static frame method for computing lateral forces, and applications of the method. Because the static frame method considers stiffness of deck, it gives more realistic distribution of lateral force than the reaction force method. Because in the reaction force method, reaction forces are only requirements for design of substructures, it was likely that the design of substructures was made without considering total safety of bridge structures. By adopting the static frame method, it is hoped that attention is given to how bridges behave during destructive earthquakes.

The static frame method was adopted in the Part V Seismic Design of the Design Specifications of Highway Bridges[4] issued from the Japan Road Association in February 1990.

ACKNOWLEDGEMENT

For developing the static frame method presented in this paper, various suggestions were made in the Bridge Committee of the Japan Road Association. Special thanks are to Mrs. Yasuo Tada, Tatuo Asama, Syouichi Saeki, Kaname Yahagi, and Yoshiyuki Enami. The authors would like to express their sincere thanks for valuable guidance and discussions for the committee members.

REFERENCES

1) Asanuma, H. : Damage Report on the Shizunai Bridge, Civil Engineering Journal, Vol. 25-11, 1983
2) Part V Seismic Design of Design Specifications of Highway Bridges (previous version), Japan Road Association, 1980
3) Clough, R.W. and Penzien, J. : Dynamics of Structures, MacGraw-Hill, 1975
4) Part V Seismic Design of the Design Specifications of Highway Bridges (new version), Japan Road Association, 1990

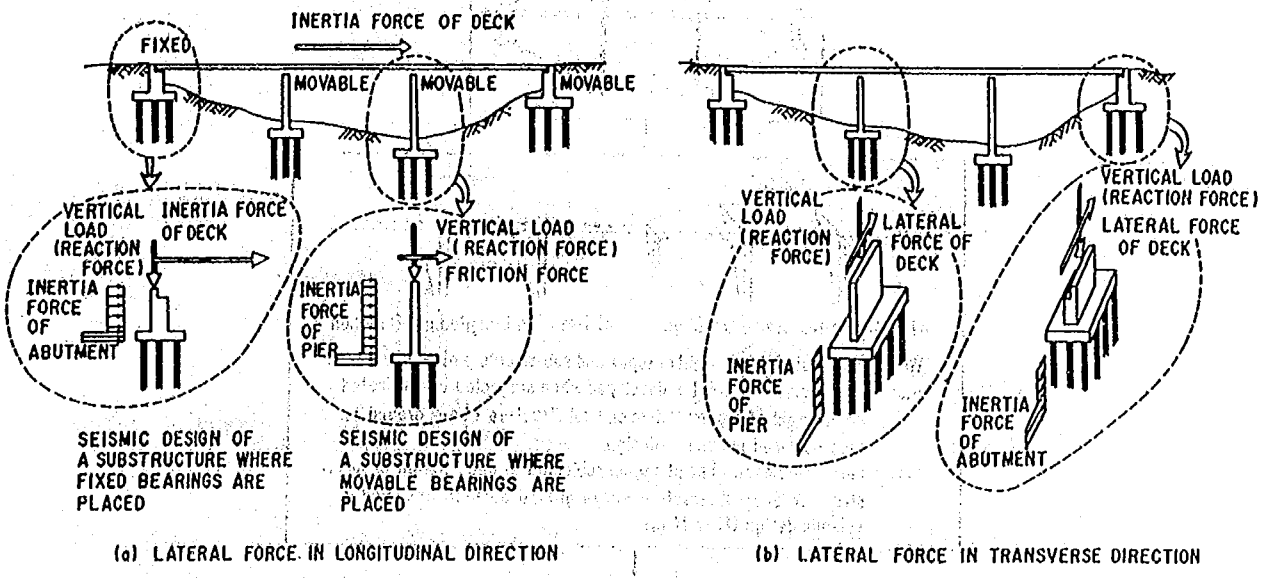

Fig.1 Evaluation of Lateral Force by Reaction Force Method

Table 1 Design Structural Units

	Longitudinal			Transverse			Design Structural Unit
Simple Girder Bridges	F M F			A Part of Superstructure which Develops a Reaction Force at the Relevant Substructure			Regarded as A Design Structural Unit Consisting of A Substructure and A Part of Superstructure Supported by the Substructure
Continuous Girder Bridges	Support Condition in Longitudinal Direction: Fixed at One Support	M F F M M F M		Difference of Natural Period between Piers: Small	A Part of Superstructure which Develops a Reaction Force at the Relevant Substructure		
	Fixed at Multiple Supports	M F F M	F F F	Large			Regarded as A Design Structural Unit Consisting of Substructures and the Superstructure Supported by the Substructures
Arch, Frame and Other Types of Bridges							

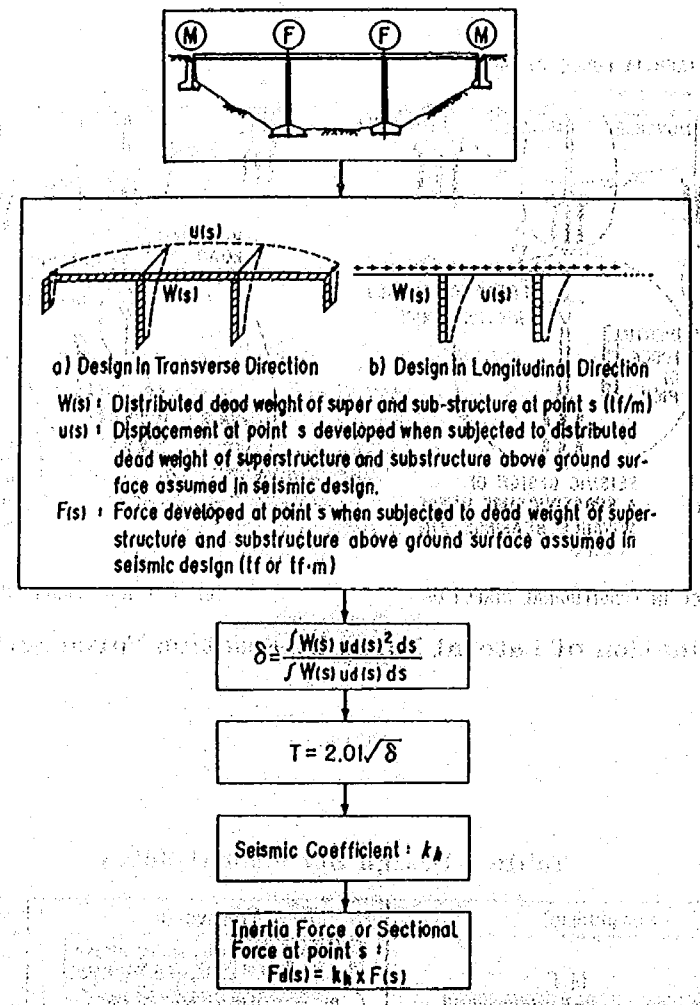

Fig.2 Flow of Static Frame Method

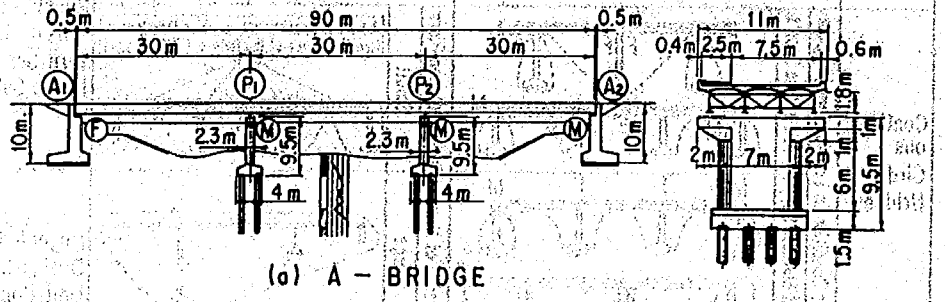

(a) A – BRIDGE

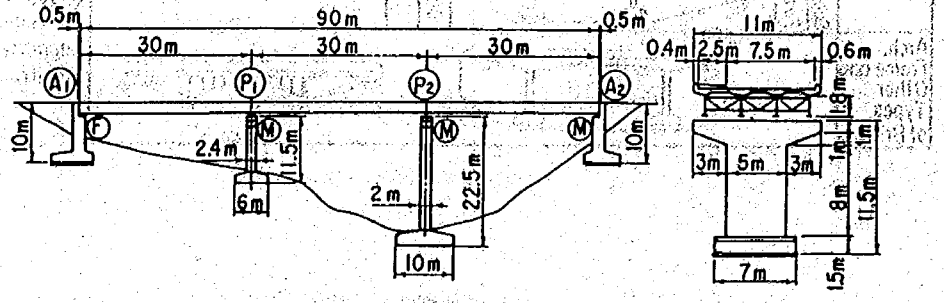

(b) B – BRIDGE

Fig.3 A- and B-bridges Analyzed

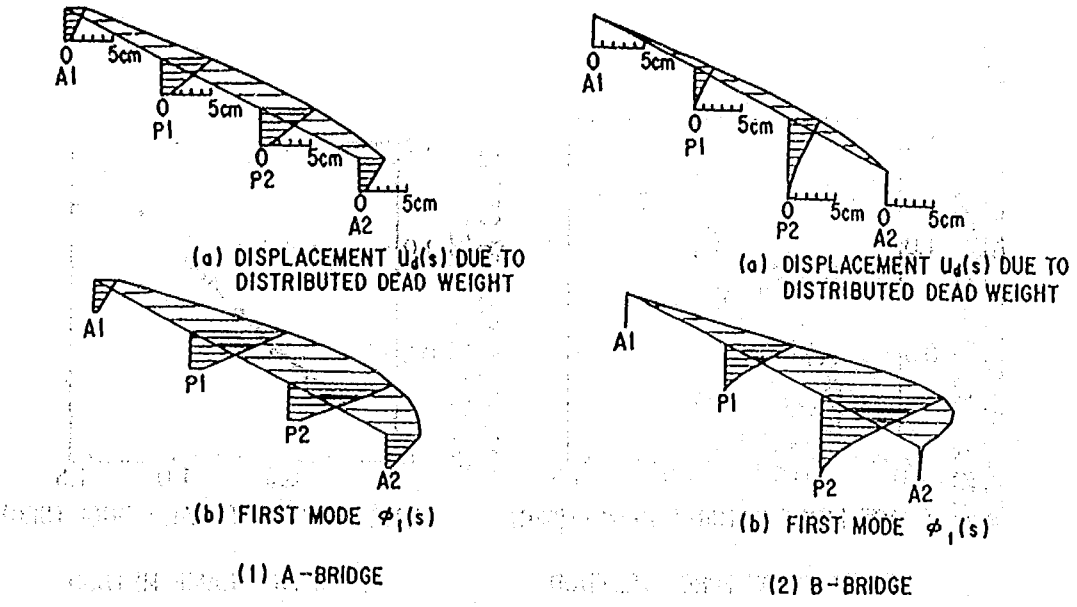

Fig.4 Comparison of Static Deformation and First Mode Shape

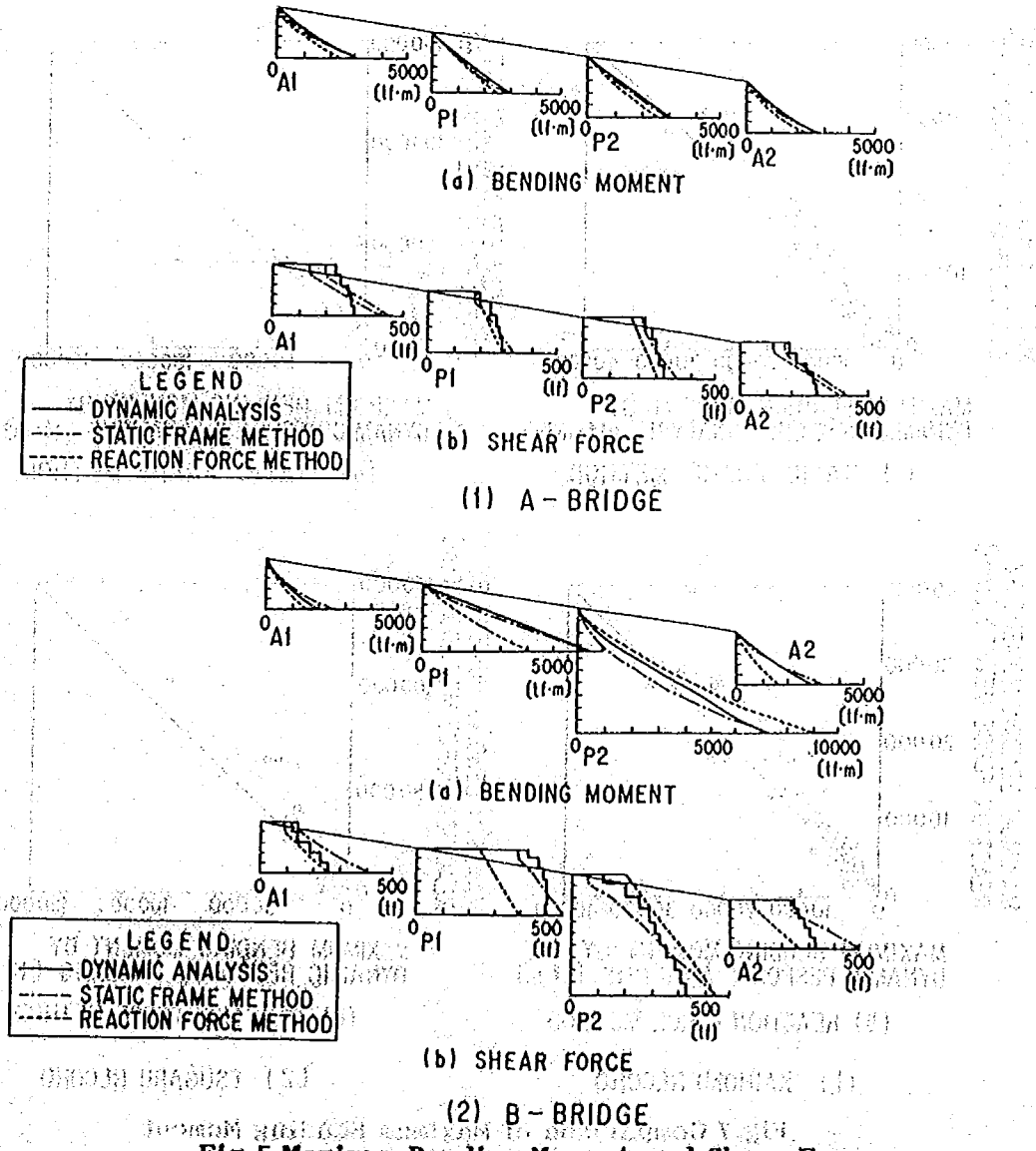

Fig.5 Maximum Bending Moment and Shear Force

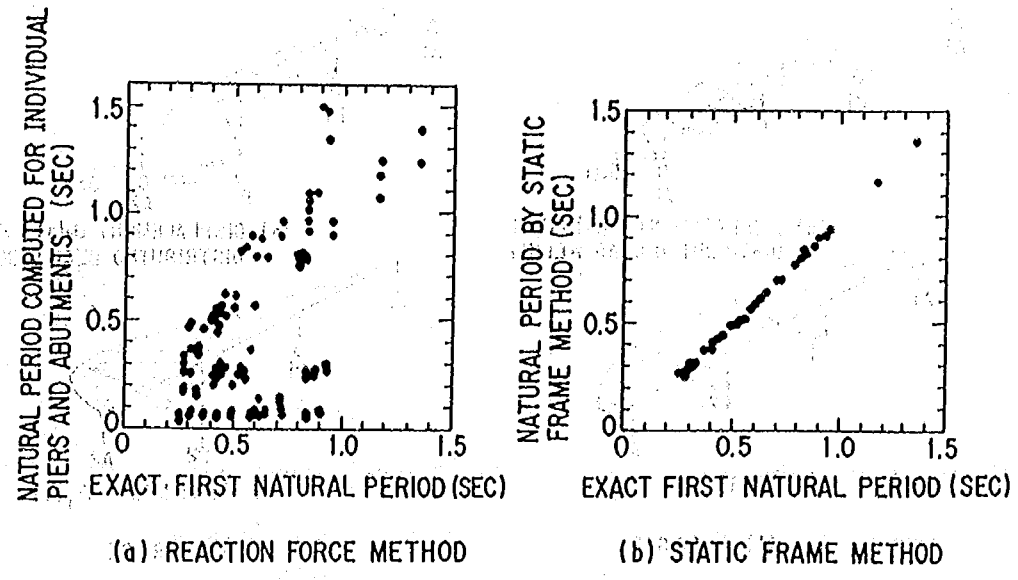

Fig.6 Comparison of Natural Period

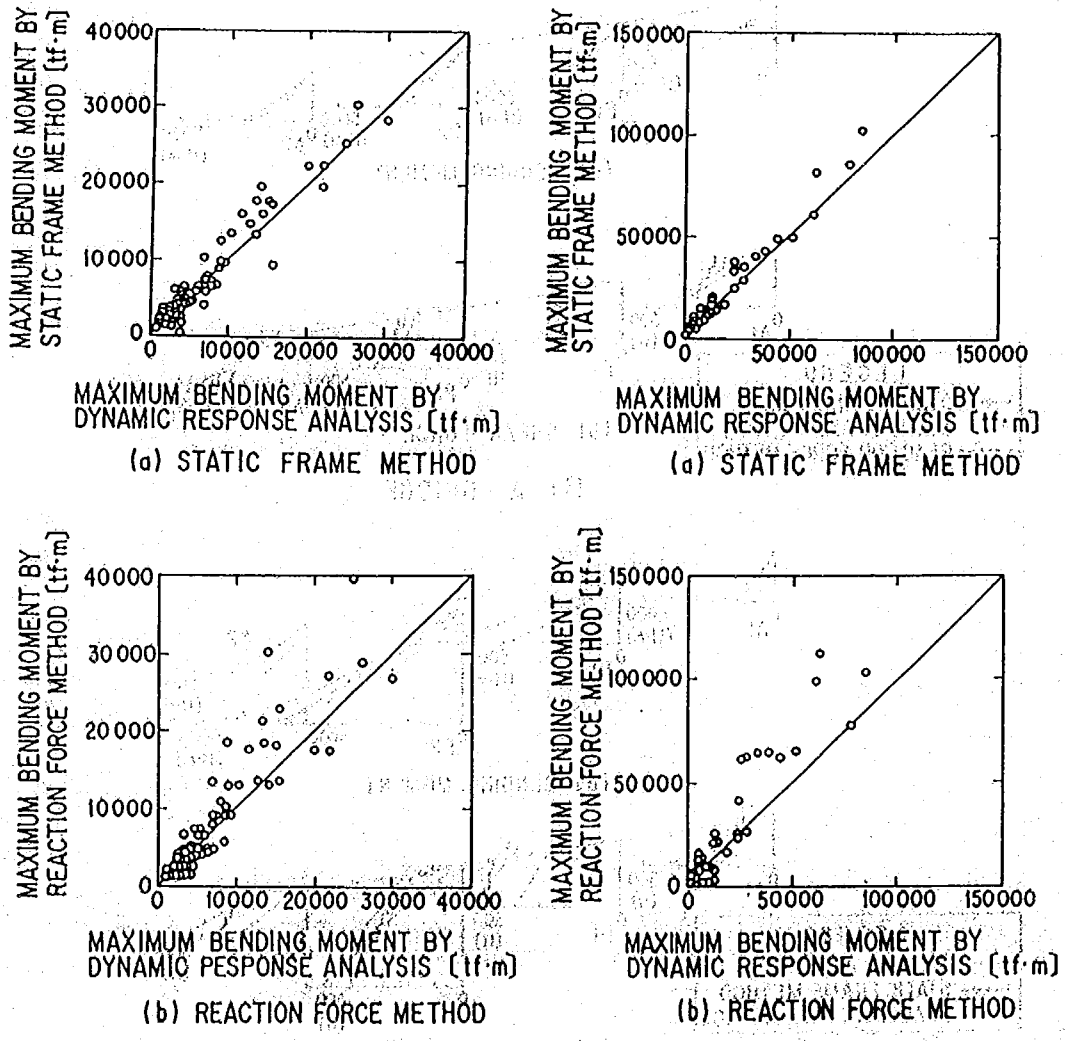

Fig.7 Comparison of Maximum Bending Moment

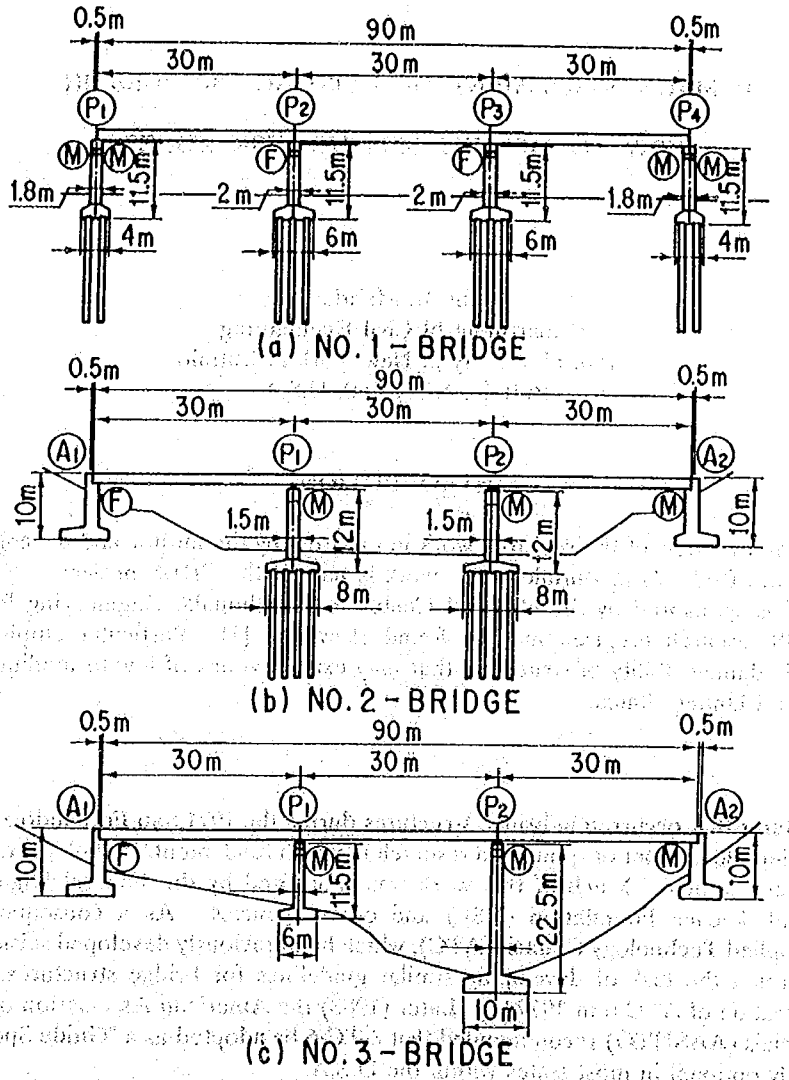

Fig.8 Three Bridges Analyzed by Static Method

Table 2 Distribution of Lateral Force

BRIDGES	ANALYTICAL METHODS	A1 (P1)	P1 (P2)	P2 (P3)	A2 (P4)
NO.1-BRIDGE	REACTION FORCE METHOD	27.6	75.9	75.9	27.6
	STATIC FRAME METHOD	25.4	78.1	78.1	25.4
NO.2-BRIDGE	REACTION FORCE METHOD	27.6	75.9	75.9	27.6
	STATIC FRAME METHOD	54.7	48.0	50.5	53.9
NO.3-BRIDGE	REACTION FORCE METHOD	27.6	75.9	75.9	27.6
	STATIC FRAME METHOD	32.5	101.4	9.8	63.1

DAMAGE ASSESSMENT OF EXISTING BRIDGES IN LOW TO MEDIUM SEISMIC RISK ZONES

John B. Mander
Department of Civil Engineering
State University of New York at Buffalo
Buffalo, NY 14260, U.S.A.

INTRODUCTION

This paper presents an overview of the research work in progress by the author and his colleagues at the State University of New York (SUNY) at Buffalo. This work is part of the ERBS project -- Earthquake Resistant Bridge Systems, and is sponsored by the National Center for Earthquake Engineering Research (NCEER). Details of the ERBS research program may be found elsewhere [1]. Particular emphasis is given to the assessment of seismic damageability of structures that may exist in zones of low to medium seismicity such as the eastern and central United States.

Research Context

The catastrophic failures that occurred in bridge structures during the 1971 San Fernando earthquake in United States led to a considerable amount of sponsored research in which fundamental problems relating to the seismic design of bridges were studied. Much of this work was sponsored by the Federal Highway Administration (FHA), the National Science Foundation (NSF) and other agencies. As a consequence of the ensuing investigations the Applied Technology Council (ATC), which had previously developed seismic design guidelines for buildings, performed the task of developing similar guidelines for bridge structures. This subsequently resulted in the publication of ATC-6 in 1979 [2]. Later (1983) the American Association of State Highway and Transportation Officials (AASHTO) recommended that ATC-6 be adopted as a "Guide Specification". The use of ATC-6 is currently optional in most states within the U.S.A.

In addition to the above mentioned research efforts undertaken in the U.S. considerable work has been also done in New Zealand. Based on governmental and university research work the N.Z. National Society for Earthquake Engineering published in 1980 a series of papers concerned with the seismic design of bridges [3]. That work plus subsequent efforts, such as that by the author [4] and others [5], now forms the basis of seismic design practice for both road and railway bridges in New Zealand.

By virtue of the fundamental nature of these past research efforts, a better understanding now exists for the seismic design and response of ductile bridge substructures (piers) as well as the span seating and bearing requirements of bridge superstructures. Although considerable research progress has been made since the 1971 San Fernando earthquake many questions remain unanswered. For example past research efforts have principally concentrated on the seismic design of new bridges in regions of high seismic activity, such as California. Only a limited research effort has been directed to the evaluation and seismic rehabilitation of the numerous bridge systems that already exist.

CONVENTIONAL WISDOM AND ITS SHORTCOMINGS

The present state-of-the-art requires that to minimize the hazard to life and limb in the event of strong earthquake ground motions, bridges may suffer damage but the prevention of structural collapse must be

ensured. To meet this underlying design philosophy two approaches have evolved by which seismic resistance can be provided; either through a ductile sub-structure; or through an isolated superstructure. These two approaches together with their shortcomings are described below.

Ductile Design of Bridge Sub-Structures

It is generally uneconomical to design bridges to respond elastically to inertia forces induced by earthquakes. Therefore, the seismic resistance of bridges is normally achieved by designing the sub-structure for both strength and ductility. Thus ductile piers (the above ground portion of the sub-structure) are designed to dissipate seismic energy by the formation of flexural plastic hinges. For a satisfactory design checks should be made to ensure the ductility CAPACITY exceeds the ductility DEMAND under the design ground motions. In concrete structures the ductility capacity is achieved by providing sufficient transverse reinforcement to; (a) adequately confine the core concrete; (b) prevent buckling of the longitudinal reinforcement; and (c) prevent shear failure. This conventional wisdom for bridge sub-structure design overtly makes the requirement that seismic damage be concentrated only in those locations where damage can be easily seen and repaired. Designers are penalized by being required to design for significantly high forces if any hinging forms beneath ground or water level.

Other forms of damage in sub-structures, such as pier shear failures, or foundation-pile hinging, are unacceptable. Although such principles may be seen to be commendable for the design of new structures, their application may be overly harsh if not impossible to implement for the rehabilitation of existing vulnerable bridge systems. For example, many existing bridge sub-structures have been predominantly designed for gravity (dead plus live) load effects, and often tend to have squat stiff piers on either shallow or piled foundations. Due to the absence of a capacity design procedure under earthquake loading, such sub-structures may fail due to: either degradation of shear strength in the piers; or foundation footing overload, pile hinging beneath the capping beam; or a combination of these factors.
Past research has expended only a minimal effort on the role foundations play during a seismic event. It is well known that soil-structure interaction will significantly influence the seismic response of bridges. The beneficial or detrimental effects of such interaction remain a moot point. For example, foundation flexibility may on the one hand increase the natural period of vibration and hence provide a beneficial reduction in design forces, and yet on the other hand a detrimental increase in deck displacements will need to be accommodated, especially at the abutments. Clearly such issues need clarification and guidance on their treatment given to designers.

Seismic Isolation of Bridge Superstructures

Isolation of the bridge superstructure from the worst effects of earthquake shaking can be achieved by mounting the bridge deck on either elastomeric or sliding bearings, or both. The additional structural flexibility will increase the natural period of vibration, which in turn will normally reduce the seismic response. A variety of specially designed mechanical energy dissipating devices can also be installed in order to minimize deck displacements (and hence seating lengths) by damping the dynamic response.

The principal disadvantage of seismic isolation is the relative displacements between the super and sub-structure can be quite large even for moderate earthquakes. This can lead to complex span seating and restrainer arrangements. Moreover, some far-field earthquakes, such as Bucharest 1977 and Mexico City 1985, exhibit response spectra in which the high frequency content has been attenuated between the epicenter and the site, while the long period content is amplified due to local site affects. This further exacerbates the large relative displacement problem. Generally, integral ductile systems are more efficient in such circumstances. Ideally a well designed and detailed bridge structure might utilize principles of both isolation and limited ductility in order to improve seismic performance by attempting to minimize both forces and displacements, respectively. However, presently there is not a clear understanding of how such a duel system would perform and design approaches have not been formulated.

Most existing short to medium span bridge decks are mounted on some sort of bearing system, rather than being built integrally with the piers. Generally, and especially is zones of low to medium seismicity, such bearings are not of the isolation type. Their principal function is to accommodate longitudinal deck expansion and contractions from thermal effects as well a transmit braking forces from the live loading. It is expected that all bearing types, including the older type of steel bearing that are used less commonly nowadays (these being largely superseded by reinforced or unreinforced elastomeric bearing pads and pot bearings), will possess sufficient intrinsic strength and/or displacement capacity to resist minor seismic events. Because such bearings are designed for service loads, their strength and stability during earthquake loading is not at all well understood by bridge engineers.

RESEARCH NEEDS

Two joint U.S.-N.Z. workshops, sponsored by NSF, were held in 1981 and 1985 to systematically identify research needs. These workshops resulted in combined researcher and practitioner opinions on research priorities, which have been documented in ATC-12 and ATC-12-1 [6,7]. Such workshops tend to be attended by engineers well versed in the practice of seismic design for the most adverse circumstances. It has only been more recently that the problem of existing non-seismically designed structures, particularly in zones of low to medium seismicity, has received more widespread attention. However, this attention has initially been focused on buildings [8]. As a result of the significant number of bridge failures and deaths in the October 1989 Loma Prieta earthquake [9], there is now a widespread awareness amongst practitioners of the problems associated with existing bridge structures not engineered for seismic resistance. Based on the aforementioned shortcomings in the present state-of-the-art, it is evident that current design and evaluation procedures need enhancing through future research initiatives. The particular motivation for extending the present state-of-the-art is to enable the large stock of existing bridges to be reliably evaluated for seismic risk, and if necessary rehabilitated.

As a result of careful identification of the research needs identified in the ATC-12 documents as well as the need to introduce earthquake engineering into zones of low to medium seismicity, the ERBS research program was proposed in 1989, only months prior to the Loma Prieta earthquake. This program has focused on regular short to medium span bridges which tend to be the most vulnerable in an earthquake, as well as the most abundant in number, thus posing a high overall level of seismic risk.

The objectives of the ERBS program are to:

(i) Evaluate the vulnerability of typical short to medium seismicity

(ii) Develop appropriate measures for rehabilitating bridges deficient in seismic resistance

(iii) Undertake theoretical and experimental research to quantify the seismic strength and deformability of entire bridge systems including the effects of soil-structure interaction.

These objectives can be translated into research needs:

Evaluation

The way in which most existing bridges may fail in the event of a strong earthquake is not well understood. An analyst needs to know the hierarchy of failure mechanisms before viable retrofitting measures can be designed. Current evaluation techniques may not capture all of the possible modes of failure. For example, analytical techniques are currently not capable of capturing the level of loading required to collapse steel bridge bearings, or to cause columns that are inadequately reinforced for shear to fail. A clear need therefore exists to identify, in terms of local seismicity and structural type, the probability of failure. That is, the return period of a catastrophic earthquake, as well as the return period of a damaging earthquake that may render a bridge system unserviceable due to a partial failure need to be determined. The role soil-structure interaction plays in bridge dynamics also needs to be included in the evaluation of existing structures. Theoretical models, in the form of transient non-linear dynamic analysis, and also seismic limit analysis approaches need further development.

These approaches need to be validated by experimental investigations. To this end, a large scale seismic soil-structure interaction testing facility, capable of testing realistic non-linear structural and non-linear soil behavior, needs to be developed. It should be noted that centrifuge testing and field testing are not suitable for such studies. Shaking table testing facilities need to be developed for such testing, preferably at a large as practicable scale in order to minimize gravity similitude problems.

Rehabilitation

Abutment bearings and girder seats often tend to be the most vulnerable elements in earthquakes. In high risk seismic zones, current practice would require retrofitting with isolation bearings and providing shear keys or restrainers to limit seat width demand. However, retrofitting the vulnerable superstructure may only move the problem to the sub-structure. As mentioned previously herein, bridge piers in many eastern and central U.S. bridges have not been designed for seismic resistance and would generally exhibit a non-ductile post-yield behavior. Retrofit methods which principally add ductility to piers are currently under development in California [10]. There is a need to develop appropriate measures of improving the ductility capacity of bridge columns in low to medium seismic zones where the demands are more modest.

If either the deck seating and/or the piers are retrofitted, it may leave the foundation system vulnerable. This could include spread footings and pile foundations as well as the abutments. These components in a bridge may be more tolerant to damage than the piers or deck bearings. However, the damage potential of the foundation system is clearly important and needs to be definitively assessed.

RESEARCH PLAN

It can be concluded form the above discussion on research needs that although the importance of new bridges should not be diminished, a consistent rehabilitation philosophy must unify various approaches to retrofitting different portions of a bridge. A capacity approach is necessary in which a desirable hierarchy of failure mechanisms for the entire bridge system is achieved by the rehabilitation process.

Before such a rehabilitation philosophy is finally established an evaluation phase is to be undertaken. This is to assess the seismic vulnerability and damage potential of existing short to medium span bridges in low to medium seismic risk zones. As part of the evaluation phase, theoretical developments will be made to improve the analytical reliability of current evaluation techniques. Particular emphasis is being given to the behavior of existing poorly detailed bridge components, including bearings, piers and foundations, as well as aspects of soil-structure interaction. Theoretical developments are being corroborated by experiments on the critical elements of bridges such as bearings, piers and foundation systems. These aspects are considered in the following sections.

THE INTRINSIC STRENGTH OF NON-SEISMICALLY DESIGNED BRIDGES

A survey has been carried out of typical bridges in the populace New York State [11]. Results show that for short to medium span highway bridges 69% of the superstructures are concrete slab on steel girder configurations, and 77% of the substructures are reinforced concrete column, bent or wall piers. Fig 1 presents a selection of this class of two-span bridge located in New York. These bridges were evaluated for a 0.19g peak ground acceleration (PGA) earthquake in accordance with the ATC-6-2 recommendations [12]. The resulting capacity/demand ratios listed in Table 1 serve as a guide of system strength, but should be treated with some caution. This is because in each case analysis shows that the shear strength of the system is questionable in the inelastic range. Most of the older structures provide only one #3 (10 mm) perimeter hoop at 12 inch (300 mm) spacing, regardless of the column dimensions. Lap splices are also generally found in the potential plastic hinge zone immediately above spread footings or pile caps. These detailing deficiencies will lead to a questionable seismic performance. However, the results in Table 1 indicate that such piers do possess some intrinsic strength to resist earthquakes inelastically, but their ductility capacity is unknown at this stage.

In order to assess the ductility capacity of non-seismically designed bridge pier experiments are currently in progress. A portion of a pier similar to that shown in Fig 1(c) has been recovered from a bridge during demolition and will be tested in the laboratory. Companion 1/4 scale model piers have also been constructed similar to Figs 1(a) and 1(c). All specimens will be tested under quasi-static cyclic loading at displacement amplitudes expected in a moderate seismic zone derived from the following assessment methodology.

ASSESSING THE HYSTERETIC ENERGY DEMAND ON BRIDGE STRUCTURES

In order to determine the ductility capacity required by the critical plastic hinge regions of bridge piers, the hysteretic energy demand must firstly be assessed. A study has been undertaken in which hysteretic energy spectra are derived for given ground motions using a non-linear dynamic time-history analysis. The method used in this study considers an absolute energy formulation proposed by Uang and Bertero [13]. This approach considers the accumulating components of energy resisting the total input energy from the earthquake

$$E_I = E_k + E_s + E_\xi + E_h \qquad (1)$$

in which E_k = kinetic energy in the system, E_s = strain energy, E_ξ = absorbed viscous damping energy, and E_h = hysteretic energy absorbed by the structure.

Figs 2 and 3 show the various response spectra for a sinusoidal motion which consisted of three parts: (i) an ascending ramp of five 1.0 Hz cycles to a PGA of 1.0g; (ii) 15 cycles at 1.0 Hz at a constant 1g amplitude; (iii) a descending ramp of five 1.0 Hz cycles. For both the harmonic and earthquake motion a simple elasto-plastic model was used. Single-degree-of-freedom (SDOF) systems were considered for different levels of force (strength) reduction R, defined as:

$$R = S_a / C_d \qquad (2)$$

in which Sa = normalized spectral acceleration required for an elastic response, and C_d = non-dimensional base shear strength coefficient.

It is instructive to firstly consider the results of the harmonic motion study shown in Fig. 2. The magnification of dynamic response with respect to maximum forcing displacement for an elastic system (R=1) is given by the well known relationship

$$D_e = [(1-\beta^2)^2 + (2\beta\xi)^2]^{-1/2} \qquad (3)$$

in which ξ = viscous damping factor (in this study ξ = 5%), and

$$\beta = T_o / T \qquad (4)$$

where T = natural period of vibration of the SDOF system and T_o = forcing period. By setting D = 1 in Eq 3 a separation period can be defined as

$$T_s = \frac{T_o}{\sqrt{2-4\xi^2}} \qquad (5)$$

where T_s separates displacements which are larger (when $T > T_s$) or smaller (when $T < T_s$) than the forcing displacement amplitude.

This separation period can also be used to identify zones of increased dynamic response for inelastic structures. For long period structures ($T > T_o$) it can be seen that the displacements converge for all values of R, that is

Newmark's equal displacement principle applies. It can also be seen that when $T < T_s$ there is a substantial amplification in displacements as the strength decreases (or R increases as shown in Fig. 2c). In the limit when R becomes large and the period is small the SDOF oscillators behavior is analogous to a sliding block where C_d becomes the coefficient of sliding friction. As the strength decreases the maximum displacement tends toward the maximum ground displacement.

For hysteretic systems with $T < T_o$ the dynamic magnification factor can be approximated by the relationship

$$D_h = D_e^{1/(2.5R-1.5)} \tag{6}$$

For an earthquake motion the principal excitation frequency is not clearly defined. However T_o can be found by using T_s in Eq. 5. T_s can be determined by observation as that period when damping energy is constant for all values of R as shown in Figs 2 and 3.

The structural ductility factor μ, for both sinusoidal and earthquake motion can be approximated by taking the greater of

$$\mu = R \tag{7a}$$

$$\mu = R \; D_h/D_e \tag{7b}$$

Eq 7a and 7b will be applicable for periods $T > T_s$ and $T < T_s$, respectively.

The most significant finding from this analysis is: using the hysteretic energy and displacement response spectra to derive the equivalent number of fully reversed elasto-plastic cycles. For an elastic response (R = 1) the number of cycles N_d is defined as

$$N_d = \frac{\Sigma|X|}{4S_d} \tag{8}$$

where S_d = spectral displacement; and $\Sigma|X|$ is the total displacement for the duration of the motion. As expected for the sinusoidal motion this is approximately 20 full reversed cycles. Note that the minimum value of N_d is 0.25, which is for a monotonic response.

For the 1940 El Centro N-S earthquake record this analysis shows that $N_d < 4$ for all inelastic responses. Similar analyses have been carried out for other earthquake ground motions and hysteretic models not shown here. Results from these analyses show similar trends: that the value of N_d are generally constant for a specific R value when $T < T_s$. For example when R = 6 and $T < T_s$, N_d was found to be approximately equal to 5, and 0.8 for the 1985 Mexico City and San Salvador 1986 earthquakes. These earthquakes respectively represent long-period-long duration and high-frequency-short duration events. These results can now be used, together with other earthquake motions to plan a realistic set of experiments.

ASSESSING THE HYSTERETIC ENERGY CAPACITY OF BRIDGE PIERS

It is important when assessing the hysteretic energy capacity of a system to have a clear definition of failure. For bridge piers failure can be defined as that state in which the pier is unable to sustain the gravity load of the superstructure, that is, the onset of collapse. Incipient pier collapse may occur when;
(a) The moment capacity is reduced to zero due to either strength deterioration, P-delta affects, or both. (In previous studies, investigators have sometimes defined this state as when the moment capacity reduces to say 80% of the nominal strength. Note that this may define a ductile serviceability limit state, but not a collapse state.)

(b) The transverse hoops fracture, thus leaving the column unconfined. (Although this is not a collapse state, strength deterioration is very rapid following hoop fracture.)
(c) The longitudinal bars fracture due to low cycle fatigue.

For columns with a high axial load intensity (P > 0.25 f'c Ag) failure modes (a) and (b) will prevail. Studies of bridges in the eastern and central United States have shown that the axial load intensities are typically low (P< 0.1 f'c Ag). Thus failure will be characterized by loss of shear strength leading to a type (a) failure for squat piers with low volumes of transverse steel, or type (c) failure a flexurally dominated response.

For flexural piers with low levels of axial load the strain range amplitude (e_a) the steel in alternating cycles can be determined from a fiber-model analysis. Using low cycle fatigue models such as that shown in Fig. 4 the cyclic capacity N_c, can be determined

$$e_a = M(2N_f)^m \qquad (9)$$

Supposing a reinforcing steel such as that shown in Fig. 4 was used to reinforce a bridge column, then for an El Centro type earthquake (with N_d=4) the strain range should be kept below ± 0.03 in order to avoid incipient collapse.

The hysteretic energy capacity of bridge piers can be assessed in two ways; either experimentally; or analytically. For an analyticaly assessment, reliable inelastic mechanistic micro-models are necessary. To date such models have been developed for flexural piers in which the shear span (M/VD) is greater than about 2.0. For squat piers, or columns under-reinforced transversely, inelastic shear displacements will govern the response at moderate to high ductility factors. Reliable models for this class of bridge pier are not fully developed at this stage. It is one of the objectives of this research to continue development in this area.

In the meantime, an experimental approach is the most viable means of assessing the post-elastic performance of bridge piers in which shear will control the behavior. When testing such piers this raises the question; What displacement history should be used? Many laboratory performance tests histories on columns and piers have in the past been ductility based. The main problem with this approach is explicitly defining the yield displacement. This problem is trivial for flexurally dominated systems. However, for multiple element subassemblages (such as the entire piers shown in Fig. 1) or when the nominal strength cannot be reliably defined, then it is not practical to use ductility based loading histories. Instead, drift based displacement histories can be adopted. For example, the displacement history currently in use on many NCEER projects consists of two complete reversed cycles of lateral loading at drift amplitudes of ±0.25%, ±0.5%, ±1.0%, ±2.0% ±3%..until failure occurs.

A viable alternative testing approach being adopted in this project is using a low cycle fatigue type of test for the columns themselves. Unfortunately to calibrate fatigue models similar to Eq. 9 a large number of tests are necessary which is time and cost prohibitive. Instead, such models can be calibrated directly and inexpensively with the use of reliable analytical models using a hysteretic energy approach.

INELASTIC DAMAGE ASSESSMENT

In energy terms, damage at time t, during a seismic excursion, can be defined as:

$$D(t) = \frac{E_h(t)}{E_c} \qquad (10)$$

in which D(t) = the cumulated damage up to time t, $E_h(t)$ = absorbed hysteretic energy to time t, and E_c = total energy absorption capacity to failure. Clearly when D(t) = 1 then failure (incipient collapse) occurs.

Alternatively, an identical result at the end of a seismic event can be obtained by

$$D_t = N_D/N_c \tag{11}$$

in which D_t = total damage at the end of the event, N_D = the number of full reversed cycles of demand determined from an analysis similar to that described above, and N_c = the number of cycles (capacity) that an element can sustain to failure (at the same displacement amplitude to the demand cycles).

Thus for a given bridge structure "Inelastic Damage Assessment" is summarized as follows.

(1) Using the appropriate ground motion for a desired return period, determine the hysteretic DEMAND using a non-linear time history analysis. This analysis should use the appropriate hysteretic model for member behavior.

(2) Using either experimental or analytical techniques determine the hysteretic energy CAPACITY.

(3) Using Eq 10 determining the damage index. If $D_t > 1$ then collapse will be expected for the target ground motion, and the pier should be seismically retrofitted.

CONCLUSION

Based on the issues raised in this paper the following conclusions are made:

1. The seismic performance of bridges designed in accordance the practice established following the 1971 San Fernando earthquake should generally be satisfactory.

2. Non-seismically designed bridges may possess some intrinsic strength that can be utilized for earthquake resistance. However, an adequate seismic performance will depend largely on the reinforcing steel detailing. Squat piers and columns with low volumes of transverse reinforcement may fail in shear.

3. Seismic performance may be improved by rehabilitating the bridge by providing either isolation bearings, ductile columns, or both.

4. For the type of bridge that exists in low to medium seismic risk zones, existing seismic evaluation techniques are inadequate. Further development is needed.

5. An energy based evaluation and rehabilitation philosophy is presently being explored and shows great promise.

ACKNOWLEDGEMENTS

The author wishes to acknowledge his SUNY at Buffalo colleagues and co-investigators in the ERBS program and in particular Dr S. S. Chen, and graduate students F. Panthaki and G. A. Chang for help with preparing this paper. The financial support of NCEER is gratefully acknowledged.

REFERENCES

[1] Mander, J.B., "ERBS -- Earthquake Resistant Bridge Systems, A Coordinated Research Initiative," Proc. Second Workshop on Bridge Engineering Research in Progress, Reno, Nevada, October 29-30, 1990 pp. 197-200.

[2] "Earthquake Resistance of Highway Bridges," Proc. Workshop ATC-6, Applied Technology Council, January 1979.

[3] 20 authors, "Papers resulting from deliberations of the Societies' discussion group on seismic design of bridges". Bulletin of the N.Z. National Society for Earthquake Engineering, Vol. 13, No. 3, September, 1980, pp 226-309.

[4] Mander, J.B., Priestley, M.J.N., and Park, R., "Seismic Design of Bridge Piers," Research Report 84-2, Department of Civil Engineering, University of Canterbury, Christchurch, New Zealand, February 1984, 442 pg.

[5] Priestley, M.J.N., and Park., R., "Strength and Ductility of Concrete Bridge Columns Under Seismic Loading," ACI Structural Journal, Jan.-Feb. 1987, pp 61-76.

[6] "Comparison of U.S. and N.Z. Seismic Design Practice for Highway Bridges", Proc. Workshop ATC-12, Applied Technology Council, December 1981.

[7] "Seismic Resistance of Highway Bridges," Proc. of Second Joint U.S.-N.Z. Workshop ATC 12-1-1, Applied Technology Council, May 1985.

[8] Poland, C.D., White, R.N., Malley, J.O., Gergely, P., "Seismic evaluation of buildings in the eastern and central United States," in Seismic Engineering Research and Practice, ed. C.A. Kircher and A.K. Chopra, ASCE, NY, May 1989, pp 546-555.

[9] "Loma Prieta Earthquake Reconnaissance Report," Earthquake Spectra, Supplement to Vol. 6, May 1990, pp 151-187.

[10] Priestley, M.J.N., Seible, F., Chai, Y., and Sun, Z., "Steel Jacketing of Bridge Columns for Enhanced Flexural Performance," Proc. Second Workshop on Bridge Engineering Research in Progress, Reno, Nevada, October 29-30, 1990, pp 205-208.

[11] Chen, S.S., and Mander, J.B., "Seismic Classification, Modeling and Testing of Existing Bridge Systems," Proc. Second Workshop on Bridge Engineering Research in Progress, Reno, Nevada, October 29-30, 1990, pp 253-256.

[12] "Seismic Retrofitting Guidelines for Highway Bridges," Report ATC-6-2, Applied Technology Council, 1983.

[13] Uang, C-M., and Bertero, V.V., "Evaluation of Seismic Energy in Structures," Earthquake Engineering and Structural Dynamics, Vol. 19, 1990, pp 77-90.

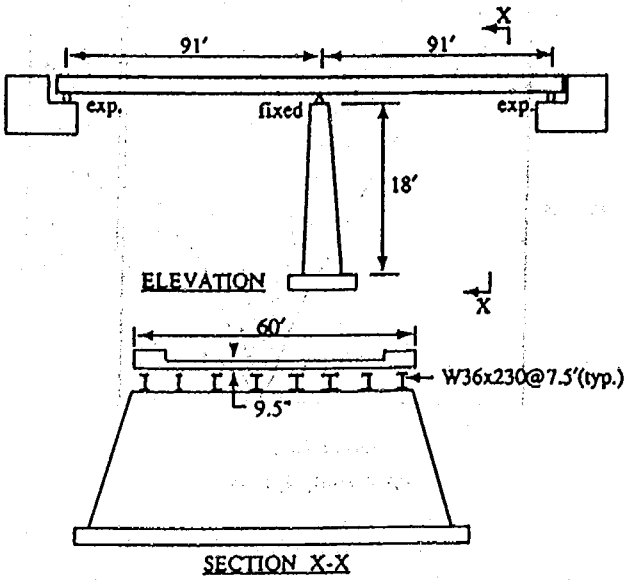

Fig 1a Sweet Home Road Bridge

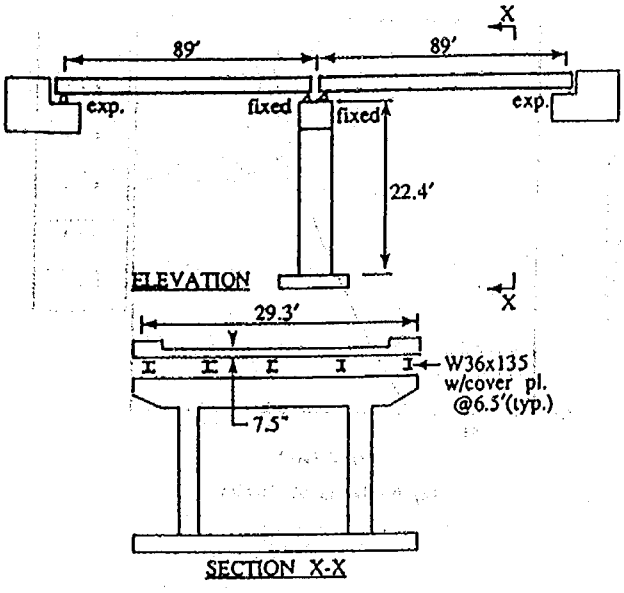

Fig 1b) Salamanca Bridge

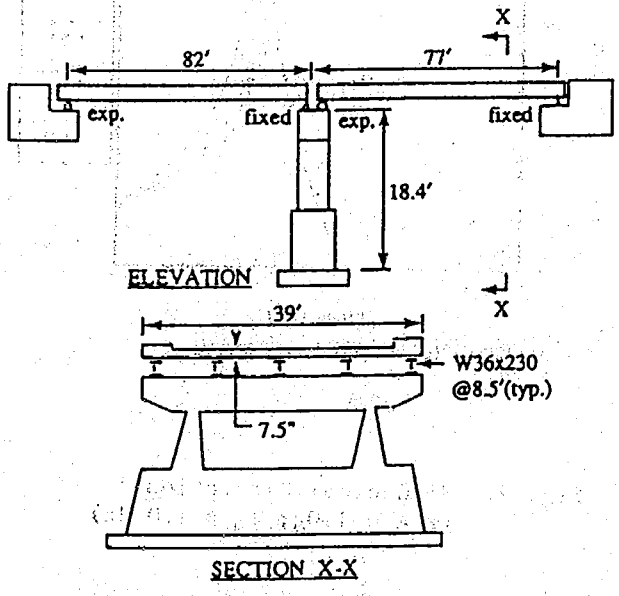

Fig 1c) Jewett-Holmwood Bridge

	Sweet Home	Salamanca	Jewett-Holm.
year built	1982	1967	1957
pier type	solid wall	2 circular cols	2 square cols.
pier height	18'	22.4'	18.4'
reinforcement	0.00175	0.0111	0.0101
period (long.)	0.20	0.89	0.24
period (trans.)	0.02	0.35	0.06
C/D Ratios (critical, for longitudinal ground motion):			
col. moment	0.562	0.411	1.49
fig. moment	0.651	1.91	1.40
col. reinf. splice	1.05	0.822	2.31

Table 1 Partial Analytical Results for 3 2-Span Bridges

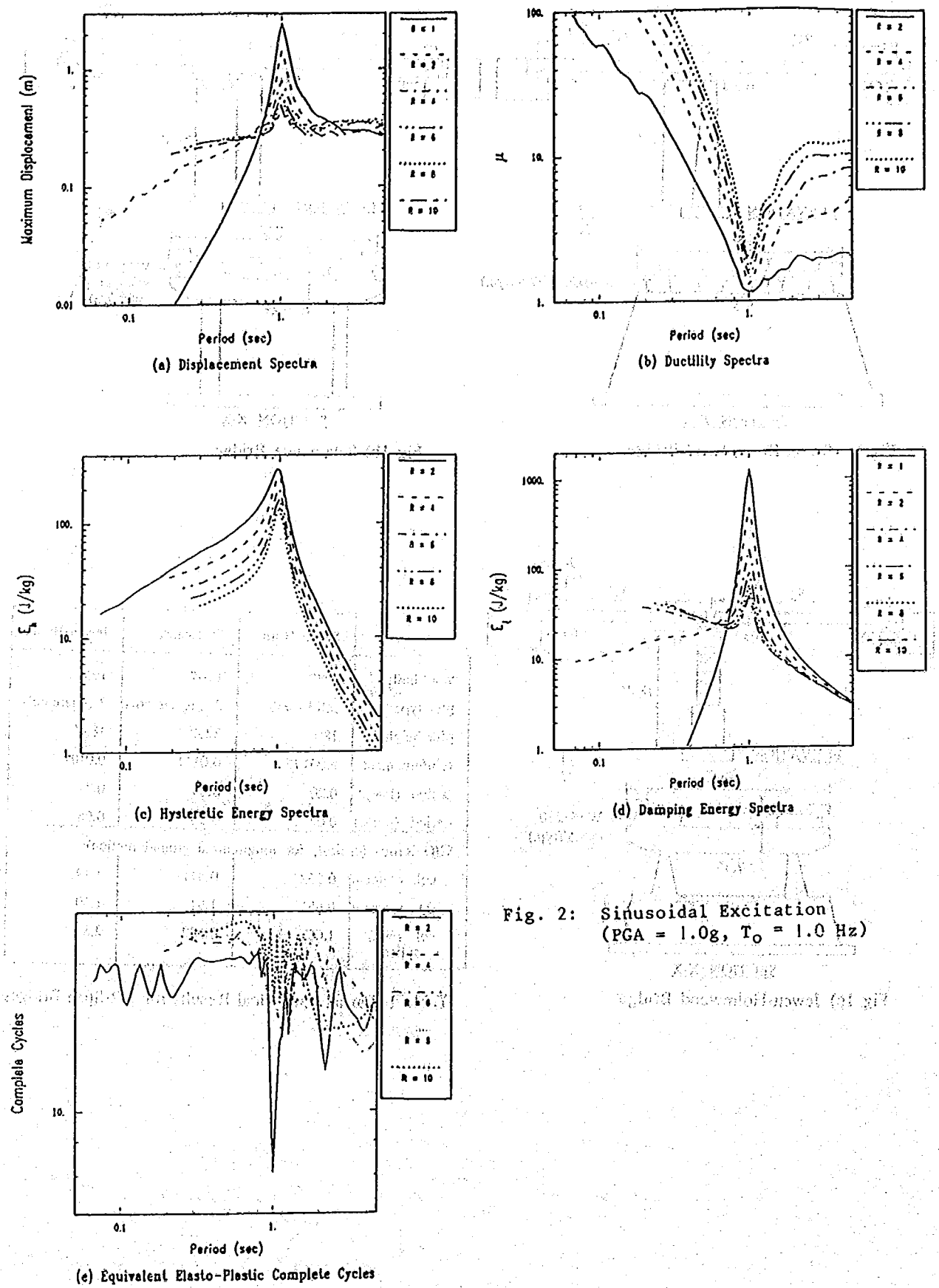

Fig. 2: Sinusoidal Excitation
(PGA = 1.0g, T_o = 1.0 Hz)

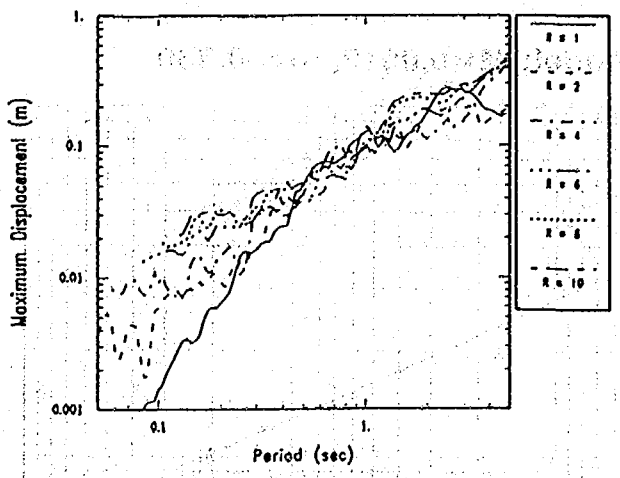

(a) Displacement Spectra

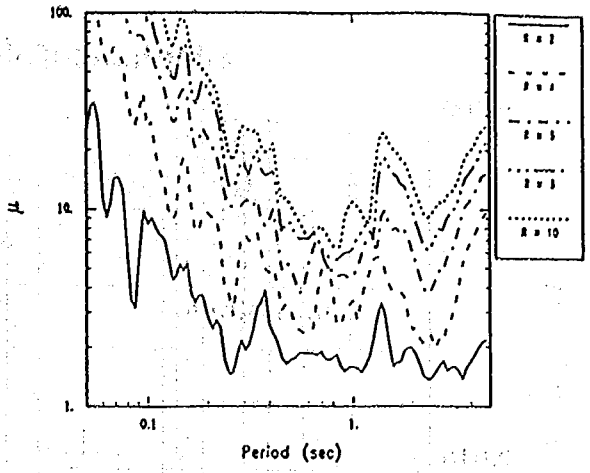

(b) Ductility Spectra

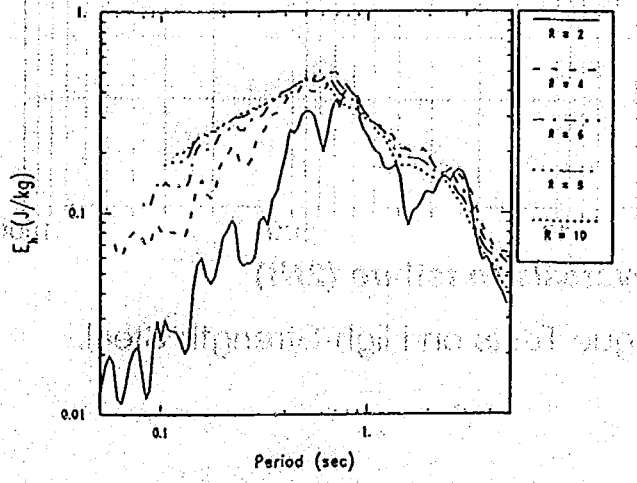

(c) Hysteretic Energy Spectra

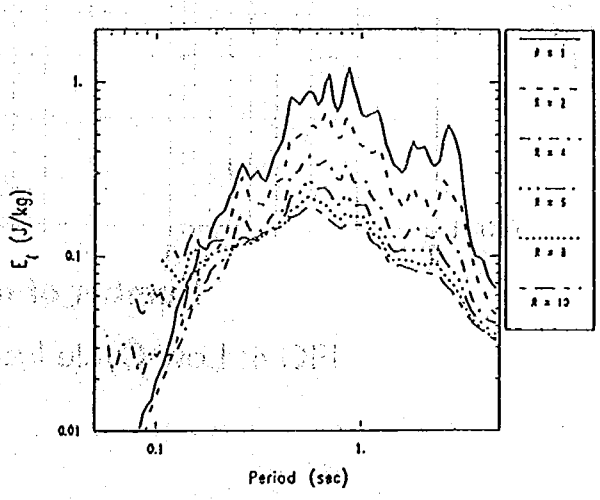

(d) Damping Energy Spectra

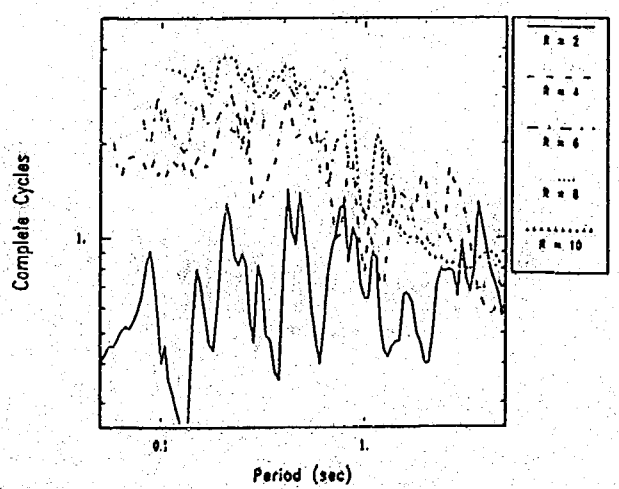

(e) Equivalent Elasto-Plastic Cycles

Fig. 3: El Centro 1940 N-S Earthquake Motion

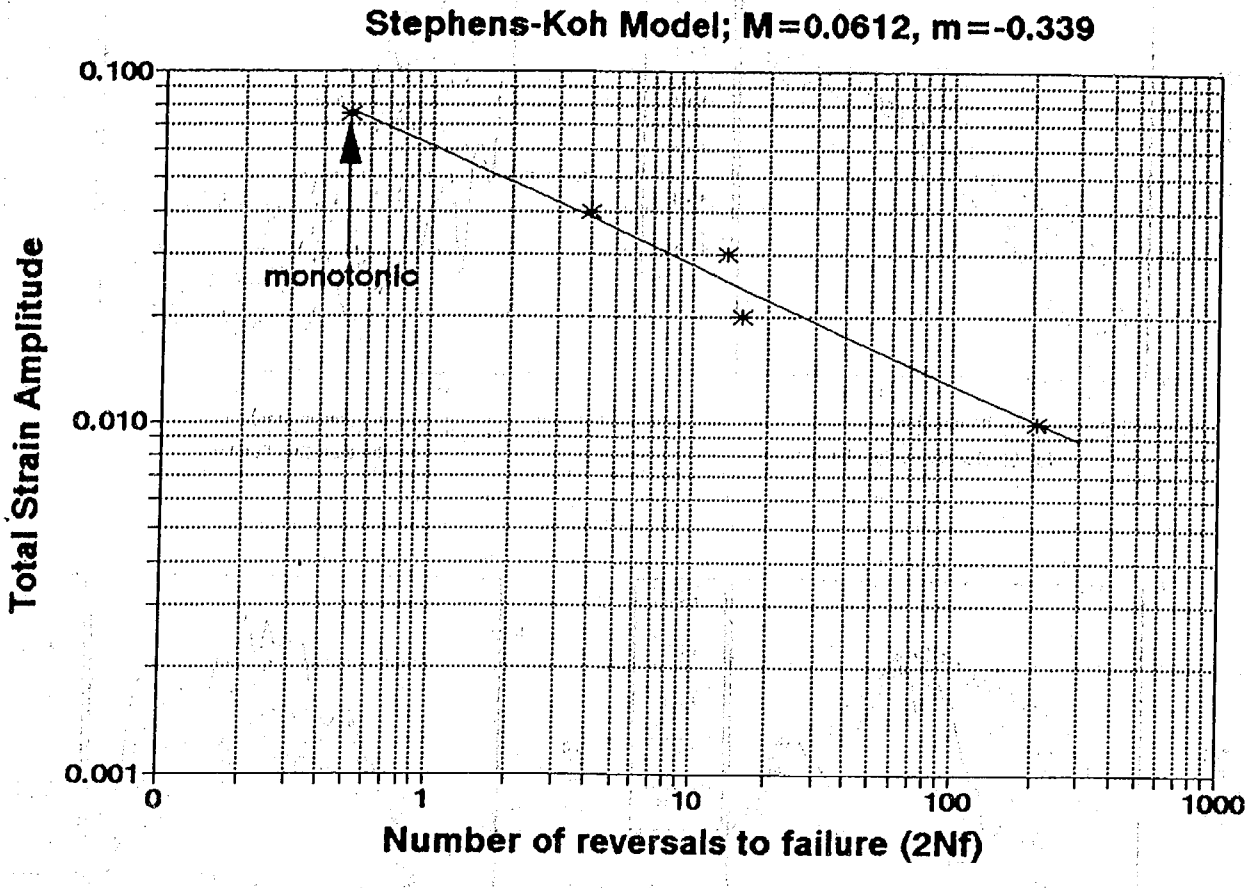

FIG 4: Low-Cycle Fatigue Tests on High-Strength Steel.

(4) Session 4

SESSION 4: SEISMIC DESIGN(3) 1:45pm～3:05pm
(Co-Chairmen: K. Tokida, I. Buckle)

(9) G. A. MacRae* , K. Kawashima, K. Hasegawa, T. Ikeuchi and K. Ohshima: Behaviour of Stiffened Box-Section Steel Bridge Piers in Seismic Regions from Model Tests
(1:45pm～2:00pm)

(10) J. H. Gates* and M. Yashinsky: Performance of Retrofit Bridges in California
(2:00pm～2:15pm)

(11) K. Tokida, K. Tamura* and K. Aizawa: Experimental Study of Phase-Different Ground Motion Effects on the Response of a Suspension Bridge
(2:15pm～2:30pm)

(12) A. F. Goldschmidt: Foundation Considerations for the Seismic Retrofit of CALTRANS Bridges
(2:30pm～2:45pm)

DISCUSSION
(2:45pm～3:05pm)

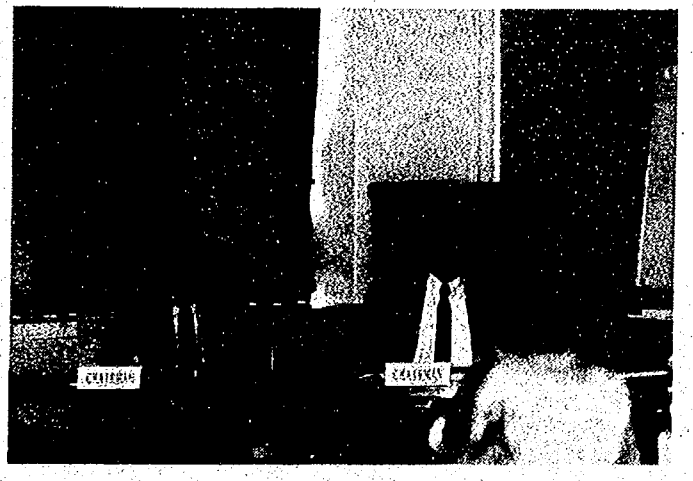

Behaviour of Stiffened Box-Section Steel Bridge Piers in Seismic Regions from Model Tests

by Gregory A. MacRae[1]

Kazuhiko Kawashima[2]

K. Hasegawa[3]

T. Ikeuchi[4]

and K. Oshima[5]

ABSTRACT

Twenty-two model stiffened box-shape steel bridge pier specimens of the type commonly used in Japan were tested in order to obtain their strength and ductility capacity and to understand their behaviour. Hollow specimens and specimens partially filled with concrete were tested both under applied lateral loading and shaking table testing. It was found that the specimens failed by overall buckling of one side as well as local panel buckling and fracture. The strength of specimens with concrete infill was increased however their deformation capacity was decreased. Specimens tested on the shaking table sustained yielding predominantly in one direction with little absorption of energy. This was different from that assummed by the applied lateral loading regimes. Specimens with greater section slendernesses generally had lower ductility capacities. A method for estimating the strength of these specimens which was independent of the effect of the section slenderness was found to be satisfactory.

INTRODUCTION

Steel bridge piers, which are constructed by welding thin plate together, have been used over the past 30 years for the construction of bridges in Japan. The construction cost of these piers is generally more than that of reinforced concrete piers but their section size is significantly less making them ideal for use in city locations where land prices are high and where there are restrictions on construction space. In some cases concrete is placed inside these piers to provide extra protection if a vehicle collides into them. Damage has not been observed in these sort of piers to date and few tests have been carried out to investigate their likely behaviour during an earthquake.

Twenty-two steel pier specimens were tested in order to assess their strength and ductility capacity because it is realized that accelerations greater than the design level may be developed in bridges during a major earthquake. Applied loading tests and shaking table tests were performed on hollow pier specimens with different configurations of internal stiffeners and on specimens which were partially filled with concrete. In this paper some of the more important aspects of the behaviour of these specimens are summarized.

SPECIMEN CONSTRUCTION, DESIGN REQUIREMENTS AND TESTING METHODS

The test specimen sizes were selected to be scaled down versions of real piers. The box-shaped sections consisted of 4 major plates to which ribs and diaphrams were welded for stiffening and strengthening. Real piers are generally large enough that a person may enter and weld from the inside but this construction technique was unable to be used on the smaller pier specimens. The specimen was therefore constructed in stages as shown in Figure 1. Weld was applied to the inside of the specimen before the final web-plate was welded into place from the outside. The diaphrams extended outside the section on one side to facilitate the welding of the final web plate to the specimen. The longitudinal stiffeners on the inside of the final web plate were discontinuous at the diaphram positions and at the base.

[1] Overseas Researcher, Earthquake Engineering Division, Public Works Research Institute, Tsukuba
[2] Head, Earthquake Engineering Division, Public Works Research Institute, Tsukuba, Japan
[3] Senior Researcher, Earthquake Engineering Division, Public Works Research Institute, Tsukuba
[4] Chief Design Engineer, Metropolitan Expressway Public Corporation, Tokyo, Japan
[5] Construction Division Manager, Hanshin Expressway Public Corporation, Kobe Construction Bureau, Osaka, Japan

Design was carried out according to the Japanese bridge design code [1] which is based on elastic design considerations. The background to the buckling design criteria for these piers is published in design guidelines [2]. There are two important section slenderness ratios which are required to be greater than certain values in order that premature buckling does not reduce their strength. They are:

1) The **panel slenderness ratio, b/(nft)**, which must be less than 28 or 24 for Grades SS41 or SM50 steel respectively. This check ensures that local panel buckling will not occur before the yield strength of the section is reached. Local panel buckling refers to buckling panels between the vertical stiffeners. In this ratio b is the width of the section (cm), t is the plate thickness (cm), n is the number of panels divided by vertical stiffeners, as shown in Figure 2, and f is given as $f = 0.65(\phi/n)^2 + 0.13(\phi/n) + 1.0$, ϕ is the stress gradient given as $\phi = (\sigma_2 - \sigma_1)/\sigma_1$, and σ_2 and σ_1 are the stresses at each edge of the plate, where $\sigma_1 > \sigma_2$, and compressive stress is defined as positive. It was conservatively assumed that $f = 1.0$ in the panels which yielded.

2) The **gamma ratio, $\gamma_1/\gamma_{1,req}$**, which must be greater than unity. This check ensures that overall buckling of one side of the pier will not occur before the yield strength of the section is reached. The stiffness of each panel and longitudinal stiffener was used to obtain an equivalent stiffness for the side as a whole and the effect of the lateral stiffeners was also considered. The value of γ_l, which is the relative stiffness of the longitudinal stiffeners, was able to be calculated as $\gamma_l = I_l/(bt^3/11)$ where the value of I_l is given below. The value of $\gamma_{1,req}$ was able to be calculated using the appropriate value from Equations 1 or 3 as described below.

i) Equation 1 should be used to calculate $\gamma_{1,req}$ when α is not greater than α_0 and the moment of inertia I_t (cm^4) of a transverse stiffener satisfies Equation 2.

$$\gamma_{l,req} = 4\alpha^2 n\left(\frac{t_o}{t}\right)^2(1 + n\,d_l) - \frac{(\alpha^2+1)^2}{n} \quad (t \geq t_o)$$

$$\gamma_{l,req} = 4\alpha^2 n(1 + n\,d_l) - \frac{(\alpha^2+1)^2}{n} \quad (t < t_o) \qquad (1)$$

$$I_t \geq \frac{bt^3}{11}\cdot\frac{1 + n\gamma_{l,req}}{4\alpha^3} \qquad (2)$$

ii) Equation 3 should be used in all other cases such as when the effect of the transverse stiffeners in the computation of $\gamma_{1,req}$ is insignificant and their effect is ignored.

$$\gamma_{l,req} = \frac{1}{n}\left[\left\{2n^2\left(\frac{t_o}{t}\right)^2(1 + n\,d_l) - 1\right\}^2 - 1\right] \quad (t \geq t_o)$$

$$= \frac{1}{n}\left[\{2n^2(1 + n\,d_l) - 1\}^2 - 1\right] \quad (t < t_o) \qquad (3)$$

where

α is the aspect ratio of stiffened plate, $\alpha = a/b$,

α_0 is the critical aspect ratio, $\alpha_o = \sqrt[4]{1 + n\gamma_l}$

a is the spacing of transverse stiffeners (cm)

b is the width of stiffened plate (cm)

d_l is the ratio of the longitudinal stiffener cross sectional area to that of the main plate, $d_l = A_l/(bt)$, (cm)

A_l is the area of each longitudinal stiffener, $A_l = b_s t_s$

I_l is the second moment of area of each longitudinal stiffener. The code requires that the moment of inertia of stiffeners such as those used in steel piers be calculated about the surface of the stiffened plate on the stiffener side. The value of I_l is therefore given as $I_l = b_s^3 t_s/3$.

t_o is the minimum thickness of plate which is given as b/(28fn) for SS41 and b/(24fn) for SM50 plate. A more general expression for the allowable buckling ratio of compact sections using the allowable yield stress is given in Equation 4.

$$\frac{b}{t_o \cdot n \cdot f}\cdot\frac{\sqrt{F_y}}{1047.7} = 1.0 \qquad (4)$$

t_s is the thickness of each longitudinal stiffener

A further ratio, the **gamma* ratio** [2], γ_1/γ_1^*, is able to be used to predict whether local panel buckling or overall buckling of one side will occur first as shown in Figure 3. If $\gamma_1/\gamma_1^* > 1$ then local buckling of the panels between the longitudinal stiffeners is the expected initial buckling mode but if $\gamma_1/\gamma_1^* < 1$ then overall buckling of one side is expected. The value of γ_l^* is given in Equation 5.

$$\gamma_i = 4\alpha^2 n(1+n d_i) - \frac{(\alpha^2+1)^2}{n} \quad (\alpha \le \alpha_o)$$
$$= \frac{1}{n}\left[\{2n^2(1+n d_i)-1\}^2 - 1\right] \quad (\alpha > \alpha_o) \qquad (5)$$

Typical test setups are given for the applied lateral loading and shaking table testing at the laboratory facilities of the Public Works Research Institute in Figures 4 and 5. The levels of axial load, N, used were in all cases less than 11% of the yield axial load, N_y. The applied loading tests were carried out by controlling the displacement of the lateral loading ram. This displacement was later corrected to take account of the rotation at the base. Cyclic loading tests of larger specimens was performed at a frequency of 0.013 Hz while for the smaller specimens a frequency of about 0.33 Hz was used. In the shaking table testing, the shaking table was initially excited with sine-waves of different frequencies and low amplitudes to determine the elastic response period of the specimen on the table. Scaled versions of the acceleration record obtained at Hachiro-gata during the Nihon-kai-chubu earthquake of 26 May 1983 were used as the basic input ground motions. The time-axis was reduced to one-half of the actual time to adjust the predominant frequency of the records so that the relationship between the period and the response spectrum shape would be more like that expected for a real bridge pier.

The yield displacement, d_y, was defined as the displacement at which yielding first occurred in an extreme fibre of the section. The yield load, H_y, and yield displacement, d_y, were able to be calculated before the test started from the measured section properties and from the results of the material tests. The same loading regime, yield load, H_y, and yield displacement, d_y, were used in the concrete infilled specimens as in the hollow specimens in order to investigate the effect of the concrete infill. The ultimate displacement, d_u, was calculated as the point at which the backbone curve of the hysteresis diagram became less than the yield load, H_y. The backbone curve was constructed by connecting the points of maximum displacement in the cycle with the highest load for each displacement ductility. The ductility capacity, μ, was defined as the ultimate displacement, d_u, divided by the yield displacement, d_y.

SPECIMENS TESTED

The differences between the twenty two tests on steel specimens which were conducted at the Public Works Research Institute are described in summary form in Tables 1 and 2 where the section size, main plate thickness, size of longitudinal stiffeners, number of longitudinal stiffeners, lateral stiffener spacing and size, gamma ratio ($\gamma_1/\gamma_{1,req}$), panel slenderness ratio (b/nft), gamma* ratio (γ_1/γ_1^*), distance from the base of the specimen to the point of application of the load and to the level of concrete infill, the grade of the steel, the properties of the steel obtained from material tests, the specimen axial load ratio (N/N_y), the number of cycles of loading applied to each specimen as well as the calculated and actual periods of the specimens on the shaking table are given. The calculated yield strength and yield displacement are given in Table 3. The section properties for all of the specimens tested satisfied the current recommendations of the present Japanese code "Specifications for Highway Bridges" [1].

Specimens S1 to S12 had sections of the same size. Specimen S1 is shown in Figure 6. Specimen S2 was the same as Specimen S1 except that the weld size was 4.5mm rather than 3mm and Specimens S3 to S12 all had 3 to 4mm weld sizes. Specimens S1 and S3 to S9 had the same internal construction but were subject to different loading regimes. Specimens S3, S4, and S5 were tested on the shaking table with 2x, 3x and 4x the earthquake record magnitude while all other specimens of this size were subjected to applied lateral loading. Specimen S7 was the same as Specimen S6 except that the loading regime applied to Specimen S7 was of decreasing magnitude (1 cycle to μ = 5, 4, 3, 2 and 1). All other specimens in applied load tests were subjected to increasing displacement ductilities. Specimens S1, S6, S8, and S9 were subjected to 10, 1, 3 and 5 cycles to each displacement ductility respectively. Specimens S13 to S18 were larger specimens which were tested by applied lateral loading. Specimens S16 and S17 were partially filled with concrete and Specimen S17 was the same as Specimen S16 except that it had a "T"-shaped internal longitudinal stiffener. Specimens S19 to S22 were smaller specimens with the same internal steel construction. Specimens S20 and S22 were partially filled with concrete. Specimens S19 and S20 were tested by applied lateral loading and Specimens S21 and S22 were tested on the shaking table. Specimens S13 to S18 were larger specimens constructed from SM50 steel with a specified allowable yield stress of 1900kgf/cm^2 [1]. All other specimens were constructed from SS41 steel with a specified allowable yield stress of 1400kgf/cm^2 [1].

TEST RESULTS

Hysteretic Behaviour

Test results for all specimens showing the yield and maximum loads, specimen overstrength factor ($\phi_S = P_{max}/P_y$), yield and ultimate displacements, ductility ($\mu = d_u/d_y$) and mode of failure are given in Table 3. The hysteretic behaviour, strength, mode of failure and deformation capacity are described below.

The hysteretic behaviour of all hollow specimens subjected to applied lateral loading was similar. From the hysteresis loops of Specimen S1, shown in Figure 7, it may be seen that little energy was absorbed before the cycles to a displacement ductility, μ, of 2. At $\mu = 3$ the loop size increased and was fat showing that a large amount of energy was absorbed. Buckling was first observed during these cycles. A large amount of strength degradation was developed during the cycles to $\mu = 4$ as the buckling deformation of the plate increased. The strength continued to decrease after the defined failure point.

The concrete-filled specimens generally had stable hysteresis loops with a post-elastic stiffnesses of about 14% of the initial stiffness before fracture occurred. At this point there was a sudden loss of load carrying capacity as shown for Specimen S16 in Figure 8.

The behaviour of Specimen S5, which was subjected to shaking table testing with four times the Hachirogata record, is shown in Figure 9. This behaviour was typical of all of the specimens tested on the shaking table. The loop followed the shape of the backbone curve of the specimens tested by applied lateral loading. Yielding occurred almost entirely in one direction resulting in the energy absorbed being similar to that in a monotonic test. The maximum displacements observed were larger than those estimated by the equal energy assumption and there were large residual displacements at the top of these specimens at the end of the tests.

Effect of Loading Type

The curve shape and ductility capacity of Specimens S1, S8 and S9, which were obtained using regimes with 10, 3 and 5 cycles of loading to each displacement ductility respectively, had similar results as shown in Figure 10. The deformation capacity of Specimen S6, which was subjected to only 1 cycle of loading to each displacement ductility, had a greater ductility capacity. Dependence of ductility on the number of load cycles was smaller in these steel pier tests than in reinforced concrete piers [3]. The strength of the specimens on the shaking table dropped off more slowly than those tested by applied lateral loading because they were subjected to only a small amount of yield reversal. Specimen S7, which was subjected to decreasing displacement ductilities, did not fail but had a backbone curve similar to that of monotonically loaded specimens because the first cycle of loading determined this curve.

It would normally be expected that the number of cycles of loading would strongly influence the deformation capacity of members subjected to both axial load and cyclic loading because axial shortening occurs and increases the damage [4]. This axial shortening is proportional to the cumulative inelastic rotation within the region of yielding before buckling becomes severe [5]. The fact that there was little difference in the behaviour of the pier specimens which were subjected to between 3 and 10 load cycles to each ductility is thought to be because low levels of axial load were applied in these tests.

The behaviour of Specimens S1 and S2 were almost identical. The 3.0mm welds of Specimen S2 were strong enough to develop the full section strength but were insufficient to form a truly composite section. However, the welds remained together long enough to achieve the same ductility as that attained by Specimen S1 which had a 4.5mm weld.

There was a large difference between the monotonic type of hysteresis loop observed in the shaking table testing and the hysteresis loop from the applied loading tests. A research program is presently underway at the Public Works Research Institute to understand why very little reversal of yielding occurred in the shaking table tests by running dynamic analyses of piers with different bilinear stiffness factors.

Mode of Failure

1) Overall Buckling of One Side

Specimens with a gamma* ratio up to about 2.0 had a failure mechanism of overall buckling of one side after several load reversals. While the specimens with gamma* ratios less than 1.0 failed by pure overall buckling of one side, the specimens with gamma* ratios between 1.0 and 2.0 sustained buckling of the panels between the longitudinal stiffeners before the longitudinal stiffeners carried the load and overall buckling of one side caused strength loss. The maximum amplitude of buckling generally occurred mid-distance between the base of the specimen and the first lateral stiffener and the wavelength of the buckle was spread over the whole base panel. The web of the section also started to buckle as the longitudinal stiffeners twisted. Strength was rapidly lost during the later stages of buckling and finally the weld connecting the flange and

web together fractured. This mode of "overall buckling of one side" is shown for Specimen S1 in Figure 11 where Face 1 and Face 3 are the flanges. In the shaking table tests, in which yielding occurred predominantly in one direction, it was found that buckling generally became severe on only one side of the specimen.

While buckling was generally concentrated in the base section of most of the specimens there were cases where some buckling was also observed in the adjoining section. In Specimen S13 it was found that buckling was concentrated in the second section up from the base on one flange and on the opposite flange deformation in the two bottom sections caused twisting of the first lateral stiffener from the base. Buckling was observed in the adjoining section as well as the base section of Specimen S14 and also slightly in Specimens S1 and S19. Deformation in more than one section would be expected to increase the overall deformation capacity of these specimens.

2) Panel Buckling and Fracture

Limited panel buckling occurred in specimens with large gamma* ratios and fracture of the steel near the base of the specimens caused final failure. When the gamma* ratio is large the gamma ratio is also required to be high in order that the panel buckling limits are not violated. Therefore, local panel buckling will not generally occur until a large amount of inelastic strain has been sustained. The buckle wavelength was much smaller than when overall buckling of one side occurred. Fracture occurred in Specimen S11 at the centre of the buckle where the strain was concentrated and fracture near or in the weld at the base of both Specimens S11 and S12 was also observed. These types of fracture are very dependent on the strength of the weld, on the amount of welding residual stresses in the plate, the fracture strengths of the steel and the weld, and on any material discontinuities which may initiate fracture.

The concrete-filled specimens suffered little buckling and failed by fracture of the weld or of the steel beside the weld at the base. It seems as though the concrete cracked at the base of the specimen causing concentrated localised deformation in the steel plate beside the concrete crack which eventually resulted in fracture. This mode of behaviour is especially likely to occur if the uncracked section strength is considerably greater than the overstrength of the cracked section because only one crack will occur giving the behaviour shown in Figure 12. The use of the "T"-shaped longitudinal stiffener in Specimen S17 was of no benefit as the mode of failure of concrete-filled specimens was fracture near the base rather than buckling. It seems as though filling the specimens with concrete to 1/3 of their height was satisfactory to ensure that the major amount of the deformation occurred at the base rather than above the level of concrete infill.

Strength

The specimen overstrength, ϕ_s, which was calculated as the ultimate specimen strength, P_{max}, divided by the initially calculated strength, P_y, ranged from 1.27 to 2.14 times as shown in Table 3. The increase in the strength of the hollow specimens above the yield strength was thought to occur for the following reasons: the section stresses may be more like that assumed by plastic behaviour in which all the fibres in the section are at yield, strain hardening increases the strength, and the axial load on the section will allow even larger overstrength values to be obtained [5]. The strength of concrete-filled specimens were 1.26 and 1.34 times greater than that of the identical hollow specimens because the concrete also resisted load. The average overstrength values were 43% and 84% for hollow and concrete-filled specimens respectively.

Lay [6] has proposed an empirical method, based on the results of experiments on steel beams, to estimate the maximum strength of a steel member, P_{max}, as a function of the material overstrength, $\phi_{om} = \sigma_{max}/\sigma_y$, and plastic load, P_p, as $P_{max} = (\phi_m + 1)/2.P_p$ where $P_p = S/Z.P_y$ and S and Z are the plastic and elastic section modulii respectively. When this method was used on Specimen S13 it was found that the ratio of the plastic strength to the yield strength, P_p/P_y, considering the effect of axial load was 1.155 and the maximum stress, σ_{max}, divided by the yield stress, σ_y, of the steel material used in this specimen was 1.43. The predicted strength was therefore $(1.43 + 1)/2 \times 1.155P_y = 1.40P_y$ which was close to the actual strength of $1.38P_y$. It may be seen in Figure 13 that this method estimated the strengths of the specimens to ±10%. The strengths of Specimens S1 to S5 were not included in this figure because it was considered that there were some gross errors in the material tests for these specimens. The maximum strengths of Specimens S1 to S5 were even greater than $\phi_{om}P_p$. The slenderness of the sections did not seem to effect the maximum strengths because these members were compact.

Deformation Capacity

The ductility capacity was generally greater in the more compact sections than in those with more slender characteristics as may be seen from the results of Specimens S13, S14, S15 and S18, in which the ductilities were 4.21, 3.05, 3.99 and 3.13, as well as Specimens S10, S11 and S12, in which the ductilities were 3.34, 4.11 and 4.31. However, the ductility of Specimen S1, which was 4.33, was higher than for Specimens S10, S11, and S12. This is possibly because some buckling occurred in the section above the base as well as in the base section in this specimen.

The specimens tested on the shaking table had large maximum displacement and ductility capacities because they were subjected to little reversal of loading and their behaviour was almost monotonic. Similarly, the ductility capacity of Specimen S6 of 5.04 was larger than that of Specimens S1 of 4.33, S2 of 4.02, S8 of 3.67 and S9 of 3.81 as a result of it only being subjected to one cycle of loading at each ductility step.

Placing concrete inside these specimens did not increase the ductility capacity due to the difference in the mode of failure. The ductility capacity of the Specimen S16, which was filled with concrete was 10% less that of Specimen S15 which was identical but hollow. Similarly the ductility capacity of Specimen S20, which was filled with concrete was 23% less that of Specimen S19.

The backbone curves of specimens tested with 10 cycles of applied loading to each ductility are given in Figure 14. It may be seen that the ductility capacities of these specimens, calculated from the point when the backbone curve became less than the yield strength, ranged between 3 and 5. A method for predicting the deformation capacity of steel specimens has also been produced from the testing described herein which considers the maximum strain in an equivalent plastic hinge length and the resistance against buckling [7].

SUMMARY

The results of 22 tests on hollow and concrete-filled steel specimens with different configurations of internal steel using applied lateral loading and shaking table testing were described in this paper. The major findings are given below:

1) The ductilities of the specimens tested with between 3 and 10 cycles of loading to each displacement step ranged from 3.67 to 4.33. These ductilities increased with the number of cycles of loading. However the specimen subjected to one cycle of loading to each displacement step and the specimen tested on the shaking table had increased ductilities of 5.09 and 12.9 respectively.
2) The specimens tested on a shaking table sustained little reversal of yielding. Their load history was therefore different from the assumed lateral loading regime in the applied lateral load tests.
3) The final mode of buckling of specimens with a gamma* ratio less than about 2.0 was overall buckling of one side. The major buckling deformation in these specimens generally occurred midway between the base and the first lateral stiffener.
4) Severe local panel buckling and fracture were observed in specimens with a gamma* ratio greater than 2.0.
5) Concrete infill increased the strength and decreased the deformation capacity of specimens in these tests.
6) The maximum strengths of the compact hollow sections could be estimated satisfactorily without considering the effects of section slenderness.
7) The ductility capacities of specimens tested by applied lateral loading ranged from about 3 to 5.
8) The displacement ductility capacity generally decreased for members with greater section slendernesses.

REFERENCES

1. Japan Road Association, "Specifications for Highway Bridges", Part II : Steel Bridges, English Edition, 1987.
2. Subcommittee on Stability Design, "Guidelines for the Stability of Steel Structures", edited by Fukumoto Y, Committee on Steel Structures, Japan Society of Civil Engineers, 1987.
3. Kawashima K. and Koyama T., "Effect of Number of Cycles of Loading Cycles on Dynamic Characteristics of Reinforced Concrete Bridge Piers", Proc. JSCE, Structural Eng., Earthquake Eng., Vol. 15, No. 1, 1988.
4. Popov E. P., Bertero V. V. and Chandramoulli S., "Hysteretic Behaviour of Steel Columns", UCB/EERC 75-11, September 1975.
5. MacRae G. A., Carr A. J. and Walpole W. R., "The Seismic Response of Steel Frames", Research Report 90-06, Department of Civil Engineering, University of Canterbury, 1990.
6. Lay M. G., "Flange Local Buckling in Wide-Flange Shapes", *Journal of the Structural Division*, ASCE, ST6, December 1965, p95-116.
7. MacRae G. A. and Kawashima K., "Estimation of the Deformation Capacity of Steel Bridge Piers", US-Japan Workshop on Cyclic Buckling of Steel Structures and Structural Elements under Dynamic Loading Conditions, Osaka, 1-3 July 1991.

Table 1. Pier Characteristics (a)

Pier	Section Size (mm) b+2t	b	Plate Thick. t (mm)	Longitudinal Stiffeners Size (mm²)	No. n-1	Lateral Stiffener Spacing (mm)	Size (mm²)	Gamma Ratio >1.0	b/Ey tfn <1047	Gamma' Ratio
S1	409 x 400		4.5	35x3.2	3	350	65x3.2	1.659	831	0.950
S2	409 x 400		4.5	35x3.2	3	350	65x3.2	1.659	831	0.950
S3	409 x 400		4.5	35x3.2	3	350	65x3.2	1.659	831	0.950
S4	409 x 400		4.5	35x3.2	3	350	65x3.2	1.659	831	0.950
S5	409 x 400		4.5	35x3.2	3	350	65x3.2	1.659	831	0.950
S6	409 x 400		4.5	35x3.2	3	350	65x3.2	1.659	831	0.950
S7	409 x 400		4.5	35x3.2	3	350	65x3.2	1.659	831	0.950
S8	409 x 400		4.5	35x3.2	3	350	65x3.2	1.659	831	0.950
S9	409 x 400		4.5	35x3.2	3	350	65x3.2	1.659	831	0.950
S10	409 x 400		4.5	40x3.2	3	350	65x3.2	2.259	831	1.38
S11	409 x 400		4.5	50x3.2	3	350	65x3.2	4.155	831	2.64
S12	409 x 400		4.5	50x10.	3	350	65x3.2	8.110	831	5.01
S13	800 x 820		10.	64x6.0	5	300	112x4.5	8.409	580	1.746
S14	800 x 820		10.	64x6.0	5	660	112x4.5	1.127	580	0.294
S15	800 x 820		10.	64x6.0	5	390	112x4.5	3.583	580	1.017
S16	800 x 820		10.	64x6.0	5	390	112x4.5	>3.583	580	1.017
S17	800 x 820		10.	64x6.0	5T	390	112x4.5	>3.583	580	1.017
S18	800 x 820		10.	64x6.0	4	390	112x4.5	3.117	699	1.290
S19	329 x 320		4.5	30x3.2	3	260	50x32	2.299	666	0.854
S20	329 x 320		4.5	30x3.2	3	260	50x32	>2.299	666	
S21	329 x 320		4.5	30x3.2	3	260	50x32	2.299	666	0.854
S22	329 x 320		4.5	30x3.2	3	260	50x32	>2.299	666	

Table 2. Pier Characteristics (b)

Pier	Height to Load (m)	Height of Concrete (m)	Steel Strength Grade	Youngs Modulus (x10⁶ kgf/cm²)	Yield Stress (kgf/cm²)	Material Over-strength ϕ_{om}	Axial Load (tf)	Axial Load Ratio	Load Cycles	Calculated Period (sec)	Actual Period (secs)
S1	2.40	-	SS41	1.321	2133	1.045	20	0.110	10	-	-
S2	2.40	-	SS41	1.321	2133	1.045	20	0.110	10	-	-
S3	2.40	-	SS41	1.321	2133	1.045	20	0.110	x2H	.422	.490
S4	2.40	-	SS41	1.321	2133	1.045	20	0.110	x3H	.422	.481
S5	2.40	-	SS41	1.321	2133	1.045	20	0.110	x4H	.422	.476
S6	2.40	-	SS41	1.736	2089	1.349	20	0.083	1	-	-
S7	2.40	-	SS41	1.736	2089	1.349	20	0.083	1 (decr)	-	-
S8	2.40	-	SS41	1.848	2977	1.318	20	0.079	3	-	-
S9	2.40	-	SS41	1.848	2977	1.318	20	0.079	5	-	-
S10	2.40	-	SS41	1.736	2089	1.349	20	0.083	10	-	-
S11	2.40	-	SS41	1.736	2089	1.349	20	0.078	10	-	-
S12	2.40	-	SS41	1.736	2089	1.349	20	0.054	10	-	-
S13	6.00	-	SM50	1.729	3845	1.432	105	0.092	10	-	-
S14	6.00	-	SM50	1.729	3845	1.432	105	0.092	10	-	-
S15	6.00	-	SM50	1.729	3845	1.432	105	0.092	10	-	-
S16	6.00	2.00	SM50	1.729	3845	1.432	105	0.092	10	-	-
S17	6.00	2.00	SM50	1.729	3845	1.432	105	0.092	10	-	-
S18	6.00	-	SM50	1.729	3845	1.432	105	0.092	10	-	-
S19	2.40	-	SS41	1.591	2418	1.54	20	0.078	10	-	-
S20	2.40	0.78	SS41	1.591	2418	1.54	20	0.078	10	-	-
S21	2.40	-	SS41	1.591	2418	1.54	20	0.078	3&3.5H	0.46	0.500
S22	2.40	0.78	SS41	1.591	2418	1.54	20	0.078	3&3.5H	0.46	0.454

Table 3. Calculated and Experimental Loads and Displacements

Pier	Calculated Yield Load P_y (tf)	Maximum Load P_{max} (tf)	Specimen Overstrength ϕ_s	Calculated Yield Displ. d_y (mm)	Maximum Displ. d_u (mm)	Ductility d_u/d_y μ	Mode of Failure
S1	8.6	13.8	1.60	13.5	56.5	4.93	Buckling
S2	8.6	14.2	1.65	13.5	54.3	4.02	Buckling
S3	8.6	-	-	13.5	-	-	No failure
S4	8.6	-	-	13.5	-	-	No failure
S5	8.6	15.9	1.85	13.5	173.5	12.9	Buckling
S6	11.7	16.5	1.41	13.9	70.0	5.04	Buckling
S7	11.7	16.9	1.44	13.9	-	-	Buckling
S8	12.4	17.3	1.40	13.9	61.0	3.67	Buckling
S9	12.4	17.1	1.38	13.9	53.0	3.81	Buckling
S10	12.4	15.0	1.27	13.9	46.7	3.34	Buckling
S11	12.4	17.2	1.41	13.9	57.5	4.11	Buckling-Base Weld Failure
S12	12.4	23.7	1.43	13.9	62.1	4.31	Base Weld Failure
S13	59.4	81.7	1.38	62.1	261.3	4.21	Buckling
S14	59.4	79.1	1.33	62.1	189.2	3.05	Buckling
S15	59.4	80.0	1.35	62.1	247.7	3.99	Buckling
S16	59.4	100.0	1.69	62.1	221.9	3.57	Base Weld Failure
S17	59.4	101.0	1.70	62.1	222.1	3.57	Base Weld Failure
S18	59.4	76.1	1.33	62.0	194.2	3.13	Buckling
S19	6.5	10.4	1.60	16.3	85.1	5.19	Buckling
S20	6.5	13.9	2.14	16.3	65.3	3.98	Base Weld Failure
S21	6.5	12.4	-	16.3	116.	-	Buckling
S22	6.5	14.5	-	16.3	88.	-	Base and Side Weld Failure

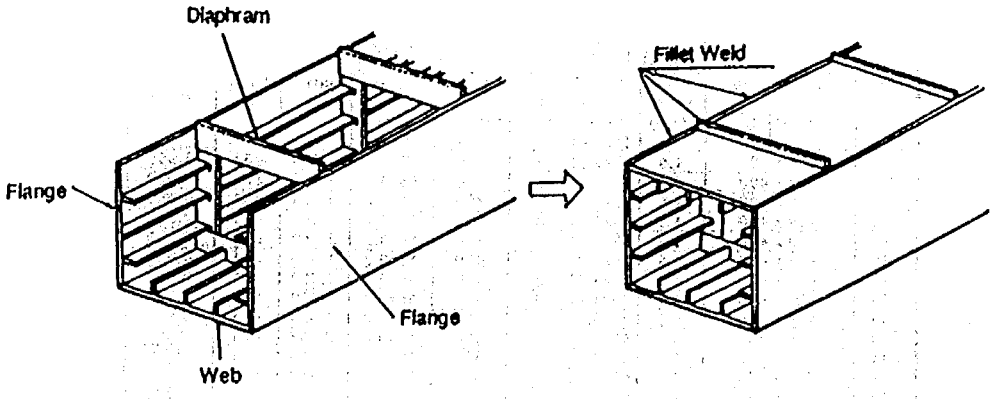

Figure 1 - Pier Construction

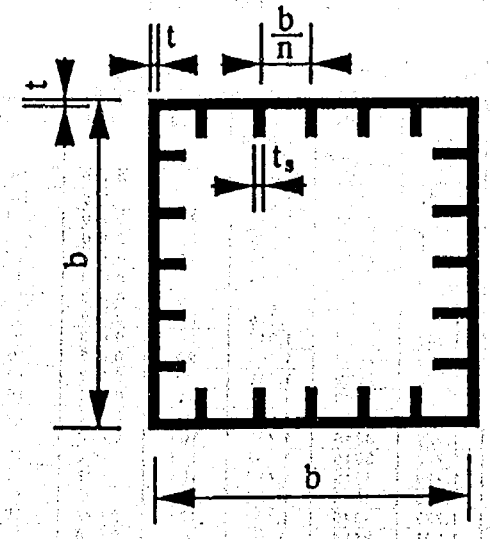

Figure 2 - Section Dimensions

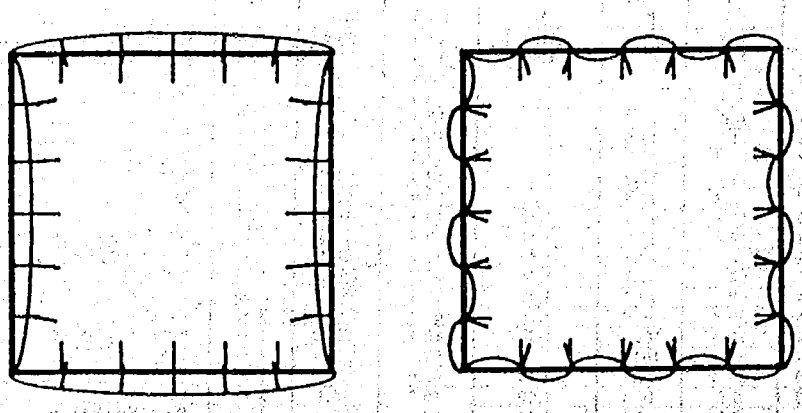

(a) Overall buckling of One Side

(b) Local Panel Buckling

Figure 3 - Modes of Deformation

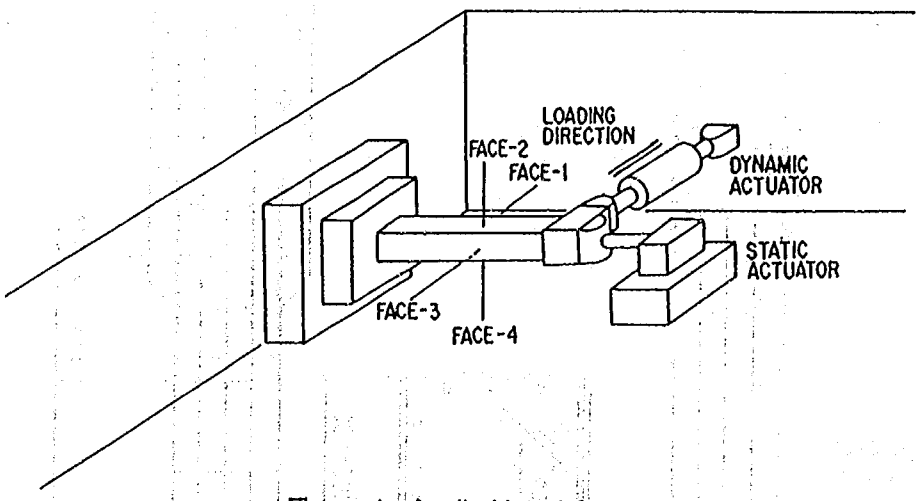

Figure 4 - Applied Load Setup

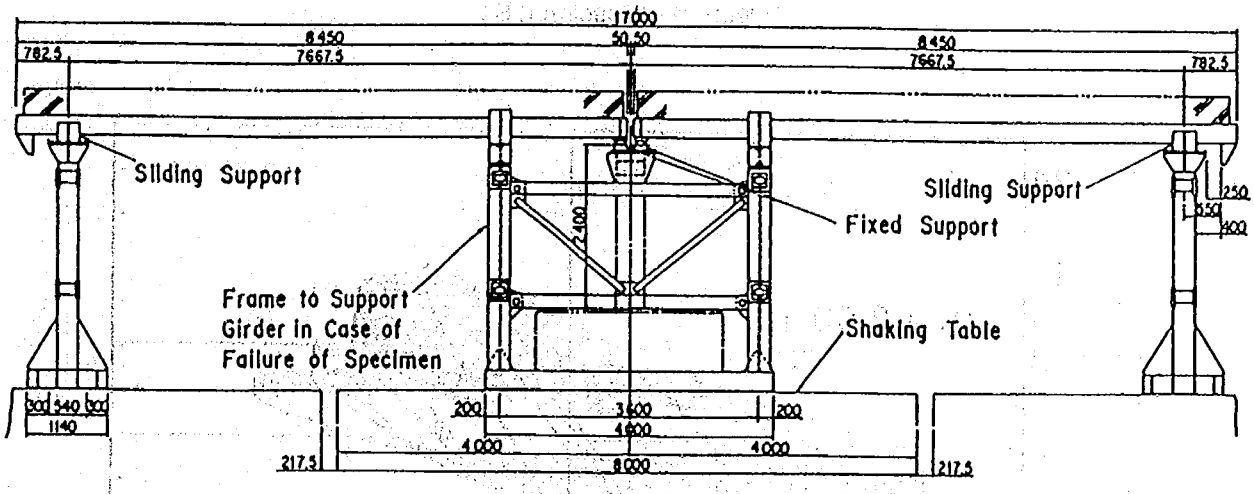

Figure 5 - Shaking Table Setup

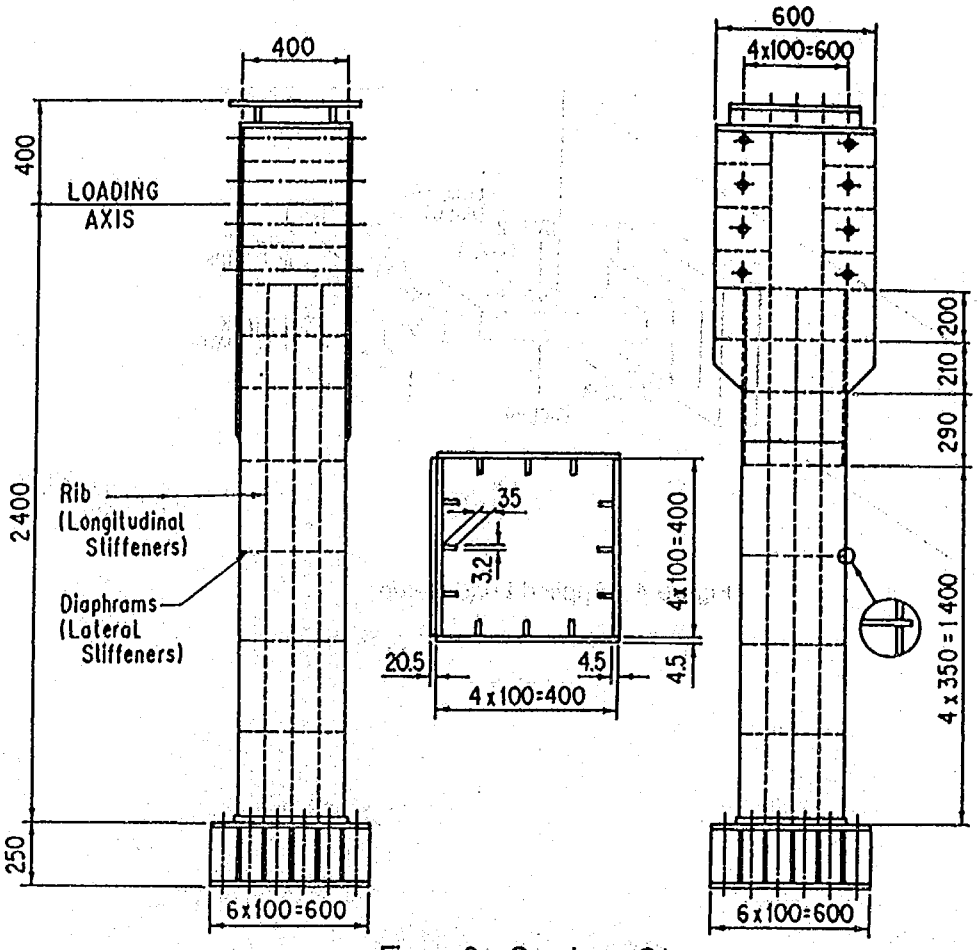

Figure 6 - Specimen S1

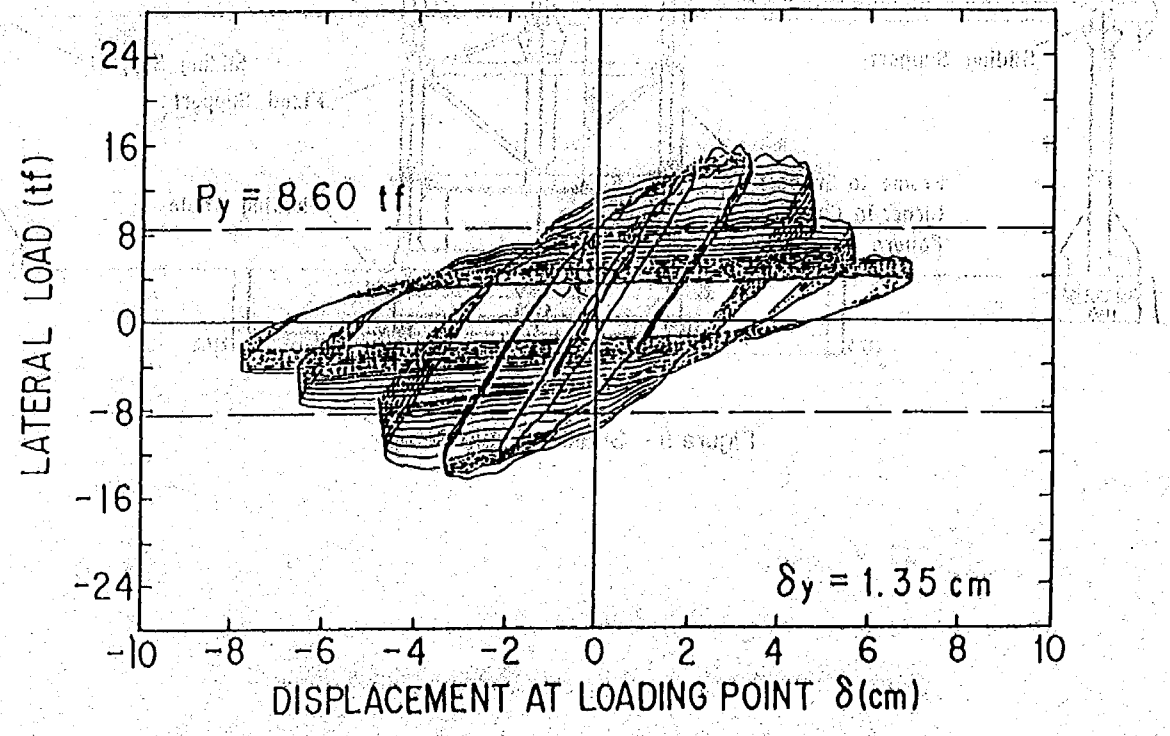

Figure 7 - Hollow Specimen Hysteresis Curve - Specimen S1

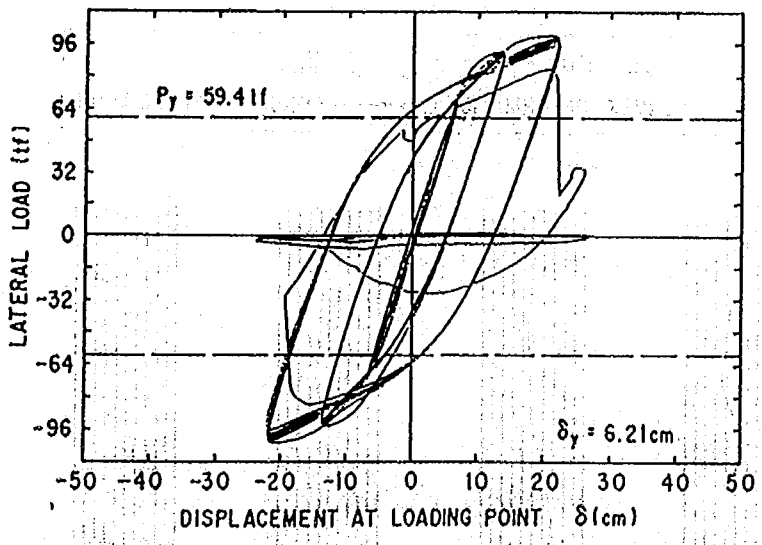

Figure 8 - Concrete-Filled Specimen Hysteresis Curve - Specimen S16

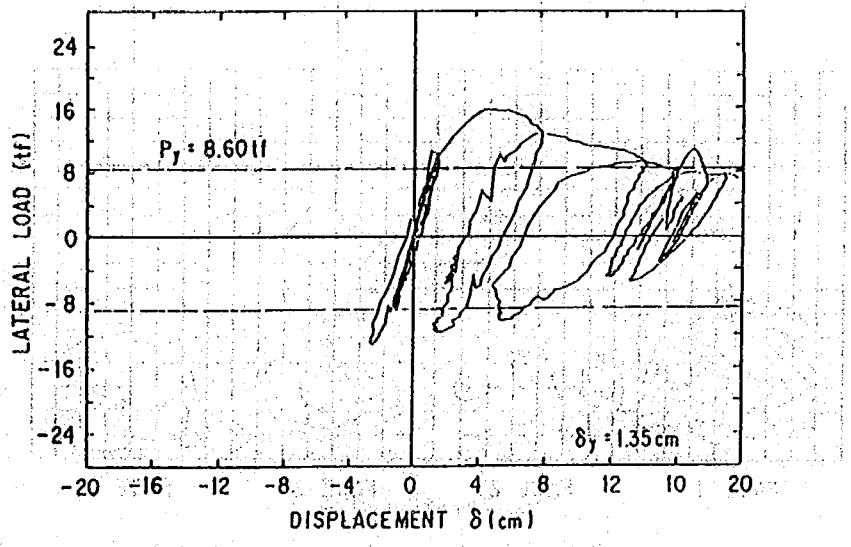

Figure 9 - Hysteresis Loop of Specimen on the Shaking Table - Specimen S5

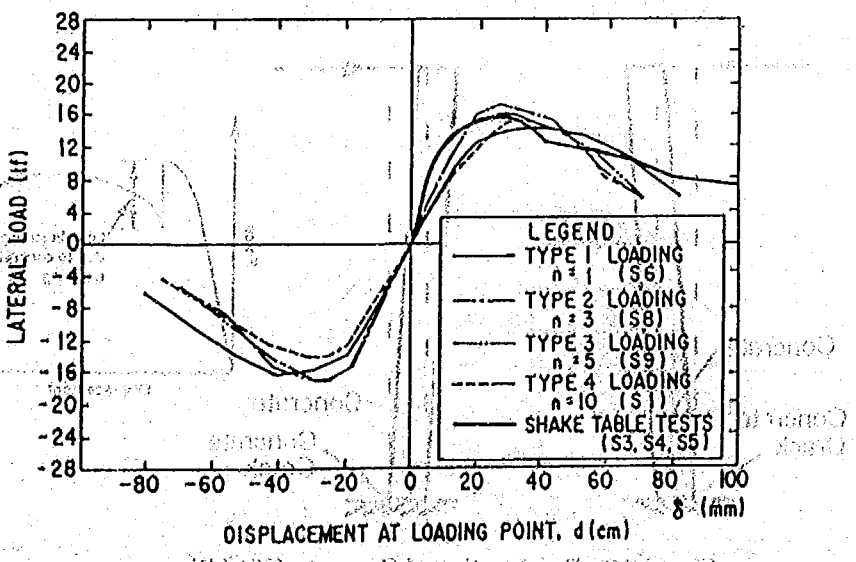

Figure 10 - Backbone Curve of Specimens S1, S6, S8, S9 and Shaking Table Tests

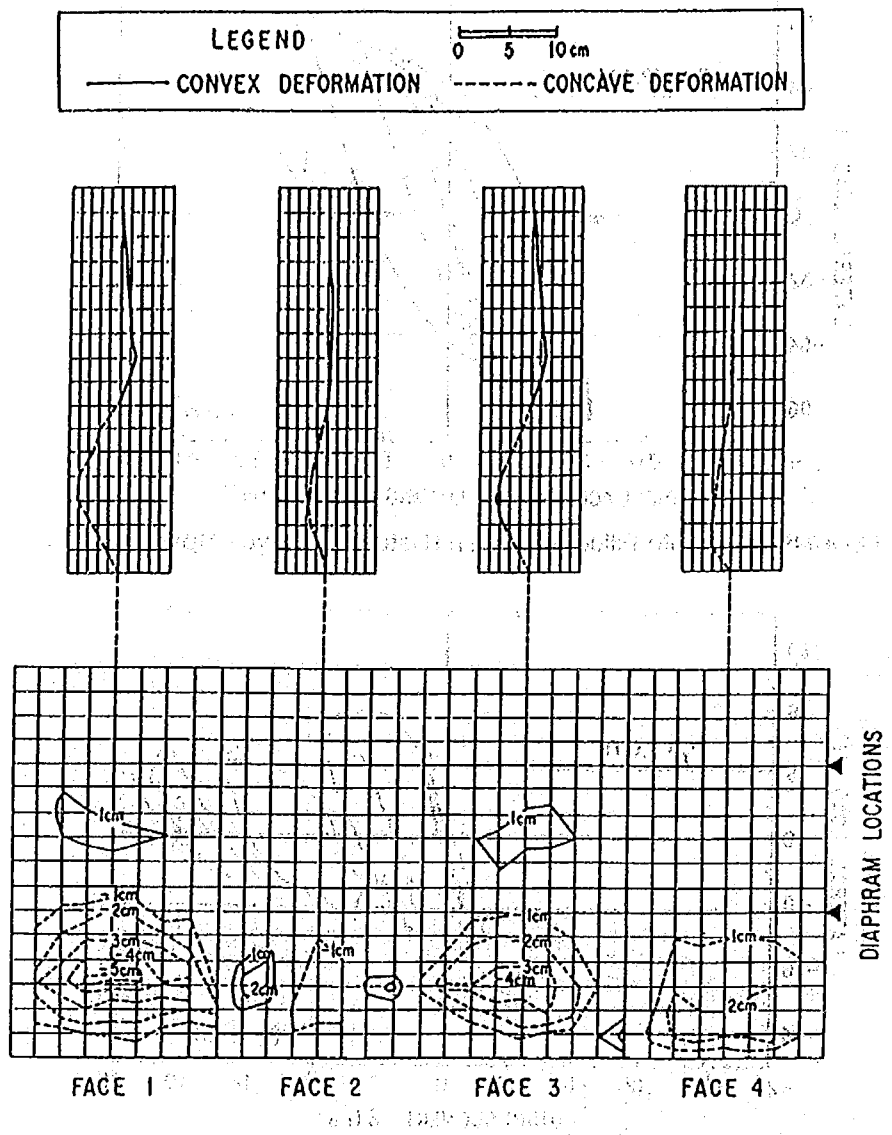

Figure 11 - Buckling of Specimen S1 at the End of the Test

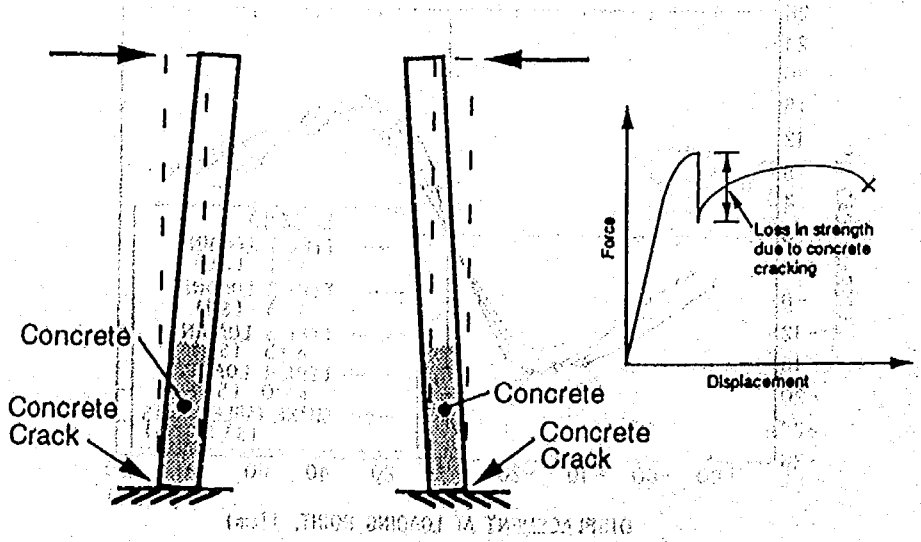

Figure 12 - Deformation of Concrete-Filled Piers

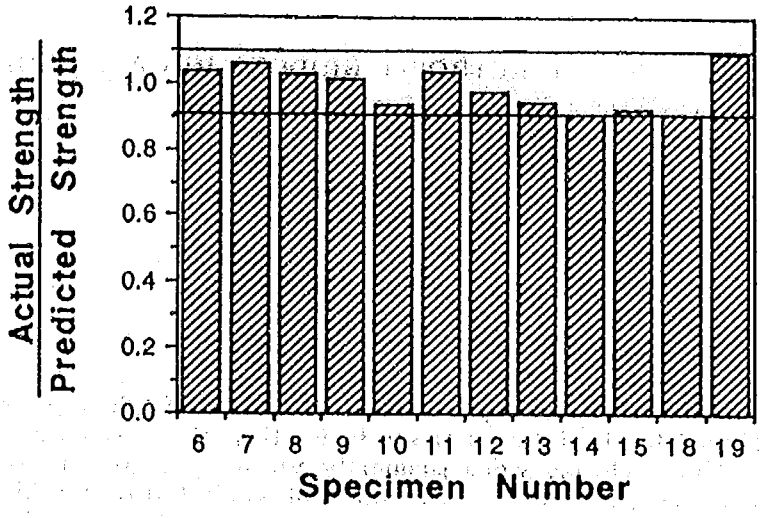

Figure 13 - Comparison of Overstrengths

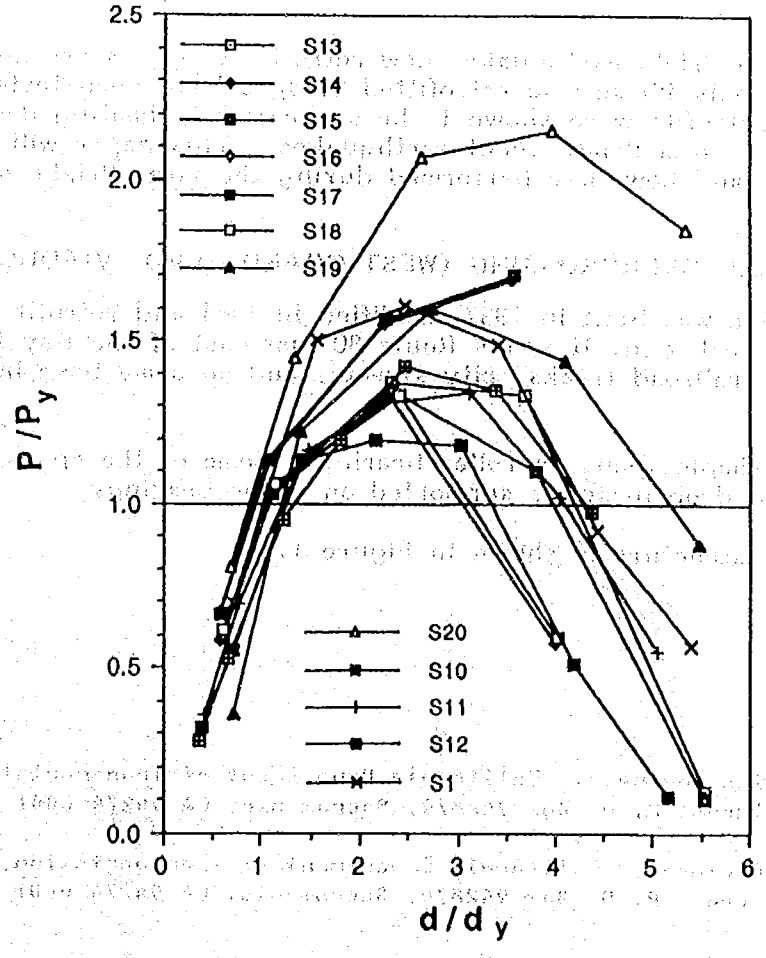

Figure 14 - Comparison of Specimen Backbone Curves

PERFORMANCE OF RETROFIT BRIDGES IN CALIFORNIA

BY

James Gates 1
Mark Yashinsky 2

INTRODUCTION

The California Department of Transportation, (CALTRANS) has pursued a seismic retrofit program since the 1971 San Fernando Earthquake. Damage from that earthquake showed that bridges were primarily vulnerable to collapse from their joints pulling apart. To prevent reoccurrence of such failures CALTRANS began a major seismic retrofit program for bridges. Structures were selected for retrofitting after examining the 13,000 bridge inventory for poor expansion joint details such as narrow seats and weak bearings. Since then, 1261 bridges have been retrofit at a cost of 54.2 million dollars. This is what was called the Phase One Retrofit Program. It was concerned with limiting movement of the superstructure.

Phase Two retrofits began in response to the 1987 Whittier Earthquake which emphasized that bridges were also susceptible to earthquake damage to nonductile columns.

As a result of the Loma Prieta earthquake, new retrofit strategies are being developed. However, only Phase One retrofitted bridges have been tested by earthquakes. These retrofits were shown to be successful in limiting damage and saving lives during the Loma Prieta event earthquakes. This paper will examine four of these retrofits and how they performed during the Loma Prieta earthquake.

THE PORT OF OAKLAND OVERCROSSING (WEST GRAND BLVD. VIADUCT)

This steel girder bridge was built in 1937, modified in 1964 and retrofit in 1976. The structure is 5445 feet long. It spans Route 80 just east of the Bay Bridge toll plaza and also crosses railroad tracks, city streets, and an army base in the City of Oakland.

The bridge is mostly simple spans on roller bearings. Some of the spans consist of cantilever girders with drop in spans supported on roller bearings.

A General Plan of the structure is shown in Figure 1.

1 Structural Mechanics Engineer, California Department of Transportation, Division of Structures, P. O. Box 942874, Sacramento, CA 94274-0001

2 Associate Bridge Engineer, California Department of Transportation, Division of Structures, P. O. Box 942874, Sacramento, CA 94274-0001

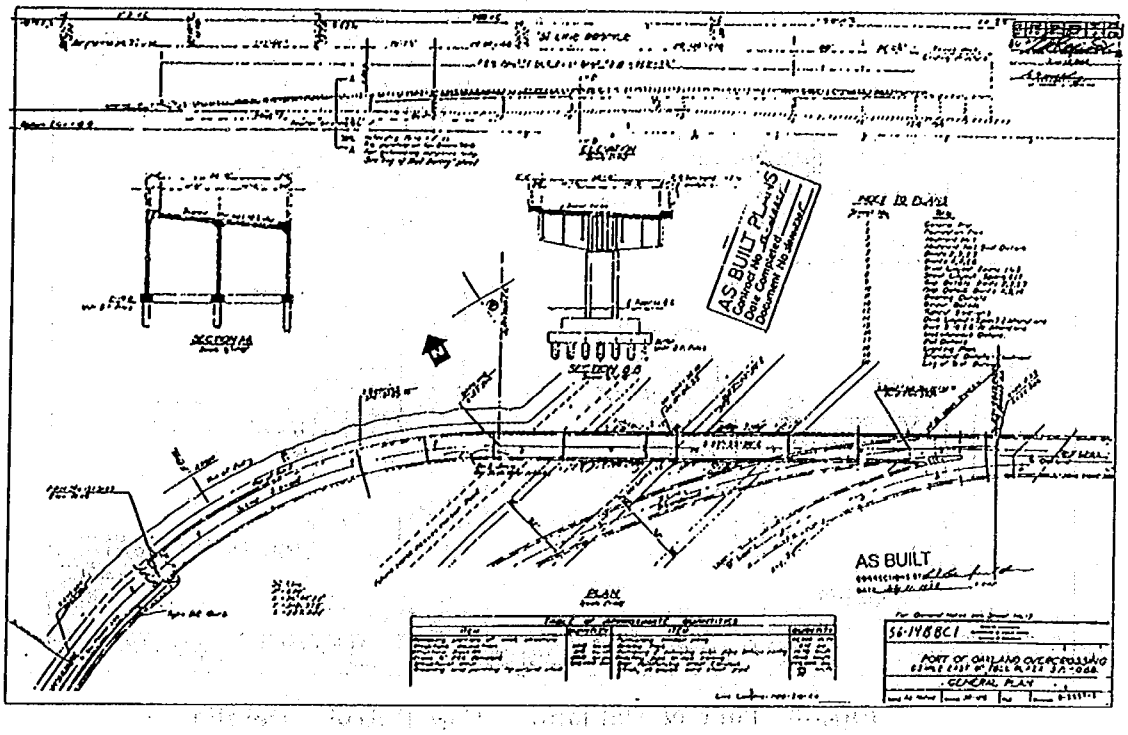

Fig. 1 Port of Oakland Overcrossing - General Plan

This bridge was seismically retrofitted in 1976. The retrofit consisted of longitudinal restrainers at each joint connected by steel brackets to the bottom girder flange or web on each side of the web.

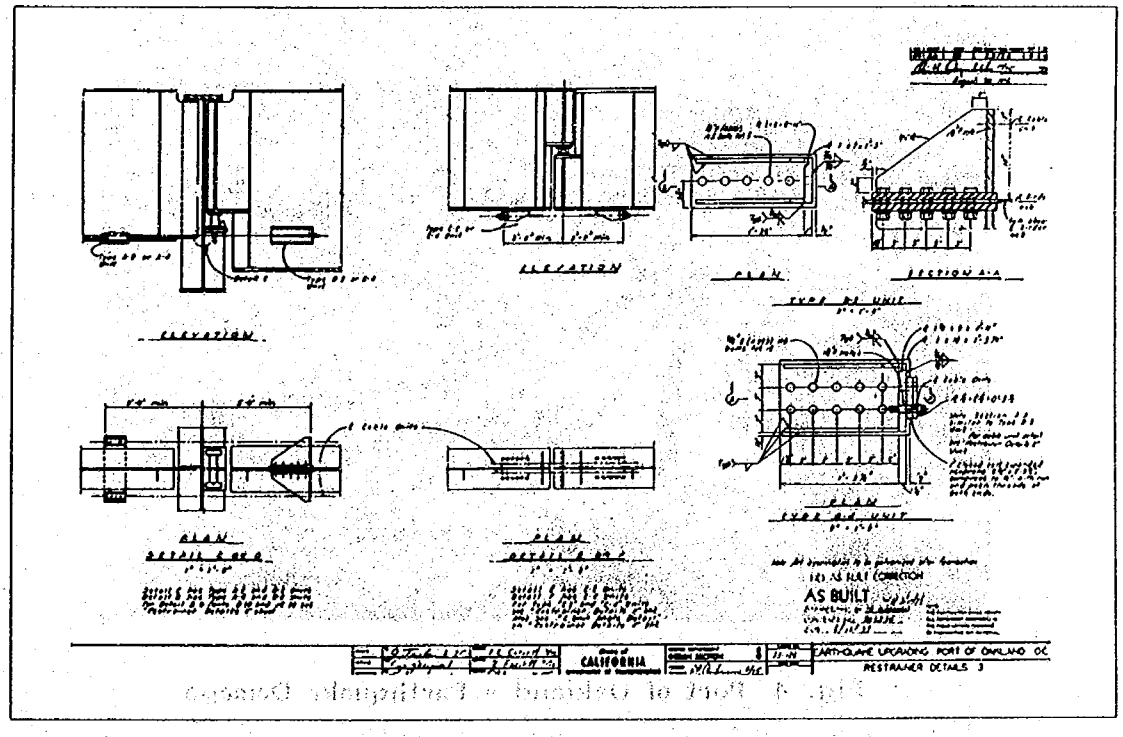

Fig. 2 Port of Oakland - Seismic Retrofit Details

At a couple of locations the bent cap was widened to provide a seat to catch the girder ends.

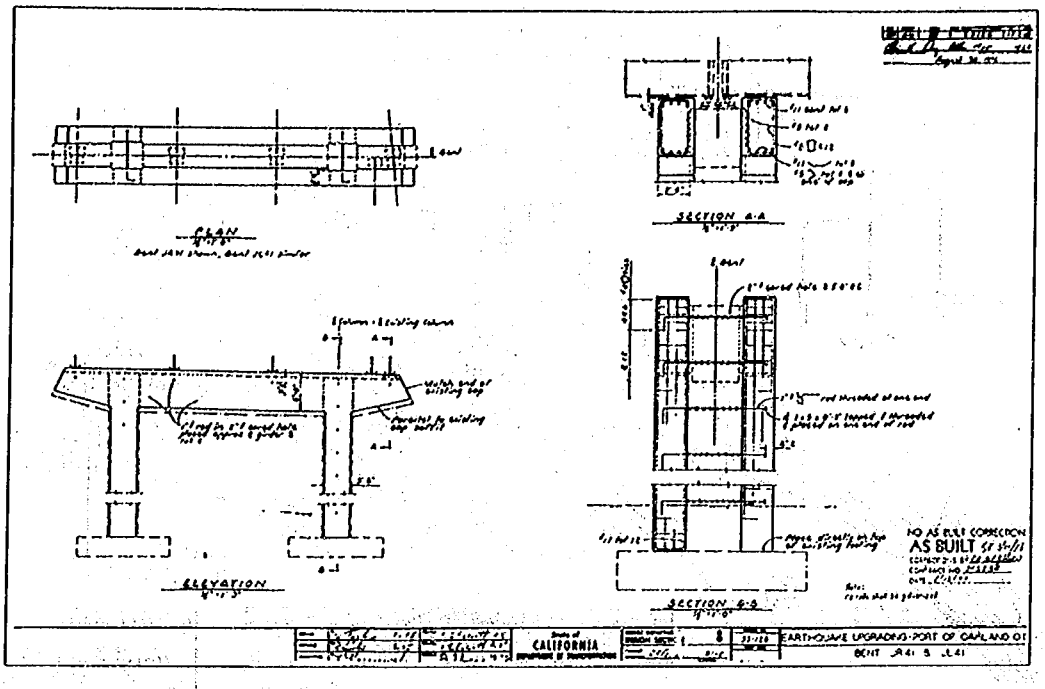

Fig. 3 Port of Oakland - Cap Retrofit Details

Although this bridge is about 80 miles north of the epicenter of the Loma Prieta Earthquake, the soft sediments of this area seem to have accentuated shaking of this bridge.

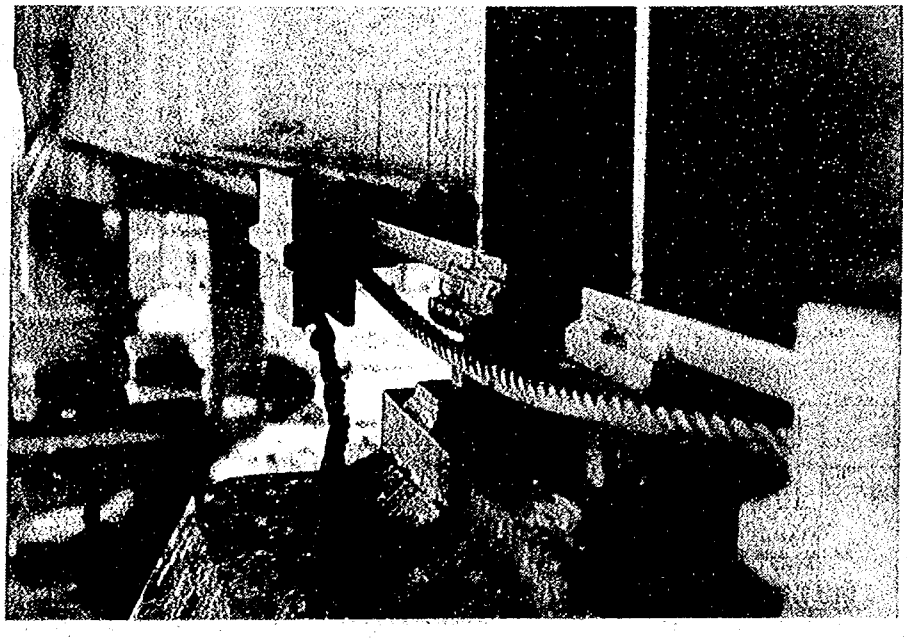

Fig. 4 Port of Oakland - Earthquake Damage

We estimate a maximum ground acceleration for the area of about 0.30g. However, cable restrainers were routinely designed for 0.25g in the mid 70's. During the earthquake the girders moved diagonally up to 14 inches with most anchor bolts and keeper plates broken, buckled cross-bracing, and most cable restrainers broken or overstressed.

The bridge was closed to traffic for several weeks, although it could have been used for emergency traffic. Considering the soft soil conditions in this area and the tremendous damage to nearby structures this retrofit appears to be a success. The restrainers were all activated, absorbing energy and holding the structure together.

EAST BAY BRIDGE (SAN FRANCISCO-OAKLAND BAY BRIDGE)

We are all aware of the fallen span at Pier E9 during the Loma Prieta Earthquake. However, an elegant retrofit strategy prevented considerably more damage at Piers E17 through E22 at the east end of the bridge. At these piers the East Bay Bridge is a series of steel trusses on alternating pin and rocker supports.

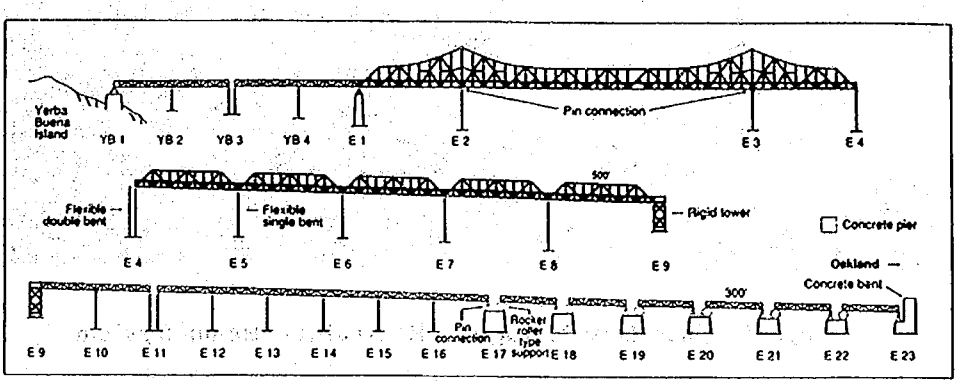

Fig. 5 East Bay Bridge

The bridge was built in 1936 and retrofitted in 1976. The portion of the retrofit discussed here are the steel restrainer beams that were installed at piers E17 to E22.

Fig. 6 East Bay Bridge - Pier E17

The trusses at this end of the bridge rest on shoes that are bolted to the concrete piers at one end of the truss and are free to move longitudinally on the piers at the other end of the truss. The retrofit consists of steel restrainer beams located 4" east of the free shoes allowing the span to move 4" to the east before coming in contact with the 24 W 68 beam. The beams are connected to the piers by steel anchor fixtures. The attachment is made with 4-1" bolts at each end of the beam. Elastomeric pads cushion the bolt forces at the anchorage. (see Fig. 5).

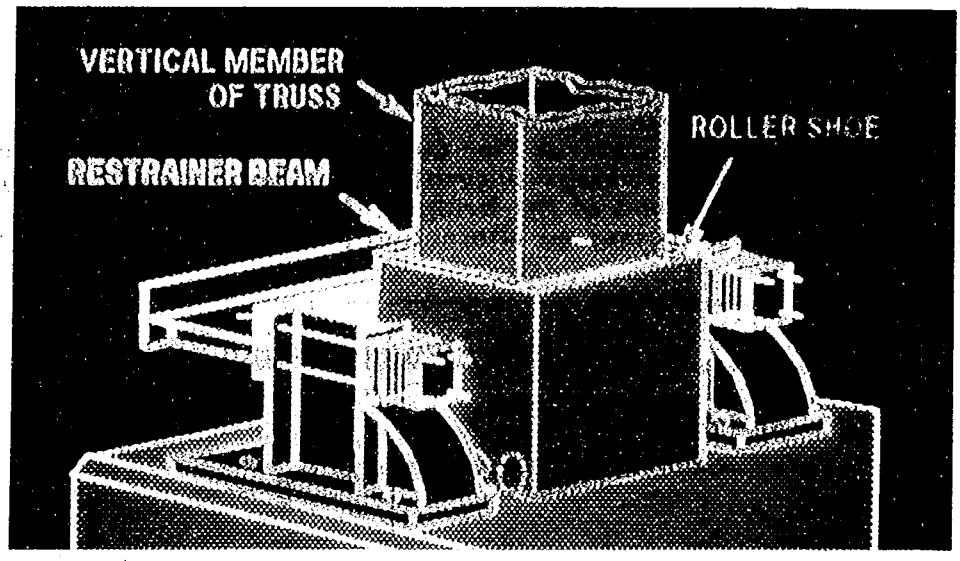

Fig. 7 East Bay Bridge - Restrainer Beam System

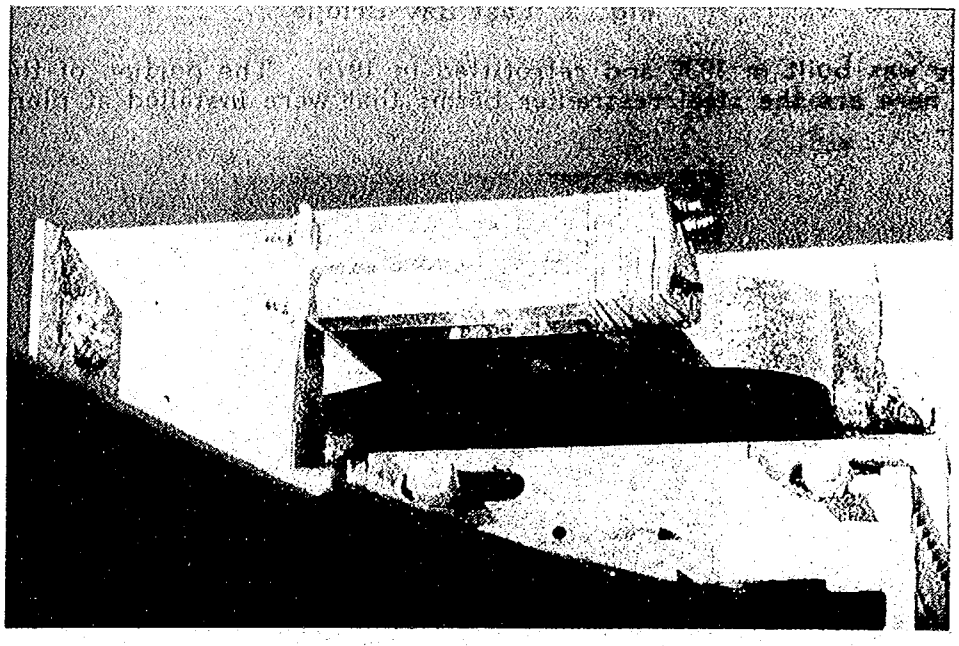

Fig. 8 East Bay Bridge - Restrainer After Earthquake

During the Loma Prieta Earthquake the north and south fixed shoes at piers E18 to E22 moved, shearing off the 24 one inch bolts that held each of them to their supports. Keeper plates prevented movement in the transverse direction. The steel restrainer beams at the free shoes prevented movement beyond four and a half inches to the east. The shoes moved back and forth about 10 inches and came to rest about 5 inches west of their original position.

The repair of damage at these locations was simple. The trusses were first jacked back into place. The damaged restrainer beams were then removed. New beams were then attached at the anchorages with new high strength bolts.

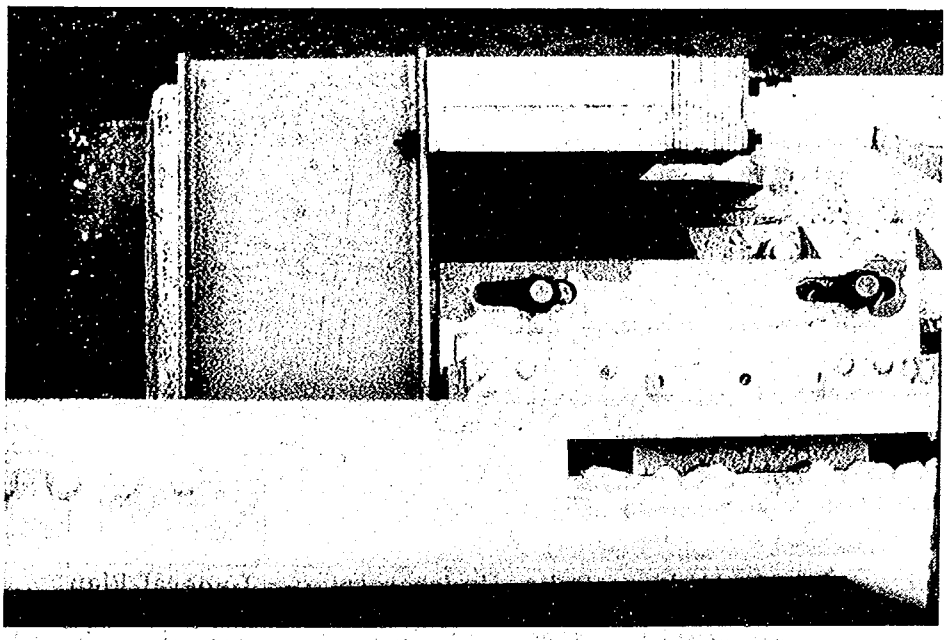

Fig. 9 East Bay Bridge - Repaired Restrainer

This was a clean and effective retrofit design. The use of elastomeric pads cushioned and protected the bridge from large impact forces during the earthquake allowing only minor damage that was easy to repair. The restrainer units were designed to consider the load paths and were economical to replace. The support assemblies were undamaged.

MADRONE DRIVE UNDERCROSSING

Madrone Drive U.C. is located south of San Francisco on State Route 17 in Santa Cruz County. It was built in 1938. It is a three span reinforced concrete T-beam bridge about 134 feet long with a steel mesh and gunite soffit. It has a hinge with a 5 inch seat in each end span. The superstructure sits on unstable rockers at the abutments. It has a 20 degree skew. There is no transverse restraint. This bridge was a perfect candidate for retrofitting. It could easily fall off its hinge or abutment seats during an earthquake.

This bridge is located approximately 8 miles north of the epicenter of the Loma Prieta Earthquake. We estimate ground accelerations at the site were approximately 0.65g. The motion during the earthquake was strongly transverse. All of the retrofitted interior shear keys were severely damaged.

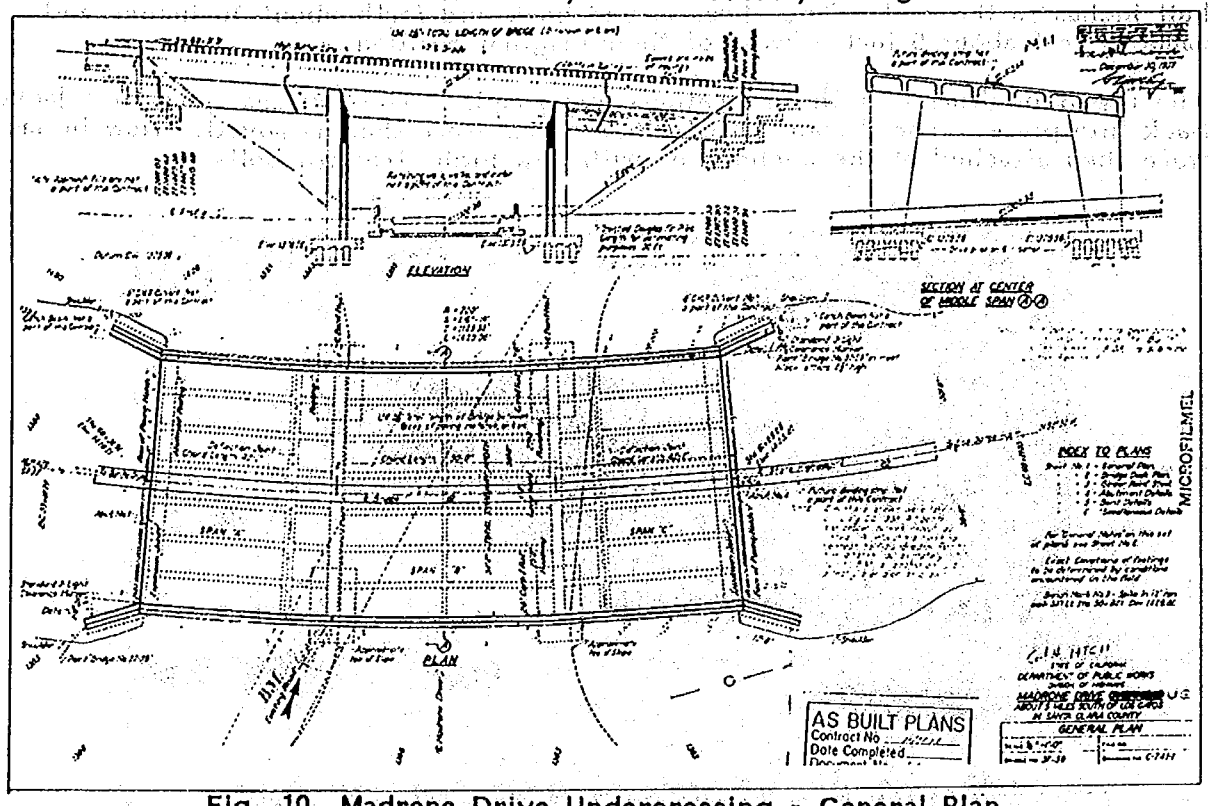

Fig. 10 Madrone Drive Undercrossing - General Plan

Madrone Drive was retrofitted in 1985. The retrofit consisted of the addition of four reinforced concrete bearing seats at each abutment and two cable loop restrainers at each hinge. Two of these bearing seats act as shear keys restraining the superstructure longitudinally and transversely. The loop restrainers were installed through 3 inch holes in the first interior T-beam webs on both sides of the hinge. Turnbuckles were installed on each side of the web which were torqued to 20 ft-lbs, then backed off 1-1/2 turns to permit thermal movements.

Deep cracks, large spalls, and exposed reinforcement were much in evidence. The structure still remained well contained by the keys. There is no doubt that the retrofit prevented a catastrophic failure of the end spans and permitted the structure to be used to carry traffic on this vital corridor.

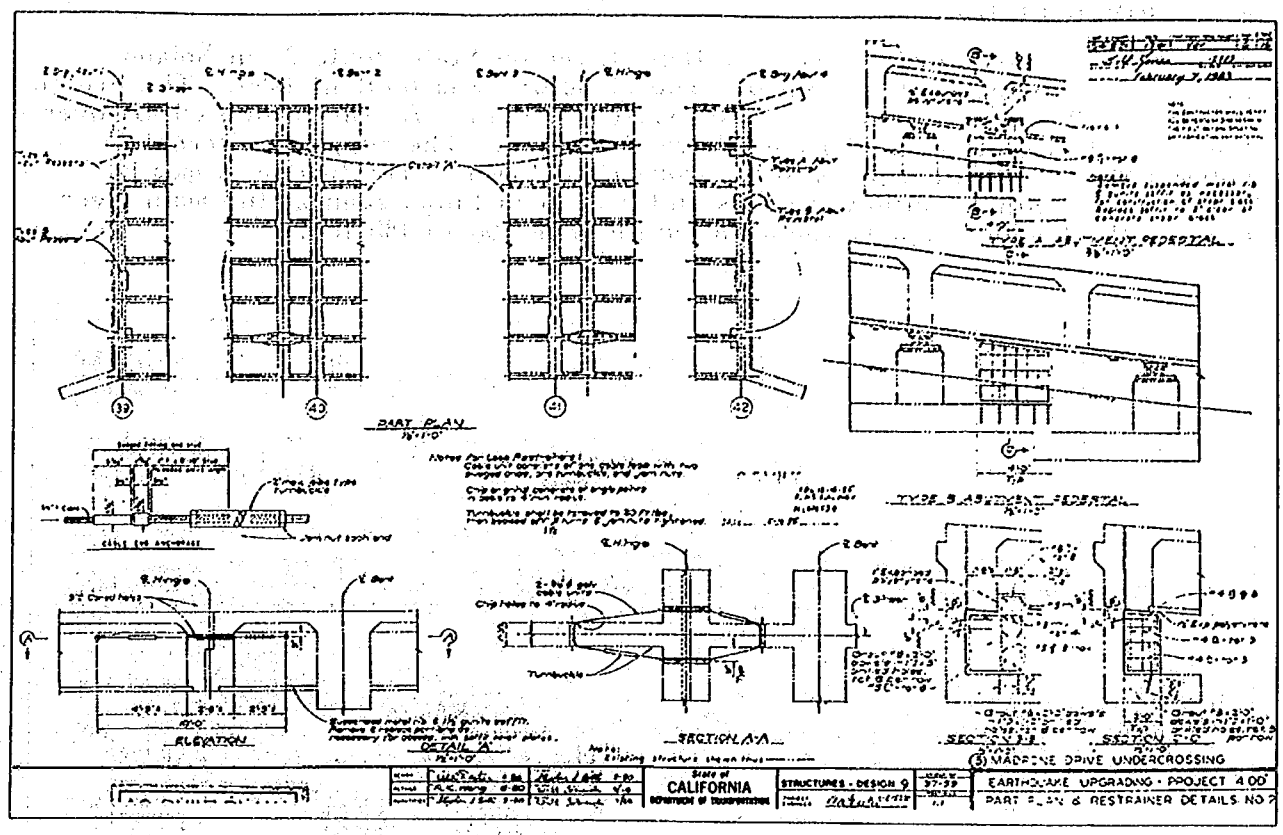

Fig. 11 Madrone Drive U.C. - Retrofit Details

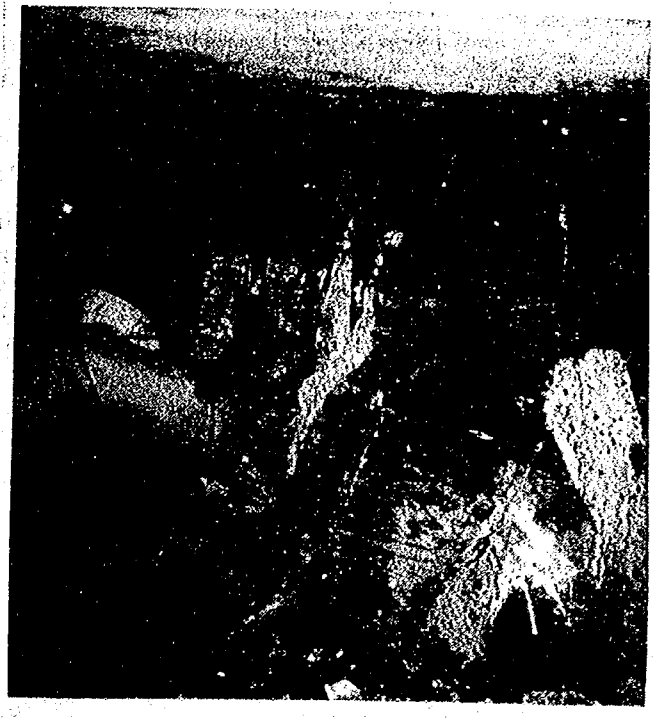

Fig. 12 Madrone Drive U. C. - Damaged Shear Key

NAPA RIVER BRIDGE

This 3280 foot structure crosses the Napa River on State Route 37 in Solano County west of the City of Vallejo. The structure was built in 1966. The bridge consists of 25 spans of precast prestressed I girders. As the bridge climbs over the river it rises to over 100 feet above the water. The supports alternate between 3 or 4 flexible piers and a more rigid tower. The bridge is mostly simple spans with 2 cantilever spans and a drop in hinge span at the main river span of the bridge. Spans range in length from 100 to 185 feet.

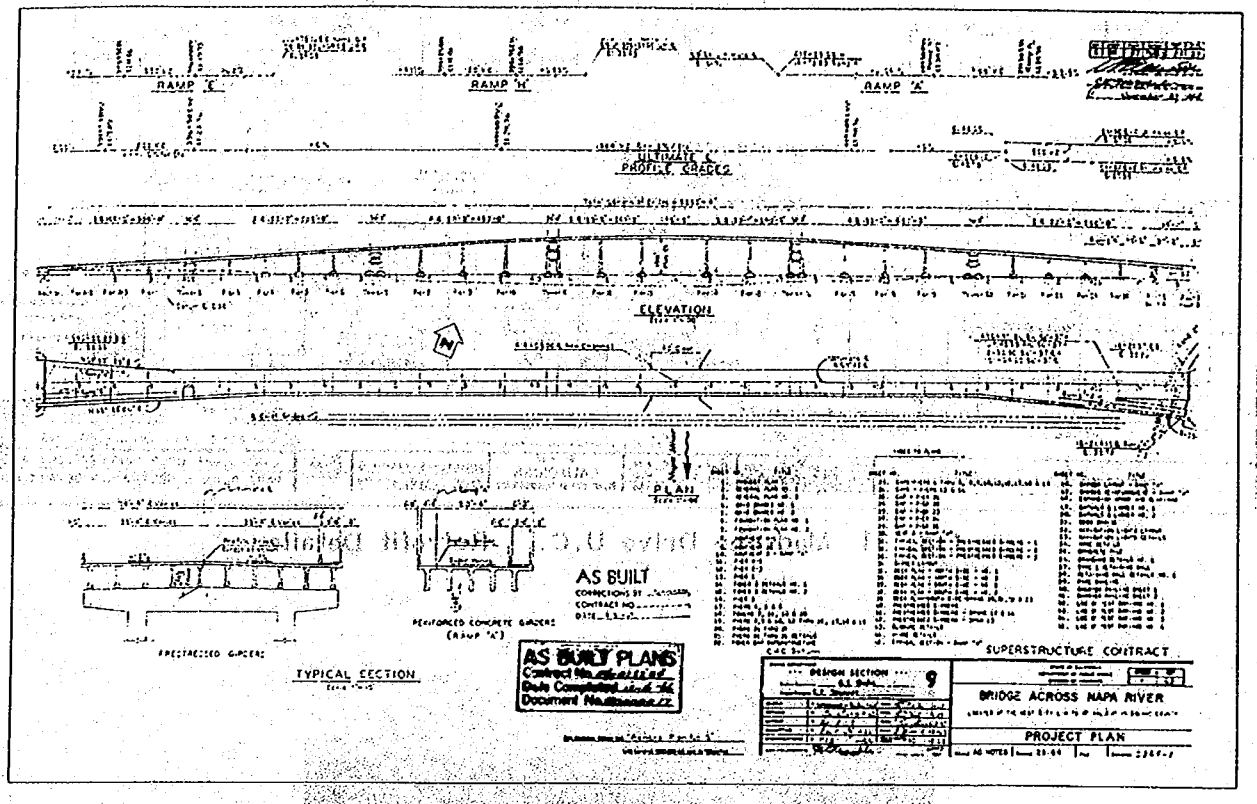

Fig. 13 Napa River Bridge - General Plan

During construction two inch cored holes were formed in the ends of the precast I girders and #6 bars were inserted. The bent caps were then poured around the ends of the girders. At 8 locations an expansion joint was placed between the I girder spans. In these locations one of the girder end spans rests on a rocker bearing and 1-1/2" bolts were placed in each bay to hold the spans together.

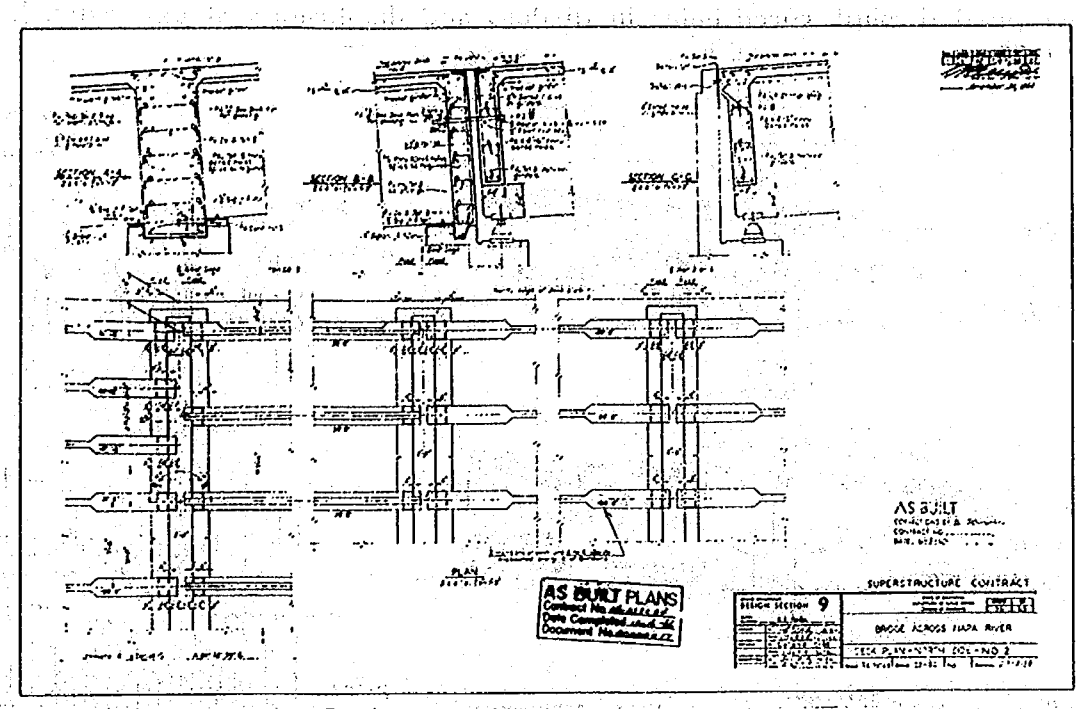

Fig. 14 Napa River Bridge - Precast Girder End Details

This bridge was seismically retrofitted in 1983. The retrofit consisted of restrainers at the expansion joints and the two hinges. Rocker bearings at abutments were replaced with concrete blocks that also acted as shear keys.

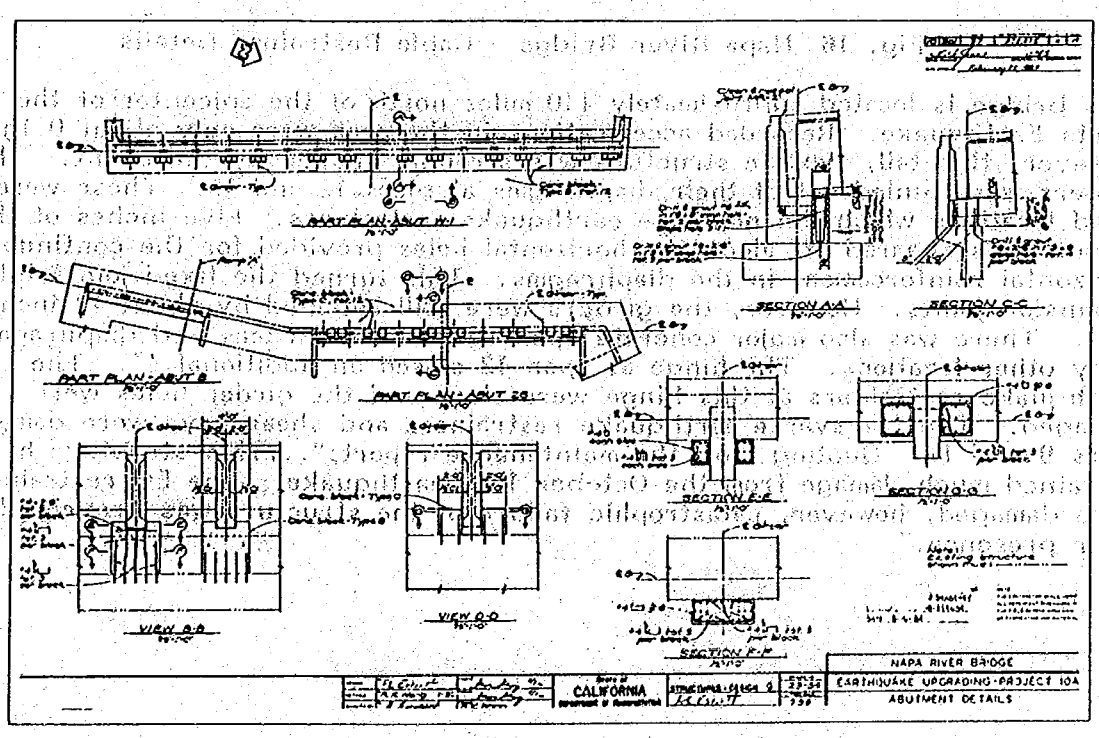

Fig. 15 Napa River Bridge - Retrofit Details at Abutments

The rocker bearings at the piers were replaced with elastomeric pads on new concrete pads doweled into the cap. Longitudinal and transverse cable restrainers were wrapped through cored holes in girders and diaphragms at expansion joints and hinges.

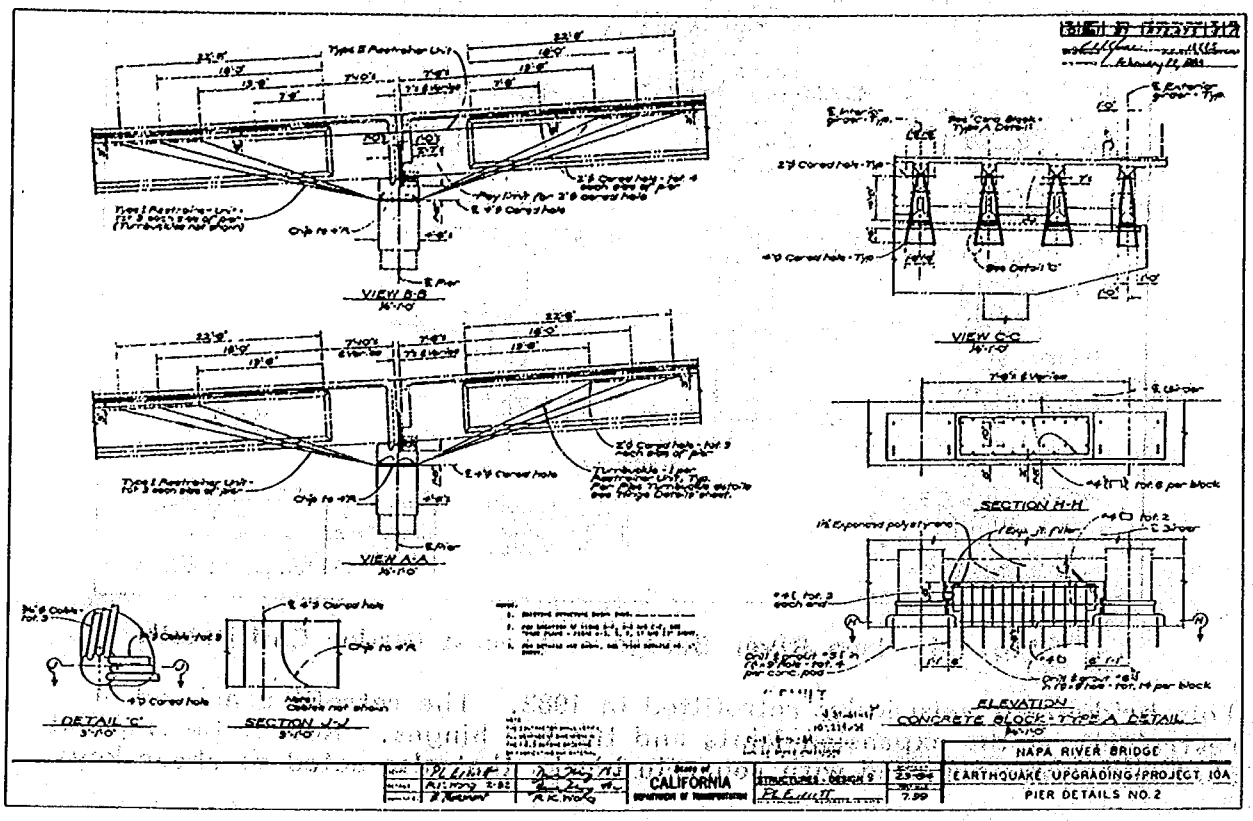

Fig. 16 Napa River Bridge - Cable Restrainer Details

This bridge is located approximately 110 miles north of the epicenter of the Loma Prieta Earthquake. Recorded accelerations in the area were only about 0.1g. However, this tall, flexible structure was strongly shaken by the event. The girders were pulled out of their diaphragms at piers 12 and 15. These were at fixed locations which did not have earthquake restrainers. Five inches of the girder ends sheared off along the horizontal holes provided for the continuous horizontal reinforcement in the diaphragms. This turned the fixed joints into expansion joints. However, the girders were still retained by about 12 inches of seat. There was also major concrete spalling between girders and diaphragms at many other locations. The hinge at span 13 closed an additional 4". The earthquake restrainers at this hinge were slack and the girder holes were damaged. The transverse earthquake restrainers and shear keys were damaged at piers 9 and 17. Quoting from the maintenance report;"...This structure has sustained much damage from the October 1989 earthquake. The EQ restrainers were damaged, however, catastrophic failure of the structure was prevented by their presence."

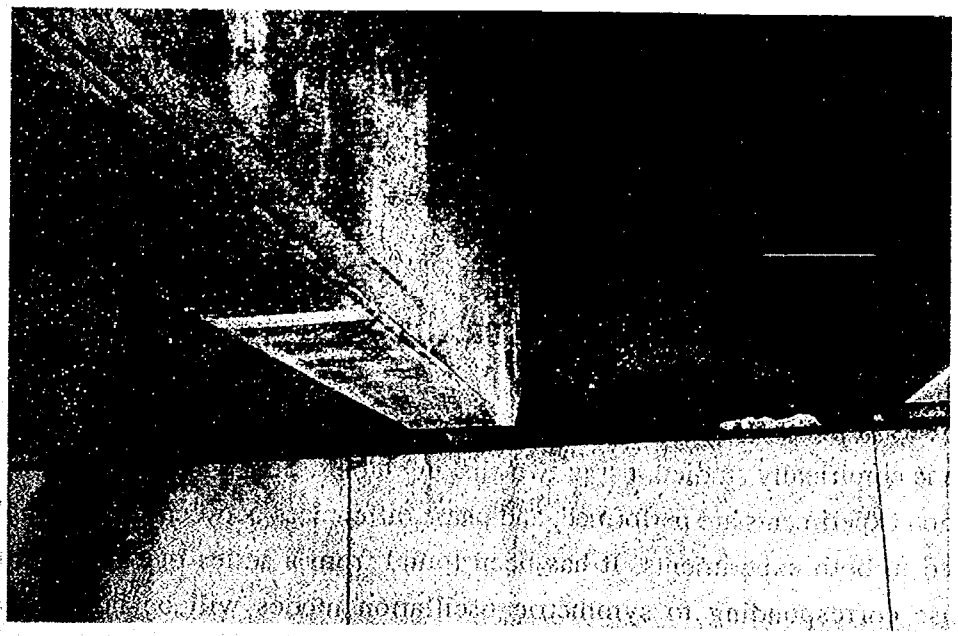

Fig. 17 Napa River Bridge - Earthquake Damage at Fixed Joint

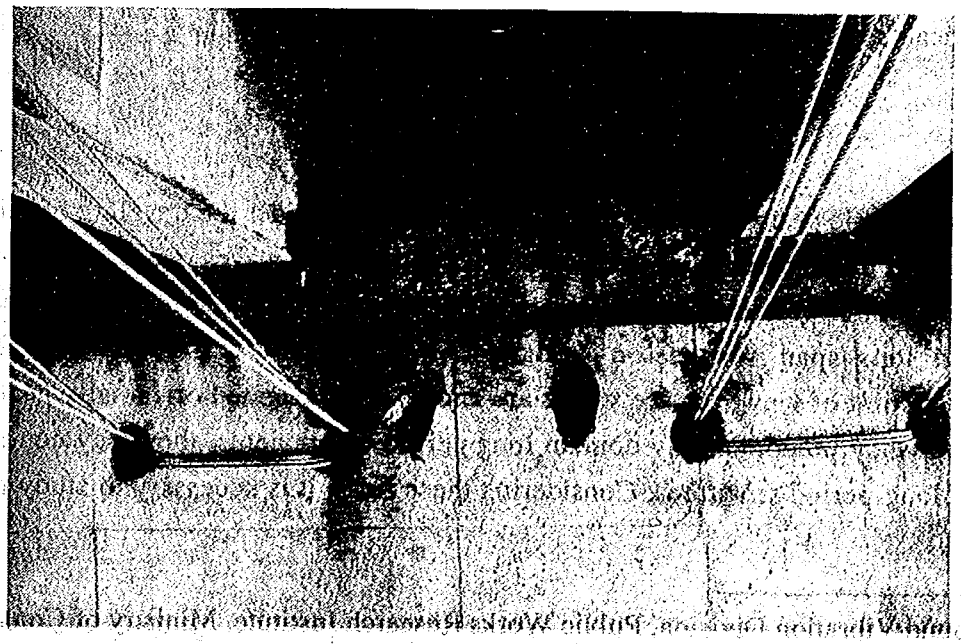

Fig. 18 Napa River Bridge - Earthquake Damage at Expansion Joint

EXPERIMENTAL STUDY OF PHASE-DIFFERENT GROUND MOTION EFFECTS ON THE RESPONSE OF A SUSPENSION BRIDGE

Ken-ichi Tokida[1], Keiichi Tamura[2] and Koh Aizawa[3]

ABSTRACT

The effects of phase-different input ground motions on the response of Akashi Kaikyo Bridge is empirically studied, using two shaking tables. Sine wave and seismic wave excitation experiments are performed, and phase differences between shaking tables are changed in both experiments. It has been found from a series of experiments that response corresponding to symmetric oscillation modes will be large, and that corresponding to anti-symmetric oscillation modes will be small, as phase difference between foundations becomes large. Response to a ground motion record, which is determined as an input motion in the seismic design of the superstructure of Akashi Kaikyo Bridge, becomes small as phase difference becomes large, except for the case of vertical displacement at the midpoint of the center span.

INTRODUCTION

In the seismic design of bridges, it is not general to consider the traveling of seismic waves from one support to the other. However, the traveling of seismic waves may cause different effects on the response of structures from uniform ground motions in case of multiple-span continuous bridges and long-span suspension bridges (Abdel-Ghaffar and Rubin, 1982). From a seismological point of view, surface waves are known to propagate horizontally near the ground surface. Since they predominantly contain long period components, they may contribute to the response of long-period structures. Considering these facts, it is necessary to study the response

[1]Head, Ground Vibration Division, Public Works Research Institute, Ministry of Construction 1 Asahi, Tsukuba-shi, Ibaraki-ken 305 Japan
[2]Senior Research Engineer, ditto
[3]Research Engineer, ditto, Presently, Kofu Construction Office, Kanto Regional Construction Bureau, Ministry of Construction

characteristics of long-span suspension bridges subjected to phase-different ground motions and traveling seismic waves.

From this point of view, the effects of phase-different input ground motions on the response of Akashi Kaikyo Bridge is empirically studied, using two shaking tables. This bridge will be the world's longest suspension bridge with a 1990m center span and two 960m side spans. A 1/500 scale model of the Akashi Kaikyo Bridge is designed and used in shaking table tests. The right anchorage and tower are set up on one shaking table, and the left anchorage and tower are set up on the other shaking table. Two kinds of experiments are conducted; sine wave excitation experiments and seismic wave excitation experiments. A ground motion record which is determined as an input motion in the seismic design of the superstructure of Akashi Kaikyo Bridge is used in the latter experiments.

EXPERIMENTAL MODEL AND METHOD

Establishing a similarity law for experimental model, the scale factors for length, acceleration and density are first decided. Considering the purpose of experiment, model erection and the performance of experiment facilities, length scale factor is decided as 1/500. Since experiments are conducted in the 1-G field, acceleration scale factor is taken as 1/1. Density scale factor is set as 1/1, taking account of model materials. Based on these conditions, the basic scale factors are decided as shown in Table 1.

Since seismic effects may virtually contribute to determining dimensions only at the bases of towers in longitudinal direction, similarity law is basically considered only for longitudinal direction. Shaking direction is also taken for longitudinal direction. As shown in Fig.1, the anchorage 1A and the pier 2P are set up on the shaking table No.1, and the pier 3P and the anchorage 4A are set up on the shaking table No.2. Twenty four accelerometers, seven displacement-meters and six strain gauges are mounted on the experimental model to mainly measure the response of girder and towers.

Natural frequency and damping ratio to the critical for the first vertical oscillation mode of model are estimated as 1.48Hz and 0.005, respectively, from a free oscillation test. Fig.2 shows main mode shapes obtained from modal analysis of the prototype bridge. Fundamental natural frequency scaled to the model is 1.47Hz and it agrees well with that obtained from a free oscillation test. Mode shapes estimated from free oscillation tests and modal analysis also agree well.

The shaking tables No.1 and No.2 can be operated independently. Two kinds of experiments are carried out; sine wave excitation experiments and seismic wave excitation experiments, and phase differences between two shaking tables are systematically changed in both experiments.

SINE WAVE EXCITATION EXPERIMENTS

Experiments are conducted for 10 frequencies; 1.47, 2.65, 4.55, 5.00, 6.84, 7.60, 9.53, 9.90, 10.4 and 13.0Hz, which are predominant frequencies obtained from resonance tests. Phase difference ϕ between two shaking tables is changed from 0 to π by every $\pi/8$ step. Response amplification is defined as dividing each maximum response value by the maximum acceleration on the shaking table. To express effects of phase difference of input motions on structure response, response amplification ratio is defined as dividing the response amplification for phase-different input motions by that for the same phase motions. Results for the following frequencies are shown in this paper; f=1.47[Hz], f=2.65[Hz] and f=9.90[Hz]. They correspond to the first symmetric vertical oscillation mode of girder, second symmetric vertical oscillation mode of girder and the first anti-symmetric longitudinal oscillation mode of towers, respectively.

Fig.3 shows response amplification ratios of vertical displacement at the midpoint of the center span. Response amplification ratios for f=1.47, 2.65[Hz] increase as phase difference ϕ becomes large. Response amplification ratios for out-of-phase motions ($\phi=\pi$) are 12 and 9 for f=1.47 and 2.65[Hz], respectively. This may be due to a fact that mode shapes for f=1.47, 2.65[Hz] correspond to symmetric vertical oscillation modes of girder, and out-of-phase motions acting on tower bases will excite oscillation of girder. On the other hand, response amplification ratio for f=9.90[Hz] decreases as phase difference becomes large. The response amplification ratio for $\phi=\pi$ is approximately 1/7. This may be because a mode shape for f=9.90[Hz] is anti-symmetric vertical oscillation mode for girder, and in-phase motions at tower bases will excite oscillation of girder.

Fig.4 shows response amplification ratios of horizontal acceleration at the midpoint of the center span. Response amplification ratios for f=1.47, 2.65[Hz] are seen to increase as phase difference increases. The degree of increase is not so remarkable as compared with the case of vertical displacement. Response amplification ratios for $\phi=\pi$ are 1.4 and 2 for f=1.47 and 2.65[Hz], respectively. Response amplification ratio for f=9.90[Hz] decreases as phase difference becomes large, and it is 1/10 for out-of-phase motions.

Response amplification ratios for horizontal acceleration at the top of towers are shown in Fig.5. Their dependence on phase difference is basically similar to those of vertical displacement and horizontal acceleration at the midpoint of the center span. The response amplification ratio for f=1.47[Hz] shows higher value than that for f=2.65[Hz] over the phase difference range of 0 to π, for example, the former for $\phi=\pi$ is 8 to 15, the latter for $\phi=\pi$ is 2 to 3.

Fig.6 shows response amplification ratios of bending moment at the bases of towers. Response amplification ratios for f=1.47, 2.65[Hz] increase as phase difference becomes large. As for $\phi=\pi$, the former is 9 to 15, and the latter is 3 to 7. Response amplification ratio for f=9.90[Hz], which corresponds to an anti-symmetric longitudinal oscillation mode of towers, decreases as phase difference becomes large. The response amplification ratio for $\phi=\pi$ is about 1/10.

SEISMIC WAVE EXCITATION EXPERIMENTS

The input motion used in seismic wave excitation experiments is the Muroran record shown in Fig.7, which is determined as an input motion for dynamic analysis of the superstructure of Akashi Kaikyo Bridge. This record was originally obtained by a displacement-type seismograph, and its amplitude characteristic is modified to meet the design acceleration response spectrum determined for spectral analysis of the superstructure of the bridge. Note that time axis is scaled to $1/22.4(=1/\sqrt{500})$ in experiments, considering the similarity law. Assuming two levels of propagation velocity of traveling seismic wave as shown in Table 2, time lags between 1A-2P (shaking table No.1) and 3P-4A (shaking table No.2) are taken as 0, 2, 3, 4, 6 and 8 seconds for prototype-base. These time lags are also scaled to 1/22.4 in experiments. An experiment with out-of-phase input motions is also conducted. Prototype-base time lags are used in the followings for convenience.

The response amplification is defined same as the case of sine wave excitation experiments, and the response amplification ratio is defined as dividing the response amplification for time lag input motions by that for simultaneous motions.

Fig.8 shows the response amplification ratio of vertical displacement at the midpoint of the center span. It increase as time lag τ becomes 0 to 6 seconds. The response amplification ratios for τ=6, 8[s] are approximately 10. Fig.9 shows the response amplification ratio of horizontal acceleration at the midpoint of the center span. It decreases as τ becomes long. The response amplification ratio for τ=6, 8[s] is about 1/3. Response amplification ratios of horizontal

acceleration at the top of towers are shown in Fig.10. Their dependence on time lag is similar to that of horizontal acceleration at the midpoint of the center span. Fig.11 shows response amplification ratios of bending moment at the bases of towers. They decrease as τ becomes up to 6 seconds, and then they increase a little at τ=8[s]. From these results, the vertical displacement at the midpoint of the center span becomes large as time lag becomes large, however, other response values become small as time lag becomes large, for the input ground motion employed in the seismic design of the superstructure of Akashi Kaikyo Bridge.

Table 3 compares the prototype-base maximum response values estimated from experiment results and those calculated from dynamic analysis. It is assumed in dynamic analysis that seismic wave propagates from 4A to 1A at the velocity v=1, 0.5[km/s], therefore each foundation is supposed to be subjected to different phase ground motion according to location. However, it is simplified in the experiments that 1A and 2P are subjected to same ground motion, and 3P and 4A are subjected to another same motion. Considering these facts, experiment results are shown only for simultaneous input motions, which can be directly compared with analytical results.

Comparing the prototype-base response values for simultaneous input motions, those estimated form experiment agree well with analytical results except for vertical displacement and horizontal acceleration at the midpoint of the center span. According to dynamic analysis results, vertical displacement at the midpoint of the center span increases as time lag becomes large (propagation velocity becomes small), horizontal acceleration at the midpoint of the center span and at the top of towers decreases as time lag becomes large. These characteristics also coincide with experiment results.

CONCLUSIONS

The effects of phase-different input ground motions on the response of Akashi Kaikyo Bridge is empirically studied and their results are compared with dynamic analysis results. The following conclusions may be deduced from this study.

1) Response to phase-different sine wave excitations depends on the relationship between excitation frequencies and mode shapes which are excited for the input frequencies. Response corresponding to symmetric oscillation mode will be large, and that corresponding to anti-symmetric oscillation mode will be small, as phase difference between foundations becomes large.

2) Response to the input ground motion, which is employed in the seismic design of the superstructure of Akashi Kaikyo Bridge, becomes small as phase lag becomes large, except for the case of vertical displacement at the midpoint of the center span. Prototype-base maximum response values for simultaneous input motions estimated from experiment results agree fairly well with those derived from dynamic analysis. The response dependence characteristics on phase lag also coincide well with results of dynamic analysis.

ACKNOWLEDGEMENTS

This research was supported by the Honsyu-Shikoku Bridge Authority. The authors would like to express their sincere thanks to the Authority personnel concerned.

REFERENCE

1. Ahmed M. Abdel-Ghaffar and Lawrence I. Rubin, "Suspension Bridge Response to Multiple-Support Excitations", Journal of Engineering Mechanics Division, Proc. of ASCE, Vol.108, No.2, 1982

Table 1 Basic Scale Factors

Item	Scale Factors
Length	$\lambda_L=n=1/500$
Time	$\lambda_T=\sqrt{n}$
Density	$\lambda_\rho=1$
Frequency	$\lambda_f=1/\sqrt{n}$
Acceleration	$\lambda_\alpha=1$
Flexure Rigidity	$\lambda_{EI}=n^5$
Tensile Rigidity	$\lambda_{EA}=n^3$
Spring Constant	$\lambda_{KR}=n^4$
Mass	$\lambda_M=n^3$

Table 2 Time Lag Assumed between Foundations of Akashi Kaikyo Bridge

	Time Lag [s]	
	v=1km/s	v=0.5km/s
1A-4A (4km)	4	8
2P-3P (2km)	2	4
$\frac{(1A-4A)+(2P-3P)}{2}$	3	6

Table 3 Comparison of Prototype-base Maximum Response Values

Point	Unit	Experiment	Dynamic Analysis		
		τ=0[s]	τ=0[s]	v=1.0[km/s]	v=0.5[km/s]
LD-3	cm	11.8	0.30	98.4	145.2
A-13	gal	120.0	50.2	46.4	37.2
A-8	gal	62.6	68.3	54.0	48.9
A-16	gal	61.2	68.5	62.8	57.6
S-4	t×m	168,000	128,738	43,533	127,435
S-6	t×m	146,000	121,144	48,420	122,220

LD-3: Vertical Displacement at the Midpoint of the Center Span

A-13: Horizontal Acceleration at the Midpoint of the Center Span

A-8: Horizontal Acceleration at the Top of 2P

A-16: Horizontal Acceleration at the Top of 3P

S-4: Bending Moment at the Base of 2P

S-6: Bending Moment at the Base of 3P

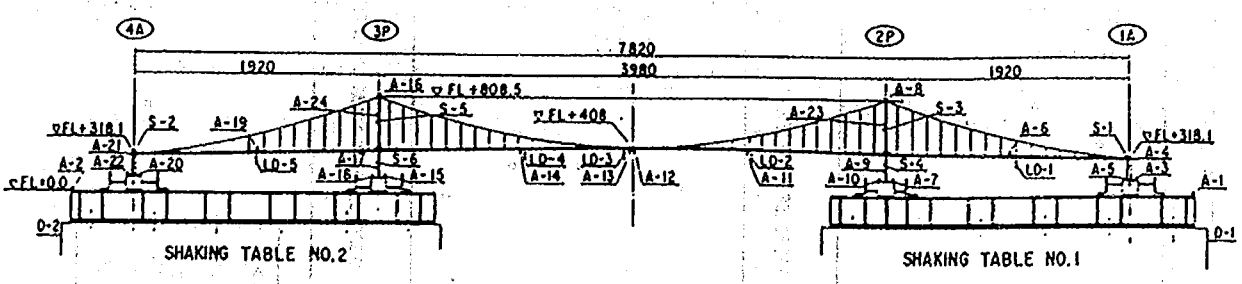

Note; A-*i*: Accelerometer, D-*i* and LD-*i*: Displacement-meter, S-*i*: Strain Gauge

Fig.1 General Plan of Experimental Model

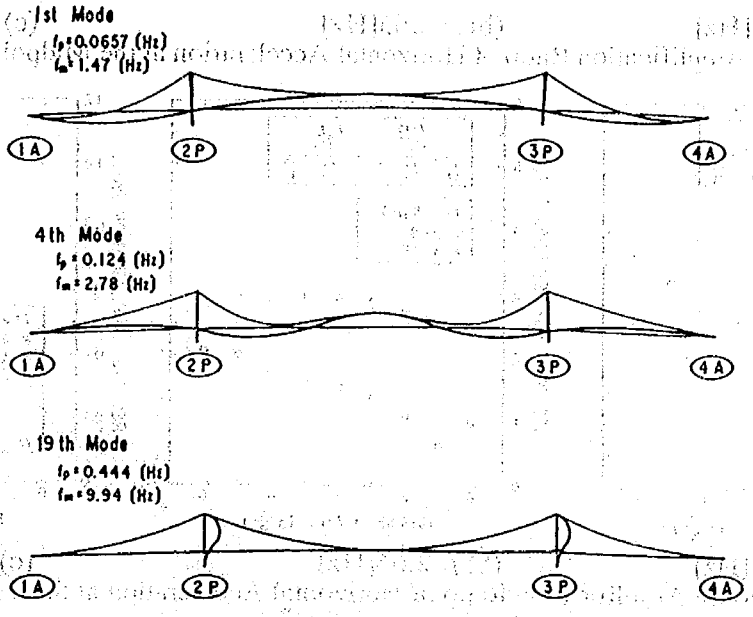

Fig.2 Mode Shapes Estimated from Modal Analysis

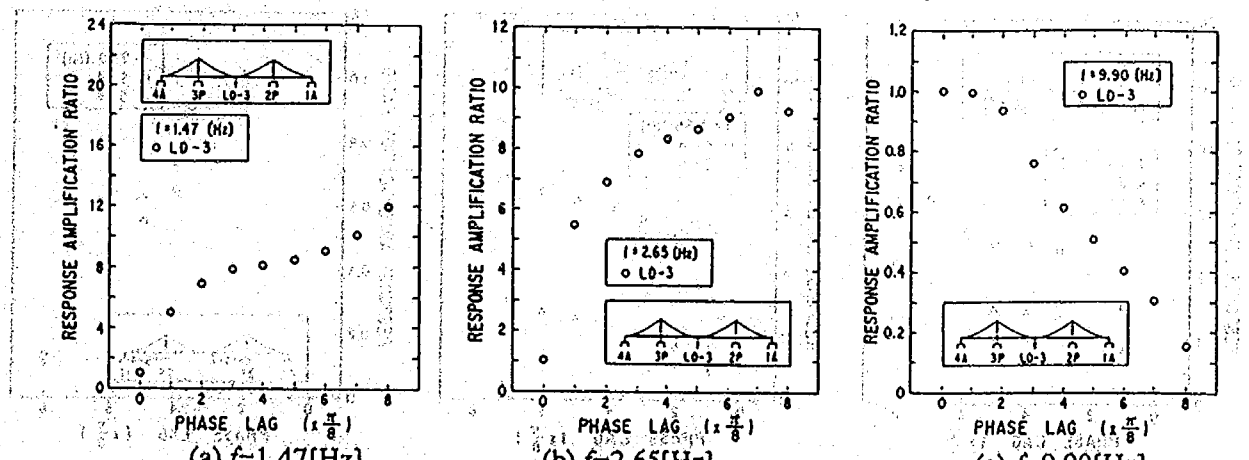

(a) f=1.47[Hz] (b) f=2.65[Hz] (c) f=9.90[Hz]

Fig.3 Response Amplification Ratio of Vertical Displacement at the Midpoint of Center Span

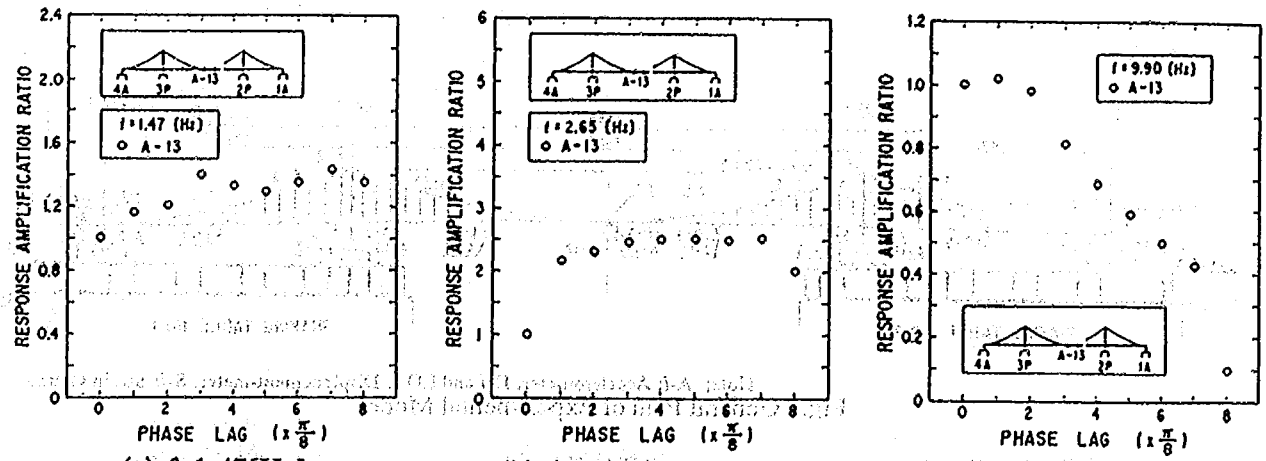

(a) f=1.47[Hz] (b) f=2.65[Hz] (c) f=9.90[Hz]

Fig.4 Response Amplification Ratio of Horizontal Acceleration at the Midpoint of Center Span

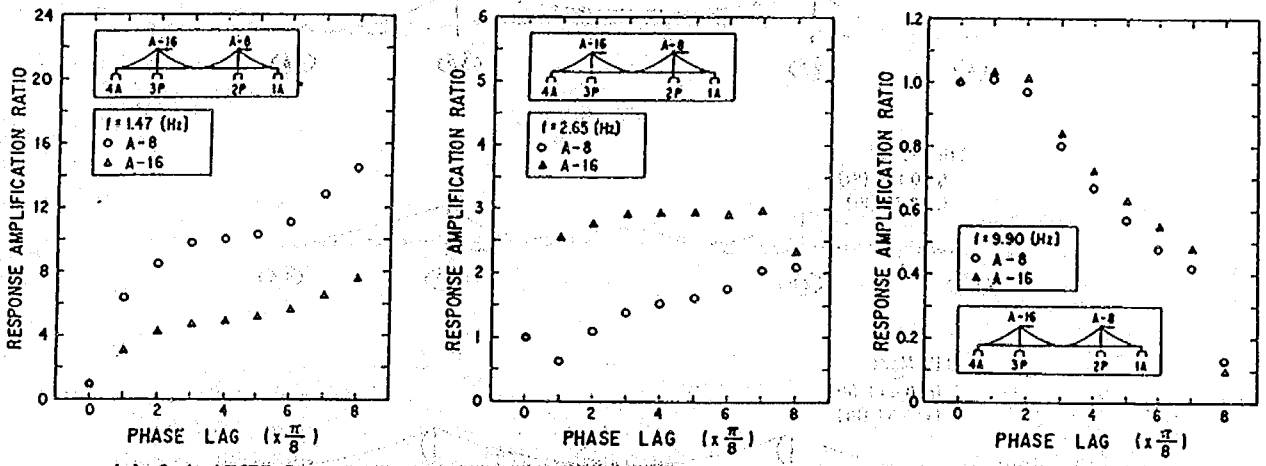

(a) f=1.47[Hz] (b) f=2.65[Hz] (c) f=9.90[Hz]

Fig.5 Response Amplification Ratio of Horizontal Acceleration at the Top of Towers

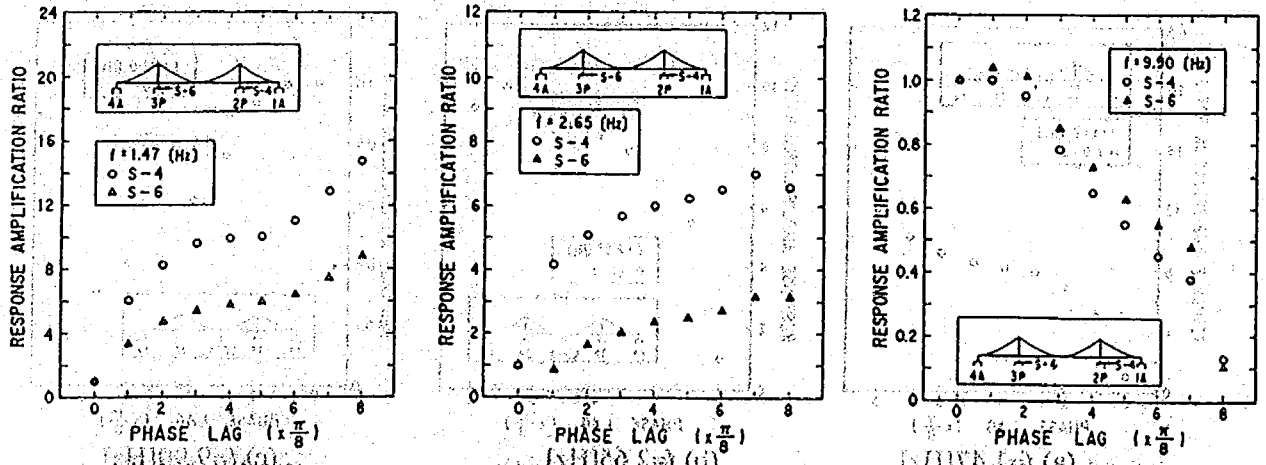

(a) f=1.47[Hz] (b) f=2.65[Hz] (c) f=9.90[Hz]

Fig.6 Response Amplification Ratio of Bending Moment at the Bases of Towers

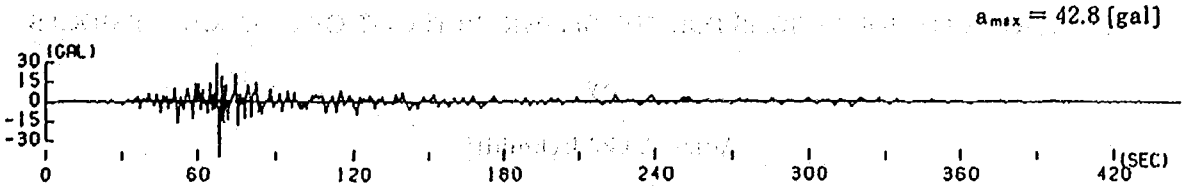

Fig.7 Input Ground Motion for Dynamic Analysis of the Superstructure of Akashi Kaikyo Bridge

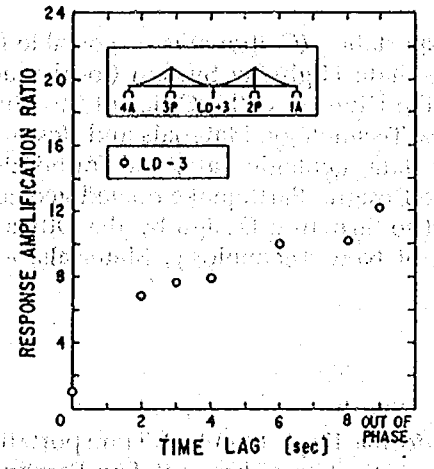

Fig.8 Response Amplification Ratio of Vertical Displacement at the Midpoint of Center Span

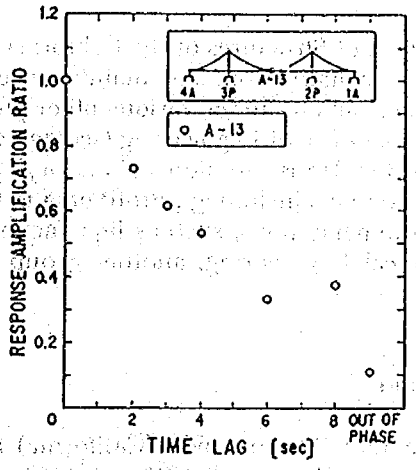

Fig.9 Response Amplification Ratio of Horizontal Acceleration at the Midpoint of Center Span

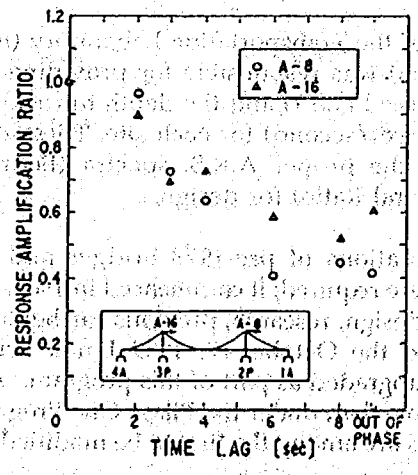

Fig.10 Response Amplification Ratio of Horizontal Acceleration at the Top of Towers

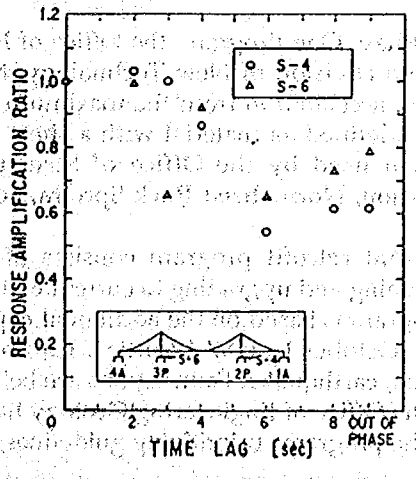

Fig.11 Response Amplification Ratio of Bending Moment at the Bases of Towers

FOUNDATION CONSIDERATIONS FOR THE SEISMIC RETROFIT OF CALTRANS BRIDGES

By

Adlai F. Goldschmidt*

Introduction

The Division of Structures of the California Department of Transportation (Caltrans) is responsible for the design, construction, and maintenance of structures of the State Highway System (local roads within the state are under various other jurisdictions). Within the Division is the Office of Structure Design. The Office of Engineering Geology of the Division of New Technology, Materials and Research (formerly the Transportation Laboratory) provides earthquake data, geologic data, and foundation recommendations including retrofit data to the Office of Structure Design. Earthquake related geotechnical recommendations, such as liquefaction data, are furnished to Structure Design by the Office of Geotechnical Engineering, another group within the Division of New Technology, Materials, and Research.

Background

Since the 1971 San Fernando (California) Earthquake, The California Department of Transportation (Caltrans) has been retrofitting bridges of the State Highway System. The post San Fernando Earthquake retrofit program (Phase One Program) consisted of reinforcing existing superstructure elements by connecting hinges and joints with restrainers, by anchoring girders, and by completing other modifications to prevent superstructure collapse. Over $50 million was spent to retrofit about 1300 bridges. The program was completed during 1988.

For the Phase One Program, the Office of Engineering Geology of the Transportation Laboratory (now called The Division of New Technology, Materials and Research) was responsible for providing the peak rock acceleration from the maximum credible earthquake (see Plate 1) and the depth to rock-like material (defined as material with a shear wave velocity >2500 feet/second) for each site. These data were then used by the Office of Structure Design to select the proper A.R.S. spectra (Bedrock Acceleration, Normalized Rock Spectra, Soil Amplification Spectral Ratio) for design.

The current retrofit program consists of total structural evaluations of pre-1978 bridges and the strengthening and upgrading to current earthquake standards where required; it commenced in 1987. The new program is based on the additional experience gained from design, research, previous earthquakes, and the October 1, 1987 Whittier, California, earthquake, and the October 17, 1989 Loma Prieta, California, earthquake. Foundations are being strengthened and upgraded as part of this program. As a result, the Office of Engineering Geology has a more significant role than under the Phase One Program. Under the programs prioritizing guidelines, single column bridges are among the first to be modified.

* Senior Engineering Geologist
California Department of Transportation
Division of New Technology, Materials and Research
P.O. Box 19128, Sacramento, CA 95819

During the past year, intensive retrofit design and construction projects have been underway. Single column structures, which the prioritizing process identified, are currently being retrofitted. As experience has been gained in both areas, changes have been implemented in an ongoing process to improve retrofit designs (including foundations).

The single column program includes pedestrian overcrossings and connector ramps. These long and high curved ramps are usually located at major freeway interchanges. There are many interchanges and they can have as many as four connector ramps. Because of their length, the connectors often pass over varying geologic material and, as a result, usually have several foundation types, all of which must be considered in the retrofit design.

Connector ramps and other bridges which cross active faults have recently been identified. The retrofits for the fault crossings are presenting special problems for both the engineering geologist and the bridge designer.

Procedure For Providing Engineering Geology Retrofit Data

The Office of Structure Design uses an involved screening process to rate and identify the earthquake damage potential of bridges. The risk algorithm assigns almost one-fourth of the criteria to geologic related items, 12% to peak rock acceleration and 12% to soils at the site. Over 24,000 bridges have been screened during the program. Structures selected during this process are then prioritized to be retrofitted. After a structure has been selected to be retrofitted, preliminary foundation data are requested by the Office of Structure Design from the Office of Engineering Geology. The request for foundation data includes "As Built" plans for the existing bridge such as the General Plan, the Foundation Plan, and the Log of Test Borings.

The Office of Engineering Geology also maintains its own data base which contains valuable foundation information such as the notes from the field investigation, pile driving records, and other information relating to the structure's foundation. In addition, other useful sources of geologic information are available in California such as the California Division of Mines and Geology, the United States Geological Survey, the California Department of Water Resources, and university publications.

After the engineering geologist has completed a review of the existing site/foundation data, a preliminary information memorandum is prepared for the retrofit designer. The memorandum, "Preliminary Seismic, Geologic, and Foundation Information" (see Plate 2), is sent to the retrofit designer so that an initial design proposal can be made for presentation at a "retrofit design strategy meeting". In addition, as experience has been gained from ongoing retrofit projects and as a result of comments from the newly instituted peer review process (by experts outside of Caltrans), extensive field investigations are being conducted at some sites, mostly at large bridges. Detailed foundation recommendations are then provided to the designer.

Retrofit Design Strategy Meeting

Retrofit design concepts are developed at the start of a project and, as a result, the engineering geologist must work very closely with the designer. Part of this process is the Design Retrofit Strategy Meeting. The retrofit designer and those engineers closely associated with the project hold a meeting with supervisory level design, construction, and maintenance engineers plus specialty engineering personnel including engineering geologists experienced in the retrofit process. The object of the meeting is to agree on a retrofit design that meets all earthquake resistance criteria. Information on traffic control (a major consideration in urban areas), alternate design approaches, overhead clearances, and solutions used for similar problems at other bridges are also discussed. Of most interest to the engineering geologist are foundation problems and their solutions.

Site Problems

Site related geologic/soils problems which must be considered for foundation retrofit design include "soft soils" (clays, silty clays, and clayey silts), liquefaction, and the crossing of an active fault or a supposed active fault. Lacking and insufficient foundation/soils information also presents problems. Obviously, if there is a lack of sufficient subsurface geologic/foundation data, additional field work is required to supplement the available information.

Existing Bridge Foundations

Caltrans bridges utilize many foundation types and combinations of foundation types consistent with structure geometry, terrain, and foundation materials. Spread footings, standard concrete piles (driven and cast-in-drilled-hole), steel "H" piles and pipe piles, high capacity driven piles, and column piles/pile shafts have all been used for bridge support.

Foundation Loads-Piles

For a total retrofit design, the compression loads on piles can be increased up to four times the design load for earthquake loads. This is because some limited damage is allowed to occur during an earthquake as long as the structure does not collapse. At this, point several items must be mentioned concerning Caltrans pile foundation designs. Due to the large number of bridges designed at Caltrans, many standard designs have been developed. These include pile types such as the 45 ton or the 70 ton design load driven concrete pile and cast-in-drilled-hole (CIDH) pile which support many of the bridges being retrofitted. The normal ultimate compression load used for design is twice the design or service load (safety factor = 2). The uplift service load used is 40% of the design load.

For comparison and review are the 1967 and 1987 (currently being used) Caltrans Standard Plans (see Plates 3 through 7) for concrete piles. For the purpose of obtaining competitive bid prices (Caltrans construction work is done by contractors), the plans for driven piles indicate several "generic" alternates. For many of the older bridges the alternate "Z" pile (the Raymond Concrete Pile) was the predominant pile type. Today the alternate "X" pile (the precast prestressed pile) is the pile type most often chosen by contractors (based on price and availability). Many of the bridges being retrofitted are supported by piles similar to the 1967 designs while current practice is to use the earthquake resistant 1987 designs. Caltrans bridges are not supported by batter piles except at abutments. Batter piles are also used for retaining wall support.

Currently, the tension capacity of a pile used for earthquake forces is 50% of the ultimate pile load (equal to the design load when using a safety factor of 2) of the pile. Tension loads are based on empirical data gathered from the hundreds of pile load tests conducted throughout California for many years by Caltrans engineering geologists. Piles are load tested to at least their ultimate capacity. The two reaction or anchor piles in a three pile test group are subject to the design load of the test pile as a tension load (see Plate 7). Where a pile obtains much of its capacity from "end bearing", the engineering geologist gives the designer an appropriate reduced value for uplift capacity.

Example Pile Capacity Problems

A problem that has presented itself with the older Alternate "Z" pile (the Raymond Pile) and the CIDH pile is the lack of full length reinforcing needed to utilize the full uplift capacity of these pile types. As a result, these pile types are not adequate for resisting the earthquake induced design tension loads. The designer much also check the piles attachment details to be sure uplift loads will be transmitted from the footing to the piles.

Another problem occurred at a retrofit project just completed. The existing steel "H" piles did not have the tension characteristics that were anticipated. These piles had been load tested during original construction. The available data indicated that additional retrofit piles (pipe piles) required would support the uplift loads at the "As Built" tip elevations. During retrofit construction, piles attained bearing "under the hammer" when they were being installed, but refused above the specified tip elevation. As a result, a "Wave Equation" analysis was made and an uplift load test was performed. The results indicated that loads were inadequate. Driving refusal due to end bearing and contractual agreements dictated the use of additional piles. Uplift pile load tests will be used more frequently on future retrofit projects. Additionally, the Office of Engineering Geology is recommending the use of higher capacity pile hammers where full pile uplift loads are required and where predrilling is to be limited.

Foundation Loads-Footings

Spread footings, when applicable, are commonly used for support of bridges on the state highway system. To accommodate the increased compression loads required for retrofit design, the ultimate load of the footing (three time the design load) can be utilized if consistent with the settlement which the structure can tolerate. Compressional loads even higher than the ultimate unit load can be used for seismic retrofit design if the increased settlement, which will probably occur, does not cause excess structural distress. To accommodate excessive compressional loads, the footing can be enlarged to provide a larger bearing area with or without piles.

Little or no load is assigned to spread footings for uplift. For retrofit, the footing is usually reinforced and piles or soil/rock anchors are added to resist uplift forces.

Additional Load Capacity

Basic to foundation retrofit design is determining the additional load capacity, if any, that the existing foundation can support. This capacity can be found by using the information available on "As Built" General Plans, Foundation Plans, and Log of Test Borings which are available for most bridges. For bridges supported by piles, the critical pile driving records required are usually available. An excellent source of information on existing bridges is available through the Office of Structure Maintenance. Their library of bridge maintenance records contains not only maintenance reports but also the Engineers Final Construction report for each bridge. This source of information has been invaluable in many cases where the "As Built" data were insufficient.

Piles used for support of older bridges are of a lower capacity than the piles used for newer bridges. As a result, these piles are shorter. Thus, the subsurface information available for these structures and for structures supported on spread footings may not extend to the depths required for retrofit analysis. In cases where there is no boring data, or there is a need for deeper data, and where soils information is needed for bridge approach embankments which were not present at the time of the initial investigation, an additional subsurface investigation is required.

Foundation capacity, for earthquake forces, at the bents/piers can be improved by using several techniques or combinations of the various methods. Just as structures vary from site to site, so do foundations and soil types. Each structure presents specific foundation retrofit requirements. For increased compression loads at pile supported piers/bents, additional piles are used. These piles can be either driven or of the CIDH type. Under bridges where low clearance is a problem, special pile installation equipment is available that can operate with less than 13 feet of headroom. The recommended pile type for these locations is the steel pipe pile which can be driven in short sections welded together.

For spread footing supported bents/piers where horizontal clearance and soil bearing capacity is adequate, an enlarged or modified footing can be used. Piles, if required, can be installed through or outside of the existing footing depending on design requirements.

When additional uplift loads have to be considered, they can be handled by piles or by soil/rock anchors. Piles used for compression loads are normally used for tension loads. A distinct advantage of anchors is they can be more easily installed through existing footings due to their smaller diameter.

Foundation retrofit at abutments consists of limiting transverse and longitudinal movement. This is accomplished by using CIDH piles three to four feet in diameter installed adjacent to and outboard of the abutment to control transverse movements. To control longitudinal movements, anchors (they can be "dead men" or large CIDH piles) are installed next to or within the roadway behind the abutment in original ground or embankment. The anchors are then attached to the abutment with connectors such as high strength reinforcing rods.

Foundation Types Being Considered

A tiedown system currently being evaluated incorporates the use of a steel casing extending from the footing to the anchor zone of the tiedown. This casing allows the tiedown tendons to be stressed without adding additional downward load on the existing footing. The primary advantage of this system is that the tiedown elongation under seismic loading is reduced, the footing rotation is practically eliminated, and the overall stability of the footing is increased.

Another method for providing uplift resistance for existing column footings is being evaluated. It consists of driven pipe piles with battered fins welded to the tip. The "Spin-Fin" piles were developed and used in Alaska. When these piles are loaded and torsional restraint is provided, the fins mobilize additional resistance over that provided by smooth pipe piles. However, in pile load tests made recently by Caltrans, the pile displacement necessary to mobilize this additional resistance was significant. Therefore, more study will be required before guidelines can be developed for use of these piles.

Conclusions

During 1990 and early 1991, many retrofit construction contracts were started and several were completed. In addition, the Office of Structure Design has held numerous strategy meetings and is in the process of designing numerous additional retrofits. At present, a large portion of the investigations conducted by the Office of Engineering Geology are for retrofits. As retrofit projects are processed, problems arise and are solved. Concepts change and the process is not as difficult as it was a year or more ago.

In addition to the standard foundation types being used, there are new pile types and variations on existing foundation systems which have been, or will be, tested for use on Caltrans projects.

Acknowledgements

Richard C. Wilhelms of the Caltrans Division of New Technology, Materials and Research, and James H. Gates of the Caltrans Office of Structure Design, are acknowledged for their contributions and help in the preparation of this paper.

References

1. Caltrans, Division of Structures, Seismic Design References, 1990.

2. Gates, James H., California's Seismic Design for Bridges, ASCE, Journal of the Structural Division, ST12, December 1976.

3. Roberts, J. E., Recent Advances in Seismic Design and Retrofit of California Bridges, 1990.

4. Wilhelms, R. C., Column Retrofit Projects, Discussion and Comments, 1991.

5. Yashinsky, Mark, The Seismic Retrofit of Bridge Foundations, (Unpublished), 1991.

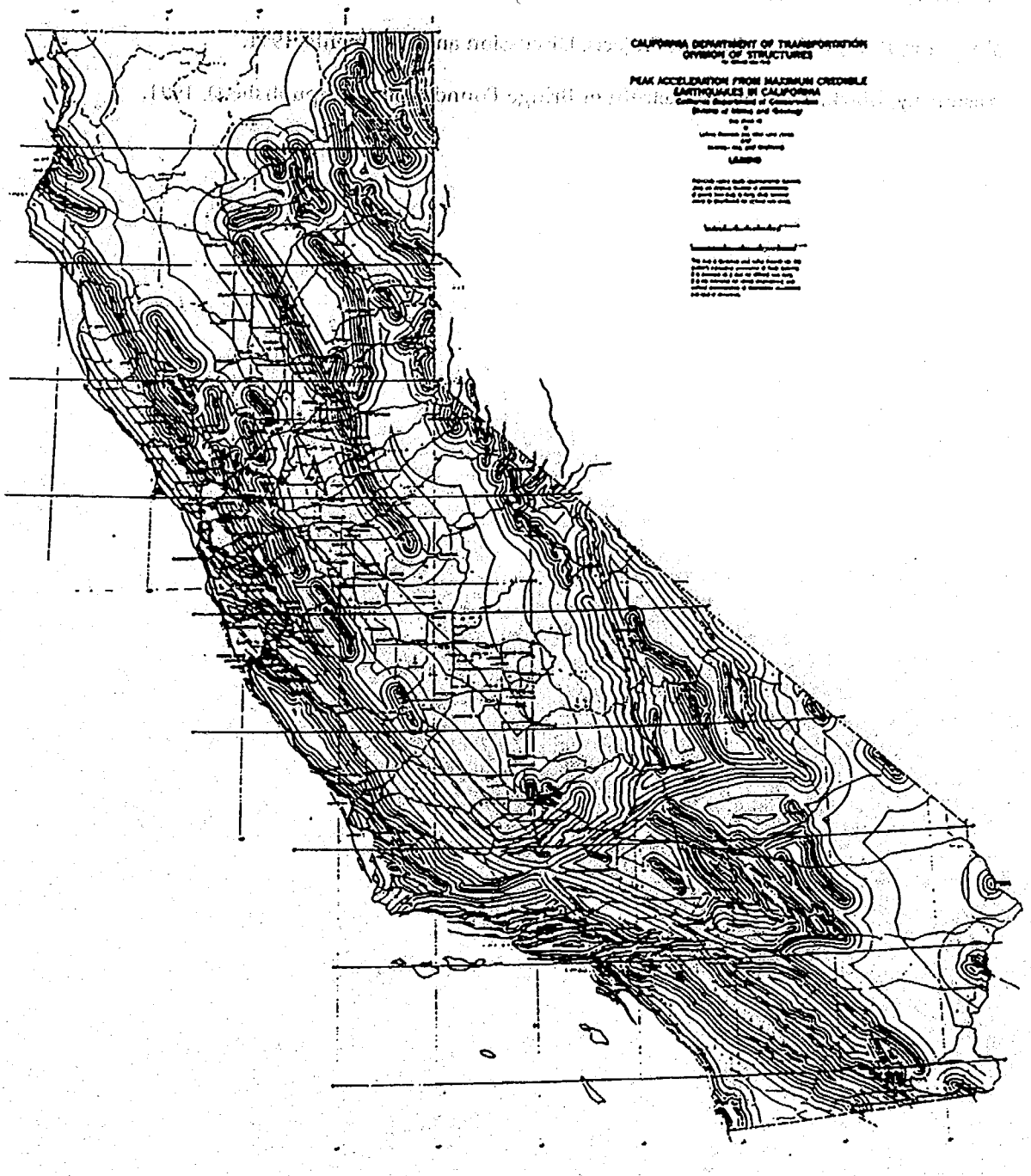
CALIFORNIA DEPARTMENT OF TRANSPORTATION
DIVISION OF STRUCTURES
PEAK ACCELERATION FROM MAXIMUM CREDIBLE
EARTHQUAKES IN CALIFORNIA

State of California — Business, Transportation and Housing Agency

Memorandum

To: Bill Jones, Chief
Office of Structure Design

Attention _____

Design Section _____

Date:

File No.: RETROFIT PROJECT NO. _____

From: DEPARTMENT OF TRANSPORTATION - 739-2483
Office of NT, M&R

Subject: PRELIMINARY SEISMIC, GEOLOGIC, AND FOUNDATION INFORMATION _____

Br. No. _____

Geologic Data

Based on "As Built" Log of Test Borings dated _____

GWS _____

Earthquake Data

Fault: Magnitude: _____.____

Distance to Site from Fault: _____.____ miles

Horizontal Bedrock Acceleration (max): 0.____g

Use Design Force Coefficient Curve for Depth:

0 - 10, 10 - 80, 80 - 150, >150

Liquefaction Potential: Low____ Med.____ High____

"As Built" Foundation

Piles — Spread Footings

Pile Type(s) _____

Design Load _____

Est. Ultimate Compression Load for Retrofit Design _____

Est. Ultimate Uplift Load for Retrofit Design _____

Scour Potential N/A____ Yes____ No____

Remarks

Additional Drilling Required: Yes____ No____

Prepared by: _____

cc: Office of Engineering Geology
MLMcCauley

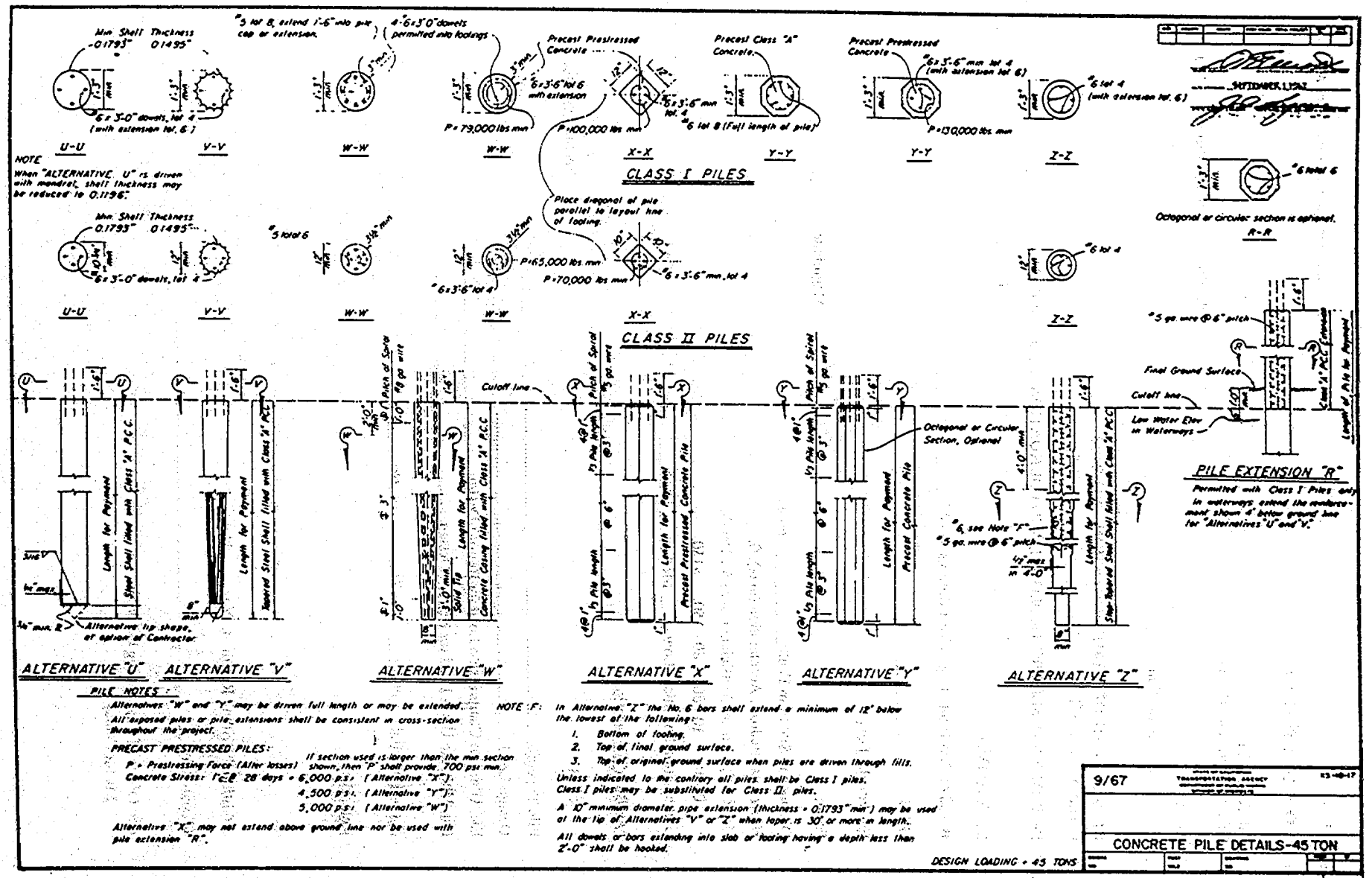

PILE NOTES :

Alternatives "W" and "Y" may be driven full length or may be extended.

All exposed piles or pile extensions shall be consistent in cross-section throughout the project.

PRECAST PRESTRESSED PILES:

P = Prestressing Force (After losses) If section used is larger than the min section shown, then "P" shall provide 700 psi min.

Concrete Stress: f'c @ 28 days = 6,000 p.s.i (Alternative "X")
4,500 p.s.i. (Alternative "Y")
5,000 p.s.i. (Alternative "W")

Alternatives "X" may not extend above ground line nor be used with pile extension "R".

NOTE F: In Alternative "Z" the No. 6 bars shall extend a minimum of 12" below the lowest of the following:

1. Bottom of footing.
2. Top of final ground surface.
3. Top of original ground surface when piles are driven through fills.

Unless indicated to the contrary all piles shall be Class I piles. Class I piles may be substituted for Class II piles.

A 10" minimum diameter pipe extension (thickness = 0.1793" min) may be used at the tip of Alternatives "V" or "Z" when taper is 30' or more in length.

All dowels or bars extending into slab or footing having a depth less than 2'-0" shall be hooked.

DESIGN LOADING - 45 TONS

9/67

CONCRETE PILE DETAILS-45 TON

B2-1

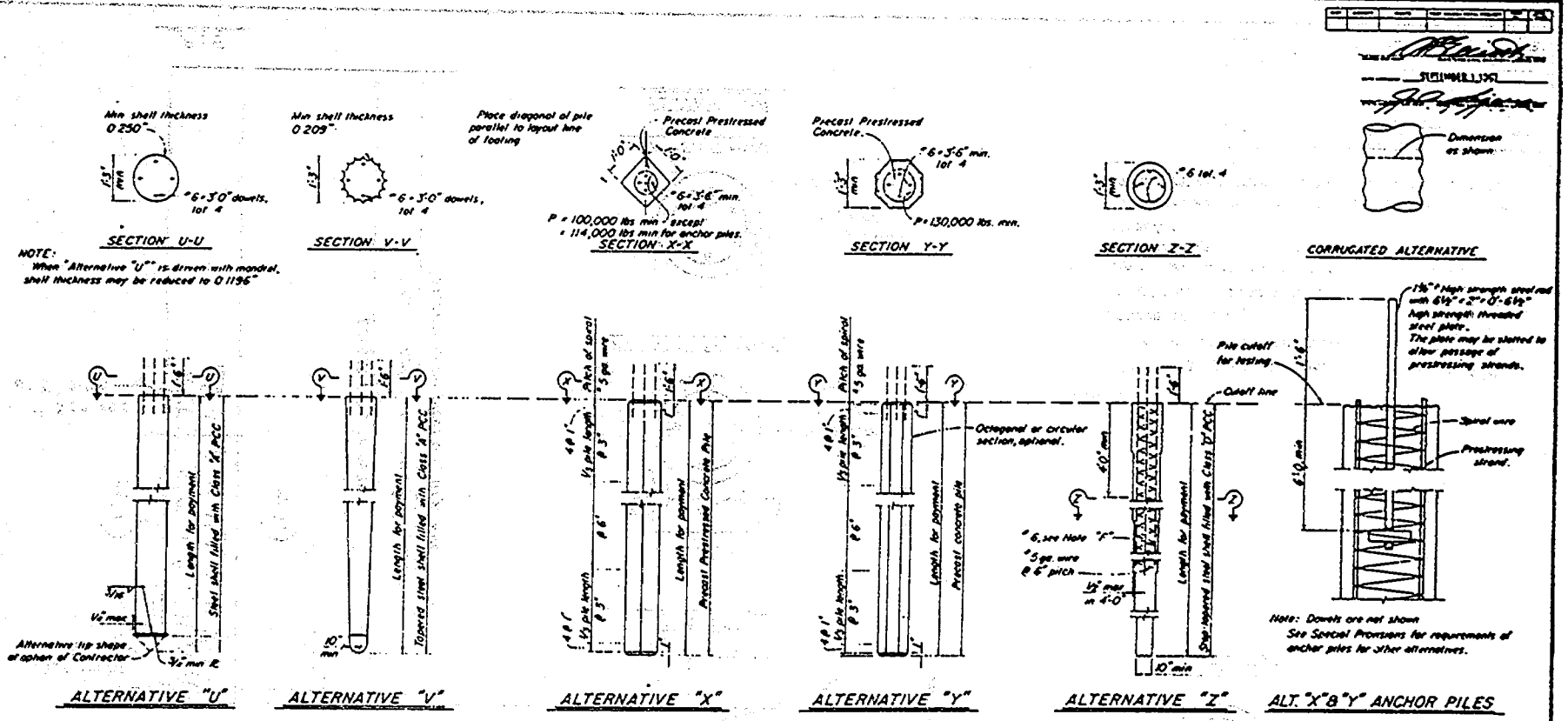

A 10" minimum diameter pipe extension (thickness = 0.250" min.) may be used at the tip of Alternatives "V" or "Z" when taper is 30" or more in length.

PRECAST PRESTRESSED PILES:
P = Prestressing Force (After losses)
Concrete Stress: f'_c @ 28 days = 6,000 psi (Alternative "X")
5,000 psi (Alternative "Y")

All dowels or bars extending into slab or footing having a depth less than 2'-0" shall be hooked

NOTE: "F"
(In ALTERNATIVE "Z" the No 6 bars shall extend a minimum of 8' below the lowest of the following:
1. Bottom of footing.
2. Top of final ground surface
3. Top of original ground surface when piles are driven through fills

DESIGN LOADING - 70 TONS

9/67

CONCRETE PILE DETAILS - 70 TON

82-5

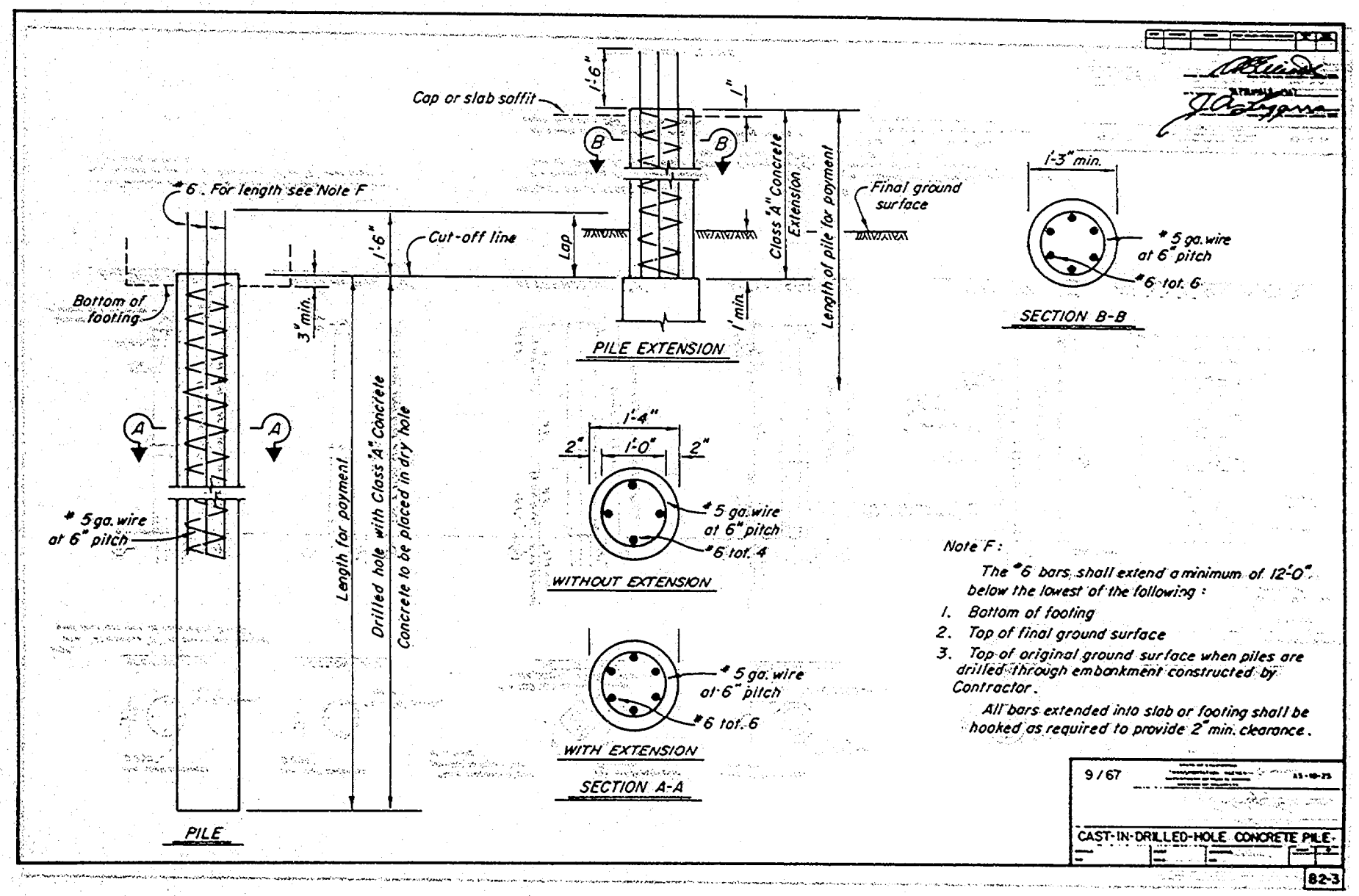

Note F :

The #6 bars shall extend a minimum of 12'-0" below the lowest of the following :

1. Bottom of footing
2. Top of final ground surface
3. Top of original ground surface when piles are drilled through embankment constructed by Contractor.

All bars extended into slab or footing shall be hooked as required to provide 2" min. clearance.

9/67

CAST-IN-DRILLED-HOLE CONCRETE PILE

82-3

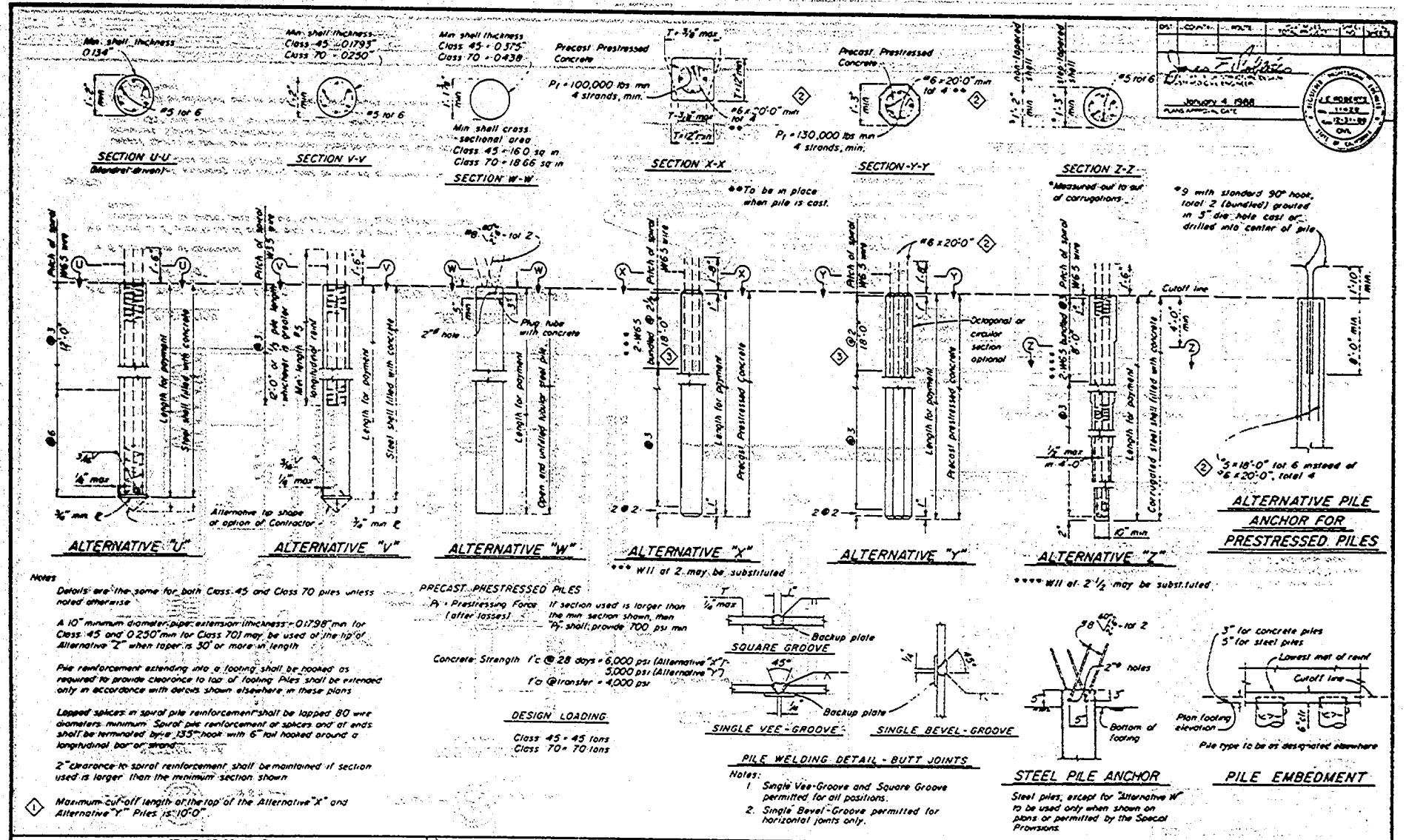
SECTION U-U
(Mandrel driven)
SECTION V-V
SECTION W-W
SECTION X-X
SECTION Y-Y
SECTION Z-Z
ALTERNATIVE "U"
ALTERNATIVE "V"
ALTERNATIVE "W"
ALTERNATIVE "X"
ALTERNATIVE "Y"
ALTERNATIVE "Z"
ALTERNATIVE PILE ANCHOR FOR PRESTRESSED PILES
Notes
Details are the same for both Class 45 and Class 70 piles unless noted otherwise
A 10" minimum diameter pipe extension (thickness = 0.1798" min for Class 45 and 0.250" min for Class 70) may be used at the tip of Alternative "Z" when taper is 30' or more in length
Pile reinforcement extending into a footing shall be hooked as required to provide clearance to top of footing. Piles shall be extended only in accordance with details shown elsewhere in these plans
Lapped splices in spiral pile reinforcement shall be lapped 80 wire diameters minimum. Spiral pile reinforcement at splices and at ends shall be terminated by a 135° hook with 6" tail hooked around a longitudinal bar or strand
2" clearance to spiral reinforcement shall be maintained if section used is larger than the minimum section shown
Maximum cut-off length at the top of the Alternative "X" and Alternative "Y" Piles is 10'-0"
PRECAST PRESTRESSED PILES
Pi = Prestressing Force (after losses)
If section used is larger than the min section shown, then Pi shall provide 700 psi min
Concrete Strength f'c @ 28 days = 6,000 psi (Alternative "X") 5,000 psi (Alternative "Y")
f'c @ transfer = 4,000 psi
DESIGN LOADING
Class 45 = 45 tons
Class 70 = 70 tons
SQUARE GROOVE
SINGLE VEE-GROOVE
SINGLE BEVEL-GROOVE
PILE WELDING DETAIL - BUTT JOINTS
Notes:
1. Single Vee-Groove and Square Groove permitted for all positions.
2. Single Bevel-Groove permitted for horizontal joints only.
STEEL PILE ANCHOR
Steel piles, except for "Alternative W" to be used only when shown on plans or permitted by the Special Provisions
PILE EMBEDMENT
Pile type to be as designated elsewhere
STANDARD DRAWING
3/87
State of CALIFORNIA
DEPARTMENT OF TRANSPORTATION
DIVISION OF STRUCTURES
STRUCTURE DESIGN
PILE DETAILS - CLASS 45 & CLASS 70
82-5

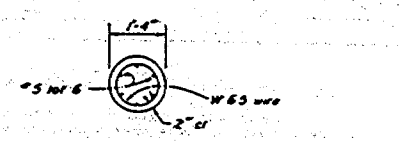

SECTION A-A
3/4" = 1'-0"

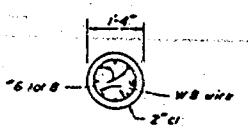

SECTION B-B
3/4" = 1'-0"

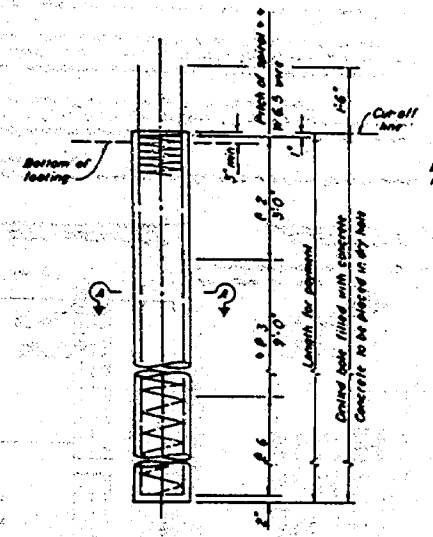

ELEVATION
45 & 70 TON DESIGN LOAD
3/4" = 1'-0"

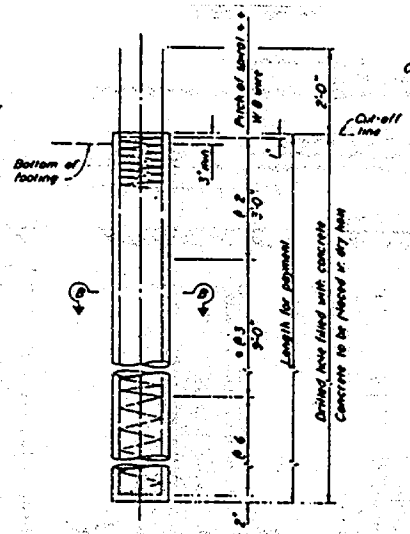

ELEVATION
100 TON DESIGN LOAD
3/4" = 1'-0"

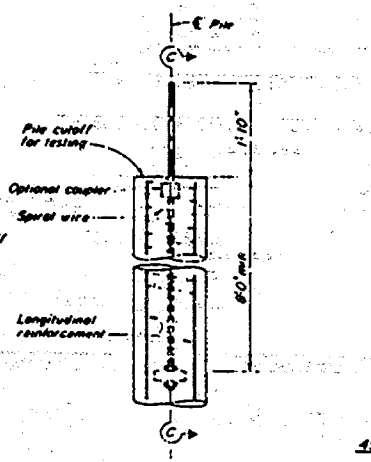

ANCHOR PILE CONNECTION

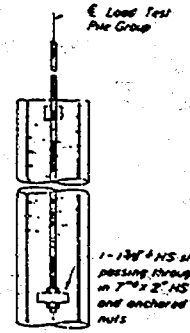

45 TON and 70 TON DESIGN LOAD

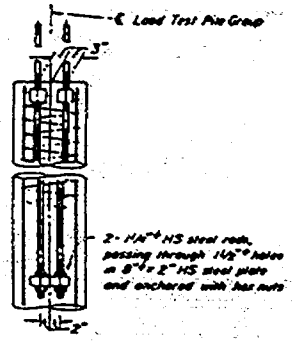

100 TON DESIGN LOAD

SECTION C-C

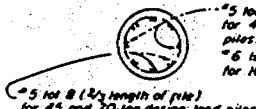

SECTION D-D

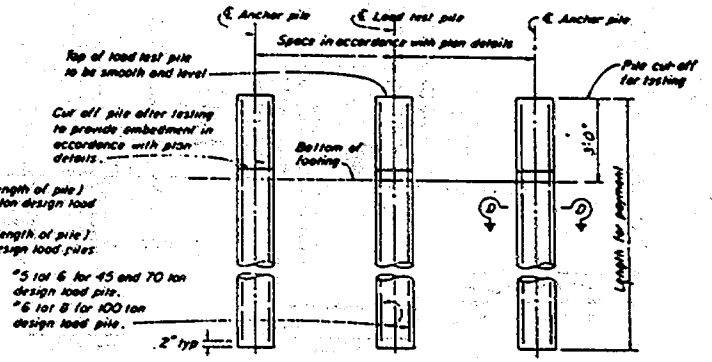

LOAD TEST PILE GROUP

* ℄ 2 at option of contractor

** Extend at 2" pitch to top of anchor piles and load test piles. For longitudinal reinforcement for anchor piles and load test piles, see "Load Test Pile Group" detail.

NOTES:

Reinforcement extending into footing shall be hooked as required to provide clearance to top of footing.

Lapped splices in spiral pile reinforcement shall be lapped at least 80 wire diameters. Spiral pile reinforcement at splices and at ends shall be terminated with a 135° hook with a 6" tail hooked around a longitudinal bar.

Piles shall be extended only in accordance with details shown in the Project Plans.

STANDARD DRAWING

3/87

State of CALIFORNIA
DEPARTMENT OF TRANSPORTATION

DIVISION OF STRUCTURES
STRUCTURE DESIGN

16" CAST-IN-DRILLED-HOLE CONCRETE PILE

82-3

(5) Session 5

SESSION 5: WIND RESISTANT DESIGN(I) 3:20pm～4:20pm
(Co-Chairmen: K. Yokoyama, Abdel-Ghaffar)

(13) E. Sato, H. Tominaga*, K. Namikawa, R. Kiyota, K. Tanida and T. Nose : A Damping Device on Main Tower Erection (The Suspension Bridge in Metroporitan Expressway Route No. 12) (3:20pm～3:35pm)

(14) N. P. Jones, R. H. Scanlan and F. Ehsan : Effect of Sidewalk Vents on Bridge Response to Wind (3:35pm～3:50pm)

(15) M. Niiyama, H. Kawasaki and Y. Saito* : Resistance/Stability to the Wind of Hakucho-Ohhashi (3:50pm～4:05pm)

DISCUSSION
(4:05pm～4:20pm)

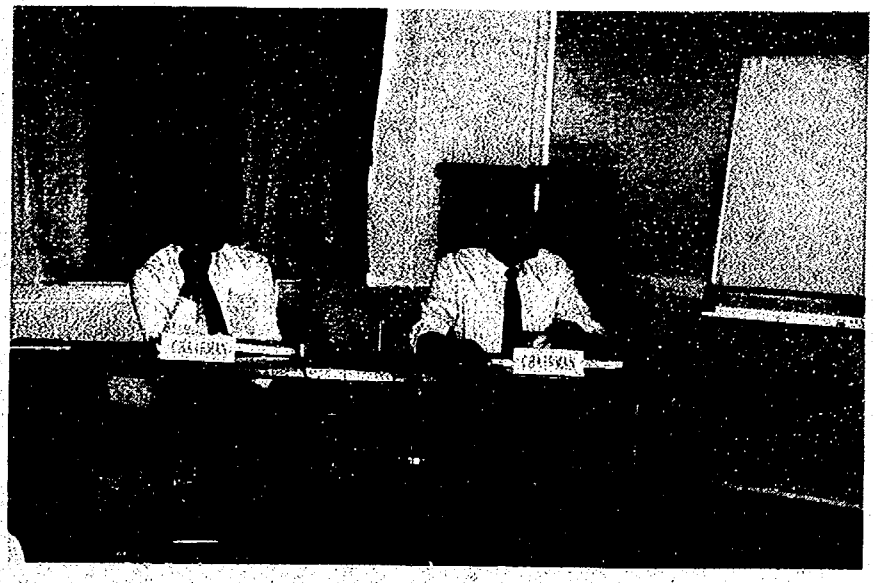

A DAMPING DEVICE ON MAIN TOWER ERECTION FOR THE SUSPENSION BRIDGE IN METROPOLITAN EXPRESSWAY ROUTE NO.12

Eisaku Sato[1], Hiroo Tominaga[2], Kenji Namikawa[3], Renji Kiyota[4], Kouji Tanida[5], Takashi Nose[6]

1) Assistant Section Manager, Design Section, No.3 Construction Department, Metropolitan Expressway Authority
2) Group Leader, -Ditto-
3) Engineer, -Ditto-
4) Deputy General Manager, Research Institute, Yokogawa Bridge Works, Ltd.
5) Section Manager, Vibration Reserch Dept., Reserch Institute, Ishikawajima-Harima Heavy Industries Co.,Ltd.
6) Acting Section Manager, Design Dept., Bridge Division, -Ditto-

EPITOME

It is widely known that free standing towers of suspension bridges, during construction suffer from vibration due to wind action. In this connection, review on aerodynamic stability through wind tunnel tests for the towers of this bridge was inevitably carried out as occurrence of vibration was foreseen at the early stage of the bridge planning.

In consequence of the tests, it was confirmed that three (3) kinds of vortex excited vibration will be generated and a damping device should be installed, accordingly. Considering the erection methods as well as the site conditions, a damper was mounted at the top of the tower.

This paper will outline the results of the wind tunnel tests and introduce the mechanism of the damper which was employed in conformityto the results of the test.

1.PREFACE

The Metropolitan Expressway Route No.12 is a 4.5 km long overpass bridge crossing the Tokyo Bay.It links Shibaura District of Minato-ku to the Bayshore Subcenter of Tokyo. A section over the Channel No.1 is a three span (two-hinged) suspension bridge with a trussed stiffening girder, having an overall length of 798 m and a center span of 570 m. (See Figs 1.1 and 1.2.)

The top deck of stiffening girders is to carry a four-lane highway, while the bottom deck provides a four-lane bayside road, pedestrian walkways, and a rail track for a new transportation system. As Figs. 1.4 and 1.5 express, a rigid structure, that does not need either lateral or diagonal members, was adopted to the tower above the road surfaces. The columns have rounded corners, and welding was employed for most of the field splices in consideration of aesthetics.
From the beginning of the project, wind observation followed by

such extensive wind tunnel tests for tower, partial stiffening girder and entire bridge models, were implemented to ascertain site wind characteristics around the site.[1)-6)]

This preparatory studies revealed that carefull attentions must be paid to the aerodynamic stability of a free standing tower. At the free standing condition, the vortex excited vibrations of out-plane deflection and torsional oscilation would occur at low speed wind transverse to the bridge axis, and also galloping of in-plane deflection by wind longtudinal to the bridge axis expected to occur at high wind speed.

This paper reports the results of the wind tunnel tests implemented during construction for a model with ultimate geometry of the towers, and introduces the damping device provided in accordance with the results of the test.

2.REVIEW ON AERODYNAMIC STABILITY

2.1 OUTLINE OF WIND TUNNEL TEST

In general, aerodaynamic unstability due to wind transverse to the bridge axis is a traditional program for a free standing tower of suspension and cable-stayed bridges. Also, it becomes into a subject of discussion that in-plane galloping by wind transverse to the bridge axis is highly expected to occur as advantage in aesthetics encourages rigid sturactures to increase in numbers. In this project as well, generation of out-plane deflection, vortex excited torsional oscillation, and galloping of in-plane deflection during erection had been confirmed through the tests in the planning phase. Further, the test reported that, at completion, in-plane oscillations (galloping) is possible to be generated in case when structural damping is not more than 0.02 though this does not menace structural safety.

Viewing the above preliminary information, the wind tunnel tests attempting to catch up the aerodynamic stability upon tower erection and completion of the suspension bridge as well as the requiredcapacity of the damping device was carried out prior to the commencement of tower fabrication.

The Eiffel type wind tunnel owned by Research Institute of Ishikawajima-Harima Heavy Industries Co.,Ltd. was used for the test. 1/60 scale elastic models representing three conditions of tthe tower,basic, free-standing, and completed, as sketched in Fig.2.1. were experimented. Among the three, the basic model is to understand the Reynolds effects by the rounded portions of the tower columns. Besides, equipments to be utilized for the erection of cable and stiffening girders were arranged on the free-standingtower model. The completed tower model was designed to ascertain in-plane deflection vibration. The effects of the mass of the cable and the girder were modelled by substituting equivalent masses at the top of the tower.

Logarithmic decrement was assumed to be δ=0.01 for the free

standing condition and δ=0.02 for completion. The dampimg was varied by degrees. In the test to decide capacity of the damper for a free-standing tower, a wind flow was set uniform from a standpoint of safety. Fig.2.2 shows the vibration modes of the free-standing tower, while Fig.2.3 provides the observed wind characteristics around the site and Table 2.1 shows the design wind velocities.

2.2 AERODYNAMIC STABILLITY OF TOWERS DURING CONSTRUCTION

As the results of the test for the free-standing tower model, the amplitude-horizontal wind derection curve (A-β), the wind speed-amplitude curve (V-A), and the amplitude-damping curve (A-δ) are shown in Figs. 2.5-7. And the characteristics of tower vibration during the erection of the cables and the girders are listed in Table 2.2. In this table, characteristics of completed catwalk system and completed main cable are estimated from free-standing experiment results.

Aerodynamic stability during construction surmised by these terms will be stated hereinafter.

1) Tower Out-Plane Oscillation

The 1st mode vortex excited vibration of out-plane deflection takes place under the wind velocity of 10m/sec for all wind direction except the bridge axis direction. Assuming vibration during erection, amplitude is below 30cm. As amplitude will be further decremented when turbulent flow is considered, no safety caution against this vibration is required. However, since the vibration appears under such low wind velocity during daily erection work is carried out and frequently occurs, a countermeasure to sufficiently manage affects on workers was imperative.
Hence, it was determined to provide the damper during the erection of the towers and stiffening girders.

The 2nd mode vortex excied vibration of out-plane deflection takes place under the wind velocity of 50m/sec for the horizontal wind direction within β=0°-45°. As the vibration appears when wind speed is above the design wind velocity of erection and amplitude is not more than 20 cm, no safety caution was considered.

2) Tower In-Plane Oscillation

The 1st vortex excited vibration of in-plane deflection takes place under wind velodity of V=22-40 m/sec for all wind direction except transverse direction to the bridge axis. Therefore, this vibration will affect on the safety of the tower. On the other hand, the test result with the completed model has found the vibration never occur under a condition of the structural damping of δ=0.02 and an addition of the 37.6% mass of girder and cable. However, it is impossible to clearly pursue when the aforementioned condition is established. Consequently, it was determined to provide the damper against this vibration during the erection of the towers and girders.

3) Torsional Oscillation
During the test, torsional oscillation has happened under terms of β=0°-45° and V=35-45m/sec. The vibration to require the damping device both upon tower's free-standing and completion of catwalk was anticipated. However, the wind velocity upon completion of the catwalk is just below the wind velocity at erection, and the structural damping under this condition is expected to be beyond δ=0.01. Accordingly, damping measure for the duration from tower free-standing till completion of catwalk installation is provided.

2.3 AERODYNAMIC STABILITY AT COMPLETION

As the result of the in-plane deflection of the completed model, Fig.2.7 shows amplitude-added mass (A-Δm) curve. The vibration disappeared when the 37.6% of the mass of the cables and the girders was added under a condition of the structural damping of δ=0.02. Therefore, no precaution is required on aerodynamic stability at the bridge completion.

3.REVIEW ON CAPACITY OF THE DAMPER

3.1 ALLOWABLE VIBRATION

Allowance of vibration shall be determined subject to safety for structures, facilities and erection operation. Generally, safety for structures shall be studied on both aspects of strength and fatigue, however, only the strength aspect was reviewed on this particular bridge since only erection peiod was considered. The ultimate wind velocity for erection works was determined to be 16m/sec and the vibration to be induced within this velocity was reviewed.

3.2 REQUIRED DAMPING CAPACITY

After reviewing from multiple angles, a mass damper type has been adopted to set on the towers. The required damping capacity (mB) and required structural damping (δa) were computed and listed in Table 3.2, where m is the mass of the damper and B is the the volume of the movement of the damper.

4.DAMPER AT SHIBAURA SIDE

The damping device set on the Shibaura-side tower is shown on Fig.4.1. The device is prepared to correspond to all of the vibration mode for which damping is required.

1) Mechanism
The device is a mass damper of an active control system to detect vibration by accelerometers, and control it by giving external force corresponding to the level of acceleration. The mechanism is schematized in Fig.4.2. The rotation of the motor is shifted and the crank is rotated in accordance with the tuned frequency. And the sliding block located on the crankshaft makes a rectilineal motion along the slit together with making a rotary

motion. Therefore, the moving mass will make a rectilineal motion the rail. The amplitude of the moving mass is controlled by changing length of the crankshaft.

2) Method of Damping
Damping system is expressed in Fig.4.3. Accelerometers 1 and 2 detect vibrational acceleration of the tower out-plane while accelerometer 3 detects that of tower in-plane. The detected acceleration is sorted in in-plane, out-plane, and torsional vibration through a differential amplifier. Each data is transmitted to a waveform analyzer, then shape of the vibration wave is transmitted to a computer as amplitude, cycle and phase information. The computer will choose a vibration mode to cope with the vibration of the tower and wind data, and control amplitude of the moving mass in order to generate damping that has reverse phase from the external force. Flow chart of damping is shown in Fig.4.4.

Damping force is controled by adjusting amplitude of the moving mass. The moving distance of the mass is so regulated that amplitude of the tower is to be within the allowable amplitude. Namely, the moving distance of the mass is obtained by tower's responding acceleration. Difference in motion of the moving mass and vibration in tower feed-backed recurrently and adjusted.

3) Features
This device features;
a) Damping to correspond to the vibration mode of a structure is possible.
b) Consequently, damping for three modes of out-plane, in-plane, and torsional is available.

The device can be utillized as a generator of vibration and applied to experiments concerning vibration characteristics when a tower is under erection.

5.DAIBA SIDE TOWER

Arrangement of a damping device for Daiba side tower is shown in Fig.5.1 and an outline of the device is figured in Figs.5.2-4. HMD (Fig.5.2.) and TMD(A) (Fig.5.3)are arranged in the center of the top horizontal strut. The former is to correspond to the vibration of out-plane deflection generated within the ultimate wind velocity for erection works, and the latter is to correspond to the vibration of in-plane deflection.

TMD(B) mounted outside the tower-top saddle is to correspond to the torsional oscillation generated during tower free-standing condition and till completion of catwalk installation as well as out-plane vibration occurring under wind velocity over the ultimate wind velocity for erection works after completion of catwalk installation. Outlines of the each component are as follows.

5.1 HMD (Hybrid Mass Damper)

1)Mechanism
A damping device by a mass damper is generally classified if the device controls the movement of the mass or not, and the former is called AMD (Active Mass Damper) and the latter is called TMD (Tuned Mass Damper).

HMD is a combination of the both dampers, and controls mass movement by actuator while a mass is added to have restoring force as same as TMD.

The device is composed of motor, reducer, pinion drive, circumferential counterweight (damping body), and roller to support counterweight.

A counterweight is functioned to swing on roller by forwarding or reversing a motor. And as a counterweight is circumferential, passive mechanism to naturally swing in accordance with tower vibration is equipped.

2) Control Method
The damping device is comprised of sensor (accelerometer) to detect tower vibration, computer to direct most appropriate control of counterweight after receiving signal from sensor and actuator (electric servomotor) to work counterweight based on computer's directive.

The counterweight works most effective when moving with 90° topology delay from tower.
In this case, vibration speed of tower and accelaration of the device have same phase and are adverse from displacement of the device. (Fig.5.6)
The device applies the avobe theory, and the flow chart of damping control is shown in Fig.5.7.

3) Features
HMD features;
a)As passive mechanism requires smaller damping force from the outside.
b)Less trouble and easy maintenance.
c)Damping is kept effective even when power is suspended.

5.2 TMD(A), TMD(B)

In this device, movement of the counterweight consumes energy induced by wind. An essential composition is similar to a pendulum and the counterweight is hung by 4-lifting members from a frame. Also, a spring put in spring case is attached so as to accord an inherent frequency of the device with that of the tower, and its position can be adjusted by several steps.
Furthermore, hydraulic dampers are placed between lifting members and a frame to give required damping in the device.
The following two (2) counterplans are considered to cope with variation of an inherent frequency of the tower during erection

of the suspension bridge.

a)Damping is capable of regulating 5 % of a gap of an inherent frequency.
b)Changing spring location to attach enables to adjust an inherent frequency.

Afterword

Recent sky-scraperization of such tower-shaped structures as those in suspension bridges, cable stayed bridges and buildings is more and more remarkable. And consideration of aesthetics for structures causes aerodynamically unstable vibration.

A variety of damping devices equipped in these structures has been in use. However, application of the device with active mechanism as introduced in this paper is seldom. This is because the damping device is still under development, and complicated phenomenon of vibration requires complex damping mechanism. From this point of view, it is the authors' pleasure if the report would help further development of the damping device.

REFERENCES

1)Terayama & Hasegawa :"Meteorological Observation on Metropolitan Expressway Route No.12", No.41 Annual Speech in Japan Society of Civil Engineers (JSCE)
2)Yamamoto & Sato :"Investigation Report on Aerodynamic Stability of Yokohama Bay Bridge", Materials of Public Works Research Institute (1980, 1981)
3)Ito, Fujino, Ki & Iwamoto : Response Characteristics on Wind Stability of Main Towers in Tokyo Port Bridge", No.42 Annual Speech in JSCE
4)Itakura, Ito, Fujino & Ki : "Review on Aerodynamic Stability of Stiffening Girders in Tokyo Port Suspension Bridge", No.43 Annual Speech in JSCE
5)Hanno, Kosaka & Ki : "Wind Tunnel Tests on Entire Span of the Suspension Bridge with Double-Decked Stiffening Girders", No.44 Annual Speech in JSCE
6)H.Kosaka, H.Hanno and Y.Fujino : "Wind Tunnel Test on Tokyo Port Bridge", 5th U.S.-Japan Bridge Workshop, 1989
7)Ohnuki, Kosaka & Hanno : "Review on Aerodynamic Stablity of Tokyo Port Bridge (Suspension Bridge Section)", Bridge and Foundation (1990.10)

Table 2.1
Desigh Wind Velocity for Tower

	Wind Velocity (m/s)	Remarks
Bridge Completion	V_D= 69.2	
During Construction	V'_D= 48.9	$V_D/\sqrt{2}$

Table 2.2 Tower Vibration during Erection

		Inherent Freq f (Hz)	Wind Velocity V (m/s)	Ampl. A	Acc. α (gal)
1st mode of 0-P Defle.	Free-Standing	0.260	7.5	28 cm	75
	With Catwalk System	0.504	14.6	23 cm	231
	With Cable	1.058	30.8	17 cm	751
1st mode of 0-P Defle.	Free-Standing	0.610	25.2	133 cm	1 954
	With Catwalk System	0.610	25.2	133 cm	1 954
	With Cable	0.610	25.2	133 cm	1 954
Torsional Osccillation.	Free-Standing	0.951	41.4	2.4 °	2 178
	With Catwalk System	1.021	44.4	2.3 °	2 387
	With Cable	1.308	56.9		

Table 3.1 Allowable Vibration

		Structure		Facility		Erection Work	
		Ampl. A (cm)	Acc. α (gal)	Ampl. A (cm)	Acc. α (gal)	Ampl. A (cm)	Acc. α (gal)
1st mode of 0-P Defle.	Free-Standing	306	817	112.7	300	18.5	50
	With Catwalk System	251	2 517	29.9	300	4.5	50
	With Cable	288	12 727	6.5	300	*	*
1st mode of 0-P Defle.	Free-Standing	50	734	20.0	300	*	*
	With Catwalk System	50	734	20.0	300	*	*
	With Cable	50	734	20.0	300	*	*
Torsional Osccillation.	Free-Standing	50	464	8.0	300	*	*
	With Catwalk System	13	535	7.0	300	*	*
	Ultimate Wind Velocity for Erection Work	13	650	6.0	300	*	*

Table 3.2 Required Damping Capacity

		Allowable Ampl. Aa (cm)	Required Structural Damping δa	Required Damping Capacity mB (ts²/m)
1st mode of 0-P Defle.	Free-Standing	18.5	0.015	0.0428
	With Catwalk System	4.5	0.015	0.0932
	With Cable	6.5	0.026	0.1269
1st mode of 0-P Defle.		20.0	0.066	0.6093
Torsional Osccillation.	Free-Standing	8.0	0.076	0.3197
	With Catwalk System	7.0	0.083	0.3250
	Ultimate Wind Velocity for Erection Work	6.0	0.097	0.3476

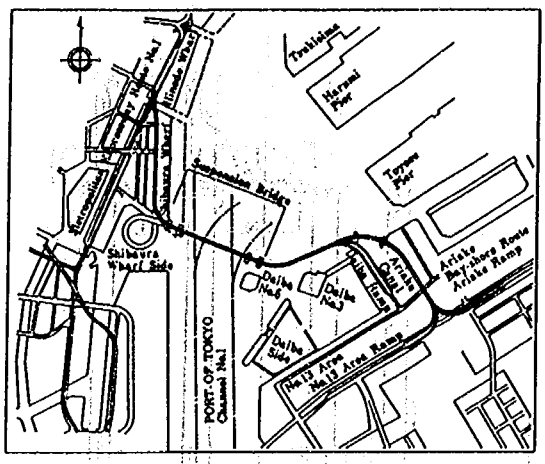

Fig.1.1 Location

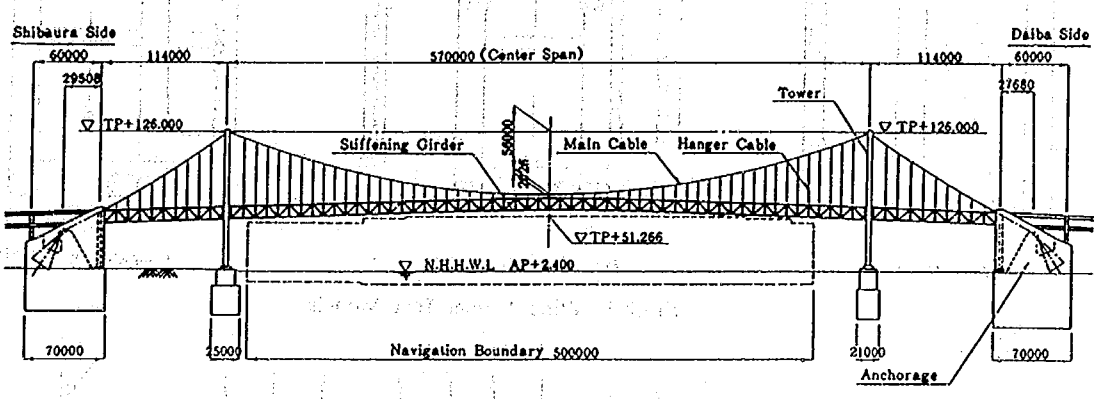

Fig.1.2 Side Elevation

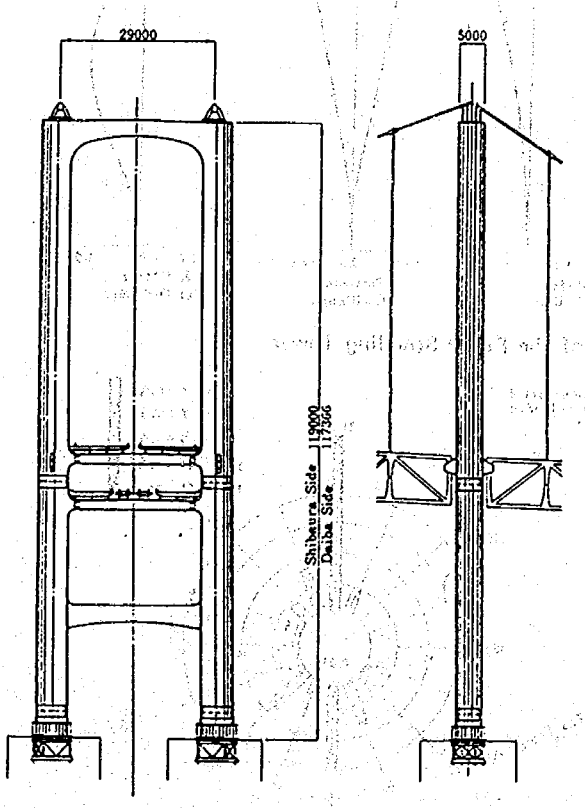

Fig.1.4 Tower Elevation

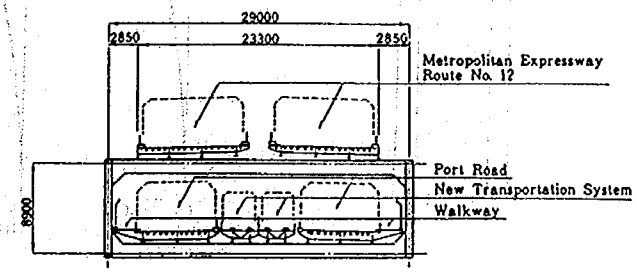

Fig.1.3 Stiffening Girder Cross Section

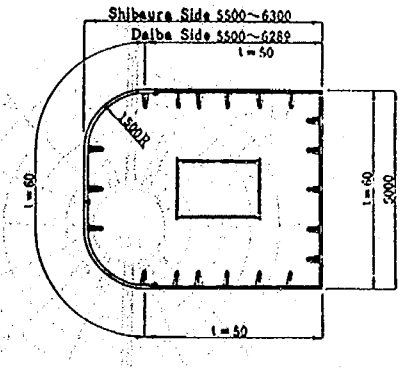

Fig.1.5 Tower Cross Section

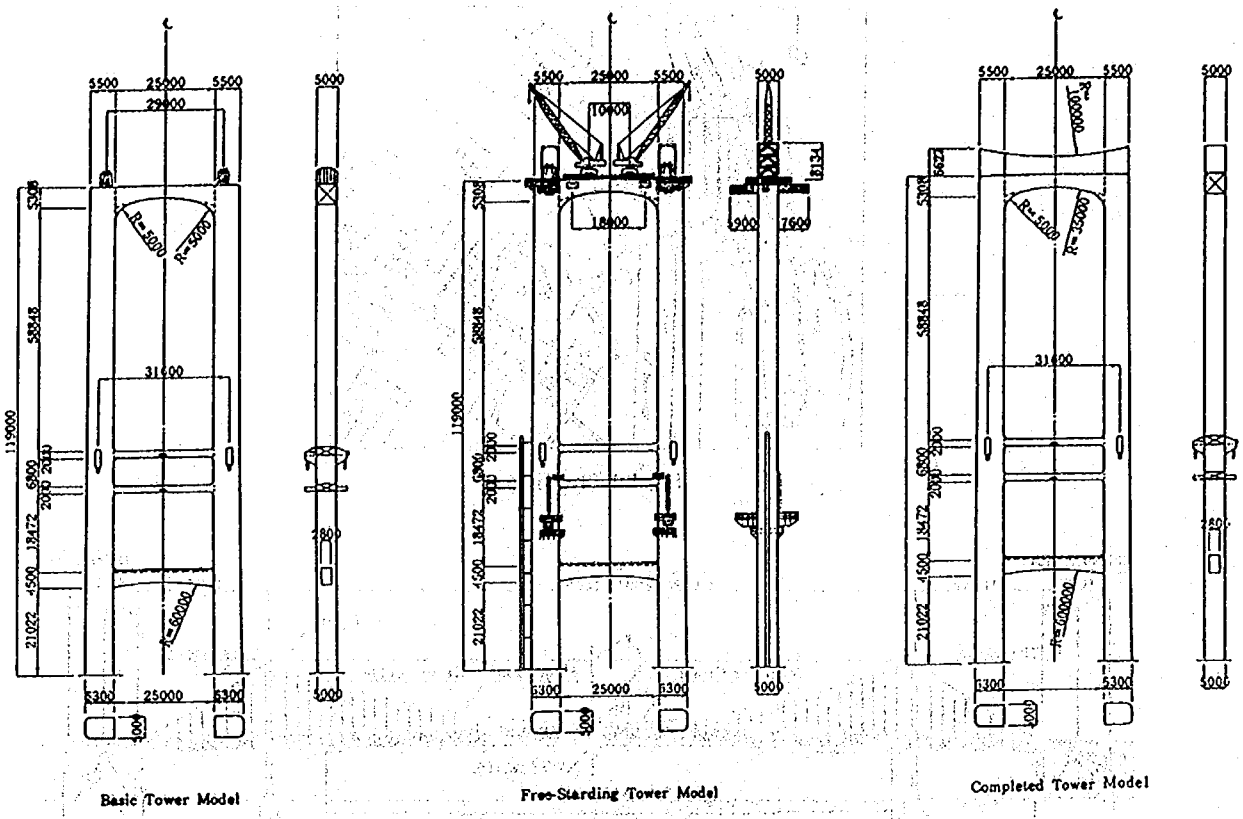

Fig.2.1 Wind Tunnel Test Models

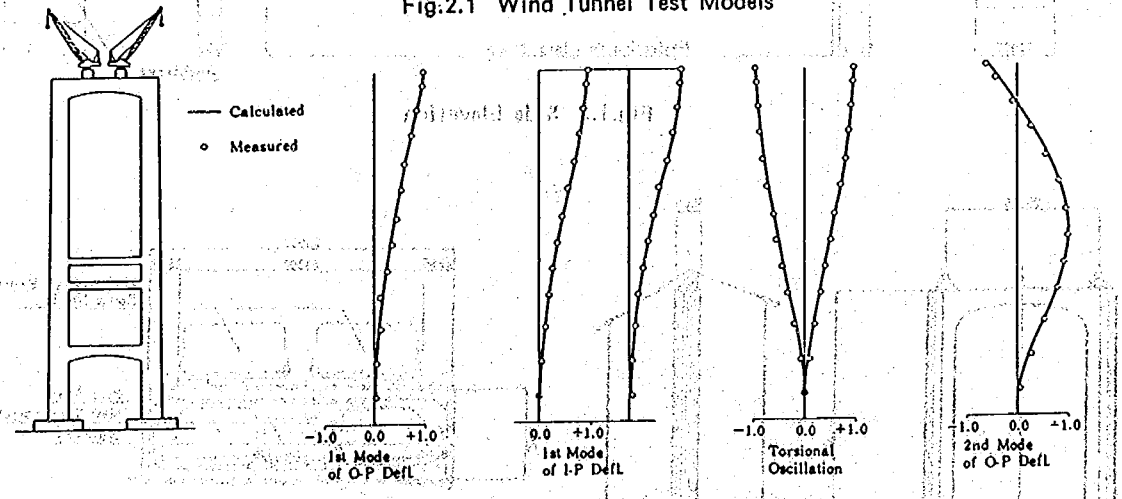

Fig.2.2 Vibration Mode of the Free-Standing Tower

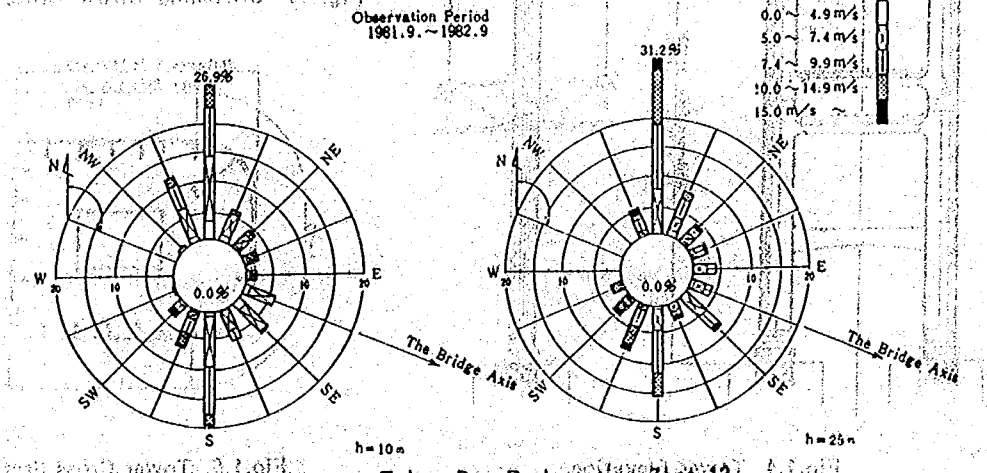

Fig.2.3 Windrose at Tokyo Bay Reclamation Zone 13

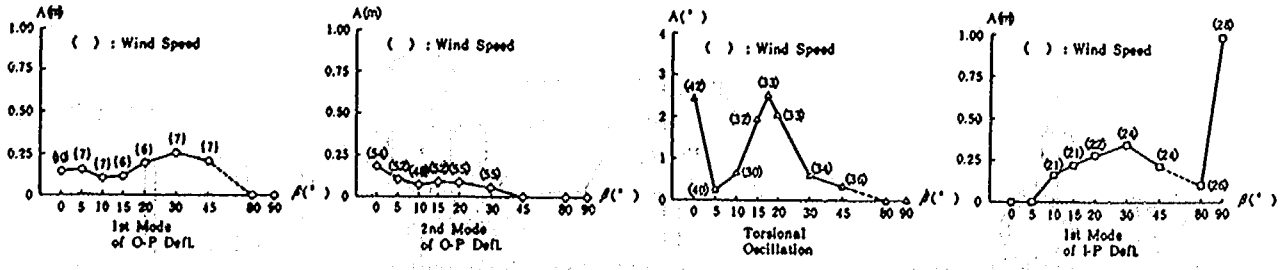

Fig.2.4 A-β Curve of F-S Model

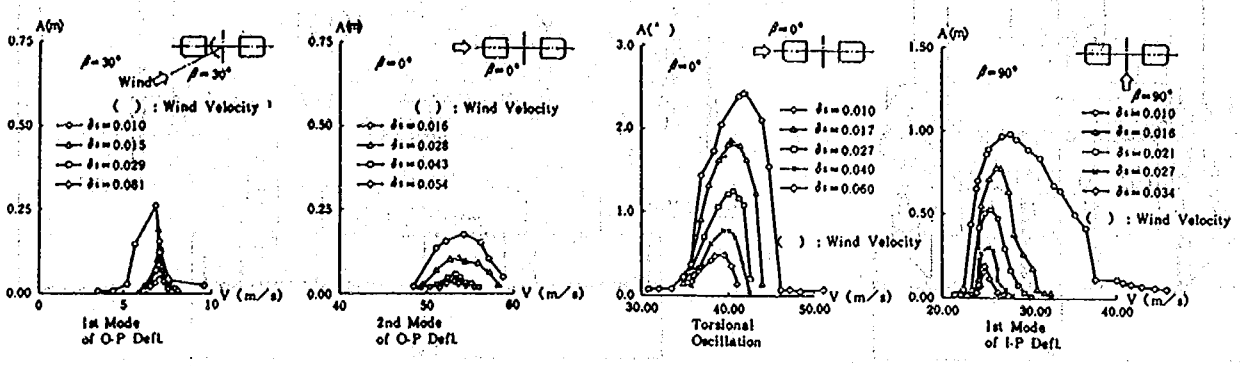

Fig.2.5 V-A Curve of F-S Model

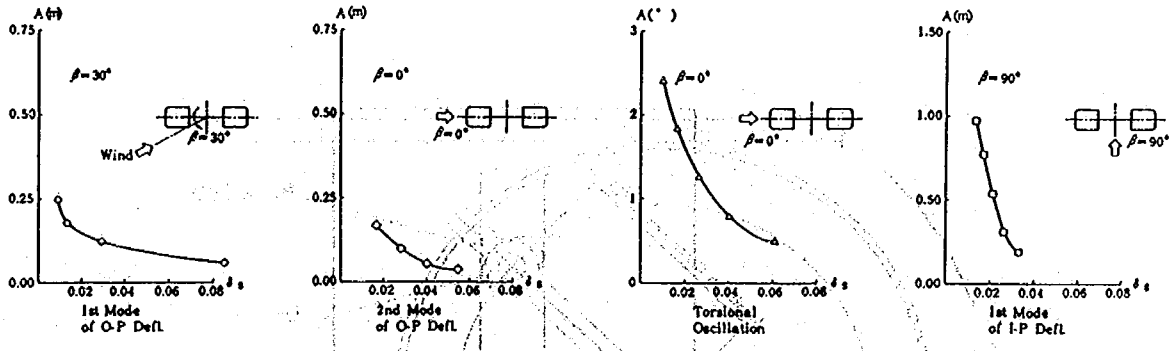

Fig.2.6 A-δ Curve of F-S Model

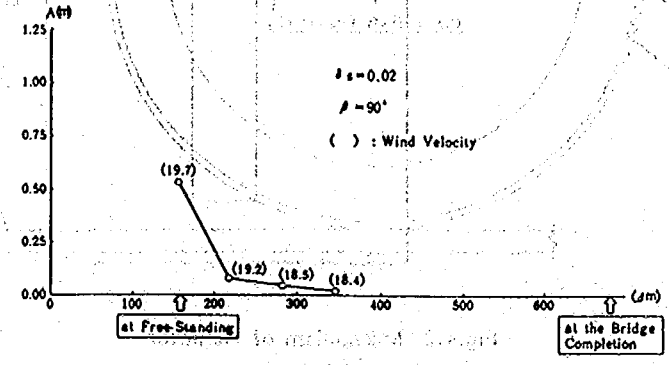

Fig.2.7 A-Δm Curve of Completed Model

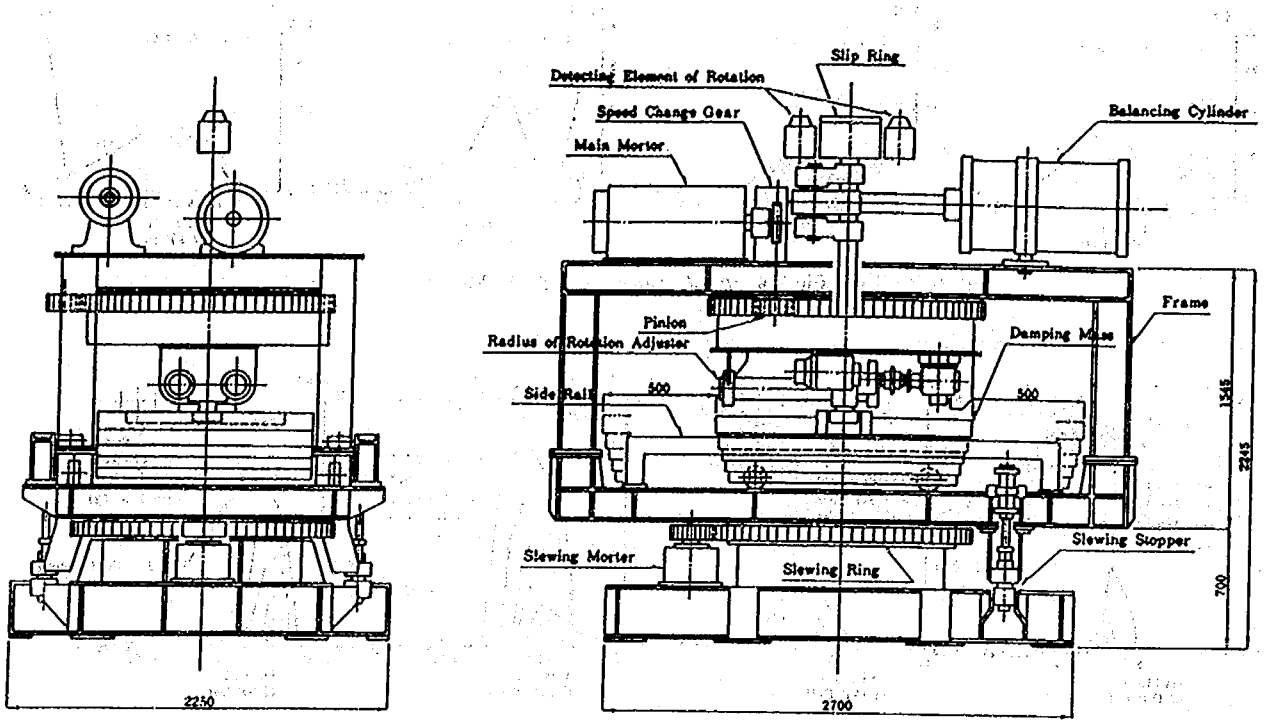

Fig.4.1 Outline of the Damping Device for Shibaura Side

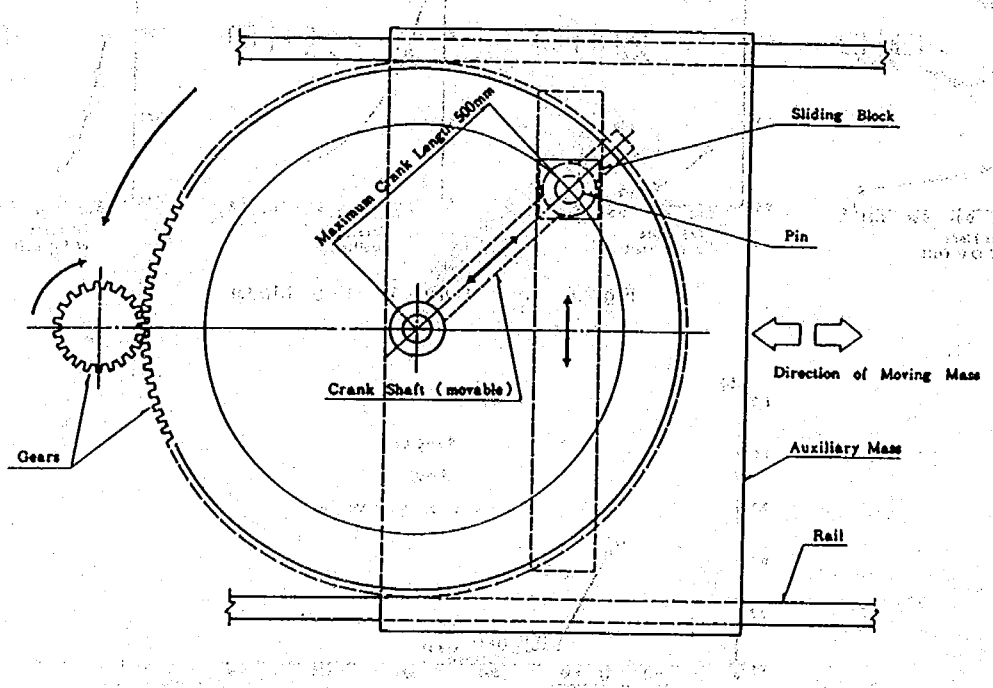

Fig.4.2 Mechanism of Actuator

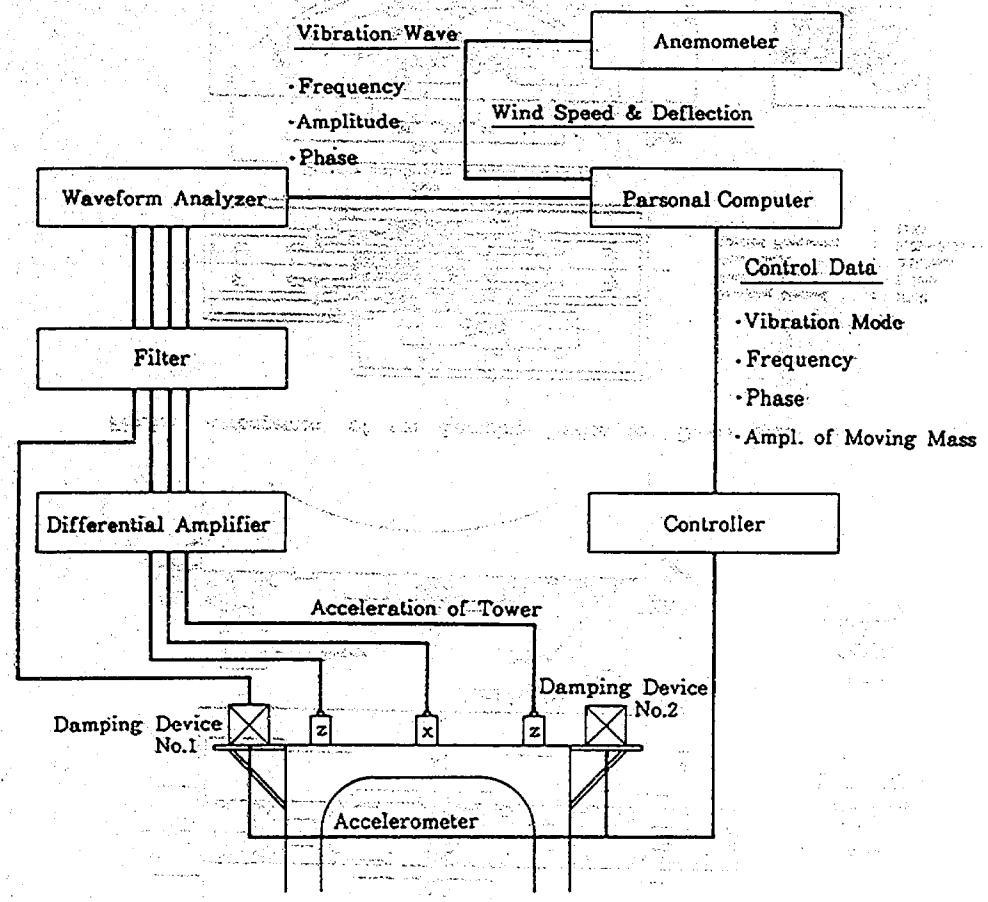

Fig.4.3 Control System

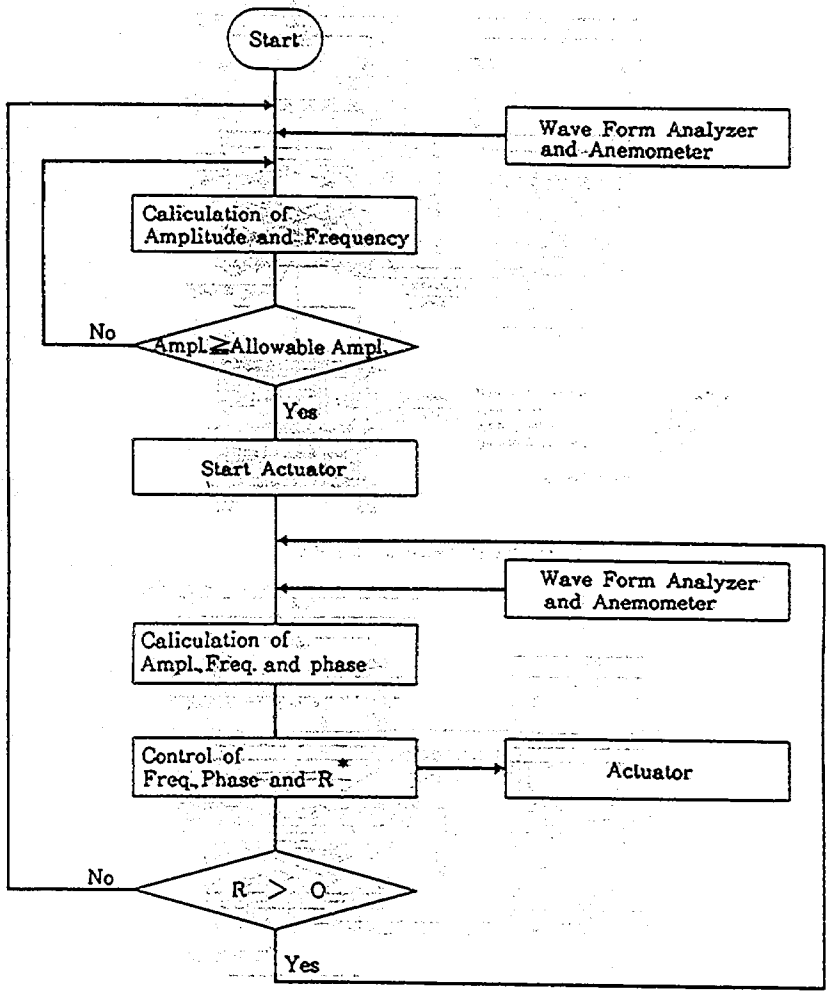

* R·····Amplitude of Mass

Fig.4.4 Flow Chart of Damping Control

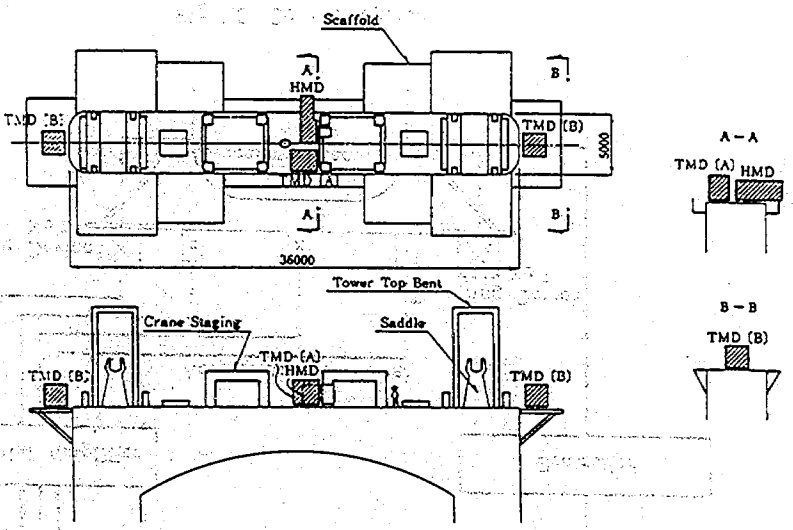

Fig.5.1 Arrangement of the Damping Device for Daiba Side

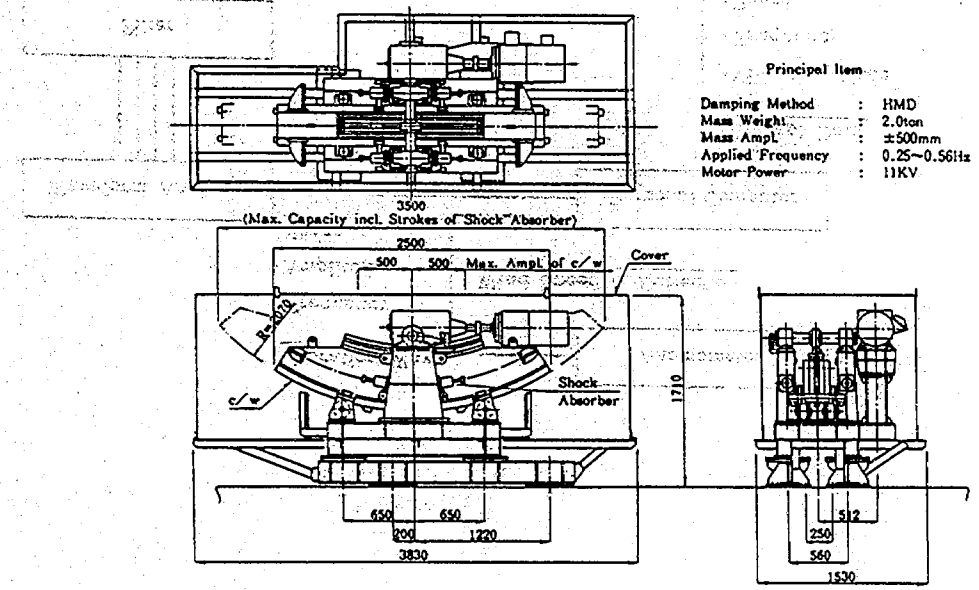

Fig.5.2 Outline of HMD

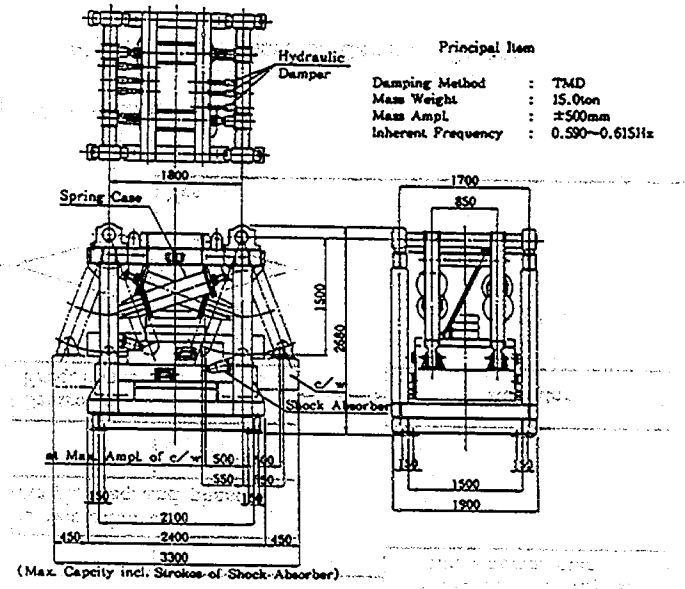

Fig.5.3 Outline of TMD (A)

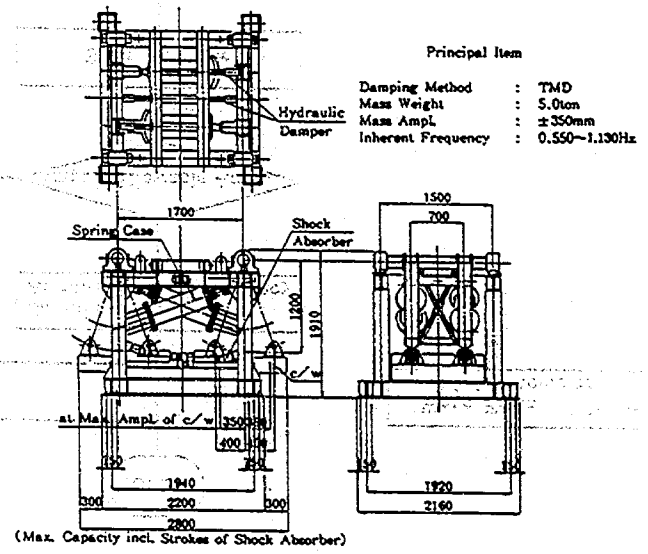

Fig.5.4 Outline of TMD (B)

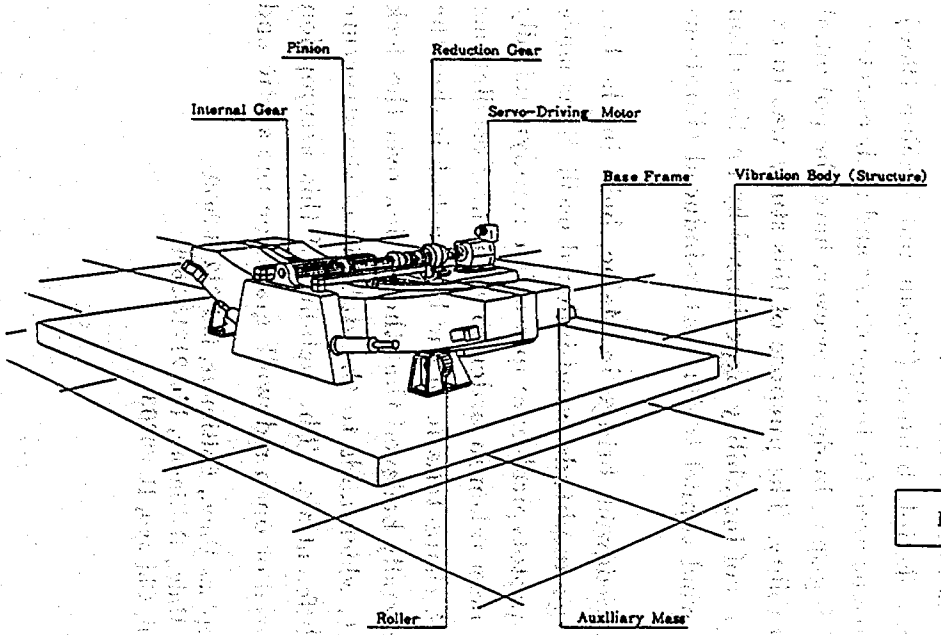

Fig.5.5 A General Idea of HMD

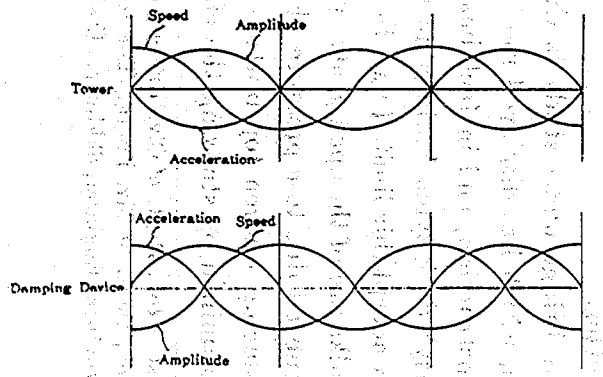

Fig.5.6 Vibration Wave of Tower & Damping Device

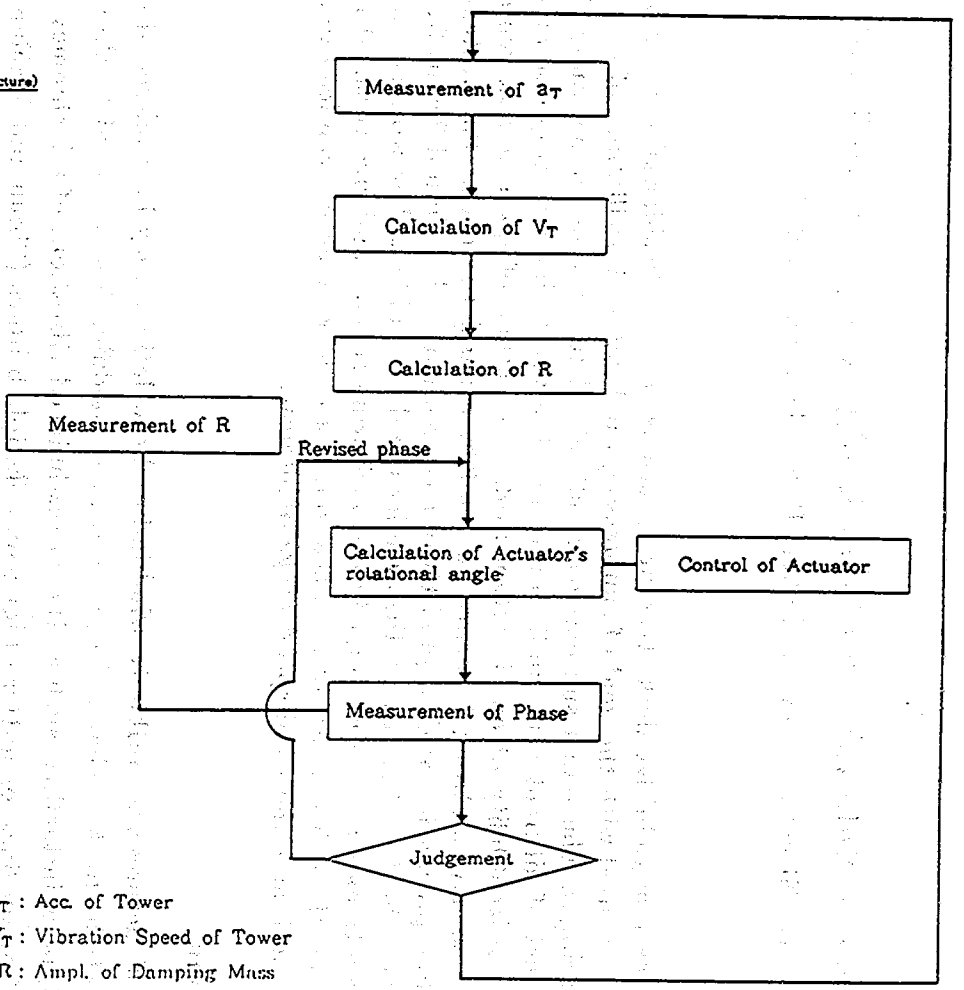

Fig.5.7 Flow Chart of Damping Control

Effect of Sidewalk Vents on Bridge Response to Wind

By Nicholas P. Jones,[1] Robert H. Scanlan,[2] and Fazl Ehsan,[3]

Abstract:

Modifications to bridge deck structures, such as open-grate sidewalks or vents, have been used with the goal of suppressing wind-induced oscillations of long-span bridges. This paper summarizes results of a detailed wind-tunnel study of the effect of different vent configurations on the vortex-induced response and flutter susceptibility of an H-section bridge. Presence of the sidewalk vents is seen to have a strong influence on the flow around the deck. The vortex-shedding process is not disrupted but merely reorganized around different frequencies. Vent configurations that render the deck stable at low wind speeds are seen to have a destabilizing effect at high wind speeds, and vice-versa. It is seen that the judicious use of modifications to the deck structure can lead to a stable section in the wind-speed range of interest.

Introduction

Slender structures susceptible to wind-induced oscillations may be rendered stable using modifications to their shape. In general, these modifications are used to eliminate a particular type of instability, such as the vortex-induced vibrations of tall chimney stacks, galloping of power lines, or flutter of long-span flexible bridges (Simiu and Scanlan 1986). A comprehensive summary of shape modifications used for bridge decks and their effectiveness is provided by Reinhold et al. (1989). Long-span bridges however, have the potential of displaying more than a single type of instability. The purpose of this study was to examine the effect of sidewalk vents on two types of instability experienced by an H-section bridge deck in smooth oncoming flow using wind tunnel tests: vortex-induced vibrations and flutter.

The bridge under study is the Deer Isle-Sedgwick bridge in Maine, built in the late 1930's, which has displayed moderate- to large-amplitude wind-induced oscillations since its construction, and in fact has become a prototypical example of an aerodynamically "uneasy" deck type. Various measures have been taken in order to keep these oscillations within acceptable limits (e.g., Bosch 1987). A characteristic of the bridge deck is that the sidewalks are of the open-grate type. It is generally believed that the air flow over the deck is disrupted due to a pressure bleeding effect, which adds to the stability of the structure by reducing uneven top-bottom pressure differentials. The validity of this assumption was examined by studying the effect of covered or open sidewalk grates on the static and

[1]Asst. Prof., Dept. of Civ. Engrg., The Johns Hopkins Univ., Baltimore, Md 21218-2699
[2]Prof., Dept. of Civ. Engrg., The Johns Hopkins Univ., Baltimore, Md 21218-2699
[3]Structural Engineer, Skidmore, Owings & Merrill, Chicago, IL 60603

aeroelastic behavior of a scaled section model of the bridge deck. All experiments were conducted in the Corrsin Wind Tunnel at The Johns Hopkins University in Baltimore, Maryland.

This paper presents brief descriptions of the experiments, summary results of the static and aeroelastic tests, and discussion of these results. Overall patterns that emerged from this study are summarized at the end of the paper.

Description of Bridge Deck and Cases Studied

The Deer Isle-Sedgwick Bridge is a girder-stiffened suspension bridge in Hancock County, Maine. The structure consists of a 329.2m main span, 147.5m side spans, and 39.6m long approach spans giving a total length of 703.5m. The two-lane roadway consists of a 0.11m deep reinforced concrete slab having a width of 6.1m. The 2m deep stiffening girders are spaced 7.2m apart. The sidewalks of the deck are of the open-grate type. Fig. 1 is a sketch of the deck cross-section. Further details of the bridge and the various modifications made to improve its aerodynamic performance are provided by Bosch (1987).

The present wind tunnel study was carried out using a section model, which is a scaled, geometrically faithful, rigid model representing a spanwise section of the deck. A section model may be mounted on a force balance in order to measure steady-state aerodynamic forces, or suspended from springs in order to obtain its aeroelastic response. Information about fundamental aerodynamic characteristics of a bridge deck obtained from section model tests is used in comprehensive analytical studies of the prototype.

The section model used in this study was built to a geometric scale of 3/125. The model was 0.914 m long, 0.185 m wide and 0.048 m deep. The section model was enclosed between two end plates to minimize aerodynamic end effects. Measurements of the wind speed between the end plates with the model removed showed that the spanwise wind velocity profile was uniform (Kumarasena 1989). Four cases were studied, as defined in Table 1.

Table 1: Definition of Cases Studied

Case	Description
1	Both Sidewalk Grates Open
2	Both Sidewalk Grates Covered
3	Only Windward Grate Covered
4	Only Windward Grate Open

Results of Static Tests

The static tests consisted of measurements of steady-state lift, moment, and drag, as

well as force and moment spectra. Tests were conducted in smooth oncoming flow at zero angle of attack, with maximum wind speed corresponding to a Reynolds number value of $Re = 1.1 \times 10^5$, based on section width.

Force and Moment Coefficients

Measured lift, moment, and drag coefficients for the four cases are shown in Fig. 2 as functions of Re. These dimensionless quantities are defined as follows:

$$C_L = \frac{F_L}{\frac{1}{2}\rho U^2 b}; \quad C_M = \frac{M}{\frac{1}{2}\rho U^2 b^2}; \quad C_D = \frac{F_D}{\frac{1}{2}\rho U^2 b} \tag{1}$$

where F_L and F_D are the net wind pressure forces in the lift and drag direction respectively, M is the net flow-induced moment, ρ is the air density, U is the speed of the oncoming flow, and b is a reference dimension of the structure. In this study, b was taken as the width of the model deck B. In order to obtain, for example, the drag coefficient with respect to section depth D, the C_D values shown in Fig. 2 should be multiplied by $B/D = 3.87$. The following observations may be made from Fig. 2:

(i) The lift coefficient is lowest when both vents are uncovered (Case 1) and is close to zero. For the remaining cases, the magnitude of C_L is at least an order of magnitude greater, indicating that any closure of the vents leads to a significant net increase in the lift force. The negative sign implies that the net force is in a downward direction.

(ii) The moment coefficient takes on similar values for Cases 1 and 2 (except at the lowest Re value) and is about one half that obtained for Cases 3 and 4. Thus, the two cases in which the vent openings are asymmetric (Cases 3 and 4) have larger moment coefficients than the symmetric cases (1 and 2). The positive sign in all cases indicates that the resultant lift force acts in a plane downstream of the longitudinal axis.

(iii) The drag coefficient takes on very similar values for all cases. However, it is seen that C_D is lowest for Case 2 where both vents are covered. This may be due to the fact that the flow suffers the least amount of disruption in this case.

Force and Moment Spectra

The following discussion will focus on the lift and moment spectra. Representative spectra of the lift and moment, at a wind speed of $U = 6.1$ m/s ($Re = 74{,}200$) for the four different vent configurations are shown in Figs. 3 and 4. It is evident that the frequency content of the forces and moment on the rigidly mounted section is strongly dependent on the vent configuration. The lift and moment spectra appear to be similar at each wind speed, and show two distinct peaks at all wind speeds for Cases 1, 3 and 4. For Case 2,

a single peak is observed except at the highest wind speed tested where a second peak appears.

This indicates that when both vents are covered (Case 2) the vortices shed from the deck concentrate around a single frequency, while when *at least* one vent is open - as in Cases 1, 3, and 4 - the shedding occurs at two distinct frequencies. The spectra in the latter cases are of a wider band. It is of interest to note however, that the open vents do not lead to a greatly disrupted flow around the deck, but rather result in a flow that remains organized, only in a different manner.

The presence of two peaks in the spectra for Cases 1, 3, and 4 suggest that two Strouhal numbers should be computed for each of these cases. This is more easily visualized in Fig. 5, which shows the frequencies of peaks of the lift spectra (shedding frequencies) as functions of the wind speed. The corresponding values of the Strouhal number, defined as:

$$S = \frac{f_s D}{U} \tag{2}$$

where f_s is the frequency of vortex-shedding, D is the depth of the section, and U is the wind speed, are listed in Table 2.

Table 2: Strouhal Numbers

Case	High Frequency	Low Frequency
Case 1	0.153	0.101
Case 2	0.185	-
Case 3	0.189	0.047
Case 4	0.143	0.085

Strouhal number values are generally based on velocity measurements in the wake of a bluff body. In the case of the unmodified Deer Isle section (Case 1), Huston (1986) reported a value of 0.11, while Ehsan (1988) obtained a value of 0.12, based on spectra of wake velocity fluctuations. These spectra showed a single dominant peak at each wind speed, which allowed a single Strouhal number value to be computed. The values listed in Table 2, which were obtained from spectra of the fluctuating *forces* on the Deer Isle model itself, differ significantly from the previously reported results not only in magnitude, but in the fact that two shedding frequencies could be clearly observed and hence, on a "force" interpretation of Strouhal number, two values of S could be computed.

It is evident that the characteristics of the wake do not accurately reflect the details of the flow around the deck for sections with complex shapes. In the present case, the

frequency content of the wake possibly combines the effect of the vortices shed from the leading and trailing edges, as well as the effect of the vents.

It may be noted from Table 2 that the high-frequency Strouhal number for Case 1 is only 6.5% greater than the corresponding value for Case 4, while the low-frequency Strouhal number is about 16% greater. In addition, the high-frequency Strouhal number for Case 2 is only 2% smaller than that of Case 3. Low-frequency shedding is observed for Case 2 only at the highest test speed, while the low-frequency Strouhal number for Case 3 is quite small (0.047).

These observations indicate that the four different cases may be conveniently reduced to two basic cases:

- Case A: Windward vent open/leeward vent open or closed (Cases 1 and 4).
- Case B: Windward vent closed/leeward vent open or closed (Cases 2 and 3).

These comments are based on static tests alone. Whether the dynamic behavior suggests such groupings remains to be discussed.

Results of Aeroelastic Tests

Vortex-Induced Vibrations

Vortices shed from an elastic or elastically mounted bluff body immersed in a fluid flow subject the body to periodic excitations, which may cause it to vibrate. These oscillations are generally quite small. However, within a range of shedding frequencies bracketing a natural frequency of the body, large-amplitude oscillations may occur which apparently control the shedding of vortices in a fluid-structure interaction phenomenon known as "lock-in" or "synchronization". Motion in this range is both self-excited and self-limiting. A detailed study of the lock-in phenomenon for bridge decks, and a mathematical model that can be used to predict prototype response were presented by Ehsan and Scanlan (1990).

For the present study, the torsional frequency of the elastically sprung model was 7.625 Hz, while the measured mechanical damping ratio varied from $\zeta = 0.0044$ to 0.0046. The maximum wind speed used was approximately 5 m/s which corresponds to a Reynolds number value of $Re \doteq 6.1 \times 10^4$. This wind speed was sufficient to obtain shedding frequencies equal to or greater than the torsional frequency for all the observed shedding modes described above, except the one corresponding to $S \doteq 0.047$ for Case 3.

The tests were conducted by increasing the wind speed in small steps, allowing the oscillation to build up and reach steady state (in case of lock in), and recording the data. The model was not released from rest at each wind speed increment. The tests were

repeated for gradually decreasing values of the wind speed as well to seek evidence of response hysteresis effects.

Fig. 6 shows the double amplitude of the steady-state torsional vibration at lock-in as a function of the reduced velocity for each of the four cases studied. The reduced velocity is a dimensionless quantity defined as U/NB, where U is the wind speed, N is the natural frequency and B is the deck width. The following points can be noted:

Case 1: Large-amplitude, locked-in oscillations are obtained in this case where both vents are open. Lock-in occurs at a wind speed of 2.5 m/s and ends at 4.6 m/s. From Fig. 5, synchronization with the high-frequency shedding would be expected to occur in this case at $U = ND/S_{11} = 2.53$ m/s, since lock-in occurs when the shedding frequency f_s is equal to the torsional frequency N in equation 2. The wind speed for lock-in at the lower frequency shedding can similarly be computed to be $U = ND/S_{12} = 3.84$ m/s. Both these values lie within the observed lock-in range of 2.5 m/s to 4.6 m/s. Thus, even though the moment spectra for the fixed model clearly show two distinct shedding frequencies, indicating two potential lock-in ranges, only a single, overlapping range is observed.

Case 2: In this case (also in Fig. 6), where both vents are covered, the lock-in wind speed is $U = ND/S_{21} = 2.1$ m/s. Tests spanning the wind speed range of 1.9 m/s to 4.3 m/s showed relatively low-amplitude locked-in vibrations occurring only in a very narrow lock-in range (2.29 – 2.62 m/s). This result is counter-intuitive considering that the moment spectra for the fixed model (Fig. 4) suggest that the vortex shedding is strongly organized at a single frequency. In addition, the mechanical damping in this case was very low – less than 0.5%. Most of the other response power spectra over the wind speed range tested showed two distinct peaks – one at the shedding frequency and a second one at the natural frequency indicating that the vibrations were of the forced type.

Case 3: In this case (Fig. 6), only the windward vent is covered, while the leeward vent is open. The model appeared to be completely stable over a wind speed range of 2.2 m/s to 4.4 m/s. Spectra of response over this range showed two distinct peaks, with the peak corresponding to shedding initially at a lower frequency than the natural frequency. As the wind speed was increased, the two peaks merged resulting in the slightly larger amplitude at 2.54 m/s. At higher wind speeds, the shedding peak was at a frequency greater than the natural frequency of the model It appears that lock-in did not occur at all in this case and that the response consisted of forced oscillation at the Strouhal frequency combined with a turbulence-induced oscillation at the natural frequency.

Case 4: Large-amplitude vibrations were observed for this case, in which the windward vent is open while the leeward vent is covered, over the same wind speed range as in Case

1. Comments about the overlapping lock-in ranges for Case 1 apply here as well. Tests had to be stopped at a wind speed of 4.5 m/s because it appeared that the model was beginning to display very large-amplitude, coupled torsional-vertical oscillations. (The vertical restraint resulted in an across-wind frequency of approximately 19 Hz.)

The similarity in the low-speed aeroelastic response of Cases 1 and 4, and of Cases 2 and 3, support the proposition suggested earlier about the existence of two basic cases A and B, comprised of the pairs mentioned above.

Torsional Flutter Behavior

In the torsional flutter of a bridge deck, the local flow around the deck becomes strongly modified by deck action. Vertical oscillation of the leading edge of the section due to model rotation is accompanied by an increased vortex discharge during flutter. These vortices, as they traverse the deck, give rise to locally destabilizing pressures which tend to enhance the motion that initiated them. This motion dominates the production of vorticity into the wake, and Strouhal effects become submerged. There is no loss of synchronization with increasing velocity as in the case of passing through lock in, and the motion grows to catastrophic proportions with increasing wind speed (Scanlan 1979).

It should be noted that flutter is a "high" wind-speed phenomenon. A flutter vortex wake is shed at or near a natural frequency of body, but this is quite distinct from the Karman vortex trail which may in fact continue to be shed at the Strouhal frequency computed from (2) at high wind speeds, though largely submerged in the more dominant flutter phenomenon.

The aeroelastic equation of motion for a balanced section model constrained to oscillate in the torsional degree of freedom α only, and neglecting flow turbulence effects, is written as (Simiu and Scanlan 1986):

$$I\left[\ddot{\alpha}+2\zeta_\alpha\omega_\alpha\dot{\alpha}+\omega_\alpha^2\alpha\right]=M_\alpha(t) \tag{3}$$

where the motion-dependent aerodynamic moment is written in the well-known flutter-derivative formulation:

$$M_\alpha(t)=\frac{1}{2}\rho U^2(2B^2)\left[KA_2^*(K)\frac{B\dot{\alpha}}{U}+K^2A_3^*(K)\alpha\right] \tag{4}$$

In these equations, I is the torsional moment of inertia per unit span, ω_α and ζ_α are the circular natural frequency and damping ratio in the α degree of freedom, M_α is the self-excited aerodynamic moment per unit span about the rotation axis, and K is the reduced frequency defined as $K=B\omega_{\alpha,e}/U$ (see below). The "flutter derivatives" A_2^* and A_3^* are nondimensional functions of K. Eqs. 3 and 4 can be written as:

$$\ddot{\alpha}+2\zeta_{\alpha,e}\omega_{\alpha,e}\dot{\alpha}+\omega_{\alpha,e}^2\alpha=0 \tag{5}$$

where

$$2\zeta_{\alpha,e}\omega_{\alpha,e} = 2\zeta_\alpha\omega_\alpha - \frac{\rho U^2 B^2}{I}\left[\left(\frac{KB}{U}\right)A_2^*(K)\right] \tag{6}$$

$$\omega_{\alpha,e}^2 = \omega_\alpha^2 - \frac{\rho U^2 B^2}{I}\left[K^2 A_3^*(K)\right] \tag{7}$$

The additional subscripts "e" define "effective" quantities. In (6) and (7), the reduced frequency K is computed using $\omega_{\alpha,e}$. The flutter derivatives are generally extracted from tests that measure the effective mechanical damping ratio and the natural frequency of the aeroelastic section model in air flow (Jones and Spartz 1990). In this study, effective system properties were calculated from transient response records obtained by providing the section model with an initial displacement and releasing it in an air flow. A magnetic release system, operated from outside the tunnel, was used to eliminate any disturbance to the flow during the release procedure.

For these tests, it was found that the flutter derivatives can be approximated by:

$$A_2^*(K) = \frac{2I}{\rho B^4}\left[\zeta_\alpha - \zeta_{\alpha,e}\right] \tag{8}$$

and

$$A_3^*(K) = 0 \tag{9}$$

Fig. 7 shows the variation of the coefficient A_2^* with reduced wind velocity U/NB for the four cases examined. Single-degree torsional flutter is imminent when A_2^* changes sign from negative to positive with increasing values of reduced wind velocity U/NB. The following observations can be made from Fig. 7:

(i) The large-amplitude lock-in response observed for Cases 1 and 4 in the approximate reduced velocity range $U/NB = 1.75$ to 3.5 (Fig. 6) is reflected in the relatively high positive values of the coefficient A_2^* in this range. Cases 2 and 3, which did not display large-amplitude locked-in vibrations, have lower values of A_2^* in this range of the reduced wind velocity.

(ii) The situation is exactly reversed at higher wind speeds. The configuration which was most stable at lower wind speeds (Case 3) begins to show flutter tendencies first. On the other hand, Case 4, which displayed the largest amplitudes of vortex-induced vibration, appears to be the most stable at higher wind speeds.

It may be mentioned here that the unmodified deck (Case 1) was also observed to be stable at higher wind speeds. The values of the flutter derivative A_2^* are consistent with those reported by Kumarasena et al. (1990). However, Huston (1986) observed that the section displayed flutter tendencies immediately following the end of lock-in vibrations at

$U/NB \simeq 3.5$. Tests by the latter were carried out on the larger-scale model used by Bosch (1987). A wire mesh was used in that model to simulate the sidewalk grates. It is possible that the mesh generated sufficient impedance to the flow so that the model behaved in a manner closer to Case 2 of the present study (vents closed) than the unmodified case. This indicates that local Reynolds number modeling for wind tunnel testing may be critically important in certain cases, and requires further study.

A conservative estimate of the prototype flutter speed is found by assuming zero damping, so that the critical value of A_2^* is zero. Table 3 compares these "conservative flutter speeds" for model and prototype. The latter quantities are computed for the first torsional mode, with $N_p = 2.336$ Hz, and $B_p = 7.2$ m (Kumarasena et al. 1989). (iii) The

Table 3: Conservative Flutter Speeds

Case	Model	Prototype
Case 1	> 9.4 m/s	> 113 m/s
Case 2	7.0 m/s	84 m/s
Case 3	6.4 m/s	77 m/s
Case 4	> 10.7 m/s	> 128 m/s

hypothesis that there are actually *two* basic cases, rather than four, as proposed earlier is supported by these results. Thus, Case A (which consists of Cases 1 and 4) is more stable at higher wind speeds, while Case B (which consists of Cases 2 and 3) is more unstable.

Conclusions

A number of observations have been made in the present discussion. These are summarized below:

1. The vortex shedding induced by irregular bluff bodies such as bridge deck sections is richer in detail than that induced by regular shapes and needs further study.
2. The presence of vents in the bridge deck does not wholly disrupt the flow around the deck. The flow is merely reorganized, and the energy is concentrated around different frequencies for different vent configurations, as seen for example, in Fig. 3.
3. The aeroelastic response shows a very strong dependence on vent configuration (Figs. 6 and 7) while the static force coefficients are relatively insensitive to it.
4. Both the static and the aeroelastic behavior of the model depend mainly on whether the windward vent is open, as in cases 1 and 4, or closed, as in cases 2 and 3. The

leeward vent appears to play a secondary role.

5. The vent configurations effective in quelling the low-speed vortex-induced vibration lead to high-speed flutter instability, and vice-versa as shown in Fig. 7.

6. The lowest value of the conservative flutter speed of the prototype bridge is 77 m/s (Case 3) which corresponds to 172 mph. This indicates that the bridge would be relatively stable against flutter, even in the "worst case". It should be expressly noted that this favorable result is a direct consequence of the high torsional frequency incorporated into that bridge by the post-erection cable modifications effected by its original designer, D.B. Steinman (Kumarasena et al., 1989). If further alleviation of that bridge's "uneasiness" is desired, it may thus be reasonable to focus mainly on deck modifications that minimize or eliminate the low-speed instability due to lock-in rather than to be concerned with high-speed instability within the range of wind speeds expected in the field.

It is clear from the preceding discussions that motional instabilities of a particularly unstable configuration can be controlled to some degree by judicious use of modifications to the deck structure. Further study is needed to assess the detailed extent of modifications needed for prototype structures, and the possible consequences of deck modifications for nonaerodynamic purposes.

Acknowledgements

The authors would like to thank Mr. Harold Bosch of the Turner Fairbank Laboratory of the Federal Highway Administration who made available the data from the Deer Isle Bridge which was used in the analysis.

The financial assistance of the National Science Foundation (Grant Nos. MSM-8707902 and CES-8705467) in support of this project is gratefully acknowledged.

Appendix I. – References

Bosch, H. R. (1987). *A Wind Tunnel Investigation of the Deer Isle-Sedgwick Bridge (Phase 1)*, Report No. FHWA/RD-87/027, Federal Highway Administration, Research, Development, and Technology, Turner-Fairbank Highway Research Center, McLean, VA.

Ehsan, F. (1988). *The Vortex-Induced Response of Long, Suspended-Span Bridges*, Doctoral Dissertation, The Johns Hopkins University, Baltimore, MD.

Ehsan, F., and Scanlan, R.H. (1990). "Vortex-Induced Vibrations of Flexible Bridges", *J. Engg. Mech.*, ASCE, Vol. 116, No. 6, pp. 1392-1411.

Huston, D.R. (1986). *The Effects of Upstream Gusting on the Aeroelastic Behavior of Long Suspended-Span Bridges*, Doctoral Dissertation, Princeton University.

Jones, N. P. and Spartz, C. A. "Structural Damping Estimation for Long-Span Bridges." Journal of Engineering Mechanics, ASCE, 16(11), November, 1990. 2414 – 2433.

Kumarasena, T. (1989). *Wind Response Prediction of Flexible Bridges*, Doctoral Dissertation, The Johns Hopkins University, Baltimore, MD.

Kumarasena, T., Scanlan, R.H., and Ehsan, F. (1990). "Recent Observations in Bridge-Deck Aeroelasticity", submitted to *J. Wind Engg. Ind. Aerodyn.*

Kumarasena, T., Scanlan, R.H., and Morris, G.R. (1989). "Deer Isle Bridge: Field and Computed Vibrations", *J. Struct. Engg.*, ASCE, Vol. 115, No. 9, pp. 2313-2328.

Reinhold, T.A., Huston, D., and Scanlan, R.H. (1989). *Structural Modifications for Enhanced Aerodynamic Performance of Long Span Bridges*, Report No. FHWA/RD-89/200, Federal Highway Administration, Offices of Research & Development, Washington, D.C.

Scanlan, R.H. (1979). "On the State of Stability Considerations for Suspended-Span Bridges under Wind", *Proc. Symposium on Practical Experiences with Flow-Induced Vibrations*, Univ. of Karlsruhe, W. Germany, pp. 595-618.

Simiu, E., and Scanlan, R.H. (1986). *Wind Effects on Structures*, 2nd ed., John Wiley & Sons, Inc.

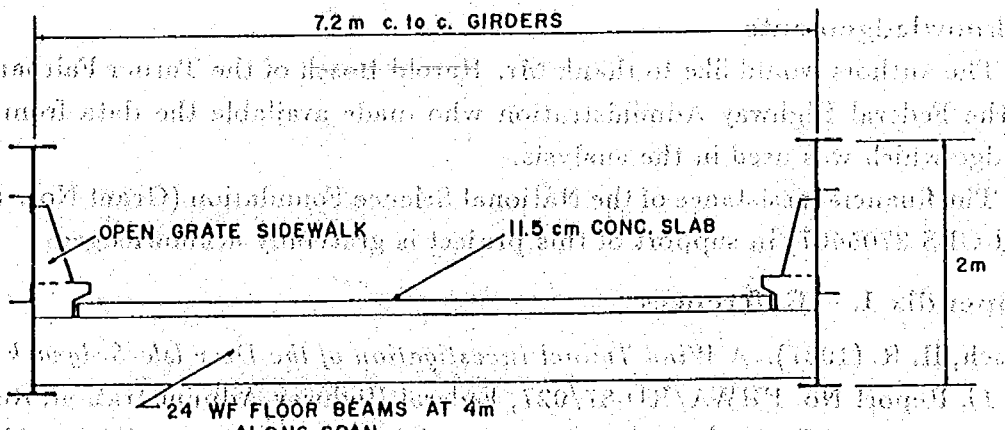

Figure 1: Deck Cross Section — Deer Isle Bridge

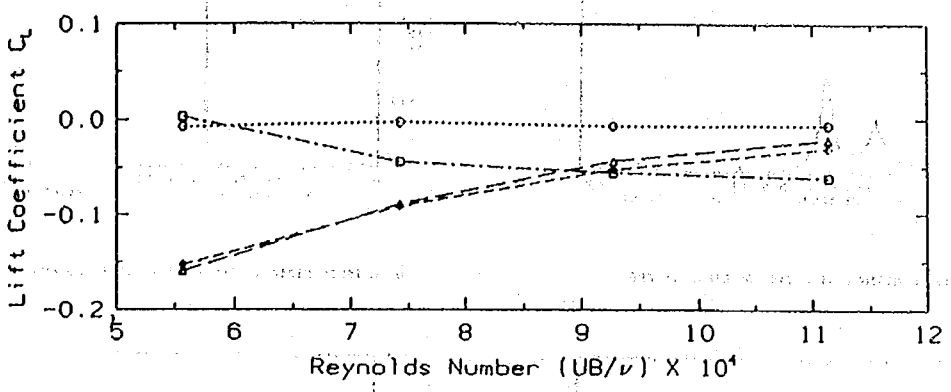

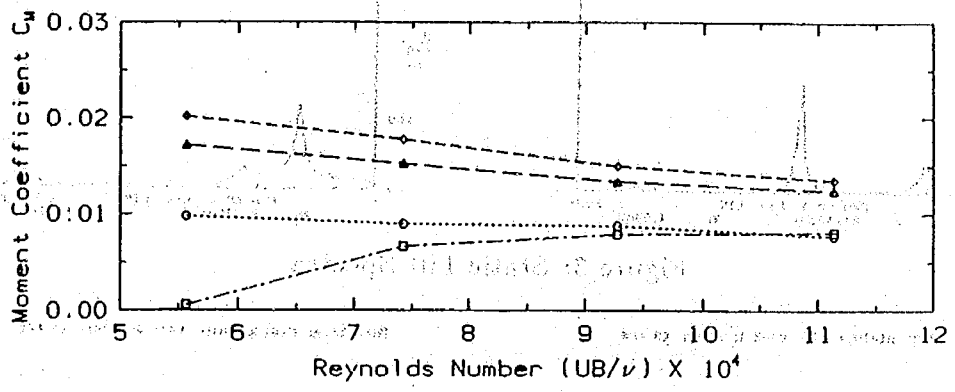

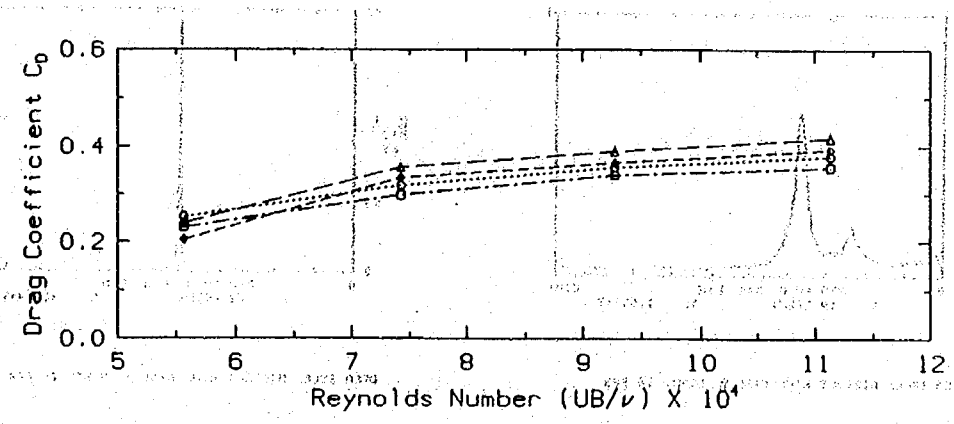

Figure 2: C_L, C_M, C_D based on Deck Width (Smooth Flow, Zero Angle of Attack)

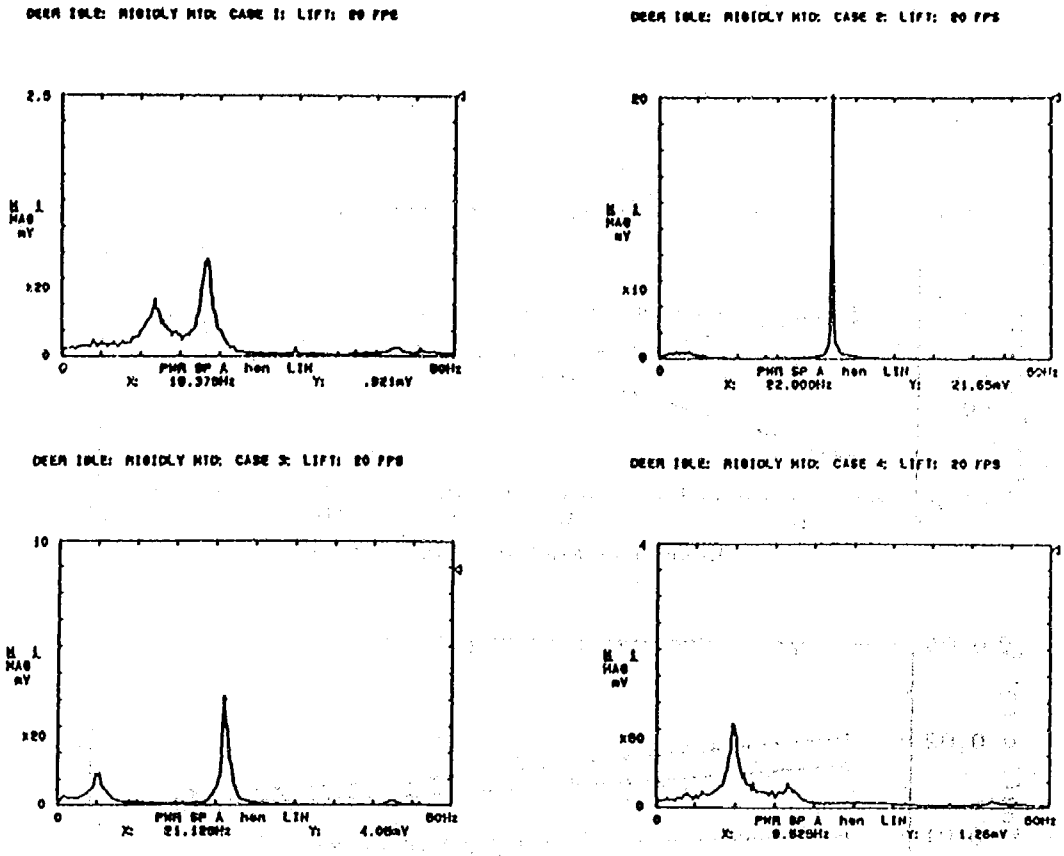

Figure 3: Static Lift Spectra

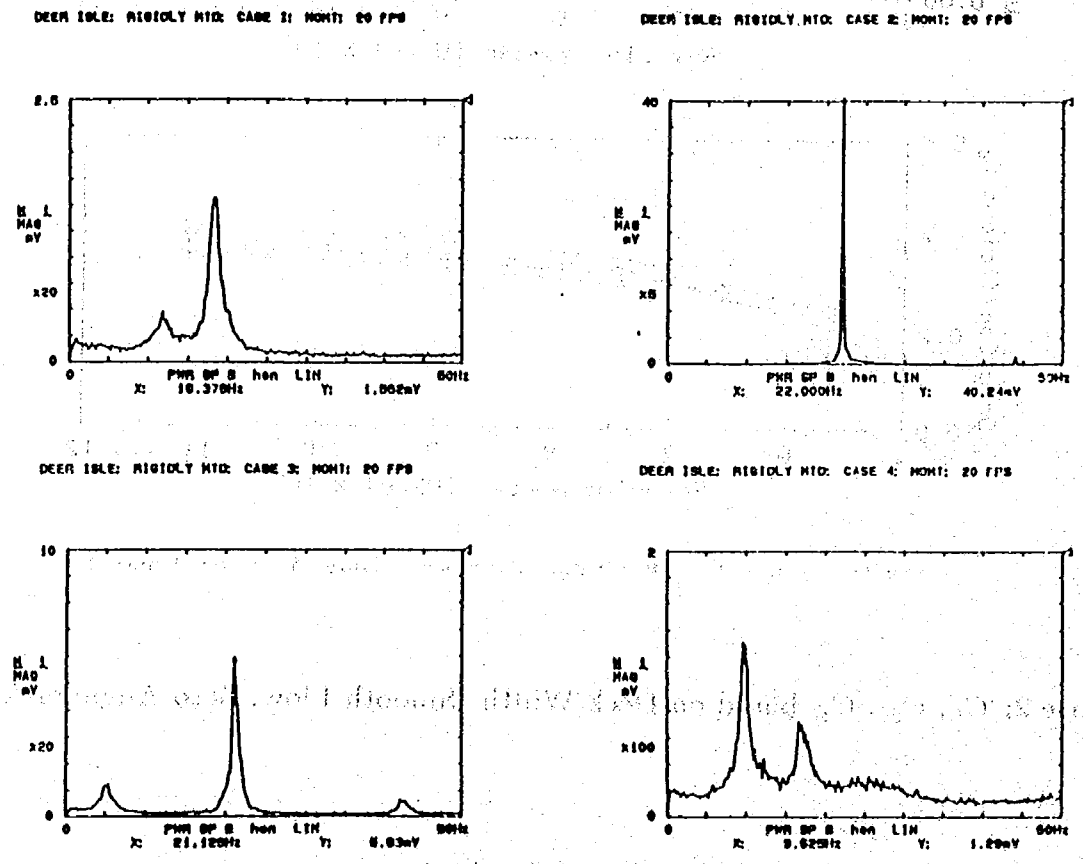

Figure 4: Static Moment Spectra

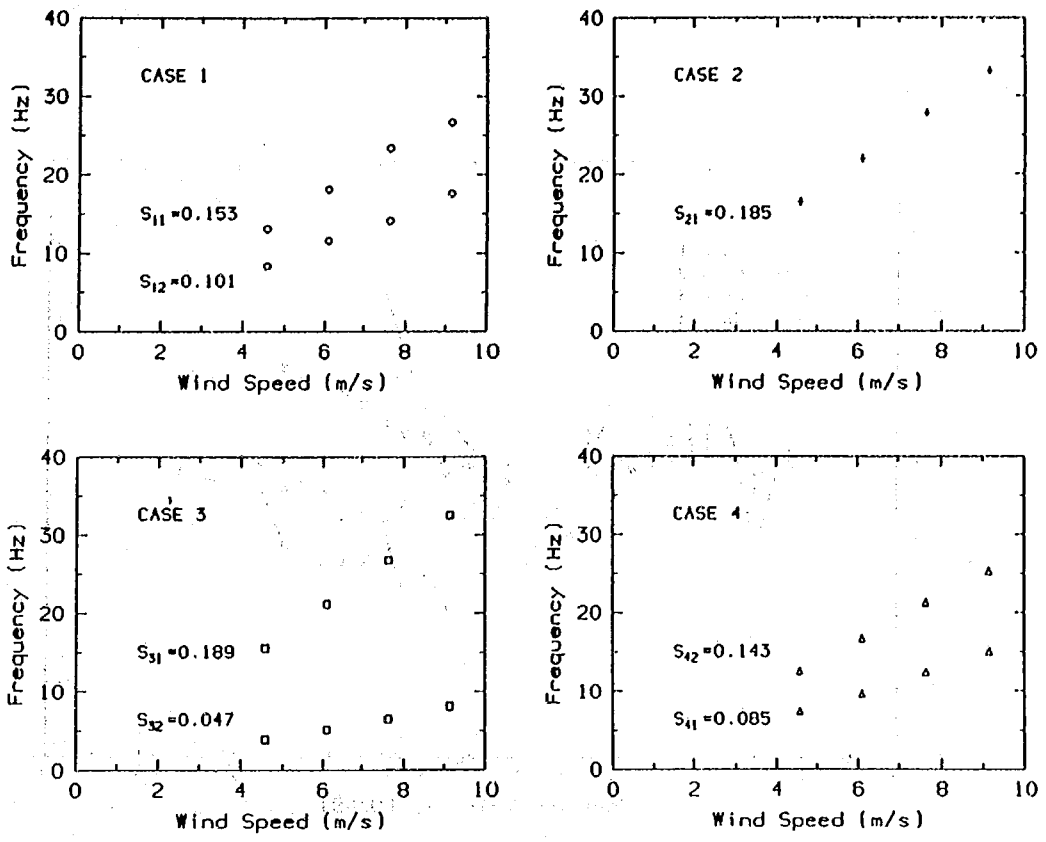

Figure 5: Frequency of Spectral Peaks (Lift) for Different Vent Configurations

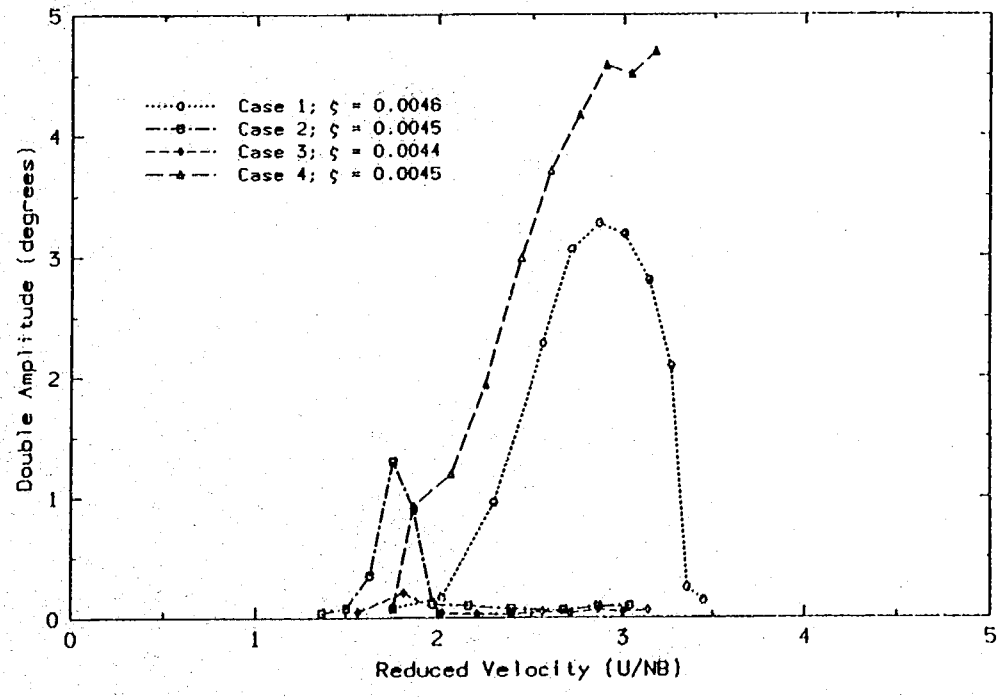

Figure 6: Amplitude of Torsional Oscillation — Deer Isle Section Model

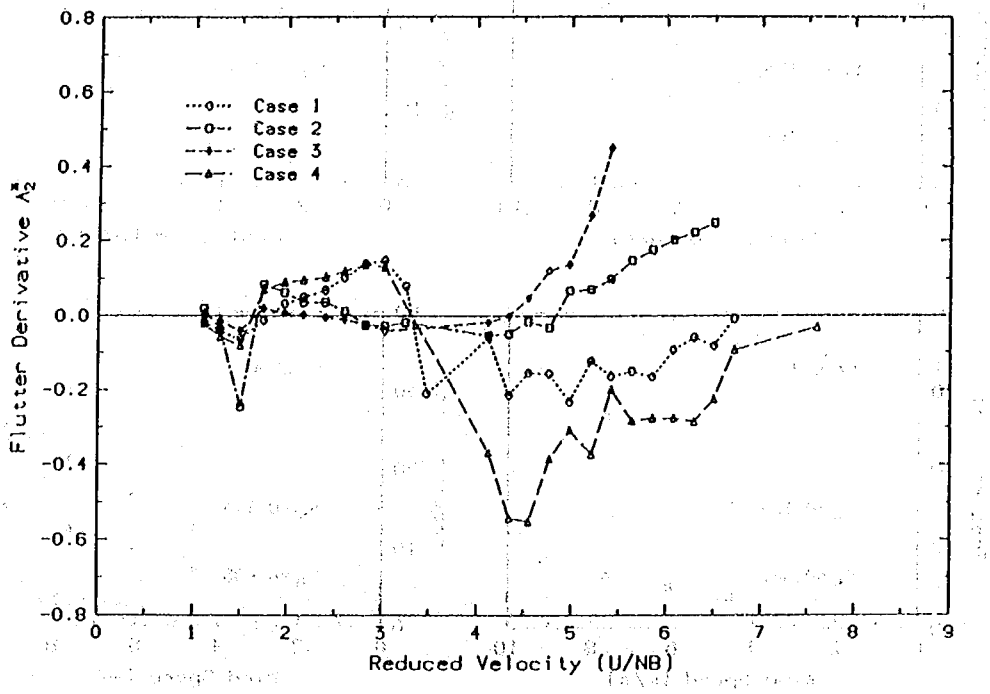

Figure 7: Effect of Vents on Flutter Derivative A_2^*

RESISTANCE/STABILITY TO THE WIND OF HAKUCHO-OHHASHI

by

Makoto Niiyama[1], Hiromi Kawasaki[2], and Yoshiyuki Saito[3]

ABSTRACT

This report briefly gives the essentials of design and construction of Hakucho-Ohhashi, a giant suspension bridge which recently started to be built as Japan's first in her cold snowy districts, the procedures and results of model tests to check its aerodynamic stability.

Rounds of wind tunnel testing, these have been conducted as is generally the case with structures of this type and with a view to serving to validate structural innovations, including measures against snow incrustation, introduced in the planning of the bridge; under assumed conditions of its being erected and after its completion, particularly to help ensure adequate behavior of its stiffening girder and main towers.

INTRODUCTION

A southwest port of Hokkaido as its prime industrial city usually called "Iron Town", Muroran has greatly contributed to its economic and industrial development by the known staple manufacture of steel as well as a mass supply of cement, oil refining and other prime production (Fig. 1).

Geographically Muroran's contours may be comparable with those of a key, as in Fig. 2, while their deep indentation, conducing to clemency of the inland sea, has enhanced functions of the major industrial harbor. But on the other hand this topography can be said to have greatly obstructed traffic flow between the north and the south of the city as well as further development, industrial or other.

Such problems are expected to be solved to significant degrees by the Hakucho New Bypass whose construction recently started with Hakucho-Ohhashi, literally The Great Swan Bay Bridge, forming its principal segments.

It was designed with many innovations embodied therein some of which will lead to its overall relative slenderness with functional beauty. They include the use of a streamlined box section for its stiffening girder and the adoption of a four-story rigid frame as structure of its main towers.

Also notable is its projected procedure of construction in which its stiffening girder is to be erected by an all-hinge erection method for the first time at home. It consists of lifting up girder segments one after another to permit their pin-connection to assure between them no moment transfer in the vertical plane, finally to reconnect them, after they have reached a certain large number, successively into an overall continuous system.

The bridge extends over a total distance of 1,380 m, comprising a central span of 720 m and two collateral spans on its sides as the world's twentieth or Japan's ninth of the same type, which primarily is a partially stiffened two-hinge three-span structure (Fig. 3).

WIND CHARACTERISTICS ON THE SITE

Since 1981 wind observation has been conducted at a steel tower (20 m

[1]Head of Road Construction Work Division, Construction Department, [2]Acting Director, [3]Member of Design Group, 2nd Construction Section, of Muroran Road Office, Muroran Development/Construction Department; Hokkaido Development Bureau, Hokkaido Development Agency

high) for meteorological observation set up (at an altitude of 60 m) adjacent to the site of the bridge. Fig. 4 shows the predominent wind direction normal to the structural axis of the bridge, with a large frequency of almost 40%. Notably the relative frequency of occurence of the WNW wind with a velocity of over 10 m/s amounts to about 10 % of the total relative frequency.

The reference velocity for the usual wind resistant design is defined as an average, V_{10}, of the velocities measured for ten minutes at a height of 10 m from the ground surface. At this time V_{10} is assumed to be 41m/s. It was calculated by such an equation of vertical distribution of wind velocity as is based on the correlation of the governmental local meteorological station's data and the above-mentioned in-situ observed data for maximum diurnal wind velocity, on assuming a period of V_{10}'s reccurence of 100 yr. (Specifically in-situ observed data were used for calculating $V_{h2} / V_{h1} = (h_2 / h_1)^{0.09}$)

Based on in-situ observed data, turbulence characteristics are shown in Table 1.

TYPES OF WIND OSCILATION

The probable types of wind oscillation are broadly classified into the following three.

1) Divergent oscillation caused by the oscillation of a structure (flutter)

The motion of a body subject to the wind is attended with its proper damping behavior plus a damping motion owing to the wind forces proportional to the wind velocity. When the above additional is a negative damping action (in the direction of the body motion), that of the total system also turns negative with increases in wind velocity.

The above situation can lead with time to the fracture of a structure resultant from progressive increases then in amplitude of the oscilation followed by its enhanced divergence.

2) Restrictive oscillation by the vortex (vortex excitation)

A vortex generated on the leeward of a structure causes alternate cyclic forces to act thereon. When the period of its generation, proportional to wind velocity, coincides with the natural frequency of the system, non-divergent resonance can occur, possibly leading to its fracture due to fatigue. Most susceptible to this in a suspension bridge is known to be its main towers.

3) Forced oscillation by turbulence (buffeting)

Any enduring aerodynamic turbulence of the wind may impose forced powers on a structural system and its attendant oscillation. Any structural response to this phenomenon is difficult to analyze owing to its input naturally being irregular.

WIND RESISTANCE/STABILITY OF STIFFENING GIRDER

1. Test model, procedure and assumption

Procedure: according to "Manual of Wind Tunnel Testing and Commentary" by the Honshu-Shikoku Bridge Authority (used throughout the tests currently concerned)

Test model: a 1/35 scale model representing two-dimensional partial rigid bodies (Fig. 5)

Structural damping factor: 0.02 (constant through all tests)

Wind stream: uniform current

Wind direction: direction normal to the longitudinal structural axis

Angles of wind attack: 0°, ±3° and ±5°

Wind velocity: design velocity = $V_D = V_{10} \times v_1 \times v_2$ = 56 m/s

with ν_1 = 1.17 for structural altitude (60m)
ν_2 = 1.16 for correction due to horizontal structural length
as to wind velocity for divergent oscilation: critical wind velocity $V_{CR} = 1.2 \times V_D$ = 67 m/s

2. Test results

Adopted as reference stiffening girder of this bridge is a box girder of rectangular section with fairings attached to it (Fig. 6), preferred to hexagonal or trapezoidal one, for their preliminarily tested wind resistance and stability proved best with this design section. An elaborate series of wind resistance tests was made on the corresponding girder models.

2.1 Optimal position of medial strips and of inspection car rails

Introduction of medial strips proved advantageous to structural wind resistance. The rails of an inspection car were placed inside, with this location practically best for wind resistance of the total system, while their gauge was adopted to be 12 m in consideration of structural and other details of the car.

2.2 Snow effects

The snow effects were considered duly in the light of the nature of the bridge as the domestically first gigantic suspension system to stand in the snowy cold regions as well as the northernmost.

The assumed modes of snow incrusted on stiffening girder, on the snowfall heaviest possible, resulted from simulating pertinent governmental meteorological records, obtained in 1963 through 1986, on the basis of the data of in-situ performed snow-incrusted-model tests.

In this case traffic lanes are regarded as cleared of snow while it has fallen to clog the top guard rails and the lower sections of the railings of the medial strip (Fig.7).

As was then noted, in case of trying the wind that blows up (with an angle of attack of +3°, the minimum wind velocity for flutter abruptly reduced, so that the original section of the stiffening girder was altered by bulging its fairing and accordingly increasing its in-situ width from 21 m to 23 m. This enabled flutter inducing velocity to be kept in excess of the critical velocity.

The stiffening girder consequently adopted for the actual bridge is shown in Fig. 8. And major test results on their section given in Fig. 8 are provided in Fig. 9; where angles of attack and wind velocities when flutter starts are respectively taken as abscissas and ordinates.

As for vortex excitation, one induced somewhere at an angle of attack of +5° and a wind velocity of 3.9 m/s with an amplitude of 0.25 m was the most noticeable but was judged to be negligible in view of the frequency of its occurence and its amplitude being low enough.

WIND RESISTANCE/STABILITY OF THE MAIN TOWERS

A main tower of a suspension bridge has generally been designed to cause no discernible oscilation at its top after — if not during — its erection. However, Hakucho-Ohhashi's main towers are anticipated to oscilate slightly after its being constructed though different in mode from those induced under construction. Wind tunnel testing was carried out in three assumed cases of the main towers under construction, those having been erected and the entire bridge completed. The following refers to the last case.

1. Test model, procedure and assumption

Test model: a 1/90 elastic scale model of the bridge in its entirety
Air currents: both uniform and turbulent currents
Angle of attack of wind: direction taken as 0° when normal to the longitudinal structural axis
Wind velocity: design wind velocity $V_D = V_{10} \times \nu_1 \times \nu_3 = 60$ m/s
where $\nu_1 = 1.22$ for correction due to structural altitude (65 % of tower height)
$\nu_3 = 1.19$ for correction due to longitudinal structural length

2. Test results

Simulation of an assumedly solely completed main tower by its scale model consists of fastening it at the top to piano wires which enabled the adjustment of oscilation modes by applying them any appropriate amount of additional mass (Fig. 10).

The adopted rectangular reference section is shown in Fig. 11. Oscilation that arose in the test was vortex excitation alone, free from any divergent oscilation, i.e., flutter. Problem amplitudes for structural design were induced by a first order lateral oscilation whose observed modes are diagramed in Fig. 12. Maximum amplitude of one-sided sway was 0.43 m in a consistent current and 0.30 m even in a turbulent current which is said generally to result in reduced amplitudes, respectively threatening first passage and fatigue types of fracture at the base of the tower and hence requiring any oscilation controls.

Accordingly introduced were aerodynamic oscilation controls, best fit for the preferentially considered removal of the cause of the problem oscilations. For this the specific means eventually used was corner cutting of the section of the main tower, a device well-documented and rich in examples. Actually, as shown in Fig. 13, combinations of parameters B and H were considered, with them kept constant throughout the tower height. The main tower's section thus adopted is given in Fig. 14. Major test results thereon are provided in Fig. 15 wherein the maximum amplitude in consistent current, 0.13 m, is to be sufficiently conservative, even with fatigue fracture allowed for.

WIND RESISTANCE/STABILITY OF STIFFENING GIRDER AMID ITS ERECTION

Mainly because the bridge under discussion is to be built using the initially introduced all-hinge erection method for the first time at home, wind tunnel testing was implemented so that wind resistance/stability of the stiffening girder of the bridge could be confirmed on a scale model of the entire structure during its supposed erection.

1. Test model, procedure and assumption

Model: a 1/145 space scale model of the entire bridge (Fig. 16)
Current: consistent current
Wind direction: direction normal to the longitudinal structural axis
Angles of wind attack: 0°, ±3° and ±5°
Wind velocity: 1) reference velocity during erection
$V_{1e} = V_{10}/\sqrt{2} \doteqdot 29$ m/s
2) reference velocity for divergent oscilations
$V_{CR} = 1.2 \times V_{1e} \times \nu_1 \times \nu_2 = 47$ m/s
3) reference velocity for restrictive oscilations
$V_D = V_{1e} \times \nu_1 = 34$ m/s

2. Test results

The erection of the girder of the bridge has been planned to follow its

course sketched in Fig. 17. of the erection stages, the wind tests covered three, each illustrated in Fig. 18, chosen as the most critical for wind resistance and stability.

1) Flutter

The flutter observed in the test was flexure-torsion type (coupled flutter); when vertical bending and torsional oscilation are concurrent. Fig. 19 shows the relation between wind velocity and angle of attack both induced by this flutter. Since such observed was relatively high velocity and admissible, covering the critical level, the desired stability can be considered to have been acquired.

2) Vortex excitation

In the stage (Fig. 18) of execution by 94 % of the plan of completion of the bridge, or 94% stage for short, no vortex excitations generated. 55 % and 29 % stages saw them (Fig. 20) in stiffening girder segments, of the central span, cantilevered from collateral spans; the former at velocities about 50 through 60 m/s with angles of attack of 3° and 5° and the latter 35 through 40 m/s with angles of attack of 5°.

However, vortex excitations in both cases were not stable but irregular. They are probably caused because hanger tension and aerodynamic characteristics of the stiffening girder in the collateral spans were reduced as a result of its torsional and vertical upward deformation by blowing-up winds which are most likely to inflict such deformations on those spans.

In sum, as for vortex excitations of stiffening girder the present testing has shown no stable but irregular oscilations, with the girder proving virtually exempt from any possiblity of fatigue fracture.

Also, being larger than the reference velocity (V_D = 34 m/s), the observed maximum wind velocities are considered to lead to none of problem vortex excitation during the erection.

3) Buffeting

Turbulent current testing showed irregular oscilations not observed on consistent currents. These have arisen not just in vertical but horizontal directions, causing relatively large amplitudes. Such phenomena are incidental to bridges like this, while being seen as a tendency of its notably large horizontal responses to turbulent currents in the present test of it supposedly under construction, when the elements of its stiffening girder was less stable—simply suspended from the main cables.

Nonetheless, no divergent oscilations were witnessed and responces to turbulent currents had only initiated at an on-the-site velocities of about 20 m/s. Therefore, the effects of buffeting on the erection works are considered only slight.

SUMMARY AND CONCLUSIONS

A series of wind tunnel testing was conducted whereby to simulate the possible effects of oscilation of the main towers and stiffening girder of the bridge supposedly after its completion and during its erection.

Notably tested was the behavior of the stiffening girder against the wind during its erection since for that the hinge erection method is destined to be employed for the first time in this country. The test results are summarized as follows.

Firstly, the stiffening girder model, while being significantly sensitive to such substructures as inspection car rails etc. as well as to modes of snow, was tested referring to variolus parameters. The test ensured the girder a sufficiently wind resistent/stable section, since:

1) Flutter-inducing wind velocity exceeded the critical value of 67 m/s.

2) Vortex excitations are not problem since they occured at an angle of attack of +5°, whose frequency of occurence is generally small enough as well as the corresponding amplitude.

Secondly, respecting the main towers, despite oscilations in both states of their being erected and having been erected, they could be held down to 0.13 m inmaximum amplitude by corner cutting whereby to change aerodynamic characteristics.

Lastly, the resistance/stability of the stiffening girder during its erection was experimentally validated by their scale models, for:

1) The flutter-inducing oscilations surpassed the reference velocity of 47 m/s.

2) Any consistent vortex excitations were not observed except irregular oscillations, whose velocities also exceeded the reference velocity of 34 m/s for restrictive oscillations.

3) There were to be seen no oscilations due to turbulent currents; with responses to them being considerably high, reaching about 20 s/m in terms of on-the-site velocity.

Namely, for oscilations of such three types the critical levels of wind velocity are found to be sufficiently excelled; hence wind resistance/stability of the structure after its completion and during its erection has been checked on its models.

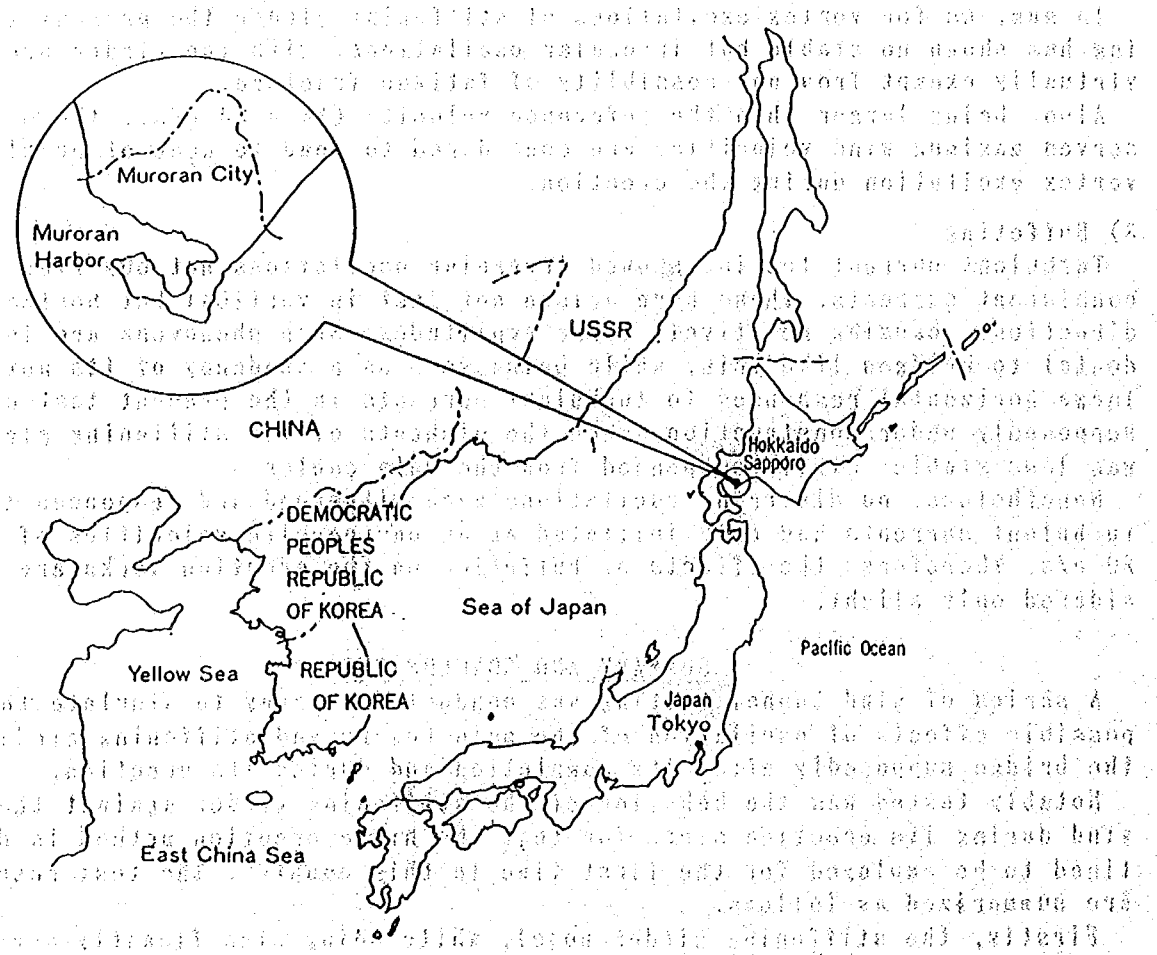

Fig. 1 Computer generated image of Muroran and Hakucho-Ohhashi

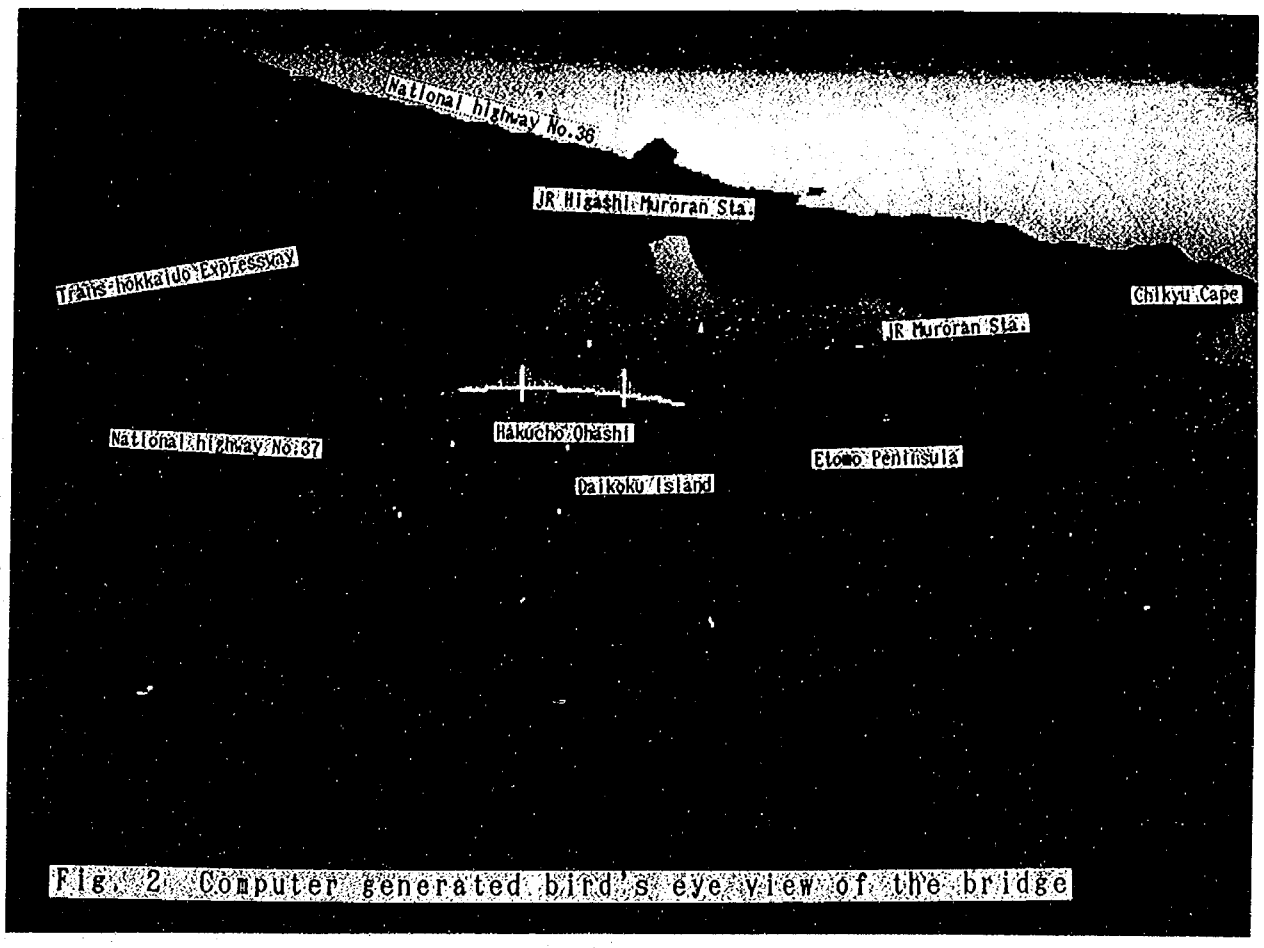

Fig. 2 Computer generated bird's eye view of the bridge

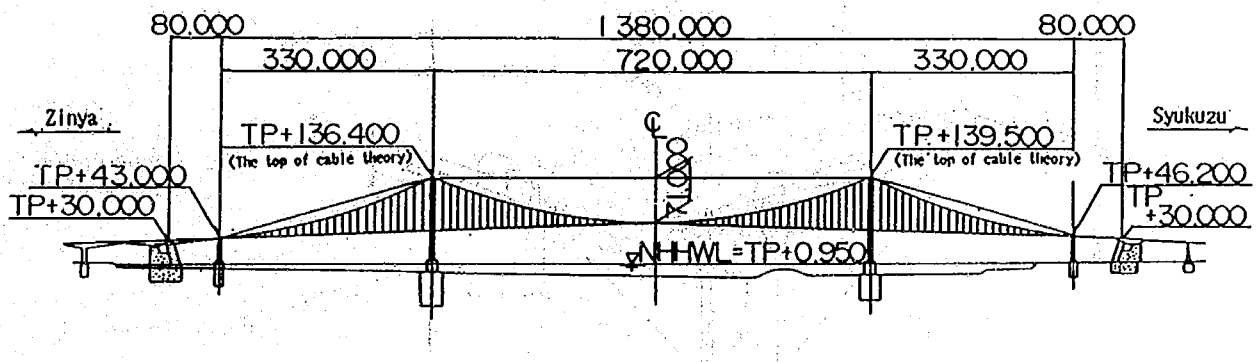

Fig. 3 Side elevation

Table.1 field observatron results of turbulen flow character

	intensity of turbulence Iu (%)	scale of turbulence Lu (m)	remark
west wind	6 ~ 9	200~700	sea wind
east wind	8 ~ 12	100~300	land wind

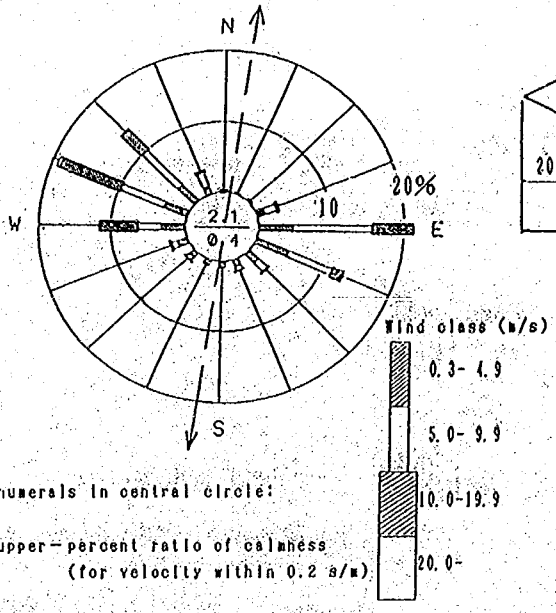

Fig. 4 Annual wind direction percentage diagram

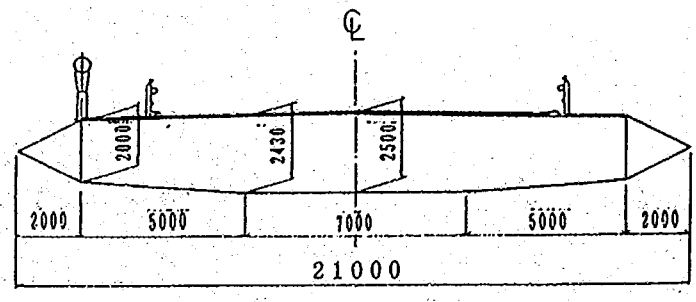

Fig. 6 Reference sectional dimensions of the stiffening girder

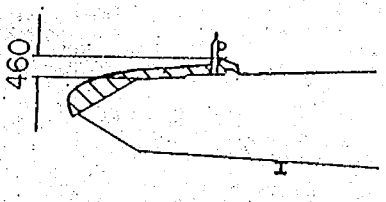

Fig. 7 Sectional mode of incrusted snow

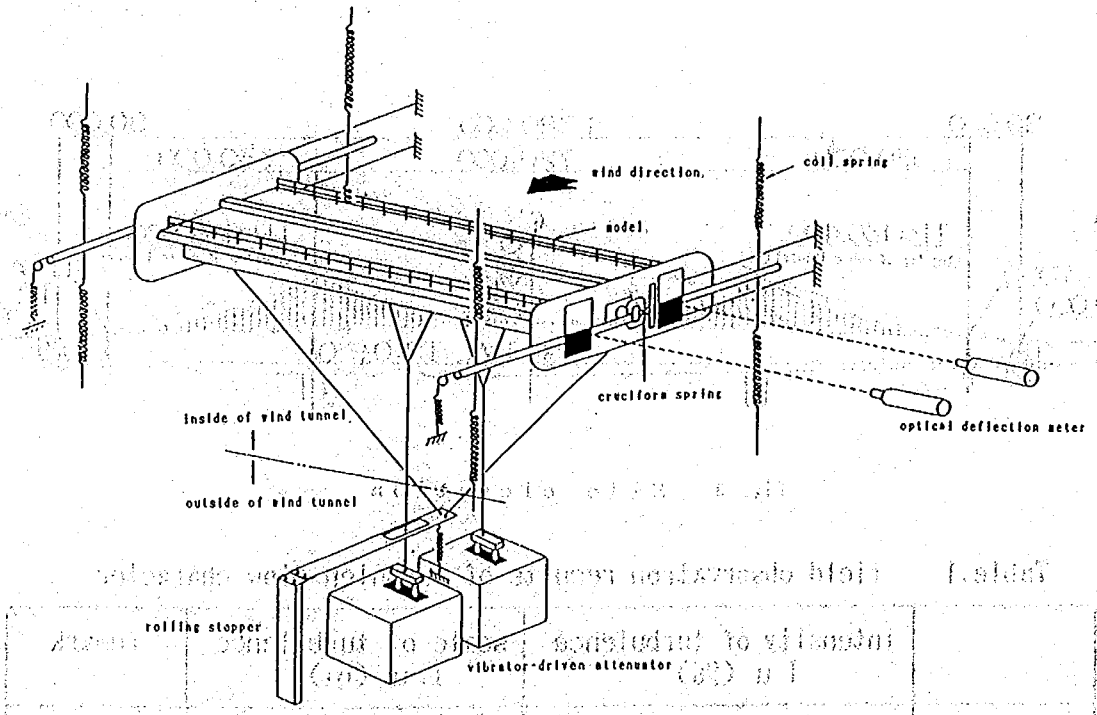

Fig. 5 Illustated conception of stiffening girder model testing

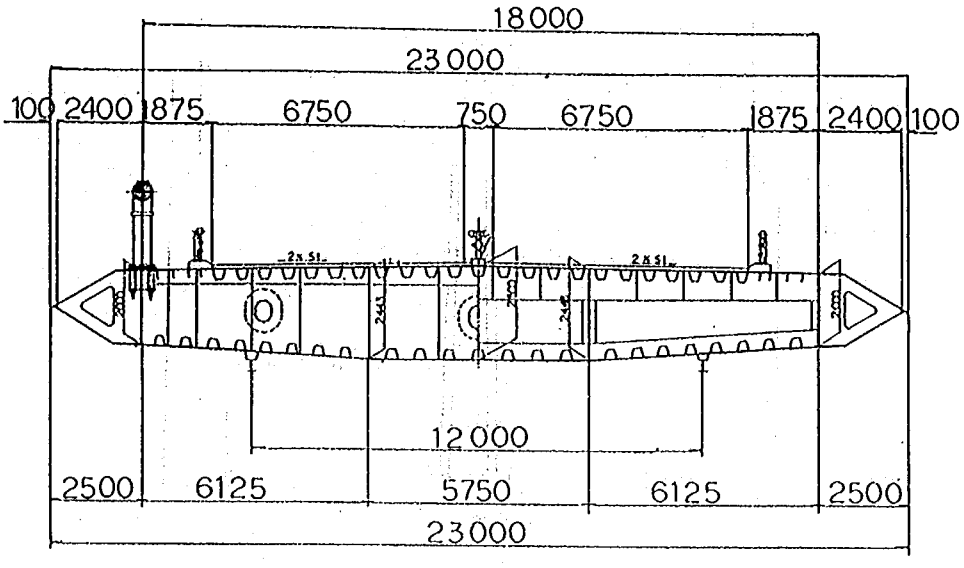

Fig. 8 Sectional detail of the stiffening girder center-to-center distance of cables

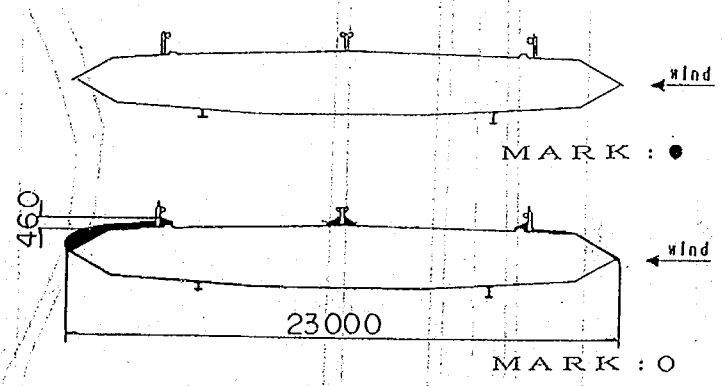

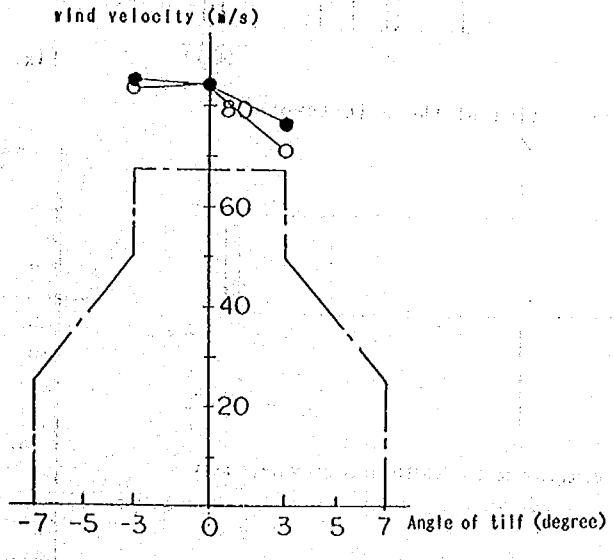

Fig. 9 Results of wind tunnel testing of model stiffening girder

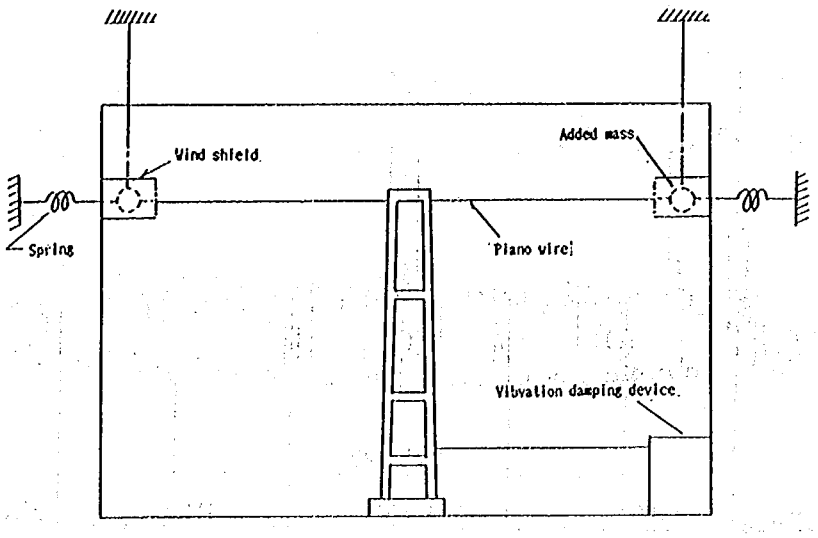

Fig. 10 Model idealization of the main tower

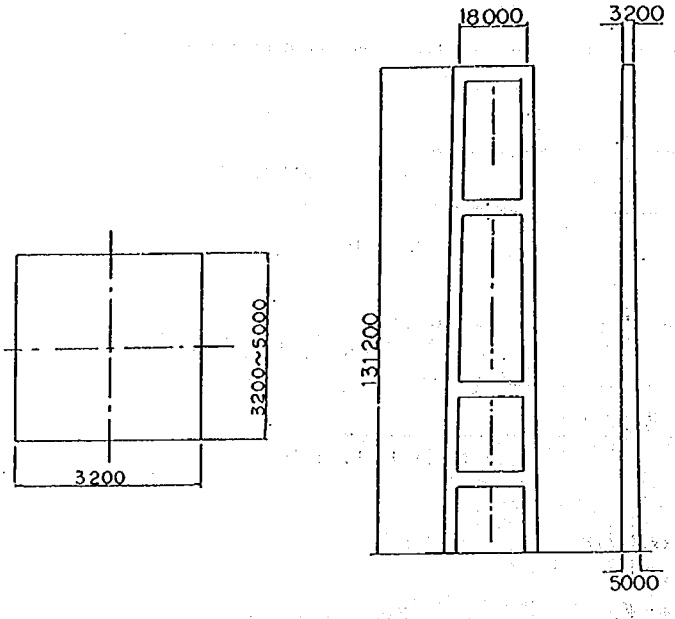

Fig. 11 Reference section of the main towers

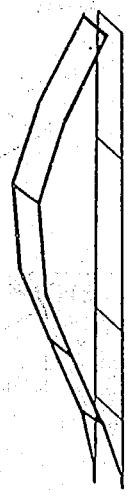

Fig. 12 Mode of deflection of the main tower

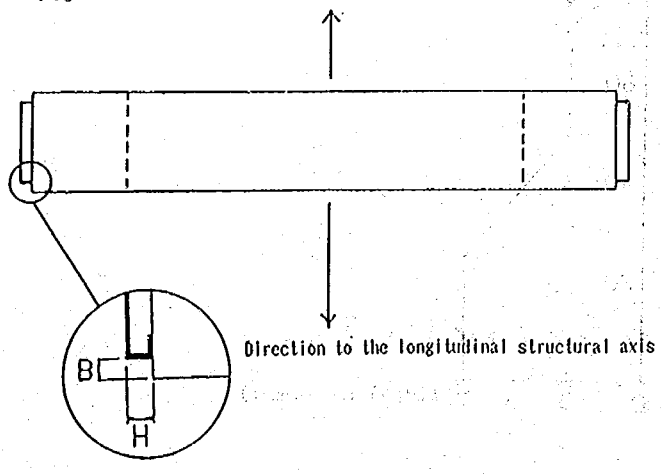

Fig. 13 Parameters for corner cutting on the main tower

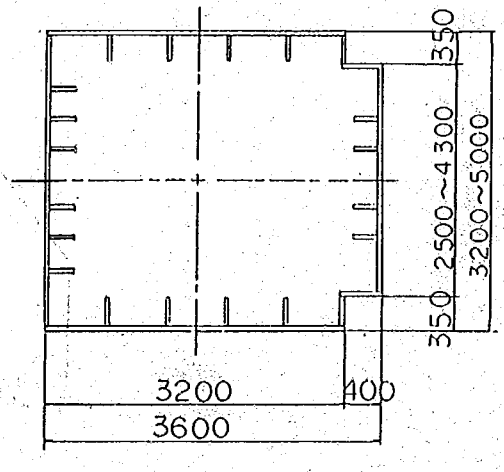

Fig. 14 Section of vertical members of a main tower

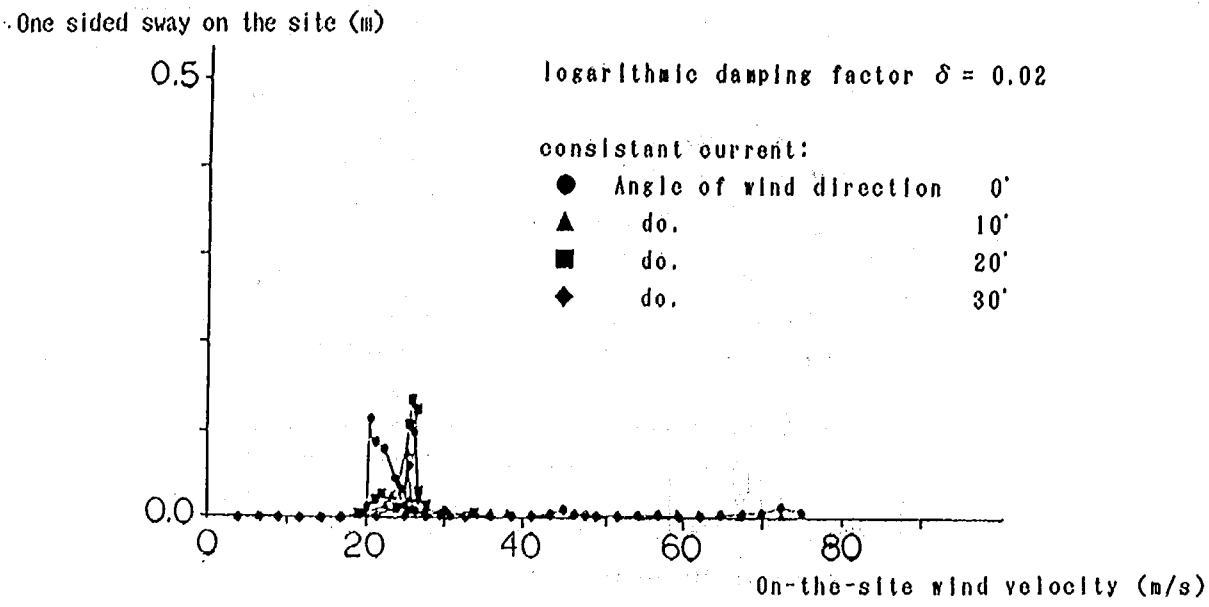

Fig. 15 Wind tunnel test results

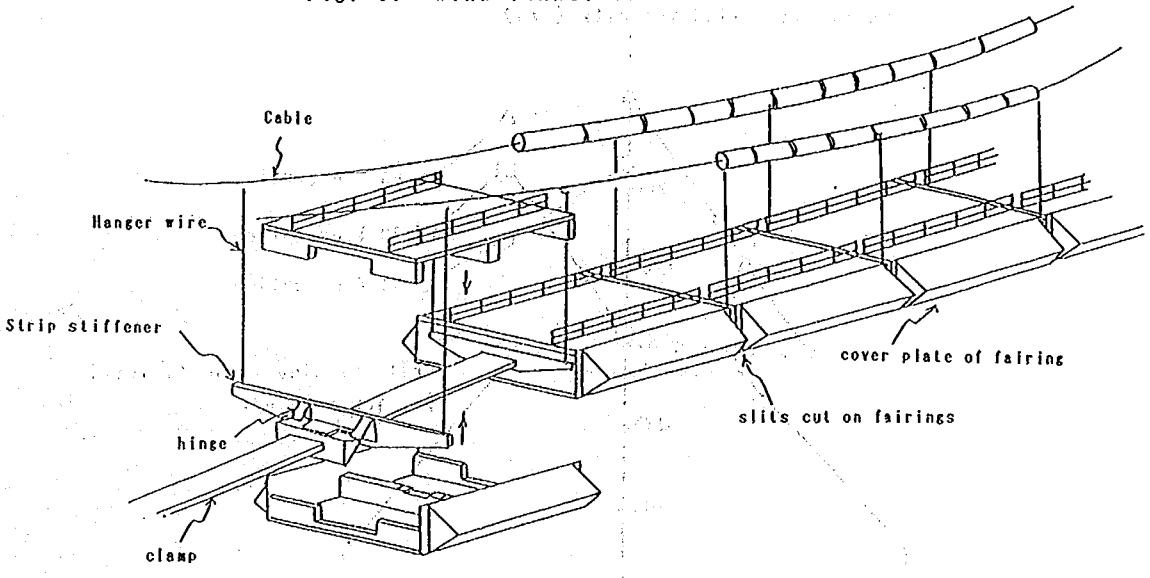

Fig. 16 Adopted modelling of the entire bridge under construction

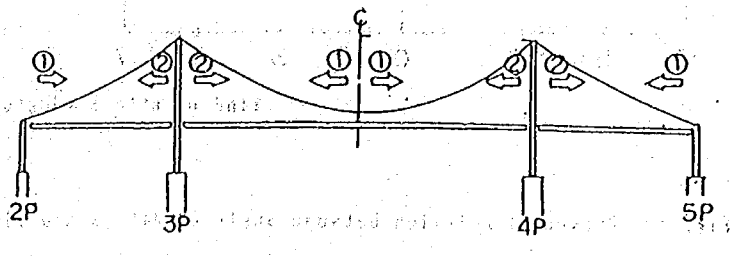

Fig. 17 Course of erection of the stiffening girder

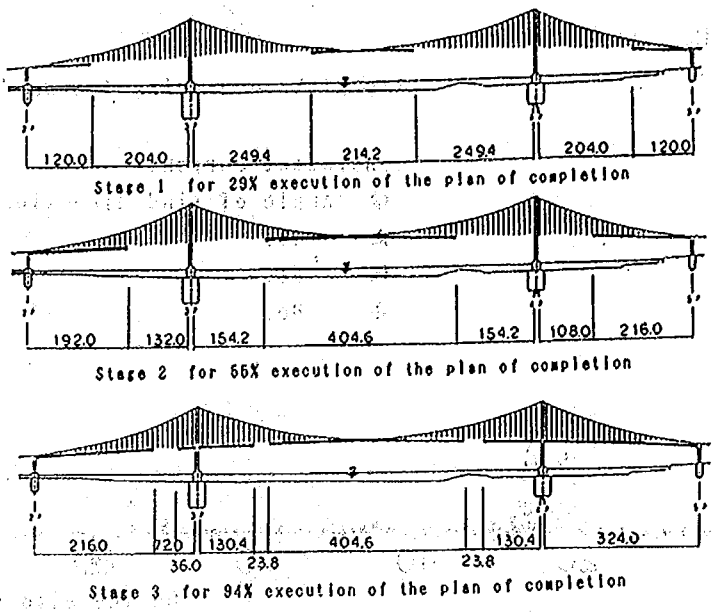

Fig. 18 Considered erection stages

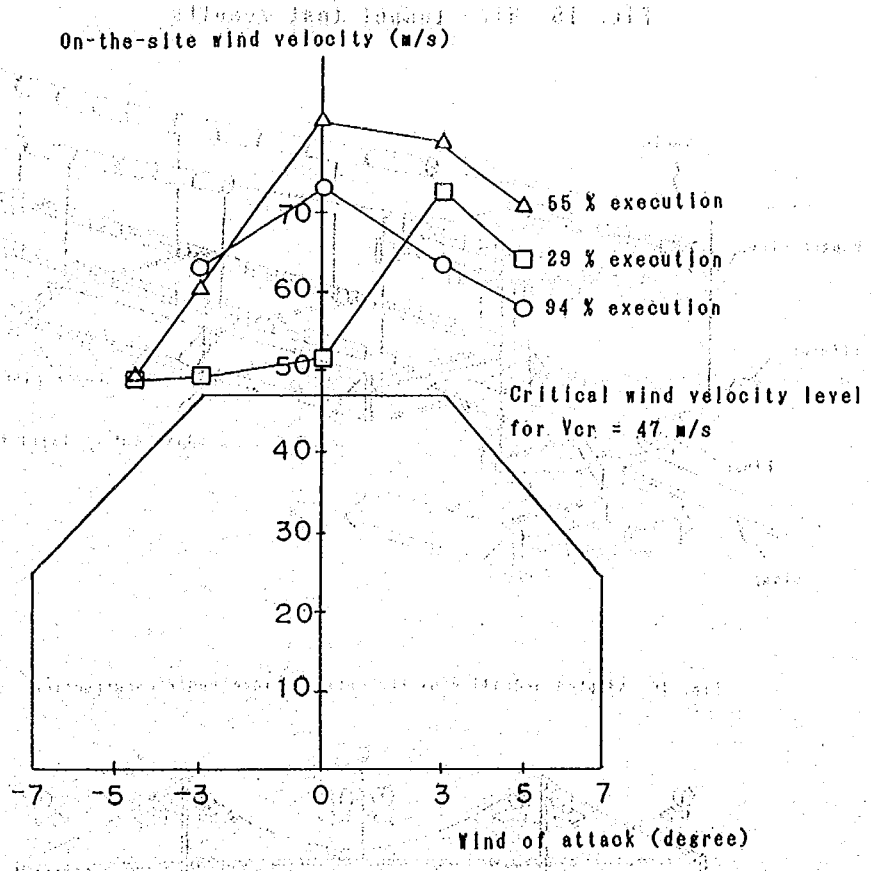

Fig. 19 Curves of relation between angle of attack and flutter-inducing velocity

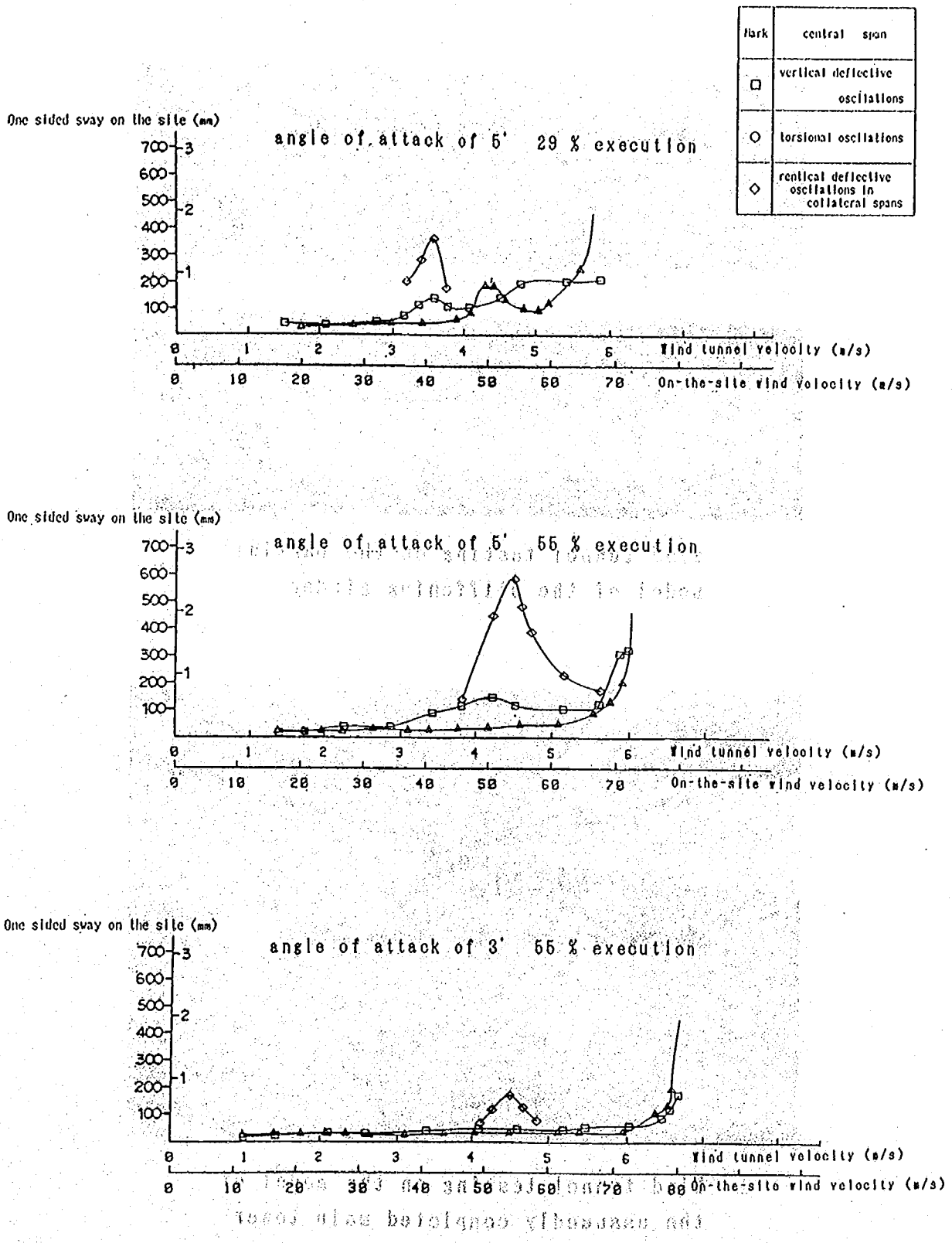

Fig. 20 Curve of amplitude vs. velocity for the stiffening girder

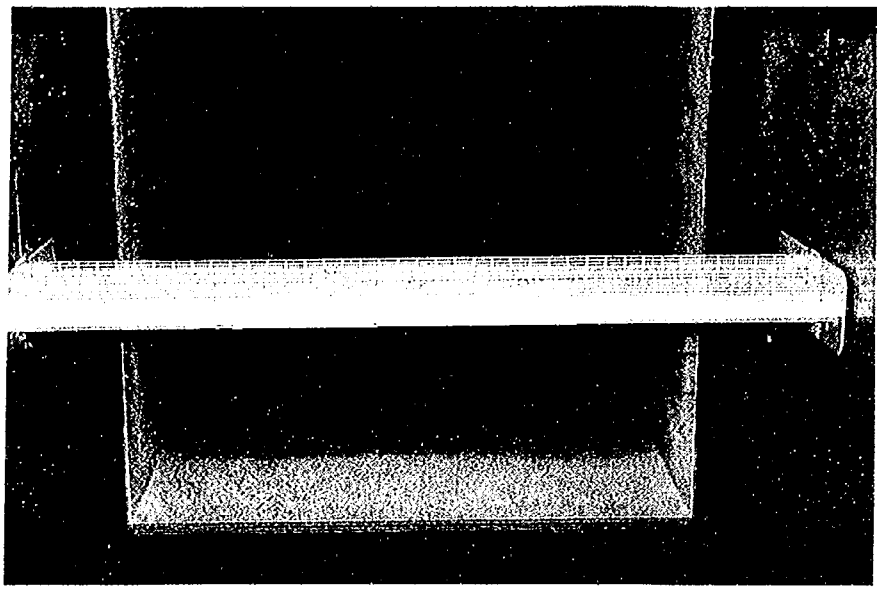

Wind tunnel testing on the partial model of the stiffening girder

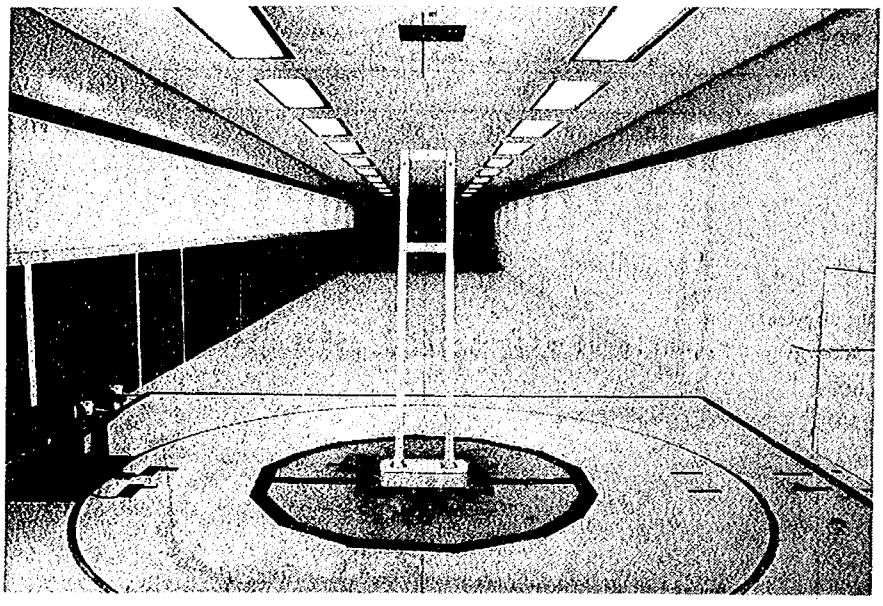

Wind tunnel testing on the model of the assumedly completed main tower

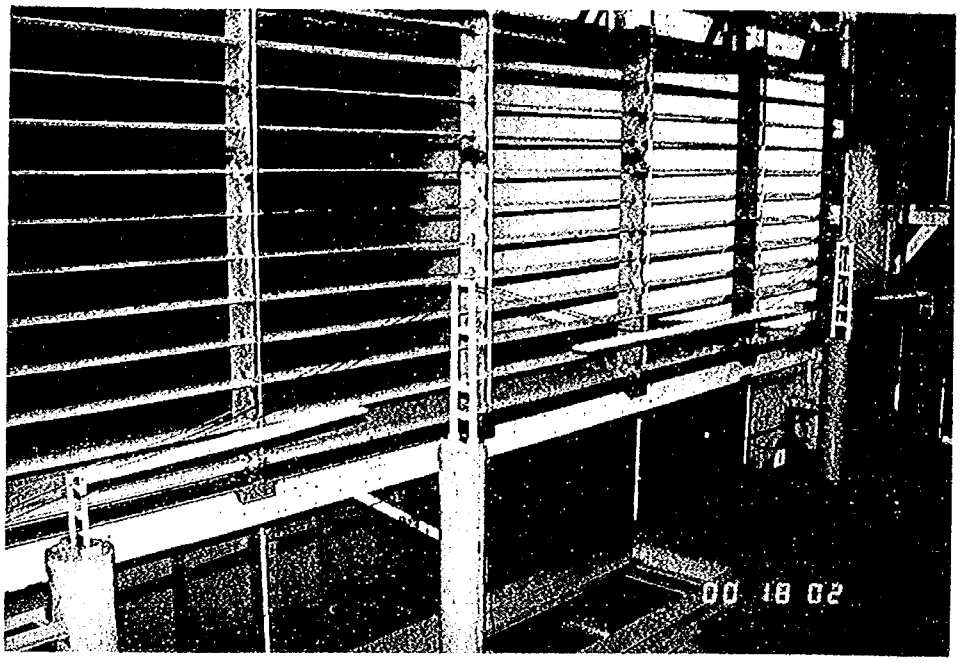

Wind tunnel testing on the model of the entire bridge assumedly being erected

(6) Session 6

SESSION 6: WIND RESISTANT DESIGN(2)
(Co-Chairmen: K. Yokoyama, N. P. Jones)

4:35pm～5:20pm

(16) Y. Fuse, N. Takahashi and T. Kobayashi* , T. Ujihara and K. Tamura: Measurement of Antivibration Effects by TMD Used in Steel-Decked Box-Girder
(4:35pm～4:50pm)

(17) K. Yokoyama and T. Kusakabe* : Preliminary Study on Active Control for Wind-Induced Oscillation of Long Span Bridges
(4:50pm～5:05pm)

DISCUSSION
(5:05pm～5:20pm)

MEASUREMENT OF ANTIVIBRATION EFFECTS BY TMD USED IN STEEL-DECKED BOX-GIRDER

by

Youichi Fuse *1, Noboru Takahashi *2, Tetsuhisa Kobayashi *3,
Takazumi Ujihara *4 and Kazumi Tamura *5

ABSTRACT

To confirm the tuning and antivibration effects of TMD (Tuned Mass Damper) installed on steel-decked box-girders of Kansai International Airport Access Bridge on the Airport Island side, sine-wave excitation tests were performed using an exciter during the erection of the bridge. As a result, it has been proved that the function of TMD in action is capable of permitting the box-girders to ensure a logarithmic decrement of damping of 0.1 or higher which is required for aerodynamic stability of these girders. The effects of TMD have also been demonstrated in an actual wind by measuring the girder vibration in an approaching typhoon.

INTRODUCTION

The Kansai International Airport Access Bridge on the Airport Island side becomes a three-dimensional type of construction including 2 roadway bridges and 1 railway bridge being constructed in parallel creating a curve in the longitudinal direction of each bridge as they change their relative positions with one another alternately.In such a case, there will be a fear of complicated aerodynamic vibration which is caused due to interference between the girders of the 3 bridges. A series of wind tunnel tests was performed to examine their aerodynamic stability [1]. The result indicated possible generation of vortex-induced oscillation, although limited, in a range of low wind velocity (20-40 m/sec) from the early stage of the bridge erection. TMDs were installed as vibration absorber.

The total of 26 TMDs has been installed on 2-span and 3-span steel-decked box-girders (for all 5 bridges). Using an exciter with a weight of 5 tons, a vibration test was performed on each TMD to confirm their tuning and effects in the early stage of the bridge erection. In the test, the natural frequency of the bridge itself was measured with the TMD locked (not in effect). This natural frequency was used to adjust the frequency of TMD to an appropriate position. Then, with the adjusted TMD put into operation, the logarithmic decrement of damping was obtained by exciting the bridge and measuring its free vibration.

An advantage was taken of an approaching typhoon during this vibration test to prove the TMD's effects by measuring vibration of girder in a gale.

This report describes the results of the above tests with some consideration added thereto on the antivibration effects of TMD installed on a box-girder.

---

*1 Executive Director, Kansai International Airport Company, Ltd. Japan
*2 Special Assistant to General Manager, ditto
*3 Sectional Chief, ditto
*4 Manager, Mitsubishi Heavy Industries, Ltd. Japan
*5 Senior Research Engineer, ditto

Outlines of the Bridges and TMD

Outline of the bridges

The subject bridges on the Airport Island side consist of 5 bridges including an eastward and a westward roadway bridge of 2-span steel-decked box-girder type, an eastward and a westward roadway bridge of 3-span steel-decked box-girder type and a railway bridge, as shown in Fig.1. All the bridges are still under construction pending such related works as asphalt pavement, electric cable erection, etc., to be performed.

Outline of the TMDs

On the basis of the wind tunnel test results [1], TMDs were designed so that the logarithmic decrement of damping, δ, might be more than 0.10. On this occasion, the following requirements had to be met :

(1) As a TMD is installed in the extremely narrow spaces in the box-girder bridges, due consideration should be taken that the weight of a TMD not hit against the bridge member in case of the TMD vibrating.

(2) In the M21,M22 and M31,M32 modes (see Fig.4), the vibration frequencies are relatively near to each other. Compared with the installation of two TMDs corresponding to the respective mode, the TMD which actuates effectively to both M21, M22, and M31, M32, mode is more economical.

With regard to (1), (2), TMD, designed to have a damping ratio much greater than the optimum value, is utilized. Such TMD has following characteristics [2]:

(1) The absorber mass is capable of restricting its amplitude to nearly that of the girders. Therefore it can be installed in the extremely narrow spaces in the box-girder bridges.

(2) There is little deterioration in the antivibration effect with changes in frequency of TMD or the bridge. This provides wider frequency ranges to be utilized effectively and wider allowable error ranges of frequency to make for easier tuning and maintenance as well as greater structural safety.

(3) There is also little variation in the antivibration effect with changes in the damping ratio of TMD.

As the investigation results, the installation places and types of TMD has become as shown in Fig.1. As shown, TMDs have been installed, 2 each, at the middle of the span of each bridge, totalling 26. Table 1 indicates the particulars of TMD of various types and the appearances of TMD is indicated in Fig. 2. Furthermore Fig. 3 shows the arrangement of TMDs inside the box-girder.

As shown in Fig. 2, this TMD is of a cantilever type consisting of a fulcrum, a cantilever, two oil dampers, two coiled springs, and a weight as a damping mass. Its frequency can be controlled freely by moving the weight horizontally.

As shown in Fig. 3, this device is installed on the lateral rib in the box-girder bridge, and it vibrates in the vertical direction, in case of the bridge vibrating.

Vibration Test

Test Method

The following procedure was used in the test.

Step 1: TMD was locked to prevent it from being operated. Using an exciter (weight: 5 tons), a sine-wave excitation test and a free vibration test were performed to obtain the natural frequency and the logarithmic decrement of damping of the bridge.

Step 2: Based on the natural frequency of the bridge measured in Step 1, the frequency of TMD was adjusted to an appropriate frequency by moving the weight of TMD.

Step 3: With TMD put into operation, the free vibration test was performed to measure the logarithmic decrement of damping of the bridge. By comparing this logarithmic decrement with that of the bridge itself as measured in Step 1, it was proved that the effect of antivibration of TMD had been obtained, as desired.

Table 2 shows the specification of the exciter used for exciting the bridge. The exciter was set at the middle of the span between P3 and P4 for the 2-span roadway bridge and between P6 and P7 for the 3-span roadway bridge. The acceleration of the girders were measured with a servo-type accelerometers that were set at the middle of each span.

Vibration Modes

Fig. 4 shows the subject vibration modes. As shown, the first- and second vibration modes were subjected for the 2-span bridge, and the first-,second- and third vibration modes, for the 3-span bridge.

Test Results and Discussion

Table 3 shows the results of the measurements of natural frequency and logarithmic decrement of damping. Also shown in the table are the results of the analysis of natural frequency performed at the time of designing TMD. Typical examples of the results of the sine-wave response measurement and the free vibration wave shapes are shown in Figs. 5, 6 respectively.

As shown in Table 3, the measured values of natural frequency are approximately in agreement with the analysis values with a difference of several per cent at a maximum.

The logarithmic decrement of damping of the bridge itself with TMD as locked was considerably scattered although all the bridges are almost of the same span construction. One of the reasons for this may be attributable to the difference in movement of the shoes. However, the visual observation indicated sufficient movement of the shoes on all bridges. This will remain to be examined in a detailed vibration measurements including the shoes at the time of the TMD tuning test for the completed bridge which will be performed when all the bridges have been completed.

All logarithmic decrements of damping of the bridges with TMD in operation were higher than that of 0.1 as required for aerodynamic stability. This indicates that TMD has developed its effect sufficiently.

Measurement of Girder Vibration in Actual Wind

General

Girder vibration was measured in an actual wind while Typhoon 28 was approaching (November 30, 1990). As a result, the effects of TMD have also been demonstrated in an actual wind.

Measuring Points

Table 4 and Fig.7 show the measuring points and the operating condition of TMD at the time of measurement. The instantaneous wind velocity and the wind direction were measured using an anemometer of propeller blade generator type that was installed on the railing over P4 of the 2-span westward roadway bridge.

Results of Measurement and Discussion

(1) Wind Velocity and Wind Direction

The wind velocities measured were about 18 m/s at a maximum averaging about 10 m/s. The wind blowing in the north (perpendicular to the bridge axis) before the typhoon's landing shifted suddenly to the west immediately after landing.

(2) Acceleration Response of Girder

Fig. 8 shows the major part of measurement results of acceleration response of the girders. The data in the figure were taken at about 12:35 November 30 when the wind velocity was about 18 m/s at a maximum in the direction almost perpendicular to the bridge axis.

The maximum values of acceleration at each measuring point are shown in Table 5 and Fig. 9, and examples of fourier spectra, in Fig.10.

A comparison from Table 4 and Fig.7 indicates that the maximum acceleration of the 2-span westward highway bridge (TMD locked) is 62.4 gal while that of the eastward roadway bridge (TMD in operation) is 16.7 gal, about 1/4 of the former, and also that the maximum acceleration of Fourier spectra of the westward roadway bridge is 10.0 gal while that of the eastward roadway bridge is 1.7, about 1/6 of the former as shown in Fig.10.

The results of the wind tunnel test that was performed before designing the bridges indicated that the bridge on the lee side would show almost the same amplitude as that of the bridge on the upwind side. From these reason, it follows that the difference between the results of the acceleration amplitude measurements of both bridges is attributable to TMD.

CONCLUSIONS

(1) Using an exciter, excitation tests were performed on steel-decked box-girders, which were equipped with TMD for aerodynamic stability, of Kansai International Airport Access Bridge on the Airport Island side. With TMD put into operation, it has been demonstrated that the logarithmic decrement of damping of 0.1 as required for such a girder for aerodynamic stability can be secured sufficiently.

The observation of vibration of the girders in an actual wind has also proved that TMD can develop its effect sufficiently.

(2) The logarithmic decrement of damping of the bridges themselves with TMD locked showed considerable scattering although they are almost of the same construction. From this fact, it is considered not only important to confirm the safety of a bridge by performing a field measurement but also necessary to reflect the results in the design by accumulating these data.

REFFERENCES

(1)Honda, A., Shiraishi, N., Motoyama, S. ; Aerodynamic Stability of Kansai International Airport Access Bridge, J. of Wind Engineering No.37 Oct.1988.

(2)Abiru, H., Matsumoto, H. ; Prevention of Induced Vibration of Steel Chimney by Heavily Damped Vibration Absorbers, Pre-print of 6-th International Chimney Conference, Brighton-England, 1988.

Table 1. Particulars of TMD

Type of TMD	E1~E8	A1~A8	B1~B4	C1~C4	D1~D2
Weight of damper mass (ton)	7.5	7.5	8.0	10.4	8.0
Frequency (Hz)	0.92	0.94	1.40	1.12	1.66
Vibration mode	M21, M22	M31, M32	M33	M31, M32	M33
Kind of bridge	Roadway bridge of 2-span portion	Roadway bridge of 3-span portion		Railway bridge of 3-span portion	

Table 2. Specifications of exciter

Shaking method	Electro-hydraulic servo system
Exciting force: Vertical and horizontal direction	3 ton · g and 3 ton · g
Frequency range	0~50 Hz
Maximum amplitude	± 200 mm
Mass	5 ton
Total weight	6 ton
Size	2300 x 1350 x 2800H

Table 4. Measuring points and the operating condition of TMD

Bridge		No. of accelero-meter	Measuring points	Operating condition of TMD
2-Span portion	East ward roadway bridge	EG2	center of span (P3~P4)	In operation
		ED2N	weight of TMD (P3 ~P4)	
	West ward roadway bridge	WG1	center of span (P2~P3)	Locked
		WG2	center of span (P3~P4)	
3-Span portion	East ward roadway bridge	EG3	center of span (P4~P5)	In operation
	West ward roadway bridge	WG3	center of span (P4~P5)	In operation
	Railway bridge	TG3	center of span (P4~P5)	In operation

Table 3. Natural frequency and logalithmic decrement of damping

Bridge		Vibration mode	Natural frequency (Hz)		Logalithmic decrement of damping	
			Measured	Calculated	TMD locked	TMD in operation
2-Span portion	East ward roadway bridge	M21	0.945	0.923	0.029	> 0.2
		M22	1.487	1.542	0.037	0.11
	West ward roadway bridge	M21	0.925	0.894	0.036	> 0.2
		M22	1.450	1.496	0.045	0.14
3-Span portion	East ward roadway bridge	M31	0.977	0.952	0.020	0.36
		M32	1.225	1.216	0.041	0.16
		M33	1.701	1.798	0.053	0.19
	West ward roadway bridge	M31	0.976	0.955	0.012	0.27
		M32	1.213	1.220	0.037	0.21
		M33	1.708	1.803	0.045	0.15
	Railway bridge	M31	1.283	1.267	0.110	0.26
		M32	1.507	1.553	0.021	0.12
		M33	2.216	2.254	0.073	0.12

Table 5. Maximum acceleration response measured (gal)

Bridge		No. of accelero-meter	Maximum acceleration	Maximum acceleration on Fourier Spectra	Operating condition of TMD
2-span portion	East ward roadway bridge	EG2	16.7	1.7	In operation
	West ward roadway bridge	WG1	62.4	10.0	Locked
		WG2	58.4	10.4	
3-span portion	East ward roadway bridge	EG3	14.5	1.5	In operation
	West ward roadway bridge	WG3	29.2	2.4	In operation
	Railway bridge	TG3	6.2	0.3	In operation

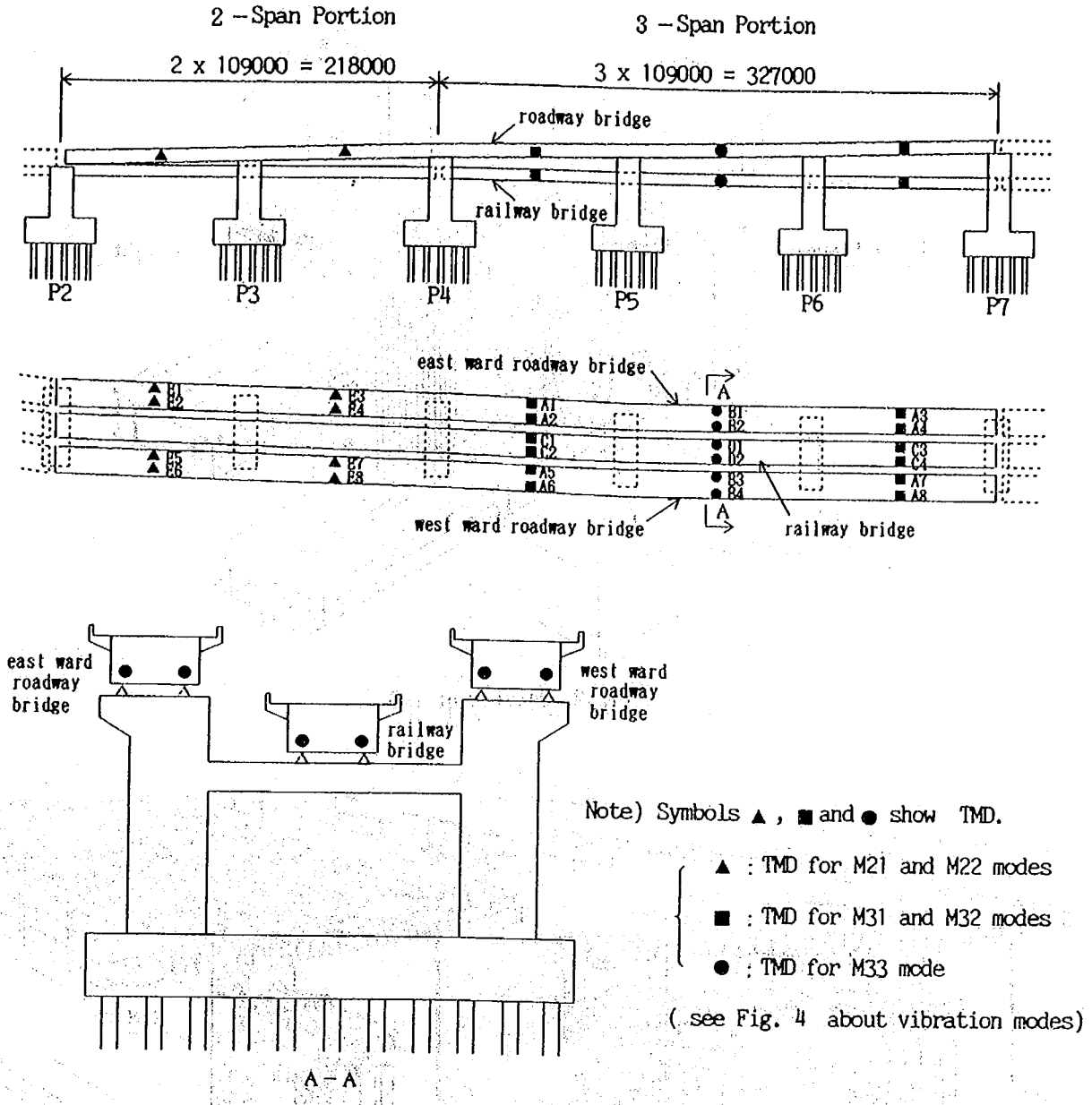

Fig. 1 Outline of Kansai International Airport Access Bridge and installation places of TMD

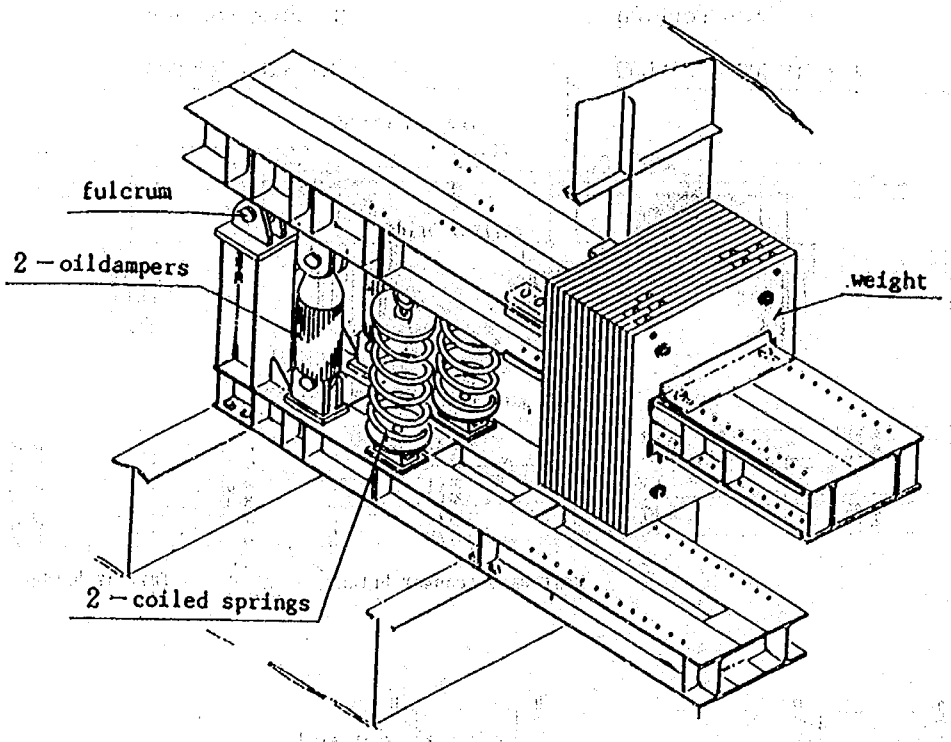

Fig.2 Outview of TMD

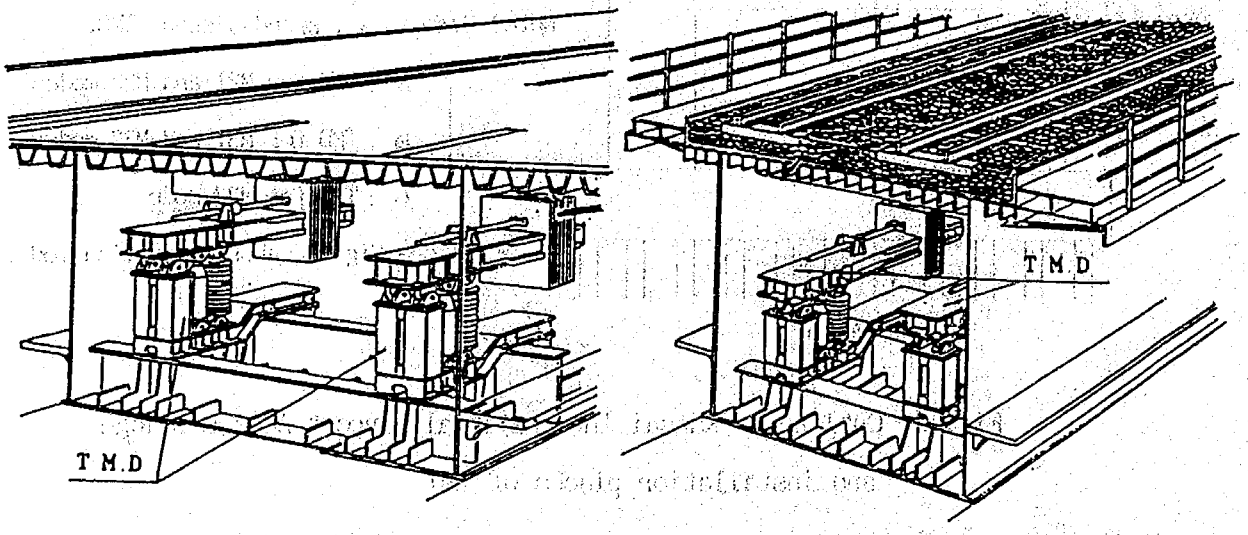

(a) Roadway bridge

(b) Railway bridge

Fig.3 Outview of TMDs inside box-girders

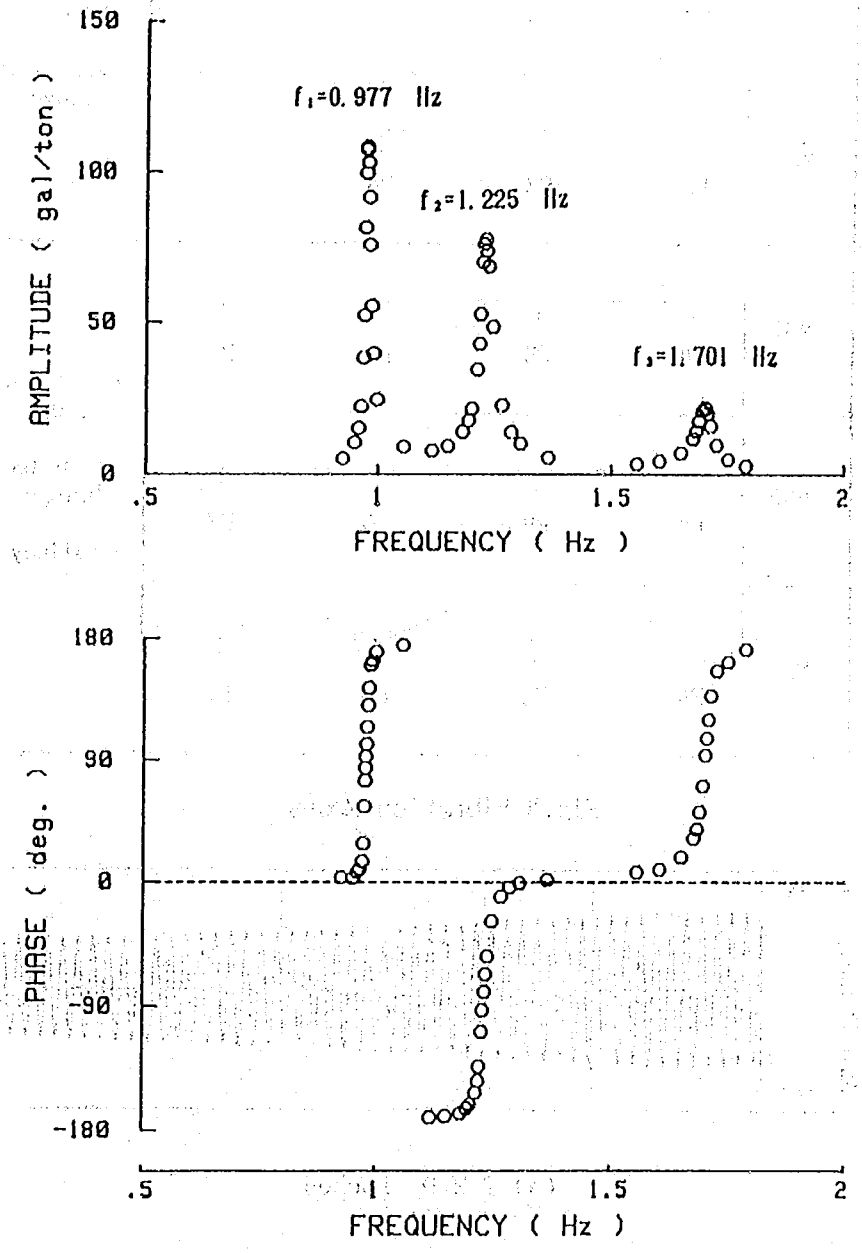

Fig.5 Examples of sine-wave response and phase curves

Bridge	Modes		Remarks
2 – Span portion	M21	P2 P3 P4	• east ward roadway bridge • west ward roadway bridge
	M22	P2 P3 P4	
3 – Span portion	M31	P4 P5 P6 P7	• east ward roadway bridge • west ward roadway bridge • railway bridge
	M32	P4 P5 P6 P7	
	M33	P4 P5 P6 P7	

Fig.4 Vibration Modes

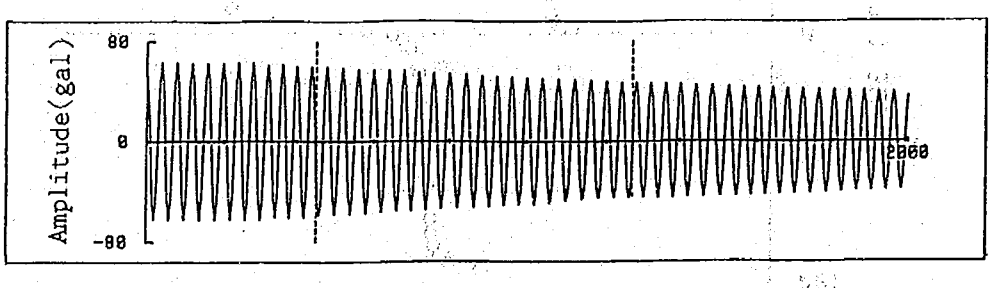

(a) T M D locked

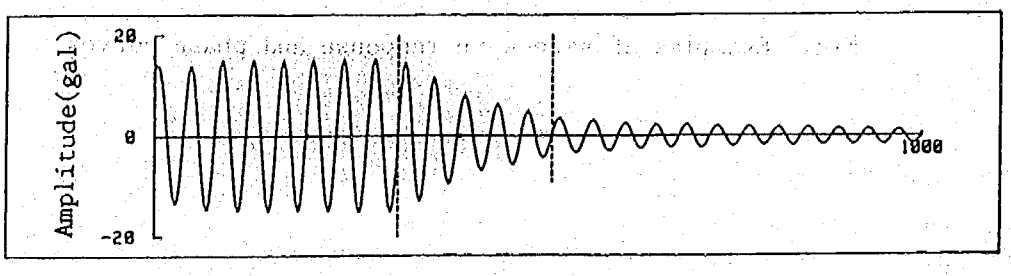

(b) T M D in operation

(3-span east ward roadway bridge)

Fig.6 Examples of Wave shapes of free-damped vibration

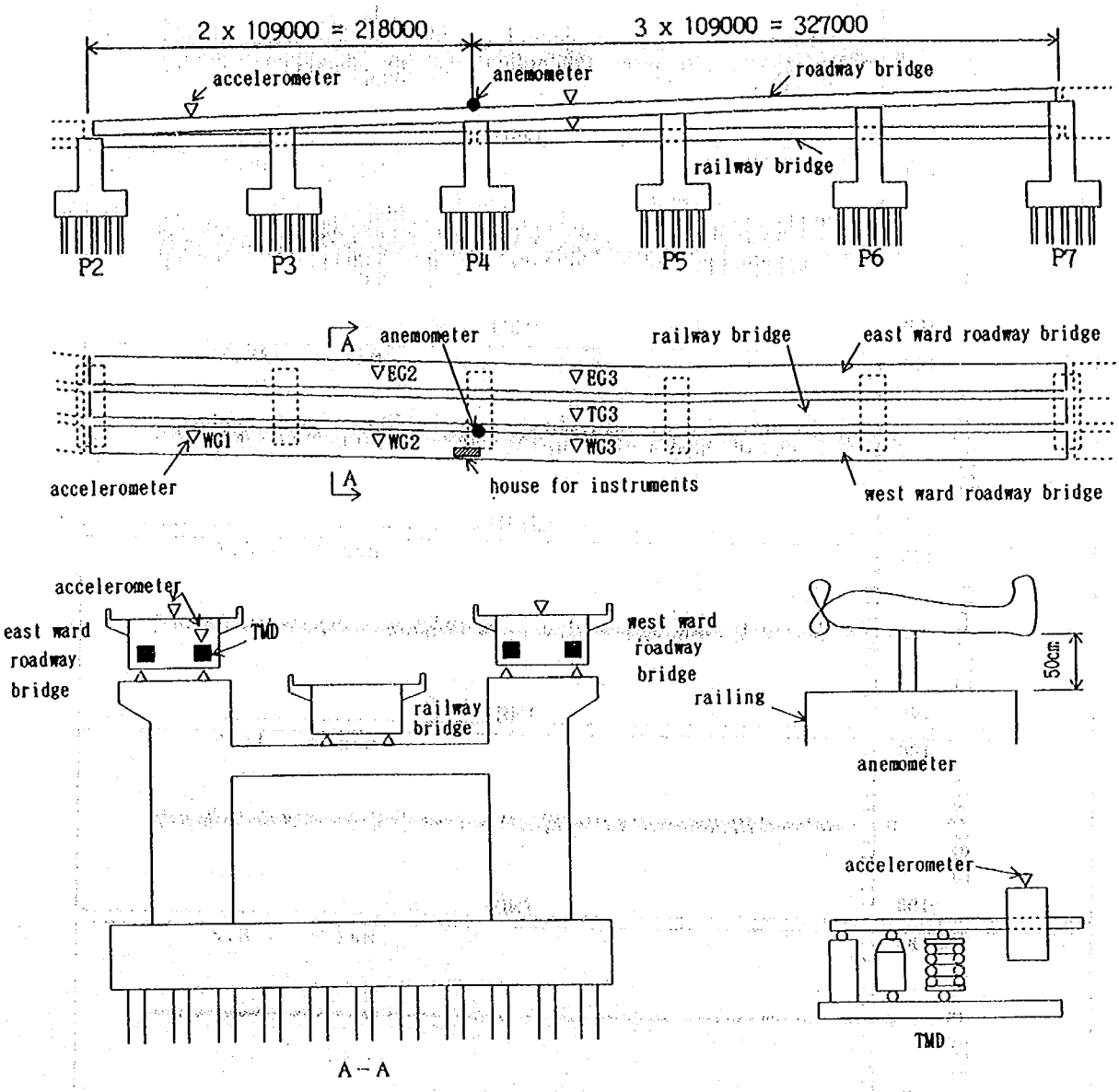

Fig.7 Measuring Points

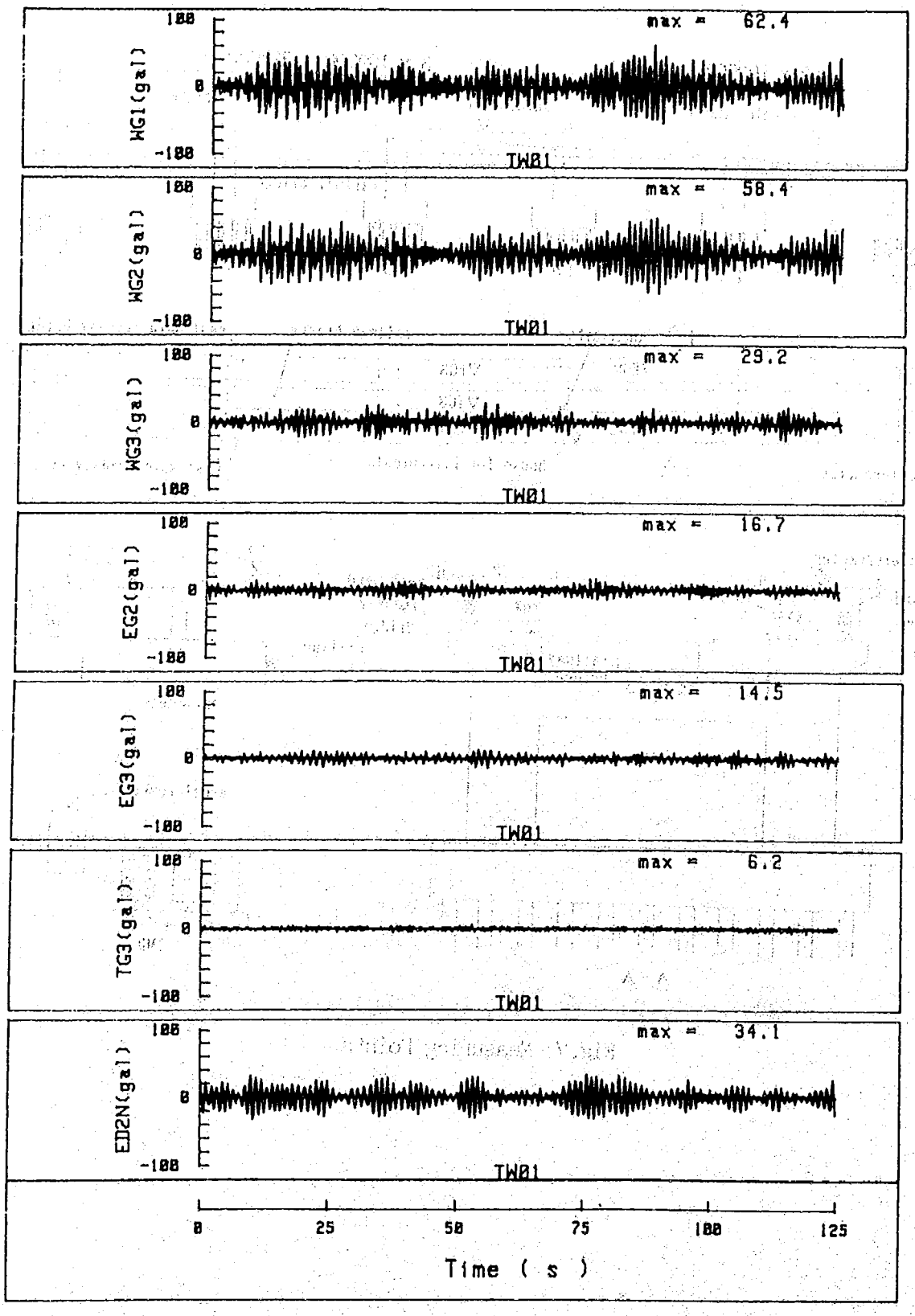

Fig. 8 Examples of acceleration response

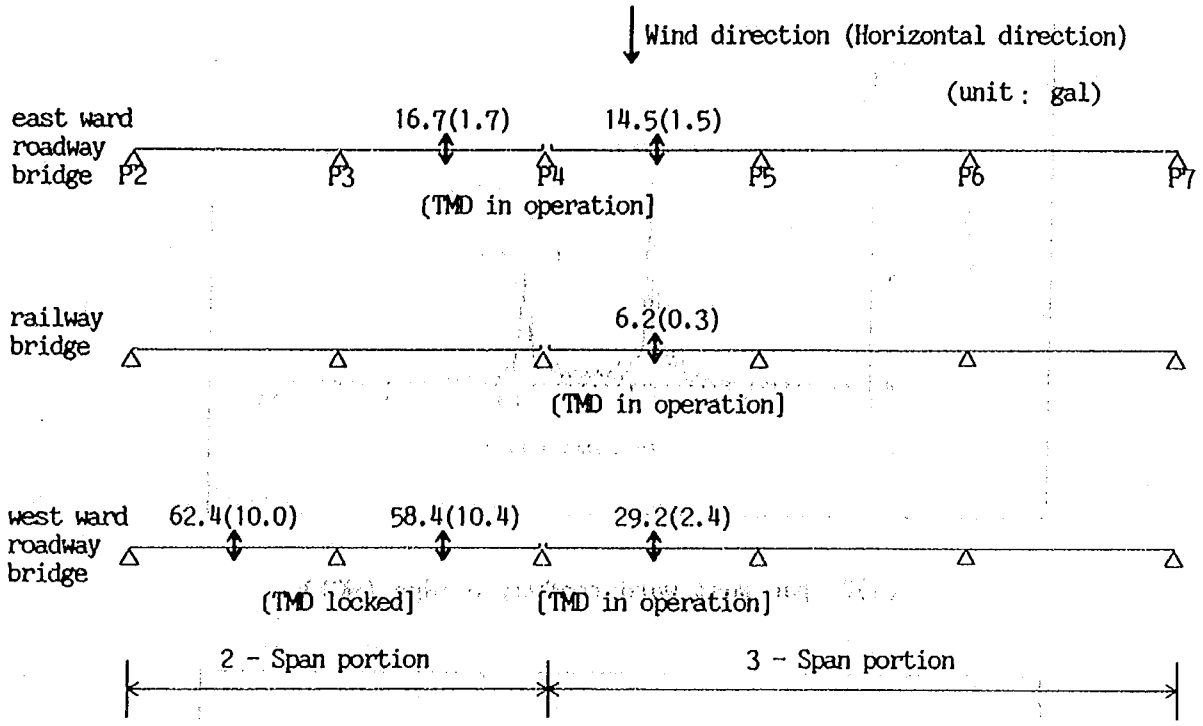

Note: The Values in parentheses '( )' show the acceleration on Fourier spectra.

Fig.9 Maximum values of the acceleration measured

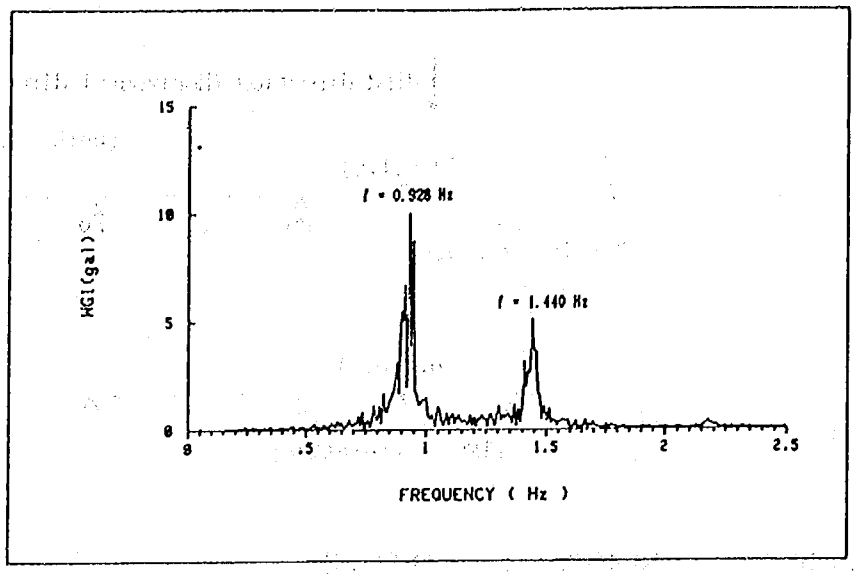

(a)2-span west ward roadway bridge (WG1)

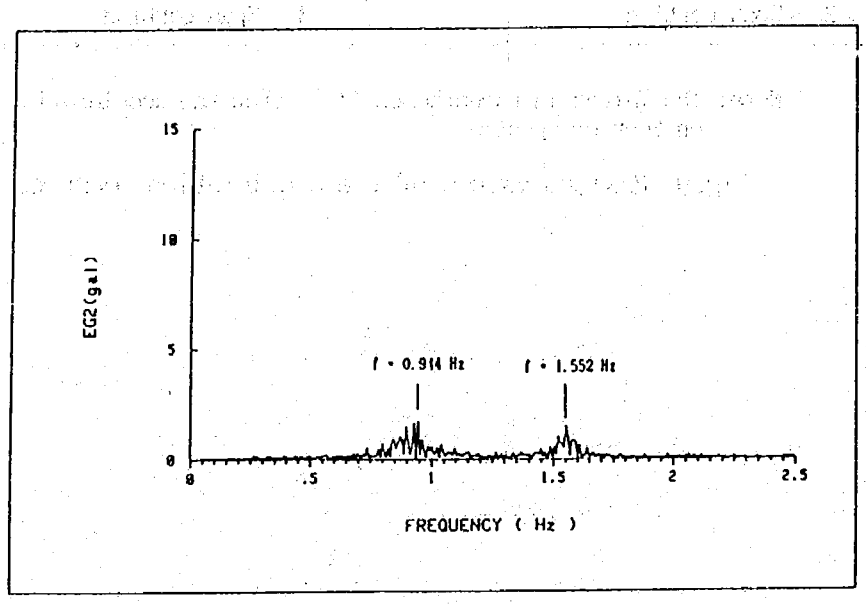

(b)2-span east ward roadway bridge (EG2)

Fig.10 Examples of Fourier spectra

PRELIMINARY STUDY ON ACTIVE CONTROL FOR WIND-INDUCED OSCILLATION OF LONG SPAN BRIDGES

by

Koichi Yokoyama[1] and Takaaki Kusakabe[2]

ABSTRACT

There are some ideas in the world to construct super-long span bridges whose center span length exceeds 2000m. As wind-induced oscillation is one of the critical problems for those bridges, it seems essential to develop new design methods and countermeasures to confirm the safety against strong wind. Aerodynamic improvement of cross section of girder and traditional passive control are not enough effective for super long span bridges. This report focuses on active control for bridges. Though the active control itself is not a new method, its application to long span bridges is a new theme. New concepts of control will be applicable, because mechanism of wind-induced vibration is different from that of other vibrations due to earthquakes and traffics. In this report, some concepts of active control and some results of investigation are introduced.

1. Introduction

In Japan, a large number of long span bridges have been constructed since the Wakato Bridge was constructed in 1962. The Akashi-Kaikyo Bridge, whose center is 1990m and will be the longest suspension bridge in the world near future, is under construction and the Tatara Bridge, which will be the longest cable-stayed bridge in the world, is also under construction.

There are some ideas of construction project of super-long span bridges whose center span length exceeds 2000m as next term big projects in Japan and in the world.

The design experience of the Akashi-Kaikyo Bridge reveals that the wind resistant design becomes one of the critical problems for such super-long span bridges, and a great amount of efforts and time will be expended on solving it. It seems for wind engineers in Japan that the Akashi-Kaikyo Bridge would be the longest bridge that is designed by traditional method, because no bridge whose center span length exceeds 2000m will be able to clear the problem of wind stability by means of traditional method. So now, it seems essential to develop new design methods or countermeasures for wind-induced oscillation of super-long span bridges.

There would be many approaches to solve the problem in order to realize super-long span bridges, for example, installation of devises to increase the frequency of structure, improvement of form or mode shape of vibration and development of methods to make use of wind force generated by 3-dimensional flow around girder. All methods described above are worth studying. Active control is one of the methods to solve the problem of wind-induced instability.

---

1 Head, Structure Division, Public Works Research Institute, Ministry of Construction, 1, Asahi, Tukuba-Shi, Ibaraki-Ken, 305, Japan

2 Research Engineer, ditto

This paper presents the results of the preliminary study on active control for wind-induced oscillation of bridges conducted by PWRI in order to evaluate feasibility of its application to the long span suspension bridges.

2. Active Control for Wind-Induced Oscillation of Long Span Bridges

Regarding the wind-induced vibration, there have been many studies which dealt with active control for application to gust response of buildings[1)-5)]. Also many reports are published on active control of buildings and structures for earthquake[6)7)] and traffic-induced vibration[8)]. These research results are valuable for study of active control of wind-induced oscillation, because some methods can be studied only converting the acting force from seismic force to aerodynamic force.

On the other hand, there are some differences between active control of wind-induced oscillation of bridges and active control of wind-induced oscillation of buildings as well as active control of earthquake-induced oscillation of bridges. Remarkable differences are described below.

a. Wind-induced oscillation is the self-excited vibration. This means that characteristics of acting wind forces are stationary.

b. Since the shape of cross section affects aerodynamic forces very much, aerodynamic forces themselves are controllable.

c. Aerodynamic forces are smaller than inertia force.

d. Because main cause of strong wind is typhoon in Japan, inspection of the system is possible before arrival of typhoon. Then, it is expected that system will be reliable.

e. In addition, there is a possibility to obtain control force from wind force itself. This is different from seismic force.

3. Basic Concepts of Active Control Method

Basic ideas of active control for wind-induced oscillations are classified as follows;

a. Mechanical active control
b. Active control by means of additional aerodynamic force.
c. Active control of static wind force.
d. Active control of aerodynamic flow pattern

Here, a and b are not new concepts but c and d are proposed by the authors. The practical effects are not sure at this stage. The basic concepts of each control method are shown as follows;

(1)Mechanical Active Control

This type of active control is well known as the Active Mass Damper (AMD) or the Active Tuned Mass Damper (ATMD)[2)]. In order to control, behavior of structure is measured and control force is given to structure by actuator as a reaction of mass block. The concept is illustrated in Fig.-1. This type of active control has been already studied very well. It will be a new subject only to estimate unsteady aerodynamic forces accurately.

(2)Active Control by Means of Additional Aerodynamic Force

This method has the same concepts with the mechanical active control. Fig.-2 shows the basic concepts of control. Some reports[4)5)] have been already published for buildings and bridge girders. In this method wind force is used as the control force instead of reaction of mass block in case of the mechanical active control. The control force is brought from wind force acting on the wing which is installed on the edge of the girder. The magnitude of control force is adjusted to required value by controlling the angle of the wing.

(3)Active Control of Static Wind Force

Aerodynamic stability is sometimes sensitive to wind angle of attack as shown in Fig.-3. Consideration of this phenomenon brought a new concept of active control. It will be possible to obtain good aerodynamic stability by keeping the wind angle of attack in the best value. Fig.-4 shows the fundamental concept of this method. The wind force acting on wing becomes torsional force that is adequate to keep wind angle of attack by twisting girder. Practically, the wind angle of attack does not change so much suddenly, so that the time span of wing controlling will be long and small energy will be needed for control.

(4)Active Control of Aerodynamic Flow Pattern

Fig.-5 shows the basic concepts of the control. In case of self-excited oscillation, there is high synchronization between aerodynamic force and vibration of bridge girder. In this method, this synchronization will become lower by controlling wings installed on girder. There are variety of patterns of putting wings and methods of control. Numerical approach is impossible to study on the effects of this method. Wind tunnel test is the only method by which the effects of control are estimated. In this study, judging the feasibility is the main subject. It will become the next term subject of this method to find some rules for getting good effects. In this method wings are controlled and control force will be almost independent upon wind velocity as method b and c. It is expected that this method is more effective than method b and c.

4. Study on Mechanical Active Control

In order to study feasibility of application of active control to wind-resistant design, fundamental model was made and fundamental numerical simulation and wind tunnel test were performed.

4.1 Method of Simulation

(1) Model of Structure and Active Control

Active Tuned Mass Damper (ATMD) is mainly studied here. Numerical simulation is performed to evaluate the effect of ATMD. Bridge is modeled as a one degree of freedom(1-DOF) system. Also ATMD has 1-DOF.

The control force is determined by optimum control theory. The equation of motion of the system can be written as Eqs.(1).

$$\begin{pmatrix} m_1 & 0 \\ 0 & m_2 \end{pmatrix}\begin{bmatrix} \ddot{x}_1 \\ \ddot{x}_2 \end{bmatrix}+\begin{pmatrix} c_1+c_2 & -c_2 \\ -c_2 & c_2 \end{pmatrix}\begin{bmatrix} \dot{x}_1 \\ \dot{x}_2 \end{bmatrix}$$

$$+\begin{pmatrix} k_1+k_2 & -k_2 \\ -k_2 & k_2 \end{pmatrix}\begin{bmatrix} x_1 \\ x_2 \end{bmatrix}=\begin{bmatrix} F-u \\ u \end{bmatrix} \quad \cdots(1)$$

In which x, m, c, k, F and u is defined in Fig-1.

Vortex-induced vibration is regarded as resonant vibration and magnitude of force is dependent upon amplitude of vibration. Aerodynamic force is expressed in Eqs.(3).

$$F(t)=A(x_1)\sin(\omega t) \quad \cdots\cdots(2)$$

In which, ω is the lowest natural frequency of the structure.

Galloping is regarded as self-exited vibration. Aerodynamic force is determined by quasi-steady theory. In this theory , aerodynamic force can be evaluated by 3-component of steady wind forces, namely drag force, lift force and pitching moment. Fig.-6 shows the aerodynamic coefficients which are used for simulation. The aerodynamic force can be expressed as Eqs.(3)

$$F(t)=\rho \cdot V^2L(BC_L+hC_D\tan\alpha(t))\sec\alpha(t) \cdots(3)$$

(2) Control Force

Control force is determined to minimize the objective function J that is shown in Eqs.(4).

$$J=\frac{1}{2}\int_0^\infty (X^TQX+Ru^2)dt \quad \cdots\cdots(4)$$

In which Q is a weighting matrix associated with the component of the state vector X, and R is a weight associated with the control force. The relative magnitude of these weighting value has a physical meaning. And there is no meaning on the absolute magnitude.

The control force is determined by solving the matrix Ricatti equation that is expressed as Eqs.(5).

$$A^TP+PA+PBR^{-1}B^TP-Q=0 \cdots\cdots(5)$$

In which A: consists of m, c and k B:consists of m.

P: unknown matrix

Finally control force u is derived from Eqs.(6) and (7).

$$G=R^{-1}B^TP \quad \cdots\cdots(6)$$

$$u=GX \quad \cdots\cdots(7)$$

In which G is called gain matrix.

(3)Time history of response

To execute simulation, eigenvalue is evaluated at first. Then modal analysis is executed and time history of response is estimated. The ordinary

method is used here in this simulation.

4.2 Results of Simulation

(1) Adequate Gain

The weighting matrix Q can be expressed as Eqs.(8).

$$Q=[0\ 0\ Q\ 0] \cdots\cdots (8)$$

This equation means that only the deflection of structure is the object of control but velocity of structure and behavior of mass block are not. Fig.-7 shows the relation between Q and effect of control. Here, the mass ratio m_1/m_2 is one hundred. Amplitude of structure decreases and control force and stroke of mass block increase with increasing weighting parameter Q. Same tendency is shown in the cases in which mass ratio is 500 and 1000. Finally, adequate Q is determined as 10^{12} and 10^{13} for AMD and ATMD respectively.

(2)Effects for Vortex-Induced Vibration

Results are shown in Fig.-8 and Table-1. For comparison of effect, simulation is also performed on Tuned Mass Damper (TMD). The stationary amplitude is 85cm without damper. TMD suppresses the amplitude to 7cm. With regard to the active control, the amplitude is decreased to 4cm by AMD and to 1cm by ATMD. On the other hand, active control causes a little larger stroke to the mass block than TMD.

Decrease of the weight of mass block makes no effect on suppressing vibration. On the other side, the stroke of mass block, which brings a practical limit of active control, becomes large value. It is also interesting result that ATMD has good stability against tuning error. Fig-9 shows the relation between effect and rigidity of spring. It seems that the effect of TMD depends on tuning very much but the effect of ATMD does not.

(3)Effects for Galloping

The effect is estimated by onset velocity of galloping. Results are shown in Fig.-10 and Table-2. Without damper, the onset velocity of galloping is 8m/s. TMD and AMD raise it to 72m/s and 132m/s respectively. ATMD suppresses galloping completely.

Practically, it is considered that TMD is not so effective to self-exited vibration. In quasi-steady theory, increase of damping is effective to raise onset velocity of galloping. It is often true that increase of damping improves wind resistance. It will be adequate to understand that the results of simulation suggests the better effects of active control than that of TMD.

Though effects are estimated by onset velocity in above discussion, stroke of mass block is not negligible. Good effects of AMD and ATMD means that control force is acting and mass block is moving to suppress the vibration. Probably, the stroke of mass block becomes one of critical conditions of design. In the next term study, this problem will be solved by advanced simulation or wind tunnel test.

5. Study on Active Control of Static Wind Force

As explained 3.(3), control force in this method is derived from a wing that is installed on girder. The magnitude of control force is adjusted by controlling the height or angle of a wing. 3-component wind forces were measured to estimate the effects of wing as the first step of this research. The cross section of bridge girder is selected from models which have poor aerodynamic stability. Also investigated is influence of wing to aerodynamic behavior of girder.

Fig.-11 shows definition of wing state. Fig.-12 shows the relation between additional aerodynamic moment and state of wing. Horizontal wing produces the largest control force. Since the control force varies continuously with changing of the state of wing, it will be easy to obtain adequate control force by adjusting state of wing. There is no remarkable change on the dynamic response of girder against wind. Practically, it is not clear whether bridge is controlled to optimal angle of attack or not, before amplitude of vibration develops. Wind tunnel test in which active controller is installed on model is necessary to solve this problem.

On the capacity of the control, there is a serious problem. A trial calculation applied to the Akashi-Kaikyo Bridge shows that 2m height plate should be equipped with a range of 500m longitudinal length in the center span, whose length is 1990m, to obtain 1 degree torsional displacement at midpoint of the center span in wind velocity of 70m/s. To put it simply, additional aerodynamic moment is too small to control the angle of attack well. This is serious and negative results for the feasibility of this method.

6. Concluding Remarks

In this report, some concepts of active control and some results of investigation are introduced. Since some concepts are new concepts and aerodynamic forces are not clear enough, the feasibility of active control is not discussed enough in this report. However preliminary study in this report presents interesting results.

Numerical simulation of AMD and ATMD suggests that they work more effectively than TMD. However it is shown that mass ratio of 100 is lowest value to obtain enough effect. This mass ratio seems to be a little heavy to equip ATMD or AMD on prototype bridge. As for flutter, no simulation is performed. It is necessary for simulation of flutter to estimate aerodynamic force and to increase the DOF of numerical model. Also on galloping, actual aerodynamic force is not evaluated. Final conclusion must be derived from farther study by wind tunnel test with active controller.

With regard to the active control of static wind force, additional force seems to be too small to obtain enough effect. On super long span bridge, torsional rigidity will become relatively small. So it is still too early to reject the feasibility of this method.

In PWRI, model of active control system will be produced in trial this year and wind tunnel test will be performed with using it. The authors also study other methods that have not been investigated yet.

References

1. J. Roorda, "Tendon Control in Tall Structures",Journal of the Structural Div., ASCE, Vol. 101, ST3, March, 1975
2. J.C.H. Chang and T.T. Soong, "Structural Control Using Active Tuned Mass Dampers", Journal of the Engineering Mechanics Div., ASCE, Vol. 106, EM6, December, 1980
3. T.T. Soong and G.T. Skinner, "Experimental Study of Active Structural Control", Journal of the Engineering Mechanics Div., ASCE, Vol. 107, EM6, December, 1981
4. M.A. Rohman, "Optimal Control of Tall Buildings by Appendages", Journal of the Structural Engineering, ASCE, Vol. 110, May, 1984

5. M.A. Rohman, "Feasibility of Active Control of Tall Buildings Against Wind", Journal of the Structural Engineering, ASCE, Vol. 113, February, 1987
6. J. Rodellar, A.H. Barbat and J.M. Martin-Sanchez, "Predictive Control of Structures" Journal of the Engineering Mechanics Div., ASCE, Vol. 113, EM6, June, 1987
7. T. Kobori, M. Sakamoto, et al, "Application Study on Active Mass Driver (AMD) System (Part1 and 2)", Proceedings of the Eighth Japan Earthquake Engineering Symposium, December, 1990
8. K. Yahagi and K. Yoshida, "An Active Control of Traffic Vibration on the Urban Viaducts", Proceedings of JSCE, No.356/I-3, April, 1985

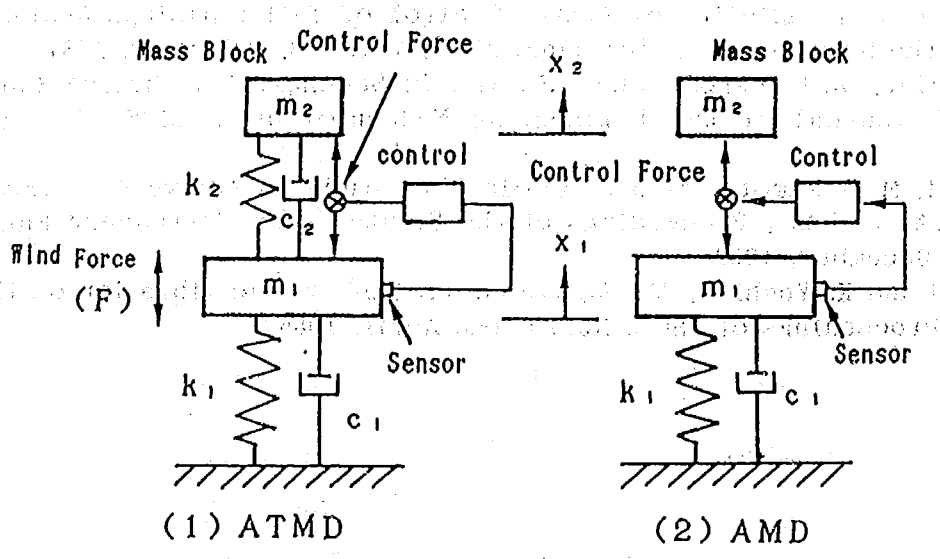

Figure-1. Mechanical Active control

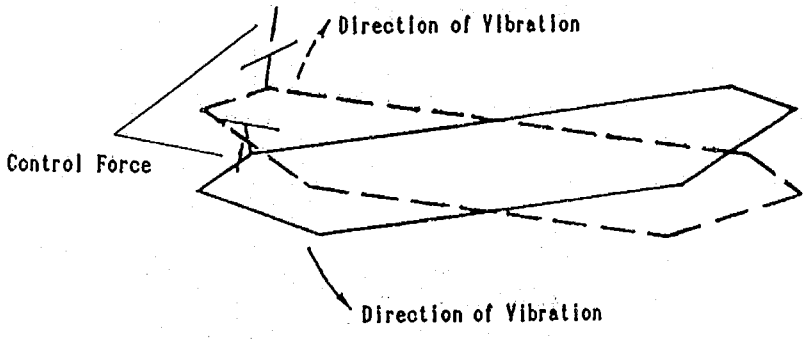

Figure-2. Active Control With Additional Aerodynamic Force

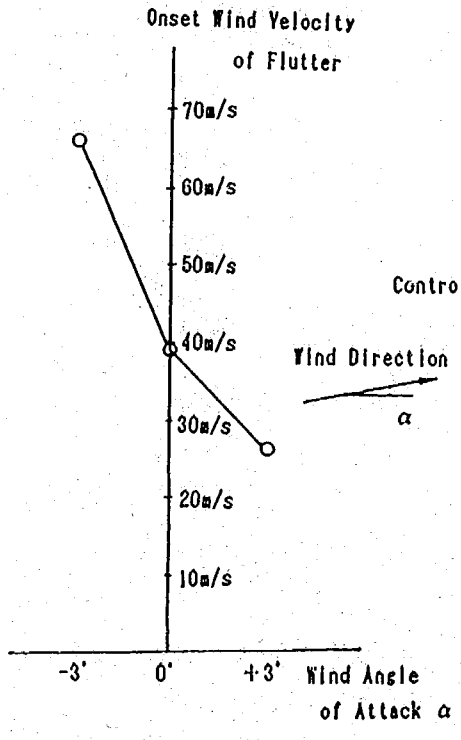

Figure-3. Effects of Wind Angle of Attack on Flutter of Bridge girder

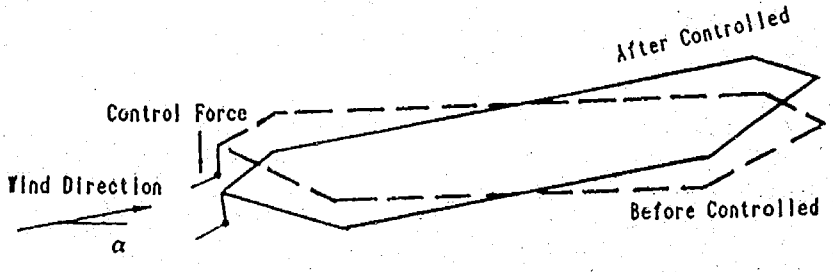

Figure-4. Active Control of Static Wind Force

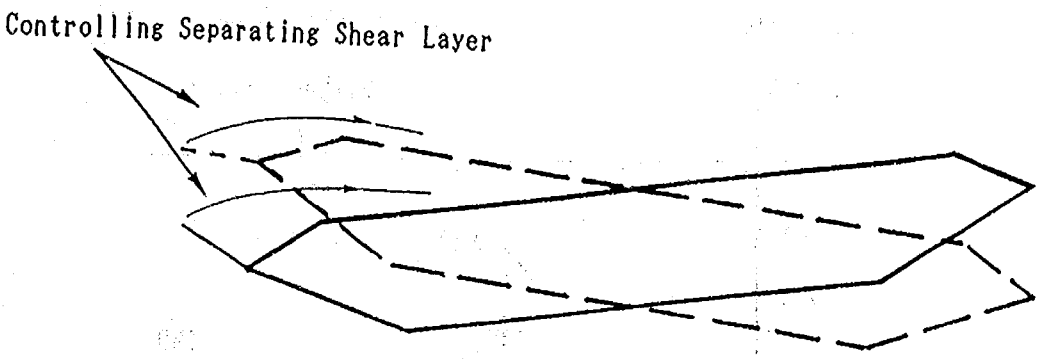

Figure-5. Active Control of Aerodynamic Flow Pattern

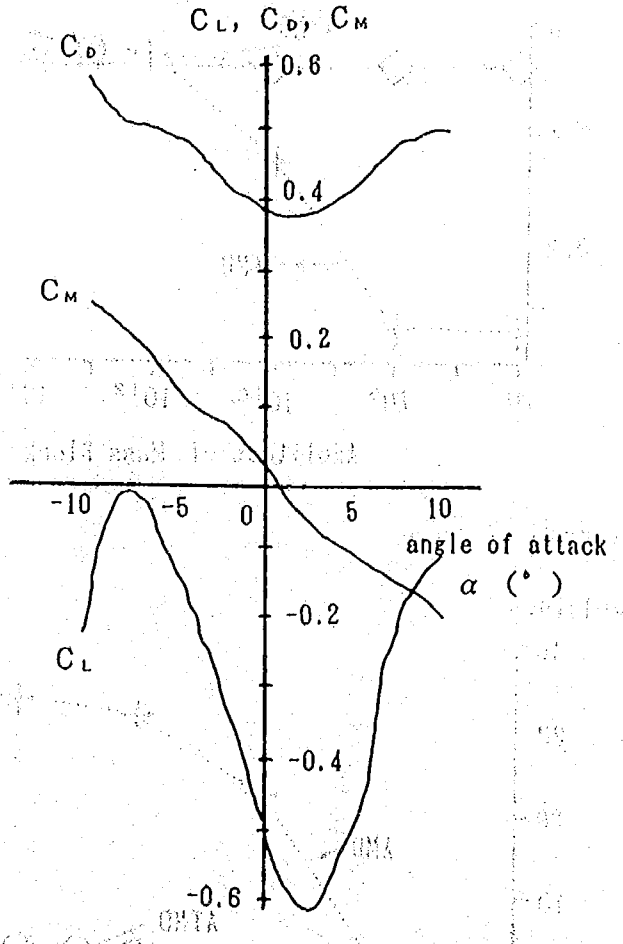

Figure-6. Aerodynamic Coefficients C_L C_D C_M

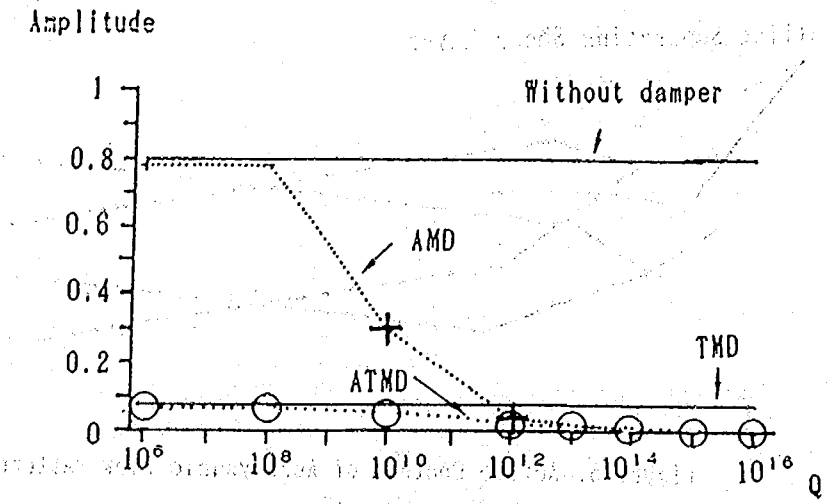

Amplitude of Structure

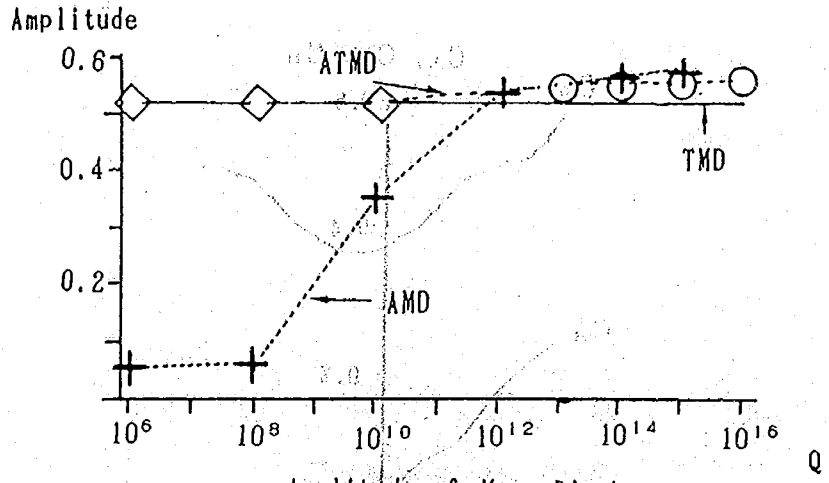

Amplitude of Mass Block

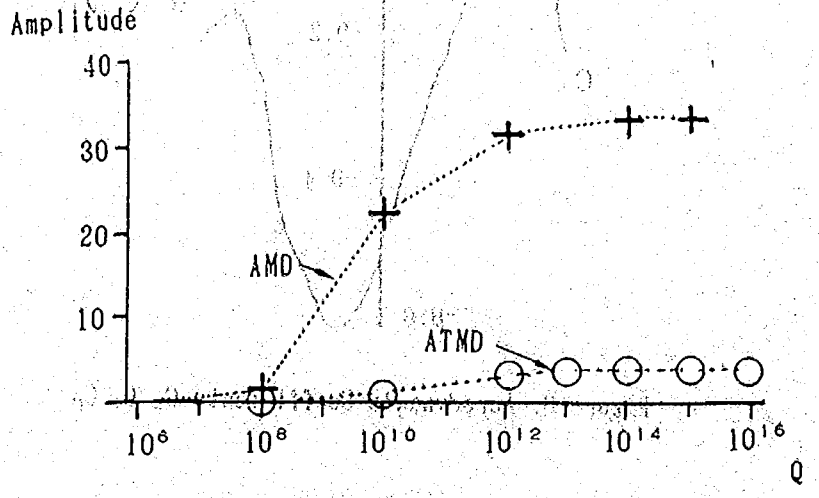

Control Force

Figure-7. Relation between Q and effect of control

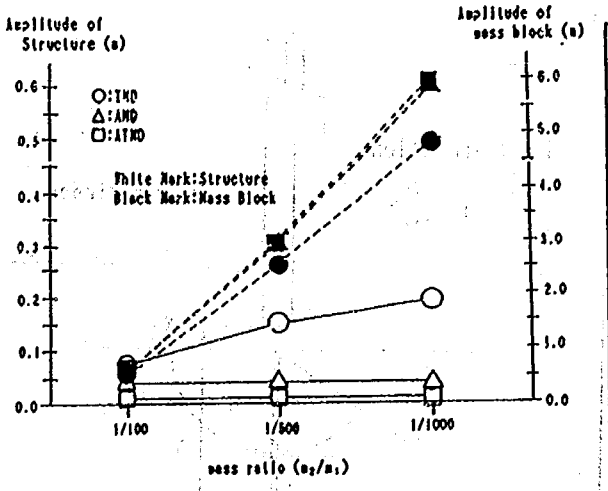

Table-1. Effects on Voetex Induced vibration

Method	Mass Ratio m_2/m_1	Amplitude	
		Structure(m)	Damper (m)
TMD	1/100	0.07	0.57
	1/500	0.15	2.59
	1/1000	0.19	4.89
AMD	1/100	0.04	0.60
	1/500		2.98
	1/1000		5.98
ATMD	1/100	0.01	0.61
	1/500		3.02
	1/1000		6.13

Figure-8. Control Effects on Vortex-Induced Vibration

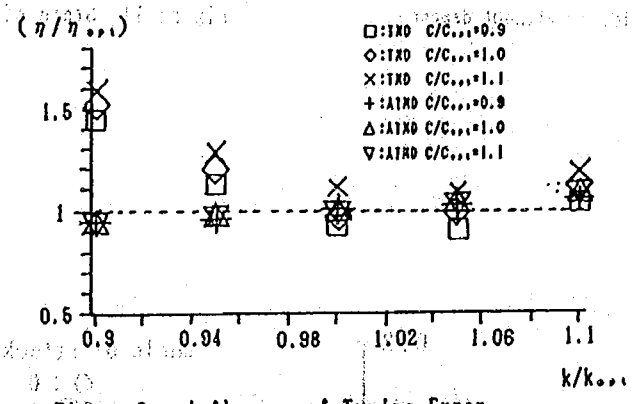

Figure-9. Influence of Tuning Error

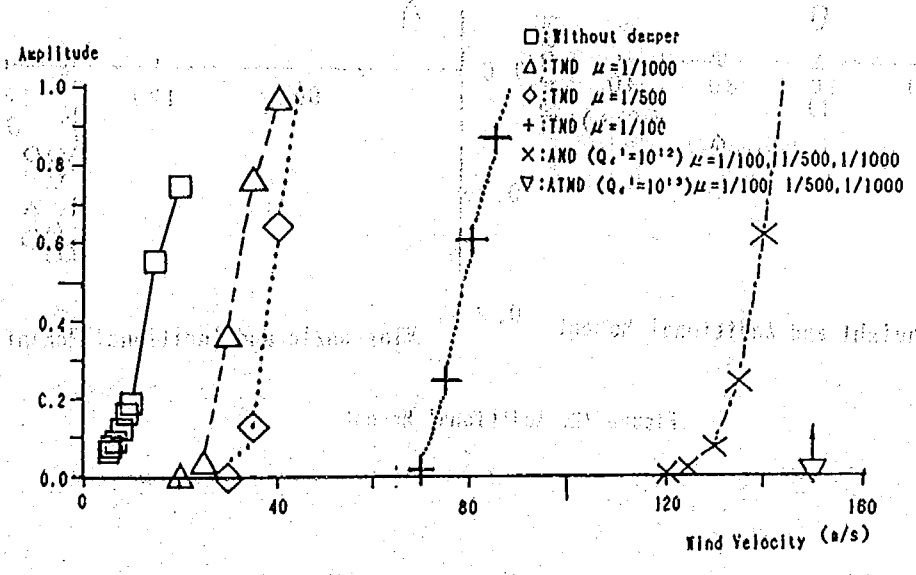

Figure-10. Onset velocity of Galloping

Table-2. Effects on Galloping

Method	Mass Ratio m_2/m_1	V_{cr} (m/s)	V_{cr}/V_{cro}
TMD	1/100	72	8.0
	1/500	35	4.4
	1/1000	26	3.3
AMD	1/100	132	16.5
	1/500		
	1/1000		
ATMD	1/100	発現せず	—
	1/500		
	1/1000		

V_{cr} : Onset Wind velocity of galloping
V_{cro}: Onset Wind velocity without damper

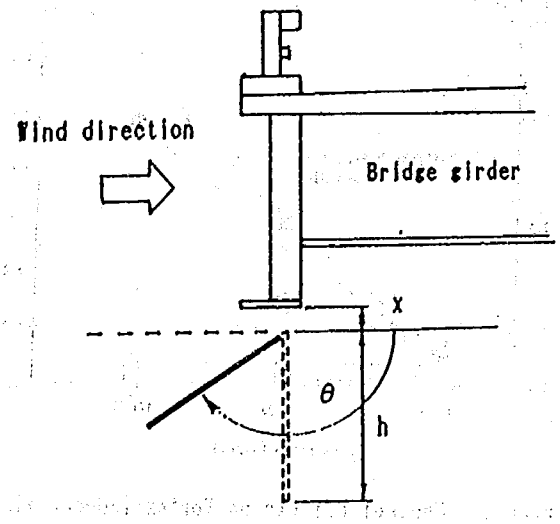

Figure-11. State of Wing

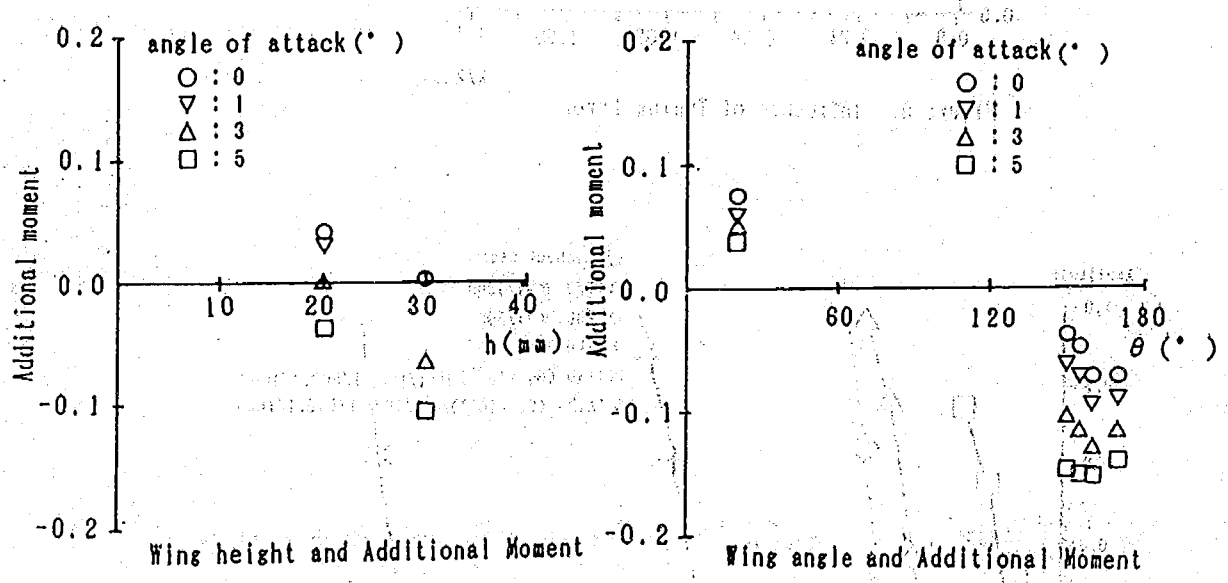

Figure-12. Additional Moment

(7) Session 7

Thursday, May 9, 1991 — Place: Conference Room (8F) PWRI

SESSION 7: DESIGN METHOD(I) — 9:15am～10:35am
(Co-Chairmen: H. Kawano, J. Clark)

(18) M. Okahara, S. Takagi and Y. Kimura* : Non-Linear Horizontal Bearing Characteristics of Column Type Foundation
(9:15am～9:30am)

(19) C. W. Roeder: Accommodation of Movements in Bridge Design
(9:30am～9:45am)

(20) H. Watanabe* and H. Kawano: Estimation of Ultimate Deformation of Column-Footing Joint
(9:45am～10:00am)

(21) T. Hashimoto, A. Makita* and K. Kobayashi: Design, Construction and Model Experiments on Corner Parts of Y-Shape Steel Bridge Piers
(10:00am～10:15am)

DISCUSSION
(10:15am～10:35am)

NON-LINEAR HORIZONTAL BEARING CHARACTERISTICS OF COLUMN TYPE FOUNDATIONS

by

Michio Okahara*, Shoji Takagi** and Yoshitomi Kimura***

ABSTRACT

With the introduction of limit state design method, it is necessary to establish an analytical method of horizontal behavior of column type foundations in areas with a large displacement. Characteristics of ground reaction within horizontal foundation resistance are shown by a bi-linear type perfect elasto-plastic model. The results calculated from this model were compared with those of the horizontal load test, and the establishment of a ground resistance constant of elasto-plastic type was investigated.

1. Introduction

A design method used in bridge foundation in Japan assumes that the ground is an elastic body. As non-linear characteristics of ground resistance cannot be expressed by this method, its application is restricted to areas with a small displacement. So it is difficult to estimate the final strength of foundations, it is impossible to use this model for the limit state design method which is under investigation as a future design system. In this study, the ground resistance is expressed using an elasto-plastic model and the behavior of column type foundations is analyzed in the scope of large displacements. Here, the ground resistance is expressed in a bi-linear type perfect elasto-plastic model disregarding the tensile spring. Using this model, horizontal load test results for each column type foundation (single pile, steel pipe pile foundation, diaphragm wall foundation, and wall pile) were compared, and the establishment of a ground resistance constant for culumn type foundations design was investigated.

2. Resistance Characteristics of the Ground

When putting horizontal resistance of piles into model form for use in design, the following views exist according to the evaluation method of ground resistance (ground reaction).

① Ultimate ground reaction method

This method is to estimate horizontal ultimate resistance using an assumptoin on the distribution form of ground reaction under ultimate ground conditions, and the condition of equilibrium between outside forces affecting the pile. However, as the ground reaction has no connection with pile displacement, the pile displacement can not be determined.

---

*:Head, Foundation Engineering Division, Structure and Bridge Department, Public Works Research Institute, Ministry of Construction
**:Head, Investigation Division, Kagoshima National Highway Work Office, M.O.C., (Former Senior Research Engineer, ditto)
***:Research Engineer, ditto

② Elastic ground reaction method

Presuming that the ground is an elastic body, this method supposes that ground reaction occurs in response to horizontal displacement of the pile. Although the ultimate bearing capacity determined by the ground cannot be expected, pile displacement can be thus we can gain bearing capacity with respect to an allowable displacement.

The method is divided into the linear elastic ground reaction method and non-linear elastic ground reaction method according to the relationship of ground reaction with pile displacement.

③ Combined ground reaction method

When the pile is horizontally transformed, the ground begins to yield from the surface with large deformation and a plastic area gradually expands downward. This is a method where the ultimate ground reaction method shown in ① is applied to the plastic area, and the elastic ground reaction method shown in ② is applied to the ground underneath that is assumed to be in an elastic area.

The evaluation method for horizontal resistance of a pile is divided into the two methods above. When a large deformation occurs in the ground such as with an ocean structure, the combined ground reaction method has been used[1]. On the other hand, as with bridge foundation, where the horizontal displacement is generally supressed within a small limit with plastic behavior[2], the elastic ground reaction method has been used[3]. The introduction of the limit state design method for foundation design has been under consideration for these last few years, and there is now a need to express behavior at times of large transformations in bridge foundation. Due to this, it is necessary to examine the introduction of the combined ground reaction method as the ground resistance instead of the usual elastic ground reaction method.

3. Comparison with Load Test

As a model estimating behavior of the column type foundations under a large deformation, the ground resistance is considered as a bi-linear-type perfect elasto-plastic model shown in Fig.1 and the calculated result is compared with the load test. The compared load test is listed in Tab.1. When comparing with the load test, attention is paid to horizontal deformation at the foundation head. Fig.2 shows an outline of it. Comparison is conducted in such a manner that the accont of deformation in the foundation is calculated by multiplying coeffieicnt of ground reaction kH and ultimate ground reaction pr by αk and αp, respectively, and coefficients αk and αp are determined to coincide with the result of the load test. As shown in Fig.2, coefficient αk influences the initial gradient of the load-displacement curve and coefficient αp influences the ultimate value of horizontal load. These points should be considered when establishing each coefficient.

The coefficient of ground reaction kH is based on Specifications for Highway Bridges[4] and calculated from the following formula.

$$kH = kHo \left(\frac{BH}{30}\right)^{-3/4}$$

Here, kH : coefficient of ground reaction in horizontal direction(kgf/cm³)
kHo: coefficient of ground reaction in horizontal direction equivalent to the value of plate loading test by means of 30cm diameter rigid disk(kgf/cm³), when estimated from coeffieient of ground deformation, it is according to the following formula.

$$kHo = 1/30\ Eo$$

BH : equivalent loading width of foundation (cm)
Eo : modulus of deformation ground (kgf/cm²)

The ultimate ground reaction of foundation front pr is based on Coulomb's passive earth pressure coefficient.

(1) Single pile foundation

Figs.3 and 4 show the results of comparison between an actual value and a calculated value on the load-displacement curve of a cast in-situ pile of a large diameter (seven examples) and steel pipe pile (three examples). There are two parameters, αk and αp, in the bilinear type ground reaction, as mentioned above, and the combinations of these are innumerable in the present study. The coefficient of ground reaction is first determined by each load test and the ultimate ground reaction is selected against it.

Judging from the total load test, corrective coefficients αk of the coefficient of ground reaction are determined as 3 and 2 in cases of cast in-situ pile and steel pipe pile, respectively. The reason why the values of them are larger than that determined in Specifications for Highway Bridges is as follows. Although the coefficient of ground reaction in Specifications for Highway Bridges determines the deformation against 1 % of the foundation width, in this study αk is determined to coincide with the load test with very little influence from non-linear characteristics, that is within a deformation of about 0.5% of the pile diameter. The value for cast in-situ pile is larger than that of steel pipe pile. It may be because adhesion between the ground and the pile is larger in the case of the cast in-situ pile.

In Figs.3 and 4, the curve is well estimated throughout the range from small to large deformation. Comparing with other test results in the same way, values of the corrective coefficient αp of ultimate ground reaction are widely scattered in each test. When αk is determined as 3 in the cast in-situ pile, values of αp are between 0.7 and 1.4. When αk is determined as 2 in the steel pipe pile, values of αp scatter between 1.0 and 2.5.

(2) Steel pipe pile foundation

Two examples of the load test results for steel pipe pile foundation were compared with the calculated result. The steel pipe pile foundation is a foundation in which steel pipe piles are settled in a form of a closed chain and the top parts of them are joined with upper slab(Fig.5). The design calculation is necessary to determine a constant for joints other than the ground resistance. The joint part is determined as a bi-linear elasto-plastic model in a same way as with the ground, and it is represented by shear rigidity Gj (tf/m²) and yield strength to shear

qu (tf/m) of joint.

Figs. 5 and 6 show examples comparing SW2. Here, constant on the joint part is determined as the following.

$$Gj = 60,000 tf/m^2$$
$$qu = 10 tf/m$$

Fig.6 shows a comparison of stress and displacement of the sheet pile in the case of 700 tf horizontal load. Although the actual value of pile stress is lower than the calculated value of it beneath the upper slab, they correspond well. Corrective coefficients of ground resistance $\alpha k=2.0$ and $\alpha p=0.7$ correspond well in the present study. They are $\alpha k=4.0$ and $\alpha p=0.6$ in SW1. The value of the coefficient of ground reaction is larger than those values, but the value of the ultimate ground reaction is lower than them, $\alpha p<1$. It is regarded that rigidity of steel pipe pile foundation itself lessens because of the influence of the joint part, and the actual ultimate ground reaction becomes lower than the value of Coulomb's earth-pressure applied to a rigid wall.

(3) Diaphragm wall foundation

An analytical model of a diaphragm wall foundation separately evaluates the front ground resistance and the side ground resistance of the foundation (Fig.8) [6]. Ratio αF of the coefficient of shearing ground reaction in horizontal direction at the side of foundation kF to coefficient of ground reaction in horizontal direction at the front of foundation kH is determined as shown in Fig.10 from two-dimensional FEM analysis and load test data. Figs.11 and 12 show a comparison between load test values and calculated values of the diaphragm wall foundation. As it is difficult to respectively determine αk and αp for both the front and the side of foundation, although the ground resistance is separately considered to each of them as shown above, the same value is used for the front ground andthe side ground. It is recognized that actual values and calculatedvalues coincide well in both figures. Here, $\alpha k=8.0$ and $\alpha p=1.0$. These values are almost the same as those of (1) cast in-situ pile.

4. Establishment of Ground Resistance Constant

The ground resistance is represented by the bi-linear type elasto-plastic model and the calculated values and the load test are compared in section 3. The coefficient of ground reaction and the ultimate ground reaction are estimated from them in the load test for each column type foundation and they are presented as αk and αp, respectively. The result are summarized in Fig.12. Here, although they can not be simply compared, as supporting mechanism and load width are different in each foundation form, every value is at almost the same level.

The corrective coefficient of coefficient of ground reaction αk is 2 to 3 in each test. It is because the value used as the basis of the coefficient of ground reaction in Specifications for Highway Bridges is determined at a standard displacement, 1% of foundation width. It is necessary to make the value larger in the present bi-linear type elasto-plastic model. On the other hand, the corrective coefficient of ultimate

ground reaction αp scatters from about 0.5 to 1.5. The values in cases of steel pipe pile and large diameter cast in-situ pile are small and below 1, the value in cast in-situ pile of 1 m in diameter is about 1, and the value in steel pipe pile is 1 to 2.5. As a lessening in rigidity of the foundation body owing to bending deformation is not considered in the present comparative calculation, when it greatly influenced test objects, αp may be rated low.

5. Conclusion

The ground resistance is represented by the elasto-plastic model and compared with the load test to establish the analytical method of column type foundation under large deformation. The ground resistance is determined to be a bi-linear type in the present study and represented by the coefficient of ground reaction and the ultimate ground reaction. Constants which are well represented in the load test result of each column type foundation are estimated by changing these design constants. As a result, the following facts are confirmed.

(1) By using an elasto-plastic model to represent horizontal ground resitance, behavior can be estimated fairly exactly even to large scale displacement.

(2) Corrective coefficients of the ground resistance constant for each column type foundation are despersed within a comparatively small range, so we expect that it is possible to establish a contant in a general manner.

We would like to express our gratitude to those who provided the load test results which proved to be invaluable in this study.

REFERENCES

1) America Petroleum Inatitute : API Recommended Practice for Planning, Designing and Constructing Fixed Offshore Platforms, API RP 2A 7th. ed., 1976.

2) Michio Okahara, Shoji Takagi, Shoichi Nakatani et al. : Survey on Horizontal Resistance Characteristics of Piles according to Load Test Data, Public Research Institute Data No.2721, 1989.

3) Japan Road Association : Specifications for Highway Bridges, Part VI Specifications for Substructures, 1980.

4) Japan Road Association : Specifications for Highway Bridges, Part VI Specifications for Substructures, 1990.

5) Michio Okahara, Shoji Takagi, Kazuhiko Chahayashi : Supporting Structure of Cast-in-site Diaphragm Wall, Collected Papers of Structure Engineering, vo.35A, 1989.

Table 1. List of subject foundations of calculation

1. Large diameter reverse pile	
R1	φ3.0m x 69m [Honshu-Shikoku Bridge Authority-Bannoshu elevated bridge foundation pile T1]
R2	φ2.0m x 39m [Honshu-Shikoku Bridge Authority-Bannoshu elevated bridge foundation pile T2]
R3	φ2.0m x 69m [Honshu-Shikoku Bridge Authority-Bannoshu elevated bridge foundation pile T3]
R4	φ3.0m x 45m [Japan Highway Public Corporation-Shinzen-Nishi elevated bridge foundation pile]
2. Benoto pile	
C1	φ1.0m x 19m [Japan Highway Public Corporation-Shino work-elevated bridge foundation pile]
C2	φ1.0m x 7m [Japan Highway Public Corporation-Ibaraki-Nishi work-elevated bridge foundation pile]
C3	φ1.0m x 11m [Japan Highway Public Corporation-Toyonaka-Higashi work-elevated bridge foundation pile]
3. Steel pipe pile	
S1	φ813mm (t=14) x 30m [Japan Highway Public Corporation-Sakata Line]
S2	φ1016mm x 24m [Kurashiki City-composite steel pipe pile]
S3	φ813mm x 22m [Iwakuni City-composite steel pipe pile]
4. Diaphragm wall foundation	
D1	3.6m x 4.5m x 13m, wall thickness 0.8m [Metropolitan Expressway Public Corporation-D31 Construction area elevated bridge foundation]
D2	0.6m x 4.0m x 19m [Ministry of Construction-Pilot Project of Technical Application-wall pile]
D3	0.6m x 6.2m x 19m [Ministry of Construction-Pilot Project of Technical Application-wall pile]
5. Steel pipe pile foundation	
ST1	φ8.81m x 51m, steel pipe pile φ 1200 [Metropolitan Expressway Public Corporation-Construction Area BT251 elevated bridge foundation]
ST2	φ9.358m x 17m, steel pipe pile φ 800 [Japanese National Railways-Ono B113P pier foundation]

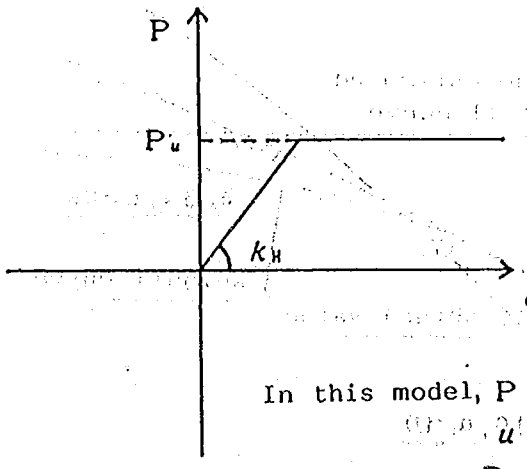

In this model, P : ground reaction
u : displacement
P_u : ultimate ground reaction
k_H : coefficient of ground reaction in horizontal direction

Fig.1. Elasto-plastic model of ground

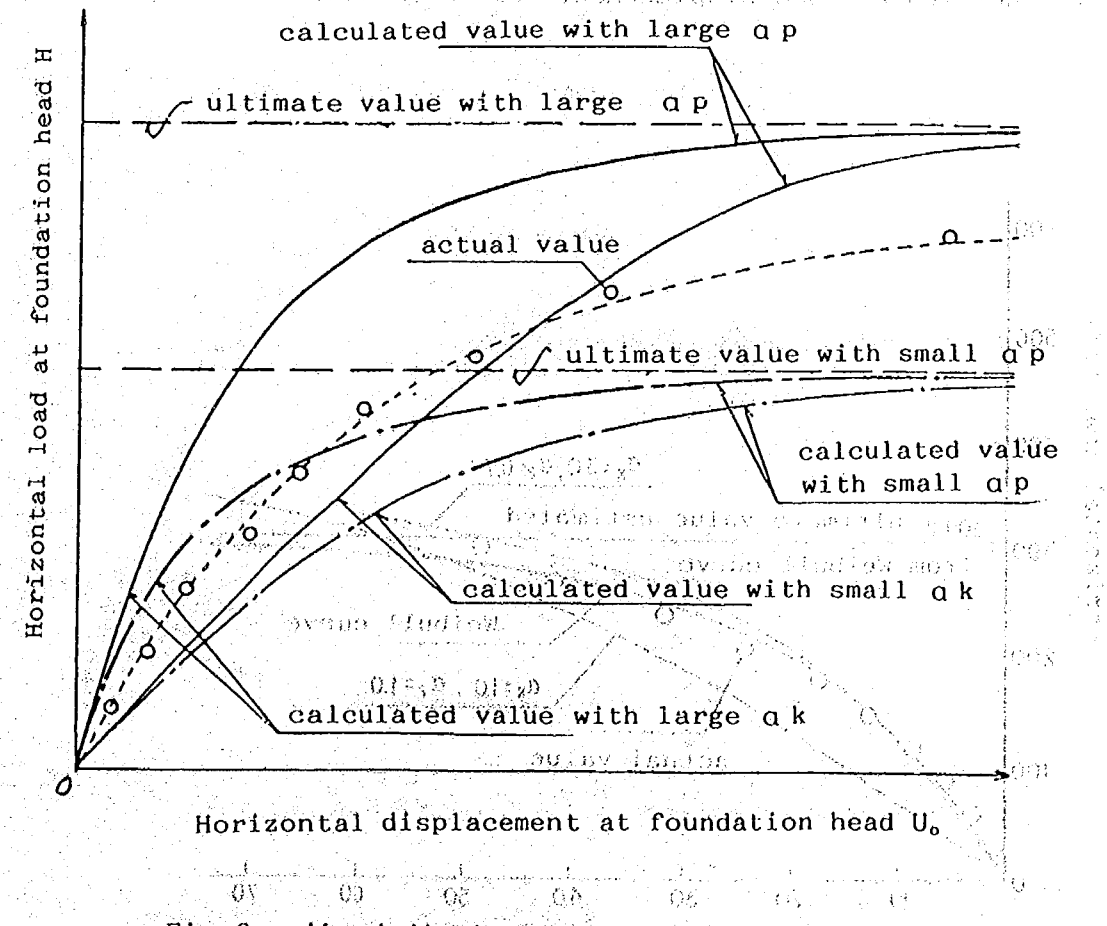

Fig.2. 'Load-displacement' curve

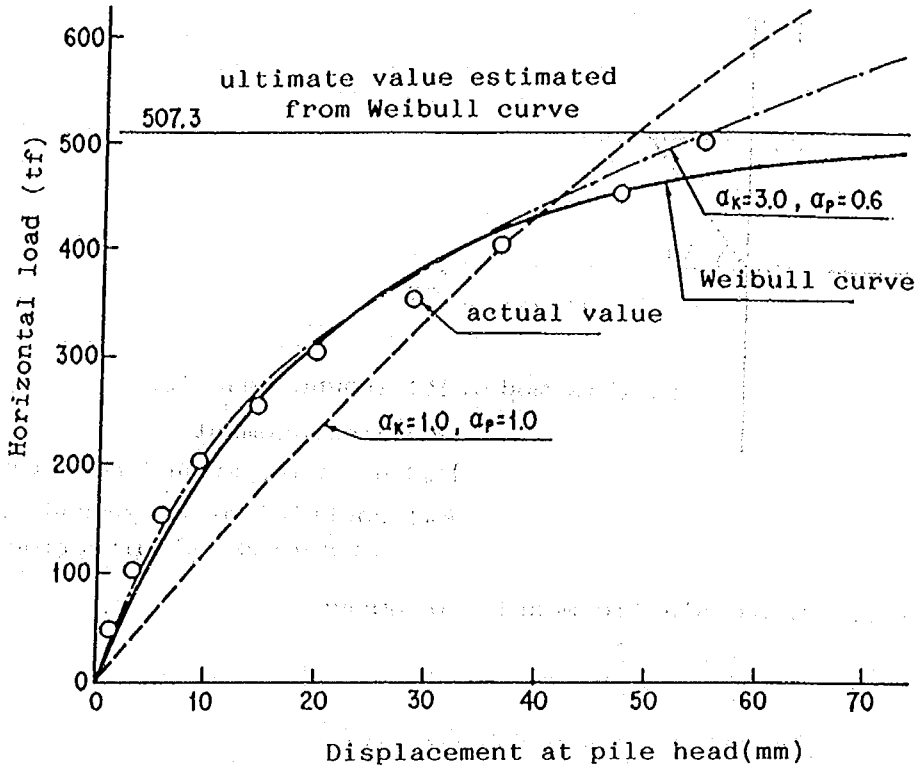

Fig.3. 'Horizontal load-displacement' curve of examination pile R1

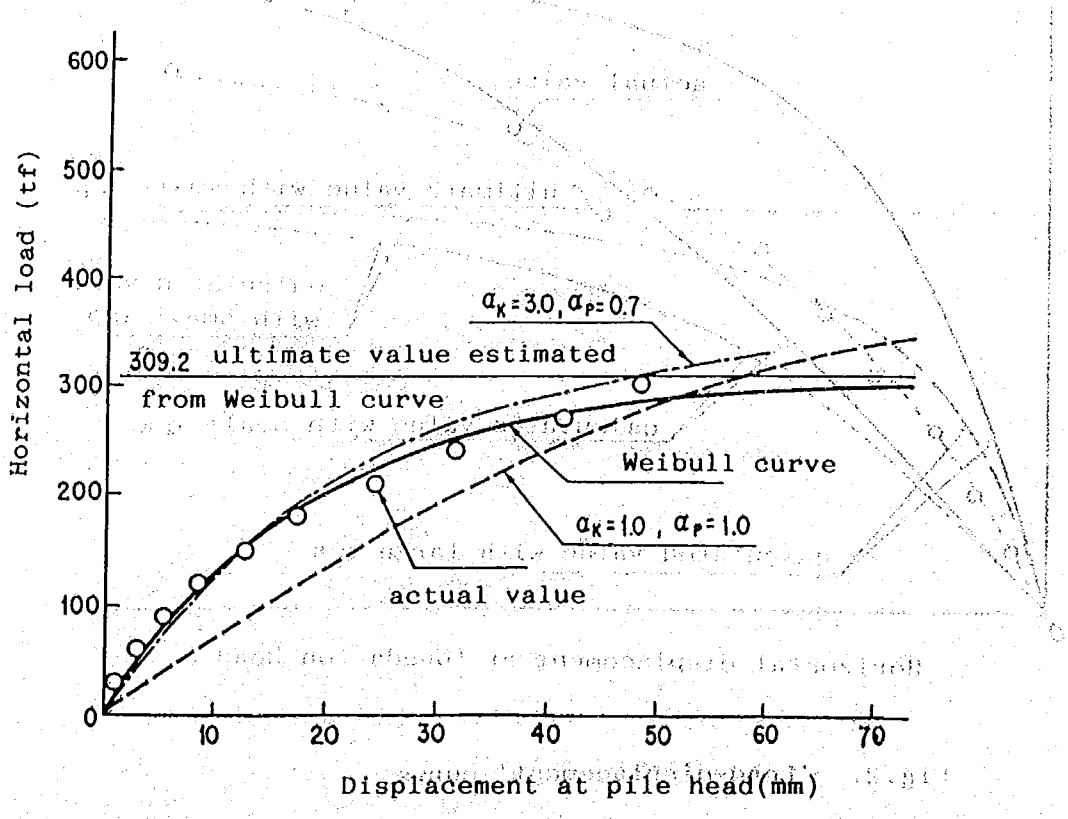

Fig.4. 'Horizontal load-displacement' curve of exmination pile R2

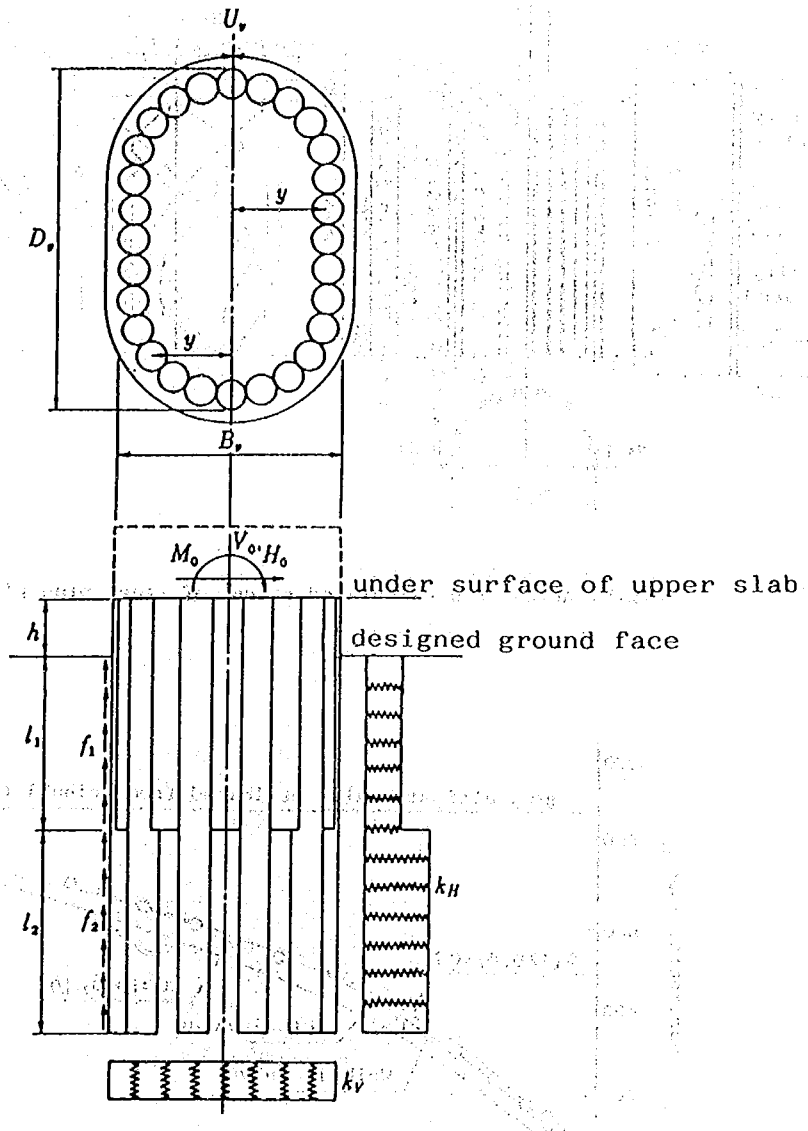

Fig.5. Design model of steel pipe pile foundation

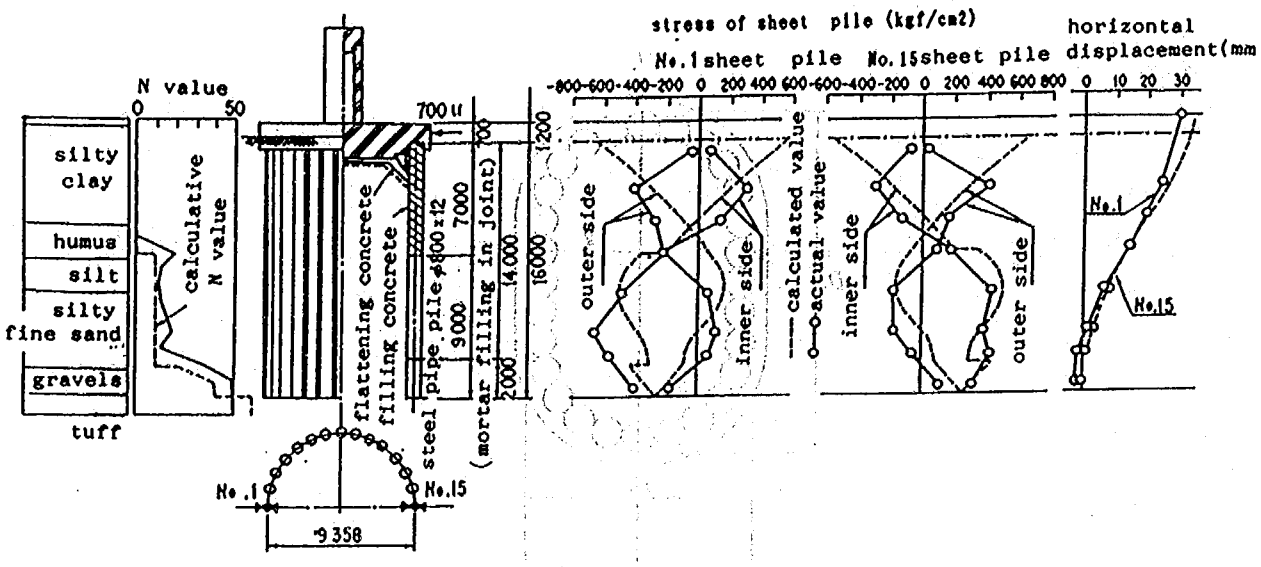

Fig.6. Actual and calculated values of steel pipe pile foundation SW2

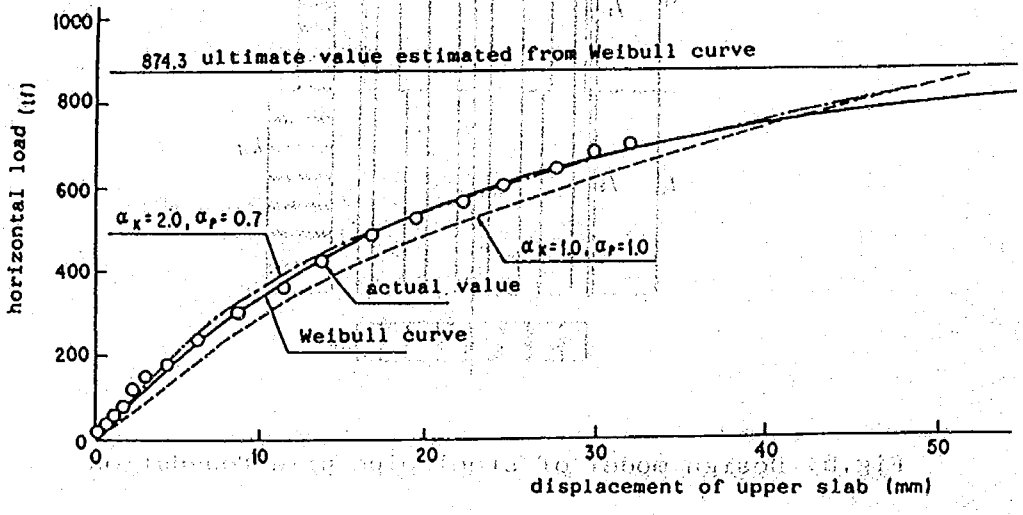

Fig.7 'Load-displacement' curve of steel pipe pile foundation SW2

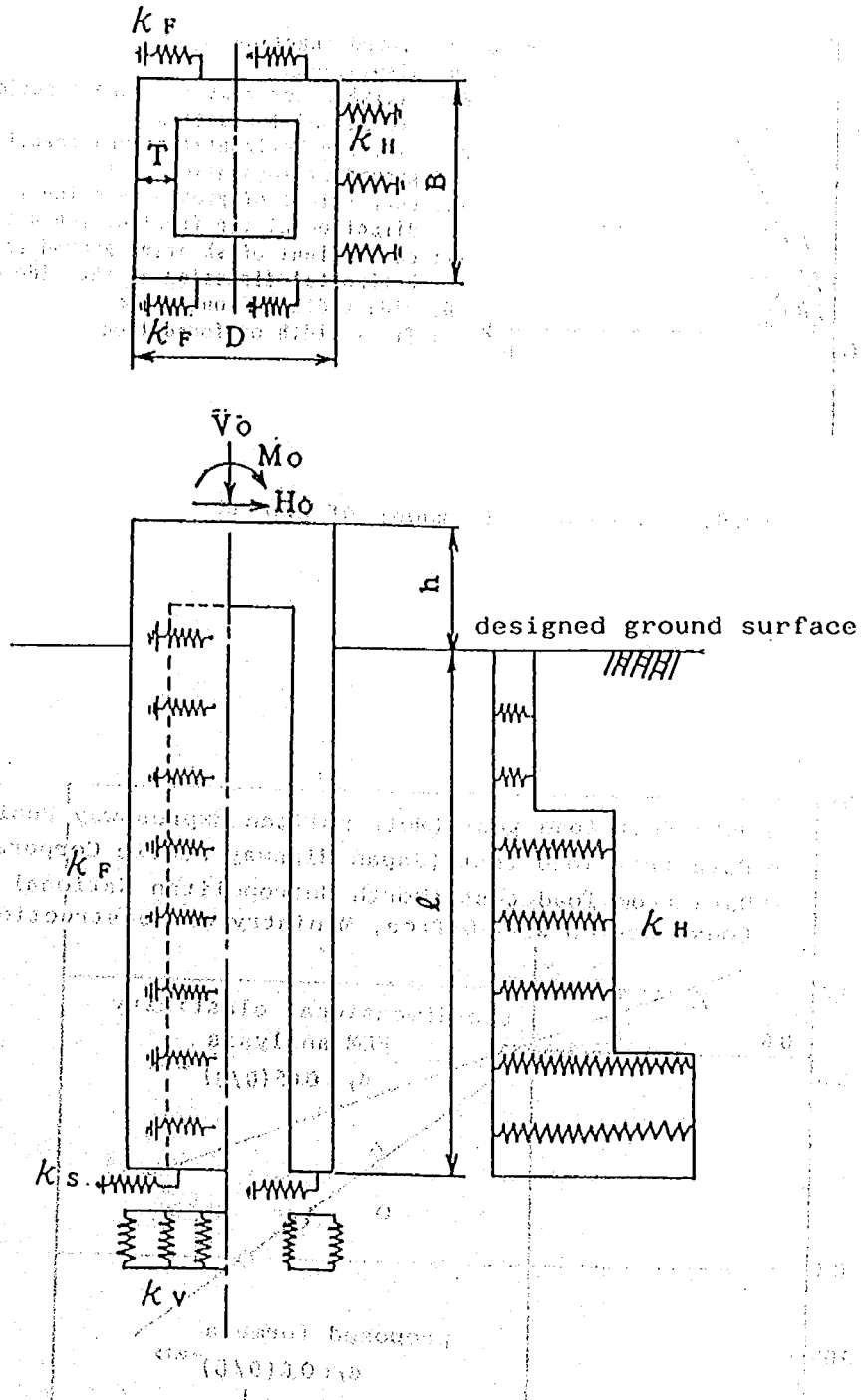

Fig.8 Design model of diaphragm wall method

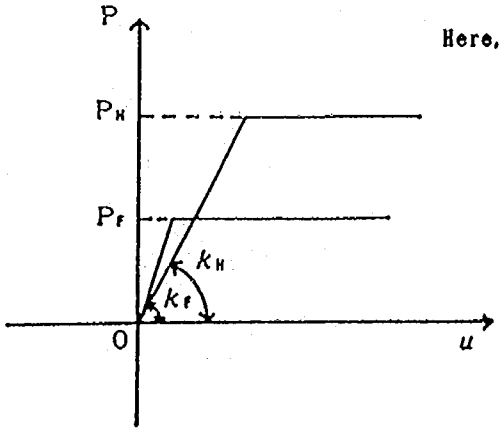

Here, P: ground reaction
u: displacement
P_H: ultimate horizontal ground reaction at front ground of foundation
P_F: ultimate horizontal ground reaction at side ground of foundation
k_H: coefficient of ground reaction in horizontal direction at the front of foundation
k_F: coefficient of shearing ground reaction in horizontal direction at the side of foundation
D: side width of foundation
B: front width of foundation

Fig.9. Elasto-plastic model of ground

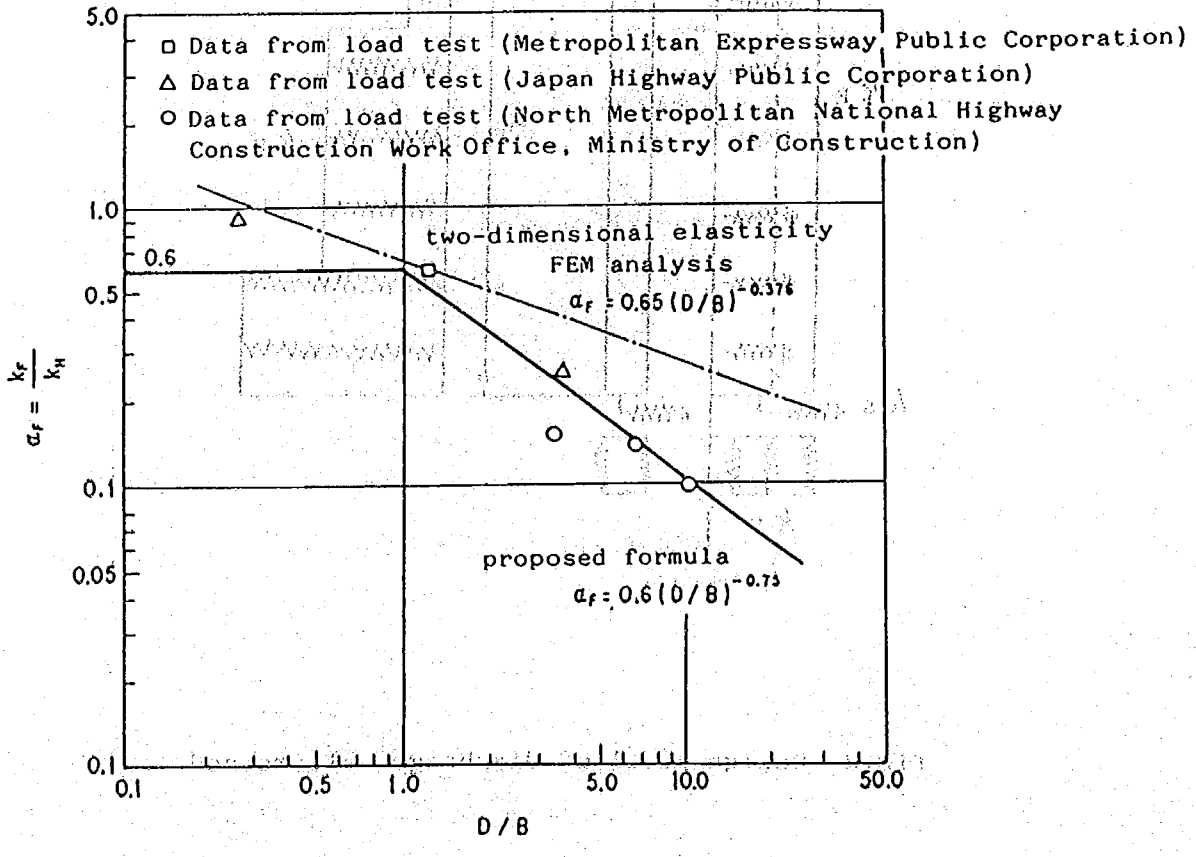

Fig.10. Relation between α_F and D/B

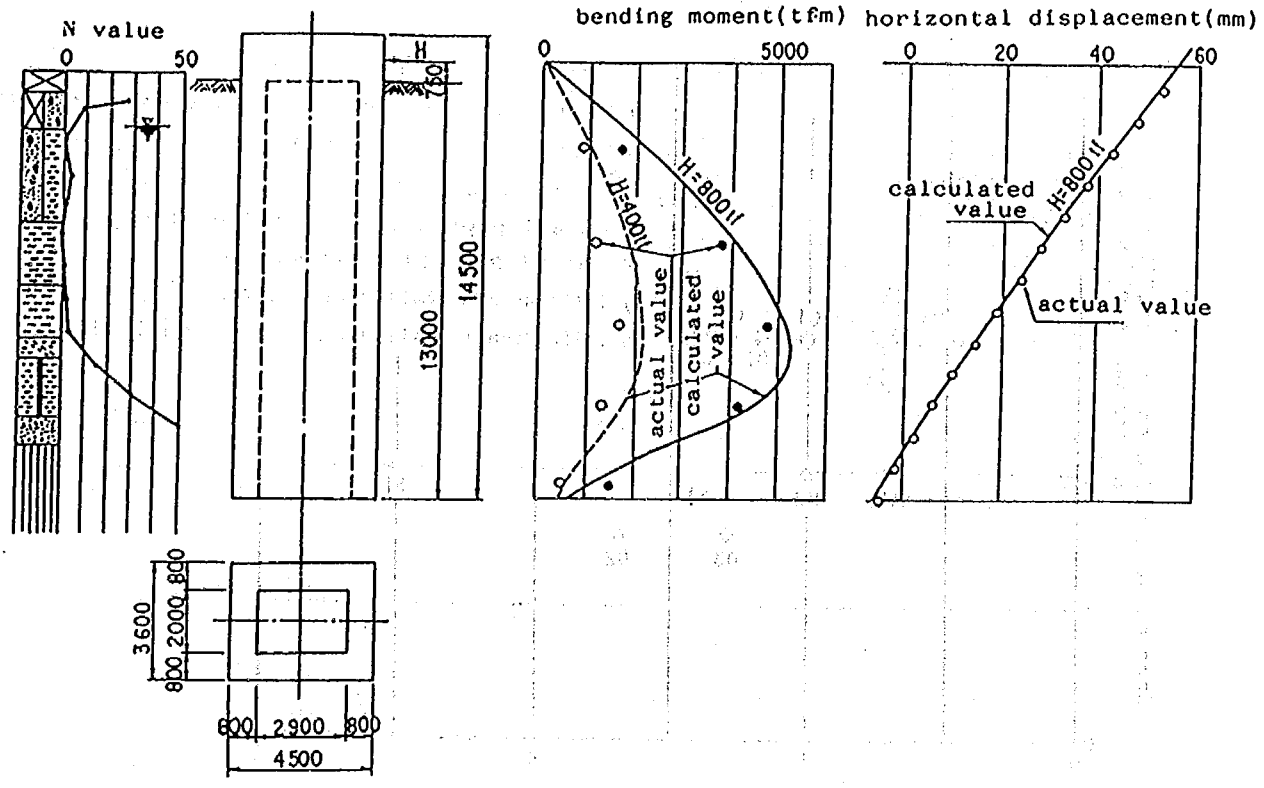

Fig.11. Actual and calculated values of diaphragm wall foundation D1

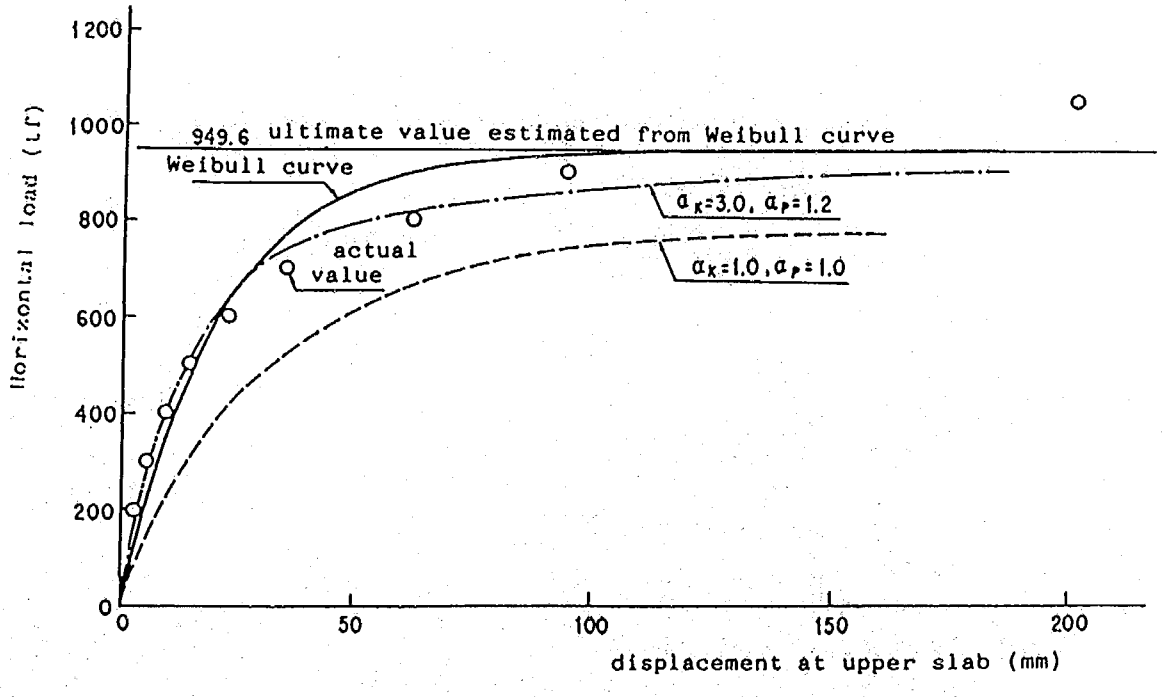

Fig.12. 'Horizontal load-displacement' curve of diaphragm wall foundation D1

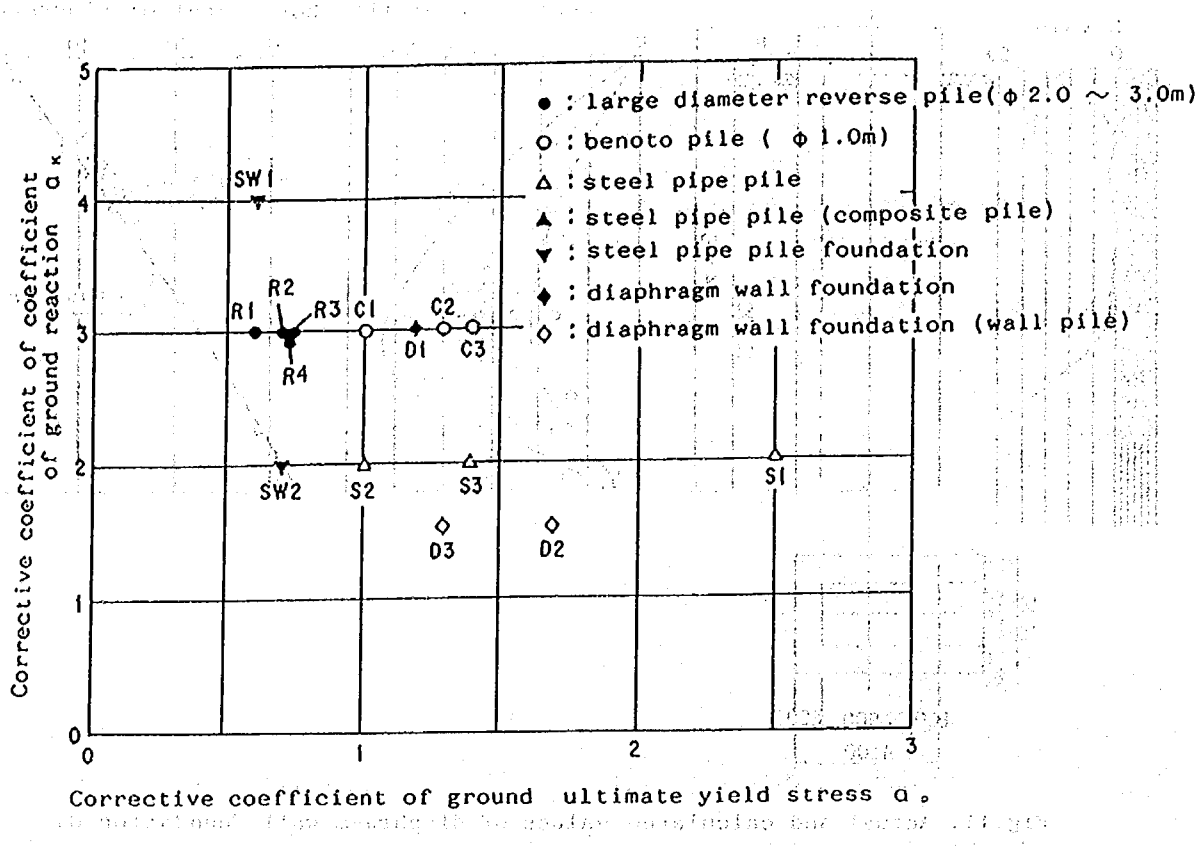

Fig.13. Corrective coefficients of coefficient of ground reaction and ultimate ground reaction

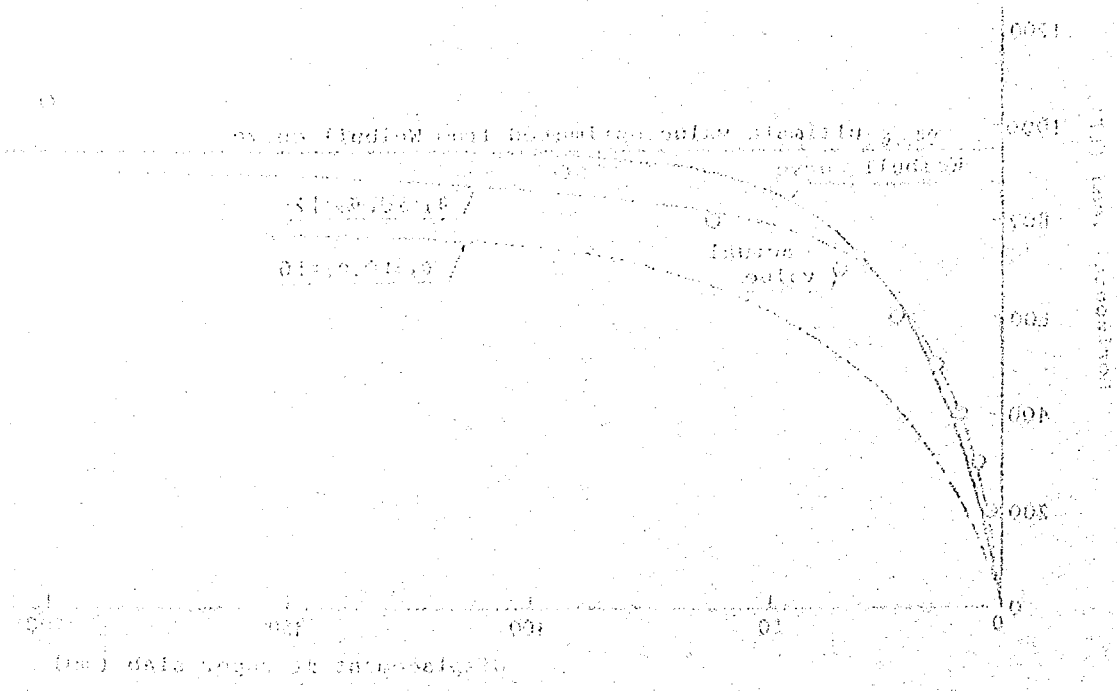

ACCOMMODATION OF MOVEMENTS IN BRIDGE DESIGN

Charles W. Roeder
Department of Civil Engineering
University of Washington
Seattle, WA 98195

INTRODUCTION

Bridges move and deform under service conditions. These movements must be accommodated in the bridge design or large forces will occur. These forces may cause damage, reduce the service life, and increase the maintenance costs of the bridge. The movements are accommodated by bridge bearings and expansion joints in most bridges, or some recent bridges are designed to have integral supports or continuous construction which minimizes the use of joints and bearings. In both cases, it is important to have a good estimate of both the magnitude and direction of the movements, since these movements affect the design of the bearings, expansion joints, piers and abutments.

Research has been performed in the United States to better understand temperature dependent bridge movements and to obtain better performance of bridge bearings in permitting these movements. These research projects are separate projects sponsored by the National Science Foundation (NSF) and the National Cooperative Highway Research (NCHRP) Program. The two projects are related and both will be summarized in this paper. The NSF grant on thermal movements will be discussed first. The standard design practice for thermal movements in the United States will be described. Theoretical calculations of temperatures which must be expected in bridges will be discussed. These temperatures will be used to examine thermal movements. It will be shown that the movements may be more complicated than suggested by the simple design models for some bridges. Specific discrepancies between the predicted behavior and the design models will be noted, and some of these discrepancies will be correlated to observed damage. A pilot study of field measurements will be briefly noted, and the future directions of the research will be discussed.

The NCHRP study on bridge bearings will then be described. The wide range of bridge bearings will be summarized, and the problems and inconsistencies commonly encountered will be discussed. An ongoing analytical and experimental research program will be described and related to the observed problems and resulting design recommendations.

THERMAL MOVEMENTS

Design Method

Thermal movements are a major aspect of bridge design. The American Association of State Highway and Transportation Officials (AASHTO) Specification[1] provides a simple method for estimating these movements. The United States is divided into two zones; a cold and a moderate climate. Larger temperature ranges are provided for the colder climate than for the moderate zone. Steel bridges are assigned a larger temperature range than are concrete bridges, because of the larger thermal mass and slower heat transfer expected in concrete bridges. The temperature range for steel bridges varies between 0°F and 120°F (-18°C and 48°C) for mild climates and -30°F

and 120°F (-34°C and 48°C) for cold climates. Concrete bridges have 70°F and 80°F (39 and 44 degrees on Celsius scale) temperature ranges for mild and cold climates, respectively. These temperatures are then applied uniformly to the bridge and expansion and contraction movements are calculated by -

$$\Delta = \alpha \, L \, \Delta T \qquad (1)$$

where Δ is the expected movement, α is the coefficient of thermal expansion, L is the expansion length, and ΔT is the difference between the extreme temperature of the bridge and the installation temperature of the bridge girders. This movement is the extreme annual movement, and it is used to establish the design requirements for the bridge bearings, expansion joints, piers and abutments. The design method has been used for many years, and most bridge engineers are generally satisfied with the method. However, there is some evidence that this satisfaction is not always justified.

Bridge Temperatures

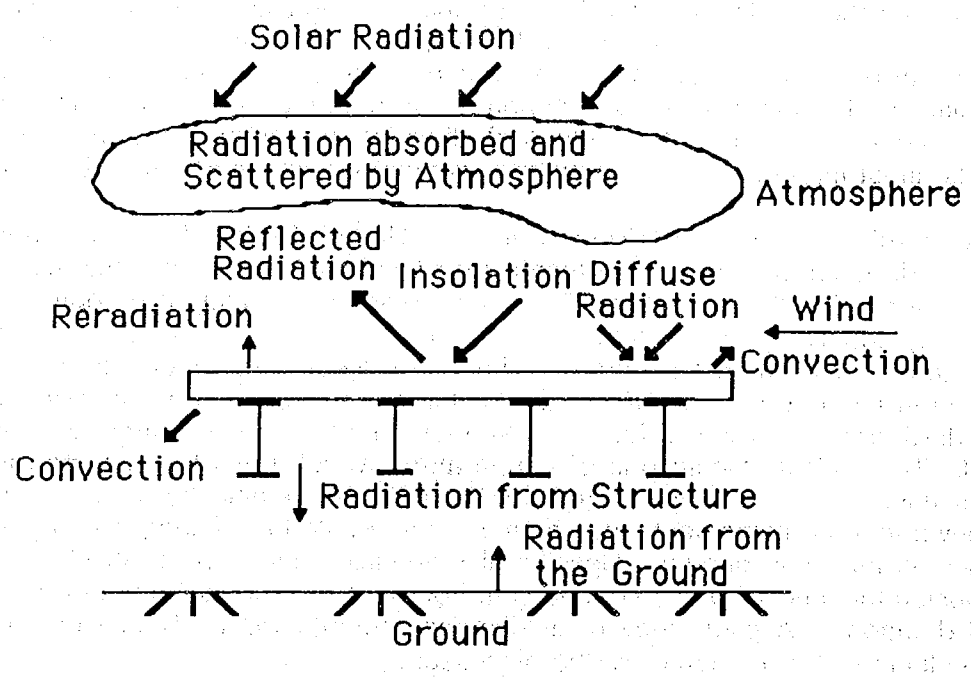

Fig. 1. Variables Affecting the Temperature in Bridges

Methods for predicting[2,3,4] temperatures have advanced in recent years. The bridge temperatures depend upon the conduction heat flow within the bridge, radiation between the sun and the bridge and the bridge and the local environment, and the convection transfer caused by air movement as depicted in Fig. 1. The temperature is very dependent upon the type of bridge and the local environment. Direct exposure of the girders to morning or afternoon sun, local shading, and numerous other factors may influence the temperature and temperature distribution. Bridge temperatures were calculated [4,5] for 10 different locations in the US and different bridge types. The calculations were started several days before the period of interest to eliminate uncertainty in the initial conditions. More complex models are required for computing the temperature distribution in some bridges than in others. The average temperature integrated over the bridge cross section is comparable to the AASHTO design temperature and is an indicator of potential for overall bridge movement. The extreme average temperatures for winter and summer were computed, and the range in the average

temperatures are plotted as a function of the range in air temperature for each location in Fig. 2. The AASHTO temperature ranges are also noted on this figure.

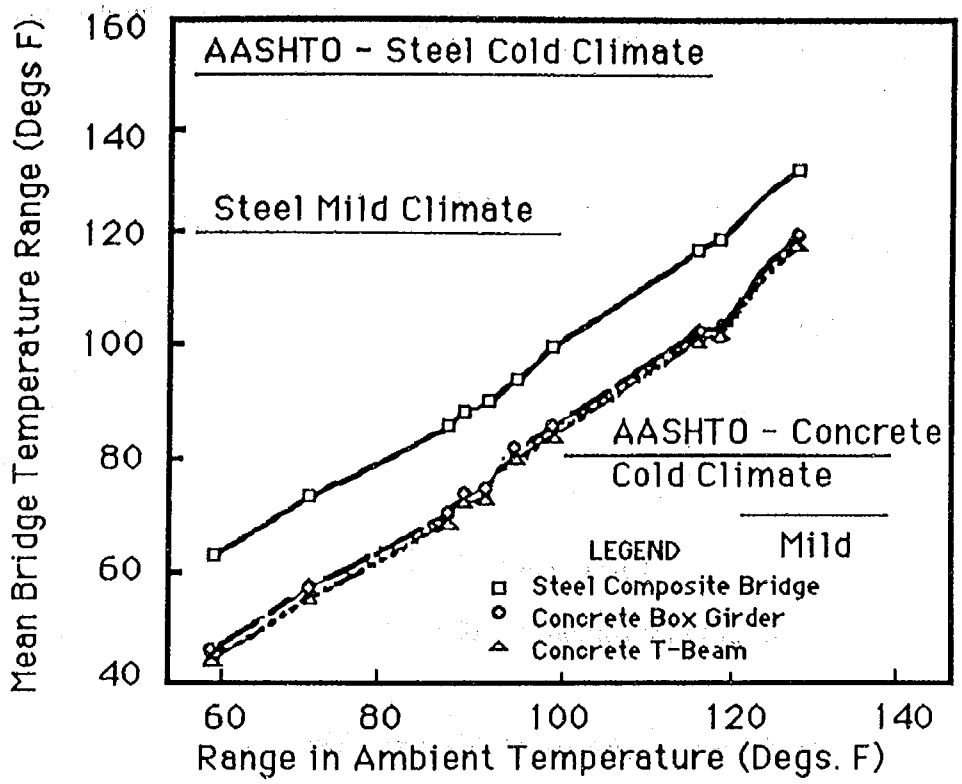

Fig. 2. Computed Temperature Ranges as a Function of the Range in Air Temperature

The temperature distribution in concrete box girder bridges is different from that predicted for concrete girder bridges, but the average temperatures for these concrete bridges are similar. The temperature range predicted for steel bridges is larger than that expected for concrete bridges. The predicted temperature range for concrete bridges is considerably larger than that defined by AASHTO for many parts of the country. This suggests that AASHTO provides inadequate thermal movement capacity for concrete bridges. However, it must be recalled that concrete bridges usually are also designed for movements due to creep and shrinkage. The figure suggests that the AASHTO provisions for steel bridges are larger than the predicted temperature ranges for most parts of the country. Thus, AASHTO may be requiring more bearings and expansion joints for steel bridges than are really necessary in some cases. This may lead to excessive cost in construction and maintenance.

Bridge Movements

Predicted bridge movements were also examined based on these temperatures. The analyses showed that the magnitude and direction of bridge movements may be appropriately estimated by Eq. 1 for straight, right bridges, but more refined analyses were often needed for sharply skew or curved bridges. The analysis for these more complex geometries often required the full three dimensional bridge geometry and the stiffness of the piers, abutments, bearings, and expansion joints. When these factors were included, movements were often more complex than suggested by the simple analysis in Eq. 1. Skew bridges frequently sustained transverse movements even though the bearings are invariably installed for longitudinal movements only. The transverse movements were relatively large on skew bridges with large skew angle and relative

width. The deflected shape of one skew bridge is compared to the undeformed shape in Fig. 3. The bearings on this bridge were aligned for longitudinal movement only, and the transverse movement caused considerable damage [6] to the bridge as illustrated in Fig. 4. Similar problems can be seen[5,7] in a number of other bridges.

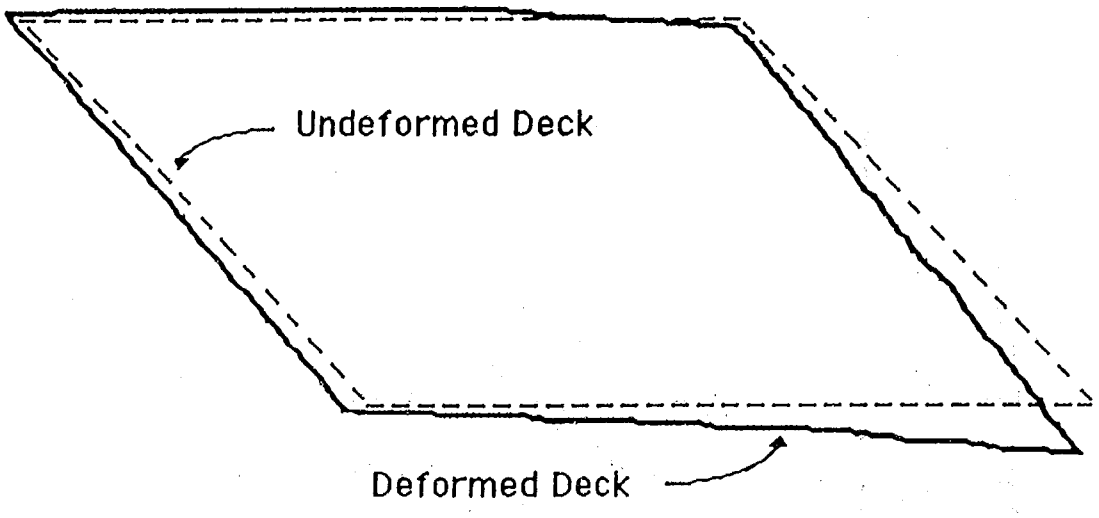

Fig. 3. Transverse Movement Predicted for a Sharply Skew Bridge

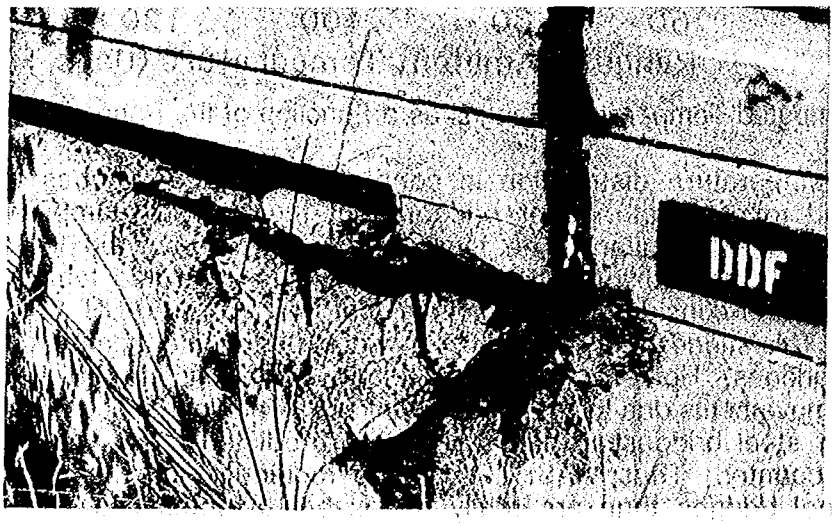

Fig. 4. Photograph of Typical Damage on a Skew Bridge with Large Transverse Movement

Curved bridges experience both radial and tangential movements. The radial movements were most significant when the radius is small. The radial movements in curved bridges are often dominated by the stiffness of piers and abutments rather than the bearings and expansion joints. The bearings on curved bridges are best oriented on the chord from the fixed point, if the fixed point is a stiff pier or abutment. The orientation of the bearing is less clear if the fixed location is over a flexible support.

Field Observations

There is very little field data on temperatures and thermal movements for bridges in the US. This research has shown that thermal movements are dependent upon the location, the local environment, the type and geometry of the bridge, and the stiffness of the bearings and substructure. Many bridges require more refined analysis than the

methods used for most bridges today. Field data is needed to substantiate these observations and to provide supporting data for making changes to design specifications and procedures.

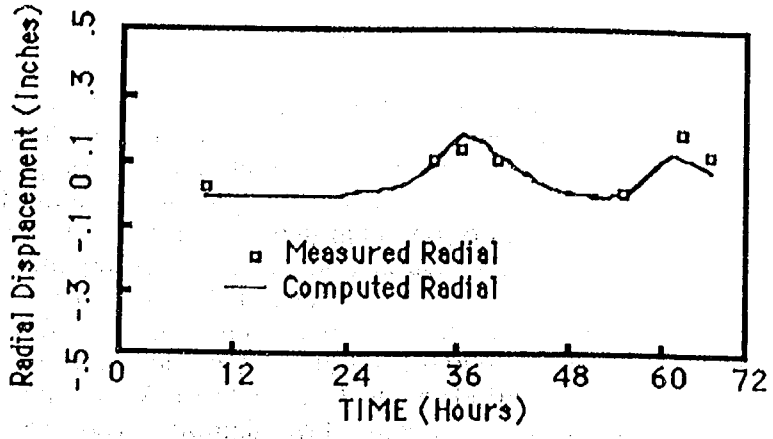

Fig. 5. Measured and Predicted Radial Movements of a Bridge Pier for Curved Bridge

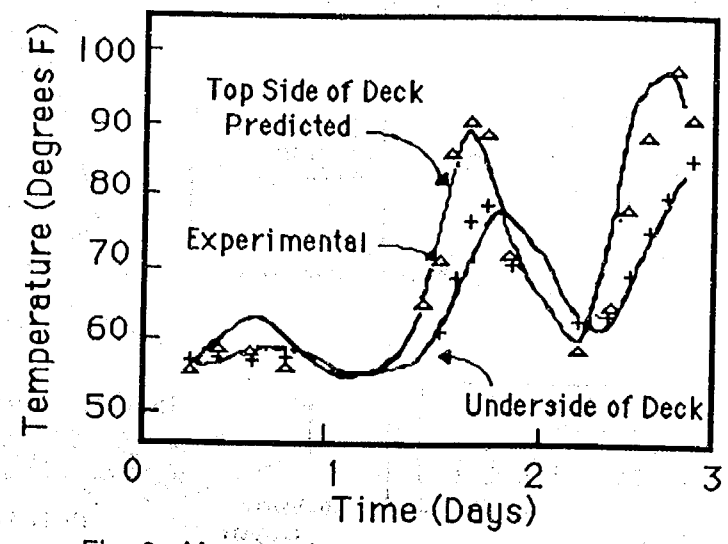

Fig. 6. Measured and Predicted Temperatures

A pilot study of field observations has been completed. The measurements were made over a three day period in July 1990 on the Sutton Creek Bridge near Eureka, Montana. The first day was a cloudy day with occasional rain. The field test consisted of measurements of the bridge and air temperatures, estimation of the wind speed and cloud cover and measurements of the bridge movements. The Sutton Creek Bridge is a continuous three span curved steel girder bridge. It has a total arc length of 657.5 ft (200.5 m) in the north-south direction and an 881.5 ft. (269 m) radius. The girders rest on fixed pin bearings at the south pier, and on rocker bearings oriented in the tangential direction at the other supports. The movement measurements were made with a theodolite and a electronic distance measurement device. Control points were place at fixed locations because they allow an evaluation of the accuracy of the measurements. The measurements recorded during this period are relatively small since they include only the movements due to the daily temperature cycle rather than the annual temperature cycle, but they were not insignificant. Figures 5 and 6 show the measured and predicted radial movement of pier 2 and the bridge temperatures, respectively. The theoretical predictions of the temperature and movement are in generally good agreement with the

measured values. Additional measurements are needed to examine the much larger movements and temperature ranges due to the annual temperature cycle, and the effects of different bridges types and climates. Further testing of this type is planned.

BRIDGE BEARINGS

Bridge bearings must accommodate movements due to thermal effects, creep and shrinkage of concrete, initial misalignment or imperfections in construction, and traffic loading. The magnitude and direction of these movements must be properly defined since they are combined with the loads to establish the design requirements for the bearing. There are a number of different types of bearings used in the US, and each has different limitations and capabilities in resisting loads and accommodating movements. If the bearing selection is improperly made, there is a mismatch between the capabilities and design requirements, and problems result. There have been problems with bridge bearings, and the NCHRP 10-20 Research Program was started in 1981 to resolve these problems. The contract was awarded to the University of Washington with Professor John F. Stanton and the author as Co-Principal Investigators. The ultimate objective of the research is to develop recommended specification provisions and design methods. This has required a wide range of experimental and analytical research. Some of this research is complete and other work is in progress.

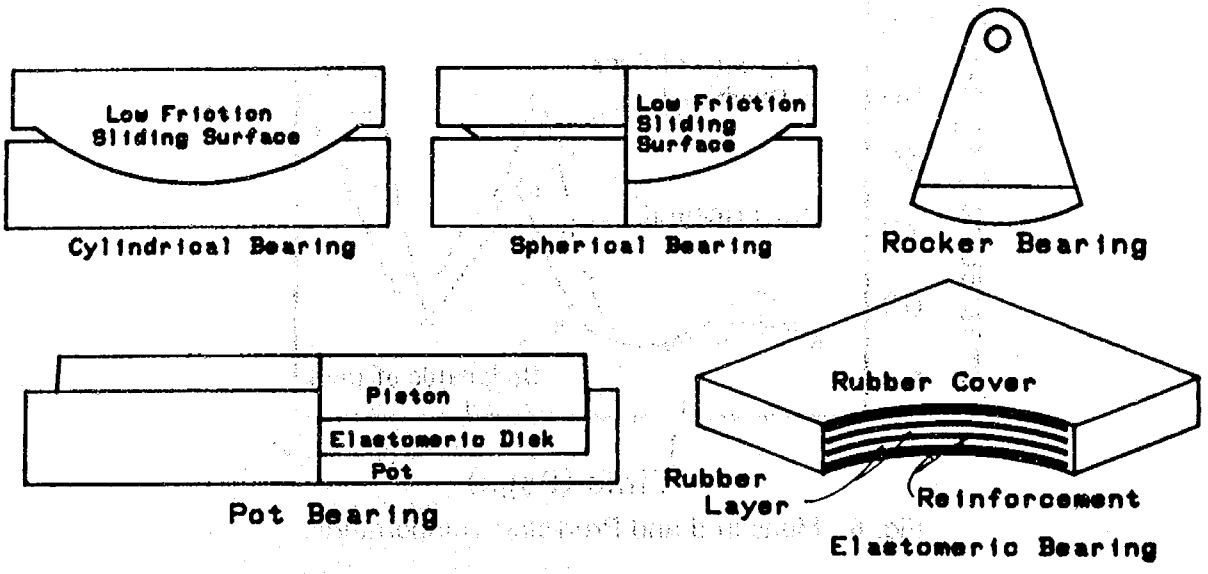

Fig. 7. Several Different Types of Bridge Bearing Used in the United States

Types of Bridge Bearing

A number of different types of bearing are used in the US, and some are illustrated in Fig. 7. Spherical and cylindrical bearings are illustrated in the upper left portion of the figure. These consist of curved sliding surfaces of lubricated bronze or PTFE. They are capable of sustaining large rotations about one axis (cylindrical bearings) or two axes (spherical bearings). The axis of rotation is the center of radius of the curved surface. They can support large gravity loads because of the relatively large compressive contact stress allowed. Since curved bearings rotate about their center of radius, they develop resistance to horizontal movement by virtue of their geometry and usually require an additional flat sliding surface to account for translational displacement. Variations between the centers of rotation of the bearing and

the bridge superstructure contribute to this translation. Curved bearings are relatively expensive and they are commonly used when the gravity load or the rotation are large.

Rocker bearings are illustrated in the upper right portion of Fig. 7 and have been used for longer than most other bearing types. Roller bearings are similar to rocker bearings, since they both accommodate movements by rolling action. Rolling resistance is small if the rolling surface is of constant radius and the surface is clean and uncorroded. Rocker bearings can also develop frictional slip resistance at the pins. They are used with pin or knuckle bearings if fixity against lateral movement is required at some location. Rocker and roller bearings are uni-directional, and they should be used only where the direction of rotation and movement are known with certainty. They may sustain large movements and rotations, but large movements require a large radius and a large bearing height. High contact stresses develop in rocker and roller bearings, and so high load bearing needs high strength steel, a large radius or both. They are commonly manufactured by steel fabricators and so they are primarily used on bridges with steel fabrication. They are less frequently used today than in the past.

Pot bearings are illustrated in the lower left portion of Fig. 7. The bearing consists of a pot, elastomeric disk, sealing rings and a piston. Rotations may occur about any horizontal axis of the bearing. PTFE sliding surfaces are used to accommodate movements, since the bearing is fixed against movement without a sliding device. The enclosed elastomeric disk is assumed to change shape readily due to its material flexibility, but to be stiff against changes in its volume. The rotational capacity of a pot bearing is controlled by the elastomer thickness and numerous clearance requirements. The standard design assumption of is that the disk behaves as a confined hydraulic fluid under compression where the sealing rings confine the highly stressed elastomer. Most bearing manufacturers in the US use 2 or 3 open flat brass rings to seal the piston, but closed circular brass rings also are used. Other patented sealing rings have been used in other countries.

Steel reinforced elastomeric bearings have uniformly spaced layers of steel and elastomer as shown in the lower right portion of Fig. 7. If properly designed they are able to support fairly large loads, and accommodate substantial movements and rotations. Unfortunately this capability has not always been recognized in the AASHTO Specification and the historic US design practice. Historic usage has limited them to less than 800 psi (5.6 MPa) average compressive stress and 7% average compressive strain and they have made little distinction between reinforced bearings and unreinforced pads. These limits have severely restricted the use of these bearings. As a result, elastomeric bearings are often poorly designed and underutilized in the US. Recent changes in the AASHTO Specifications[8] allow higher stresses and wider usage of elastomeric bearings. Recommendations have been made which would further increase these stress levels if adequate quality control is maintained. The bearing must be designed to control the stress in the steel and the strain in the elastomer. The time and temperature properties of the elastomer, fatigue, stability, delamination, yield and rupture of the reinforcement, stiffness of the elastomer, and geometric constraints must be considered in the design if the fully capabilities of the bearing are to be realized. Taller bearings are required to accommodate larger movements and rotations. The movements and rotations may occur in two directions, although special design considerations may be required with movement or rotation about more than one axis.

Low friction sliding surfaces are required for many of the bearings used in the United States. Flat surfaces are used to accommodate very large translational movement

and cylindrical (or spherical) surfaces may be used to accommodate rotation about one (or two) axes. The magnitude of the translation and rotation can be very large, since they are limited only by the dimensions of the sliding surface. The displacement may be multidirectional unless guideways or restraints are provided. The load capacity is limited only by the surface area of the bearing surface. These sliding surfaces are typically based on lubricated bronze or PTFE. Figure 8 illustrates a typical flat PTFE sliding surface

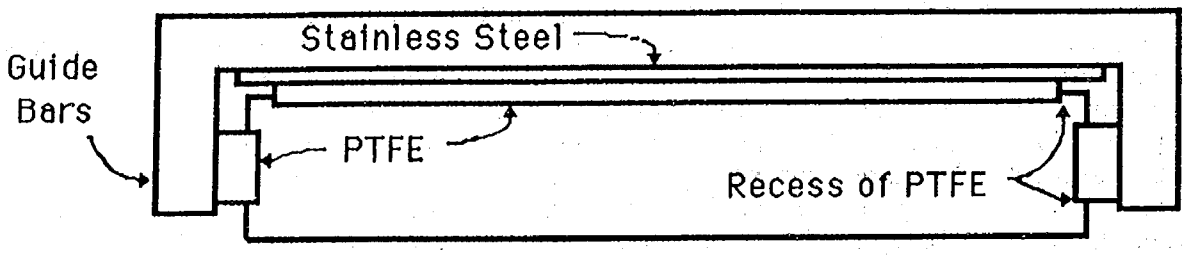

Fig. 8. Typical PTFE on Stainless Steel Low Friction Sliding Surface

Lubricated bronze bearing surfaces have been used for many years and are still used frequently. The mating surface is normally an ordinary steel surface which is not produced by the bearing manufacturer, but it should be significantly harder than the bronze surface and have a comparable surface finish. Lubricated bronze bearings typically use a regularly spaced recess pattern filled with lubricant. The recess pattern and the lubricant compound are regarded as proprietary. The coefficient of friction is in the order of .07 under initial conditions. The surface lubrication wears away with time and movement, and eventually direct contact is developed between the bronze and the mating surface. At this time, further movement causes wear or erosion of the bronze, but the lubricant in the recesses facilitates the movement and minimizes the wear of the bronze. The coefficient of friction increases at this time. Bronze bearings are relatively economical. They do not require the highly polished mating surface required with PTFE, nor do they require the tight geometric constraints since the material is thicker and significant wear is expected. However, the frictional resistance may be considerably larger than that achievable with PTFE surfaces.

If good quality control and design are achieved, PTFE (polytetrafluorethylene) sliding surfaces can develop lower frictional resistance than lubricated bronze surfaces, since coefficients of friction as low as 0.01 to 0.02 are possible. Coefficients of friction as large as 0.20 and 0.30 also are possible under other conditions, and this illustrates the importance of the design and quality control in the manufacture of the bearing. The PTFE is used with a very smooth stainless steel (typically for flat sliding surfaces) or anodized aluminium (for curved surfaces) mating surface. The friction decreases with increasing compressive stress between the PTFE and mating surface, lubrication of the sliding surface, and smoother finish on the mating surface. The coefficient of friction is larger for the first cycle of movement than for later ones. The friction increases if the mating surface is contaminated, if the PTFE contains filler such as fiberglass, or if the surface is roughened or worn. The great variability in the coefficient of friction of PTFE makes it essential that the bridge engineer use data which is appropriate for the given application, and require a certification test to assure that the design requirements are actually achieved in practice. PTFE will creep (or cold flow) laterally when subjected to high compressive stress. Creep may severely damage the PTFE and shorten the life of the bearing. The PTFE is sometimes confined in a recess to minimize this effect. Filled PTFE, which is reinforced with fiberglass or metal fibers, is sometimes used to resist cold flow, but it also increases the coefficient of friction. PTFE is sometimes woven into a mat which is placed over a metallic grid. This woven configuration is believed to

provide increased resistance to creep, while maintaining low coefficients of friction. PTFE wears with time and movement and provisions should be made for possible replacement after a period of time. The coefficient of friction of PTFE increases at very low temperatures.

Problems in US Practice

There have been a number of problems with bridge bearings in US engineering practice. Many of these problems appear to be related to the manufacturing process. Bearing manufacturers in the US tend to be widely dispersed into small firms. These firms are often entrepreneurs in their development of bearing systems. They develop slight variations in their bearings, and make substantial claims regarding the benefits their bearings over the bearings of their competitors. At the same time, most manufacturers have only a rudimentary idea of bridge design and the demands a bridge can place upon a bearing. New bearing manufacturers are continually entering the business while older firms are withdrawing, and communications between the bridge engineer and bearings manufacturer are often not good. Bridge engineers on the other hand often pay less attention to the design and selection of the bridge bearing than to other parts of the structure. They sometimes do not understand the differences in behavior and capabilities of different bearings, and they are often forced to rely on unsubstantiated claims of manufacturers in the selection process. Within this context, it is not too surprising that problems occasionally occur.

Elastomeric bearings have historically performed well in the US. They have experienced increasing usage over the past 30 years. There were a number of problems during their early usage, but these problems were resolved by early versions of the AASHTO Specification. They are economical and require minimal maintenance. However, they have historically not been utilized at anywhere near there full potential, and the AASHTO Specification has only recently begun to reflect their full design potential. These bearings have been the subject of considerable research in the NCHRP 10-20 Research Program. This research[8,9,10,11] is essentially complete and many recommendations have been made for improving their design and performance.

Spherical bearings also have performed well if they are manufactured to good tolerance control and if they use a high quality low friction sliding surface. They are expensive, and this has limited their use. This limited market means that there are few suppliers, but this has also avoided some problems with poor workmanship. Spherical and cylindrical bearings are the subject of limited ongoing research.

Rocker and roller bearings have provided variable performance. They perform poorly during earthquakes, since they may tip over or roll out of position. Their uni-directional characteristics have caused problems when used in applications requiring limited multi-directional movement or rotation. They experience corrosion and may lock up in service causing large forces and damage to the bridge. At the same time, many of these bearings have performed well for far longer than the newer bearing types. These bearings are not the subject of major research effort because of their declining usage, and the fact that the problems associated with these bearings are more often related to misuse of the bearing rather than a fundamental lack of understanding of the bearing behavior.

Pot bearings have a shorter history of usage in the US, but they have been experiencing increased usage in recent years. They are quite economical, and many engineers are enthusiastic about their capabilities. However, problems have been

reported in recent years. The confined elastomer sustains large hydrostatic stress, and the highly stressed elastomer can easily leak from the bearing as depicted in the photo of Fig. 9a. There is evidence that friction causes wear or abrasion of the elastomeric disk as shown in Fig. 9b. Elastomer thickness and clearance requirements define the rotation capacity of pot bearings. If these thicknesses and clearances are properly designed, the rotation capacity can be quite large. However, typical pot bearing designs use clearances, thicknesses and tolerances limit the rotation to .015 to .02 radians. This rotational capacity is similar to that possible with elastomeric bearings and less than the rotation possible with rocker or spherical bearings. Nevertheless, many design engineers assume that a pot bearing can sustain any large rotation. This mismatch of expectations also contributes to pot bearing failures. Pot bearings are a subject of substantial ongoing research in the NCHRP 10-20 Program.

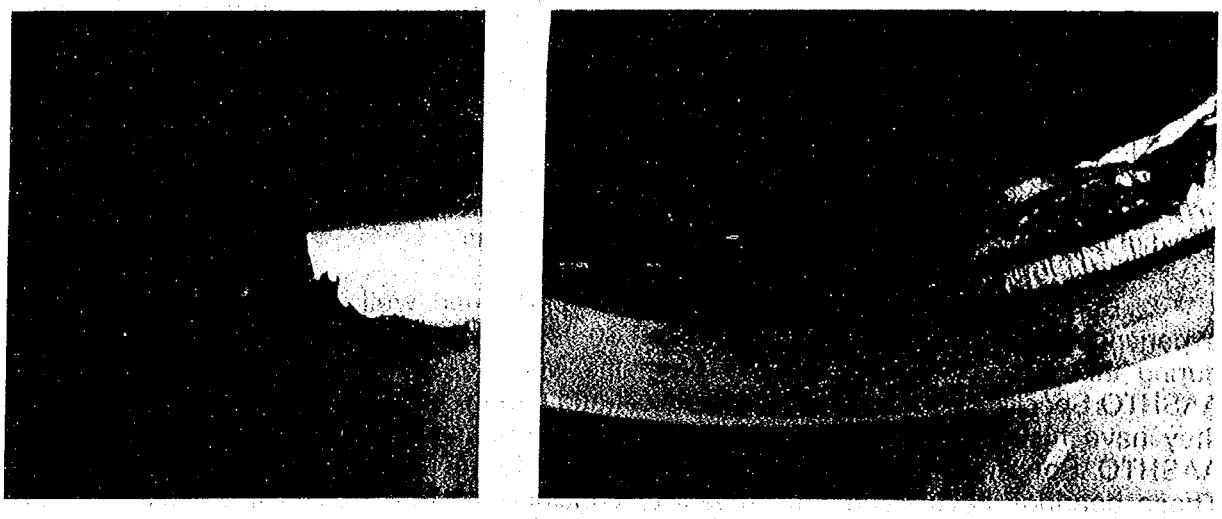

a) Elastomer Leakage b) Abrasion and Wear of Elastomeric Disk

Fig. 9. Photos of Observed Problems with Pot Bearings

Lubricated bronze sliding surfaces have been used for a number of years, and they have strong proponents in among bridge engineers. They are generally robust but there appear to be a few problems. For example, the mating surface are usually produced by a fabricator other than the bearing manufacturer, and there have been cases noted where inadequate geometric control and surface finish was provided. In some cases, the bronze has cracked or split due to stress concentrations caused by inadequate geometry control. Excessive friction has developed in some bearings with no or inadequate lubricant. They develop a fairly large coefficient of friction, and they are a relatively crude system compared to some other bearings. As a result, there is no ongoing research on these sliding systems. PTFE sliding surfaces are quite a different story, however. PTFE is used with increasing frequency, and the AASHTO Specification [1] does not provide provisions which reflect the true behavior of these elements. The deficiencies in the AASHTO Specification restrict the usage of these elements and have lead to problems and misinterpretations as to their capabilities and design requirements. PTFE sliding surfaces are also a major ongoing thrust in the NCHRP 10-20 Program.

Completed Research

The NCHRP 10-20 Research Program was started in 1980, and the major thrust of the initial work was elastomeric bearings. The initial research showed that there was

a state of the art review. It indicated that the existing design procedure was generally very conservative for steel reinforced elastomeric bearings but overly liberal for unreinforced elastomeric bearing pads. It showed that much larger allowable loads and translational movement and rotational capacities were possible with reinforced elastomeric bearings, but that specifications needed to have better control over the design and manufacture of these bearings. A draft specification[8], which restricted unreinforced elastomeric bearing pads to control the increased strain and slip and permitted increases in the load and movement capacity of some reinforced elastomeric bearings,was prepared in this phase and was adopted into AASHTO Specification in 1985.

The second phase[9] of the NCHRP 10-20 Research Program was directed toward answered questions raised in the first phase of the research and development of a more refined draft specification, and it started in 1982. Fatigue tests were performed to evaluate the fatigue life under variable shear deformation and compressive loads, and this led to rational elastomer strain limits. Buckling and stability tests were performed and led to appropriate stress limits. Force - deflection and moment - rotation tests were performed to evaluate the stiffness, and ultimate load tests were performed to examine failure modes such as delamination and tensile failure of the reinforcement. The proposed specification[9] permitted increased load capacity on some reinforced elastomeric bearings but required additional refinement in the design and manufacture of these bearings. This research showed the importance of quality control in the manufacture of the bearing and the effect of low temperature stiffness on the performance of the bridge and bearing. Extremely large forces may develop in bridges in some cold climates if the elastomer compound is not carefully selected. The third phase of the research[10,11,12] included an experimental study of low temperature stiffness of elastomers, establishment of improved tolerance requirements, development of test methods for evaluating elastomeric bearings under the increased loads and deformations, and finalization of the proposed design specification. The experimental study of low temperature stiffness showed that good low temperature compounds could be developed for neoprene and natural rubber, but that poor resistance to low temperatures was possible with both materials. The low temperature stiffness could be more that 50 times as large as the room temperature stiffness and this could lead to extremely large forces in the bridge. The low temperature behavior was very dependent upon the elastomer compound, and the time and temperature of exposure. A test method and acceptance criteria were developed to control this stiffening phenomenon.

The third phase of the research also had a second objective which was to provide a state of the art review[13] of pot bearing and PTFE sliding surfaces as used in high load multi-rotational bearings. The research brought to light many of the problems and concerns noted in the prior discussion. These findings led to the initiation of the fourth and final phase of the research program which is now in progress.

Research in Progress

The final phase of the research was started in 1989 and is scheduled for completion in 1992. This phase includes all types of high load - multi rotational bridge bearing. The first portion of this work consisted of development of a preliminary draft of a general design specification for all types of bridge bearing, development of a preliminary draft bearing selection guide and the establishment of experimental research requirements needed to finalize these documents. The preliminary drafts were developed and discussed with many bridge engineers, bearing manufacturers and the project panel. The experimental research requirements include-

- service load and rotation tests on pot, disk and spherical bearings.
- lateral load tests on pot, disk, and spherical bearings.
- coefficient of friction tests on flat dry and lubricated, woven and filled PTFE.
- low temperature friction tests on all forms of PTFE.
- analysis of leakage potential and failure mechanism of different bearings.
- establishment of acceptance test requirements for different bearings systems.
- creep and wear tests on PTFE
- analysis and material tests to support and combine the diverse efforts.

Friction tests on PTFE samples are being performed at Queen's University, Ontario, Canada. These tests show that the coefficient of friction varies with the sliding speed. The coefficient of friction is invariably larger for the first cycle of slip than it is for later cycles, and it decreases with increasing compressive stress and increases at low temperatures. The coefficient of friction is larger for flat dry PTFE than it is for lubricated material. Figure 10 shows typical results from these tests. This research is continuing and will provide considerable additional information on bearing behavior.

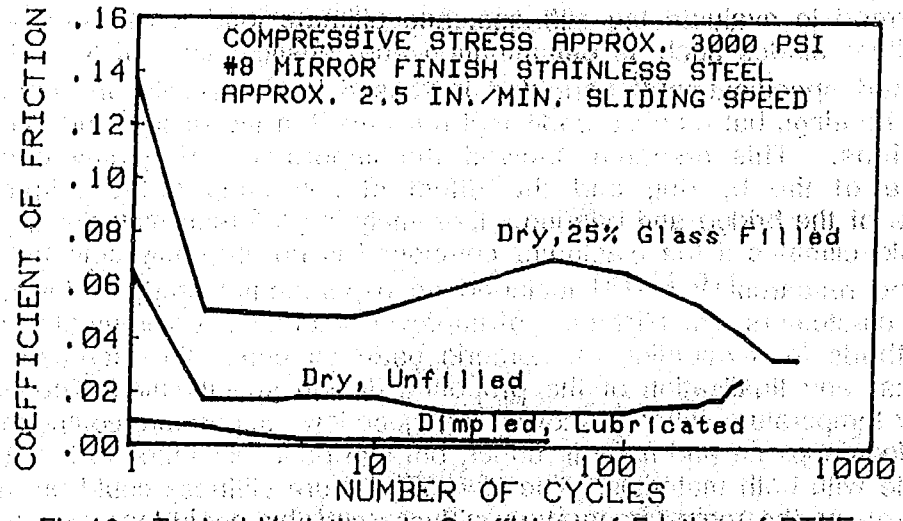

Fig.10. Typical Variations in Coefficient of Friction of PTFE

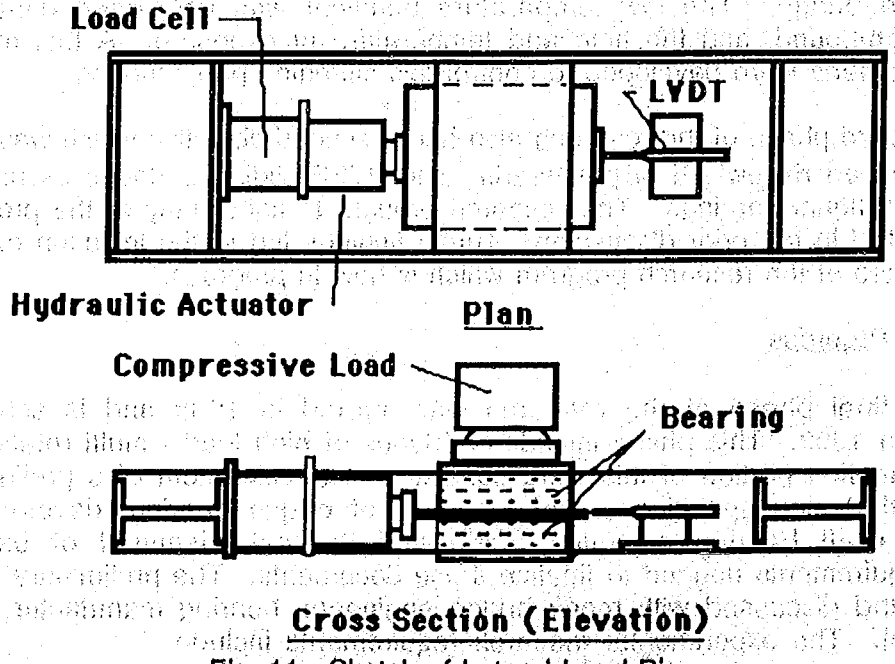

Fig. 11. Sketch of Lateral Load Rig

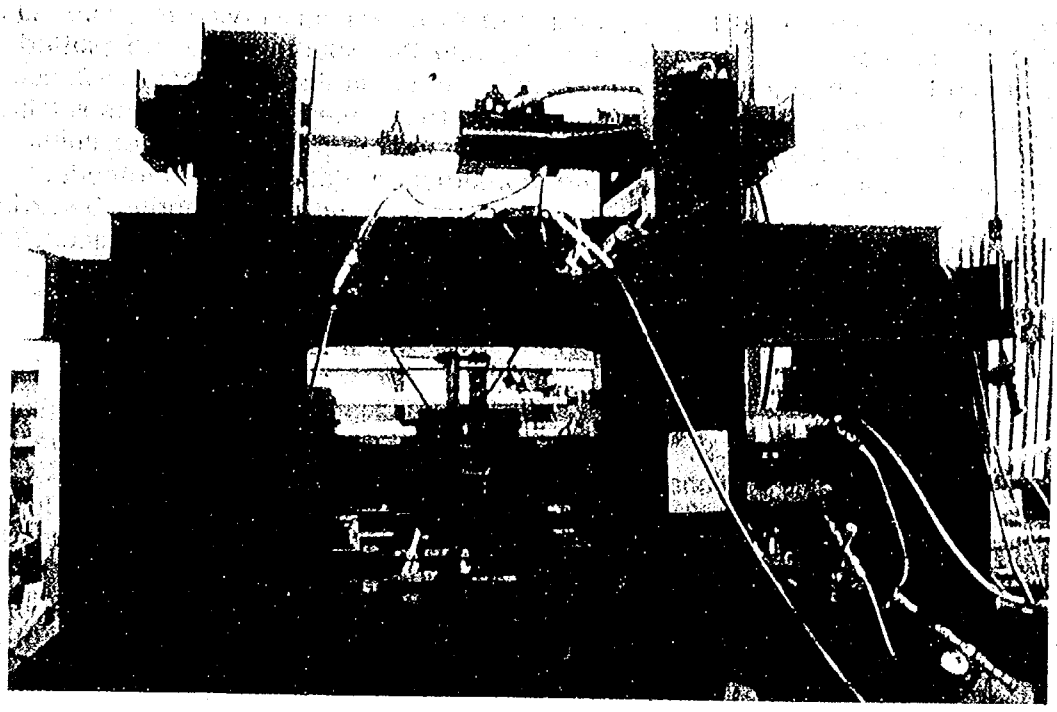

Fig. 12. Photograph of Rotational Load Rig

The tests on bearings are being conducted at the University of Washington. Separate load rigs have been built to test full size bearings under combined lateral load and compressive load and combined rotation and compressive load. Figures 11 and 12 show these two test rigs. The lateral load rig will be used to provide strength and stiffness tests of bearings, guideways and restraints. A few of these tests have been completed but a number of additional tests on spherical bearings, pot bearings, and guideways for PTFE sliding systems will be required.

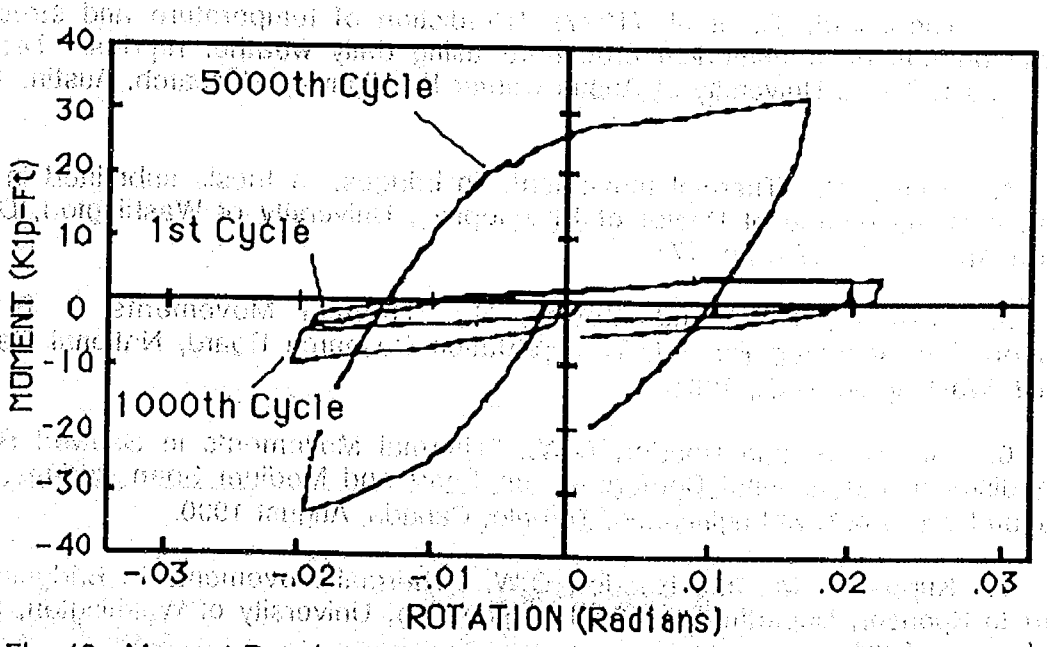

Fig. 13. Moment-Rotation Behavior Noted on one Series of Pot Bearing Test

The rotational rig will be used to apply a large number of service rotation cycles to pot bearings, disk bearings, and spherical bearings. Some of these tests are complete, but more are required. Figure 13 illustrates a typical result of a rotation test on a pot

bearing which was subjected to 5000 cycles of its maximum service rotation. Only the behavior of the first cycle, the 1000th cycle, and the 5000th cycle are plotted in the figure. It can be seen that there is a dramatic increase in the rotational resistance of the bearing as the number of cycles are increased. These measured changes illustrate the importance of the test program. Additional tests will be performed to examine factors such as lubrication, sealing rings, and construction details and methods. These comparative tests should lead to an improved understanding of bearing behavior and improved design specifications. The rig will also be used for a few maximum rotation tests to determine extreme limits on individual bearings.

ACKNOWLEDGEMENTS

The thermal movement research was funded by National Science Foundation Grant CES-8714894 with Dr. John B. Scalzi as the Program Manager. The bridge bearing research is funded by the National Cooperative Highway Research Program (NCHRP 10-20) with Ian Friedland as the Senior Project Manager. Professor John Stanton at the University of Washington, Professor Ivan Campbell at Queen's University in Canada, and the author are Co-Investigators on the present phase of the bearing research. The opinions expressed in this paper are those of the author and do not necessarily reflect the opinions of the funding agencies. The support on these projects is gratefully acknowledged.

REFERENCES

1. AASHTO, "Standard Specification For Highway Bridges", 14th Edition, Washington, D.C., 1989.

2. Potgeiter, I.C. "Response of highway bridges to nonlinear temperature distributions," a thesis submitted in partial fulfillment of the degree of Doctor of Philosophy University of Illinois, Department of Civil Engrg., Urbana, IL.

3. Thepchatri, T., et al. (1977). "Prediction of temperature and stresses in highway bridges by a numerical procedure using daily weather reports." *Technical Report* 23-1, Texas University at Austin Center for Highway Research, Austin, TX, pp. 145.

4. Moorty, S., "Thermal movements in bridges," a thesis submitted in partial fulfillment of the degree of Doctor of Philosophy , University of Washington, Dept. of Civil Engrg., Seattle, WA, pp. 171.

5. Roeder, C.W. and Moorty, S., "Thermal Movements in Bridges." Transportation Research Record, Transportation Research Board, National Research Council, Washington, D.C., 1991.

6. Moorty, S. and Roeder, C.W., "Thermal Movements in Skewed Bridges" Proceedings of International Conference on Short and Medium Span Bridges, Vol. 2, Canadian Society of Civil Engineering, Toronto, Canada, August 1990.

7. Kuppa, S. M., and Roeder, C.W., "Thermal Movements in Bridges," Final Report to Sponsor, Department of Civil Engineering, University of Washington, Seattle, WA, January 1991.

8 Stanton, J.F. and Roeder, C.W., "Elastomeric Bearings - Design, Construction and Materials," NCHRP Report 248, Washington, DC, September, 1982.

9. Roeder, C.W., Stanton, J.F., and Taylor, A., "Elastomeric Bearings - Design Construction and Materials," NCHRP Report 298, National Research Council, Washington, DC, 1987.

10 Roeder, C.W., Stanton, J.F., and Feller, T., "Low Temperature Performance and Manufacturing Tolerances of Elastomeric Bearings," NCHRP Report 325, National Research Council, Washington, DC, 1990.

11. Roeder, C.W., and Stanton, J.F., "State of the Art Elastomeric Bridge Bearing Design," ACI Journal, No. 1., Vol. 88, 1991.

12. Roeder, C.W., Stanton, J.F., and Feller, T., "Low Temperature Performance of Elastomers," ASCE, Cold Regions Journal, Vol. 4, No. 3, 1990.

13. "Pot Bearings and Sliding Surfaces, " NCHRP Research Results Digest, No. 171, September 1989.

ESTIMATION OF ULTIMATE DEFORMATION OF COLUMN-FOOTING JOINT

by

H.Kawano[1] and H.Watanabe[2]

ABSTRACT

The column-footing joint of bridge piers is the section where the bending moment caused by the lateral load to the column is maximum. And it is very important to ensure the required development length of anchorage reinforcement for preventing the bridge piers from reducing their ultimate strength due to bond failure between anchorage reinforcement and footing concrete. Presented in this paper is a method to calculate ultimate strength of anchored reinforcing bar derived from the pullout test data, and the effect of slip of anchorage reinforcement on the total deformation of column is discussed based on the result of cyclic loading test with RC column-footing specimens.

INTRODUCTION

The design of anchorage reinforcements is based on the allowable stress design method in the Design Specification for Highway Bridges. The tensile stress of the anchorage reinforcement is fixed at the allowable tensile stress and the development length is so determined that the anchorage strength which is obtained by multiplying allowable bond stress by nominal surface area of anchored reinforcing bar becomes less than the allowable tensile force of the bar. The procedure of the examination is described as following form;

$$\frac{\pi D^2}{4} \cdot \sigma_{sa} < \tau_{ba} \cdot \pi \cdot D \cdot \ell_d$$

where
σ_{sa}:allowable tensile stress of anchorage reinforcement
D :diameter of anchorage reinforcement
τ_{ba}:allowable bond stress
l_d :development length of anchorage reinforcement

It is necessary to examine the safety factor of piers in the ultimate limit state for the earthquake resistant design, and also to examine ultimate state of anchorage reinforcement. But the design method based on the allowable stress is not proper to examine the safety of anchorage reinforcement in the ultimate limit state, because the tensile stress acting to the reinforcement in the ultimate limit state is greater than the allowable stress.

---

1) Head, Concrete Division, Geology and Chemistry Dapartment, Public Works Research Institute, Ministry of Construction
2) Research Engineer, ditto

We have to use not the allowable stress (σ_{sa}) but the tensile stress in the ultimate state (σ_{su}) as the tensile stress in equation 1. The development length calculated from equation 1 by using the values σ_{su} and τ_{ba} is too conservative, and thus we have to identify the value of ultimate bond strength (τ_{bu}).

When the anchorage reinforcement is pulled out from the footing, slip occurs between reinforcement and concrete, and then the reinforcement moves upper direction. This slip causes the rotational displacement of columns (fig.1), which affects the ductility of the columns. Then we have to take into account of the rotational displacement to estimate the ductility of the column precisely.

In this paper we discussed the ultimate anchorage strength and effect of slip of the reinforcement on the ductility of the columns from the results of the eccentric pull out test using beam specimens and cyclic loading test of column-footing model.

ESTIMATION OF SLIP AND ULTIMATE STRENGTH OF ANCHORAGE REINFORCEMENT

Generals

The bond stress distribution has to be cralified to estimate the ultimate strength of anchorage reinforcement precisely. The bond stress distribution is determined by solving the equilibilium equation.2 putting the bond stress versus slip relationship into the equation. (Bond stress versus slip relationship is represented "S-S relationship" here after.)

$$\frac{D}{4} * \frac{d\sigma_s}{de_s} * \frac{d^2S}{dx^2} = \tau(x,S) \qquad \text{(equation.2)}$$

where
e_s : tensile strain of the reinforcement
S : local slip at the point $X=x$

Bond is made up of three components; 1)Adhesion, 2)Friction, 3)Mechanical interaction between concrete and steel. Bond of deformed bar depends primary on mechanical interlocking, and the mechanism of this action is very complicated and almost impossible to describe by numerical models. Thus S-S relationship must be obtained through bond tests. There are many kinds of bond tests. But as the result of S-S relationship obtained from a bond test is greatly affected by stress distribution in the concrete adjacent to reinforcement, we must choose the bond test which can represent the stress distribution in real footings.

In this study we carried out the beam pull out test specimens to obtain the parameters which represent the simplified S-S relationship model shown in fig.2.

Outline of the pull out test

Eleven specimens were tested. Dimensions of specimens are shown in fig.3. The conditions of specimen are shown in table.1. Bond isoration of the reinforcement from concrete was made by covering the reinforcing bar by a rubber hose. The pull out force was derived by bending the specimens. As anchored reinforcing bars in the footings usually have enough cover and spacing, split failure caused by the radial component of stress transferred from reinforcing bar seldom occurs. Then anchored reinforcing bars of the specimens were settled at the center of the cross section to prevent a

split failure.

Tensile strain was measured at the center of the reinforcing bar by strain gauges attached on the surface of the bar, and slip of reinforcing bar was measured at the center and end of the bar using displacement transducer. Local bond stress was not measured in this experiment for the values of bond stress calculated from measured strain difference between two adjacent strain gauges sometimes contain large error.

We assumed the simplified S-S relationship as shown in fig.2, and tried to identify the parameters S_1, S_2 and τ_{max} to fit the relationship between tensile strain of anchored reinforcing bar and slip obtained from the experiment.

Test results and discussions

Test results of the relationship between tensile strain of anchored reinforcing bar and slip are shown in fig.4. The failure of the specimens can be seldom observed except for the scale off on the surface of concrete at the center of the specimens (i.e. at the loaded end). The development length of specimens is enough for preventing anchored reinforcing bar from bond failure before tensile yielding. Slip of reinforcing bar observed at the free end was very small compared to the one at the loaded end. The slip of free end is remaining deformation.

In the previous study[1], we carried out the pull out test and have decided the parameter of the S-S relationship shown as table.2.

Table.2 The test conditions and resultant values of parameters (S1,S2,τmax) obtained in the previous study.

Test conditions	
fc':227kgf/cm^2	steel dia.:22mm
Parameters	
S1:0.03mm	S2:5mm τmax:60kgf/cm^2

As shown in table.2, the test conditions was limited to only one case. Then we tried to calculate S1 and τmax in various conditions by using results of the relationship between tensile strain of anchored reinforcing bar and slip obtained from the beam pull out test.

It was reported that the ultimate bond strength increased as concrete strength increased. In the reference (2), the relationship between concrete strength (fc') and ultimate bond strength (τu) is expressed as following form;

$$\tau u \propto fc'^{1/2} \quad \text{(equation.3)}$$

In this study we use the following equation.

$$\tau u = 60 * (fc'/227)^{1/2} \quad \text{(equation.4)}$$

According to this relationship, τmax was assumed to change proportionally to the square root of fc'. On the other hand, S1 and S2 are supposed to change proportionally to the diameter of anchored reinforcing bar. The results of the relationship between tensile strain of anchored reinforcing bar can be obtained from analysis by solving eq.2. In the calculation, the stress-strain relationship of reinforcement is assumed as fig.2. If the calculated slip at the free end exceeds S1, the integration of bond stress over the whole surface of bars gradually decreases. Then we defined that the ultimate strength of anchored reinforcing bar is equal to the pull out force at the point where the slip of free end equals S1. The result of the analysis are shown in fig.5 and fig.6. Fig.5. shows the effect of concrete strength on the tensile strain of reinforcing bar and slip at the free end. In some cases, the difference between the measured value and the calculated value is relatively large, but it is concluded that τmax is corrected well according to eq.4. Fig.6. shows the effect of steel diameter on the tensile strain of reinforcing bar and slip at the loaded end. The difference between the calculated slip and the measured one is larger in the case that S1 and S2 varies analogously to steel diameter.

Then we have concluded that τmax changes according to eq.4 and S1 and S2 can be fixed to 0.03mm and 5mm respectively.

EFFECT OF SLIP OF ANCHORED REINFORCING BAR ON THE DUCTILITY OF COLUMN OF BRIDGE PIER

Generals

It is essential to estimate ultimate strength and deformation of columns for the earthquake resistant design of bridge piers. The important points for the seismic design of anchored reinforcing bar of columns are

(1) To estimate the effect of the slip of anchored bar on the ductility of whole structure.

(2) To examine whether the ultimate anchorage strength is larger than the pull out force acting on the anchored bar when the whole structure is in the ultimate limit state.

The ultimate deformation of bridge pier consists of bending deflection of columns and rotational displacement of column caused by the slip of anchored reinforcing bar. Thus the ultimate deformation (δ) can be expressed by the following equation;

$$\delta = \delta_1 + \delta_2$$

where

δ :deformation of column

δ_1:deformation of column by bending

δ_2:deformation of column by rotation(fig.1)

Fig.7 shows the procedure to calculate δ . δ_2 is usually neglected in Japanese Earthquake Resistant Design Specifications for Highway Bridges. But as reported in the reference (3), the rotational displacement caused by slip of anchored reinforcing bar is not negligible small in some cases. In this paper, the method to calculate δ is discussed to estimate the ductility of bridge pier by taking δ_2 into account. The cyclic loading test of RC column-footing model was done to examine if the procedure of the calculation is proper.

Cyclic loading test of RC column-footing model

Five specimens of two types were prepared as shown in fig.8. The dimension and development length of specimens are shown in table.3. Footing size of column #1 and #2 was so determined that any crack could not occur in the footings. On the other hand column #3,#4, and #5 were allowed to occur cracks in footings. Ready-mixed concrete whose nominal strength is 210kgf/cm^2 was used. The maximum size of coarse aggregate was 20mm and the slump was 8cm. The results of compressive strength test of the concrete is shown in table.4. The reinforcing steel used was type SD30.(nominal yield strengh :30kgf/mm^2)

The static loading test was carried out for all specimens by the displacement control with the loading program shown in fig.9.

Tensile strain of primary reinforcement was measured with strain gauges. The displacement of columns were measured with displacement transducer whose accuracy was 1/100mm. The angle of rotation of column at the column-footing joint was also measured as shown in fig.10.

Column #1 and #2 failed by shear after the primary reinforcement yielded in tension. The ductility of both specimens were about 4. Column #3 failed by tensional failure of the primary reinforcement without causing any shear crack in concrete. The ductility was about 6. Column #4 and #5 failed by shear of the footing. Hysteretic behavior of each column are shown in fig.11. The character of hyhteretic loop obtained by cyclic loading was different between column #1,#2,#3 and column #4,#5. Column #4,#5 showed the slip type hysteresys loop which indicates that amount of absorbed energy by plasic deformation is small.

Measured and calculated ultimate strength and ductility are shown in table.5. δ_1 is obtained from the following equation;

$$\delta_1 = \int_0^H \phi(z)\,(H-z)\,dz$$

where
$\phi(z)$: curvature at the point Z=z (fig.12)

δ_2 is obtained from the following equation;

$$\delta_2 = s/(d-x)$$

where
d : effective depth of the cross section of the column
x : distance from extreme compression fiber to neutral axis of the cross section at the bottom of the column
s : slip of the anchored reinforcing bar

Slip of the anchored reinforcing bar (=s) is obtained by solving eq.2. The boundary condition of the bar on the surface of footing is assumed as the tensile strain determined from the equilibirium of the cross section at the bottom of the column.

The rotaion angle obtained from the measurement of the specimen is calculated from following equation;

$$\theta = (el1-el2)/dl$$

where
θ : rotation angle at the bottom of the column
el1,el2 : measured displacemet of the bottom of the column by slip

of anchored reinforcing bar
dl : interval of the measurement point

δ_2 is calcultated from the following equation;

$$\delta_2 = \theta * H$$

where
H : The distance from the bottom of column to the point of loading.

The effect of rotational displacement caused by slip of the anchored reinforcing bar on the total displacement of column can be estimated by δ_2/δ . Measured δ_2/δ and calculated one was compared to make certain whether the estimation is reasonable. The results are shown in fig.13. As the rotation angle is the function of the tensile strain of the anchored reinforcing bar at the bottom of the column, δ_2/δ should be expressed by the function of the tensile strain of the bar. But it is very difficult to measure the strain of reinforcing bar after yielding, then we use the plasticity of column to express the strain of reinforcing bar indirectly. δ_2/δ obtained from test data spreads more widely as the pasticity factor increses, and the minimum value of δ_2/δ after the primary reinforcement yields is almost the same as the one at the plasicity factor eaquals 1; ie,

$$\min\left(\delta_2/\delta\right) \fallingdotseq \delta_{2y}/\delta_y$$

where
p :plasicity factor of column($p=\delta/\delta_y$)
δ_y:deformation of column at the reinforcing bar yielding

Roughly speaking, calculated δ_2/δ comes near the average value of measured δ_2/δ , but the difference from the measured one becomes larger as the plasticity facter becomes larger. At the point of p=1 the calculated δ_2/δ agrees with the measured one.
Then following equation holds almost good.

$$\left(\delta_{xy}/\delta_y\right)_{cal} < \left(\delta_2/\delta\right)_{meas}$$

The ductility factor including δ_2 is expressed by following form.

$$\frac{\delta_u}{\delta_y} = \frac{\delta_{1u}+\delta_{2u}}{\delta_{1y}+\delta_{2y}} = \frac{\left(\frac{1}{1-\delta_{2u}/\delta_u}\right)}{\left(\frac{1}{1-\delta_{2y}/\delta_y}\right)}\frac{\delta_{1u}}{\delta_{1y}} \geq \frac{\left(\frac{1}{1-\delta_{2y}/\delta_y}\right)}{\left(\frac{1}{1-\delta_{2y}/\delta_y}\right)}\frac{\delta_{1u}}{\delta_{1y}} = \frac{\delta_{1u}}{\delta_{1y}}$$

Then it is concluded that the component of displacement caused by the slip of anchored reinforcing bar have to be taken into account to estimate the ductility factor precisely. And the ductility factor calculated by neglecting the rotational displacement component gives the conservative

results.

CONCLUSIONS

1) The slip of anchored reinforcing bar can be estimated by assuming the simplified bond stress-slip relationship. The parameters which determine the simplified S-S relationship can be derived from the beam pull out test.

2) The ductility factor of bridge pier can be estimated more precisely by including rotational displacement of column caused by the slip of anchored reinforcing bar. The ductility factor calculated neglecting the rotational displacement gives conservative results.

Table.1 Test condition of specimens

specimen no	nominal concrete strength(kgf/cm^2)	steel diameter(mm)	development length(*D)	Number of bar	Clear spacing bar(*D)
1	300	10	30	1	-
2	300	10	40	1	-
3	300	10	50	1	-
4	180	10	40	1	-
5	180	10	50	1	-
6	300	10	30	3	3
7	300	10	50	3	3
8	300	10	50	3	1
9	180	10	30	3	1
10	180	10	50	3	1
11	180	16	30	1	-

Table.3 Dimensions of specimens

specimen no	1	2	3	4	5
cross section(cm)	30*30	30*30	50*50	50*50	50*50
effective depth(cm)	25	25	45	45	45
primary reinforcement	D22*3	D22*3	D16*5	D22*5	D29*5
tensile reinforcement ratio(%)	1.49	1.49	0.44	0.86	1.43
stirrup	D8@6cm	D6@6cm	D10@10cm	D10@10cm	D10@10cm
column height(cm)	105	105	180	180	180
shear span ratio	4.2	4.2	4.0	4.0	4.0
development length(*D)	59D	30D	43.8D	43.8D	43.8D
dimension of footing	70*120	70*120	70*70	70*70	70*70

table.4 Compressive strength of concrete of column specimens

Specimen no	Compressive strength (kgf/cm^2)
1	252
2	234
3	326
4	318
5	324

table.5 Ultimate strength and deformation of column specimens

column no	Dispacement at the yield point(mm)	Load at the yield point (tonf)	Ultimate Deformation (mm)	Ultimate strength (tonf)	Ductility factor
1	9.5	14.8	41.5	13.8	4.4
	7.8	9.1	11.3	9.4	1.4
	4.5	9.1	5.8	9.4	1.3
2	9.6	14.9	38.4	16.0	4.0
	7.8	9.1	11.3	9.4	1.4
	7.8	9.1	5.4	9.4	1.3
3	7.9	9.3	46.1	7.2	5.8
	8.0	9.8	45.1	11.4	5.6
	6.1	9.8	23.4	11.4	3.8
4	8.8	14.7	51.5	17.3	5.9
	10.6	18.0	38.6	19.8	3.6
	6.6	18.0	15.1	19.8	2.3
5	17.8	23.5	31.6	26.2	1.8
	-	-	12.5	25.7	<1
	-	-	9.2	25.7	<1

upper value: measured
middle value: calculated value with taking into account for δ_2
lower value: calculated valee without taking into account for δ_2

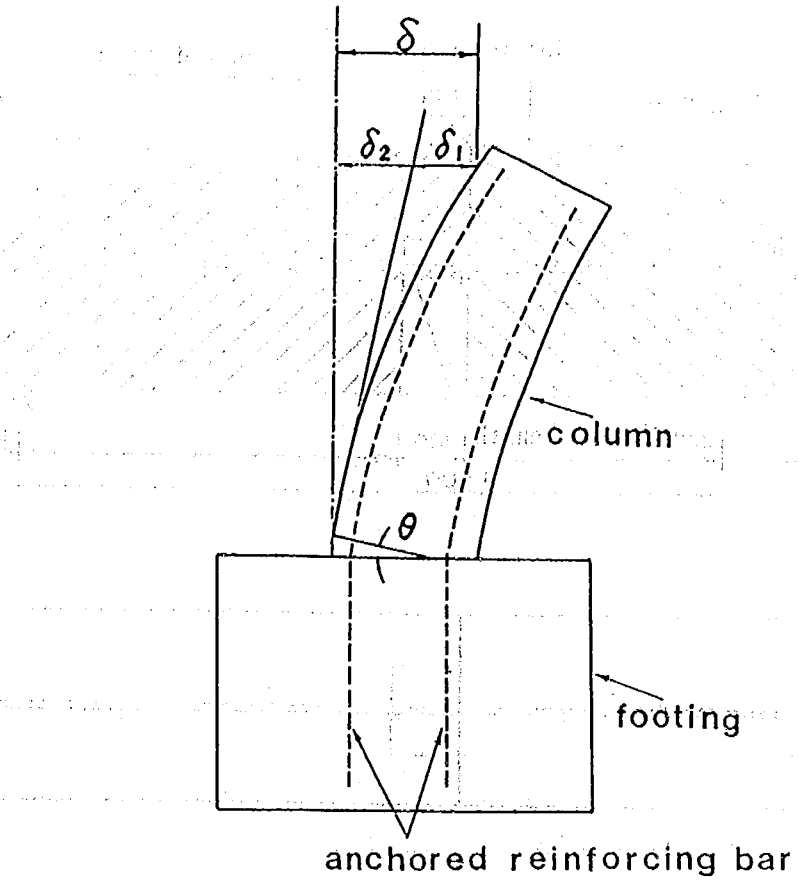

Fig.1 Deformation of column

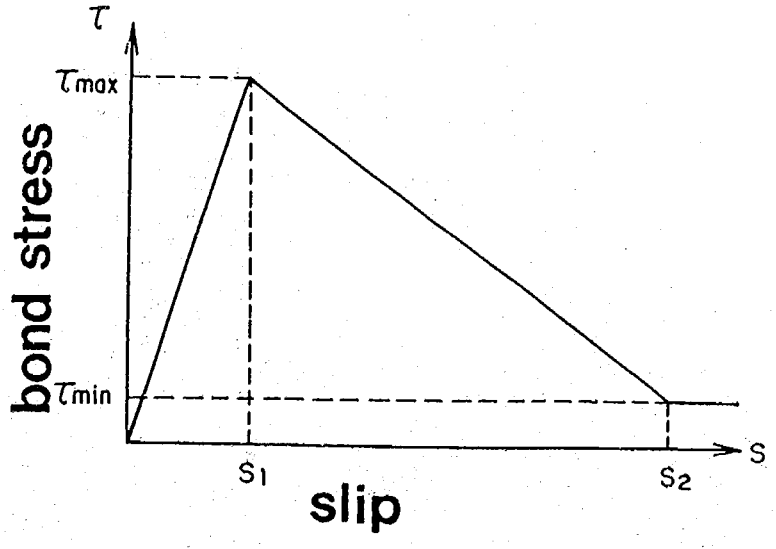

Fig.2 Simplified bond stress slip relationship

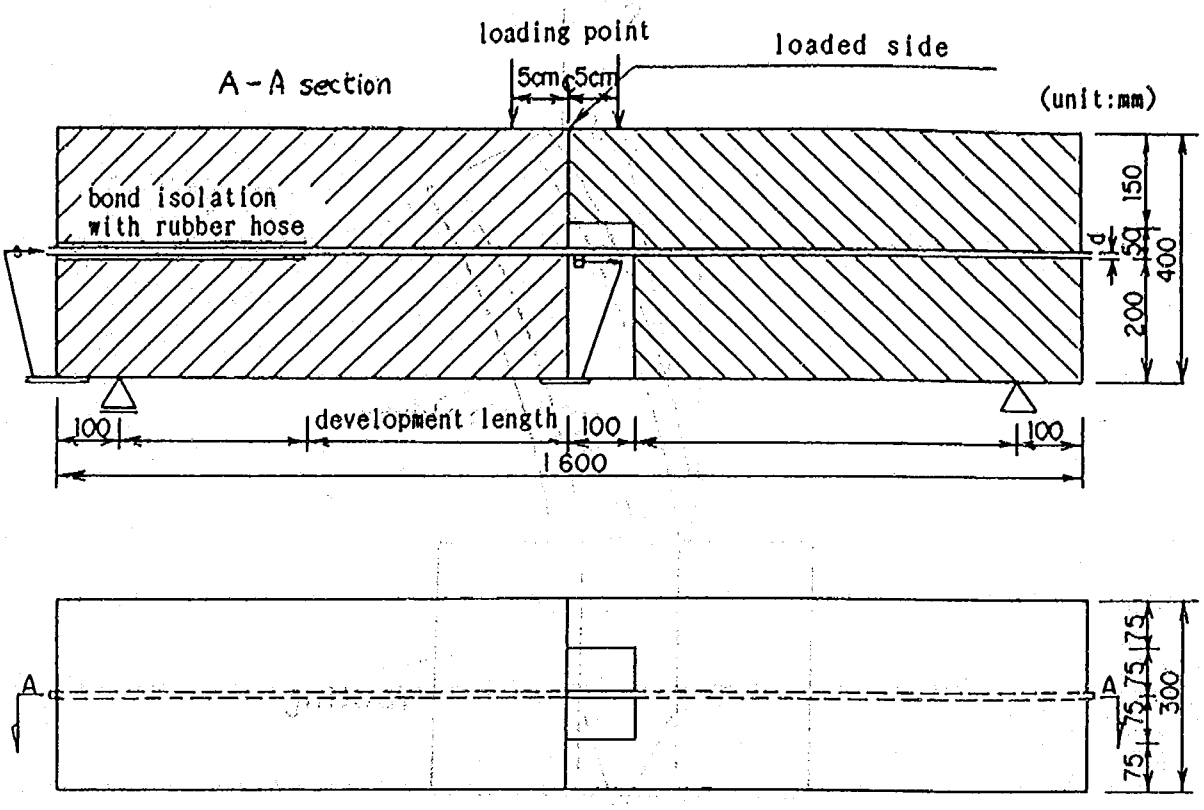

Fig.3 Dimension of beam specimen

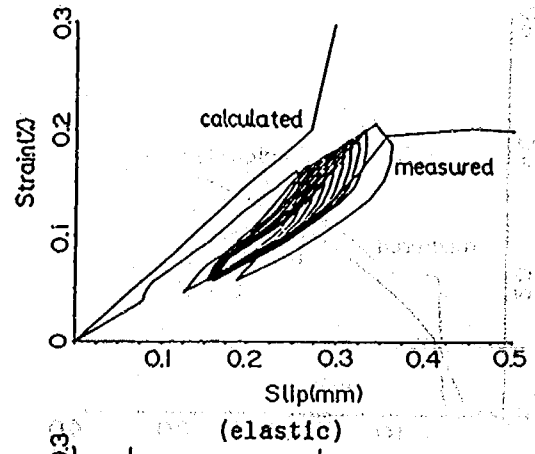

(elastic)

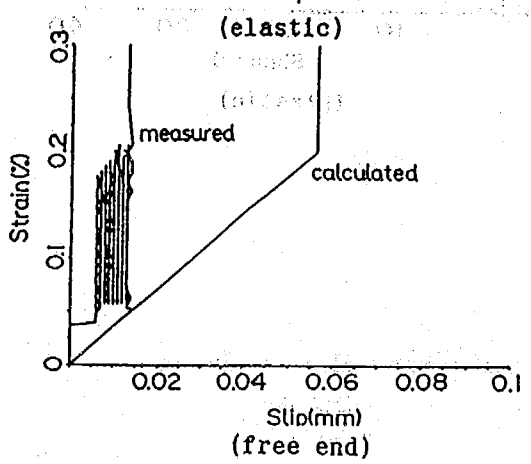

(free end)

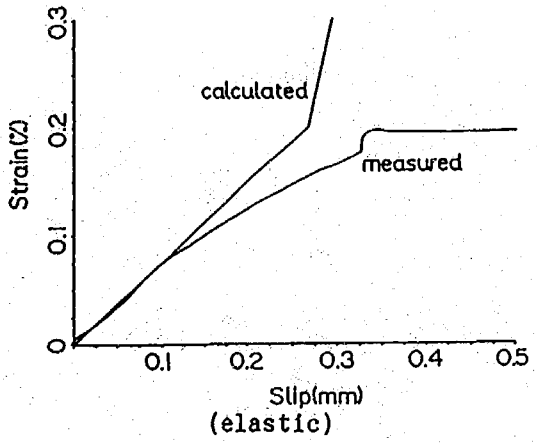

(elastic)

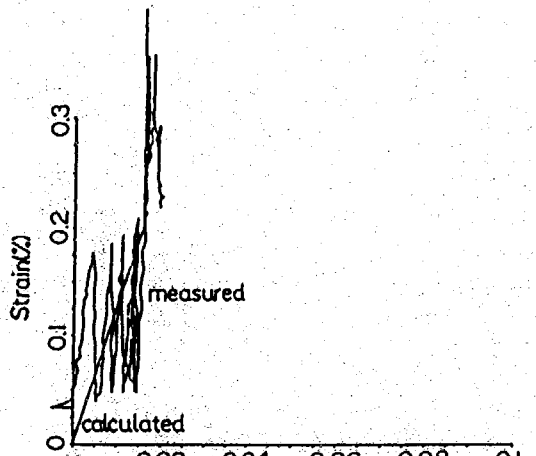

(free end)

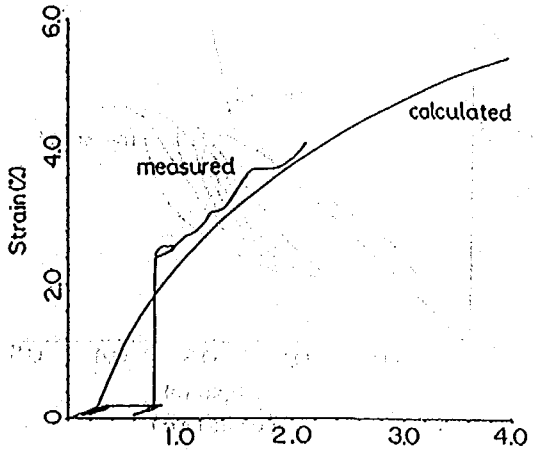

(plastic)

(1) beam #1

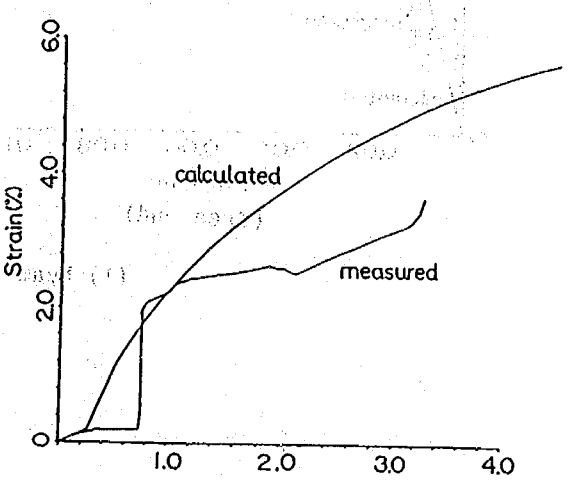

(plastic)

(1) beam #2

Fig.4 Examples of tensile strain slip diagram(test data)

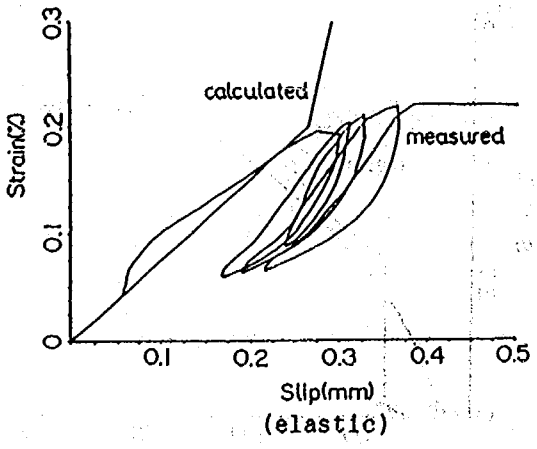
Strain(%)
0.3
0.2
0.1
0
calculated
measured
0.1
0.2
0.3
0.4
0.5
Slip(mm)
(elastic)

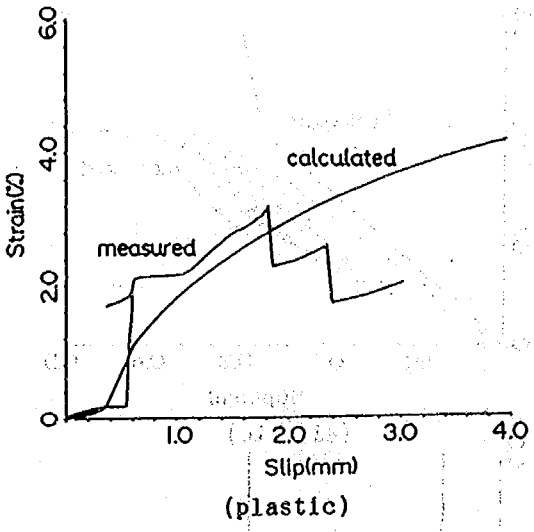
Strain(%)
6.0
4.0
2.0
0
calculated
measured
1.0
2.0
3.0
4.0
Slip(mm)
(plastic)

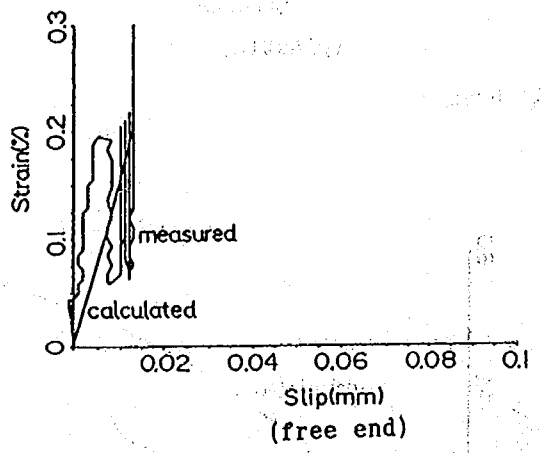
Strain(%)
0.3
0.2
0.1
0
measured
calculated
0.02
0.04
0.06
0.08
0.1
Slip(mm)
(free end)

(1) beam #3

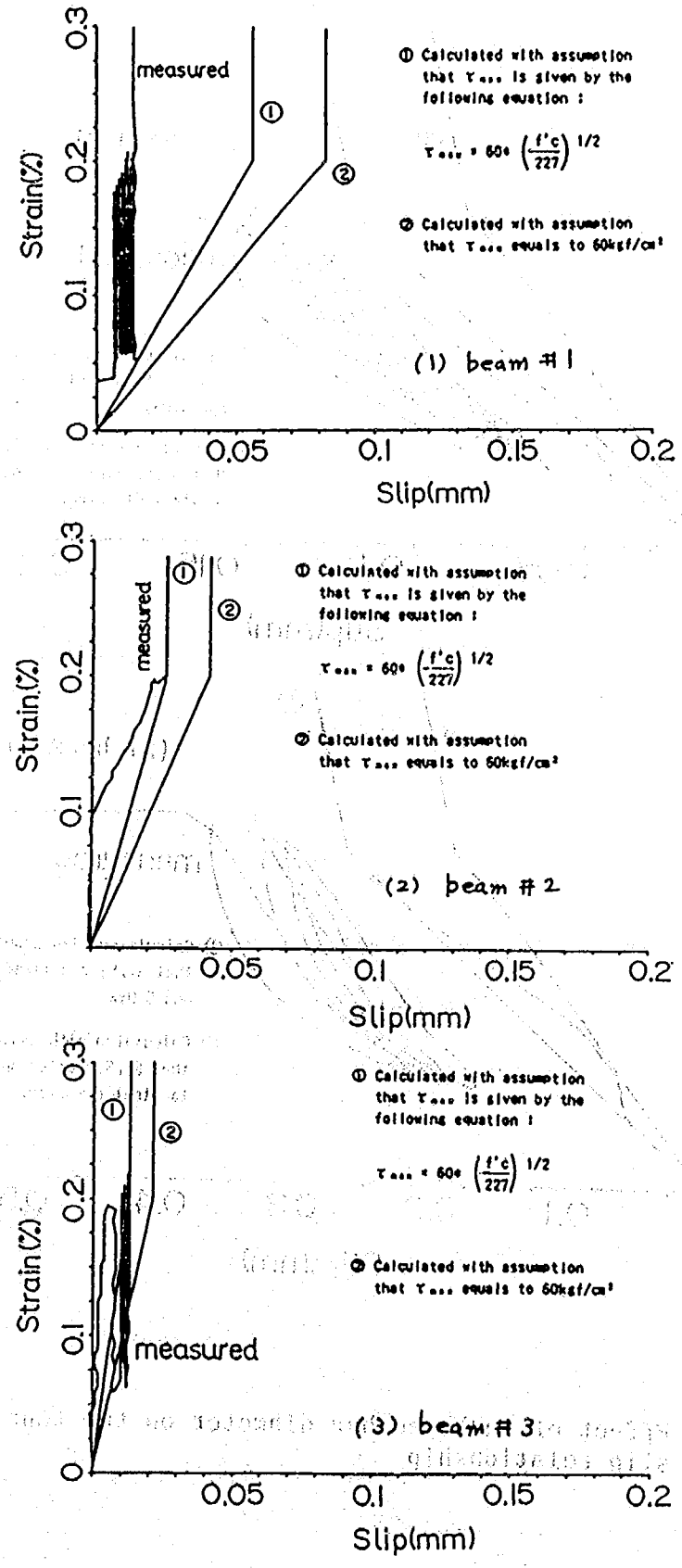

Fig.5 Effect of concrete strength on the tensile strain slip (free end slip) relationship

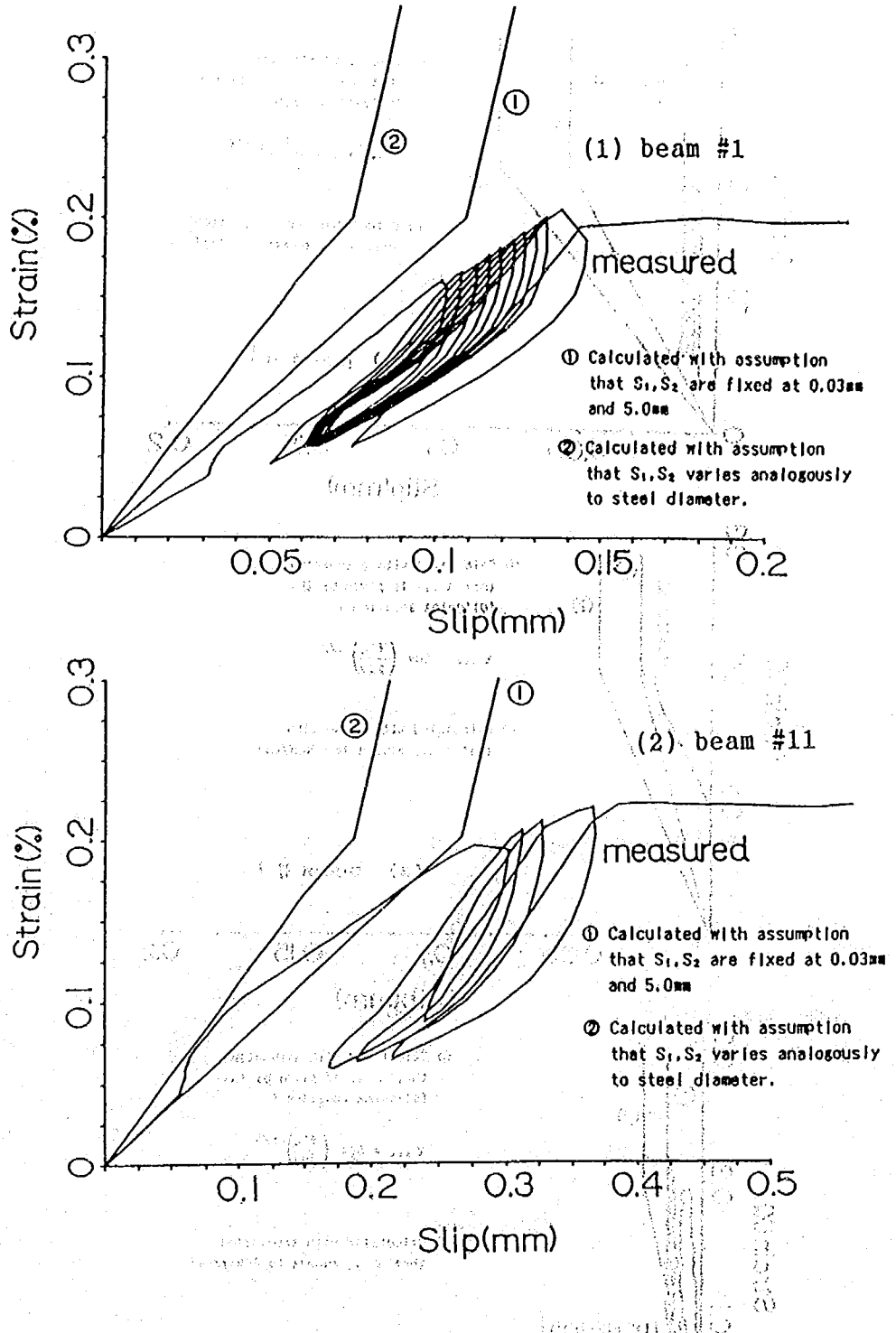

Fig.6 Effect of anchored bar diameter on the tensile strain slip relationship

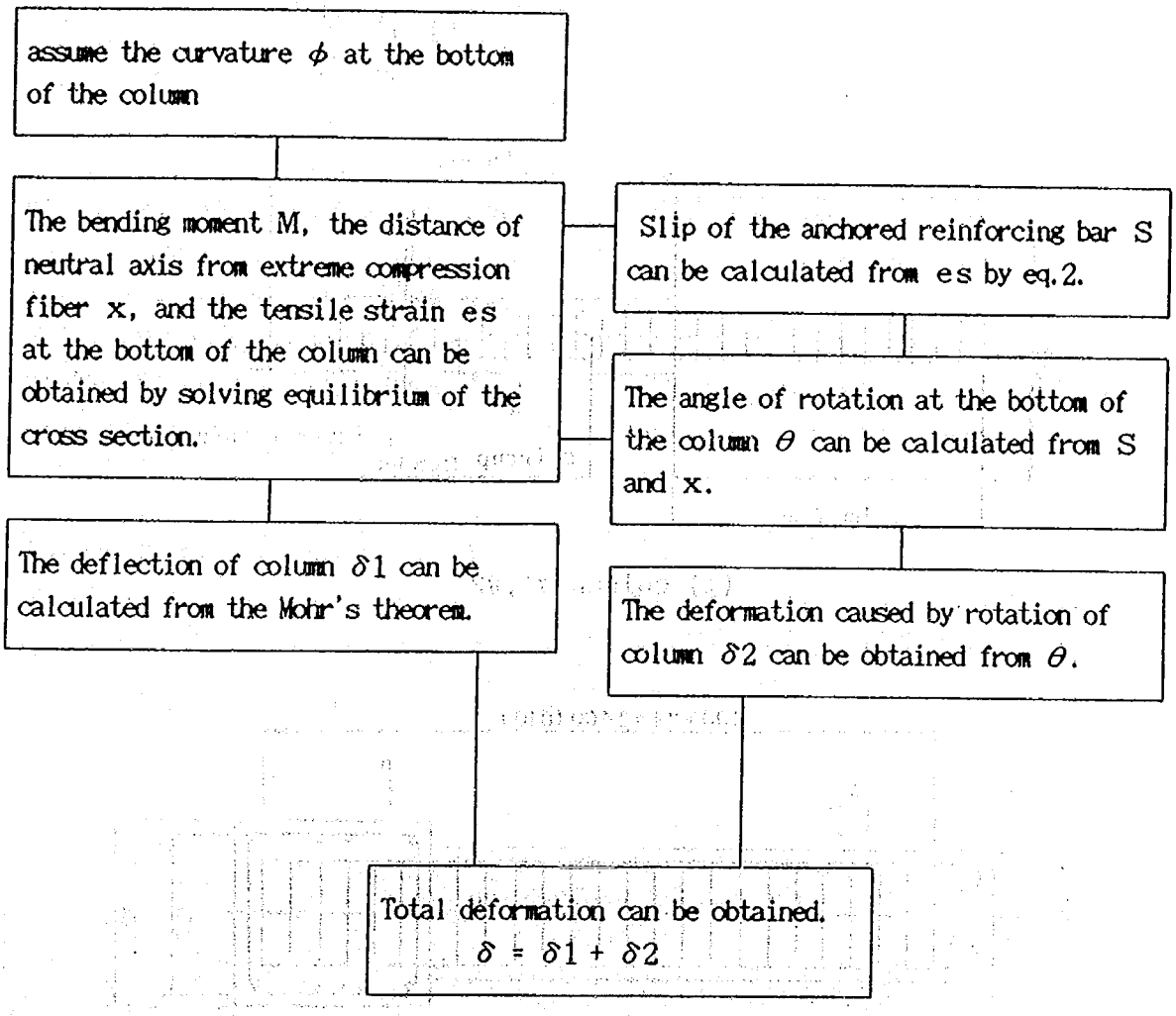

Fig.7 Calculation procedure of δ

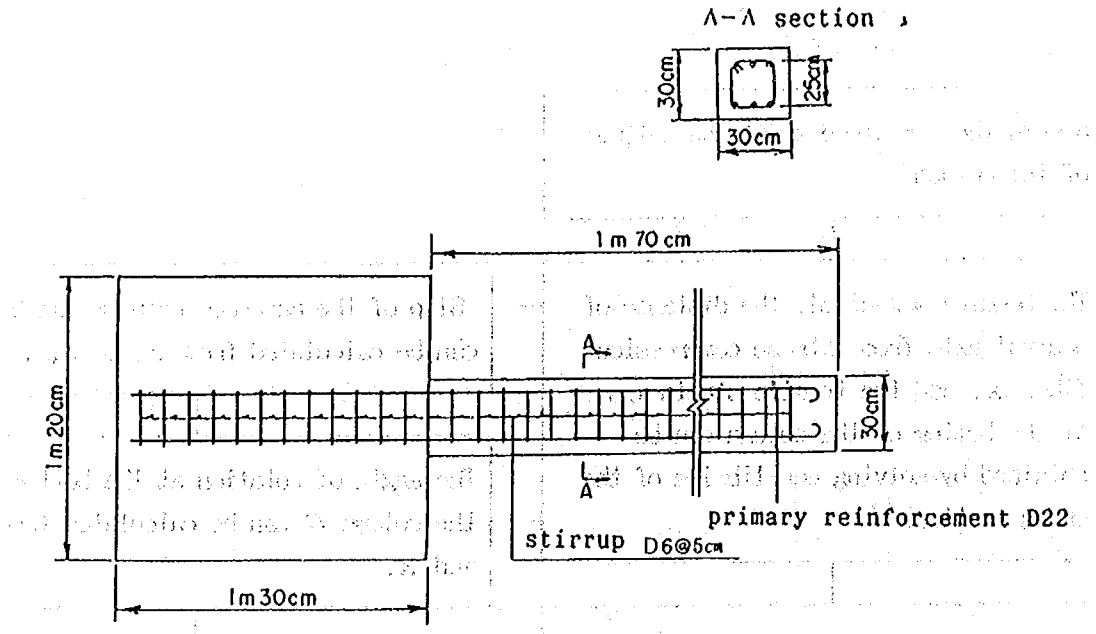

(1) column #1, #2

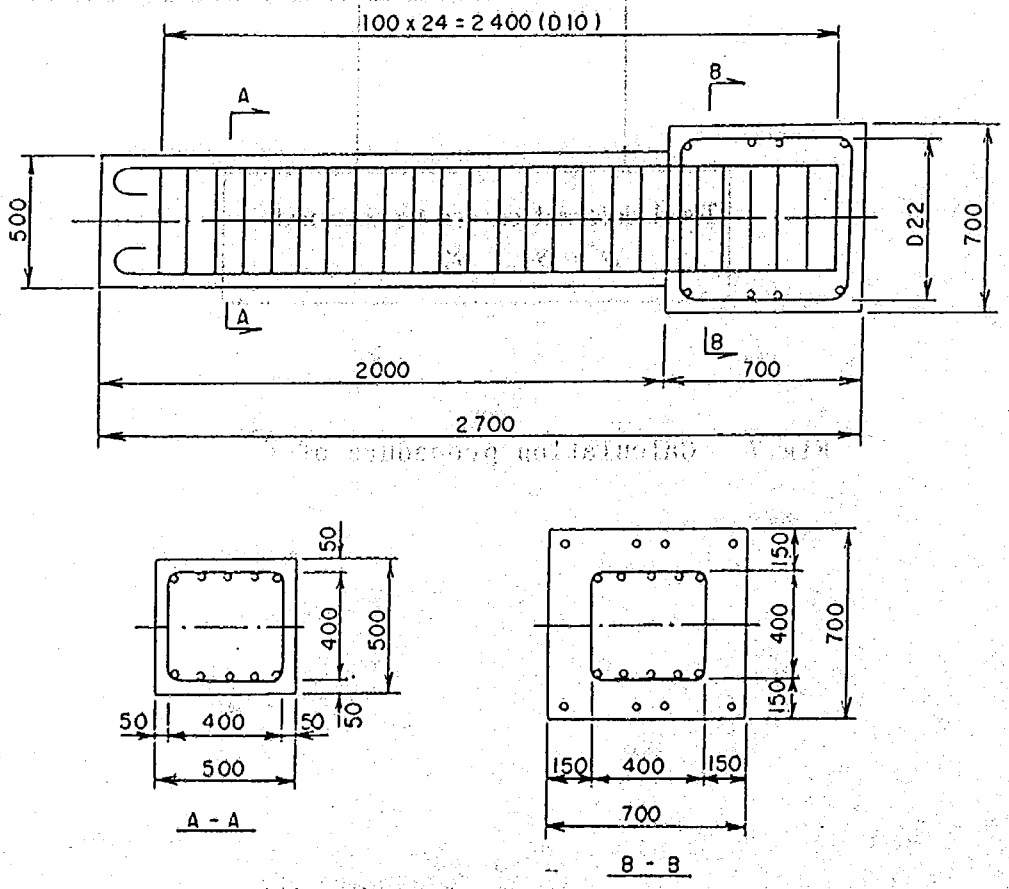

(2) column #3, #4, #5

Fig.8 Dimension of beam specimen

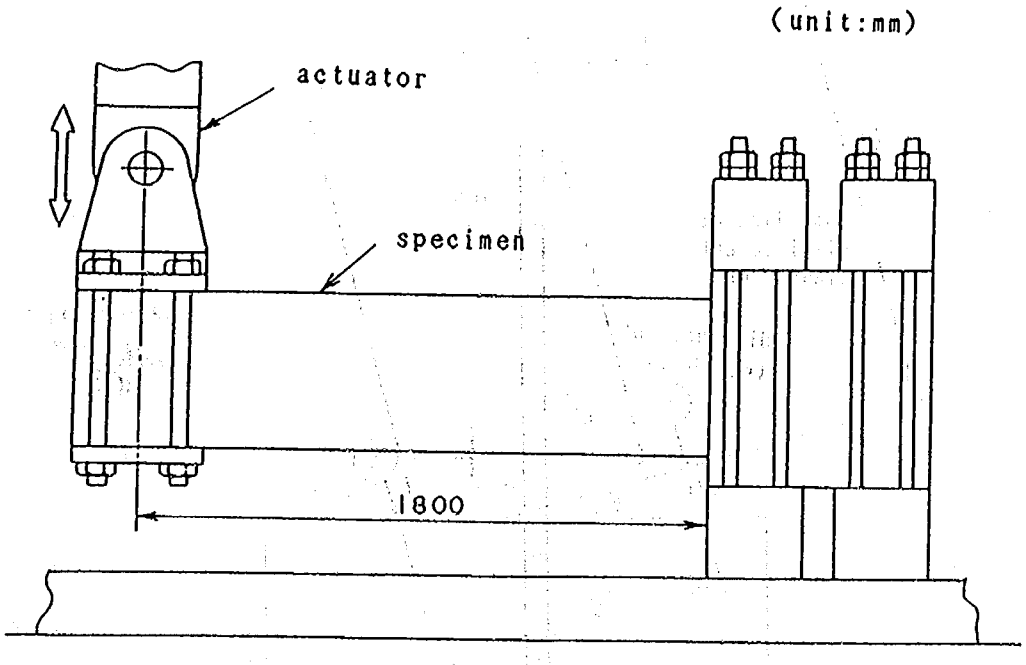

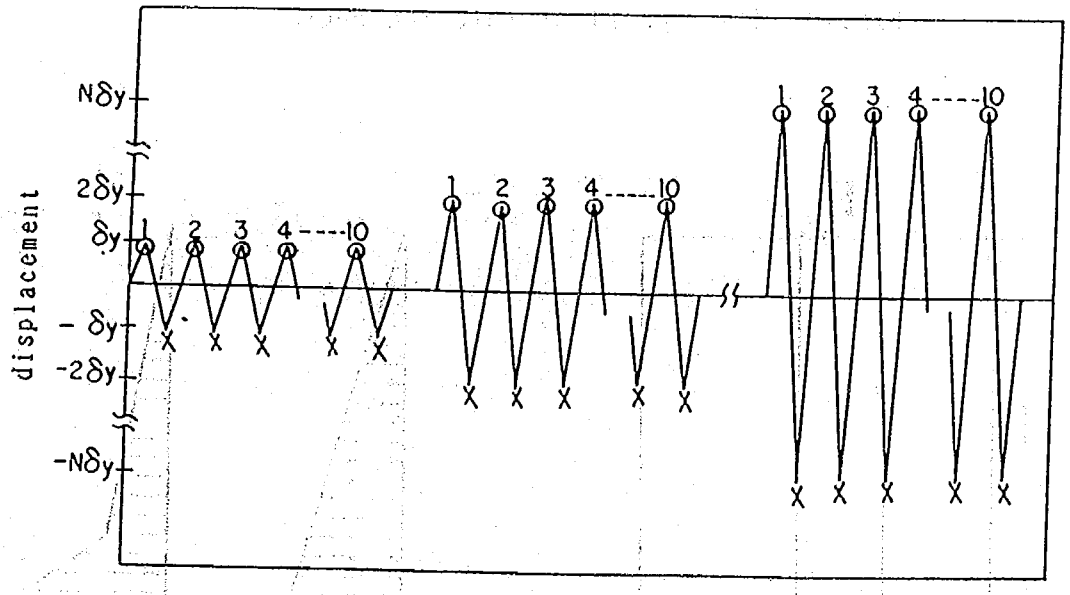

Fig.9 Loading program

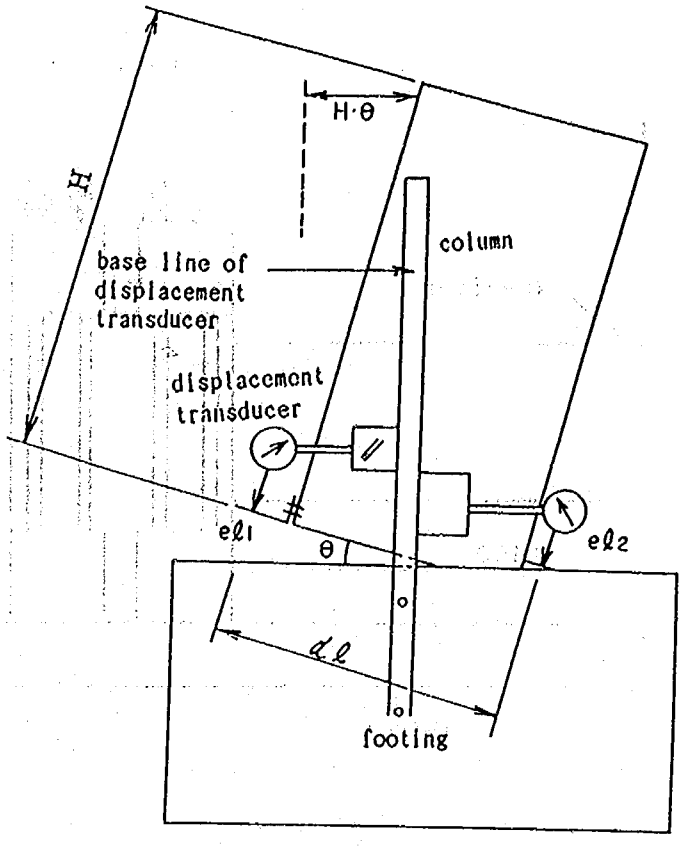

Fig.10 Measurement of rotation angle

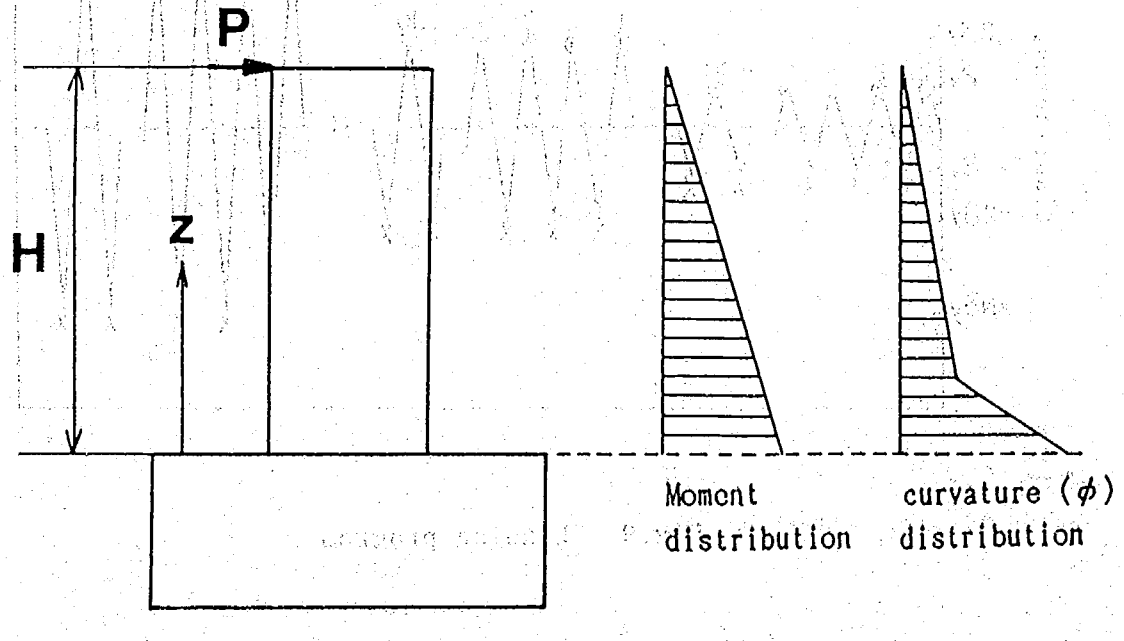

Fig.11 Curvature distribution of the column

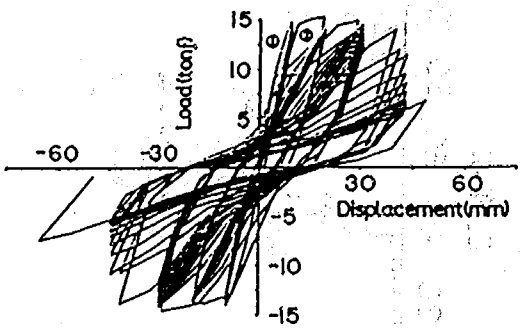

1

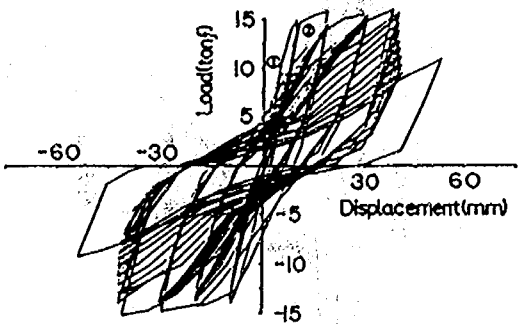

2

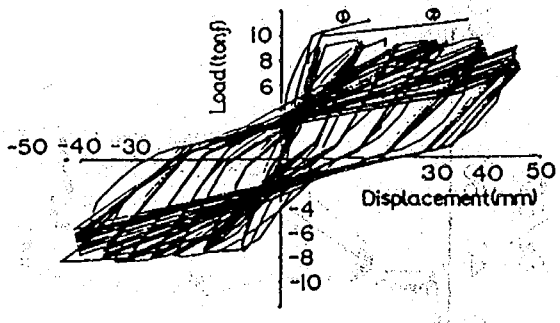

3

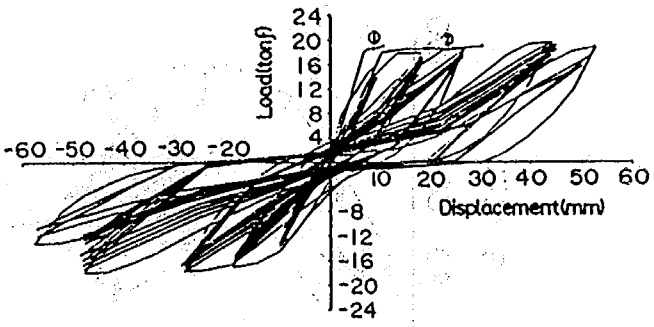

4

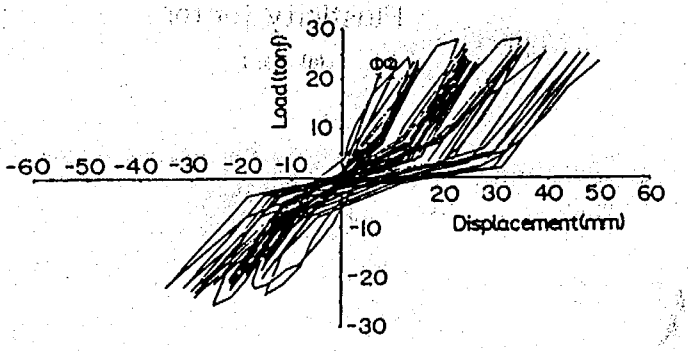

5

Fig.12 Hysteresis loop of column specimens

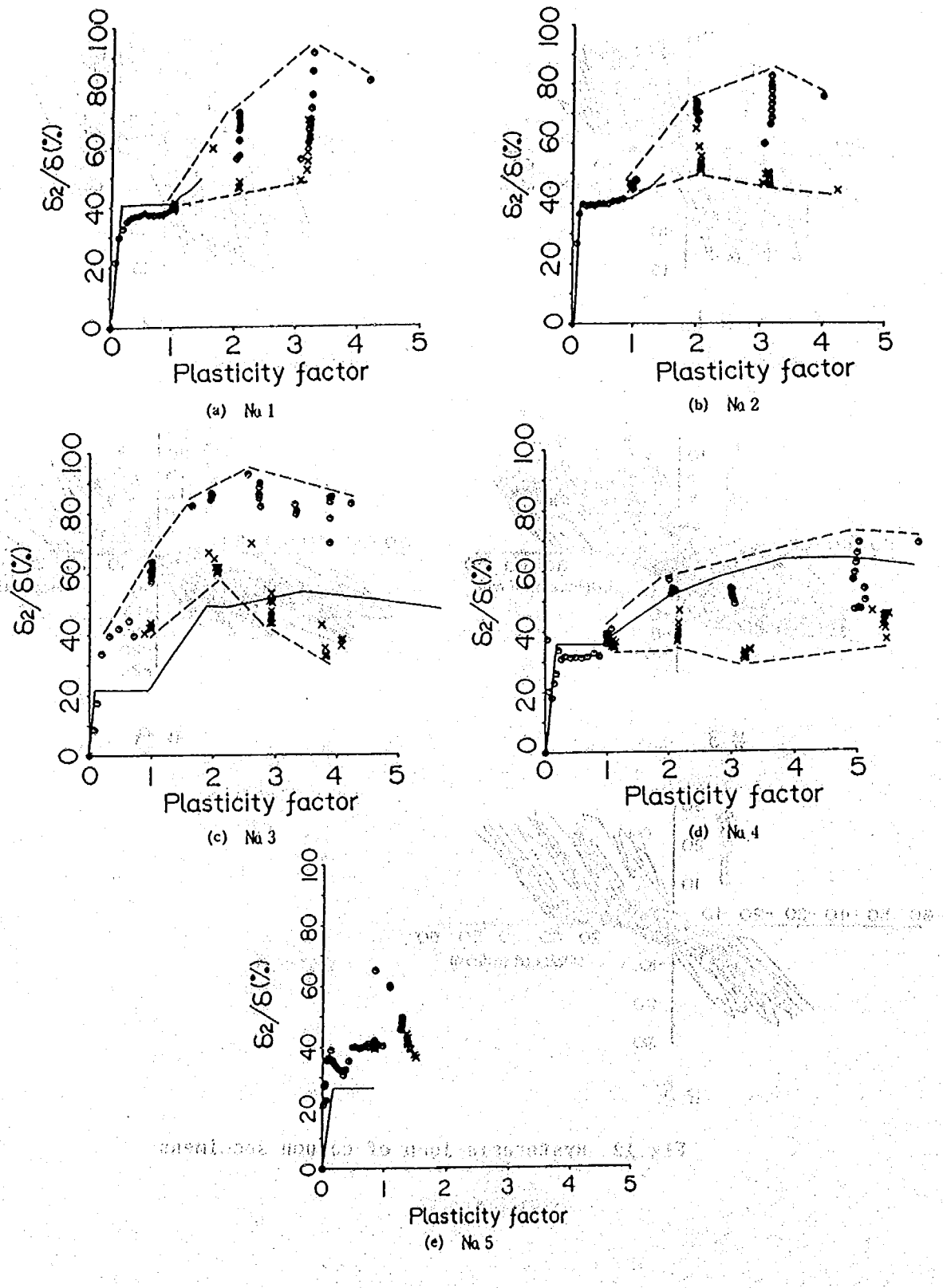

Fig.13 Measured and calcurated δ_2/δ

DESIGN, CONSTRUCTION AND MODEL EXPERIMENTS ON CORNER PARTS OF Y-SHAPE STEEL BRIDGE PIERS

by

Teruyou HASHIMOTO[1], Atsuhiro MAKITA[2], Kiyoshi KOBAYASHI[3]

ABSTRACT

In this paper, model experiments on corner parts and tests on field welding procedure for Y-shape steel bridge piers of elevated bridges for Tokyo metropolitan expressways are detailed.

In order to elucidate stress characteristics and to determine optimum structural details of the captioned corner parts, elastic and load carrying capacity experiments, and finite element analyses were carried out on the one-half scale model, in addition, tests on field welding procedure inside corner parts by using full scale model was executed.

Thus, proposed design guide (draft) for the corner parts of Y-shape steel piers was reflected in the actual design.

1. Preface

The Metropolitan Expressway Public Corp. was established in June, 1959, and in order to relieve and dissolve the road traffic congestion in the existing urban districts of the metropolitan area as well as the city center of Tokyo, the construction of expressways were planned as a complementary measure to principal highways and streets, but now, those play an important role as efficient mainstay roads.

As of January 1, 1991, 220 km as shown in Fig. 1 was put in service, and the number of the cars daily utilizing them was about 1.1 million.

Among them, Itabashi-Toda Expressway line is the route connecting to the extension of No. 5 second stage line, and is the route of 3.7 km total length, which is constructed over the national highway No. 17 (New Omiya Bypass).

The locations of the bridge piers for this route were determined taking account of the street plans of the New Omiya Bypass, underground utilization and so on, further because those cannot be installed in walkways, those were limited to the median strip.

The section concerned is straight in the alignment, but due to the branching and merging influence with the adjoining Bijogi Interchange, the width of the expressway became 20 m~30 m, therefore, with the conventional T-shape bridge piers, the beam length becomes too long, leading to a fear

1 Senior Engineer, Design Division, First Construction Department, Metropolitan Expressway Public Corp., Japan
2 Engineer, Design & Survey Division, Kanagawa Management Department, Metropolitan Expressway Public Corp., Japan
3 Reg. Consulting Engineer, Manager, Steel Structure & Civil Engineering Division, Mitsui Engineering & Shipbuilding Co., Ltd., Japan

as the deflection and vibration of the beams created by running vehicles. Therefore, by increasing the rigidity of the beams and paying attention to the esthetic beauty under bridge girders, it was decided to adopt the Y-shape bridge piers as shown in Fig. 2, and to rigidly connect the main girders with the cross beams.

2. Examination of Y-shape steel bridge piers

As for Y-shape steel bridge pier, there have been only several examples of the execution such as Tatsumi district of No. 9 route of the metropolitan expressways (see Fig. 1) and others, so, this type of bridge pier is relatively new in Japan. In the intersecting part (hereinafter, referred to as corner parts) of V-legs and a column of the pier, since the axis lines of respective members do not intersect at right angle, the conventional design method[1] for corner parts cannot be directly applied. Consequently, in respective examples of the execution,[2),3),4)] various design methods were devised to account for individual technical circumstances.

In the case of No. 9 route, a vertical diaphragm was installed at the corner parts (Fig. 3). In this case, as the five steel plates, that is, the vertical diaphragm, the inner side flanges of V-legs and oblique diaphragms intersect at a point, providing a polygonal steel bar was necessary as shown in Fig. 3 (a).

In this part, a remarkable stress concentration is caused, and installing a highly rigid member like the polygonal steel bar might promote it further. However, from the point of view of fabrication, the polygonal steel bar is necessary, requiring much consideration with respect to welding procedures such as preheating.

On the other hand, in order to omit the polygonal steel bar, it is necessary to examine the effect of the vertical diaphragm regarding the stress distribution and the load carrying capacity in the elastic region, and to examine the structural details comprising the upper flanges and oblique diaphragms as shown in Fig. 3 (b), including the selection of steel materials and welding procedure.

According to the considerations mentioned above, it was decided to carry out elastic experiment, load carrying capacity experiment and finite element analysis on the models of this corner parts (two models in total with and without the polygonal steel bar and the vertical diaphragm) in order to grasp the stress characteristics and to study on the structural details.

3. Model experiment on the corner parts

3.1 Method of model experiment

(1) Items of experiment

Two types of experiments, the elastic and the load carrying capacity, were carried out. The former was for examining the stress distribution in the corner parts, and thus obtaining the data to determine the cross sectional dimensions. The latter was aimed at examining the behavior of stress and deformation in the vicinity of the ultimate limit states and

verifying the appropriateness of the structural details of the corner parts.

(2) Design of the models

Two kinds of models were fabricated with and without the polygonal steel bar at the flange intersection of the V-legs. Hereinafter, the model without the polygonal steel bar and the vertical diaphragm is called model A, and the model with them is called model B.

As for the scale and similarity ratio of the models the general dimensions were made into 1/2, taking account of the design, fabrication and transport but as to the plate thickness, the parameter R of width to thickness ratio was adjusted. The particulars of the flange part of the models are shown in Table 1 in comparison with the actual bridge pier.

(3) Loading method and loading cases

The experiment was carried out in the large-structure testing laboratory of Research Institute of Science and Technology, Faculty of Science and Technology, Nihon University.

1) Elastic experiment

The models were placed horizontally on the test floor using skids. For loading, center hole jacks and PC steel bars were employed. Since it is difficult to directly load unit sectional force on the V-legs, the seven cases shown in Table 2 were carried out to determine the strains due to unit load by establishing the simultaneous equations. Attention was paid to axial force in cases 1~3, to shearing force in cases 4 and 5, and to bending moment in cases 6 and 7, respectively. In the cases 4 and 6, horizontal reaction skids were used, but the other cases were self equilibrium state. In respective cases, the measurement was carried out by loading twice at intervals of 0.1 times of the maximum load in Table 2.

2) Load carrying capacity experiment

A 3000 t large-structure testing machine was used for the loading case 3 of the elastic experiment. (Photograph 1). Loading was applied on the columns of the models standing upside down, and hinge shoes which can move horizontally were attached at V-legs. At the time of loading, first, two cycles of the elastic loading was carried out to confirm proper loading and bearing fitness of the shoes. Next, the load was increased at intervals of 20 t, and in the vicinity of the maximum load, the loading was carried out by displacement control.

(4) Measuring system

Referring to the results of the finite element analysis, the measuring points of strain were set up concentrating in the corner parts and the vertical diaphragm, and strain was measured at about 1,100 points per one model. In the vicinity of the maximum load in the latter half of the load carrying capacity experiment, the strain speed increased, therefore in order to improve the accuracy of the data, about 500 points were measured using a high speed data logger. The list of the measuring instruments used

for this experiment is shown in Table 2. Strain, displacement and load (by load cell) were all converted to electrical quantities by a data logger, and then transferred to a computerized measuring system.

(5) Data processing

From the above explained seven sets of loading cases, strains ϵ_M, ϵ_N and ϵ_S for unit sectional forces shown in Fig. 5 (c) can be obtained by the following simultaneous equations resulted from basic loading conditions shown in Fig. 5 (b).

$$M_1\epsilon_M + N_1\epsilon_N + S_1\epsilon_S = \epsilon_1$$

$$M_2\epsilon_M + N_2\epsilon_N + S_2\epsilon_S = \epsilon_2$$

$$M_3\epsilon_M + N_3\epsilon_N + S_3\epsilon_S = \epsilon_3$$

Stresses calculated from ϵ_M, ϵ_N and ϵ_S are defined as the upper and lower limit values for 90% reliable zone.

3.2 Numerical analysis

In order to evaluate the measured values obtained through the elastic experiments for in-plane loading and to calculate the stresses due to out-of-plane loading, the finite element analysis (using the program NASTRAN) was carried out.

Analysis models were A and B of the scale models, A of the actual bridge pier and A of the out-of-plane scale model. In the finite element analysis, rectangular plane shell element were employed for the outer plates and the diaphragms, and bar element for the longitudinal ribs. Boundary conditions were set that the column end is built in, and at the top of the V-legs, unit load was applied by converting to nodal loads. Stresses for the cases of the elastic experiments were determined by combining these unit loading cases. Examples of mesh division are shown in Fig. 6.

Moreover, in order to determine the position, at which the maximum stress occurs in the actual bridge pier, the results of the finite element analysis for unit loading and those of the space frame analysis for the actual bridge pier were summed by a personal computer.

Besides, as the analysis on the displacement which correspond to the load carrying capacity experiment, the plane frame analysis taking shearing deformation into account was carried out.

3.3 Confirmation tests on field welding procedure for corner parts

Due to the fact that the bridge construction site is located inland area, Y-shape corner parts had to be divided into the transportable size in conformity with the Law on Road Traffic, resulting in the joints of field welding, in which the weld lines of these are inclined by 30° to horizontal line, consequently, some welding work has to be executed with oblique overhead position. In this experiment, considering the specialty of the corner parts of Y-shape bridge piers, deformation characteristics due to welding, welding procedure, thermal control and quality of welded parts

were examined by using the full-scale model around the field welding parts (material: SM58, t = 33 mm). Besides, in the experiment of this time, two sets of steel jigs for preventing the distortion due to welding were installed at the time of web welding, and four sets were installed at the time of welding of inner and outer flanges (Fig. 7).

4. Experimental results and discussions

4.1 Stress coefficient

The stress condition in the corner parts is complicated due to various factors such as stress concentration, shear lag, plate bending and so on. Moreover, in this work section, since the pier is rigidly connected with superstructures, the sectional forces of both in-plane and out-of-plane arise in bridge piers, making the stress condition much more complicated. Therefore, considering the convenience for practical design, the following formula to calculate stresses in the corner parts was introduced.

(Stress in the corner parts)
= (Basic stress) x (Stress coefficient)

Basic stress is of the one obtained from the conventional beam theory by assuming the whole cross section to be effective, and stress coefficient is of the one introduced by taking the above explained complicated factors into account. Accordingly, the stress coefficient was determined by dividing the values measured at the corner parts by the basic stress.

As for the stress coefficient related to in-plane sectional force, the elastic experiment values were taken as the basis. On the other hand, considering that out-of-plane sectional force is secondary compared with the in-plane force, and in the in-plane stress coefficient, the experimental values showed good agreement with the finite element analysis values, the value by the finite element analysis was adopted as the out-of-plane stress coefficient.

Besides, as for the in-plane stress coefficient, the upper and lower limit values of the 90% reliable zone of the experimental values were adopted. This is because, in the case of using only the upper limit value or the most probable value, when the contributions from respective sectional forces act negatively, the result becomes dangerous side. The values of respective stress coefficients are shown in the next section.

4.2 Elastic experiment

The measured values were statistically processed, and the results of the stress distribution for unit sectional force are as follows.

(1 In Fig. 8, the principal stress diagrams for the webs and vertical diaphragm of the models A and B are shown together with the results of the finite element analysis. In the finite element analysis, the smallest mesh was 35 mm (about 2.7 times of lthe plate thickness 13 mm). According to Fig. 8 (a) and (b), the experimental values and the finite element analysis values agree well, and not much difference can be observed on the stress flow between A and B. In Fig. 8 (c), it is known that the stress at the middle part of the vertical diaphragm is small.

② According to the space frame analysis and finite element analysis, a dominant stress due to actual load occurred at the corner part (the element near web) of the curved surfaces of the outer flanges of V-legs (R = 3.5 m in the actual bridge piers), that is, in the vicinity of the joining parts with the oblique diaphragm (Fig. 9). In addition, the stress distribution due to the unit sectional force determined from the experimental results showed nearly the same position as shown in Fig. 9.

③ The in-plane stress coefficients at this point are shown in Table 4, and the values of A were somewhat small compared with B. Besides, the comparison between the model and the actual bridge pier of model A shows good agreement, and thus it is known that the law of similarity was realized. The stress coefficients of the model A are shown in Table 5 together with the out-of-plane stress coefficients.

④ The region of the corner parts was defined herein as shown in Fig. 10 referring to experiment and the finite element analysis.

4.3 Experiment on load carrying capacity

In the vicinity of the maximum load, the loading by displacement control was carried out, and finished at the limit, about 50 mm of the horizontal displacement of supporting shoes. The main results of the experiment were as follows.

① In Fig. 11, the load-horizontal displacement curves for the top of V-legs are shown. In the linear part, the horizontal displacement (the mean value of four supports) was somewhat small in the model B, but the difference from that of the model A was small, and both nearly agreed with the values of the frame analysis taking shearing deformation into account. As for the horizontal displacement of respective shoes of the model B, that of the right leg was small compared with the model A, and the difference between the left and right legs was large.

② The collapse made was the same in both models, and the outer flanges of V-legs buckled inward as the whole stiffened plates (Fig. 12, Photograph 2). The maximum load was 880 t in the model A, and 980 t in the model B. In this connection, the value of the trial calculation on the load carrying capacity by regarding the outer flanges as the stiffened plates subjected to pure compression, and by using the load carrying capacity curves in the Specifications for Highway Bridges was 900 t. According to the measured values in both models, the buckling deformation arose when the outer flanges nearly reached the yield strain, and it corresponded with the region of the parameter of width to thickness ratio R (= 0.342) < 0.5 for the load carrying capacity curves in the Specifications for Highway Bridges.

③ As shown in Fig. 13, the expansion of plastic region propagated faster in the model A, but both were nearly the same degree under the load level taking the difference in the maximum load in consideration. The distribution in the model B was somewhat asymmetric in the left and right legs. In both models, in the vicinity of the intersection between inner flanges of V-legs (in the model B, the polygonal steel bar portion), yielding occurred at relatively low load, but the plastic region did not expand to adjoining zone, and remained in the local

region.

④ The strain of the vertical diaphragm in the model B maintained linearity up to about 700 t, and was about 1200 μ in the vicinity of the maximum load. As to the strain of the oblique diaphragms, the difference between both models was small, and also the magnitude of strain was small.

4.4 Experiment on procedure of field welding

(1) Deformation

1) Measurement of grooves

The web plates were precedently welded, and by the contraction due to this preceding welding, in the grooves of the inner and outer flanges which are not yet welded, the root gap decreased by 0.5~0.8 mm on the average. Consequently, at the time of fabrication in the factory, a proper value of the root gap which is to be welded later is the standard root gap plus about 1 mm, and the tight fitness length at both ends for maintaining groove shape requires about 2 t a little longer than 1.5 t (50 mm) in this experiment.

2) Out-of-plane distortion

Though the jigs for preventing distortion were used, the out-of-plane distortion occurred in the vicinity of weld lines, that is, about 3 mm at maximum in the webs of 2 m long, and about 7 mm at maximum in the flanges of 3 m long, were observed.

3) Slip between splice plates and longitudinal ribs

By fastening more than 50% of the total number of high strength bolts, the slip due to welding temporary tack-welding did not occur.

(2) Welding method

1) For all three positions of oblique overhead, horizontal and flat, CO_2 one-side penetrated Uranami welding method was adopted.

2) "PICO-MAX 2" was employed for all three positions, as a multipurpose gas shield automatic welding machine.

(3) Thermal control

1) Preheating with electric panel heaters

When the atmospheric temperature was 15~23°C, in order to carry out welding above 80°C, which is the prescribed temperature, it was found that considering the time of temperature drop, it was necessary to operate heaters about 90 min before welding work, and to finish the welding within about 40 min after the heaters were removed.

2) Quantity of heat input

In the experiment of this time, the one-side Uranami welding of

CO_2 welding was employed, and the maximum quantity of heat input per one pass reached about 40,000 joule/cm.

3) Interpass temperature

As for the upper limit value, "not higher than 230°C", which is the specified temperature for HT 70 and 80 of Honshu-Shikoku Bridge Authority, was adopted.

(4) Quality assurance for welded parts

1) Appearance inspection

In the measurement of the height of weld reinforcement and the appearance inspection, there was not any problem.

2) Nondestructive inspection of welded parts

Automatic ultrasonic flow detection test and radiographic test were carried out, and the results were within specified values.

5. Conclusion — Determination of corner parts structure

First, according to the elastic experiment and the finite element analysis, the in-plane stress coefficient of the model A was small compared with the model B. Moreover, the stress at the middle part of the vertical diaphragm in the model B was small. Next, the difference in the maximum load between both models by the experiment on load carrying capacity is not considered as appreciably large inspite of the effect of the restraint of horizontal displacement at the time of initial loading. Further, considering the strain condition in each member including the vertical diaphragm, the propagation of plastic region and so on, it was judged that there is not any significant difference between A and B.

On the other hand, there are some advantages in the model A such as the reduction of excessive heat control process because of without the polygonal steel bar, the improvement of welding work conditions resulted from the omission of the vertical diaphragm and the reduction of steel weight. In addition, judging from the geometry of welding joints, or the improvement of the lamination resistant performance of steel plates, there would be no lamellar tear in the intersection between inner flanges. Accordingly, it was decided to adopt the model A which can avoid stress concentration as far as possible so that the stress flow is more smooth. Moreover, the quality of the welded parts by oblique overhead welding within the region so-called "corner parts" was about the same as compared with ordinary field welding. Based on these considerations, the design guide (draft) for the corner parts of Y-shape bridge piers including the stress coefficient and the region of the corner parts was proposed.

By the way, because this design guide (draft) aimed at reflecting it to the practical design, the various structural particulars are limited. Consequently, as the subjects for hereafter, it becomes necessary to examine the case in which the curvature of the outer flanges and the intersecting angle of the axis lines of V-legs are different.

References

1) Okumura T., Ishizawa N., "The Design of Knee Joints for Rigid Steel Frames with Thin Walled Section", The Proceedings of the JSCE, 1968.5 (in Japanese)

2) Matsumoto K., Tomizawa S., Eya S., "Design and Construction of Elevated Bridges with Y-shape Piers," "Bridge and Foundation", 1979.5 (in Japanese)

3) Metropolitan Expressway Public Corp., Kawada and Nissha No. 924 JV, "Report on Test and Analysis for Corner Parts of Y-shape Steel Piers", 1976.3 (in Japanese)

4) Nagoya Expressway Public Corp., Japan Association of Steel Bridge Construction, "Report on Test and Design Method for Corner Parts of Y-shape Piers", 1989.3 (in Japanese)

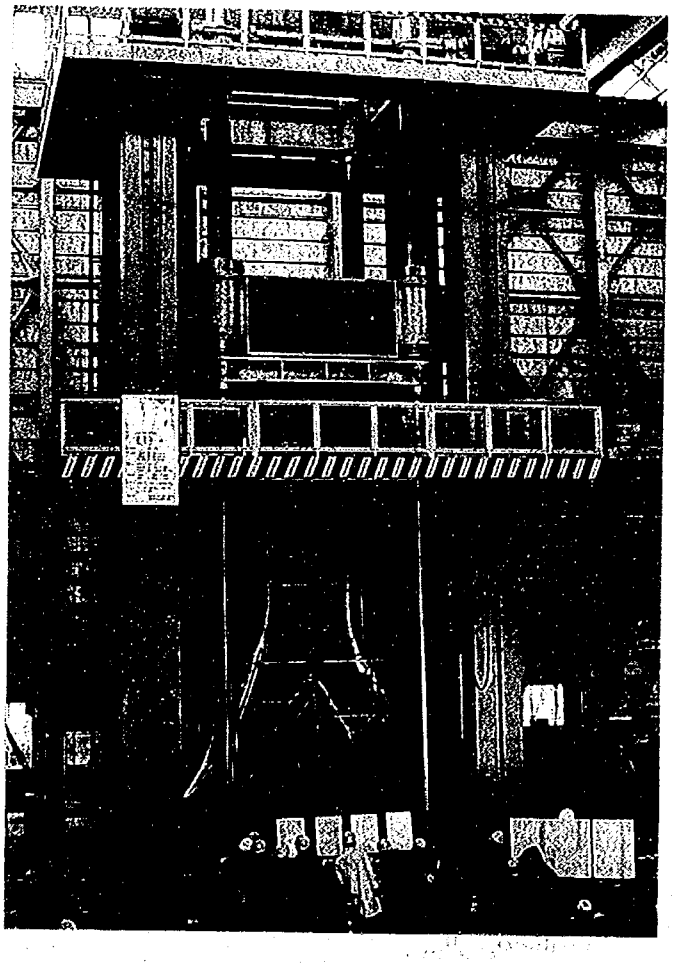

Photo-1 Experiment on load carrying capacity

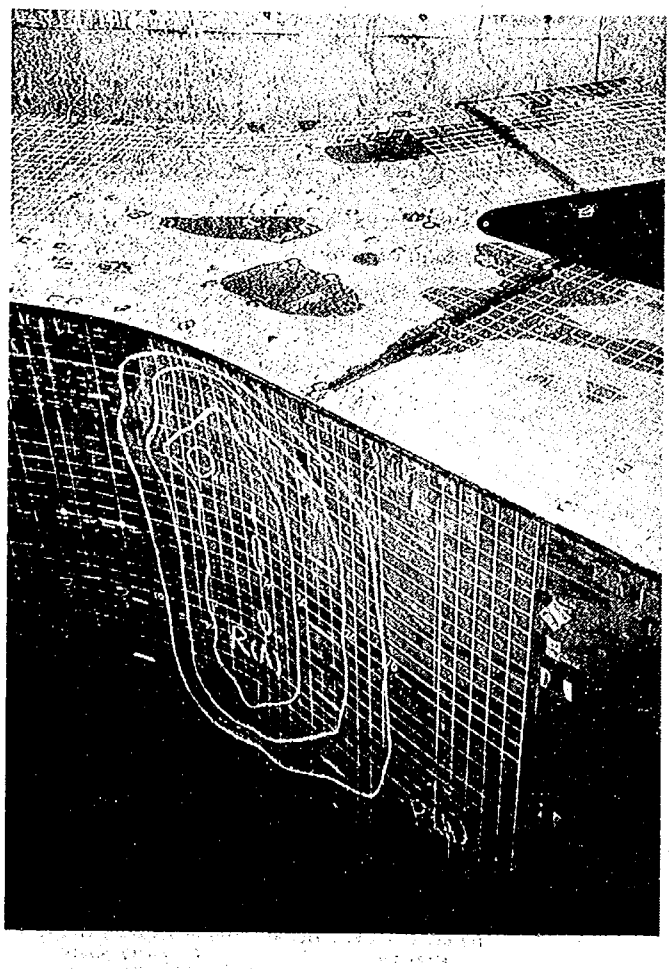

Photo-2 Deformation after buckling

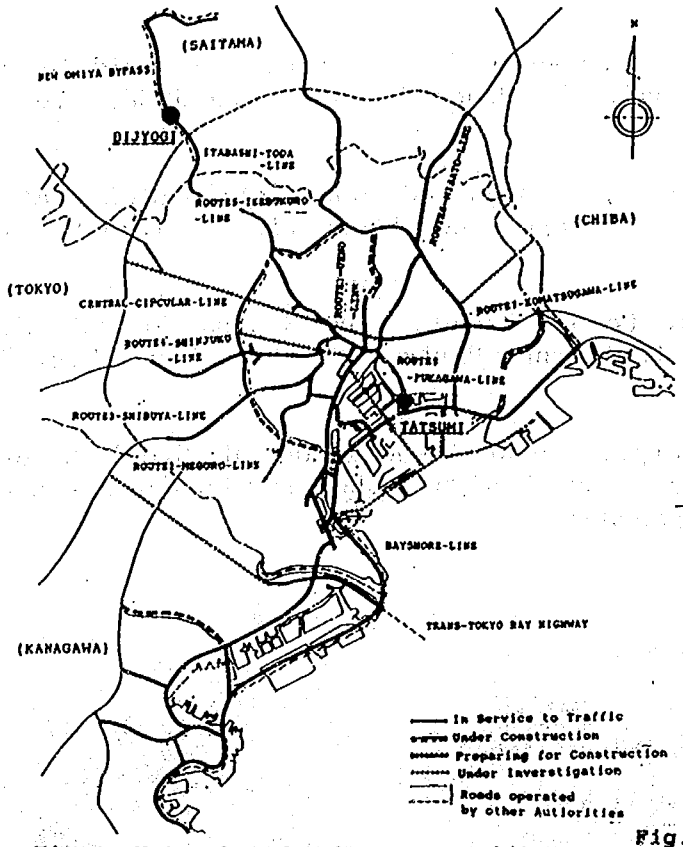

Fig.1 Networks of Tokyo Metropolitan Expressway

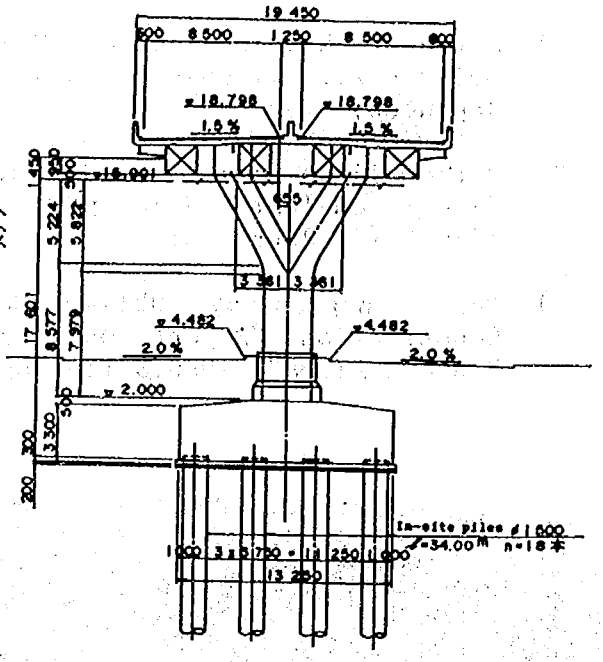

Fig.2 General view of Y-shape steel pier

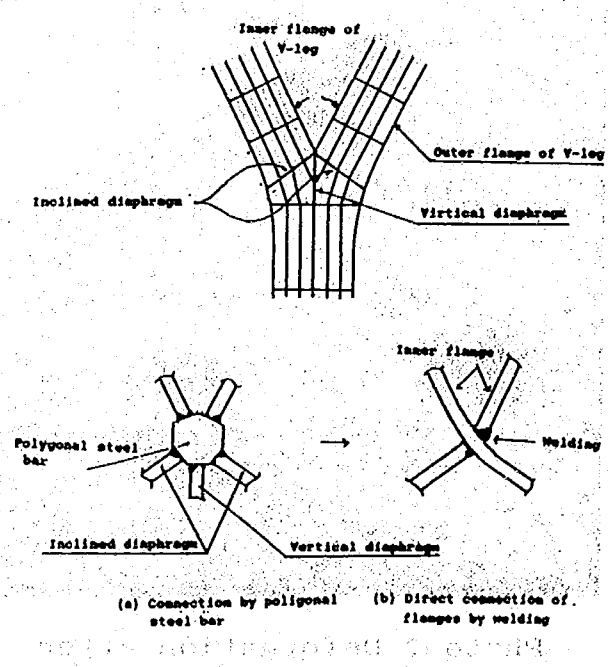

Fig.3 Details at V-leg intersection between inner flanges and diaphragms

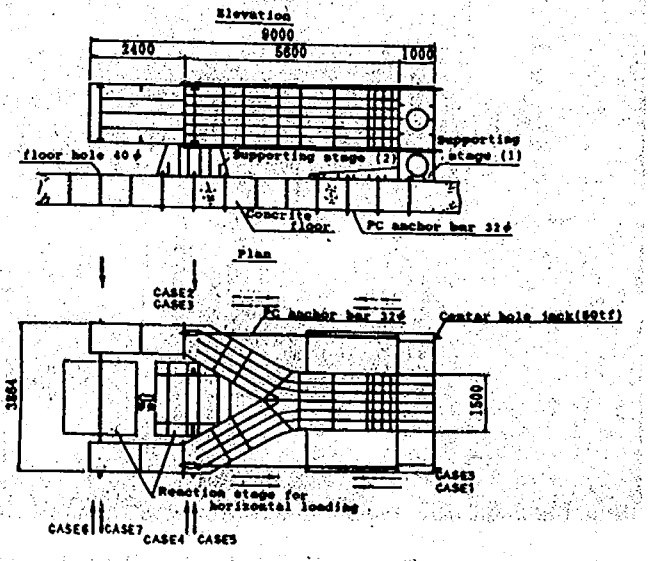

Fig.4 Arrangements for elastic experiment

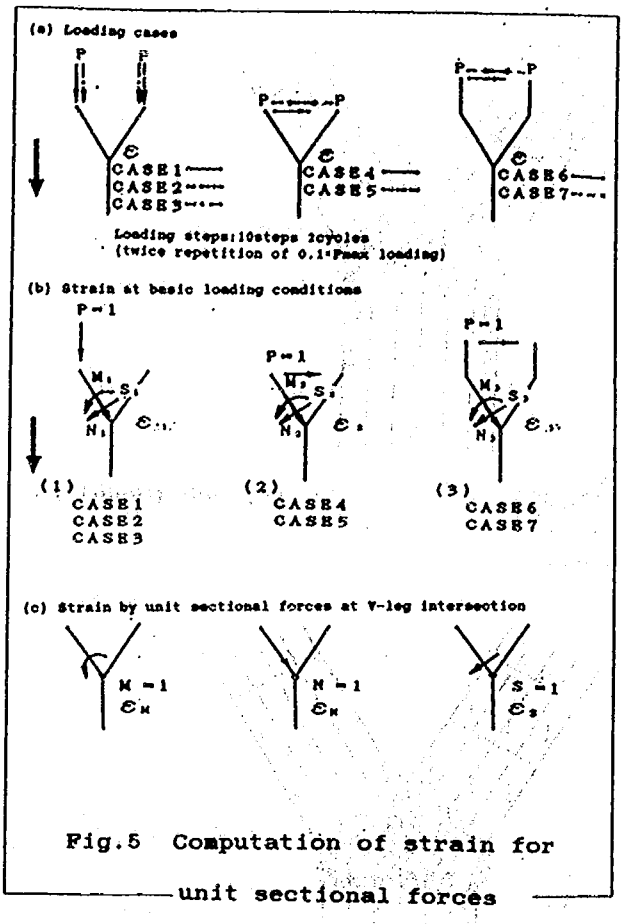

Fig.5 Computation of strain for unit sectional forces

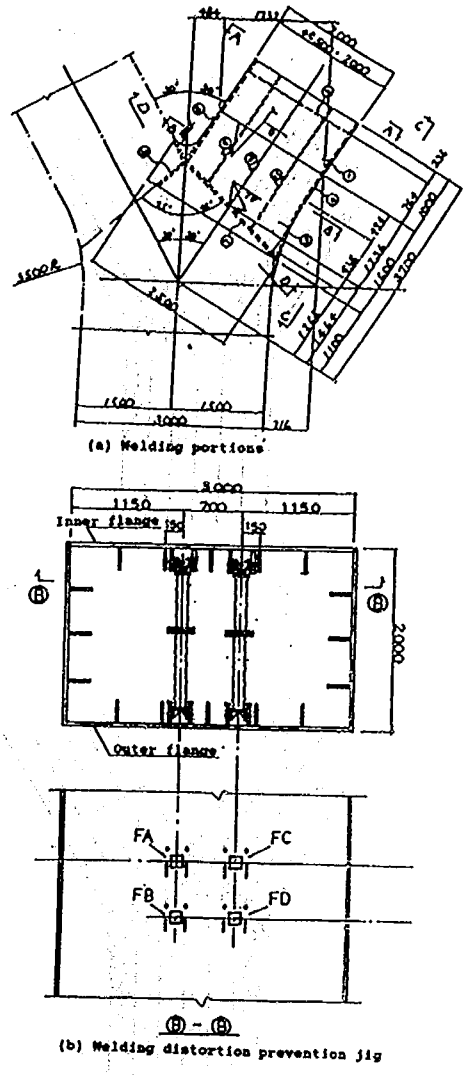

Fig.7 Experiments for site welding procedure

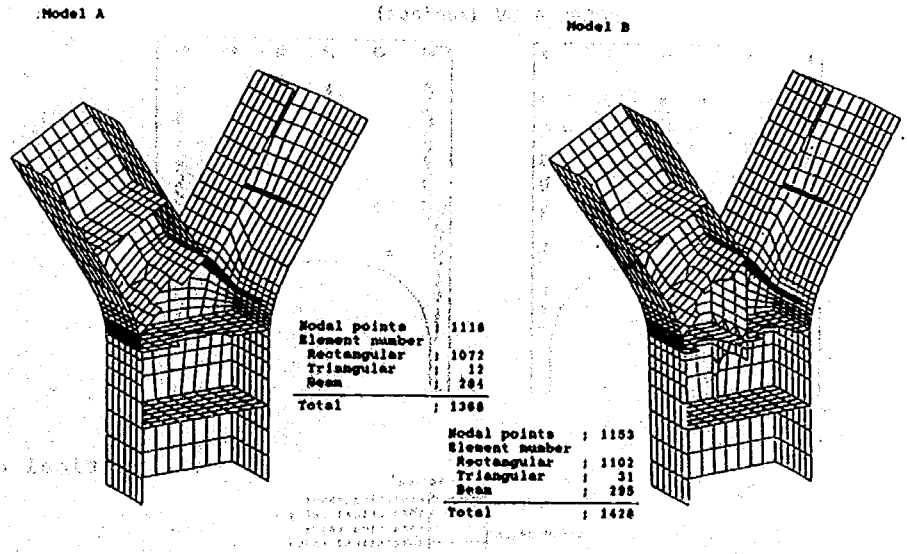

Fig.6 Meshing for FEM analysis

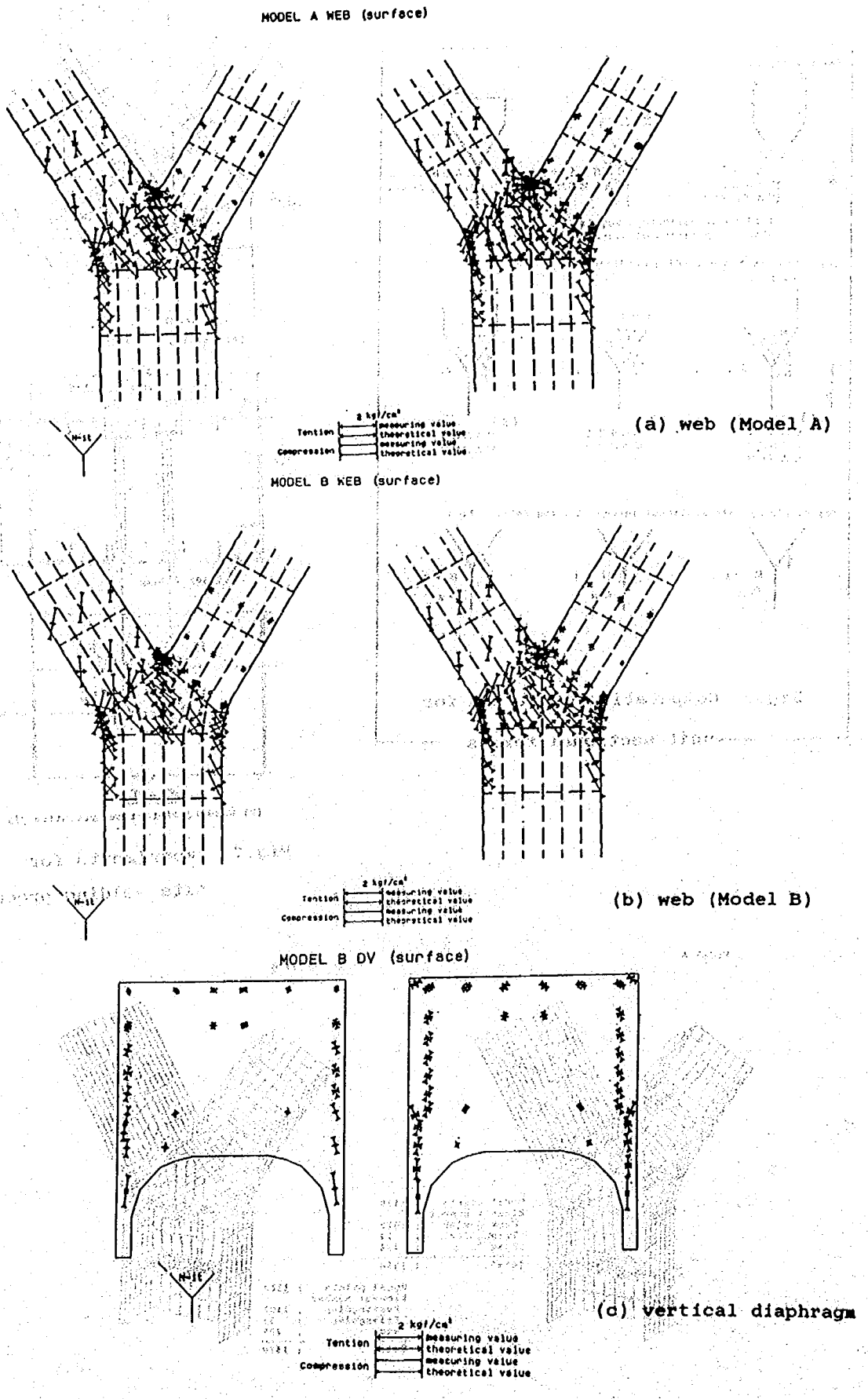

Fig.8 Principal stress diagrams

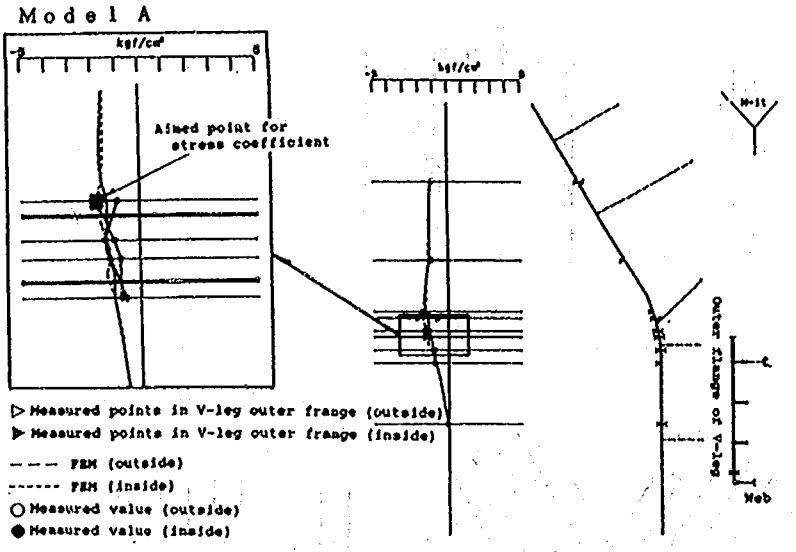

Fig.9 Normal stress distribution of outer flange at curved region

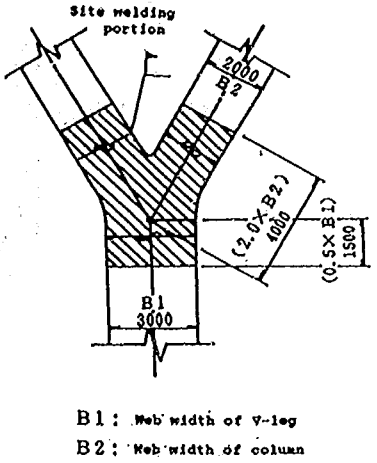

Fig.10 Definition of corner parts

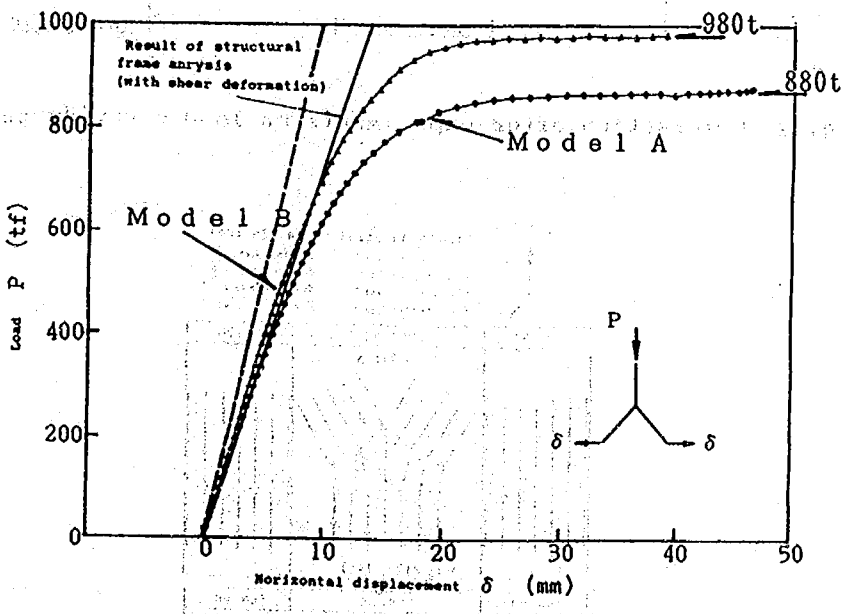

Fig.11 Load-displacement curves

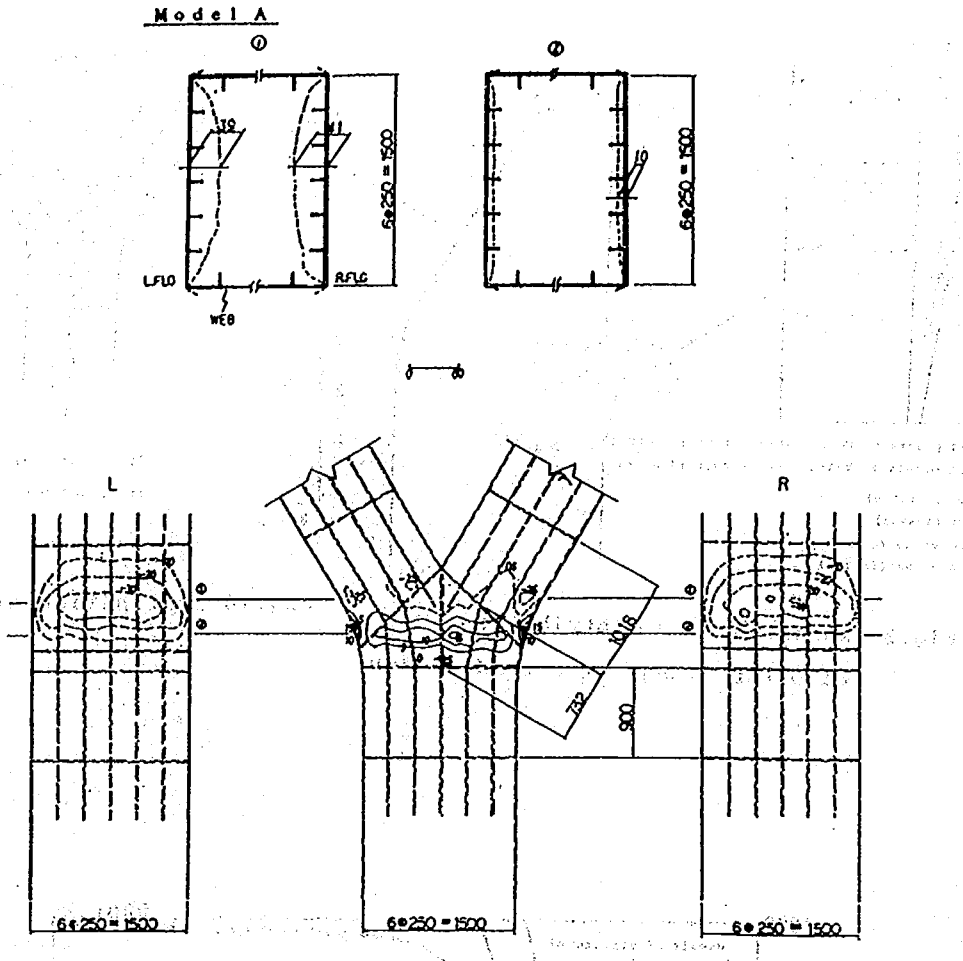

Fig.12 Deformation after experiments on load carrying capacity

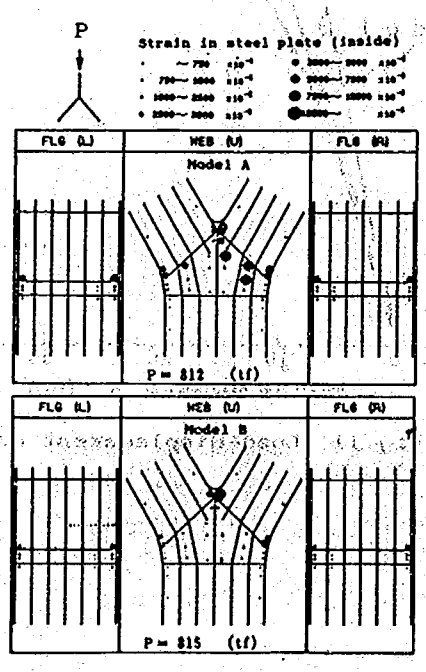

Fig.13 Distribution of plastic zone

Table 1 Comparison on main particulars between actual pier and experimental model

	Actual pier	Experimental model
Flange	3000×32	1500×13
Longitudinal rib	230×22	90×13
Panel number	6	6
Steel material	SM50Y	SS41
Width vs.thickness parameter R (R)	0.340	0.342
Width vs.thickness parameter R (F)	0.356	0.358

Table 2 Loading cases for elastic experiment

Loading case	Max. Load	Loading condition
1	80 t (40t)	
2	80 t (40t)	
3	50 t (25t)	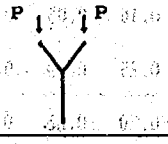
4	40 t (20t)	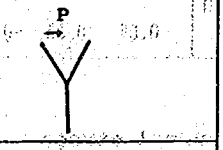
5	30 t (15t)	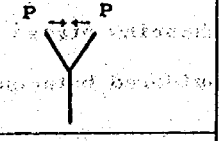
6	20 t (10t)	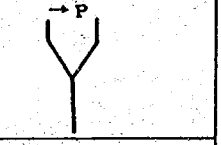
7	15 t (75 t)	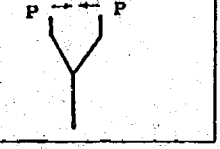

( ): Load per one PC steel bar

Table 3 Equipment list for measurement

Equipment	Typename	Quantity	Capacity
Strain gage	FLA-3-1L (1 axis gage)	306	Gage 3mm
	FRA-3-1L (3 axes gage)	617	Gage 3mm
Displacement-meter	COP100	9	100mm
	COP 50	16	50mm
	COP 25	10	25mm
	COP 10	4	10mm
Load cell	CLC-100A	4	100t
Switch box	SHH-50A	10	50
	ASH-50A(AH)		50(A, AH, B)
	[30A]orASH-50B		50
	[30B]	700	30(A, B)30
Data logger	TDS302	3	–
	THS 1000	1	–
Data processing computer	PC98 PL	4	–

Remarks:Number of gage shows total of model A and B.

Table 4 Stress coefficients on in-plane sectional forces

Loading on left leg		Experiment	FEM on model	FEM on actual pier
Model A	Bending	-1.45 ~ -1.00	-1.33	-1.23
	Axial force	-1.85 ~ -1.40	-1.78	-1.73
	Shearing force	0.15 ~ 0.60	0.62	0.62
Model B	Bending	-1.60 ~ -1.20	-1.33	
	Axial force	-2.20 ~ -1.80	-1.90	
	Shearing force	0.45 ~ 0.75	0.63	

Table 5 Stress coefficients on left leg

	For sectional forces acting on left leg			For sectional forces acting on right leg		
	In-plane sectional forces		Out-of-plane sectional forces	In-plane sectional forces		Out-of-plane sectional forces
	1 My	2 Nx	3 Sz	4 Mz	5 Tx	6 Sy	7 My	8 Nx	9 Sz	10 Mz	11 Tx	12 Sy
Kσ	1.00	-1.85	-0.80	∓1.15	±0.05	∓0.75	0.15	0.05	0.30	∓0.15	±0.35	∓0.15
	1.45	-1.40	-0.15				0.25	0.50	0.50			
Kτ	-0.25	0.00	0.00	0.20	-0.80	-0.70	-0.20	-0.25	-0.55	-0.15	-0.30	0.25
	0.00	0.05	0.55				-0.05	-0.05	-0.05			

Kσ : Stress coefficient on normal stress

Kτ : Stress coefficient on shearing stress

Conbination must be considered between section forces to obtain maximum stress.

(8) Session 8

SESSION 8: DESIGN METHOD(2)

10:50am～11:50am

(Co-Chairmen: M. Fujiwara, J. Kulicki)

(22) E. Maragakis* , M. Saiidi, B. M. Douglas, G. Norris, R. Siddharthan and D. Sanders: Bridge Engineering Research In Progress at The University of Nevada, Reno
(10:50am～11:05am)

(23) M. Fujiwara, K. Nishikawa* , K. Minosaku, J. Murakoshi, S. Yamamoto: Current Condition on Introduction of Limit State Design Method to Highway Bridge Design in Japan
(11:05am～11:20am)

(24) J. M. Kulicki* and D. R. Mertz: United States LRFD Bridge Specification
(11:20am～11:35am)

DISCUSSION
(11:35am～11:50am)

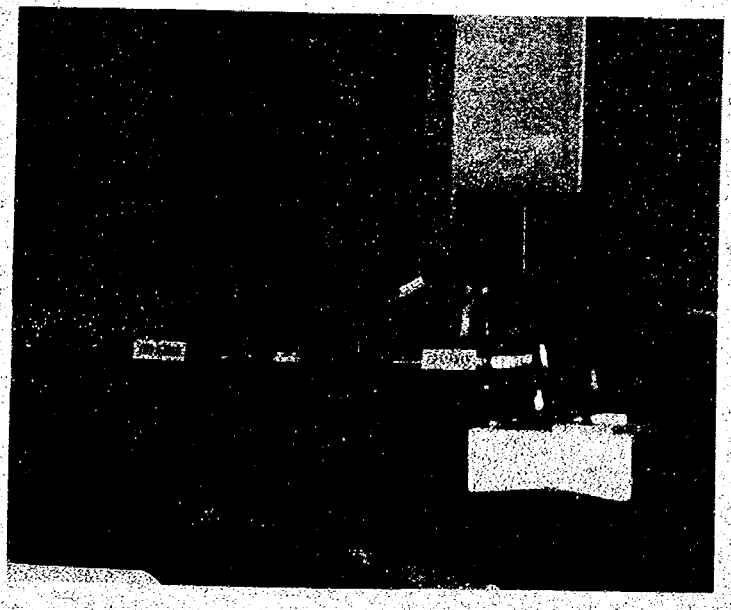

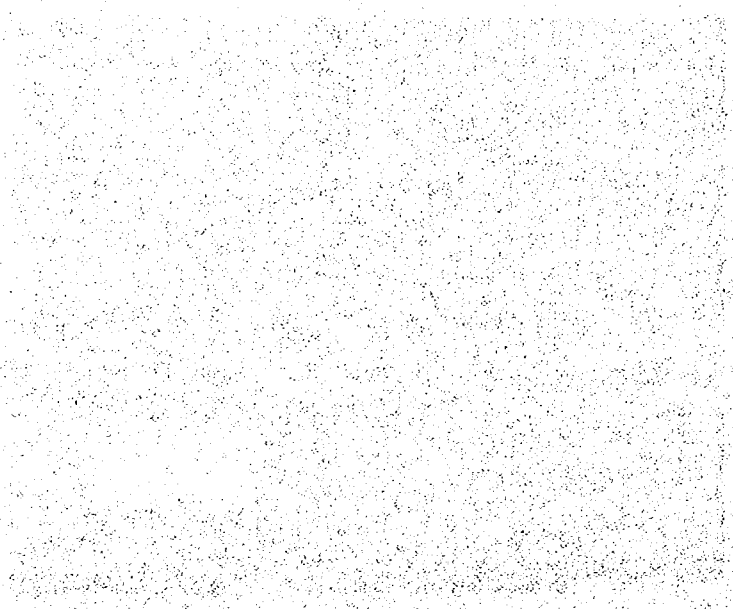

BRIDGE ENGINEERING RESEARCH IN PROGRESS AT THE UNIVERSITY OF NEVADA, RENO

by

Emmanuel Maragakis,[1] Mehdi Saiidi,[2] Bruce Douglas,[3]
Gary Norris,[1] Raj Siddharthan,[1] and David Sanders[4]

INTRODUCTION

An overview of the history of bridge damage in the United States generated by seismically induced vibrations indicates that the 1971 San Fernando earthquake revealed the vulnerability of highway bridges to earthquake loadings and, thus, presented a major turning point in the development of significant research work in this area. The recent Loma Prieta earthquake reminded both researchers and engineers that, although extensive research has been done in the past, more continuous efforts are necessary to protect existing and new bridge structures from the catastrophic effects of earthquakes. The Civil Engineering Department at the University of Nevada, Reno has focused its attention for the past fourteen years or so on research related to several aspects of Bridge Engineering with particular emphasis given to the dynamic and seismic response of bridges. The objective of this paper is to summarize some of the research projects that are currently in progress in the Department.

The research projects which are briefly presented in this paper include the following:

1. A study of prestress force losses in a posttensioned box girder bridge in Reno,

2. A study related to the cyclic response of one-way hinged bridge columns,

3. A study on the tilting and sliding of bridge abutments under seismic excitations,

4. A study on the behavior of pile group and drilled pier foundations,

5. A study on the development of deterioration models for the prediction of the remaining life of bridges,

---

1. Associate Professor, Civil Engineering Dept., University of Nevada, Reno, NV 89557

2. Professor and Chairman, Civil Engineering Dept., University of Nevada, Reno, NV 89557

3. Professor, Civil Engineering Dept., University of Nevada, Reno, NV 89557

4. Assistant Professor, Civil Engineering Dept., University of Nevada, Reno, NV 89557

6. A study on the effects of the energy losses due to the impact between the bridge deck and the abutments on the response of short-span bridges,

7. A study of the exact role of bridge cable restrainers on the seismic response of bridges,

8. A parametric study on a simple base isolated bridge system, and

9. A parameter identification study based on the data obtained from a full-scale test of Meloland Road Overcrossing which was performed in 1988.

The following colleagues and students are acknowledged for their assistance with these projects: Saber Abdel-Ghaffar, Samia Ara, Prakash Gowda, Eric Hutchens, Dr. E. Hwang, Yang Jiang, Joseph Shields, David Straw, Spiros Vrontinos, and Zia Zafir.

A. A STUDY OF PRESTRESS FORCE LOSSES IN A REAL BRIDGE

A post-tensioned box girder bridge near Reno, Nevada, has been instrumented and the changes in the prestress force, concrete surface strain, and deflection have been measured since September 1988. The primary objective of the study is to determine the prestress losses in an actual bridge in a relatively dry climate. The project is funded by the Nevada Department of Transportation.

The bridge, located at the Golden Valley Interchange, covers a simple span of 155 feet, and is a multi-cell box girder bridge with 30 degree skew. Provisions were made in the construction drawings to allow access to one of the exterior cells and to girders G1 and G2 (Fig. A1). In these girders, block outs were placed during construction to allow for the instrumentation of four of the prestressing tendons near the center of the bridge (Fig. A2). The instrumentation included twelve strain gages installed on the prestressing wires and two stress-free strain gages used for temperature compensation. In addition, six dial gages with a sensitivity of 1/10,000 inch were installed over a 30-inch gage length on the webs of two of the girders (Fig. A2). Data were collected at the time of the application of full prestressing force, and periodically thereafter over a 30-month period. A relatively short time interval was used initially to capture the rapid change of stresses. In addition to the above data, the deflection of the bridge at mid-span relative to the abutments was measured. The measured data present the time-dependent prestress losses which are due to creep and shrinkage of concrete and the relaxation of prestressing steel.

A time-step analysis method has been used to determine the prestress losses. The procedure is based on the documents prepared by the American Concrete Institute Committee 209, and accounts for the interdependency of creep, shrinkage, and relaxation losses. The total prestress losses also were estimated using the method adopted by the American Association of State Highway and Transportation Officials (AASHTO).

Results indicate that both analytical methods underestimate the actual prestress losses (Fig. A3). A possible explanation for the difference is the relatively low ambient humidity which might not have been adequately accounted for in the theoretical formulas. The measured data have shown a strong dependency of

prestress losses to seasonal changes in temperature and humidity (Fig. A3). Furthermore, the data have indicated that the time for the prestress forces to stabilize can be considerably longer than expected. The concrete surface strains (marked by squares in Fig. A3), while were useful in confirming trends of stress changes, were not sufficiently accurate to predict the prestress losses.

B. CYCLIC RESPONSE OF ONE-WAY HINGED BRIDGE COLUMNS

Reinforced concrete bridge columns with a one-way hinge at the base have been utilized in many bridges. The hinge detail eliminates moment transfer in the weak direction to the footing and reduces thermal stresses in different bridge components. When subjected to lateral loads, the hinge is subjected to flexure and shear in addition to the normal load resulting from the vertical loads. While the flexural strength of the hinge can be calculated using conventional methods, its shear strength is not well understood nor studied. The problem becomes more complicated when cyclic lateral loads are applied.

A study into the behavior of reinforced concrete hinges is in progress at the University of Nevada, Reno (Ref. B1). The research is funded by the U.S. National Science Foundation and includes both testing and analysis. The test elements have included hinged columns, pure shear specimens, and pure compression specimens. The focus of this summary article is the column specimens. Figure B1 shows the dimensions and steel distribution for typical column specimens. The steel crossing the hinge area consisted of six number 3 bars. The column specimens were one-sixth scale models of the columns in the Rose Creek bridge located in Northern Nevada. The design concrete compressive strength was 4,000 psi, and the grade of steel was 60. The maximum aggregate size was 0.5 inch. Each specimen was constructed in two steps: (1) first the concrete for the foundation was poured and cured in the moist room and (2) the column concrete was placed. The details of the construction process and material properties are presented in Ref. B2. The axial load for the specimens was selected to produce the same stress in the hinge throat as that produced by the dead load in the Rose Creek bridge. This load was kept constant for all the column specimens.

Several test variables have been studied for the column specimens. These include:

1. The loading type (monotonic versus cyclic),
2. The column aspect ratio, and
3. The detail of steel bars crossing the hinge throat.

Most of the specimens were subjected to cyclic loads. The maximum displacement corresponded to a ductility of four (with ductility defined as the ratio of displacement and the apparent yield displacement). The column aspect ratios were one and two. The steel detail was varied in some of the specimens to improve the hysteretic shear-slip behavior of the hinge region. The modified hinges included diagonal steel or bundled bars near the edges.

Figure B2 presents a typical load-deflection diagram for a specimen with a distributed straight bar and an aspect ratio of one. The results show that, up to a displacement ductility of two, the energy absorption capacity of the element was reasonably high. This would indicate that the hinge performance may be adequate in a moderate earthquake. For higher ductility ratios, however, the

response was associated with severe stiffness and strength degradation. The results for modified hinges have indicated some improvements. A detailed analysis of the data is in progress to quantify the effectiveness of these details.

C. TILTING AND SLIDING OF BRIDGE ABUTMENTS UNDER SEISMIC EXCITATION

The seismic design of bridge abutments depends on the anticipated movement of the abutment during the design earthquake. In the case of free-standing abutments that can move in excess of 0.5% of the height, the displacement based approach is desirable. In such cases, wall sliding as well as tilting modes of deformations should be considered in the design (Ref. C1 & C2). We recently developed a simple rigid plastic model to study tilting and sliding of free-standing abutments in a coupled manner (Fig. C1). Currently the abutment displacements are estimated assuming that only sliding of the abutment occurs (AASHTO Procedures).

Forces acting on a rigid wall subjected to base excitation are shown in Fig. C2. The center of rotation about which the wall rotates needs to be pre-selected. When the center of rotation is assumed to be close to the toe of the wall, the moment of inertia about the point of rotation and the stabilizing moment are higher but the resisting foundation soil moment is lower than the corresponding values associated with the center of rotation near the middle of the base. The influence of the factors mentioned above on computed total wall top displacement (sliding and tilting) can be seen in Fig. C3 for a typical wall of height 5.0m (Ref. C1).

The recent wall displacement study has clearly identified the importance of, among other factors, the yield resisting moment, vertical acceleration component, and the location of the point of rotation. The rigid plastic yield moment which was estimated based on Winkler Springs for the foundation model was found to be dependent upon the bearing capacity of the foundation and on the dimensions and reactions at the base.

Rigid plastic models are widely preferred by practicing engineers because they do not require a characterization of the stress-strain relationships for the soils. On the other hand, a small wall rotation before the limiting condition is reached can result in a large abutment top displacement. It should be noted that 1° of rotation about a base of a 6m abutment is equivalent to an abutment top displacement of about 100mm. Studies are now underway that address this issue. Validation studies are also being undertaken using field data and centrifuge data. Design implications with respect to bridge performance caused by abutment movements are being investigated.

D. PILE GROUP AND DRILLED PIER FOUNDATION BEHAVIOR

There is ongoing research at the University of Nevada, Reno relative to the static and seismic behavior of highway bridge pile groups and large diameter drilled shafts. The methodologies for assessing the nonlinear variation in the lateral and the rotational stiffnesses of a pile group were discussed in the previous report of research (Ref. D1). The methodology for the lateral stiffness evaluation included appropriate treatment of layered soil conditions, group

interference effects and the added lateral resistance provided by the embedded pile cap. The rotational stiffness evaluation included the appropriate treatment of layered soil conditions, a shifting axis of rotation associated with differing vertical pile stiffnesses in load versus unload-reload response, and the associated (permanent) rotationally settlement.

Current research supported by the California Strong Motion Instrumentation Program (CSMIP) and the Center for Infrastructure Studies (CIS) has been directed toward an improved characterization of lateral beam on elastic foundation (BEF) response based on so-called strain wedge (SW) model formulation (2). Accordingly, the subgrade modulus or (alternatively) the "p-y" curve BEF response has been found to be a function of both soil and pile conditions (i.e., besides the effect of pile size there is dependency upon pile shape, bending stiffness, and pile head fixity conditions; likewise, p-y curves are dependent upon the sequence of soil layers). In addition to an improved lateral springs characterization, there is an effort to assess the added lateral resistance arising from vertical side shear, bottom shear, and the bottom moment response of large diameter drilled shafts of intermediate to rigid flexibility. While there have been attempts by others to account for such effects relative to a rigid member, current efforts are directed at the response of a shaft of varying flexibility.

Such methodologies are being used to assess the differing responses of pile groups at the Cypress Viaduct during the Loma Prieta earthquake. It should be noted that the southern half of this structure was founded on short end bearing piles in Merritt sand while the northern portion was founded on long friction piles through Bay mud. There was a sudden change in both the lateral and rotational stiffnesses of the pile groups from bents 71 to 72 arising from the sudden change from one type of pile group to the other. This, combined with the likely difference in ground surface motions at the top of Bay mud (along the northern portion of the viaduct) and Merritt sand (along the southern end), probably contributed to the collapse of the superstructure. Any future structural modeling of the collapse mechanism of the viaduct would be remiss if such differences were not taken into account.

In addition to the evaluation of the response during the earthquake, SW modeling is being used to evaluate the observed behavior from CALTRANS lateral pile group load tests at bents 61 and 97. These unique tests were carried to structural failure of the piles and/or the cap. From a preliminary analysis, it is seen that an accurate evaluation of pile group behavior requires a consideration of the following factors: the embedment effect relative to piles in the Merritt sand (i.e., overburden pressure at the pile top [base of the pile cap] of the piles loaded at a level below the surrounding ground surface), the group interference effect which increases with load or deflection amplitude, the changing bending stiffness of the piles due to increased cracking at the higher load levels, and the development of plastic hinges in the piles. Basically, it is assessed that the pile groups exhibited a fixed head condition up to the attainment of a limiting value of moment at the pile head after which a plastic hinge developed at all such locations.

A separate analysis of the behavior of the Oakland Outer Harbor Wharf during the Loma Prieta earthquake should provide insight into the effect of developing liquefaction conditions on the ensuing response of piles for both marine and highway bridge applications.

Finally, the aforementioned consideration of side shear, bottom shear, and the bottom moment response is being pursued in relation to the CALTRANS lateral load tests of eight-foot diameter drilled shafts at the Century Freeway I-105 site.

E. DEVELOPMENT OF DETERIORATION MODELS FOR PREDICTING REMAINING BRIDGE LIFE

Deterioration of the nation's bridge system is a problem which will cost billions of dollars to repair in the coming decades. In these days of limited resources, transportation authorities must make decisions concerning which bridges need immediate repair and which ones can wait. Most states have regular schedules for inspecting their bridges. During these inspections the bridge is checked for structural damage and foundation problems and is given a rating for its general condition. In the late 1970's, inspectors were required to estimate the remaining life of the bridge. In most cases, it was found that the inspector would find the design life of the bridge by subtracting the age of the bridge from the original design life. Therefore, if the bridge had a design life of 50 years and it was 40 years old, the remaining life was 10 years. If the bridge was older than the design life, then the inspector would typically say the remaining life was either 5 years or 10 years depending on the general condition of the bridge. The objectives of the research project is the development of general deterioration models for several different bridge types and to lay the groundwork for the determination of more detailed models for individual bridge components. All states are in the process of developing or have already developed a Bridge Management System. One aspect of these systems is the use of bridge deterioration models to predict the remaining bridge life in a systematic and rational way. The investigation of deterioration models for the State of Nevada is being funded by the United States Department of Energy through the Nuclear Waste Project Office.

The focus during the first months of the project has been a literature review. Several literature searches have been conducted. Literature which addresses deterioration can be divided into three categories: case studies, deterioration studies, and modeling studies. Literature which is classified as case studies examines particular structures which had deterioration problems and explain what was done to repair the problem. Deterioration studies investigate the parameters that cause deterioration, while modeling studies try to predict the rate at which deterioration occurs. Most of the literature falls into the categories of case studies and deterioration studies. Two articles identified that are of particular interest are listed below. The report by Maser (Ref. E1) indicates the use of intelligent systems to gather deterioration data. The effective collection of data for a comprehensive deterioration model is the key to its success. West et al. (Ref. E2) developed deterioration models which show promise for steel and prestressed concrete bridges located in the State of Pennsylvania. The model developed for reinforced concrete bridges was not as accurate. The two most influential variables in the models were the age of the bridge and if any rehabilitation had been done to the bridge. Neither the current condition of the bridge nor the surrounding environment was used in the bridge life prediction. The deterioration model envisioned for this project will include current site conditions. The models developed by West et al. were correlated against bridges in Pennsylvania which had similar site conditions. Therefore, while the models were reasonable for bridges in Pennsylvania, they

would not necessarily apply to bridges in Nevada or other parts of the country.

During the next several months the project will begin to examine in detail the inspection and maintenance records for bridges in Nevada. The records will be statistically analyzed to determine if there are any trends which are important for the deterioration models. The final product will be a group of general deterioration models to be implemented in the Bridge Management System for the State of Nevada.

F. INVESTIGATION OF THE ENERGY LOSSES DUE TO THE IMPACT BETWEEN THE BRIDGE DECK AND THE ABUTMENTS

The impact between the bridge deck and the abutments, has been the source of extensive damage during the 1971 San Fernando and other recent earthquakes and has attracted research interest during recent years. One aspect that has been neglected in all the previous studies is the energy losses that occur due to this impact. In all the studies related to this phenomenon that have been performed so far as well as in most of the bridge dynamic analysis programs used by researchers and engineers, the abutments are represented with linear or nonlinear springs and, in some cases, with a combination of springs and hysteretic dampers. Although this type of representation for the abutments allows for the modeling of the foundation stiffness as well as for energy losses due to material and radiation soil damping, it does not take into account the energy losses due to the severe collision between the bridge deck and the abutments. The objectives of this project are the following:

(i) To investigate the effects that energy losses directly related to the collision between the bridge deck and the abutments have on the seismic response of bridges and

(ii) To develop simplified modeling techniques for the incorporation of these losses in already existing bridge analysis programs which can be used easily by researchers and engineers.

To accomplish these goals, simplified models of bridge structures have been developed. These models are described in Refs. F1 and F2. Some representative results of the analysis performed so far are shown in Figs. F1-F4. Figures F1-F2 show a comparison of the displacement envelopes of the bridge deck for a coefficient of restitution equal to 0.6. In both cases, the models considered have been excited by the 1987 Whittier earthquake. It can been seen that the degree of the influence of the impact on the response depends on the stiffness of the abutment soil spring. This is more obvious in Figs. F3-F4 that show the maximum displacement of the middle mass for several values of the abutment springs for different earthquake excitations. One can see that, for softer springs, the effect of the impact on the maximum response of the deck is more significant.

G. EVALUATION OF THE EFFECTS OF CABLE RESTRAINERS ON THE SEISMIC RESPONSE OF BRIDGES

The Civil Engineering Department is currently involved in two projects related to the evaluation of the role and the effects of cable restrainers on the overall

response of bridges during earthquakes. These projects are funded by the California Department of Transportation, the National Science Foundation, and the Nevada Department of Transportation. The major objectives of these projects are:

(i) To develop detailed modeling elements for the currently used cable restrainer retrofitting systems and incorporate them into available bridge dynamic analysis computers;

(ii) To perform a detailed survey of the response of cable retrofitted bridges during the recent Loma Prieta earthquake and classify these structures according to factors such as sustained damage, structural type, geometry, location, etc.; and

(iii) To analyze representative structures using the techniques developed in phase (i) and evaluate the performance of the retrofitting cables and their exact role on the overall performance of the structures.

H. AN ANALYTICAL STUDY OF THE SEISMIC RESPONSE OF BASE-ISOLATED BRIDGES

The objective of this project is the performance of analytical studies for the investigation of different aspects of the seismic response of base isolated bridges. Figure H.1 shows two simplified models of bridge isolated systems which have been developed and analyzed in the first phase of this study. Model 1 in this figure represents an isolated bridge with isolation located at the top of the bridge pier and at the abutments. This configuration, which essentially isolates the bridge deck from the bridge substructure, is currently used in the majority of isolated bridges. Model 2 of the same figure represents an isolated bridge with the pier isolation moved to the bottom of the pier. In both cases, the deck is modeled with a rigid mass while the piers and the isolation bearings are represented by linear springs.

Several parametric studies were performed using the two models. The parameters of the models were evaluated based on the properties of the Rose Creek bridge, a structure located near Winnemucca in the State of Nevada. Figure H2 shows a representative result of the parametric studies. In this figure, the absolute maximum displacement of the deck mass is plotted as a function of the ratio of the isolator and the pier stiffnesses for the 1940 El Centro Earthquake. For a better comparison between the two models, the original curves have been smoothed by using curve fitting techniques. It is obvious that there are no major differences between the maximum responses predicted by the two models. At this point, further parametric studies are in progress including bilinear springs for the isolations and hysteretic springs for the bridge piers.

I. PARAMETER IDENTIFICATION STUDIES ON THE MELOLAND ROAD OVERCROSSING

In May of 1988, comprehensive quick-release dynamic field experiments were carried out on the Meloland Road Overcrossing (MRO) near El Centro, California. This structure has been severely shaken in past earthquakes and particularly during the 1979 Imperial Valley Earthquake. Because of its proximity to the

active Imperial Fault, this bridge has been heavily instrumented to record strong earthquake motions. This two-span reinforced concrete box girder bridge with its monolithic abutments represents about 40% of the bridge inventory in the State of California.

The quick release experimental data has been analyzed to identify the mode shapes and natural frequencies. Sufficient data were collected to be able to identify the translations and rotations of the bridge deck and foundation elements. Further, the primary accelerogram data has been successfully integrated to produce reliable estimates of the static deformations of the structure caused by the quick-release loads (Refs. I1, I2).

In a preliminary parameter identification study (Ref. I3), a SAP 90 model of the bridge was used in conjunction with a pattern search optimization procedure to identify the structural parameters of interest for the MRO. Twelve independent structural parameters were found from the experimental dynamic data. The first transverse mode, the first and second vertical modes, and the first torsional mode for the bridge were used to identify these twelve parameters. All of the rotational soil-structure interaction springs at the abutments were found along with the vertical and transverse springs. At the central pier foundation, the only spring not identified was the rotational spring about the column axis. In addition, the effective moments of inertia of the deck in both directions were found along its effective torsional constant. The effective moment of inertia of the column was also found. A principal result of this preliminary study was that the structure was quite soft when the modulus of the concrete was taken to be 3,700 ksi. The structural model obtained from the dynamic mode shapes and frequencies was then used to predict the static displacements caused by the quick-release rams.

The final phase of the project is being completed. A slightly more refined model has been constructed which includes the depth of the abutment wall as a parameter. The introduction of this variable has permitted some insight regarding the value of the longitudinal soil-structure interaction springs at the abutments to be gained from the vertical dynamic modes. Along with this more refined model, a very comprehensive sensitivity study regarding the influence of each parameter has been undertaken. The primary purpose of this study is to establish the confidence limits for all of the parameters being sought. In this phase of the project, the static data is also being used to identify a structural model which will be compared to that obtained from the dynamic mode shapes.

References

B1. Saiidi, M., J. Orie, and B. Douglas, "Lateral Load Response of R/C Bridge Columns With a One-Way Pinned End," ACI Structural Journal, Vol. 85, No. 6, November-December 1988, pp. 609-616.

B2. Straw, David, "Scaled Model Testing of One-Way Reinforced Concrete Pier Hinges Subjected to Combined Axial Force, Shear, and Flexure," a thesis submitted in partial fulfillment of the requirements for the degree of Master of Science in Civil Engineering, University of Nevada, Reno, March 1991.

C1. Siddharthan, R., Ara, S., and Norris, G.M., "A Simple Rigid Plastic Model for Seismic Tilting of Rigid Walls," tentatively approved for publication in the Journal of Structural Engineering, ASCE, March 1991.

C2. Siddharthan, R., Gowda, P., and Norris, G.M., "Displacement Based Design of Retaining Walls," Proceedings, Second International Conference on Recent Advances in Geotechnical Engineering and Soil Dynamics, Missouri, Vol. I, March 1991, pp. 657-661.

D1. Douglas, B.M., Saiidi, M., Norris, G.M. and Maragakis, E. "Bridge Research at the University of Nevada," Proceedings, 3rd U.S.-Japan Workshop on Performance and Strengthening of Bridge Structures, Tsukuba, Japan, May 1987, 17 pp.

D2. Norris, G.M. and Abdollaholiaee, "BEF-Studies with the Strain Wedge Model," Proceedings, 26th Annual Symposium on Engineering Geology and Geotechnical Engineering, Pocatello, Idaho, April 1990, Paper 13, 32 pp.

E1. Maser, K.R., "Intelligent Systems for the In-situ Evaluation of Materials and Structures," National Science Foundation Report Number NSF/CEE84-60816, July 1985.

E2. West, H.H., R.M. McCure, E.J. Gannon, H.L. Riad, and B.E. Siverling, "Nonlinear Deterioration Model for the Estimation of Bridge Design Life," Pennsylvania Transportation Institute Report Number PTI-8935; University Park, Pennsylvania, September 1989.

F1. Maragakis, E.A., Douglas, B.M., Vrontinos, S.N., "Simple Modeling of the Impact Energy Losses Occurring Between the Bridge Deck and the Abutments," Proceedings of the 6th U.S.-Japan Joint Workshop on Bridge Engineering, May 1990, Lake Tahoe, Nevada.

F2. Maragakis, E.A., Douglas, B., Vrontinos, S., "Classical Formulation of the Impact Between the Bridge Deck and the Abutments During Strong Earthquakes," submitted to the 6th Canadian Conference on Earthquake Engineering, Toronto, Ontario, June 1991.

I1. Douglas, B.M., E.A. Maragakis, and B. Nath (1989). "Static Deformations of Bridges from Quick-Release Dynamic Experiments," Journal of the Structural Division, Vol. 116, No. 8, Proceedings Paper 24977, pp. 2201-2213.

I2. Douglas, B.M., E.A. Maragakis, and B. Nath (1990). "Calculating Static Deformations from Quick-Release Accelerograms," Bulletin of the New Zealand National Society for Earthquake Engineering, Vol. 23, No. 4, pp. 239-253.

I3. Douglas, B.M., E.A. Maragakis, S. Vrontinos, and B.J. Douglas (1990), "Preliminary Parameter Identification Studies on the Meloland Road Overcrossing," Proceedings of the 6th U.S.-Japan Workshop on Bridge Engineering, Lake Tahoe, Nevada, 14 pp.

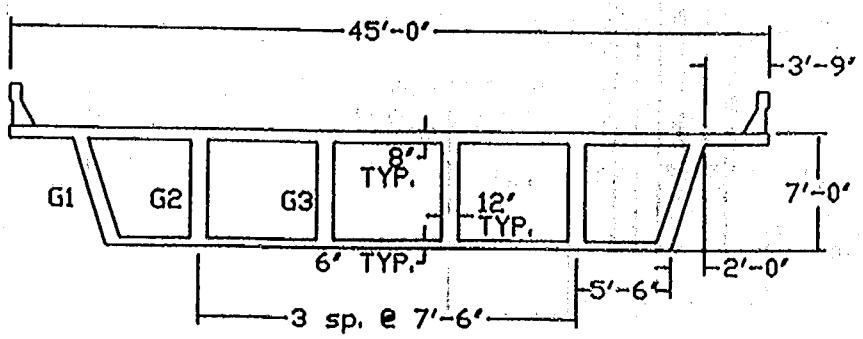

Fig. A1-Cross Section of the Golden Valley Bridge

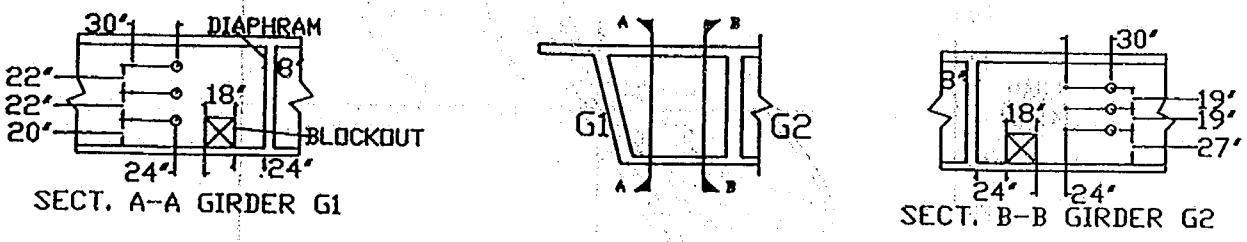

Fig. A2-Location of Access Blocks and Dial Gages

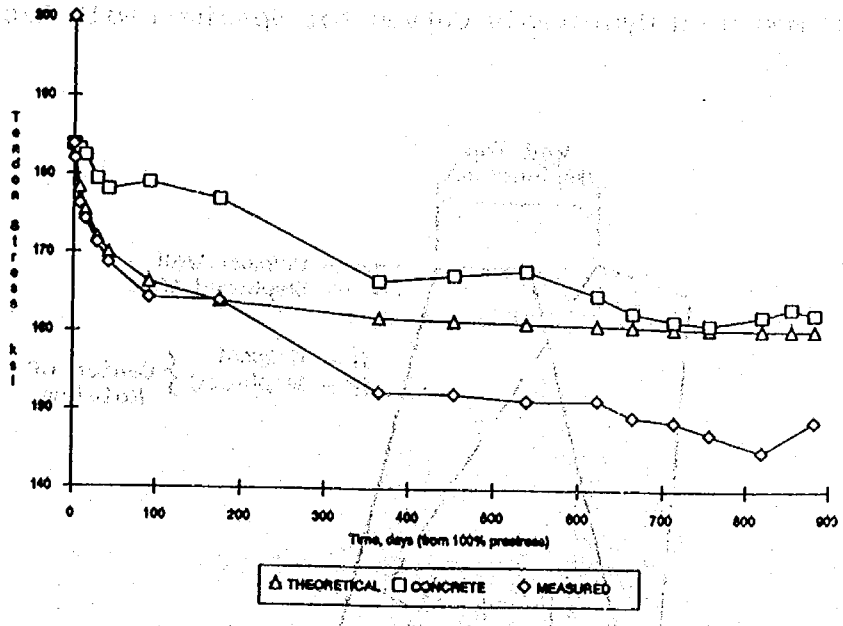

Fig. A3-Measured and Calculated Prestress Losses

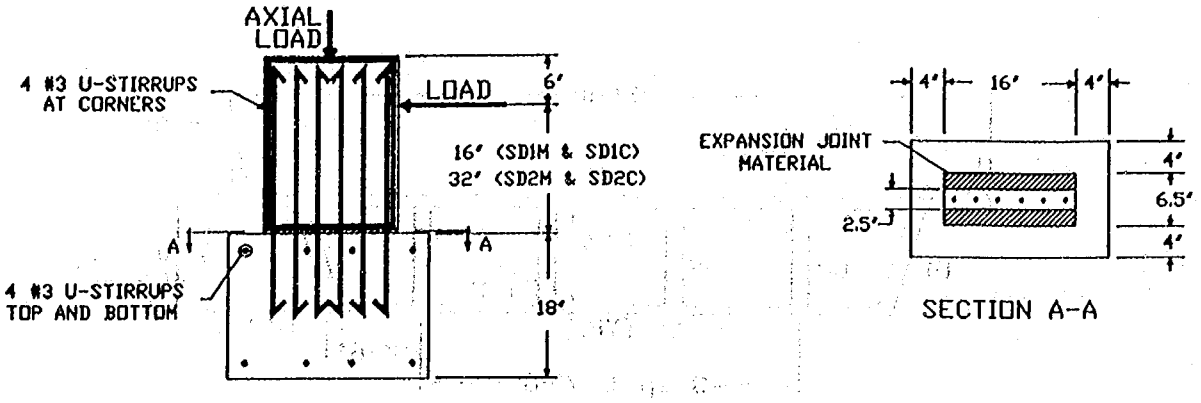

Fig. B1-Detail of Column Specimens with Distributed Bars

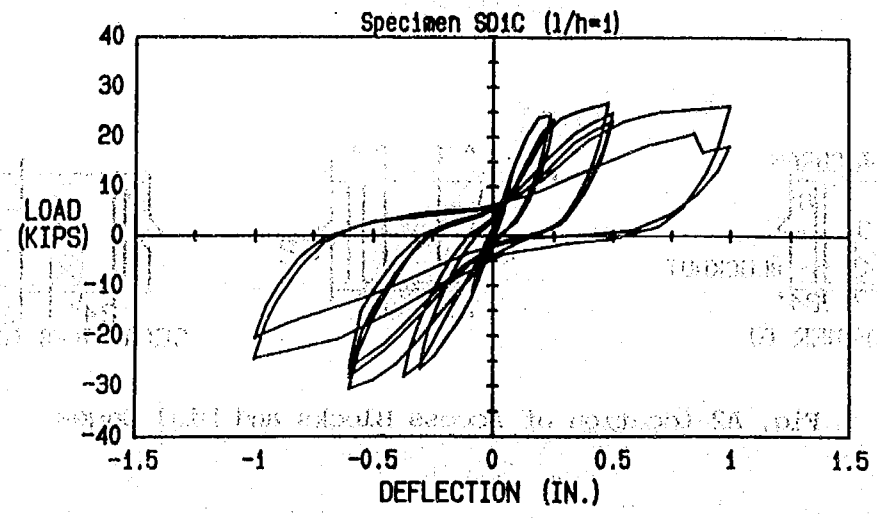

Fig. B2-Measured Hysteresis Curves for Specimen with Distributed Bars

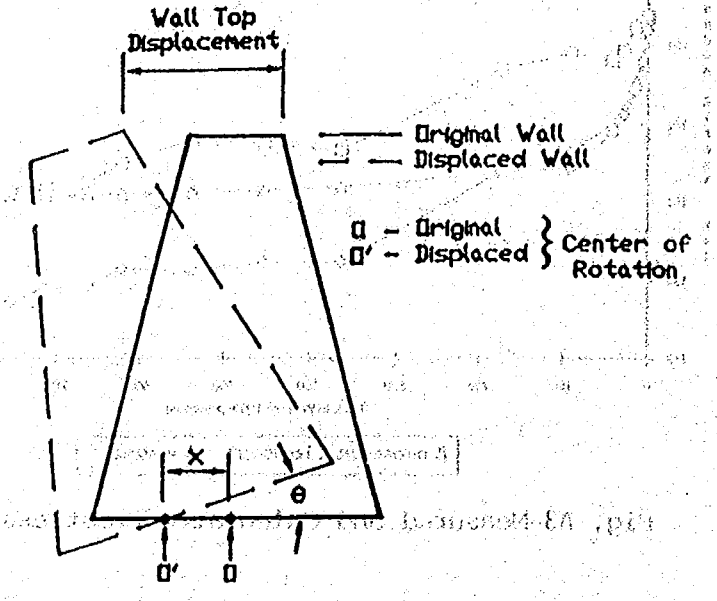

Fig.C1-Sliding and Titling Deformation Modes for Abutments

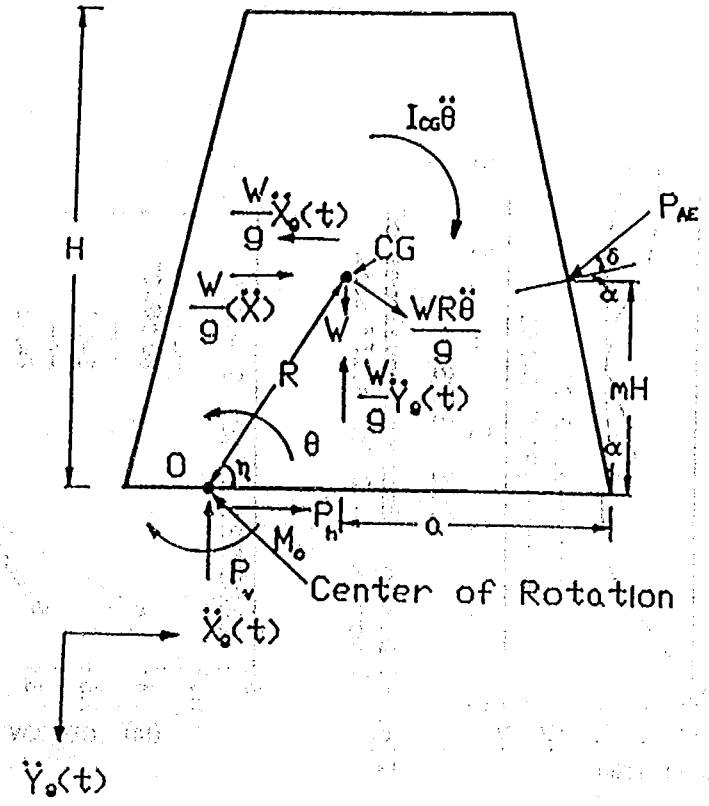

Fig. C2-Forces on a Rigid Wall During Seismic Excitation

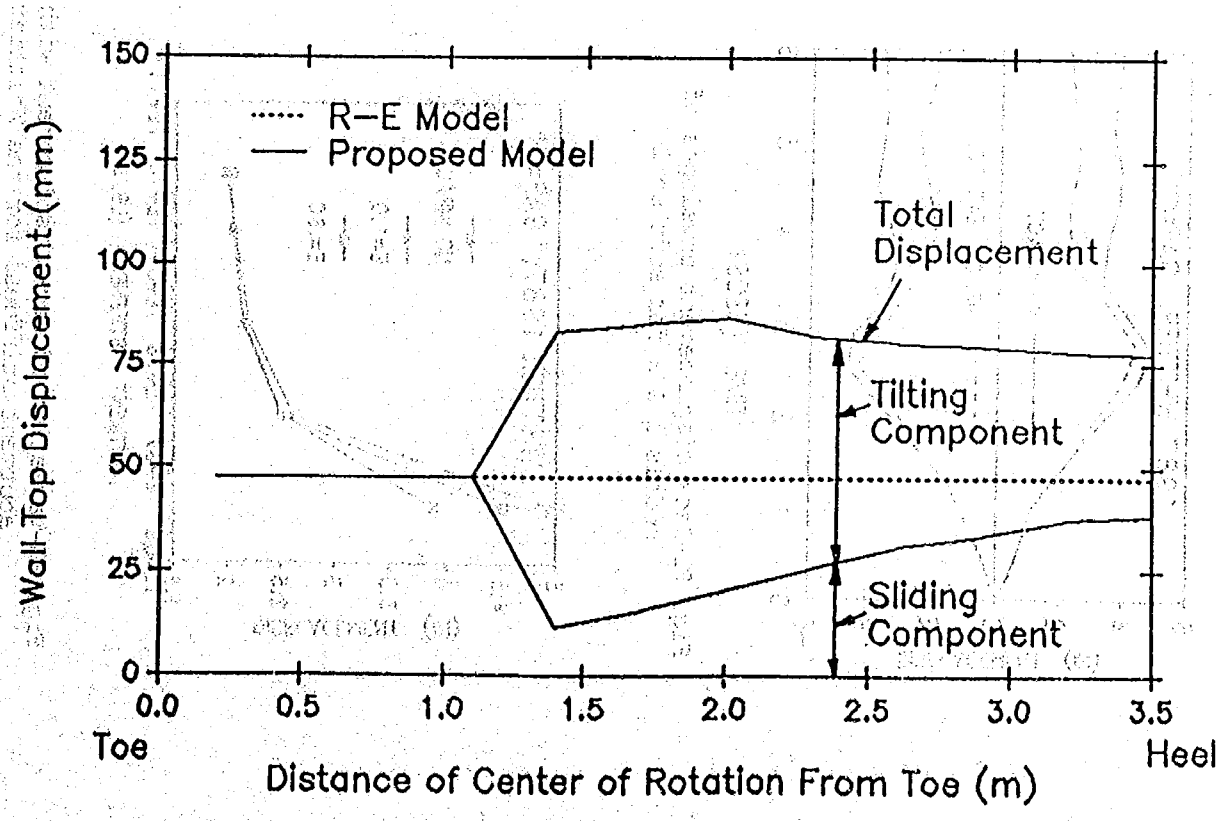

Fig. C3-Sliding and Tilting Components of Wall top Displacement for Sinusoidal Excitation

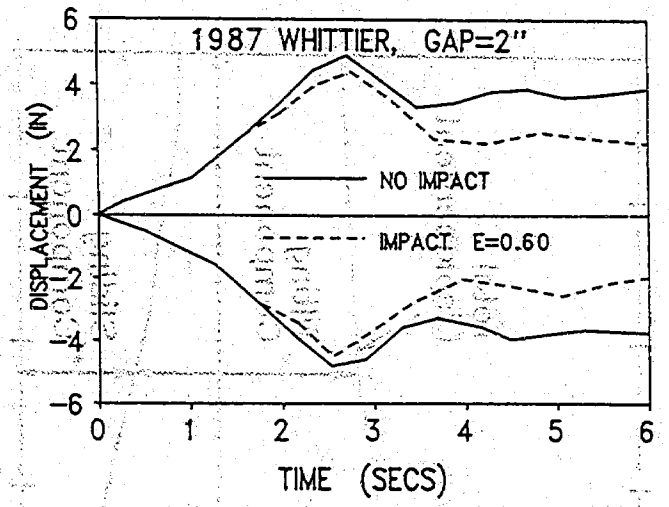

Fig. F1-Deck displacement envelopes of models 1 & 2 for soft soil

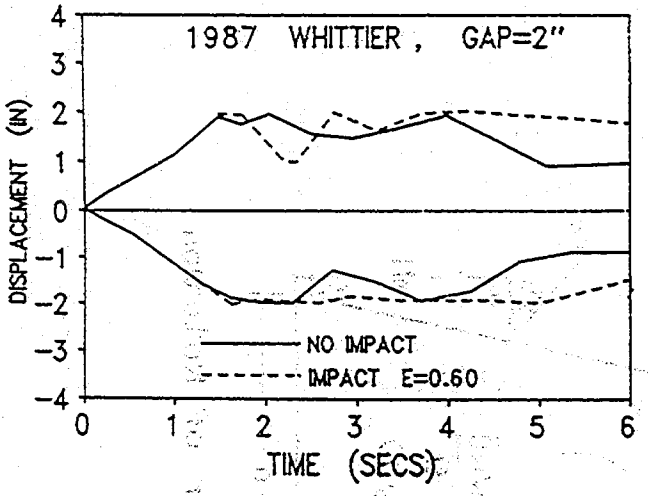

Fig. F2-Deck displacement envelopes of models 1 & 2 for stiff soil

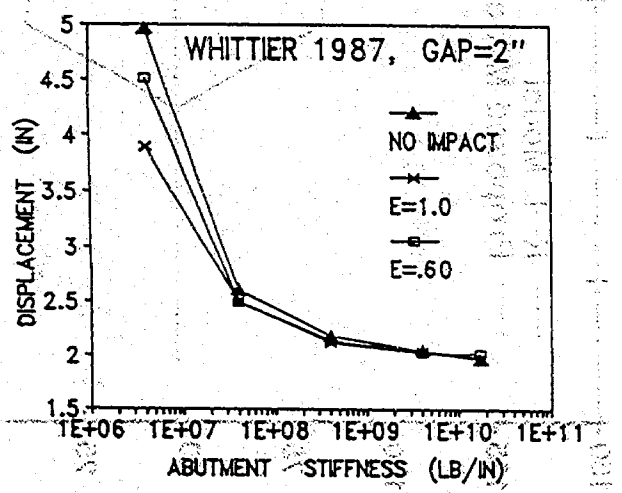

Fig. F3-Variation of deck displacement with abutment stiffness for the Whittier earthquake

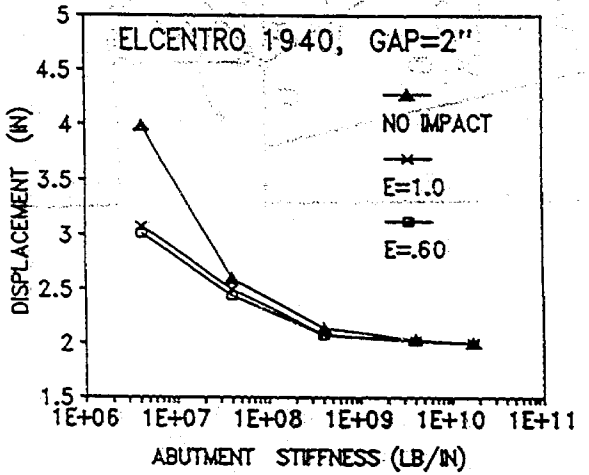

Fig. F4-Variation of deck displacement with abutment stiffness for the El Centro earthquake

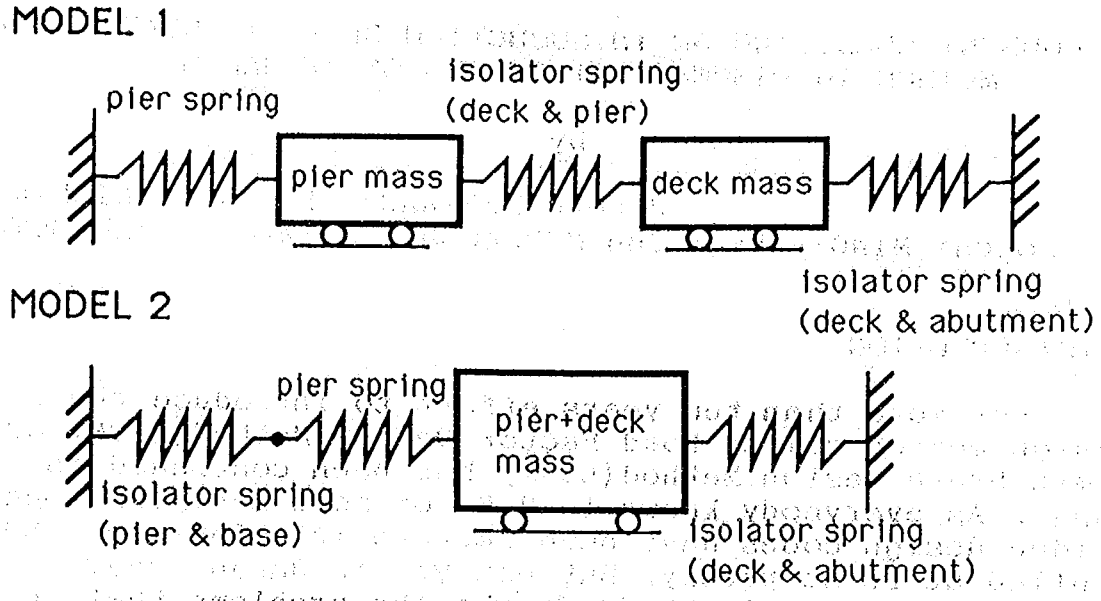

Fig. H1-Simplified models for isolated bridges

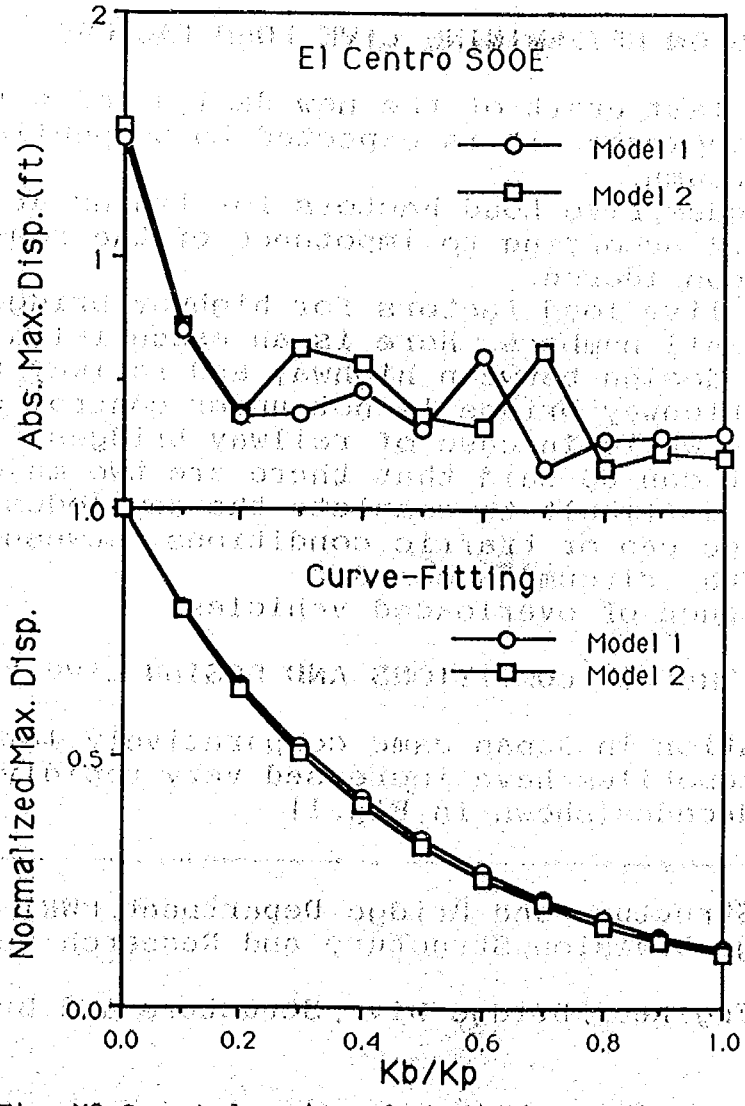

Fig. H2-Computed maximum deck displacements

CURRENT CONDITION ON INTRODUCTION OF LIMIT STATE DESIGN METHOD TO HIGHWAY BRIDGE DESIGN IN JAPAN

by

Minoru FUJIWARA*, Kazuhiro NISHIKAWA**
Koichi MINOSAKU***, Jun MURAKOSHI***, Satoshi YAMAMOTO***

1. INTRODUCTION

For more than ten years, effort to introduce the new design method called Load Factor Design Method(LFDM) or Limit State Design Method(LSDM) has been continued in Japan. As everybody knows, in U.S. or some European countries, bridge design codes have been rewrote into forms of LSDM and applied at reast partly. But not yet in Japan. Why?

This paper tries to describe the problems that we are faced with to complete the new design codes. Most problems can be thought to lie on determining Design Live Load(DLL).

2. DIFFICULTIES ON DETERMINING LIVE LOAD FACTORS

Recently, last draft of the new design codes for railway bridges was completed. It is expected to be published in this coming autumn.

In the codes, Live Load Factors for trains are set arround 1.1~1.2 according to impotance of the routes and the limit states considered.

Probably live load factors for highway bridge could not be that small numbers. Here is an essencial difference of concept in design between highway and railway bridges. Live load of highway bridge is not under control of the administrators while in case of railway bridges it is.

So far it can be said that there are two major problems that makes it difficult to complete the new codes. They are

(1)A large gap of traffic conditions between the design basis and actual circumstances, and

(2)Existence of overloaded vehicles.

3. CHANGES OF TRAFFIC CONDITIONS AND DESIGN LIVE LOADS

Motorization in Japan came comparatively late, but number of automobiles have increased very rapidly in these a couple of decades(shown in Fig.1).

---

* Director, Structure and Bridge Department, PWRI, MOC
** Head, Bridge Division, Structure and Research Dep., PWRI, MOC
***Research Engineer, Bridge Div., Structure and Bridge Dep., PWRI, MOC

Only 35 years ago, when the current DLL, called TL-20, was set up, heavy trucks were very few. Fig.2 shows the changes of proportion of heavy trucks among total trucks. Proportion of those over 8 tons (in Freight Tonnage) is only 10 percent in 1965. But now, the proportion soared up to over 90 percent.

When the current DLL are set up, it was considered a rare case that heavy trucks comparable to the DLL come one after another on a bridge and make lines on it. But looking into the current traffic condition, it is possible to occur significantly often that a bridge holds a DLL comparable load or more.

Fig.3 shows the share of freight trnsportation among various media. Though railway systems were well developped in Japan, the share of truck increased to very high level as far as freight concerns. It is considered that the prosperity of home delivery service and so called "Kanban System" for manufacturing which uses highway as a belt conveyor and storehouse contribute to increase the share.

Anyway these facts brought unexpected growth of road traffic and at the same time burden on the bridges.

On the other hand, there are 116,000 road bridges over 15 meter or longer in Japan. Since 1926, DLL has been revised three times as shown in Table 1. In spite of these revises, few bridges are posted as below 20 tons. There could be a concept that posting faithfully to the DLL was not practical or acceptable and generally old bridges have hidden safety factor due to the premitive design technics.

That had been true while traffic grew gradually. But recent bursting heavy traffic is giving bridges serious damage. Shortage of durability on bridges is getting acturized even in TL-20 bridges.

Furthermore, as Table 2 shows, almost a half of road bridges in Japan are designed by the DLL of 14 ton truck or lighter. In trunk highway, most of such bridges have already been replaced or strengthened. But a great number of bridges are still in use.

Some effective measure should be done to save those poor bridges before new design codes are introduced.

4. THE ACTUAL CIRCUMSTANCES OF OVERLOADING VEHICLES

It might not be a special problem. But current situation of overloaded vehicles in Japan can be seen abnormal to bridge engineers.

Japanese regulations for the limits of axle load and GVW are almost similar level to the major countries as shown in Table 3. Table 4 and Fig.4~7 are results of recent surveys on actual axle loads and GVWs at several points on trunk national highway.

Table 3 shows the largest axle load and GVW recorded at each survey points. Only 48 hours of survey caught 30.4 tons of axle load (three times larger than the regulation!), 69 tons of dump truck (3.5 times!) and 95.4 tons semi-trailer (3.5 times too!). Where have all the regulations gone !

If we had to set up a Live Load Factors (LLF) faithfully based on the data, it should not be below 3.5! Is it reasonable?

Fig.4 shows the spectra of axle loads and GVWs for dump trucks. There can be observed two peaks in the spectra of rear axles and GVWs. These are reflections of vacant and full loaded trucks. According to the survey, the average Gross Weight of dump trucks is about 28 tons. It is far above the reguration.

Fig.5 is those for semi-trailors. Similar tendencies are observed.

Fig.6 shows a distribution of the largest axle load recoded widely in Japan. This proves that the overload problem is not limited for the metropolitan area. And Fig.7 shows varieties of spectra. This point out the difficulties to set up a single LLF for the bridge design codes.

Of course, checking up the vehicles are enforced periodically. But by police, not by administrator of the roads. Here might be a problem.

After large scaled vehicle weight checking up, heavily violated trucks reduce. But it is also a fact that booms of construction push up the GVWs.

There might be a very difficult problem to solve, because the effect of the overloading is far larger than any other fators related to safety of bridges.

Not only technical but also administrative measure should made for these problems before or at least simultaneously the LLFs are set up. Any kind of measure should be tried so that the new design codes can make sense.

Table 1 Design truck live load of existing bridges

Grade of bridge	Year of specification			
	1926	1939	1956	1972
1 st	12ton	13ton	20ton	20ton
2 nd	8	9	14	14
3 rd	6	—	—	—
Else	—	—	—	TT-43※

※ Trailer truck with total weight of 43ton

Table 2 Number and length of existing bridges by design truck live load

Design truck live load	Number and length[1]	National expressway	National highway	Prefectural road	Municipal road	Total
20ton or more	Number	4,004	15,025	16,534	13,739	49,302
	Length(km)	573	1,307	1,376	714	3,970
14ton or less	Number	0	1,056	8,772	42,011	51,839
	Length(km)	0	49	407	1,732	2,188
Posted (Limit of load)	Number[2]	397	170	459	5,016	6,042

Note) 1)Number and length of existing bridges with bridge length of 15m or more (as of April, 1990)
2)As of April, 1989

Table 3 Axle weight limit and total weight limit for vehicle in various countries

Country		Japan	U.S.A.	U.K.	Germany
Axle weight	Single	10.0t	9.1t	10.5t	10.0t
	Tandem	According to axle space	15.4t	20.3t	16.0t
Total vehicle weight	Single	20.0t	Max:36.3t (According to wheel base and axle number)	17.0t for 2 axle 24.4t for 3 axle	16.0t for 2 axle 22.0t for 3 axle
	Semi trailer	34.0t for national expressway, 27.0t for others		32.5t	32.0t for 4 axle 38.0t for 5 axle
	Full trailer	By transit permission system for special vehicle		38.0t	38.0t

Table 4 Measured results of axle weight and total weight of vehicles

Measured point	Ariake (Port area)	Kumagaya (Local city)	Soka (Local city)	Hachinohe (Local city)	Yoga (Tokyo)
Route of road	National highway 357	National highway 17	National highway 4	National highway 45	Metropolitan expressway 3
Percentage of large size vehicles	35.0%	32.4	20.0	11.0	10.7
Maximum axle weight of vehicles	30.4 ton	23.5	28.4	28.5	17.8
Maximum total weight of dump-truck	69.0 ton	46.7	59.1	43.7	33.5
Maximum total weight of semi-trailer	95.4 ton	72.5	74.5	86.1	53.7

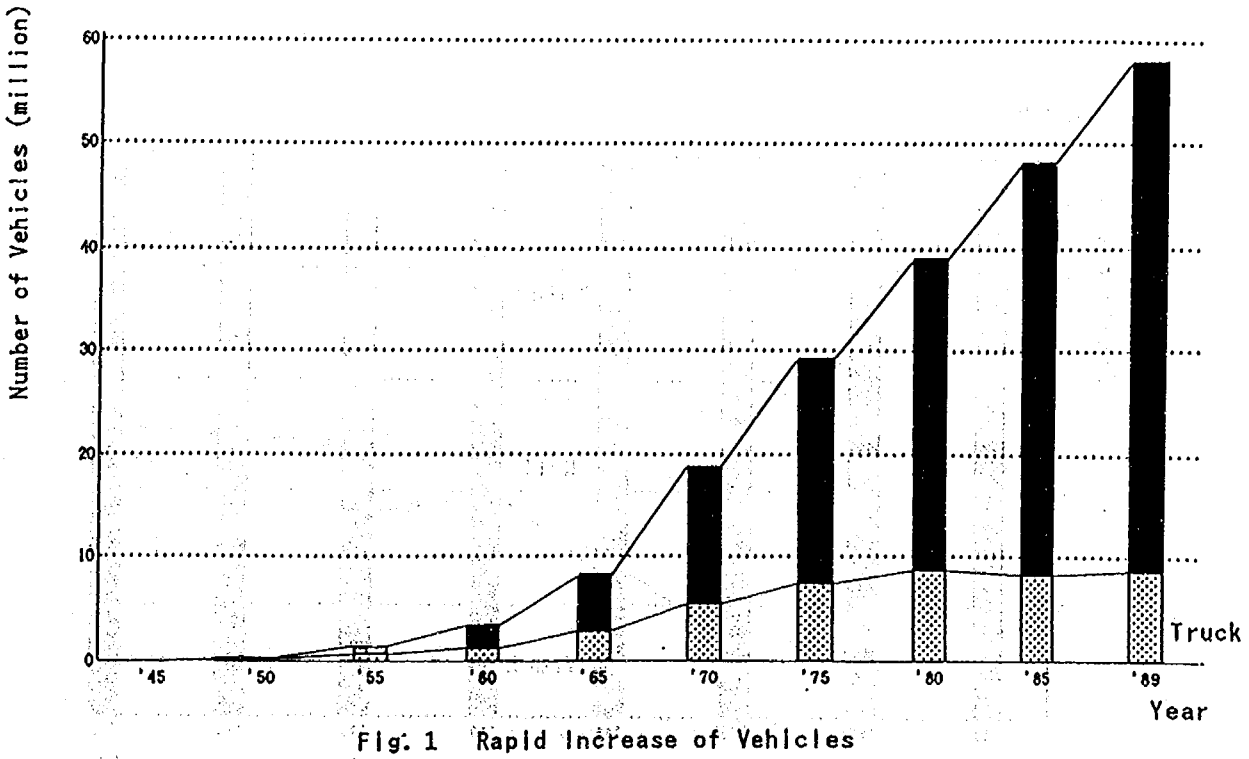

Fig. 1 Rapid Increase of Vehicles

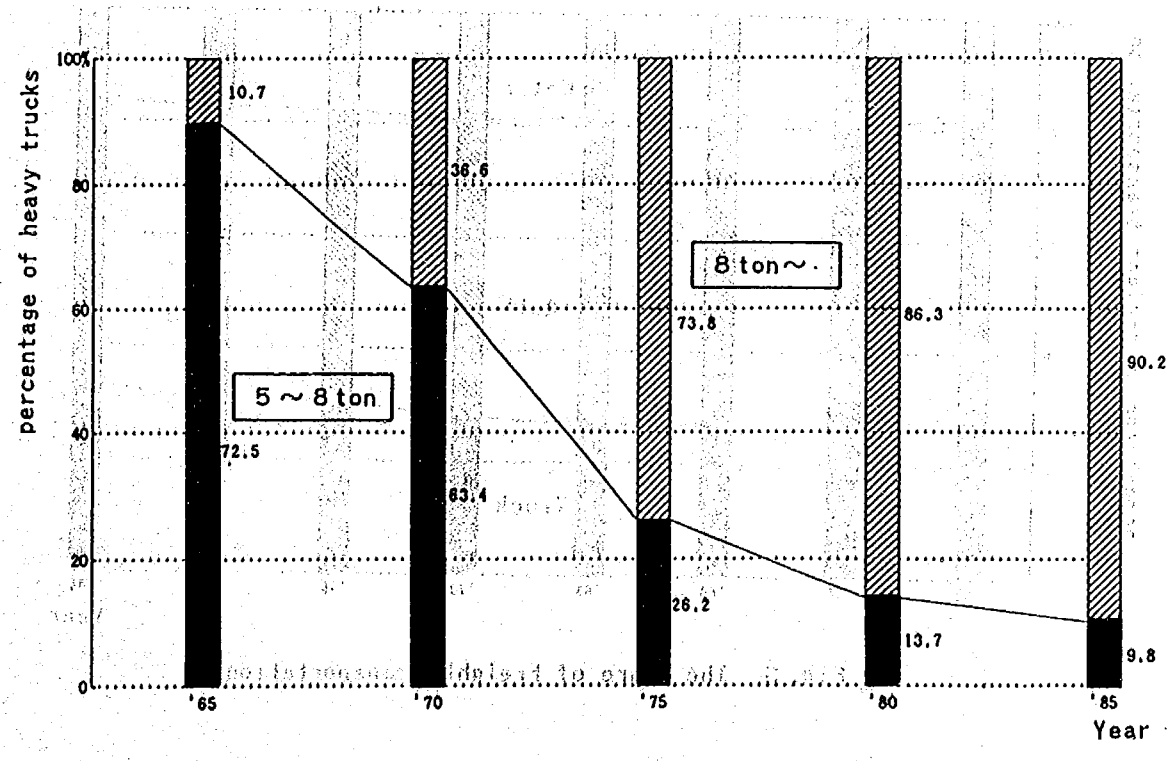

Fig. 2 Change of proportion of heavy trucks

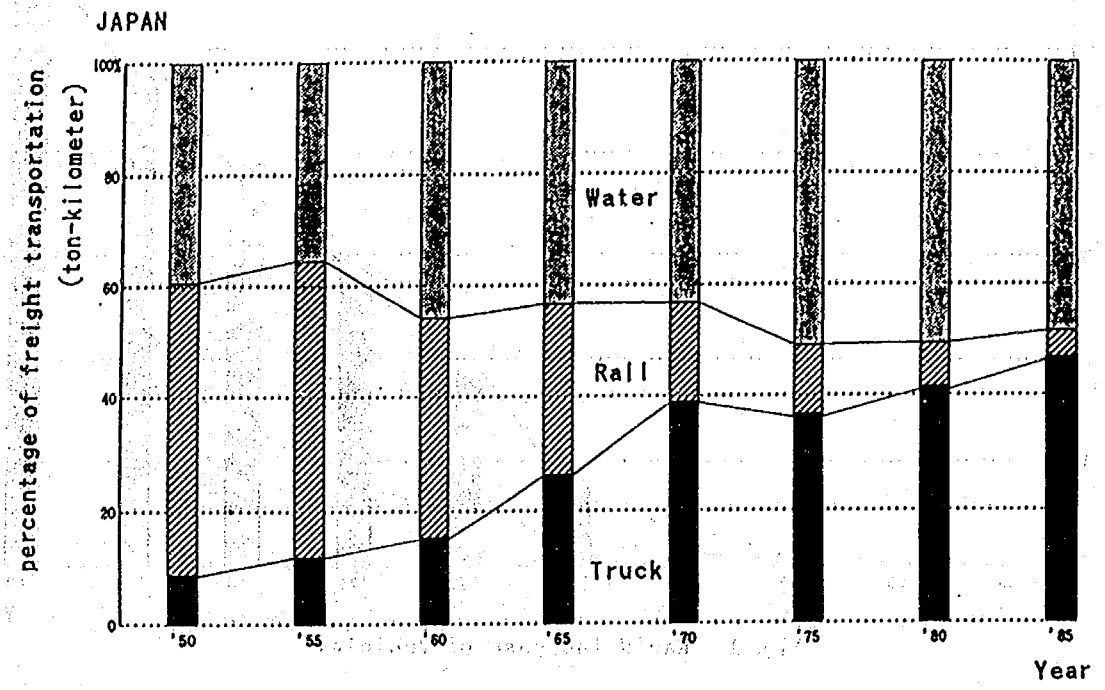

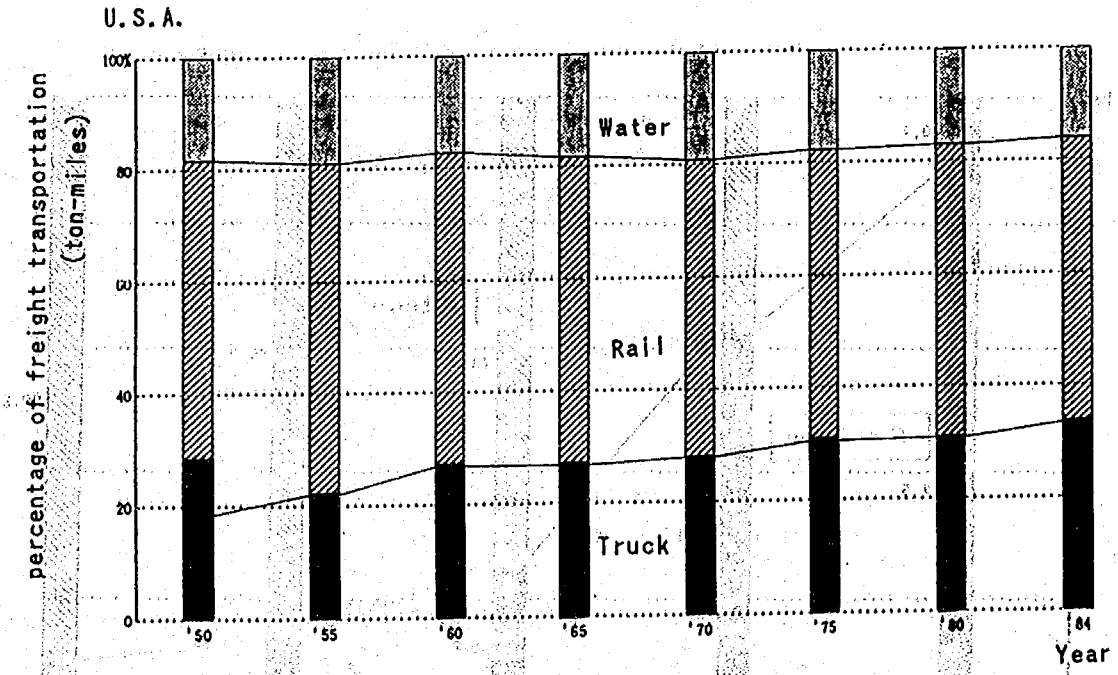

Fig. 3 The Share of Freight Transportation

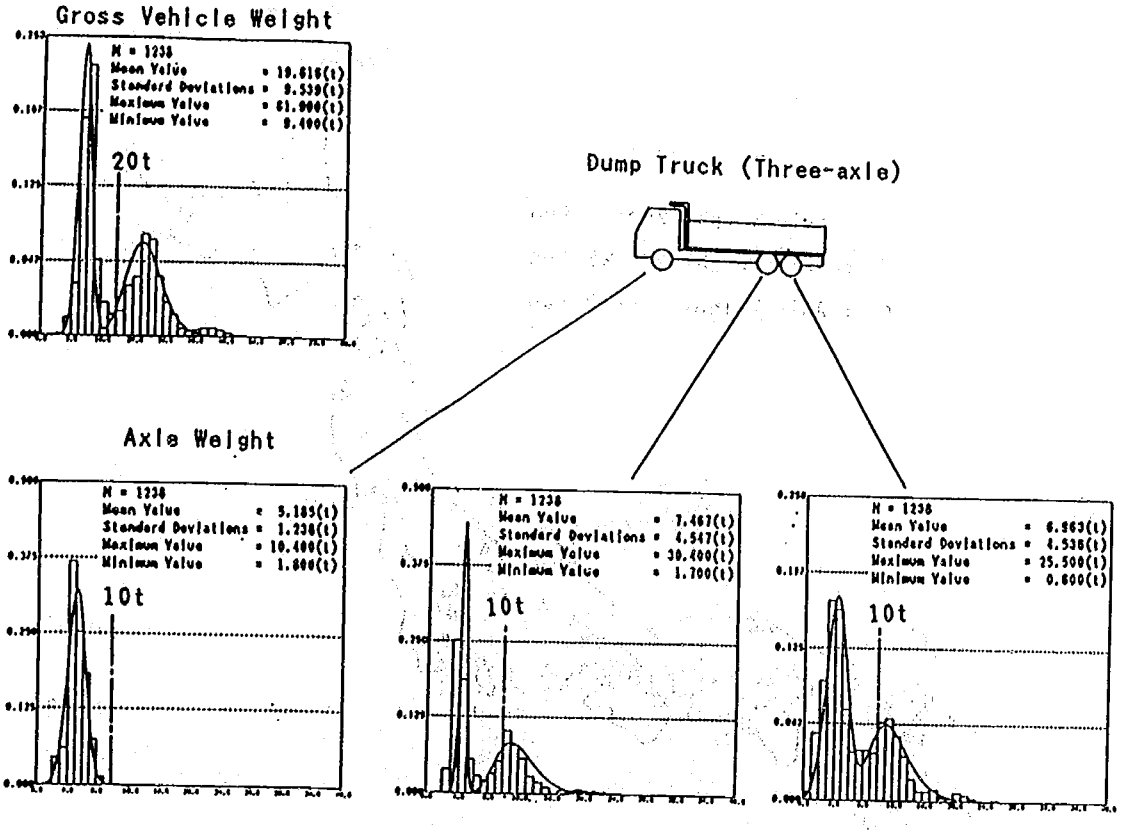

Fig. 4 Gross Vehicle Weight and Axle Weights for Dump Trucks

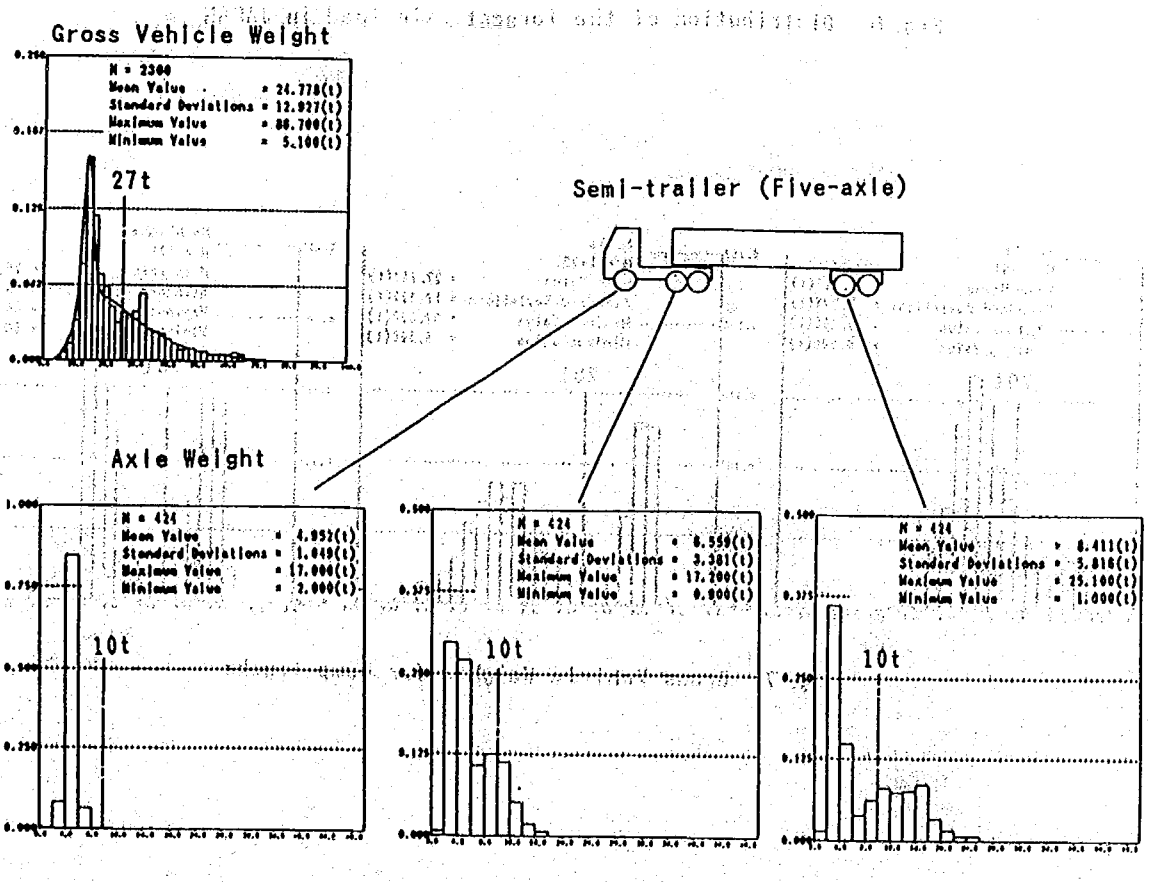

Fig. 5 Gross Vehicle Weight and Axle Weights for Semi-trailers

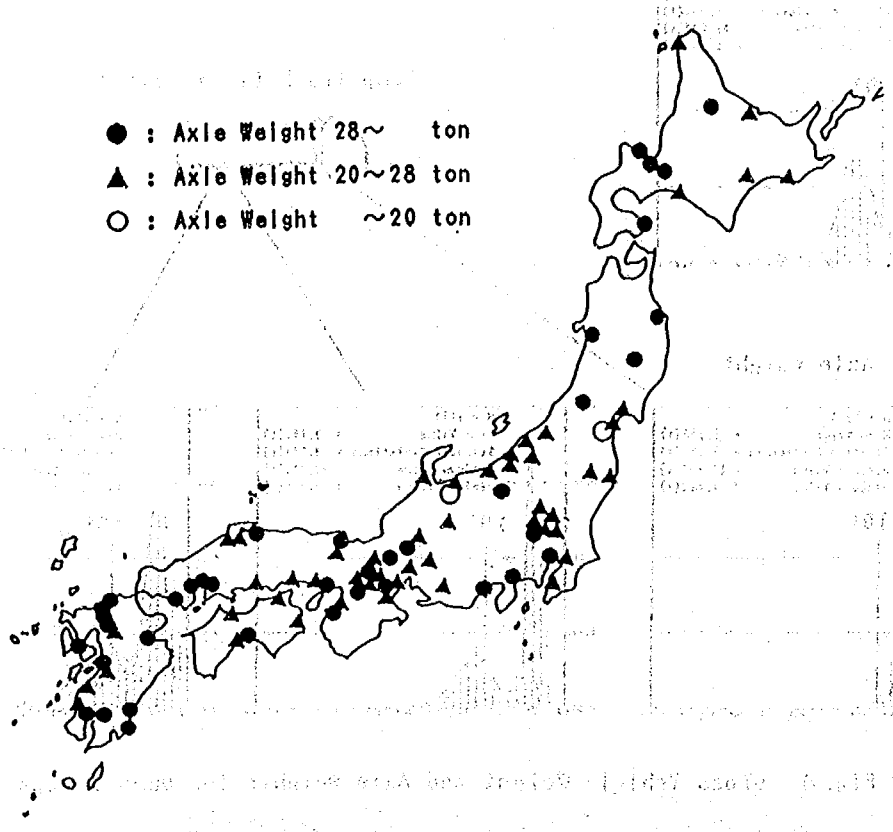

Fig. 6 Distribution of the largest axle load in JAPAN

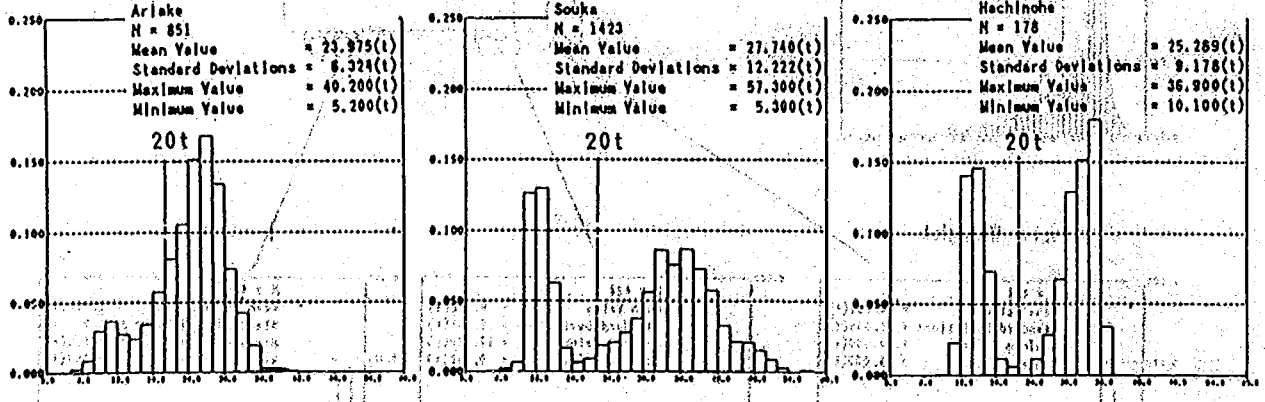

Fig. 7 Gross Vehicle Weights for Dump Trucks

7TH U. S. - JAPAN BRIDGE WORKSHOP

UNITED STATES LRFD BRIDGE SPECIFICATION

BY

JOHN M. KULICKI, Ph.D., P. E., PARTNER, MODJESKI AND MASTERS
DENNIS R. MERTZ, Ph.D., P. E., SENIOR ENGINEER, MODJESKI AND MASTERS

HISTORY

The current bridge design specification used in the United States is the Standard Specification for Highway Bridges, 14th Edition, 1989, adopted by the American Association of State Highways and Transportation Officials commonly known as AASHTO. While the specification bears a 1989 date, it in fact is a document that has gone through nearly seven decades of evolution since its first edition. After initial adoption, the specification has been maintained through the efforts of the Subcommittee on Bridges and Structures, which contributed largely volunteer effort to maintain the document and keep it relatively up-to-date by incorporating proposals from various researchers and practitioners. After nearly six decades of that process, the specification contained numerous contradictions and was becoming increasingly difficult to read and in some cases was almost incoherent.

In the early 1980's an effort was made to editorially rearrange the material, and to start to address the internal contradictions. This effort led to the 13th Edition of the specification in 1983. While a significant improvement to the wording of the specification, this edition did not change the basic philosophical approach of the specification, which involved design by either of the following methods:

- Allowable Stress Design, which treated each load on the structure as equal from the viewpoint of its statistical variability. A "common sense" approach was taken to recognize that some groups of loadings were less likely to occur than others; e.g., a loading combination involving 100 mile-an-hour wind, dead load, full shrinkage in temperature was thought to be less likely than a load combination involving dead load plus the full design live load. In this case, the former load combination was permitted to produce a stress equal to 133 percent of the latter.
- Load factor design, in which a preliminary effort was made to recognize that live load, in particular, was highly more variable than dead load. This thought is embodied in the concept of having different multipliers on dead load and live load, e.g., a load combination involving 130 percent of the dead load, plus 217 percent of the live load equal to a measure of resistance based primarily on the inelastic capacity of the cross-section.

In 1979 the Ontario Ministry of Transport Communciation released its 1st Edition of the Ontario Highway Bridge Design Code - a bridge specification based on reliability theory with load and resistance factors determined by a probabilistic process. This document was updated in 1983, and a 3rd Edition is to be released imminently. Work on probabilistically-based

bridge design specifications has also been underway in Europe, the United Kingdom and elsewhere.

In the United States, a ground swell began to develop in the middle 1980's which favored the development of a completely new AASHTO specification in order to incorporate technical advances in calculation techniques, resistance equations, and to change the underlying philosophy of safety.

Responding to this need, the National Cooperative Highway Research Program, a mission-directed, short-range research funding agency of the National Transportation Research Board, a Division of the National Academy of Science and Engineering, contracted with Modjeski and Masters in 1986 to study the principals of safety philosophy underlying the OHBDC, the current AASHTO specifications in both load factor and allowable stress formulations, as well as other key specifications such as the BS5400, specification work underway in Europe, and the specification of the Japan Roads Association.

In May of 1987 a report was submitted to the Annual Meeting of the Subcommittee on Bridges and Structures making the following recommendations:

- The AASHTO Specifications should be completely rewritten.
- The specification needed to be significantly altered to incorporate the latest research findings on 50 specific technical issues.
- The specification should be provided with a commentary for the first time in its seven-decade existence.
- The underlying safety philosophy should be calibrated load and resistance factor design (LRFD) known in some countries as probabilistic limits states design.

ORGANIZATION AND ADMINISTRATION

The Subcommittee accepted these recommendations, and in July of 1988 Modjeski and Masters was authorized to assemble a team of experts and write a calibrated, probabilistically-based design specification. A core group called the Code Coordinating Committee (CCC) was assembled and they in turn nominated experts in various disciplines of bridge engineering to work in committees called Task Groups.

Fifty-six nationally and internationally known experts were organized into the following 14 Task Groups, 13 of which were responsible for writing the text of the chapters of the specification:

- General Features
- Load and Load Factors
- Analysis of Structures
- Buried Structures
- Metal Structures
- Wood Structures

- o Decks and Deck Systems
- o Concrete Structures
- o Foundations
- o Abutments, Walls and Piers
- o Joints and Bearings
- o Bridge Railings
- o Movable Bridges
- o Calibration

The fourteenth group, Calibration, did not write a section of the specification per se. This group contains the reliability experts who produced the load factors and resistance factors for all of the rest of the working groups using probabilistically-based reliability theory calibrated to past practice.

The objective given the working groups was to produce a document which was:

- o Technically state-of-the-art
- o Comprehensive
- o Readable and practical
- o Emphasized redundancy and ductility
- o Emphasized multi-disciplinary approaches
- o Not a replacement for textbooks

MAJOR CHANGES

Perhaps the most pervasive change in the specification in terms of its impact throughout all its chapters, is the conversion to one unified design philosophy called Load and Resistance Factor Design which will replace the dual allowable stress design-load factor design in the current specification. Four limit states have been identified and they are:

- o Strength limit states involving safety for a load or combination of loads which may come on the structure once in its design life of 75 years.
- o Service limit states which involve loads which may be repeated on a weekly or even daily basis, and for which the structure must respond within the limits of certain stress, crack width, or deformation and vibration limits.
- o Extreme event limit states which deal with loadings having extraordinary return periods, such as major earthquakes, vessel or vehicle impact, or impact by large ice flows for which the structure need only survive in a stable and safe enough condition so that it may be utilized by emergency vehicles after the event, or so that occupants of the structure at the time of the event may get off safely.

- Fatigue and Fracture limit states which involves numerous applications of service load stresses for which fatigue propagation will not result in fracture. Fracture toughness is specified for the specific material and temperature zone in the material specifications rather than the design specifications.

Other areas of major change to the specification include:

- Revised load factors
- Revised resistance factors
- Entirely new design load combinations
- A new live load model
- Revised procedures and equations for analysis and load distribution
- A totally combined concrete section intergrating plain, reinforced and prestressed concrete
- Limit states presentation for soils, foundations, and retaining walls
- Increased emphasis on bridge hydraulics and scour prevention
- Minor revisions to the 1983 AASHTO guide specification for seismic design which is fully intergrated into the current specification
- Inclusion of specifications for the design of segmental concrete bridges
- A methodology for design for ship collision
- Crash testing provisions for bridge railings
- Introduction of the isotropic concrete deck as equivalent to the conventional moment design

CALIBRATION

The process of calibration to a pre-chosen reliability index will intimately interrelate the values of nominal loads and resistance, their bias, coefficient of variation of loads and resistance, the load factors and resistance factors in the specification, and the reliability index. The reliability index may be thought of as evolving from the following process. Loads and resistance are thought of as uncorrelated statistical quantities shown schematically as normal distributions in Figure 1. The nominal loads, Q, are multiplied by load factors, γ_i, and the nominal resistance, R, is reduced by a resistance factor, ϕ, to separate the distribution curves of loads and resistances so that the area of overlap,

where resistance is less than loads, is as small as desired. The nominal values of loads and resistance are related to their respective mean values by their biases.

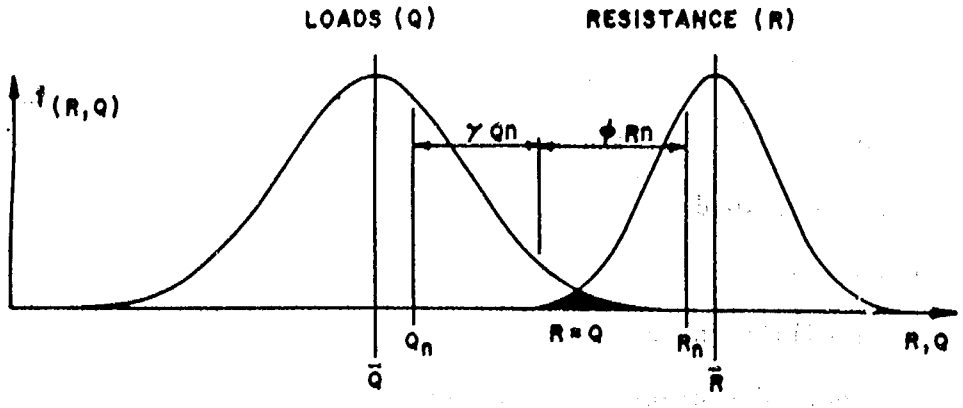

Figure 1 - Loads and Resistance as Normally Distributed Variables

One of the basic concepts of the probabilistically-based specifications is that they recognize that a societal decision is required as to the frequency of nominal attainment of the design criteria, i.e., resistance less than loads. The deterministic specifications, such as allowable stress design and load factor design methods in the current specification, do not explicitly address this question, and therefore, lead many people to believe that they absolutely preclude the situation in which resistance could be less than loads. Obviously, this can happen regardless of the philosophy of safety used in a design specification.

If the statistical variation of the combined quantity mean resistance minus mean loads was known, then that portion of the distribution of mean-resistance-minus-mean-loads which was negative could be made as small as desired by defining a design point where mean loads would be equal to mean resistance as some number of standard deviations (Beta), away from the mean value. This concept is illustrated in Figure 2. The value of Beta can be selected to make the frequency of occurrence of the design event as small as desired.

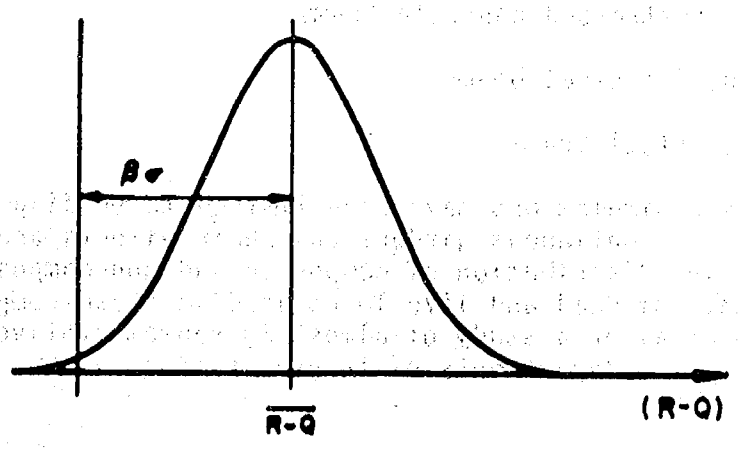

Figure 2 - Combined Distribution

The multiplier Beta is known as a reliability index and may be expressed, for the idealized case of normal distribution curves, by the following equation:

$$\beta = \frac{\lambda \Sigma \gamma_i Q_i - \phi \bar{Q}}{\phi \sqrt{\sigma_r^2 + \sigma_Q^2}}$$

where γ_i = A load factor applied to

Q_i = A nominal load

$\bar{Q}$ = Mean load

β = Reliability index

σ_r = Standard deviation of resistance

σ_Q = Standard deviation of loads

λ = Bias of loads which is the mean value divided by the nominal value

In an optimally designed structure, the resistance will be nearly equal to the sum of the factored loads divided by the resistance factor. Therefore, it can be seen that the reliability index requires accurate representations of statistically variable loads. These representations are called load models.

Preliminary calibration calculations have been undertaken by the Calibration Task Group based on computer simulation of 195 bridges involving the following combination of variables:

- Girder spacings from 4 feet to 12 feet
- Spans ranging from 20 feet to 200 feet
- Reinforced concrete beams
- Precast prestressed concrete beams
- Non-composite steel beams
- Composite steel beams

So far, these simulations have been limited to bending moments in simple span girders. Continuous girders and shear effects are currently being evaluated. The distribution of composite and non-composite loads and the relative amounts of dead and live loads used in these computer simulations were developed after a study of almost 70 representative plans submitted by several state departments of transportation.

Preliminary calibration calculations have resulted in the following tenative values of load factors:

- o General dead load, 1.25
- o Dead load of wearing surfaces and utilities, 1.50
- o Live load, 1.70

The corresponding resistance factors for bending are as follows:

- o Reinforced concrete, 0.90
- o Prestressed concrete, 1.00
- o Composite or non-composite steel, 0.95

IMPROVED LOAD MODEL

Since 1944, the AASHTO Specification has utilized the so-called HS truck and lane loading. The largest HS truck specified is the HS20-44 which is shown in Figure 3. On longer structures this truck configuration is replaced by a combination of uniform load and concentrated load also shown in Figure 3. In the 47 years since this load was first introduced, the weights and configurations of vehicles on U. S. highways have changed dramatically, as has the density of traffic which speaks to the probable occurrence of one or more trucks on the bridge.

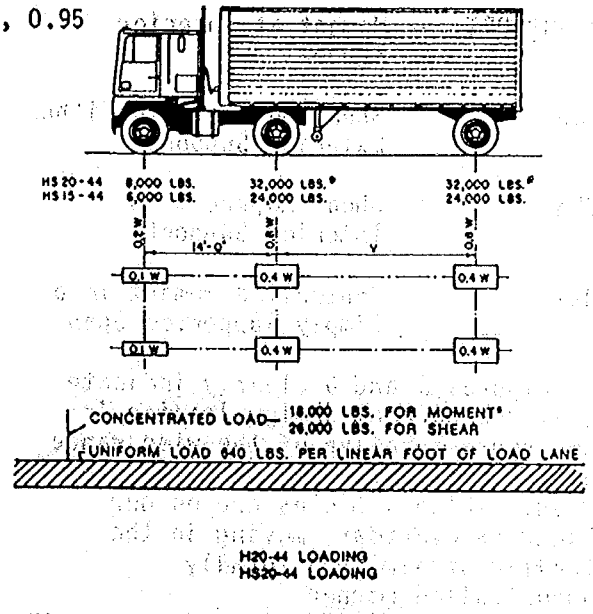

Figure 3 - Current AASHTO Live Loads

A recent study commissioned by the National Transportation Research Board entitled "Truck Weight Limits - Issues and Options" reviewed configurations of vehicles allowed on the highways by various states as exceptions to certain national weight limits. The Loads Task Group extracted 22 representative vehicles configurations from that study, the smallest and largest of which are shown in Figure 4. The results of comparing bending moments and shears in simple span and two-span continuous girders ranging from spans of 20 to 150 feet produced by the HS20 loading and the envelope of results

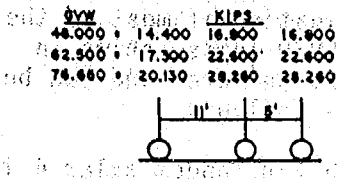

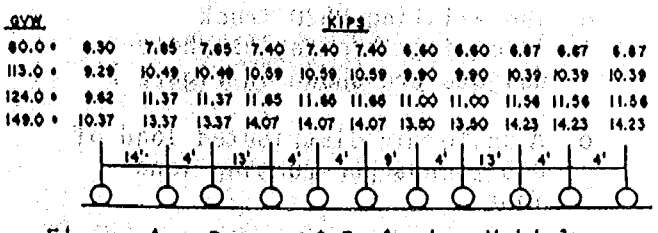

Figure 4 - Range of Exclusion Vehicles

produced by the 22 load configurations is shown in Figures 5 and 6, respectively.

The following nomenclature applies to Figures 5, 6, 8 and 9:

M POS .4L = Positive Moment at 4/10 Point in Either Span

M NEG .4L = Negative Moment at 4/10 Point in Either Span

M SUPPORT = Moment at Interior Support

Vab = Shear Adjacent to Either Exterior Support

Vba = Shear Adjacent to Interior Support

Mss = Centerline Moment in a Simply Supported Span

Figures 5 and 6 clearly indicate that the current design loading is not representative of the wide range of vehicles currently on U. S. highways. These vehicles are on our highways everyday, moving in the traffic stream in a totally uncontrolled manner.

After studies of numerous proposed live load models, the relatively simple combination of most of the existing AASHTO loads, shown in Figure 7, was selected and can be described as follows:

- Two 25 kip tandem axles 4 feet apart
- The existing HS20 truck involving three axles whose weights are shown in Figure 7
- A uniformly distributed load of 640 pounds per running lane foot

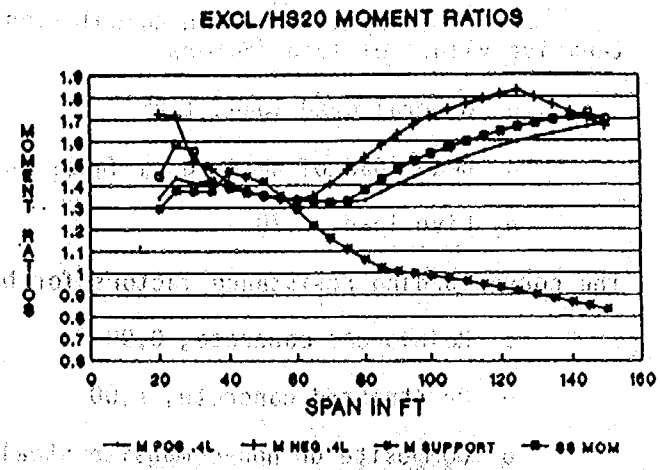

Figure 5 - Ratio of Moments - Exclusion/AASHTO

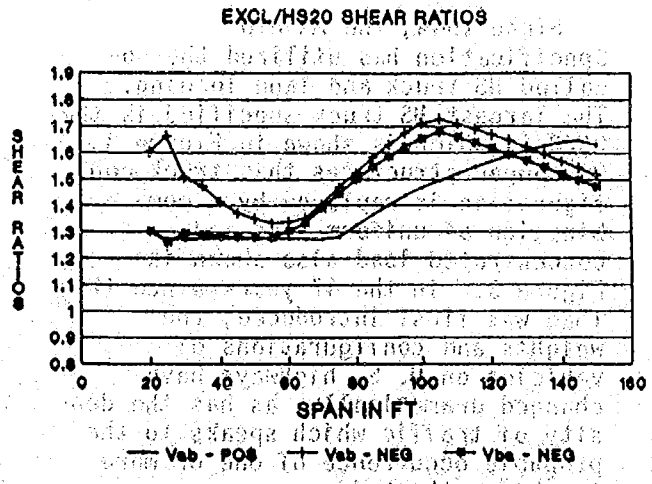

Figure 6 - Ratio of Shears - Exclusive/AASHTO

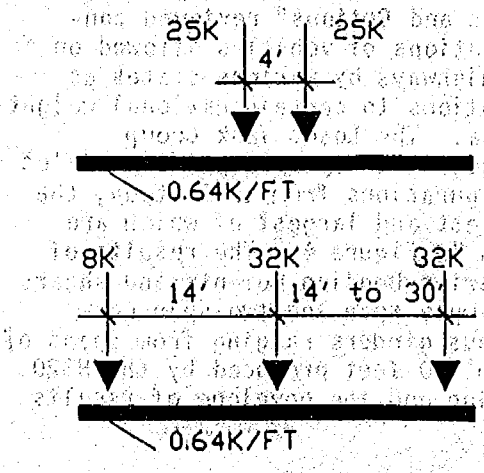

PROPOSED LIVE LOADS

Figure 7 - Proposed New Live Load

These live load models are combined in the following fashions:

- o General design load - either the tandem axles coincident with the uniform load or the HS20 truck coincident with the uniform load, whichever produces the larger result
- o Deck design load - either the tandem axle or the HS20 loading without the uniform load
- o Fatigue load - one HS20 truck regardless of the number of lanes or the length of the structure, without the uniform load, and reduced by a statistical factor based on applying Minor's Law to describe the cumulative damage of a spectrum of variable weight trucks correlated to the HS20 truck.

The results of re-analyzing the simple span and two-span continuous units described above for the basic live load are shown in Figures 8 and 9, respectively. These figures show that, with the exception of negative moment at a support, the moment and shear ratios calculated for selected points cluster much more regularly and tightly than those shown in Figure 5 and 6. The fact that the values cluster at about the same central trend for various spans indicates that a load factor can be independent of span length. That observation, taken with the tight clustering of both shear and moment about the same central trend, indicates that the load factor can be taken as a constant value for shear and moment regardless of span. As previously stated, the tentative value for that factor is 1.7 based on a comparison of the shear and moment produced by the live load model and a statistical simulation of 75-year mean maximum values utilizing measured truck weights from sta-

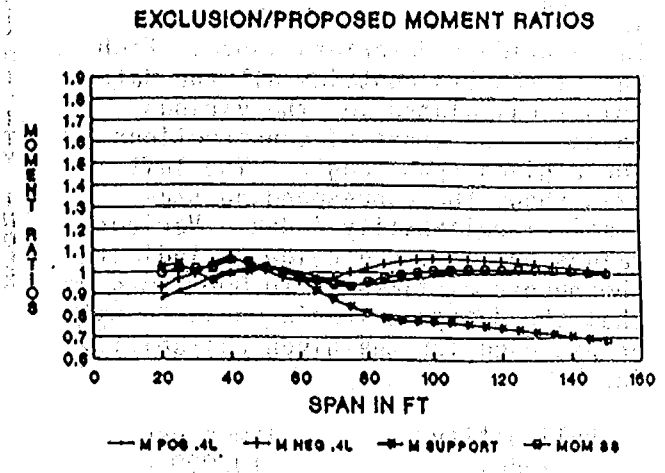

Figure 8 - Moment Ratio - Exclusion/Proposed

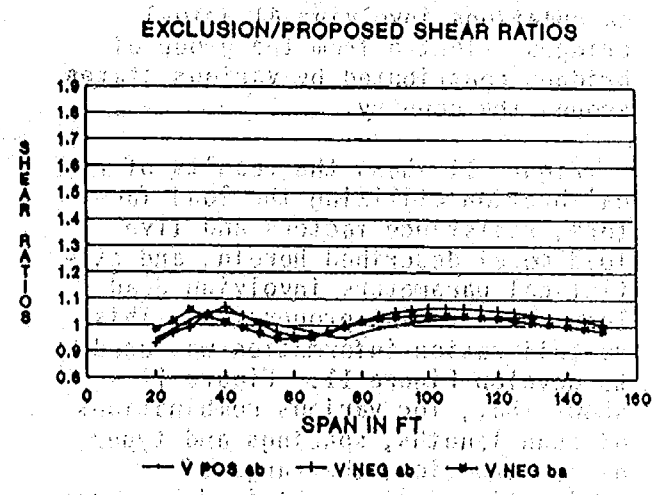

Figure 9 - Shear Ratio - Exclusion/Proposed

tionary scales, selected weigh in motion studies, and a review of overweight citations in one state.

RESULTS OF THE CALIBRATION PROCESS

Figure 10 shows the reliability indices obtained for the 195 simulated bridges described above. Each bar of results contains all the data points calculated for the various spacings and types of constructions for a given span length. The left axis shows the corresponding statistical reliability index. Various values are provided below to indicate the number of times in 10,000 times that the design criteria would be met or exceeded for the given reliability index.

Reliability Index	Times per 10,000
1	1,587
2	228
3	13
4	< 1

As can be seen, design processes, models and load factors in the existing AASHTO Specification yield to wide range of results. This range of results was also observed in calculations involving 41 actual bridges selected from the group of bridges contributed by various states around the country.

Figure 11 shows the results of re-calibration utilizing the load factors, resistance factors and live load model described herein, and statistical parameters involving dead load and material properties. This re-calibration information was used to develop Figure 11. Figure 11 shows that, for various combinations of span lengths, spacings and types of construction, the range of reliability indices obtained has been extremely reduced. This achievement of much more uniform safety in

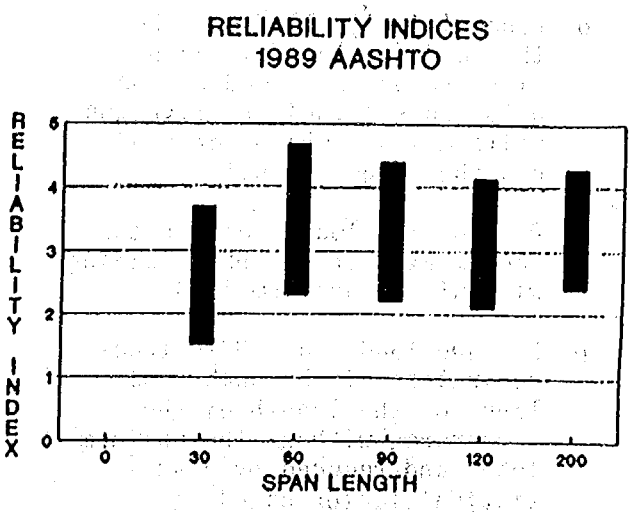

Figure 10 - Current Reliability Indicies

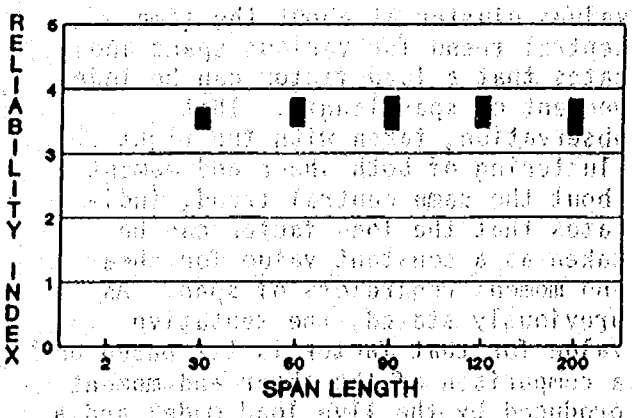

Figure 11 - Reliability Indicies Under Proposed Specification

bridges was one of the major objectives of utilizing probabilistic LRFD as the philosophical basis for the new specification.

While the compression of reliability indicies resulting from the proposed specification is gratifying, the major result of this project is that the proposed specification has a consistent, adaptable philosophical basis. As new data on the variation of loads, material properties, and construction tolerances becomes available, this information can be incorporated in a revised calibration to consistent safety. Conversely, if society determines that the target reliability factor should be raised or lowered, the process yields consistent load and resistance factors.

REVIEW PROCESS

In an open democratic society, it is vitally important that the bridge design community have an opportunity to review and comment on proposed new specifications. To that end, the first draft of the LRFD Specification was submitted to:

- All members of all Task Groups working on the project
- All members of the Oversight Panel which represented industry, academia and government
- The chief bridge engineers of all 50 states
- The Central and Regional Offices of the Federal Highway Administration, and
- Several private bridge authorities.

Their review of the first draft specification led to over 4,000 comments which were reviewed and discussed by the Task Groups. Many of the comments were incorporated in the second draft specification which has just been released.

That second draft will be available not only to the same group of approximately 250 people who received access to the first draft, but will also be made available to any bridge engineer anywhere who is willing to purchase a copy from the NCHRP. All individuals are free to submit comments on the second draft specification. Additionally, industry groups are currently assessing the impact of the new specification by comparison to past designs.

FUTURE ACTIVITIES

It is anticipated that during the summer of 1991 several state departments of transportation will voluntarily do a series of comparative designs to be developed by the Research Team to fully exercise the specification. The results of these trial designs will be presented to a special meeting of the Subcommittee on Bridges and Structures to be assembled in St. Louis in mid-September to review the results of the comparative design and to discuss the specification in detail.

Comments received from this review process will be reviewed and incorporated as necessary as the second draft is processed into third draft status - the draft which will be submitted to the Subcommittee for consideration for adoption. The earliest possible adoption date is late 1993.

ACKNOWLEDGEMENTS

The Authors express appreciation to the following individuals whose support and assistance has been most important:

Mr. Ian M. Friedland, Project Officer for the NCHRP

Mr. Veldo M. Goins, Chairman of the Oversight Panel

Mr. Clellon Loveall, Chairman of the AASHTO Subcommittee on Bridges and Structures

(9) Session 9

SESSION 9: BRIDGE CONSTRUCTION(1) 1:10pm～1:55pm
(Co-Chairmen: K. Nishikawa, E. Maragakis)

(25) T. Maruyama* , M. Kamei and H. Tanaka: Design and Erection of Mono-Cable and Self-Anchored Suspension Bridge
(1:10pm～1:25pm)

(26) J. H. Clark: West Seattle Swing Bridge
(1:25pm～1:40pm)

DISCUSSION
(1:40pm～1:55pm)

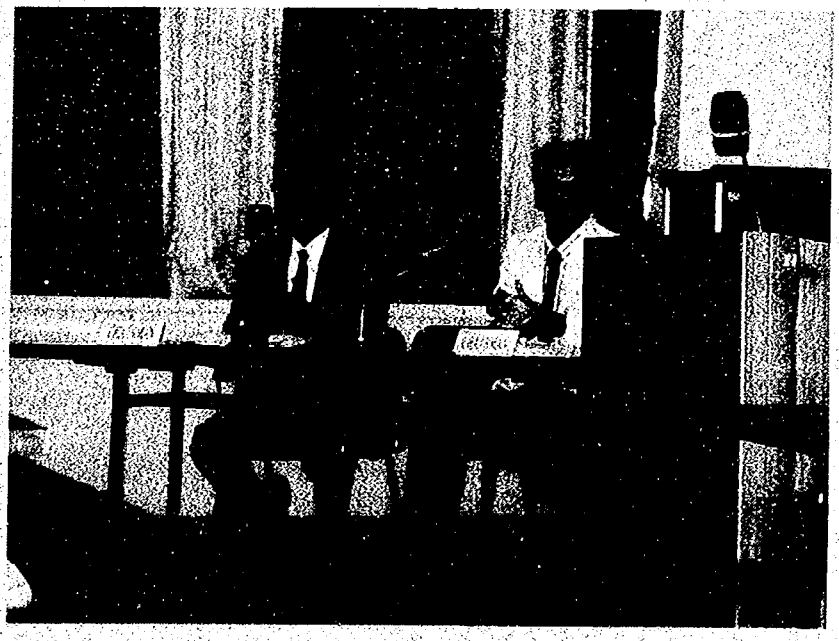

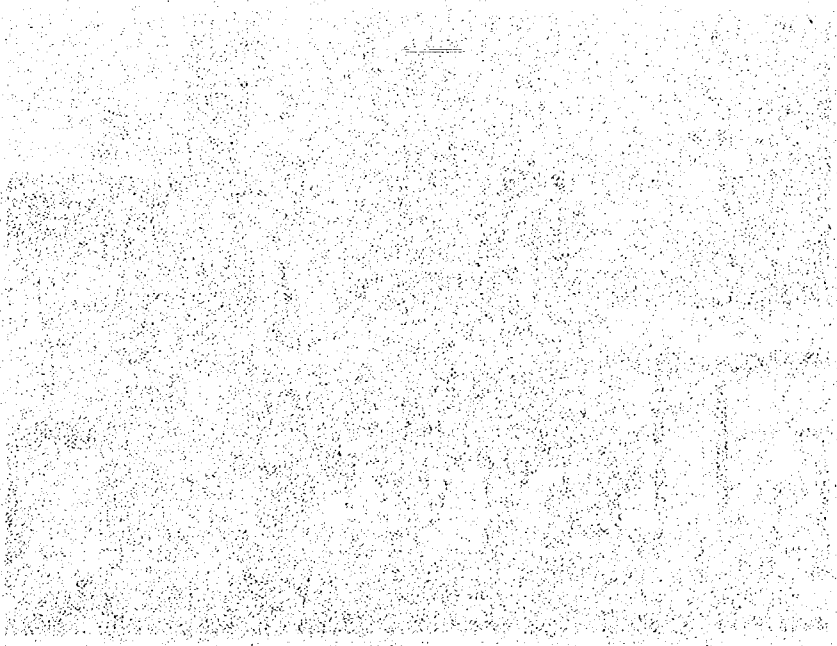

DESIGN AND ERECTION OF MONO-CABLE AND SELF-ANCHORED SUSPENSION BRIDGE

Tadaaki MARUYAMA
Chief of Bridge Dept. Public Works Bureau
Osaka Municipal Government
2-2-500, Umeda 1-Chome, Kita-Ku, Osaka 530, JAPAN

Masahiro KAMEI
Staff Officer of Elevated Crossings Dept. Public Works Bureau
Osaka Municipal Government
2-2-500, Umeda 1-Chome, Kita-Ku, Osaka 530, JAPAN

Hiroshi TANAKA
Assistant Manager of Steel Structure Design Dept.
Hitachi Zosen Corporation
3-40, Sakurajima 1-Chome, Konohana-Ku, Osaka 554, JAPAN

ABSTRACT

The Konohana Bridge is a self-anchored suspension bridge with inclined hangers. This type of bridge is the first idealization in the world. From the point of structural analysis the bridge has the similar characteristics of a cable-stayed bridge because its girder carries the portion of the dead load therefore the bending moment is caused in the girder. In addition, cable tension adjustment of hangers was necessary to keep prestress in erection. New technologies were developed by achieving numerous experiments and analyses. The construction of the Konohana Bridge marked an epoch not only in bridge technologies but also in bridge aesthetics.

1. INTRODUCTION

Construction of the reclaimed land located in the northern part of Osaka port is now taking place (Fig. 1). Its area consists of the north district (approx. 2.2 million m^2) and the southern district (approx. 3.9 million m^2). Effective land use is being planned under the name "TECHNOPORT OSAKA".

Its purpose is to build a city that provides multi-functions such as information, leading technologies and international trade. It is also intended that people will enjoy good living circumstances and culture events there.

In order to encourage this development, the Konohana Bridge (Photo 1) and its approach bridges constructed; these will have a total length of 1.7 km, as shown in Fig. 2. These bridges connect city centers with the reclaimed land.

This route will be connected to the Osaka Bay route which is simultaneously being constructed by the Hanshin Expressway Public Corporation and becoming a part of the traffic system of Osaka bay area.

Fig. 2 shows the main bridge over the sea, the approach to the northern district and to the downtown district.

The bridge type, a monocable three-span self-anchored suspension bridge, was selected considering various conditions such as economy, high-way route configuration, and navigation channel space (Fig. 3, Photo 1).

The configuration of the stiffening girder is chosen as inverted-trapezoidal because it serves as a main cable anchorage which is installed in it to resist the huge axial force introduced by the main cable.

Hangers are arranged between the single-plane main cable and a central web. Their inclined arrangement improves structural rigidity and increases dynamic damping. The hanger system disperses live load effects in the axial direction. This bridge is the first realization of its type in the world; therefore numerous experiments and analyses were performed in the course of establishing the appropriate design.

2. DESIGN DIMENSIONS

Bridge type: Mono-cable self-anchored suspension bridge
Bridge class: Class 1
Design load: TL-20 and TT-43
Design traffic speed: 60 km/hr.
Span length: $120^{m} + 300^{m} + 120^{m}$
Clear width of roadway; 23.5^{m} (4-lanes roadway with 2-side walks)
Longitudinal gradient: Center span; 1% parabola, Side span; 2% straight line
Navigation channel span: 160^{m}
Navigation under-clearance: O.P. + 33.7^{m} (above sea level)
Stiffening girder type: Steel inverted-trapezoidal box girder with two cells
Tower type: A shape
Hanger arrangement: Hung between main cable and center web, slanted
Steel weight: Approx. 11,220 ton (c.f. Table-1)
Foundation: Steel pipe pile foundation ($\phi 1.5^{m}$)
Length = 51.4^{m}

3. LOAD AND ALLOWABLE STRESS

3.1 Load

Following is explanations of some special considerations in the design of this bridge. Others not detailed here are based on the Specifications for Highway Bridges published by the Japan Road Association (hereafter called "Highway Code").

1) Live Load

The vehicle load and crowd load were determined not only by the "Highway Code" but also by the "Design Code of the Superstructure of the Honshu-Shikoku Bridge"[2] (hereafter referred to as the "Honshu-Shikoku Code").

2) Impact

The "Highway Code" refers to impact relative to hangers only but not to main cables and stiffening girders for the design of a suspension bridge. However since this bridge has self-anchorage and a box type stiffening girder, the characteristics of structure are rather similar to those of a cable-stayed bridge. Dead weight has a great influence on the main cable and tower; an impact factor (=i) was not applied to them. As to the stiffening girder and hangers, this factor was established uniformly as i = 0.10 after the case of cable-stayed bridge and this was proved adequate by the field load tests.

3) Influence of Prestress

Prestress introduced into the hangers was considered as the principal load, together with dead load and live load.

4) Temperature load

The range of temperature variations is considered to be ±35°C. This range reduces to ±15°C when combined with the wind and seismic loads.

The maximum temperature difference between parts of the structure is considered to be ±15°C. This reduces to ±7.5°C when combined with a temperature variation of ±35°.

5) Wind load

Basic design wind speed is 50^{m}/sec.

Design wind speed is determined by using a modification factor for height, and longitudinal and vertical length of structure.

For example, adopted design wind speed for the stiffening girder is 72^{m}/sec, for the main cable 77.95^{m}/sec, for hangers 77.95^{m}/sec, and for the tower, 79.2^{m}/sec, respectively.

6) Seismic load

Seismic design intensity (e.g. seismic coefficient = 0.3) was determined according to "Highway Code; Earthquake-proof Design" which refers to the method of modified seismic design. The ground condition is very weak at the site. Safety was verified by doing dynamic analyses considering soil-structure interaction.

7) Erection tolerances

Erection tolerances of towers are considered for both longitudinal and lateral directions. The value of these was set at $h_t/1000 = 7.5$ cm (h_t; tower height). For hangers, two items, T_{E1} and T_{E2}, were considered. T_{E1} is possible measurement error of instruments and is 10% of tension force of dead load. T_{E2} is ±5ton which is an allowable range for adjustment of the hanger force.

8) Influence of displacement of supports

Estimated non-uniform sinking is 10 cm.

Each pier is presumed to sink independently and the most disadvantageous combination of supporting pier sinking is considered in the static analysis.

9) Load for fatigue verification

For hanger fatigue, 50% of difference between maximum and minimum tension force by live load is considered, referred to DIN 1073.[3)]

3.2 Allowable Stress

Allowable Stress of the steel material is applied from "Highway Code". σ_{ta}; the allowable tensile stress of the main cable is 64 kgf/mm^2. Hanger σ_{ta} is determined as the rupture tensile stress using a safety factor of three. Therefore σ_{ta} of parallel wire strands (P.W.S) made of galvanized steel wire is 53.3 kgf/mm^2 (=160/3). If the secondary stress is considered, the safety factor become two. Furthermore, the fatigue allowable stress range of the hanger is 17 kgf/mm^2 taking into account past experimental values. If the secondary stress is considered, the allowable stress becomes 20 kgf/mm^2.

4. DESIGN OF SUPERSTRUCTURE WORK

4.1 Tower

The tower has the following characteristics compared with a conventional suspension bridge.

1) The tower configuration above the horizontal beam is A-shape which is adequate for the monocable as shown in figure 4.
2) The tower and stiffening girder are coupled with pins at the horizontal beam of the tower. Therefore the longitudinal direction force of earthquake is reacted at two supporting points.
3) The tower foundation is connected to the steel frame with high tension bolt (H.T.B) which is buried in the bridge pier.

When a suspension bridge tower is designed at present, it is conventional to refer to the proposal for the design of such towers and its explanation in the Honshu-Shikoku Code. Nevertheless, since this bridge has the features mentioned above, it is inappropriate for the direct apply of that code. Therefore the "Highway Code" was mainly applied, and the "Honshu-Shikoku Code" was only referred to in particular instances.

Furthermore, a load test was carried[4] out using a tower model on a scale of 1:20 to confirm the ultimate strength of inplane of the tower. Figure 4 shows that tower corner turns round at the horizontal beam and in this corner complex stresses are incurred because of the axial force and torque under girder stretching. Another load test which will be mensioned later was performed to clarify the stress distribution and ultimate strength with a corner model. Tower dimensions and typical cross sections are illustrated in figure 4.

4.2 Stiffening Girder

The stiffening girder of this bridge (Fig. 5) is an inverted-trapezoidal box with two cells. A central web is located in the box section, and connection plates of hangers are also installed on the steel deck plate every ten meters longitudinally.

The connection plates and central web plates are as one body however the thickness of the former is 38mm (SM58) and that of latter, 12mm (SS41).

Two webs act as longitudinal plates which resist the cable anchorage girder force at the main cable anchorage (Fig. 6). The height of the stiffening girder here becomes somewhat larger than the typical part to contain the main cable anchorage. The ratio of girder height to center span is about 1:100 and it is smaller than that of a conventional cable stayed bridge.

The plate thickness of main deck plate is 12mm, which is stiffened by longitudinal ribs (trough ribs) at 650mm intervals and also by lateral diaphragms at 3,333mm intervals. The plate thickness of the main deck plate is increased, however, to 25mm in the vicinity of the main cable anchorage.

As for the erection method, among several alternative erection plans, a bent construction method was chosen. This method is competent for the self-anchored bridge.

In an early erection stage, the stiffening girder was laid on temporary stagings and piers without hangers. In this stage the bridge looks, therefore, like a box girder bridge and a large moment was incurred in it. Lower flanges were determined not only for the completed stage but also for this erection stage. The lower flange thickness is from 12mm to 16mm. Fig. 7 shows the design bending moment diagram of the stiffening girder due to dead load and live load.

The main cable anchorage, which contains 30 strands, is located at the end of the girder. It differs from the case of a cable-stayed bridge. Consequently, not only a conventional analysis method[6] but also an FEM analysis were applied for its cross sectional determinations.

4.3 Main Cable

The main cable consists of 30 strands; each strand is made up of P.W.S. 184 (wire diameter 5.2mm). On the assumption that its void ratio is 20%, the diameter of the main cable is 432mm.

The stiffening girder is comparatively wide for its height. Therefore strands are easily spread in the horizontal direction; then the strand arrangement takes advantage of this at the main cable anchorage. A flat top method is used to install the main cable in the splay saddle (figure 8).

The sag ratio is the important factor in determining the structure of a suspension bridge.

A conventional truss-type suspension bridge employs a sag ratio of 1/8 – 1/10; on the other hand a box type one takes slightly less.

This bridge is self-anchored type and the main cable is anchored inside the stiffening girders.

The axial force of the cable will become too large if the sag ratio is very small, and it becomes difficult to locate its anchorage inside the girder.

By a comparative sag ratio study, changing it from 1/5 to 1/10, and focused on economy, construction, aesthetics and other factors, 1/6 (50m) was determined as the optimum sag ratio.

The maximum main cable tensile force is 7,329 tf, with the allowable tensile strength 7,501 tf.

4.4 Hangers

Since the hangers of this bridge are inclined, compression forces are introduced due to the live load position. Hangers are made of non-compression resistant material, therefore they slacken if prestresses are not introduced.

The following conditions are satisfied in the determination of how much prestress should be introduced:

1) Leave at least a 20 ton hanger tensile force under maximum compression by live load.
2) Make the bending moment distribution in the stiffening girder smooth and its absolute value small.
3) Do not deform the catenary curve (which is not catenary precisely speaking) of the main cable excessively.

HiAm hanger cable, which has superior fatigue strength, is adopted.

Furthermore, section areas satisfy the following formula.

$$T_D + T_{Lmax} + 0.2 \times T_{SDmax} + T_{E1} + T_{E2} \leqq T_a$$
$$T_D + T_{Lmin} - T_{E1} - T_{E2} \geqq 5 \quad \ldots\ldots (1)\ a, b, c$$
$$T_D + T_{Lmin} + 0.2 \times T_{SDmin} - T_{E1} - T_{E2} \geqq 0$$

where

T_D: Design dead load axial force after completion (unit: tf)
T_{Lmax}: Max. live load axial force by influence line analysis (unit: tf)
T_{Lmin}: Min. live load axial force by influence line analysis (unit: tf)
T_{SDmax}: Max. axial force due to support subsidence (unit: tf)
T_{SDmin}: Min. axial force due to support subsidence (unit: tf)
T_{E1}: Axial force measurement error during erection (unit: tf)
T_{E2}: Allowable tension force difference between measurement value and design value (unit: tf)
T_a: Allowarable axial force (unit: tf)

Two types of ϕ7mm galvanized steel wire, HiAm 127 and HiAm 163 were used as a result of the calculations. Fig. 9 shows arrangement of HiAm 127 and HiAm 163 in hangers.

Table 2 shows the hanger cross sections and their area in addition to their allowable axial force. Hangers are connected to the stiffening girder and the main cable respectively by pins. A load cell and shim plates to adjust axial force are inserted in the socket of the stiffening girder (Fig. 10).

Corrosion of hangers is prevented by galvanizing the wire, wrapping the surface of the bundled strands in polyethylene film and then wrapping two layers of butyl based rubber on top of them. An aluminum cover is used to prevent deterioration of the rubber and for a better appearance (Fig. 11).

The new tensile adjustment system was developed and tensile adjustment analysis has become easy and quick using computer software to which inputs come from load cells directly.[8)]

In addition to verifying hanger fatigue according to the DIN 1073 fatigue standards, the following investigations were also carried out.

Firstly, the stress fluctuation characteristics on the hangers were checked by computer traffic load simulation.

Secondly, a prototype HiAm 163 cable fatigue experiment was carried out (Photo 2) up to 5×10^6 fatigue cycles and the S-N curve was obtained by extreme value statics.

Finally, safety was confirmed with respect to fatigue by calculating cumulative damage based on the S-N curve.[9), 10)]

5. RESEARCH WORKS

5.1 Two-dimensional bridge model experiment

The model bridge on the scale 1:20 (Photo 3) was built to ensure the analytical method during erection, the hanger adjustment and applications of live loads.

In addition to the above, the dynamic behaviors of the suspension bridge with the inclined hangers were also examined through the vibration tests. Changing inclined hangers to vertical hangers, the following are confirmed; the stiffness and damping of the bridge with inclined hangers is larger than those of vertical ones and it is advantageous to resist earthquake or wind loads. However fluctuation of hanger force in inclined hangers is large and it is harmful to fatigue loads (Fig. 12).

5.2 Wind tunnel experiment and field observation of natural wind

The aerodynamic stability was examined by two-dimensional model on the scale 1:28 and three-dimensional model on the scale 1:59 (Photo 4) in the wind tunnel under the laminar and turbulent flows.

The aerodynamic stability and the efficiency of the stabilizer such as flaps and fairings were investigated.

As can be seen from Fig. 13, the appearance of vortex shedding was observed at low wind velocity. After many wind tunnel test, finally the vortex shedding was completely suppressed by flap and spoiler. Torsional flutter was also shifted to higher wind velocity range.[11)]

Simultaneously natural wind observation[12)] at the site has been carried out since 1982 when the erection started. As measurement tools, ultra-sonic anemometers were set on three bridge piers (P20, P21, P23) over the sea to get accurate wind velocity records. Test conditions such as wind direction, angle of attack, turbulence characteristics etc. were determined according to the results of onsite surveys.

Wind tunnel tests of a 3-dimensional model with a 1:59 ratio were conducted for both the erection and the completed stages[13].

The test results show favorably good agreement with those of the 2-dimensional model, both qualitatively and quantitatively. It was found[14] that the appearance of vortex shedding could be suppressed by a slightly turbulent wind.

In addition, bridge member fatigue and usability were analyzed according to a probabilistic theory using wind observation data and the results of wind tunnel tests. It was confirmed that the present cross section exhibited sufficient safety[15] and there was no need for special aerodynamic devices of damper.

Furthermore, the ultra-sonic anemometers have been moved to the central divider and accelerometers also have been set in the girder for long-term measurements to obtain strong wind characteristics and response characteristics of typhoons during both erection and completion stages. Measurements have been continued to get data base of wind.

5.3 Resistant experiment of tower corner

The ultimate strength of the corner parts of tower was inquired on the model specimen with scale 1:5 by using the hydraulic jack with capacity 600 tons (Photo 5).

5.4 Field measurement of vibration

Vibrational characteristics of the bridge were measured.[16] A truck-crane was used to vibrate the bridge by lifting the steel weight up and down. The frequency of the measurement agreed with calculated on in each mode. The dampings are shown in Table 3. The damping of torsion was much larger than the assumed one. Probably the movement of the main cable contributed to add damping.

6. ERECTION

The erection procedure of this self-anchored suspension bridge is different from that of a conventional suspension bridge. After the stiffening girder blocks and towers were erected, the main cable was strung and then the hangers were set in place. Figure 14 shows the whole erection procedure. The G1 block located on the downtown side was too heavy for the hoisting capacity of the 3000 ton floating crane. Therefore the weight was reduced by omitting some parts of the block, and temporary staging erection was performed to affix these parts using a 350 ton truck crane.

The stiffening girder was set on temporary staging and supports of a horizontal beam of the tower at higher elevation than the final elevation so that it became easy to attach the hangers. Prestresses were introduced into the hangers after the stiffening girder was jacked down. Tensile force adjustment in the hangers was done; the tensile force values are very close to the design ones. The main cable was wrapped after almost all the dead load was applied.

7. CONCLUSIONS

Thirty years have passed since Professor F. Leonhardt announced the idea of the monocable suspension bridge with inclined hangers. Since then his idea has partially been realized by using inclined hangers in dual main-cable type suspension bridges such as the Severn Bridge, Humber Bridge, Bosporus Bridge, etc.

The Konohana Bridge is not only of monocable type but is also self anchored. There were many points in this design that had to be overcome once again. Therefore many computer analyses and experiments were made, and the results thereof were reflected in the design.

REFERENCES

1) Matsukawa, A., Matsumura, H., Kamei, M., Nagai, Y., "Plan of Hokko Bridge (Provisional Name) and Erection of Substructure," Bridge and Foundation, January, 1986 (in Japanese).
2) Design Standard for Superstructure of Honshu-Shikoku Project, June, 1980.
3) DIN 1073, Stahlerne Straßen brücken, 1974.
4) Fukumoto, Y., Usami, S., Ito, Y., "Fundamental study on Strength of Main Tower of Hokko Bridge," Nagoya University Civil Engineering Research Report No. 8201, September, 1982 (in Japanese).
5) Nakai, H., Kamei, M., Yamagami, T., Okabe, S., "Research on Ultimate Strength of Tower Corner of Hokko Bridge," Proc. 40th Annual Meeting of JSCE, Part I-446, September, 1985 (in Japanese).
6) Kondo, K., et al. "Design of Cable Anchorage of Toyosato Bridge (Cable-stayed Bridge)," Proceedings of JSCE, No. 192, August, 1971 (in Japanese).
7) Matsukawa, A., Kamei, M., Mine, Y., "FEM Analysis of Main Cable Anchorage of Hokko Bridge," Proc. 40th Annual Meeting of FSCE, Part I-447, September, 1985 (in Japanese).
8) Matsukawa, A., Kamei, M., Tanaka, H., "Erection Control of Self-anchored Suspension Bridge (Hokko Bridge) with Inclined Hangers," Proc. 41th Annual Meeting of JSCE, Part I-198, November, 1986 (in japanese).
9) Matsukawa, A., Kamei, M., Mizoguchi, T., and Sasaki, Y., "Fatigue Strength analysis of Parallel Wire Strand Cables Based on the Statistical Theory of Extremes," Journal of Structural Engineering, Vol. 32A, April, 1986 (in Japanese).
10) Matsukawa, A., Kamei, M., Fukui, Y., Sasaki, Y., "Fatigue Resistance Analysis of Parallel Wire Strand Cable Based on Statistical Theory of Extreme," STAHLBAU, 11, 1985.
11) Matsukawa, A., Kamei, M., Ushio, M. and Ueda, T, "2-D Model Experiment of Hokko Bridge: Suspension Bridge with Inclined Hangers", Bridge and Foundation, June, 1986 (in Japanese).
12) Komatsu, S., et al, "Turbulence Characteristics of Natural Wind in Osaka North-Port," Proc. 41st Annual Meeting of JSCE, Part I-308, November, 1986 (in Japanese).
13) Matsukawa, A., Matsumura, H., Kamei, M., "Study on Aerodynamic Stability of Hokko Bridge," Proc. 39th Annual Meeting of JSCE, Part I-302, October, 1984 (in Japanese).
14) Matsukawa, A., Kamei, Yokota, T., "Study on Aerodynamic Stability of Hokko Bridge, " Proc. 41st Annual Meeting of JSCE, Part I-312, November 1986 (in Japanese)
15) Komatsu, S., Kobayashi, H., Kawatani, M., Matsukawa, A., "Influence of Vortex Shedding by Fluctuation of Angle of Attack," Proc. of 8th National Symposium on Wind Engineering September 1984 (in Japanese).
16) Kobayashi, H. and Kawatani, M.," Field Measurements of Vibtational Characteristics of Hokko Bridge", Research Report for Osaka Municipal office, 1987 (in Japanese).

Table 1 Weight of contents of Konohana Bridge

Approximate weight (Unit in tons)	Stiffening girder	8,210
	Towers	1,820
	Cable	710
	Hangers	240
	Shoes	190
	Others	50
	Total weight	11,220

Table 2 Hanger section & allowable tensile force

	HiAM 127	HiAm 163
Cross Section	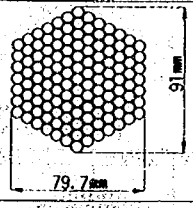	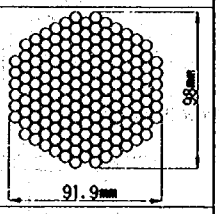
Area (cm^2)	48.9	62.7
Allowable axial force (tf)	268	365

Table 3 Field measurement of damping

Mode	Log. Decrement (δ)
1st Bending	0.02 ~ 0.025
2nd Bending	0.02 ~ 0.025
3rd Bending	0.02 ~ 0.04
1st Torsion	0.1
Cable (out of plane)	0.03 ~ 0.04

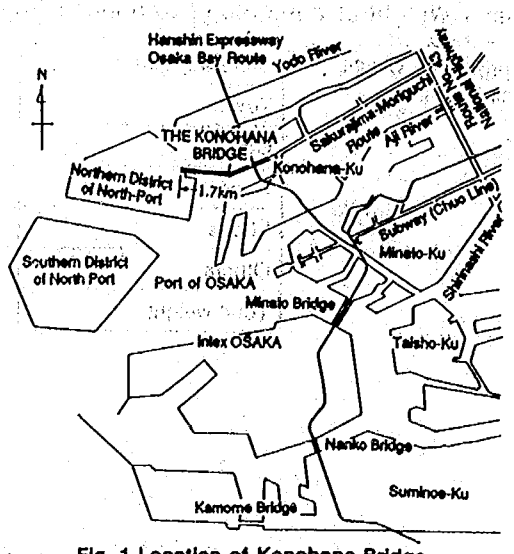

Fig. 1 Location of Konohana Bridge

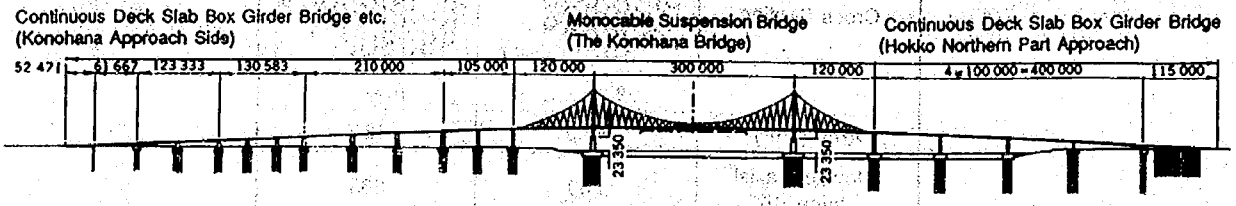

Fig.2 General view of Konohana Bridge

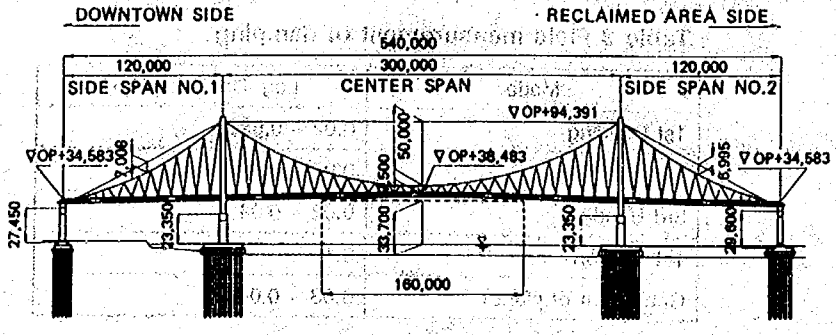

Fig. 3 Side view of Konohana Bridge

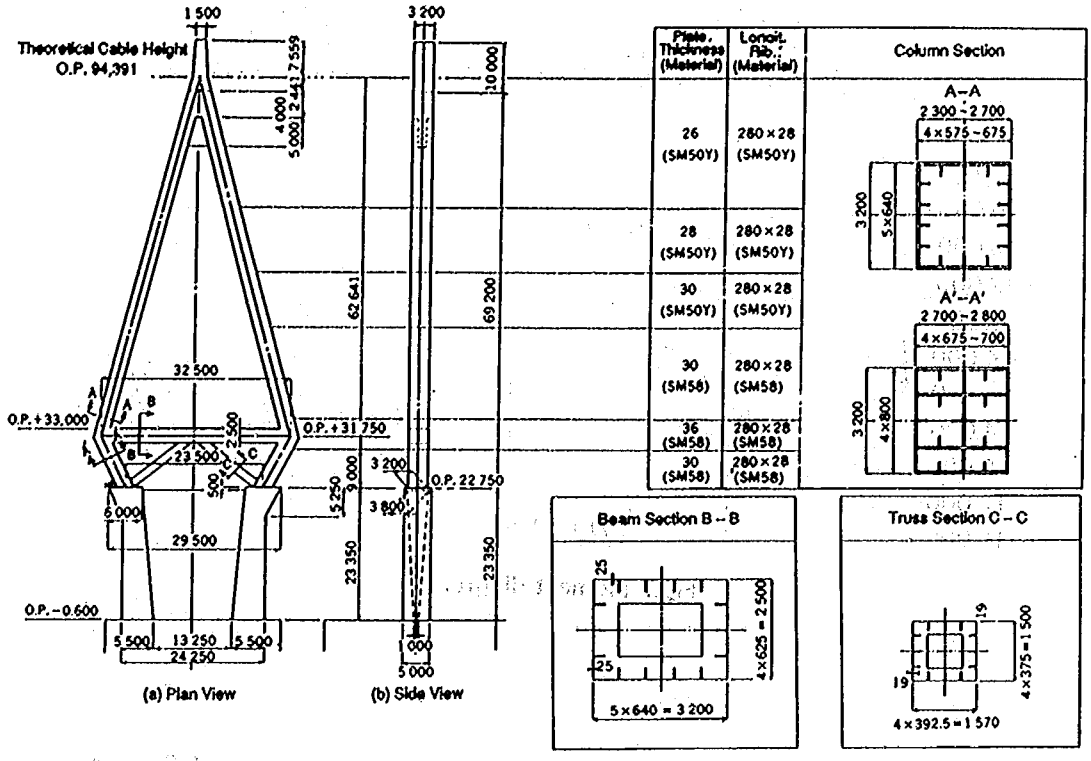

Fig.4 General view of tower

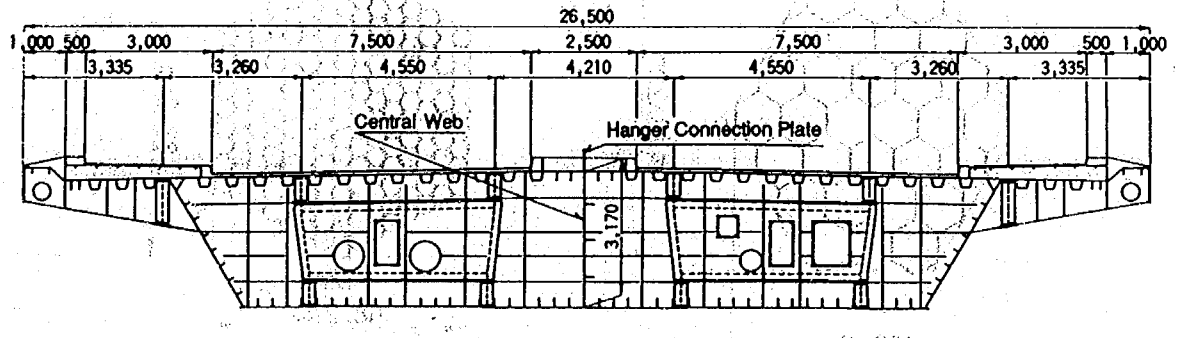

Fig.5 Typical cross section of stiffening girder

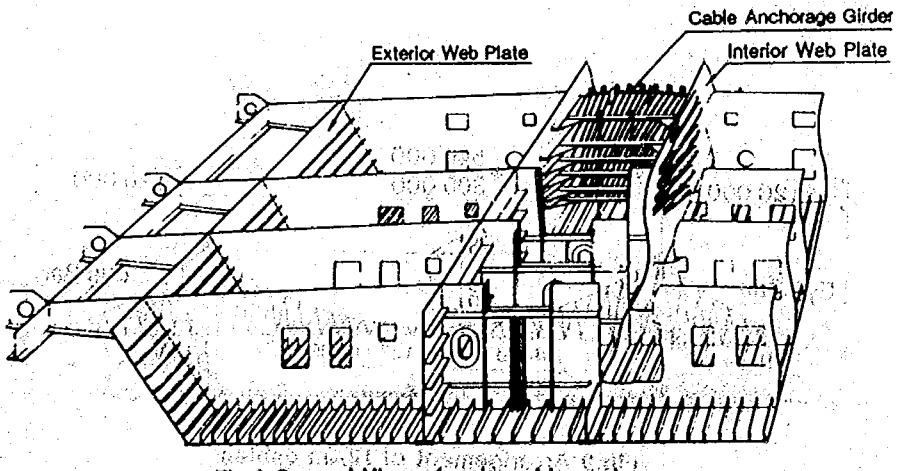

Fig.6 General View of main cable anchorage

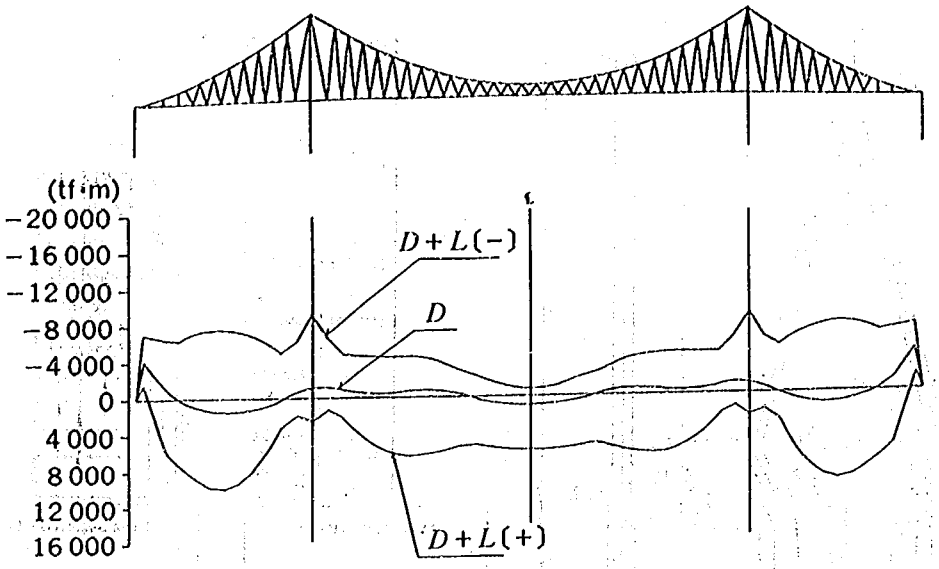

Fig.7 Moment diagram

Arrangement of Strands
at the Top of Tower (30-Strand)

Cross Section of Strand
(P.W.S.5.2ϕ x 184)

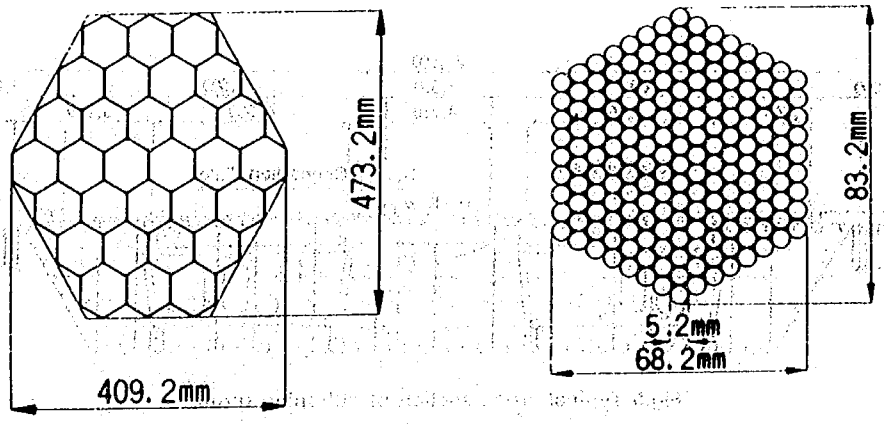

Fig.8 Cross section of main cable

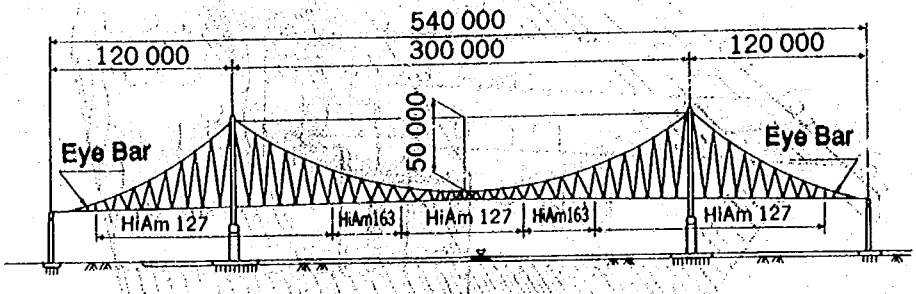

Fig.9 Arrangement of HiAm cables

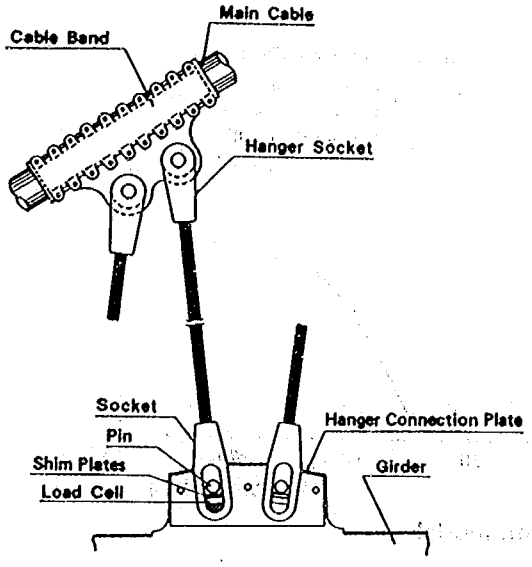

Fig.10 Hanger connection

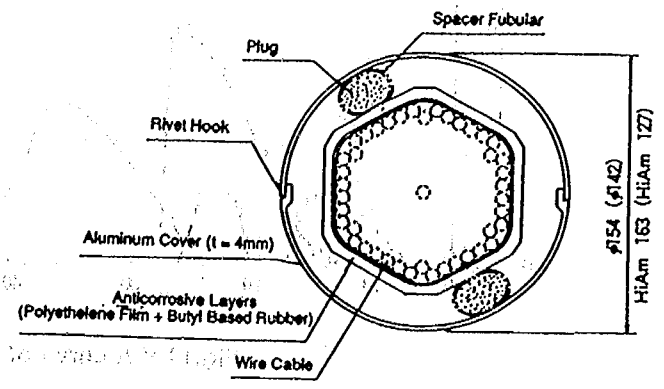

Fig.11 Hanger protection

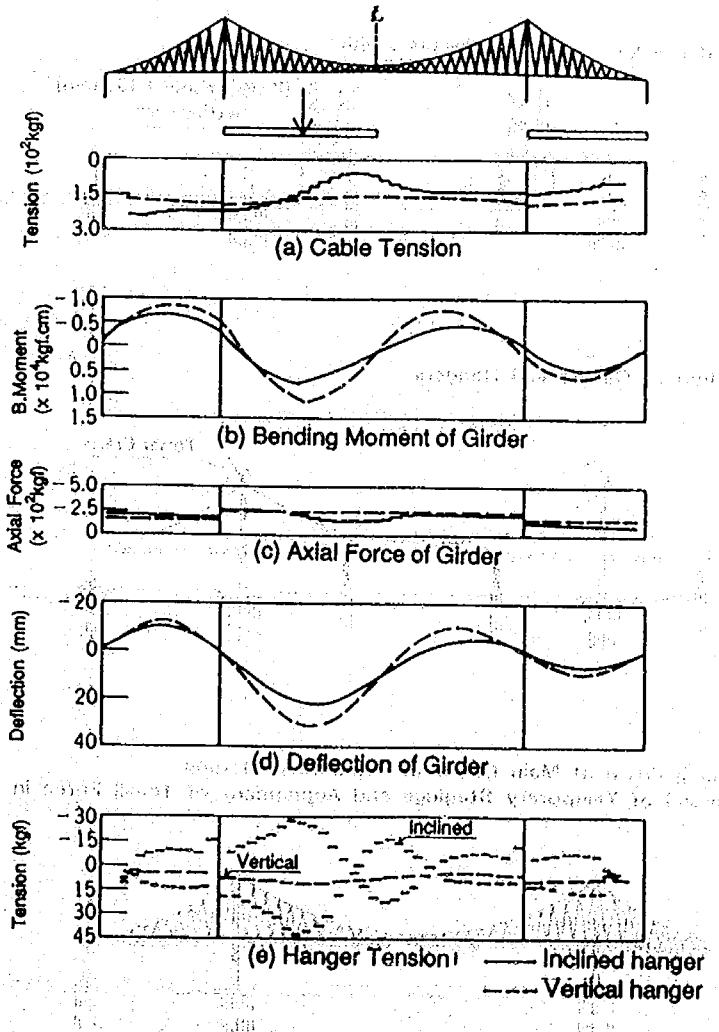

Fig.12 Response comparison of two systems

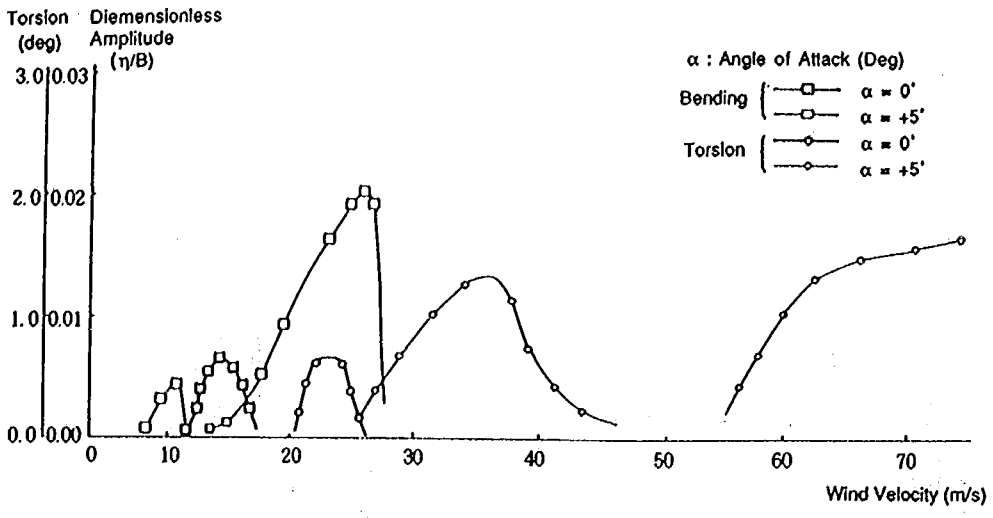

Fig.13 V-A curve of section model

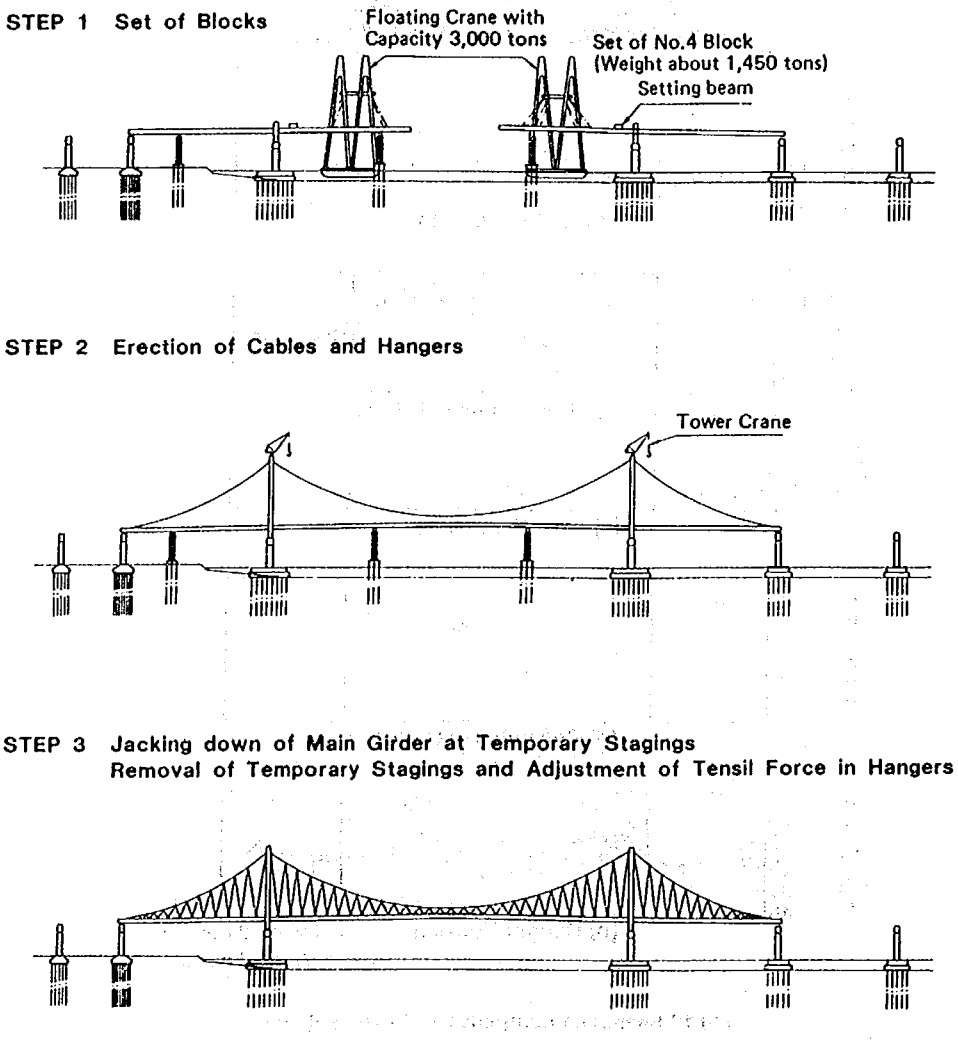

Fig.14 Erection steps of Konohana Bridge

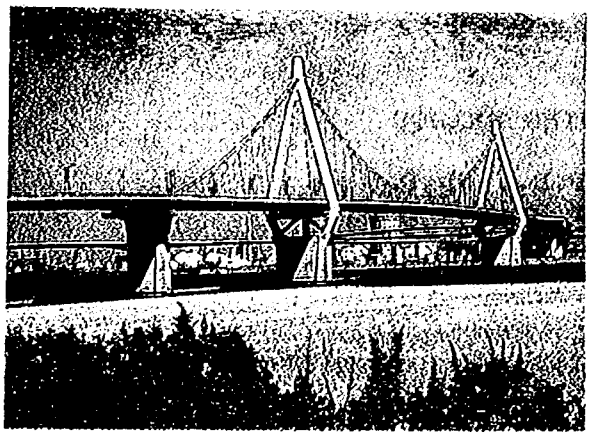

Photo 1 The Konohana Bridge

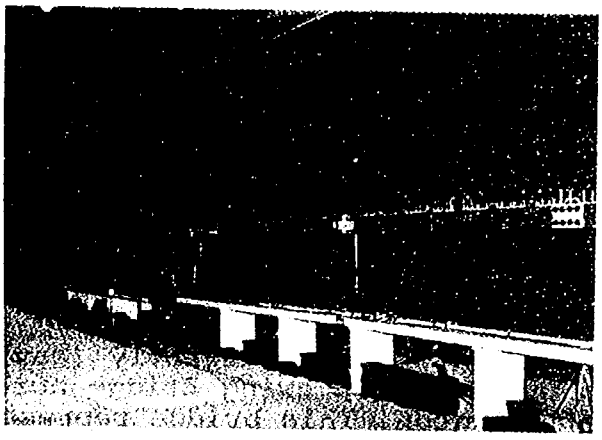

Photo 3 Two-Dimensional Bridge Model Experiment

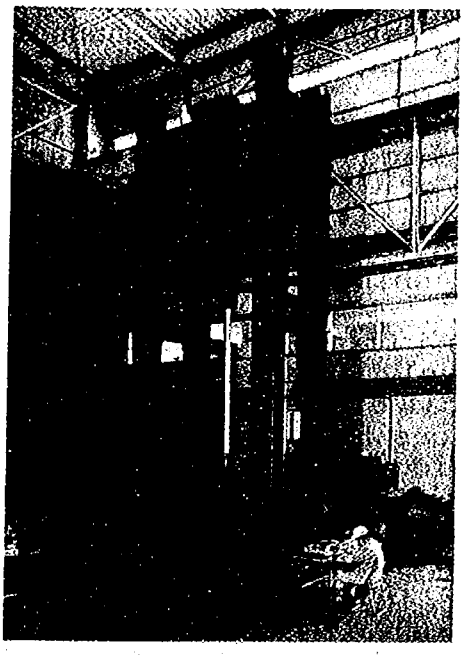

Photo 2 Hanger Fatigue Experiment

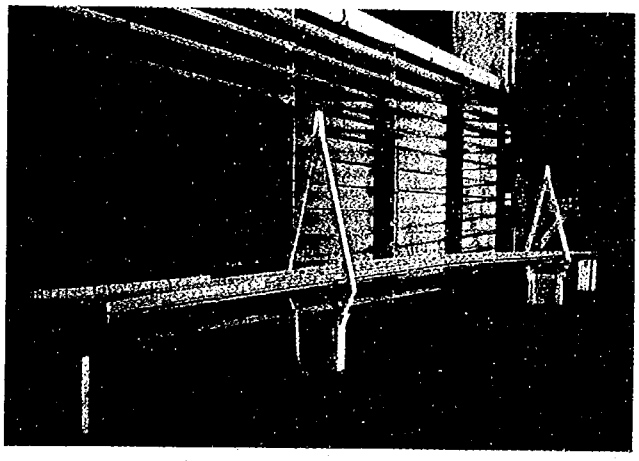

Photo 4 3-D Wind Tunnel Experiment

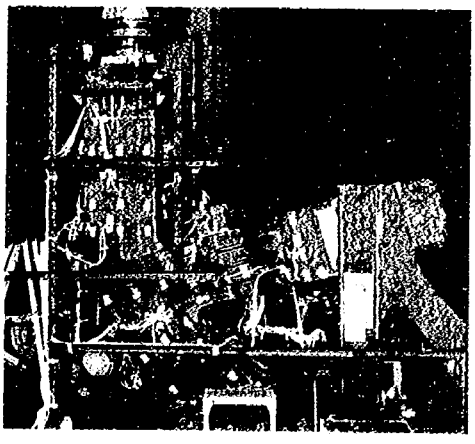

Photo 5 Resistant Experiment of Tower Corner

WEST SEATTLE SWING BRIDGE

John H. Clark, P.E., Ph.D.
Vice President & Chief Bridge Engineer

ANDERSEN BJORNSTAD KANE JACOBS, INC.

Construction is currently (May 1991) being completed on a double leaf concrete swing bridge across the Duwamish River in Seattle, Washington. This bridge represents a revival of a type of movable bridge long out of favor and incorporates some new concepts in machinery and movable bridge technology. This paper describes the structure and its site, details some of the factors which led to this novel design and the construction of the bridge.

The bridge (Figure 1) connects two portions of the industrial port area of Seattle across one of its major shipping channels. Prospects for widening the current 46m (150 feet) wide ship channel to 76m (250 feet) required replacement of the existing bascule built in 1927. Current (1988) navigation traffic required approximately 10 openings per day of the existing bridge which provided 14m (45 feet) of vertical clearance over high water. Increasing the vertical clearance from 14m for the existing bascule bridge to 17m (55 feet) for the new bridge is predicted to be sufficient to reduce the number of openings to 7 per day average, primarily for large ocean going barges and ships.

Vehicular traffic crossing the waterway bound for residential areas in the western part of Seattle had previously been routed over a new high level bridge (43m [140 feet] vertical clearance) completed in 1984. The route had been served by various bridges since early in the City's history. One of the first bridges was a steel swing bridge constructed in the early years of this century and replaced in 1927 by a bascule bridge. The first bascule bridge was paralleled by a second soon after to meet growing traffic demands. Traffic growth on the roadway coupled with increasing use of the channel created frustrating delays for the traffic when the bascules were opened during peak traffic hours. Plans for a new high level crossing were made more urgent when an inbound freighter struck a pier of the north bascule in June 1979, rendering it inoperable.

However, the high level bridge did not provide for the local traffic between the two industrial areas on either side of the waterway due to the difficulty of providing adequate ramps to the elevated structure. This local traffic was 3,500 vehicles per day, 15% trucks prior to closure of the existing bascule and is predicted to increase to 11,600 vehicles per day by 2000.

Pedestrians and bicycles are also provided for on the new swing span, but are excluded from the high level bridge. The total structure width of 15.2m (49 feet 9 inches) provides for two traffic lanes and one combined bicycle/pedestrian way of 3.66m (12 feet).

The swing bridge alignment was placed on the existing bridge alignment to minimize required right of way and revisions to the existing street network. This alignment results in the bridge axis being skewed approximately 45 degrees to the channel. A total of nineteen different alignments in the vicinity and three basic structure types were evaluated before selection of the swing bridge for final design development. Other structure types investigated in the preliminary design stages were a vertical lift bridge and a bascule bridge. The vertical lift bridge was felt to be aesthetically incompatible with the immediately adjacent high level bridge. A vertical clearance of 43m (140 feet) would have been required and the towers would have extended above the level of the deck of the adjacent bridge. The 45° skew of the channel alignment to the street alignment would have required a lift span length of approximately 140m (460 feet). A bascule bridge was also investigated. The required span length was approximately 116m (380 feet) between trunnion bearings with a skew of 30° between the channel and the roadway. The alignment shift to reduce the skew from 45° to 30° would have added two reverse curves to the street and required additional right of way.

The 146m (480 feet) span center to center of pivot piers for the swing bridge was established by the width of the open west leaf and the location of a column of the adjacent high level bridge. The east pivot pier is then placed symmetrically about the centerline of the proposed channel. The tail span length of 53m (173 feet) was also set by the column of the high level bridge. Once the alignment was chosen, the span lengths were fixed. The west approach length of 153m (448 feet) is determined by the need to cross over a railroad track and an intersecting street. The east approach length of 147m (482 feet) was determined by the maximum grade of 7% and vertical curve lengths required for proper sight distance. Stair towers for pedestrian access are provided on each approach. A control tower for the bridge operator is adjacent to, but separate from, the west pivot pier. The control tower is a 36m (120 feet) high structure so that the bridge operator has unrestricted view of the channel and all of the approach roadway.

The crossing site is near the mouth of the Duwamish River. Soils encountered at the site range from hydraulic fill and recent alluvial sands and silts to heavily pre-consolidated glacial till. Depth to the till varies from 15m (50 feet) on the west end of the project to 60m (200 feet) on the east end. Lenses of loose silt

exist erratically throughout the alluvium layer. The loose surficial silts and hydraulic fill are deemed susceptible to liquefaction in major seismic events. Densification by Vibroflotation was specified to prevent such liquefaction.

Seismicity of the area is moderately active. Site specific seismicity studies and geotechnical studies developed the following design spectrum:

Table 1

Seismic Design Spectrum

	Maximum Ground Response	Amplification Factor 5% Damping	Pseudo Spectrum Value
Acceleration	320 gals	2.2	700 gals
Velocity	32 cm/sec	1.8	58 cm/sec
Displacement	14 cm	1.8	25 cm

The seismicity studies and the seismic design of the high level bridge are discussed in a previous paper (Clark, 1982) along with details of the geology and foundation conditions at this site.

Seismic design criteria generally followed the Guide Specifications for Seismic Design of Highway Bridges, 1983 of the American Association of State Highway and Transportation Officials with appropriate modifications for the unique structure.

The main piers and superstructure comprise a structural unit which does not contain the "ductile element" upon which the Guide Specifications are predicated. The location of the piers in the sloping bank of the existing and future channel created a problem of differing transverse stiffness of the piles which would have led to eccentricity between the center of mass and center of rigidity. These two problems were addressed by the new concept of "seismic isolation" sleeves (Figure 4) described below. It is anticipated that the lateral support from the ground for the foundation piles will begin at the uniform level of the top of the granular fill. This elevation was set so as to provide the optimum balance between flexibility and pile moments from seismic response. The calculated seismic response displacements are such that the extreme corner pile which is in tension will just reach predicted yield under the design seismic event (Figure 5). Maximum seismic response at a main pier is approximately equivalent to 230 gallons acceleration and 50 cm (2 inch) displacement. Design calculations included detailed consideration of soil structure interaction.

Considerations in the choice for the superstructure design were construction economy, maintenance costs, traffic safety and aesthetic compatibility with the adjacent high level bridge (a concrete box girder). Two designs were prepared and advertised for bids, a post-tensioned segmental concrete box girder and a steel box girder with a precast prestressed concrete deck made composite after erection. Typical cross sections of the two alternatives are shown in Figure 2.

A major challenge in the design of the concrete box girder bridge was control of long term deformations. Provisions for control of both long term and short term deformations included additional post-tensioning beyond that required for stress control, provision of some unbonded tendons, provision for additional future tendons, provisions for adjustment of approach span elevation at the tail span joint, provision for vertical adjustment of each leaf as a whole, and specifications requiring nearly simultaneous construction of the two movable leaves.

The first line of defense against unwanted long term deformation was the adoption of the principle of load balancing for the design of the longitudinal post-tensioning. The amount of prestress provided is the amount required to provide 100% load balancing for the final dead load condition. This required approximately 30% more post-tensioning than the amount required to satisfy service load stress conditions. The deck of the box girder is post-tensioned transversely and vertical post-tensioning is included in the webs. The additional longitudinal post-tensioning reduced the need for vertical post-tensioning in some areas. Completion of the concrete casting operations indicate that the maximum difference between the camber of the two opposing leaves is approximately 15mm (0.6 inch).

Static balance of each leaf about the pivot pier is achieved by thickening the webs and bottom slab in the tail span and by the addition of ballast concrete and galvanized reinforcing steel bars such that the last 12m (40 feet) of the tail span is solid except for an access shaft 1.0m x 1.2m (3.3 feet x 4.0 feet). Galvanized reinforcing steel bars and precast ballast blocks are provided for adjustment of the static balance. As built measurements after casting of each section were taken so that the final static balance could be closely predicted. It was found that it was necessary to explicitly account for the measured density of the concrete (from quality control test cylinders) and the actual weight of reinforcing and prestressing steel in each segment to accurately predict the static balance. Allowable static imbalance during construction while the bridge rested on temporary service bearings was 72 MNm (53,000 kip-ft). Static imbalance during construction operations of the movable leaves was limited to 6.8 MNm (5,000 kip-ft) to avoid stick-slip chatter in the pivot shaft guide bearings.

The 12.8m (42 feet) diameter pier house (Figure 3) carries the superstructure loads to the foundations and houses the drive machinery, emergency generators, and part of the control system. Pier house walls are 81cm (32 inches) thick and are heavily reinforced.

The pier table element of each leaf is supported by a transition element which provides two load paths to the foundation. The closed position path (serving vehicular traffic) is from the superstructure pier table through a conical shell to the walls of the pier house. Service bearings made up from steel plates with reinforced elastomers separate the transition element from the roof of the pier house. These service bearings are placed on an 11.4m (37.33 feet) diameter circle. Temporary bearings were placed between the permanent service bearings to provide stability during construction of the cast-in-place segmental concrete leaves. The operating position load path is from the pier table through the center portion of the transition element to the 3.66m (12 feet) diameter pivot shaft. The pivot shaft is a concrete filled steel shell 44mm (1.75 inch) thick which in turn rests on the hydraulically operated lift-turn cylinder. The pivot shaft is maintained in the vertical position by guide bearings at the roof and operating floor level of the pier house. In the operating position, the whole movable leaf including transition element and pivot shaft are raised approximately 25mm (1 inch) to transfer the load from the service bearings to the pivot shaft. A reinforced concrete footing founded on 36 concrete filled steel pipe piles, 91cm (36 inch) diameter, completes both load paths.

The piling system incorporates 122cm (48 inch) diameter steel pipe "seismic isolation" sleeves around each foundation pile. The purpose of these sleeves is to control the elevation at which the foundation piling begin to receive lateral support from the surrounding soil. The sleeves were driven first and then the foundation piles were driven inside using a centering device to maintain the annular clearance. The foundation piles were cleaned out to a depth of 18m (60 feet) below the bottom of the footing, reinforcing steel placed, and then filled with tremie concrete. The annular space was cleaned out and 12.5m (41 feet) backfilled to below the bottom of the footing. The sleeves also support the tremie seal which is separated from the footing. The bottom of the footing was cast while supported on short posts which would not permit shear transfer between the tremie seal and the footing in a seismic event.

Heavy locks at the tail span joint and at the center joint are provided for transfer of seismic response loads and to restrain differential displacements due traffic, differential temperature, and accidental misalignment. Tail locks are 36cm (14 inch) x 58cm

(23 inch) I-shaped bars and the center lock is a 25cm (10 inch) x 32cm (12.5 inch) rectangular bar. The torsional stiffness of the box section is sufficiently high that locks were provided only on the longitudinal center line of the section. The locks are driven by hydraulic rams powered by local pumps.

Twin hydraulic slewing cylinders (56cm [22 inch] bore by 234cm (92 inch) stroke) rotate each movable leaf from the closed position to the open position to allow for passage of ships. The operational cycle is based on a normal two minute slewing time, total cycle including traffic lights and gates is approximately 4½ minutes. Friction is minimized due to the fact that the structure is supported on the hydraulic fluid of the lift-turn cylinder. The principal source of friction is the pivot shaft in vertical alignment. Indicated frictional torque is approximately 68 kNm (50 kip-feet) based on pressure readings in the slewing cylinder during temporary operation during construction with one slewing cylinder.

Power for raising and rotating the movable leaf is provided by 3-75 kw (100 horsepower), 8 liter per second (125 gpm) hydraulic pumps in each pier house. Normal operation is with two pumps, the third pump alternates as a spare. Other redundancies built into the system include the ability to slew the bridge using only one slewing cylinder (with increased cycle time) and even to slew the bridge against the friction of the service bearings should the lift/turn cylinder fail to operate. This latter redundancy is an extraordinary condition to be undertaken only in extreme emergency. It requires manual overrides of pressure relief valves in the hydraulic system and would require replacement of part of the service bearings.

Hydraulic system components are designed to operate at a normal pressure of 11.7 MPa (1700 psi) and an emergency (slewing against the service bearing friction) pressure of 41.4 MPa (6000 psi).

Hydraulic buffers are designed to stop the leaf moving at full rotation speed of 0.57 degrees per second in 0.44 degrees of travel. Open position buffers are located on the roof of the pier house and contact stops on the inner surface of the transition element core. Tail span buffers are located on the approach span piers and contact the full span. Normal closing speeds at buffer contact are 35% of normal speed, thus normal operation buffer loads are small.

The control unit is a programmable controller which sequences operations, and provides status information to the bridge operator. The primary position control is limit switches which initiate braking via the controller. The dynamics of the operating structure (large inertia, low damping) were not deemed suitable for dynamic

feedback control. The control system is essentially the same as manual operation except that the controller "pushes the buttons," checks interlocks, and announces the status on a monitor. Manual override is possible for most steps of the operation.

Diesel powered emergency generator sets (350 kw) are provided in each pier house on the lower floor. Fuel storage is placed in day tanks in the pier house.

One of the design exercises of great value was to conduct a study of maintenance action to insure provision for access for maintenance to all items. This study insured that adequate openings were provided for removal and replacement of each piece of machinery and that all pieces of equipment and areas of the bridge had a means for safe access for inspection and maintenance. Access holes 122cm x 183cm (4.0 feet x 6.0 feet) were provided in the bottom slab of the tail span for machinery replacement. Normal personnel access to the interior of the box girder is from platforms at the center joint. The interior of the box girder is provided with lights.

Bids for the construction of the project were received in September 1988. Five bids (tabulated in Table 3) were received for the concrete box girder alternative ranging from $33,526,192 to $37,560,626 including demolition of the south bascule, all approach work and site work. The contract for the concrete box girder alternative was awarded to Kiewit-Global, a joint venture, on September 28, 1988 and notice to proceed was given on March 1, 1989. Principal construction quantities are listed in Table 2 and the cost breakdown for major work categories (based on the low bid) is presented in Table 4. The contract calls for a 22 month construction schedule. Construction is nearly complete as of April 1991. Remaining operations include setting of the joint armor, placement of the latex modified concrete overlay on the segmental construction, completion of the barriers, and installation and check out of the control system. Scheduled completion date of opening to traffic is June 1991.

The project was designed by the joint venture WSB-2 Design Team comprised of Andersen Bjornstad Kane Jacobs, Inc., Parsons Brinckerhoff Quade and Douglas, Inc., and Tudor Engineering Company. Contech Consultants, Inc. was responsible for the segmental box girder design. Hamilton Engineering Inc. designed the hydraulic machinery and Elcon Associates, Inc. provided electrical design. The project sponsor is the City of Seattle Engineering Department, Frank S. Yanagimachi is project engineer for the City.

References:

Clark, John H. "Foundation Design: West Seattle Bridge" Transportation Research Record No. 982, Transportation Research Board, Washington, D.C. 1984

Robison, R., "Seattle Swing", Civil Engineering, American Society of Civil Engineers, September 1990

Table 2

Principal Construction Quantities (Structural)

Item	Unit	Approaches		Swing Spans	
		Sub Struc	Super Struc	Sub Struc	Super Struc
Structural Excavation	cy	3200		5220	
Soil Densification	cy	38600		18900	
PSC Piling 16.5" Dia	lf	19335			
PSC Piles 16.5" Dia	ea	290			
Steel Piling 36" Dia	lf			10120	
Steel Piles 36" Dia	ea			64	
Concrete Cl D	cy			1372	
Concrete Cl C	cy			186	82
Concrete Cl B	cy				
Concrete Cl AX	cy	2880	1370	3284	65
Concrete Cl PC 5000	cy	275	606	1195	
Concrete Cl PC 6000	cy			237	6604
PSC Girder S4	lf		911		152
PSC Girder S120	lf		2750		
PSC Girder M120	lf		3404		
Reinf Steel	Ton	337	115	347	420
Reinf Steel, Epoxy Ct'd	Ton		115		92
Prestressing Steel, Bar	Ton			1.3	14.6
Prestressing Steel, Strand	Ton				267
Concrete Barriers	lf		3496		2475
Metal Railing	lf		3035		
Latex Mod Concrete	sy				4450
Control System	LS				
Hydraulic System	LS				
Lift/Turn Cylinders	ea			3	
Pivot Shafts	ea		2		
Control Tower	LS				

1 cy = 0.765 m^3
1 ft = 0.305 m
1 Ton = 907 kg
1 sy = 0.836 m^2

Table 3

Bids Received (September 1988)

Bidders	Alternate A	Alternate B
Engineer's Estimate	$33,330,749.40	$36,621,554.40
Kiewit-Global, a joint venture	33,526,192.00	No Bid
General Construction Co./ 3A Industries, J.V.	33,750,799.50	No Bid
Guy F. Atkinson Const. Co.	34,854,453.00	No Bid
S.J. Groves & Sons Co.	36,803,487.00	No Bid
Paschen Contractors, Inc.	37,560,625.88	No Bid

Table 4

Cost Breakdown (Low Bid)

1.	Mobilization	$2,800,000
2.	Demolition	3,761,566
3.	Civil (Streets, Utilities, Traffic)	3,384,171
4.	Approach Spans	4,659,520
5.	Swing Piers	6,868,280
6.	Swing Spans	5,601,985
7.	Machinery	3,977,000
8.	Electrical	1,055,895
9.	Controls, Control Tower	941,000
10.	Pier Protection	476,775
		$33,526,192

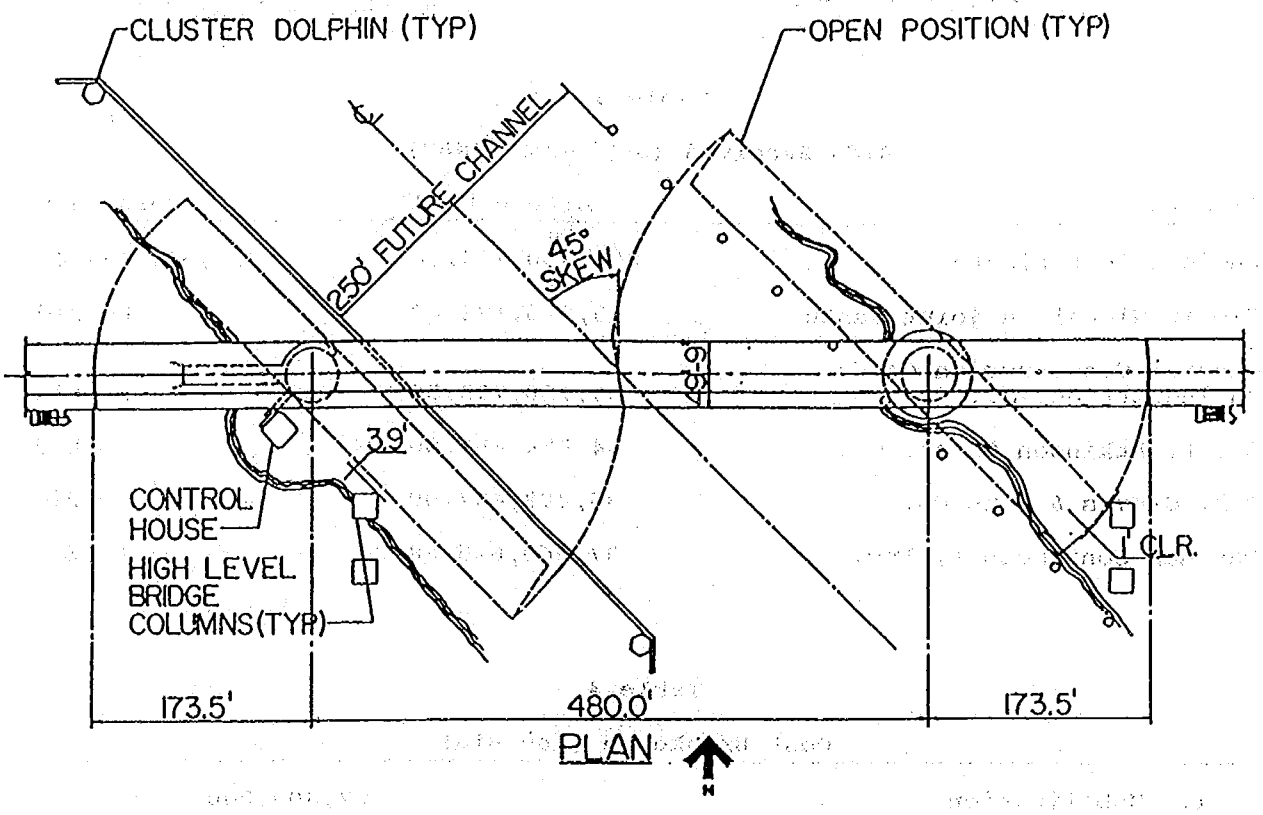

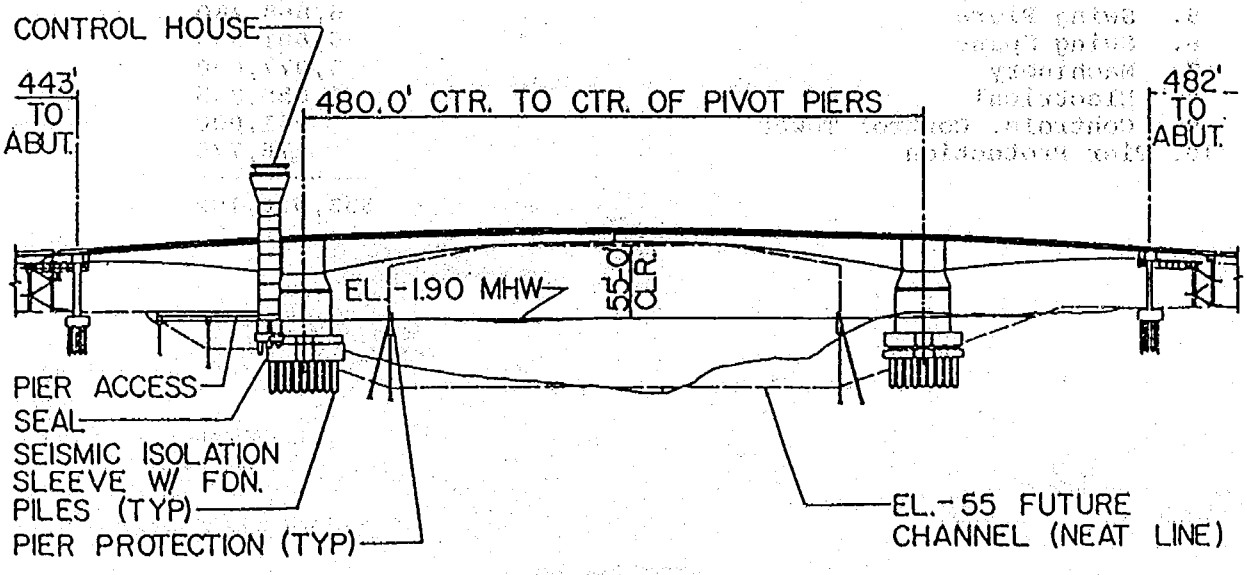

ELEVATION

NOTE: ELEVATIONS SHOWN ARE AT PROFILE GRADE LINE. FUTURE CHANNEL SHOWN.

FIG. 1

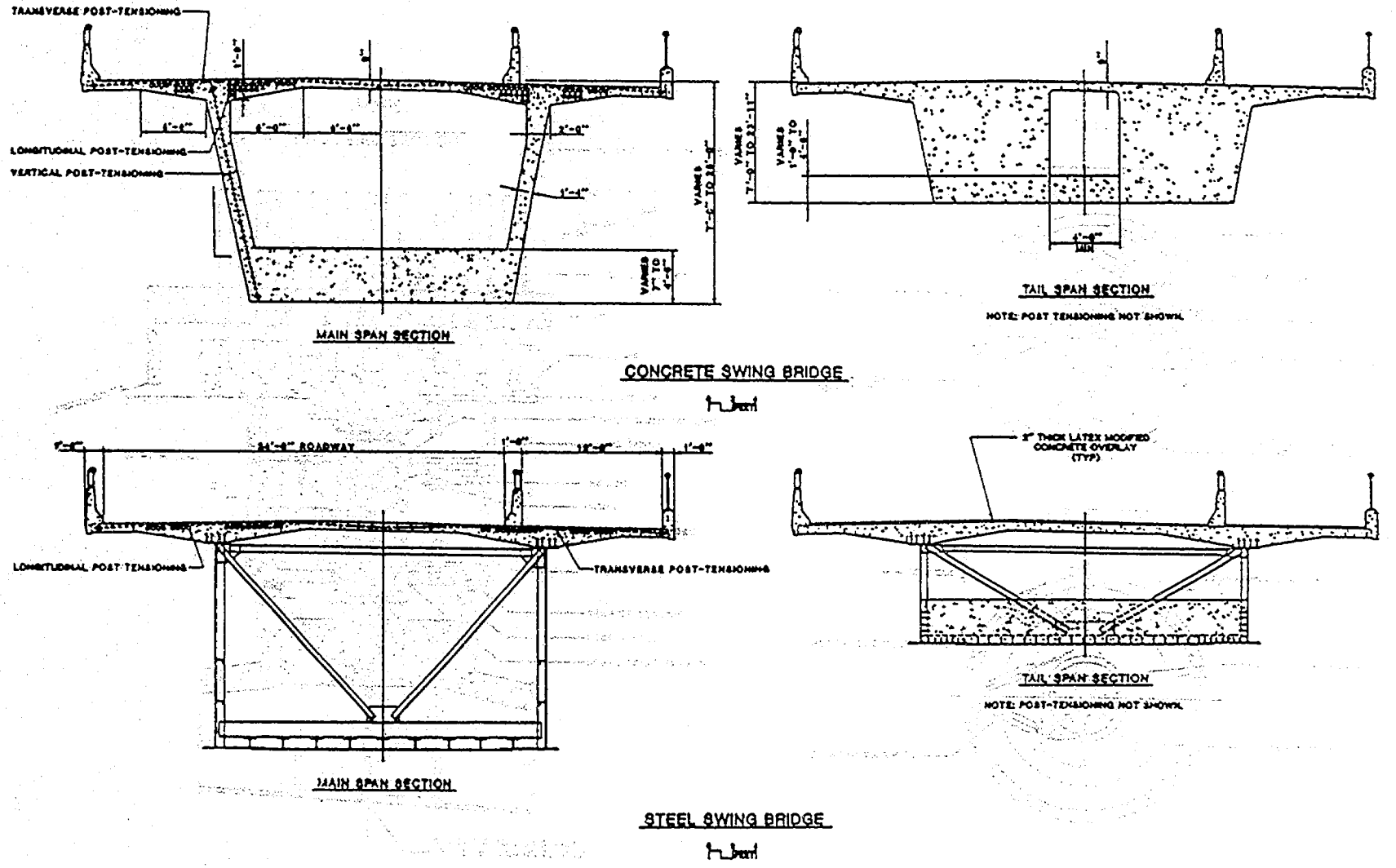
TRANSVERSE POST-TENSIONING
LONGITUDINAL POST-TENSIONING
VERTICAL POST-TENSIONING
MAIN SPAN SECTION
TAIL SPAN SECTION
NOTE: POST TENSIONING NOT SHOWN
CONCRETE SWING BRIDGE
34'-0" ROADWAY
LONGITUDINAL POST TENSIONING
TRANSVERSE POST-TENSIONING
MAIN SPAN SECTION
3" THICK LATEX MODIFIED CONCRETE OVERLAY (TYP.)
TAIL SPAN SECTION
NOTE: POST-TENSIONING NOT SHOWN
STEEL SWING BRIDGE

FIGURE 2

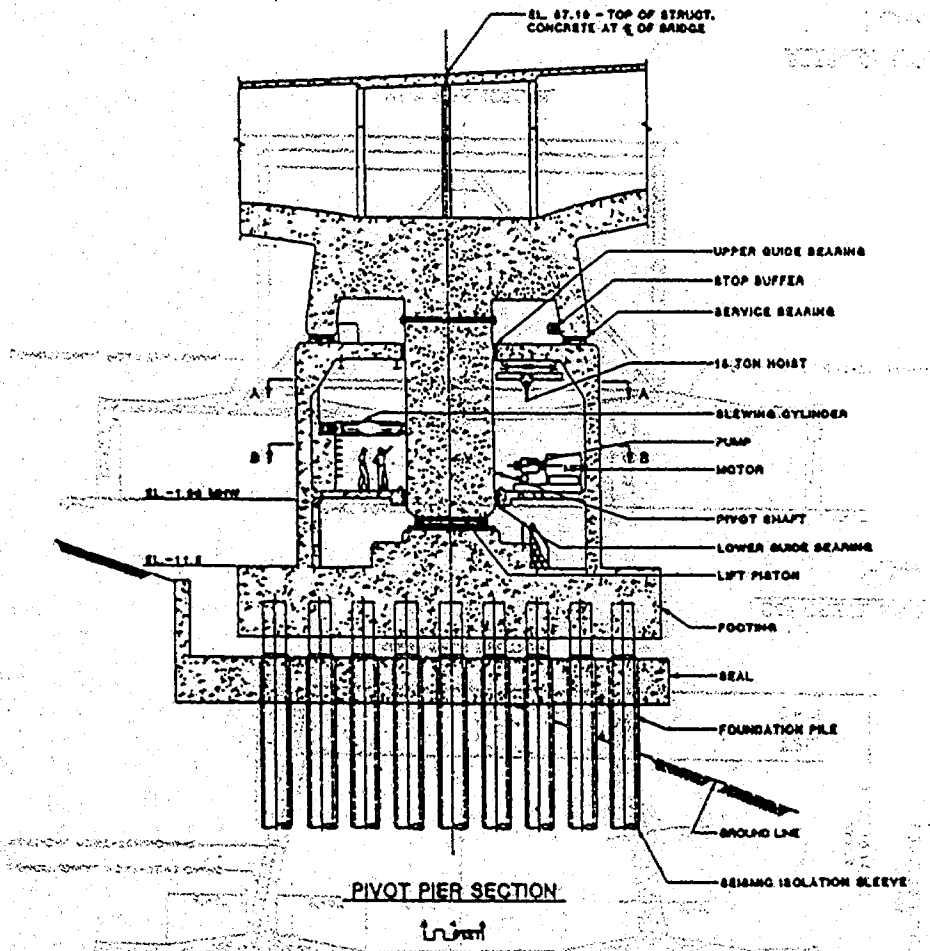

PIVOT PIER SECTION

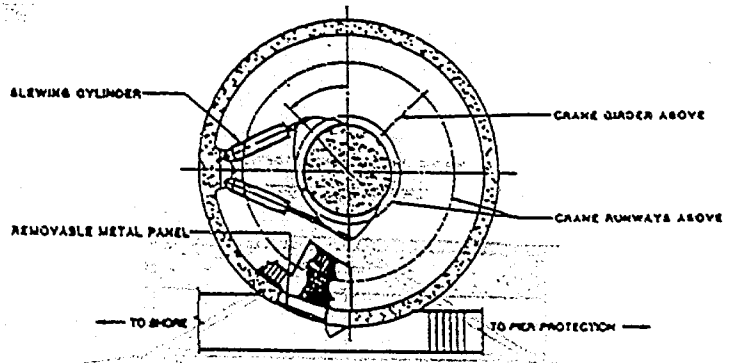

SECTION A-A

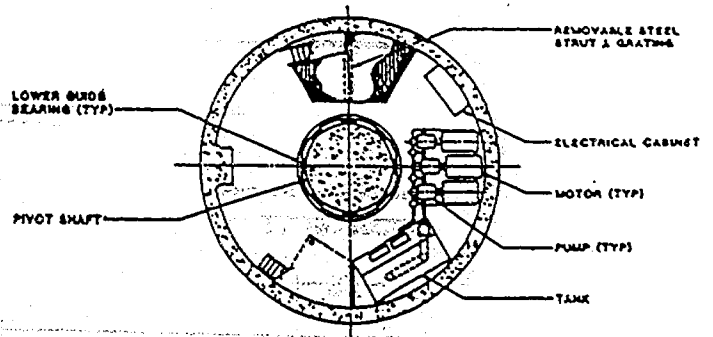

SECTION B-B

FIGURE 3

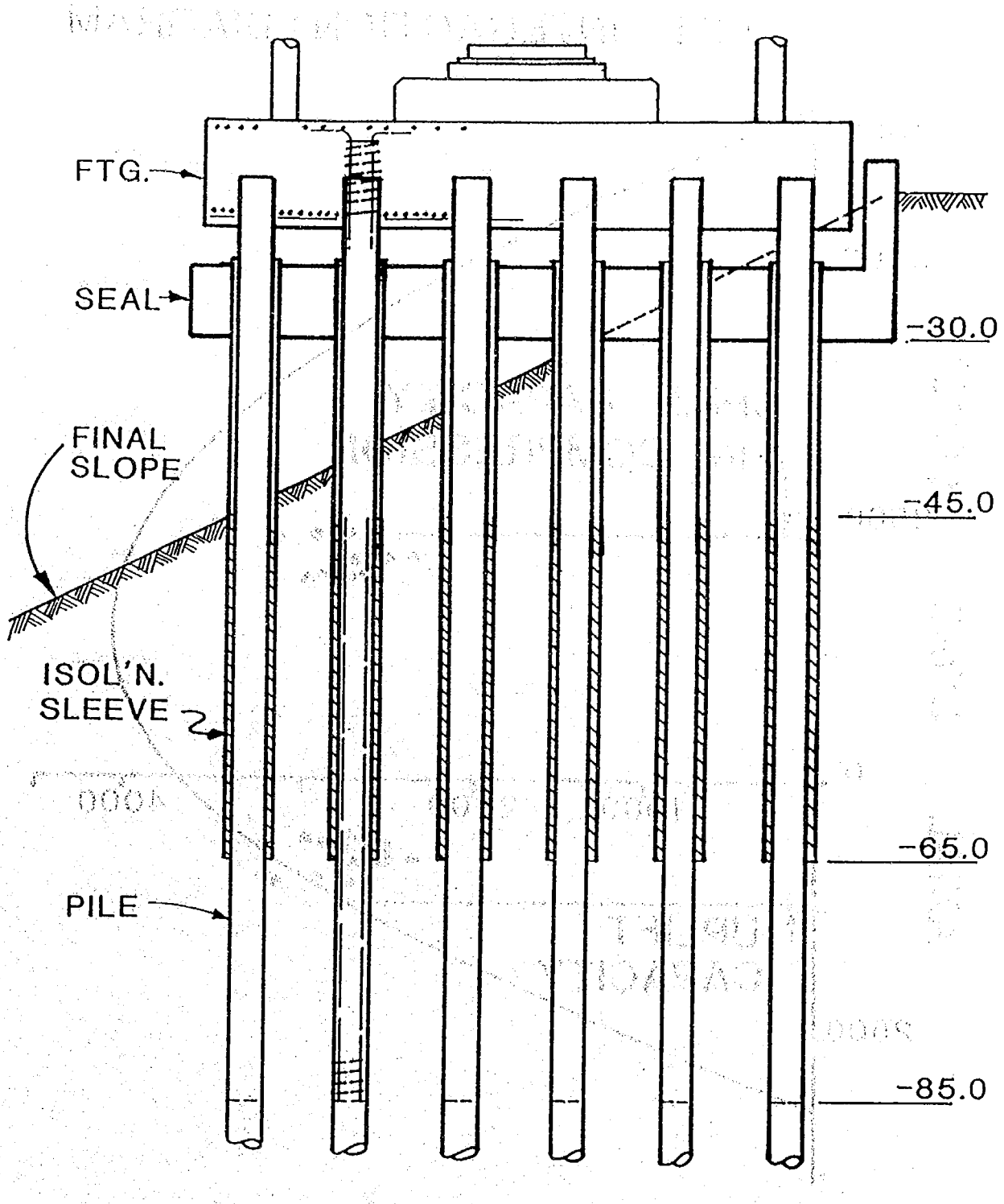

PIVOT PIER FOUNDATION

FIGURE 4

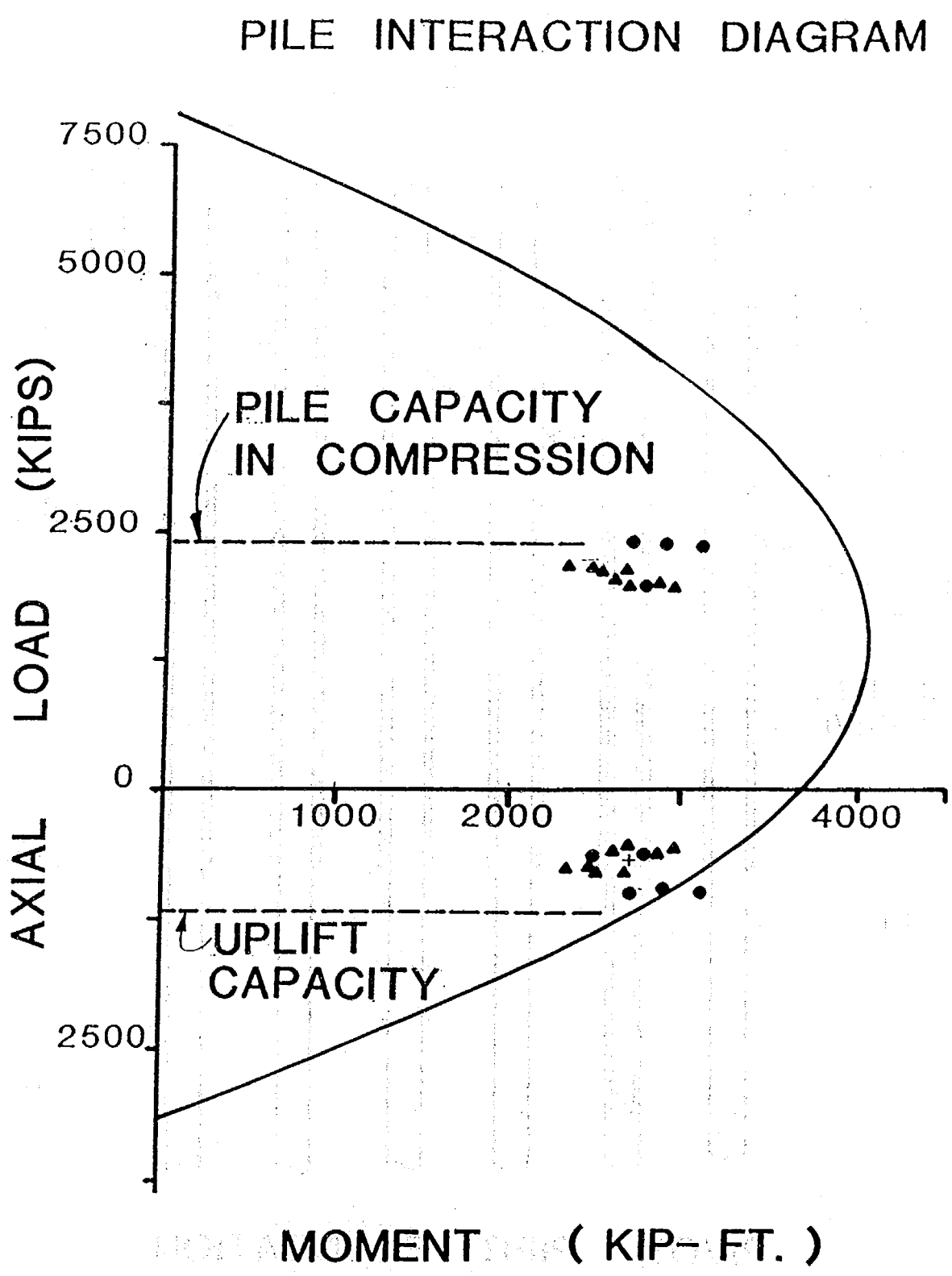
PILE INTERACTION DIAGRAM
7500
5000
2500
0
2500
AXIAL LOAD (KIPS)
PILE CAPACITY
IN COMPRESSION
UPLIFT
CAPACITY
1000
2000
4000
MOMENT (KIP- FT.)

FIGURE 5

(10) Session 10

SESSION 10: BRIDGE CONSTRUCTION(2) 2:10pm～3:10pm
(Co-Chairmen: M. Okahara, C. Roeder)

(27) N. Nomura and Y. Yoshida* : Foundation Design and Construction for the Akashi Kaikyo Bridge
(2:10pm～2:25pm)

(28) B. M. Douglas* , M. Blakely, M. Saiidi and E. A. Maragakis: Construction of the New Bridge Engineering Laboratory Facility at the University of Nevada, Reno
(2:25pm～2:40pm)

(29) Y. Kagawa, T. Meta, S. Nakamura and H. Kato* : Planning and Design of Multi-Span Continuous Bridges
(2:40pm～2:55pm)

DISCUSSION
(2:55pm～3:10pm)

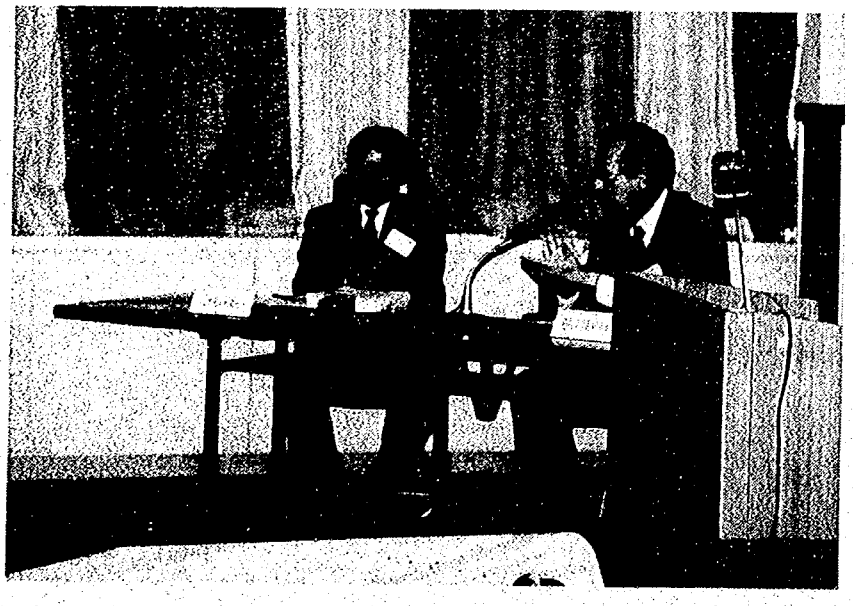

Foundation Design and Construction for the Akashi Kaikyo Bridge

Naoshige Nomura
Manager, Third Design Division, Honshu-Shikoku Bridge Authority
Yoshitaka Yoshida
Manager, Design Division, First Construction Bureau, Honshu-Shikoku Bridge Authority

1. Preface

The Akashi Kaikyo Bridge, a three-span, two-hinge stiffening truss suspension bridge, will be built between Honshu and Awajishima across the Akashi Straights on the Honshu-Shikoku route from Kobe to Naruto, and will, when completed, boast a center span of 1,990m and a bridge length of 3,910m, thus making it the world's largest suspension bridge, surpassing the Humber Bridge in the U.K, which has a center span of 1,410m. Photo 1 shows what the bridge will look like upon completion.

The economic affects of the Akashi Kaikyo Bridge's completion are expected to include increased manufacturing income between Shikoku and the Hanshin area, improved convenience, an expanded sphere of living activity, and increased tourism.

The ground-breaking ceremony was held in April 1986, with construction commencing in March 1988, and completion scheduled for 1998. As of May 1991, construction was underway for the anchorage and main tower foundations and the towers were under factory construction. Photo 2 shows the excavation of the underground continuous wall for the 1A anchorage (Honshu side).

2. Natural Conditions

2.1 Terrain

The area where the Akashi Kaikyo Bridge crosses the straight is about 4km wide with maximum depth at the center of 110m. On the Honshu side of the straight there is a gentle shelf at 40m to 50m in depth and the Awajishima side presents a mild ridge ranging from 35m to 45m in depth. The foundations for the main towers 2P and 3P are located here.

2.2 Geology

The geological conditions in the vicinity of 1A shows alluvial soil on the surface with an upper level of diluvial deposits spreading out. Beneath this are distributed the Akashi layer, the Kobe layer, and the base layer of granite. The foundation of 1A is positioned on the Kobe layer. The ocean floor in the vicinity of 2P has a thick accunmulation of Akashi layer, with Kobe layer distributed beneath. The ocean floor in the vicinity of 3P shows relatively thin alluvial and diluvial deposits, with a Kobe layer beneath. The 3P foundation is located on the Kobe layer. The foundation for 4A is on the granite located near the surface.
(Figure 1)

The Akashi layer is a stratum that was formed between the tertiary Pliocene epoch and the Quarternary Pleistocene epoch, and is composed primarily of gravel, and is a diluvial deposit of gravel with silt and sand in between, being relatively firm. The Kobe laver is a

stratum from the tertiary Miocene epoch composed of accumulated soft rock. This Kobe layer is an alternation strata of sandstone and mudstone, with the Awajishima side comprising much accumulated sandstone with feldspar (coarse particulate arkose sandstone), thus offering a very different rock facies.

2.3 Whether and Marine Phenomenon

The maximum wind velocity was recorded in September 1965 during typhoon No. 23, with gusts of 65.0m/sec., and maximum average wind velocity over 10 min. of 52.2m/sec. The maximum wind velocity for an average year is 30m - 40m/sec., being 4.0m/sec. at 3P. The average wave height is 51.4cm, with maximum wave height of about 6m.

3. Evaluation and Basic Concept of the Bearing Layer for the Akashi Kaikyo Bridge

3.1 Design Concept for the Bridge Foundation

The foundation structure of the Akashi Kaikyo Bridge has the following characteristics when compared with the previous suspension bridge linking Honshu and Shikoku.

① The main tower foundations and anchorages are beared by the Kobe layer and the Akashi layer. The Kobe layer is a poorly consolidated thin soft rock layer composed of many alternation strata of sandstone and mudstone. Further, the Akashi layer is a semi-consolidated gravel deposit, including large amounts of highly aerated gravel.

The bearing strength and deformation characteristics of this soil differ from those of the hard bed rocks comprising aerated granite and Cretaceous period Izumi layer which were the bearing rock for the previous suspension bridge linking Honshu and Shikoku.

② The main tower foundations and anchorages are set in the alluvial and diluvial deposits, and are supported at positions far below sea level.

③ The load of the bridge's superstructure acting upon the footing is larger than that in previous suspension bridges, and the structural dimensions are also large.

To make use of the above characteristics, the following points must be taken into consideration when designing the bridge foundation.

① The maximum constant soil reaction force of the main tower foundations and anchorages is over 200tf/ m^2, so the each supporting layers must be strong enough to safely bear the foundation.

② The substructure is a rigid body foundation, with a relatively large foundation width compared to the depth to which the foundation is set, and the rate at which the weight is distributed over the bottom surface is large.

③ It is possible to design the superstructure giving consideration to the affects of substructure displacement. However, the movement of the footing must be such that no damaging affects to the upper structure are caused.

Consequently, a safety survey regarding bearing, slippage, and tipping must be performed when designing the foundation, and it was decided to use various numerical analysis methods—including split plot experiments, Rigid Body Spring Method (RBSM), finite element method (FEM), etc.—for the bearing strength and displacement. (Figure 2)

3.2 Basic Soil and Rock Model for Foundation Design

The general relationship of geological surveys and foundation design is shown in Figure 3. To improve the accuracy of stability calculations for the foundation and to perform efficient foundation design, it is important to create an appropriate foundation soil model. Here appropriate soil surveys and tests were conducted giving consideration to the current soil conditions and design requirements, and a basic soil model was created to serve as the basis for design taking into consideration the scale of the foundation structure.

The soil constants and experiment methods for stability and earthquake response analysis are shown in Table 1, with the basic soil model for point 1A shown in Table 2.

4. Foundation Construction

4.1 Anchorage (1A)

The location of the 1A anchorage has a water depth of 4m to 6m, with a thick alluvial deposits and a thin Akashi layer.

Therefore, the Kobe layer found at TP- 55 to 60m was used as the bearing layer. The anchorage foundation is a round rigid body about 90m in diameter, and is deeply set. The following four construction methods were considered.

① Pneumatic caisson method
② Open caisson method
③ Underground continuous wall method
④ Rigid body foundation with underground continuous wall method

Underground continuous wall method was selected due to its extensive use in large foundations and its recent use in LNG foundations due to its reliability. The construction method procedures are shown in Figure 4.

4.2 Main Tower Foundation

The main tower foudations are located at great depths (2P: 46m, 3P: 37m), with strong tides, and are supported by gravel or soft rock in the relatively unconsolidated Akashi and Kobe layers. Consequently, large- scale caisson excavation and settling are difficult, so considerations were narrowed down to the steel pipe continuous wall caisson method and the laying down caisson method, with laboratory hydraulic experiments, on- site excavation surveys, and other investigations being performed, leading to the following conclusions.

① Pre-excavation to the Kobe and Akashi bearing layers is sufficiently possible.
② Through construction surveys, it was determined that the mounding of rubble around the caissons could be performed to prevent scouring.
③ As a result of design work based on considerations of new geological survey data, the necessary dimensions from the superstructure, and the construction characteristics that there would be no large change in dimensions between the steel pipe continuous wall caisson method (foundation with embedment) and the laying down caisson method (foundation without embedment).
④ The laying down caisson method is a simple construction method and can be performed with current equipment. It is also a method that the Bridge Authority has experience with on the Seto Ohashi Bridge, etc.

In addition to the results of these surveys and design work, a comprehensive evaluation including construction time and cost was performed, and it was decided to use the laying

down caisson method for the main tower foundation of this bridge. The construction procedure is shown in Figure 5.

Further, due to considerations of scouring resistance, stability during construction, nondirectionality, and ease of submerged work, round foundations (2P: diameter 80m, 3P: diameter 78m) were selected.

Special underwater concrete has been used in the caissons.

Figure 6 shows the general structure of 2P and 3P. On top of the special underwater concrete, the top plate directly supporting the tower is constructed using a reinforced concrete (RC) structure.

5. Measurement Results

Here are shown the measurements of bottom load and soil displacement accompanying the concrete pour for the 2P foundation. Sliding micrometers have been used for soil displacement.

Bibliography

1) Yoshida,Y., "Design Overview of the Akashi Kaikyo Bridge", Bridge, 90-11, (in Japanese)
2) Kawaguchi,K., "Design and Earthquake Resistance Design of the Akashi Kaikyo Bridge", Bridge and Foundation, 88-8, (in Japanese)
3) Yasuda,M., and Okano,S., "The Plan for the Akashi Kaikyo Bridge", Bridge and Foundation, 88-8, (in Japanese)
4) "Manual of the Akashi Kaikyo Bridge Earthquake Resistance Design (Proposal) and Explanation" by Honshu-Shikoku Bridge Authority, 88-3, (in Japanese)
5) Manual of the Akashi Kaikyo Bridge Substructure Stability Calculations (Proposal) and Explanation", by Honshu-Shikoku Bridge Authority, 88-3, (in Japanese)
6) "Manual of the Akashi Kaikyo Bridge Foundation Rock Supporting Strength and Displacement Static Calculations (Proposal)", by Honshu-Shikoku Bridge Authority, 88-3, (in Japanese)

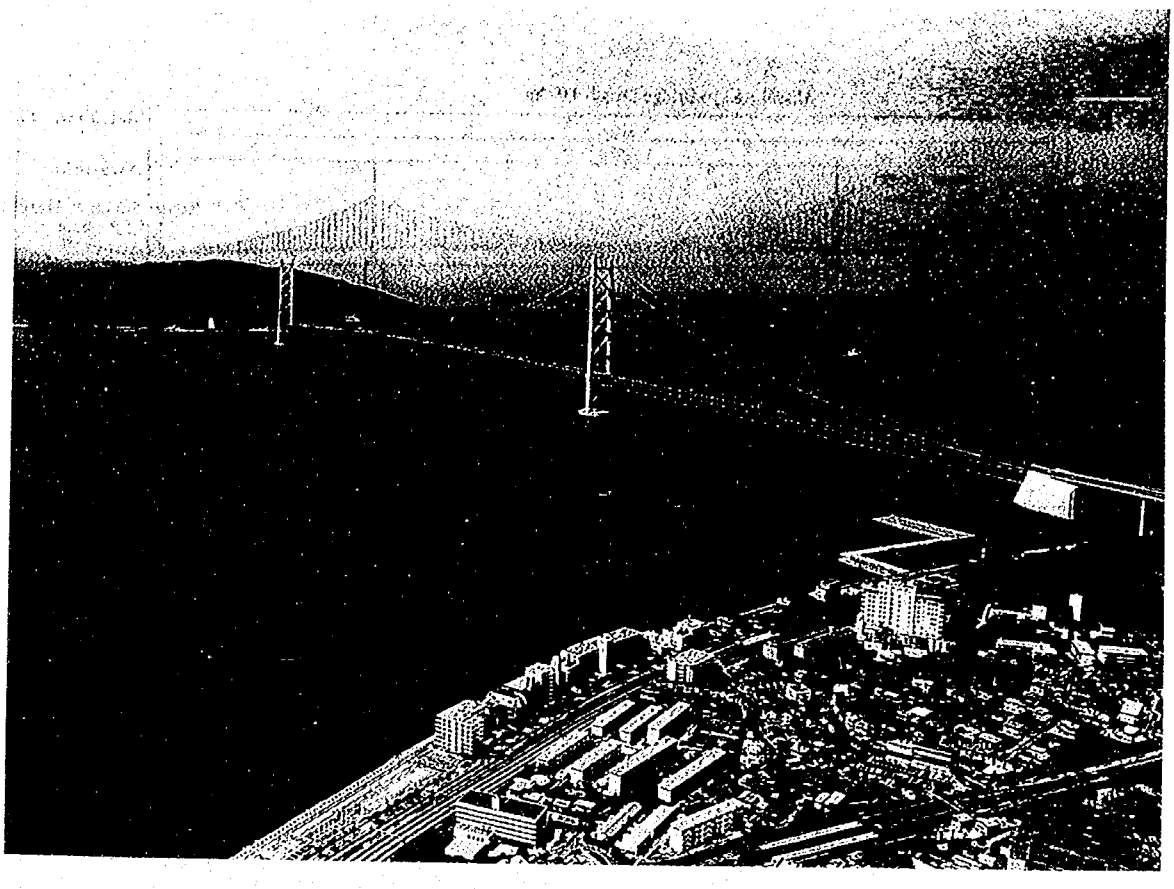

Photo 1: Conceptual view of the completed Akashi Kaikyo Bridge

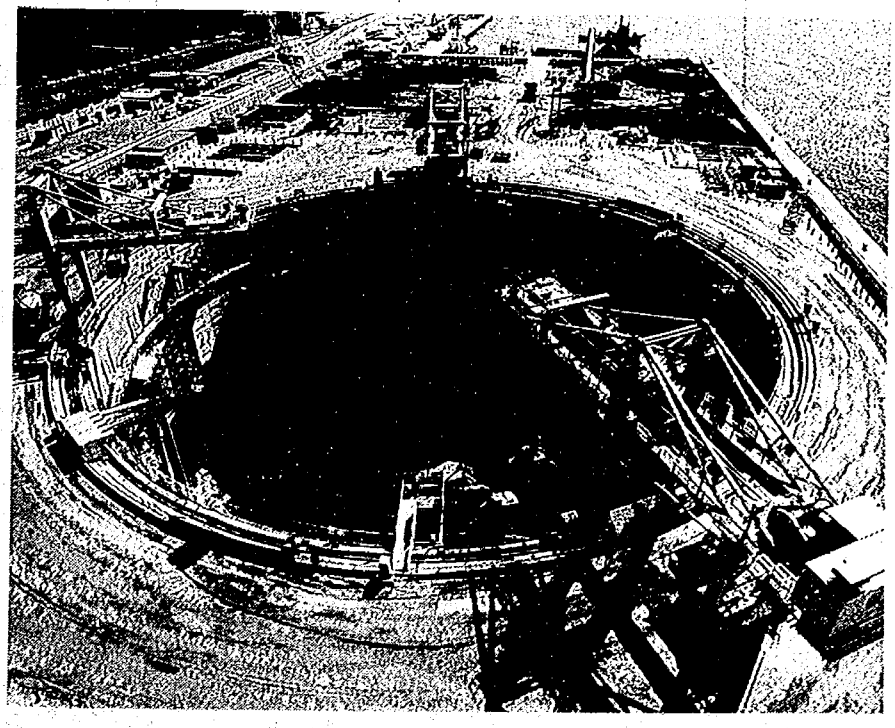

Photo 2: Excavation conditions at the 1A anchorage (March 1991)

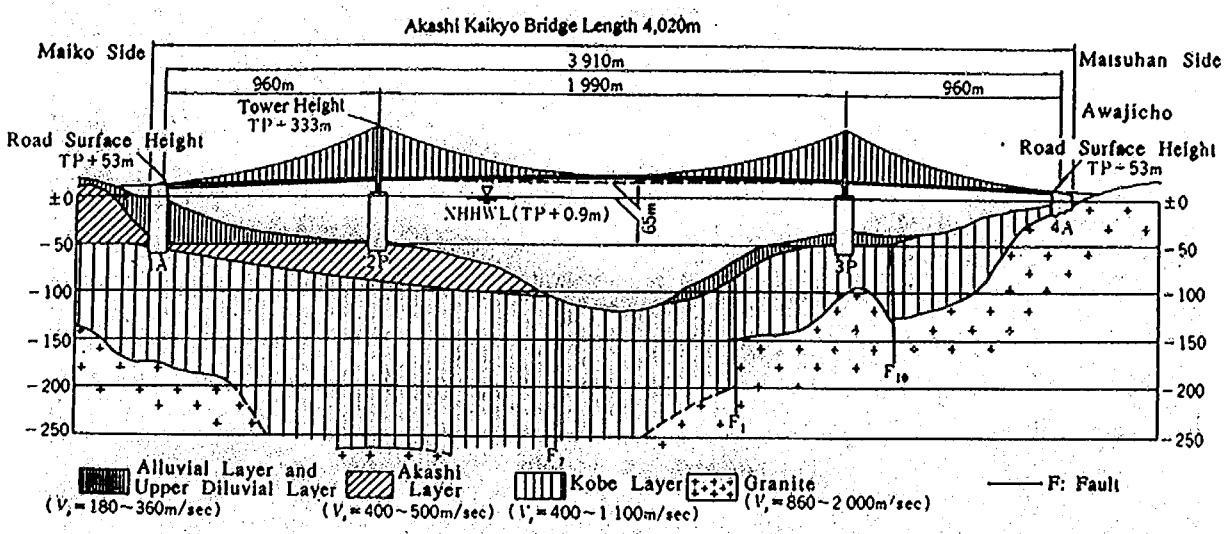

Figure 1: Section View of Akashi Kaikyo Bridge Geology

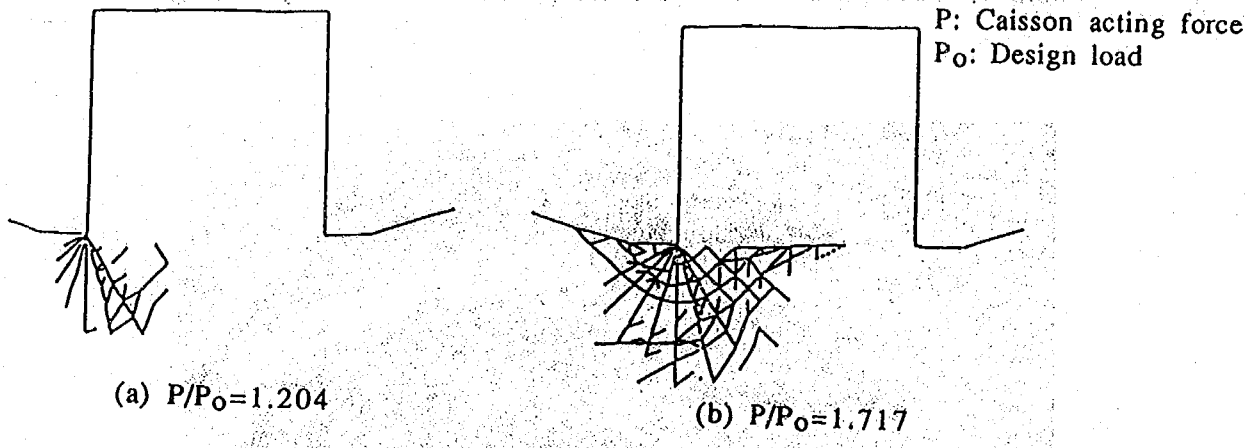

Figure 2: Example of RBSM Analysis (2P)

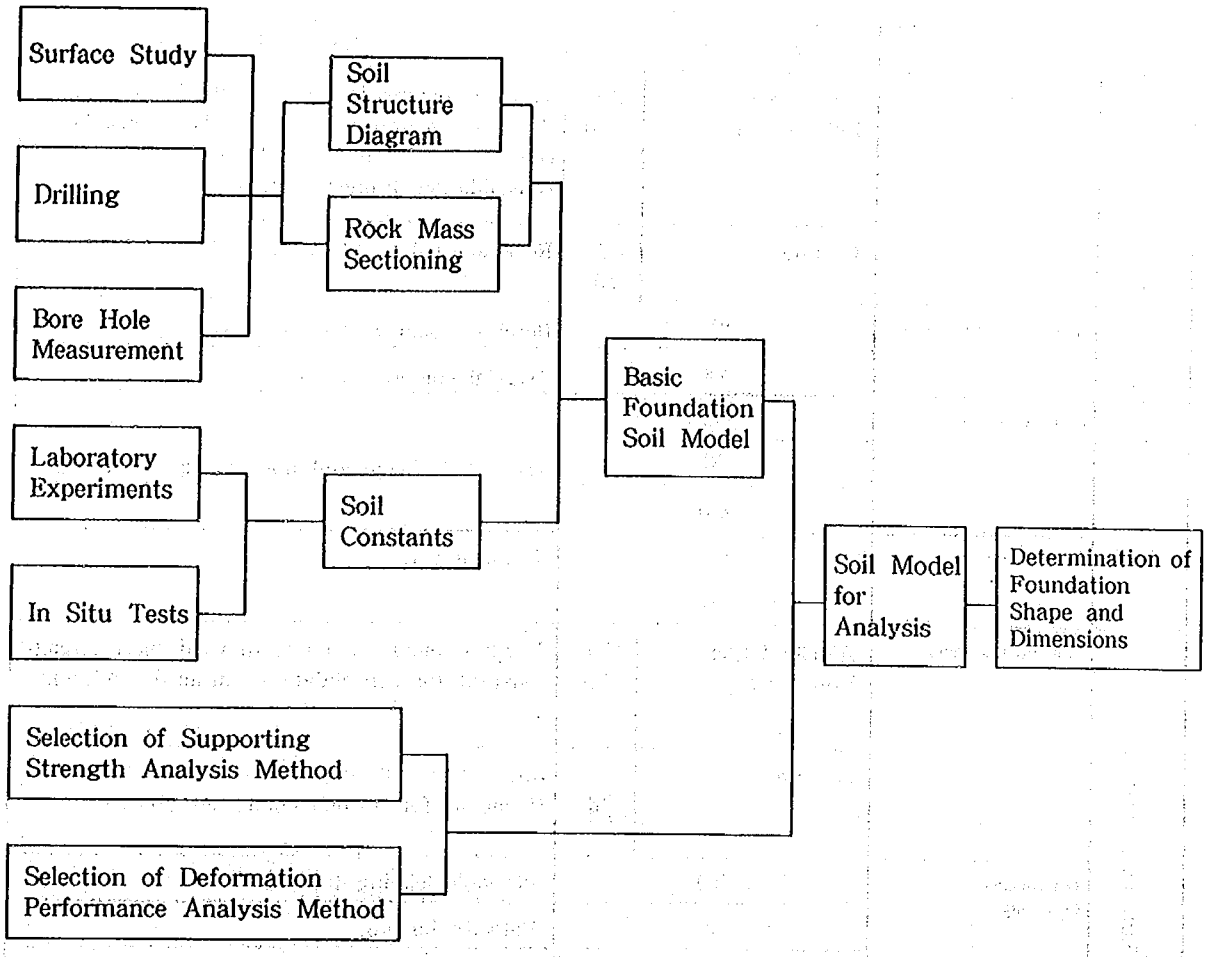

Figure 3 : The Relationship of Geological Surveys and Foundation Design

Table 1: Soil Constants Needed for Design and Associated Test Methods

		Soil Constant		Test Method
Normal Conditions	Strength Constants	Akashi Layer Kobe Layer	Ccd ϕcd	Triaxial compression tests to yield Ccd, ϕcd, or the effective stress indices C, ϕ (responsible for consolidated-drained conditions) for consolidation-drained conditions
		Granite	Cd ϕd	Rock shear test (triaxial test)
	Deformation Constants	ES		Borehole loading (triaxial test)
		Vs		Triaxial compression test
	Creep Constants	Gx		Triaxial drainage and nondrainage creep test
		G3		
		η 3		
	Unit Weight	γ γ t γ sat		Physical test
During Earthquake Constant	Strength Constants	Akashi Layer Kobe Layer	Ccu ϕcu	Triaxial compression test to yield sheer strength constant for consolidated-undrained conditions.
		Granite	Cd ϕd	Rock shear test to yield shear strength constant (Same as for normal conditions above)
	Deformation Constants	ED		Borehole loading test
		Go		Velocity logging
		G		Repeated triaxial test
	Attenuation	D		Repeated triaxial test
	Unit Weight	γ γ t γ sat		Physical test
During Strong Winds or Collision with Vessels	Strength Constants	Akashi Layer Kobe Layer	Ccu ϕcu	Triaxial compression tests to yield sheer strength constant for consolidated-undrained conditions.
		Granite	Cd ϕd	Rock shear test to yield shear strength constant
	Deformation Constants	ED		Double that of normal conditions (2Es)
		ν D		Same as for normal conditions
	Unit Weight	γ γ t γ sat		Physical test

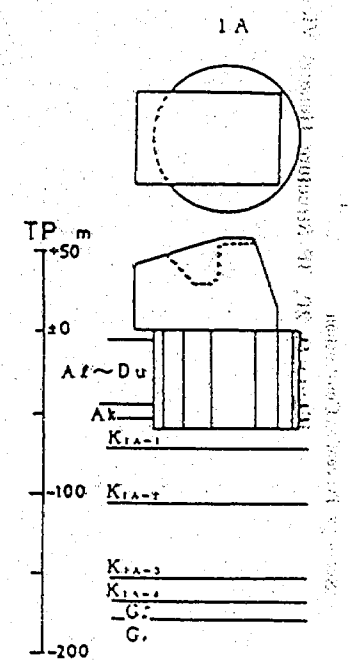

Table 2

Stratum		Altitude	Layer Thickness	Physical Characteristics					Strength Characteristics				Deformation Characteristics						
									Normal Conditions		During Earthquakes, Strong Winds, and Collisions with Vessels		Normal Conditions					During Strong Winds and Collisions with Vessels	
													Deformation Constant		Crooo Constant			Deformation Constant	
Name	Zonation	(T.P. - m)	(m)	γ_{sat} (tf/m³)	γ' (tf/m³)	V_s (m/s)	V_p (m/s)	ν_D	C_{cu} (tf/m²)	ϕ_{cu} (°)	C'_{cu} (tf/m²)	ϕ'_{cu} (°)	E_o (tf/m²)	ν_o	C' (tf/m²)	C'/C_o	$C_{v=0}$ (1/min)	E_o (t/m²)	ν_o
Alluvial Deposits	Aℓ	-4	6	1.76	0.76	180	1,300	0.49	—	—	—	—	8,400	0.38	—	—	—	16,800	0.38
Upper Diluvial Deposits	D	-10	10						0	30	0	30	11,000	0.38	—	—	—	22,000	0.38
		-20	25			300		0.47											
Akashi Layer	AK	-45	10	2.15	1.15	450	1,800	0.47	5	35	50	30	46,000	0.33	4,500	0.08	1.95×10^{-4}	92,000	0.33
Kobe Layer	K_{1A-1}	-55	17	2.25	1.25	600	2,100	0.46	30	25	130	30	66,000	0.35	12,000	0.10	0.18×10^{-4}	132,000	0.35
	K_{1A-2}	-74	35	2.23	1.23	700	2,200	0.44	40	25	60	20	83,000	0.30	21,300	0.12		166,000	0.30
	K_{1A-3}	-109	44	2.27	1.27	820	2,500	0.44	20	35	100	30	82,000	0.31	26,100	0.29		164,000	0.31
	K_{1A-4}	-153	17	2.44	1.44	1,200	3,300	0.42	30	35	150	30	89,000	0.37	27,200	0.29		178,000	0.37
Aerated Granite	Gr	-170	10	2.40	1.40	1,300	3,500	0.42	10	37	$C_{cu}=10$	$\phi_{cu}=37$	90,000	0.41	31,700	0.5	5.3×10^{-5}	180,000	0.41
Granite	Gr	-180	—	2.60	1.60	2,000	4,500	0.38	50	40	$C_{cu}=50$	$\phi_{cu}=40$	100,000	0.25	64,000	0.5	4.9×10^{-5}	200,000	0.25

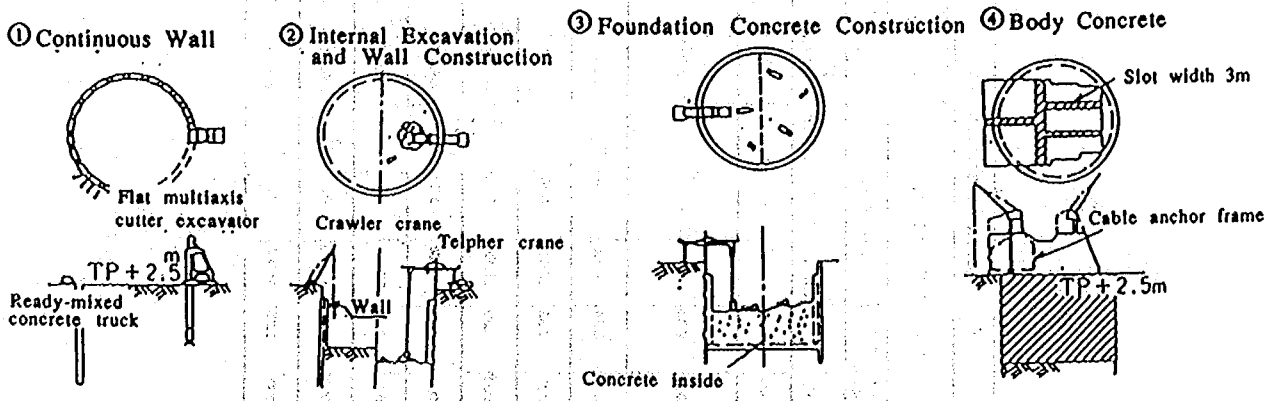

Figure 4: 1A Anchorage Foundation Construction Procedure

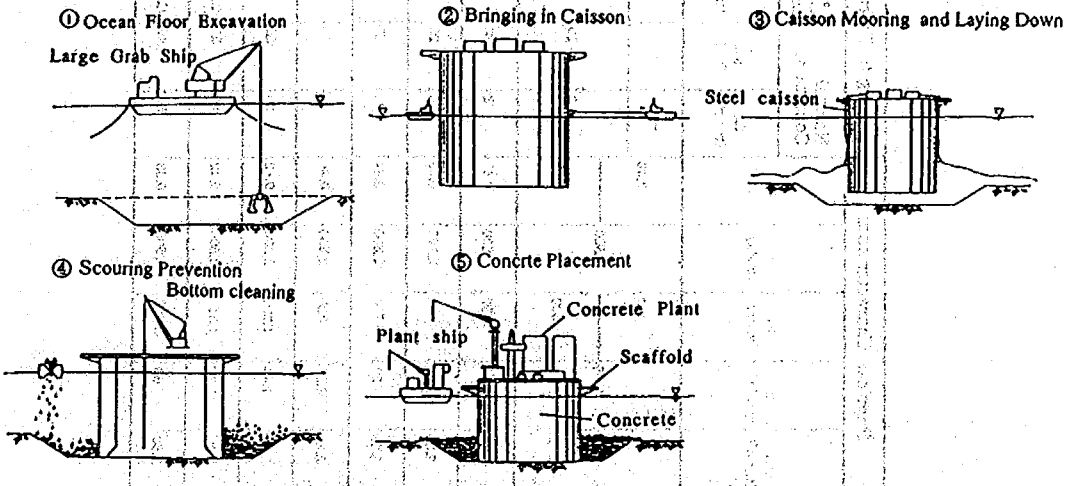

Figure 5: 2P, 3P Main Tower Foundation Construction Procedure

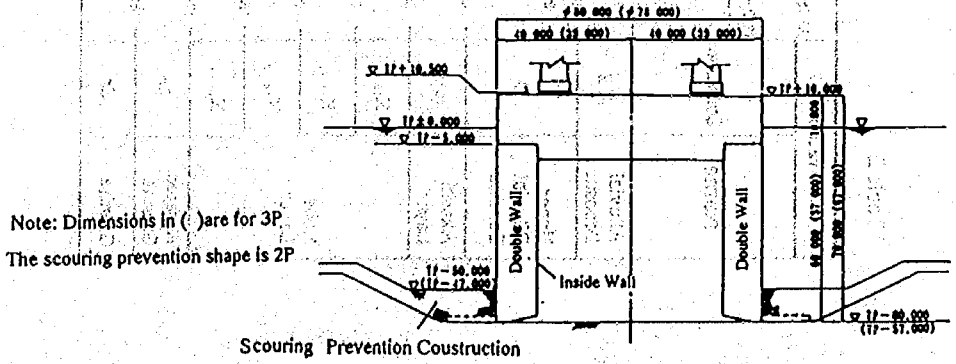

Figure 6: 2P, 3P Structure General View

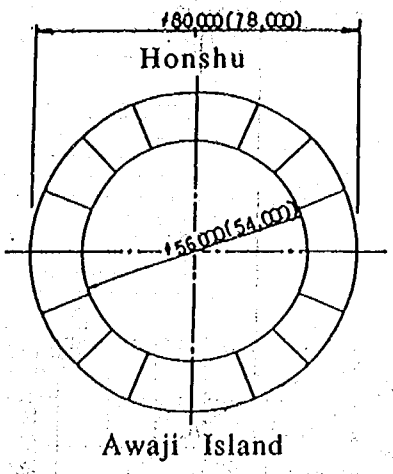

Note: Dimensions in ( ) are for 3P.

Figure 7: 2P,. 3P
Double Wall Concrete Section

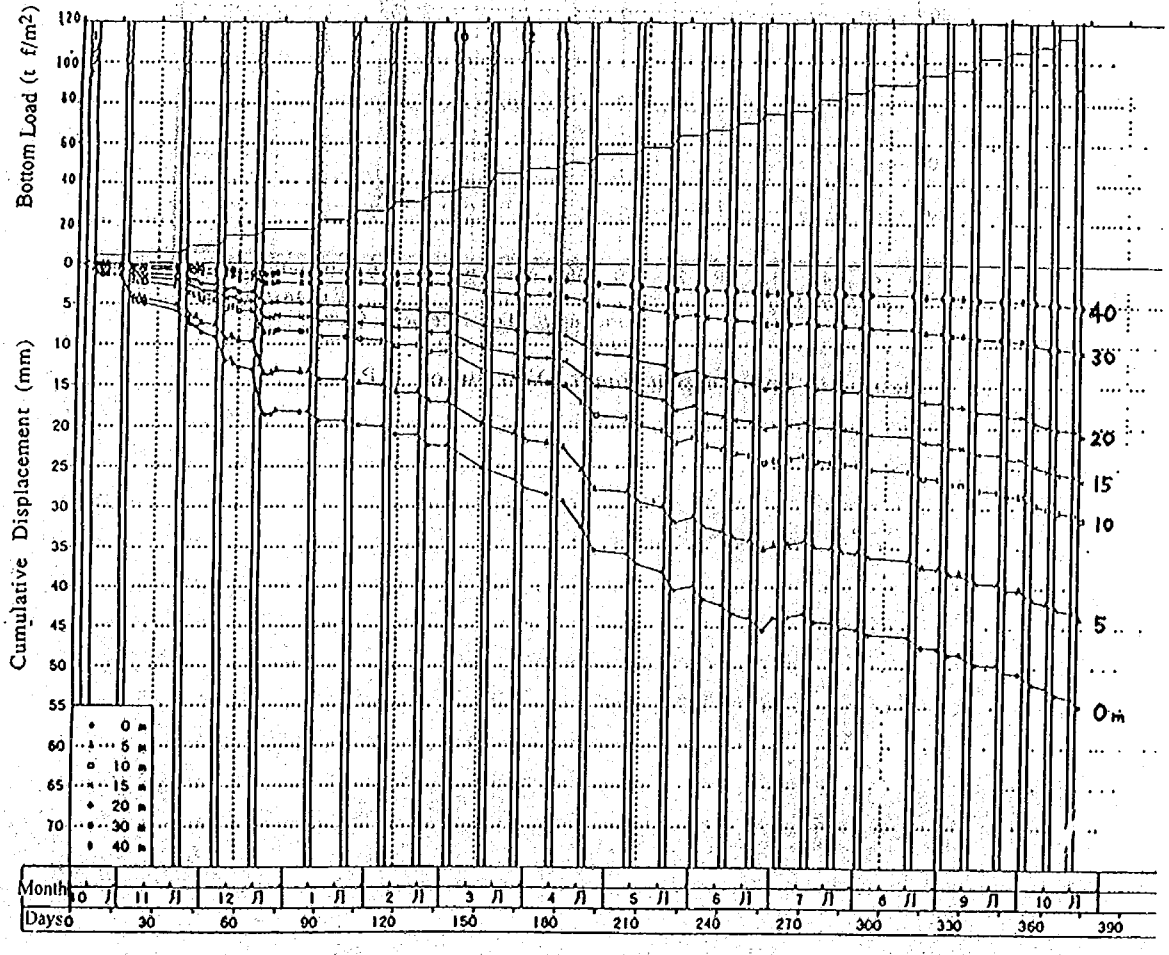

Figure 8: Time Series for Soil Displacement by Depth

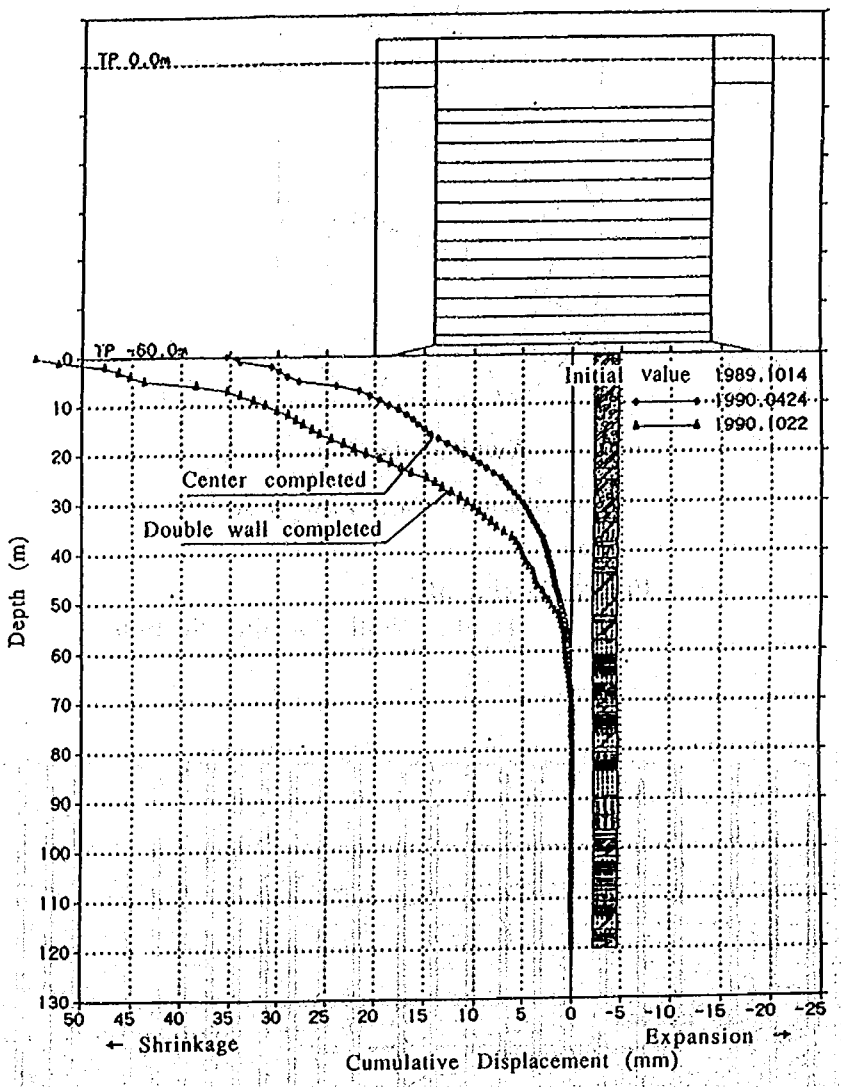

Figure 9: Soil Displacement Distribution (2P)

CONSTRUCTION OF THE NEW BRIDGE ENGINEERING LABORATORY FACILITY AT THE UNIVERSITY OF NEVADA, RENO

by

Bruce M. Douglas[1], Michael D. Blakely[2]
M. "Saiid" Saiidi[1], and Emmanuel A. Maragakis[1]

INTRODUCTION

Between 1982 and 1988, the total number of bridges in the United States increased from 571,246 to 577,710 (1,2). The number of structurally deficient bridges increased from 132,154 to 135,826; while the number of functionally obsolete bridges decreased from 121,042 to 102,531. In 1982, 44% of the total bridge inventory was either structurally deficient or functionally obsolete. In 1988, this percentage of deficient bridges declined slightly to 41% (1,2). This indicates that, unless the rate of improvement is increased dramatically, this aspect of the bridge engineering problem will continue to plague the country.

In addition to the general bridge engineering problem mentioned above, there is a great need to improve the seismic resistance of bridges in earthquake prone areas of the country. Twenty years ago, the 1971 San Fernando earthquake (3) caused significant damage to highway bridges. The heightened awareness of highway bridge vulnerability to earthquakes created by this event eventually resulted in the American Association of State Highway and Transportation Officials (AASHTO) guide specification for the seismic design of bridges (4). More recently, the 1989 Loma Prieta Earthquake (5) which caused great damage to highway bridges in the San Francisco Bay area, indicated that more structural engineering research involving experiments on large-scale bridge models and components needs to be conducted to improve the seismic design of bridges.

The need for large-scale structural and earthquake engineering experimental facilities has long been recognized (6 through 15). In particular, Japan has been a leader in developing large-scale structural testing facilities (11). As a result of the needs in the area of bridge engineering research, the University of Nevada, Reno is constructing a new Bridge Structures Laboratory as part of a 55,000 square foot Engineering Laboratory Center $10,000,000 capitol expansion project (Fig. 4). The primary purpose of this paper is to describe this new bridge structures laboratory and some of its unique features and capabilities and to briefly identify two

1. Civil Engineering Department, University of Nevada, Reno, Nevada 89557

2. Mike Blakely, Structural Engineer, 100 W. Grove Street, Suite 475, Reno, Nevada 89509

large-scale experimental projects which are in the developmental stages.

DESCRIPTION OF THE HIGH BAY BRIDGE STRUCTURES LABORATORY

Main Test Floor: Figure 1 shows a plan view of the laboratory. The 3-ft. thick main test hall slab of reinforced concrete measures 101 ft. by 56 ft. The main floor has a 2-ft. by 2-ft. gridwork of tiedown or socket holes formed by 2½-inch standard pipe sleeves perforating the test hall slab. The main 3-ft. thick slab was designed as a one-way slab supported by the two side walls of the basement and three intermediate bearing walls. The principal slab reihforcement consists of top and bottom mats of number 14 bars running in both the transverse and longitudinal directions at 12 inches on center. In addition to the one-way slab action, the whole basement/bearing wall/main test slab system also forms a very large box girder system in the longitudinal direction. The specified strength of the concrete was 4000 psi, but the test cylinder results indicate that the actual 28-day concrete strength achieved was 5000 psi. The specified ASTM flatness index for the main slab was 50 or greater and the ASTM levelness index was 35 or greater to result in a very flat floor as described in ACI 117.

Strong Wall: Figure 1 also shows the 20-ft. wide by 19-ft. high 2-ft. thick posttensioned strong wall located in the center of the east wall. This strong wall is also perforated with tiedown sockets on the same 2-ft. interval as the main floor. This interval was maintained because all of the steel test accessories which will be built for the laboratory will have this spacing, thus, allowing their reuse at any location within the facility.

Lift-out Grate: At the southeast corner of the facility, Fig. 1 shows a lift-out grate and stair section to allow heavy test equipment and fixtures to be lowered to the basement foundation slab for temporary storage. Another access stairwell to the basement is located at the northwest corner of the laboratory.

3000-psi Hardline Hydraulic Distribution System: Also shown in the plan view are the four hydraulic hardline ports along the west face of the central bearing wall. These ports provide for a 250-gpm (gallons per minute) hydraulic supply and return as well as a small drain line. These ports were designed so that an additional 250 gpm of hydraulic pumping capacity can be added in the future. The hydraulic pumps serving the bridge structures laboratory are located in a separate pump house outside the southeast corner of the building. A cooling tower to provide cold water to cool the hydraulic oil is also located adjacent to the pump house.

Roll-up Doors: The final feature indicated in Figs. 1 and 2 is the roll-up doors at the north and south ends of the laboratory to allow large trucks to pass through the laboratory. The small storage or "bone" yard at the north end of the building is currently smaller than needed, but this can be enlarged in a phase 2

expansion of the facility.

Basement: The foundation of the laboratory consists of a 2-ft. thick reinforced concrete foundation mat shown in Figs. 2 and 6. Three 16-inch thick 8-ft. high concrete bearing walls, forming four nominally equal width basement cells, rest on the foundation mat and support the main slab. These bearing walls are also shown in the longitudinal section in Fig.3. Every 10 ft., the top and bottom of the bearing walls have been perforated with 6-inch diameter PVC sleeves. These sleeves are to allow the convenient running of electrical and instrumentation cables from the experiments to the control room. The center of the bearing walls have also been perforated with a man-sized opening to allow transverse access between the basement cells, and to provide for quick egress is case of fire. A 10-ft. clearance between the ends of these bearing walls and the outer foundation walls has been provided to allow the movement of people and a forklift in this basement area. The primary purpose of this basement area is to allow access to the underside of the main slab during tiedown operations and to run power and instrumentation cables from experiments to the control room, but it will also be used for the temporary storage of laboratory equipment and test fixtures.

Bridge Cranes: The test hall is equipped with two bridge cranes, shown in Figs. 2, 3, and 5, having a clear lift of 36½ feet. These cranes each have a 25-ton main hook and a 5-ton auxiliary hook. All four hooks can be hoisted at either 6 or 20 fpm (ft. per minute). The bridges of both cranes have travel speeds of either 25 or 80 fpm, and the bridge trolleys carrying the hooks can travel across the bridges at either 20 or 63 fpm. These cranes are radio controlled in such a way that they can both be run independently or in common. When they are in the common or simultaneous mode of operation, it is possible to run all four hooks up and down at the same speed as well as have the hooks move around the laboratory floor at the same speeds. This will greatly facilitate the hoisting of large test specimens being lifted by both cranes at the same time.

Reaction Blocks: Figure 2 also shows the reaction blocks. The blocks can be used as supports or reaction abutments and to spread the loads in some experiments. They can also be ganged together to serve as posttensioned beam elements to span over or to strengthen the test floor. These 4-ft. by 4-ft. by 8-ft. reinforced concrete reaction blocks represent a unique feature of this laboratory. They are cast in a steel form to insure dimensional control and are perforated in all three directions with socket holes on the same 2-ft. by 2-ft. pattern used in the main test slab and the reaction wall. Each face of the reaction blocks will also be fitted with two or more 8-ton swivel lift anchors so that they can be placed by a single overhead crane. The blocks are designed to interlock directly with the floor and the reaction wall with the long dimension of the block either parallel or perpendicular to the reaction wall. In the perpendicular direction, the reaction blocks

will have to be shimmed with 3-inch filler blocks. The primary purpose of these reaction blocks is to be able to construct a variety of different reaction fixtures required in different experimental situations by posttensioning them with Dywidag bars to the main test hall floor and/or the strong wall. When the laboratory opens in the fall of 1991, the construction contract provides for ten blocks to be supplied along with the steel form. Having the steel form allows more blocks to be cast as needed.

Basement Access Ramp: An access ramp from the storage yard at the north end of the facility to the basement of the laboratory is shown in Fig. 1. This ramp is designed to allow long items to be moved to temporary storage in the basement and to allow a forklift to be driven down to the basement level.

Future Earthquake Simulation: The entire test facility consisting of the foundation mat, basement walls, bearing walls, and main test floor forms a rigid box structure weighing at least 5,000,000 pounds. A foundation of this size and weight can support an earthquake simulation shake table or tables along with the structural models which could weigh between 50,000 to 100,000 pounds. This would correspond to a dynamic test mass to foundation mass ratio of between 50 and 100, which should give good earthquake simulation results. In the future, it is anticipated that several horizontal single-degree-of-freedom earthquake simulators would be employed to study the effects of non-coherent earthquake ground motions on bridge models. It is anticipated that the reaction blocks mentioned above would be used to react to the structural actuators driving the earthquake simulators.

Additional Features: Natural lighting for the laboratory is provided by two large skylights in the roof of the facility as well as by a large block of windows at the north end of the laboratory. On the main test floor, 110- and 220-volt electric power outlets, 100-psi compressed air, and water spigots are located at frequent intervals around the outer perimeter of the laboratory. These utilities are also available in the basement areas except for the 220-volt electric power outlets. If necessary, the 220-volt electric power can be accessed in the basement by running power cords up through the socket holes in the main slab.

LOAD CAPACITIES AND DESIGN CRITERIA

The test floor was designed as a continuous one-way slab spanning from the exterior walls over three interior bearing walls. Two-way plate action was considered at boundaries and discontinuities and to distribute large individual point loads.

The floor system capacity is, in general, shear critical. Flexural reinforcement was designed to provide a flexural failure mode for the load case where a uniform load is applied over a large area. However, when large local point loads or line loads are applied close to supports, shear capacity becomes critical.

Based on the specified concrete strength (f'_c = 4 ksi) and the reinforcing steel strength (f_y = 60 ksi), the slab capacity in shear and flexure are $\Phi \cdot V_c$ = 40 kips/ft. and $\Phi \cdot M_u$ = 297 kips/ft. respectively. Using the load factors of 1.4 for dead loads and 1.7 for live loads, the test floor can safely support the following live loads:

1. Uniform loads and patch loads of any size in balanced or unbalanced configurations and in any direction up or down: 3.4 ksf (kips per square foot).

2. North-south line loads in any single slab span in any direction up or down: Capacity varies linearly from 35 kips per lineal foot applied at mid span to 23 kips per lineal foot at 3 feet from the supports.

3. Single point loads with no other load applied within 12 feet of the point load and which are not adjacent to the basement stair openings: 300 kips upward or 240 kips downward.

4. "Special" experimental live loads which are both controlled and measured can justify the use of an ultimate live load factor of 1.4. Thus, in this case, the above loads can be increased by 20%.

Small downward uniform loads can result from materials stacked on the floor. However, the large loads described above can only occur as a result of various experimental situations. These experiments must be designed as systems with static equilibrium. A uniform load of 3.4 ksf is equivalent to 22 feet of solid stacked concrete. An upward load of 300 kips would pick up the entire weight of a 20-ft. by 20-ft. area of slab, wall, and mat foundation. Loads of this type must have reactions of equal magnitudes but opposite directions.

Several possible experiments with very high load levels were devised in order to evaluate the versatility of the test floor. One case envisioned a vertical cantilever column which was bolted to the test floor and had a 200-kip horizontal force applied at 25 feet above the floor. A second experiment had a large column with a 400-kip axial load and reaction blocks piled on two sides which were used to jack 200-kip horizontal loads into the column 25 feet above the floor. A third experiment envisioned testing a 30-ft. by 80-ft. long concrete box beam. The beam would rest on reaction blocks at each end and 200-kip point loads would be jacked through the test floor at eight locations. All of these experiments were found to be feasible on the test floor.

The 24-inch thick concrete strong wall located on the east side of the laboratory was designed to serve as a utility reaction wall for small experiments. It is a vertical cantilever projected from the basement exterior wall. It has mild steel reinforcing and has been

posttensioned (Fig. 7) to a uniform stress of 950 psi. Thus, the wall can resist cyclic load applications while remaining elastic and uncracked. This results in a uniform wall stiffness and avoids the significant stiffness change which occurs when the concrete cracks. Experimental loads to the wall are limited by allowable tensile stress on the precompressed tensile zone and by the allowable compressive stress using simple elastic beam analysis.

EARLY EXPERIMENTS PLANNED

One of the first large experiments planned will be to determine the ultimate load capacity of some used prestressed concrete box bridge girders. These 3-ft. by 4-ft. by 69-ft. prestressed concrete box girders were removed from a bridge structure built in 1968 which was torn down and replaced with a new structure. The owner wants to investigate the structural integrity of a sample of the girders to improve their resale value.

A second project, which is in the feasibility stage, will be to test some full-scale beam/column joints from a reinforced concrete box girder bridge built in the early 1960's. This bridge was functionally obsolete and was replaced with a new structure. The now redundant bridge is slated for removal. The feasibility of removing the bridge's 16 beam/column joints and transporting them to the laboratory as part of the demolition project is currently being investigated. The purpose of the study will be to identify the seismic resistance characteristics of the existing beam/column joints, and then to study a series of seismic retrofitting schemes which would be applied to the remainder of the 16 total specimens. This knowledge will be very useful in retrofitting other similarly reinforced concrete box girder structures.

ACKNOWLEDGEMENTS

During the design phase of the laboratory, formal site visits were made to five structural laboratories. For their generous giving of their time and ideas, our thanks go to Frieder Seible of the University of California at San Diego, James Jirsa of the University of Texas at Austin, Robin Shepherd of the University of California at Irvine, Lloyd Cayse of the Turner-Fairbanks laboratory at McLean, Virginia, and Patrick Quinn of the University of California at Berkeley. Laboratories at the Public Works Research Institute and the Building Research Institute at Tsukuba, Japan; the University of Auckland, New Zealand; the University of Canterbury at Christchurch, New Zealand; the University of Illinois at Urbana; and the University of Michigan at Ann Arbor were also all visited prior to the actual detailed planning of the laboratory. James Jirsa of the University of Texas at Austin also acted as a consultant to Mike Blakely, the structural engineer for the project. In addition, we thank the design firms and the construction team who worked together to make the lab a reality. The design firms include Mentgen Associates, Architects; Peterson

& Associates, Ltd., Mechanical Engineers; MBA Consulting Engineers, Electrical Engineers; SEA, Inc., Engineers; Summit Engineering Corporation, Engineers; RFD Consultants; and Anshen & Allen Architects. The construction team was comprised of the general contractor, Clark & Sullivan Constructors and their subcontractors: Martin Iron Works, Gardner Engineering, Pioneer Electric, T.W. Construction, CB Concrete, Koffler Masonry, Sacramento Insulation, D & D Contractors, Pierce Enterprises, and Alpine Glass. The hydraulic infrastructure was supplied by MTS Systems Corporation, and the bridge cranes were supplied by Crane Services Corporation.

REFERENCES

1. "Limited Funds and Numerous Deficient Off-System Bridges Create Federal Bridge Program Dilemma," (1983), report to the Secretary of Transportation, U.S. General Accounting Office, Report No. GAO/RCED-84-66, December 8, 77 pp.

2. "The Status of the Nation's Highways and Bridges: Conditions and Performance and Highway Bridge Rehabilitation Program 1989," (1989), report of the Secretary of Transportation to the United States Congress, U.S. Government Printing Office, Washington, D.C., June.

3. Elliott, A.L. and I. Nagai, (1973), "Earthquake Damage to Freeway Bridges," San Fernando, California Earthquake of February 9, 1971, Vol. II, U.S. Department of Commerce, U.S. Government Printing Office, pp. 201-233.

4. "Guide Specifications for Seismic Design of Highway Bridges - 1983," (1983), published by the American Association of State Highway and Transportation Officials - AASHTO, 444 N. Capitol Street, N.W., Washington, D.C., 106 pp.

5. Benuska, L., editor, (1990), "Loma Prieta Earthquake Reconnaissance Report," Earthquake Spectra, Supplement to Vol. 6, May, Ch. 6.

6. "Earthquake Engineering Research - 1982," (1982), Committee on Earthquake Engineering Research, Commissions on Engineering and Technical Systems, National Research Council, National Academy Press, Washington, D.C., 266 pp.

7. "Earthquake Engineering Research - 1982, Overview and Recommendations," (1982), Committee on Earthquake Engineering Research, Commissions on Engineering and Technical Systems, National Research Council, National Academy Press, Washington, D.C., 78 pp.

8. Scholl, R.E., editor (1984), "Experimental Research Needs for Improving the Earthquake-Resistant Design of Buildings," a technical evaluation based on a workshop sponsored by the National Science Foundation, EERI Report No. 84-01, 84-02, January.

9. Jennings, P.C. and R.E. Scholl, editors (1984) "Experimental Research Needs for Improving Earthquake-Resistant Design of Buildings, Overview and Recommendations," EERI Report No. 84-02, January, 43 pp.

10. "Earthquake Engineering Facilities and Instrumentation," Ad Hoc Committee on Earthquake Engineering Facilities and Instrumentation" (1984), Committee on Engineering and Technical Systems, National Research Council, National Academy Press, Washington, D.C., 1984, 33 pp.

11. Kamimura, K., Y. Aoki, and M. Nakashima, (1984), "Register of World Large Scale Test Facilities for Building Research," Kenchiku Kenkyu Shiryo, No. 49, Building Research Institute, Ministry of Construction, Japan, March, 51 pp.

12. Hognestad, Eivind, N.W. Hanson, Ladislav B. Kriz, and Otto A. Kurvits, (1959), "Facilities and Test Methods of PCA Structural Laboratory," Development Department Bulletin No. D33, Portland Cement Association, Skokie, 32 pp.

13. Seible, F. and G. Hegemier (1986), "Full-Scale Structural TEsting," ACI Concrete International: Design and Construction, Vol. 8, No. 7, July 1986, pp. 48-52.

14. Design and Construction of the UCSD Charles Lee Powell Structural Systems Laboratory," University of California, San Diego Report SSRP-86/01, November 1986, 55 pp.

15. Douglas, B. (1984), "A National Bridge Engineering Laboratory - A Proposed Plan," Center for Civil Engineering Earthquake Research, Report CCEER No. 84-4, University of Nevada, Reno, 51 pp.

16. Woodward, K. A. and J.O. Jirsa (1977), "Design and Construction of a Floor-Wall Reaction System," CESRL Report No. 77-4, Department of Civil Engineering, University of Texas, Austin, 71 pp.

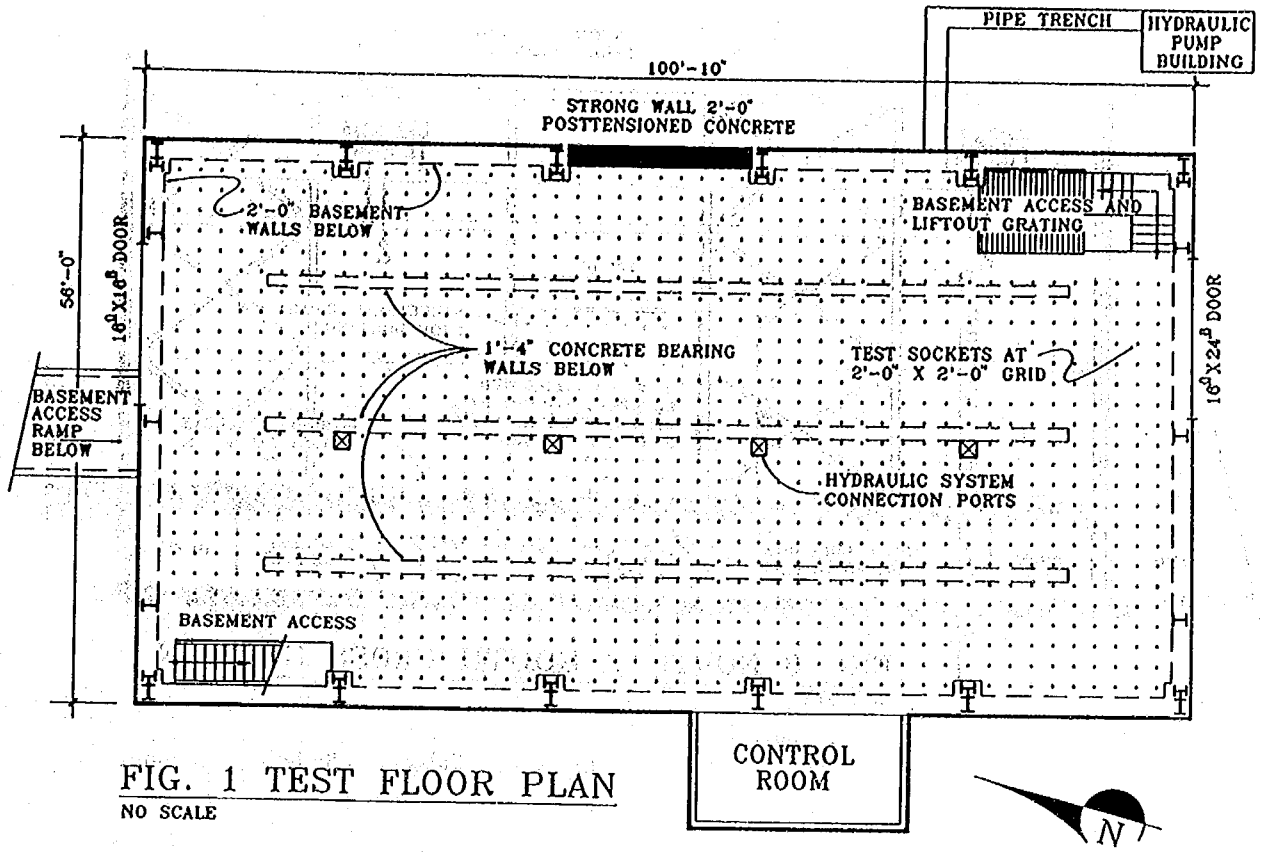

FIG. 1 TEST FLOOR PLAN
NO SCALE

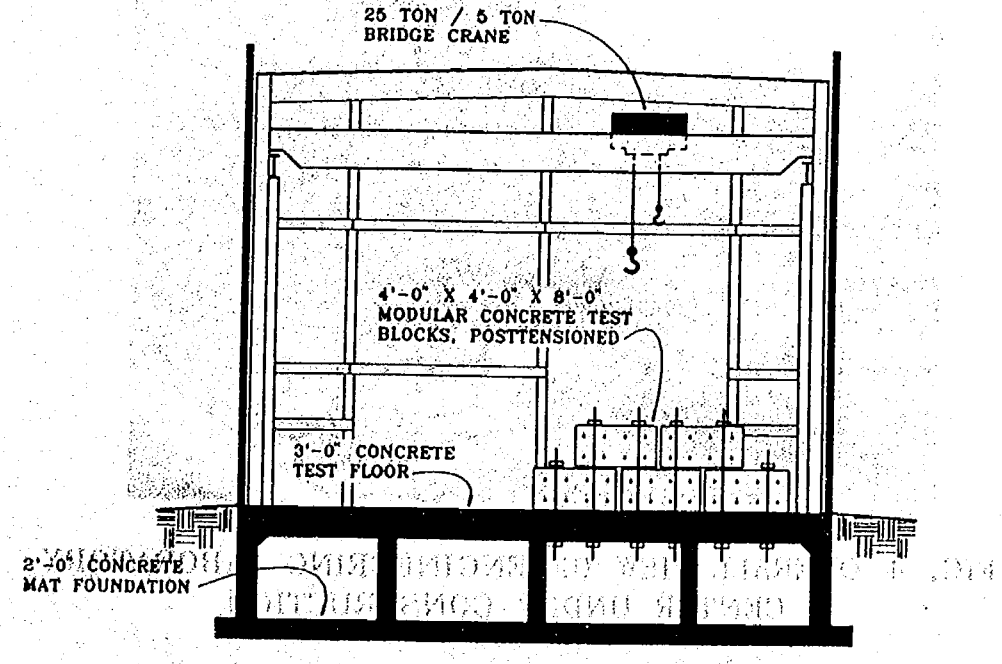

FIG. 2 EAST / WEST CROSS SECTION
NO SCALE

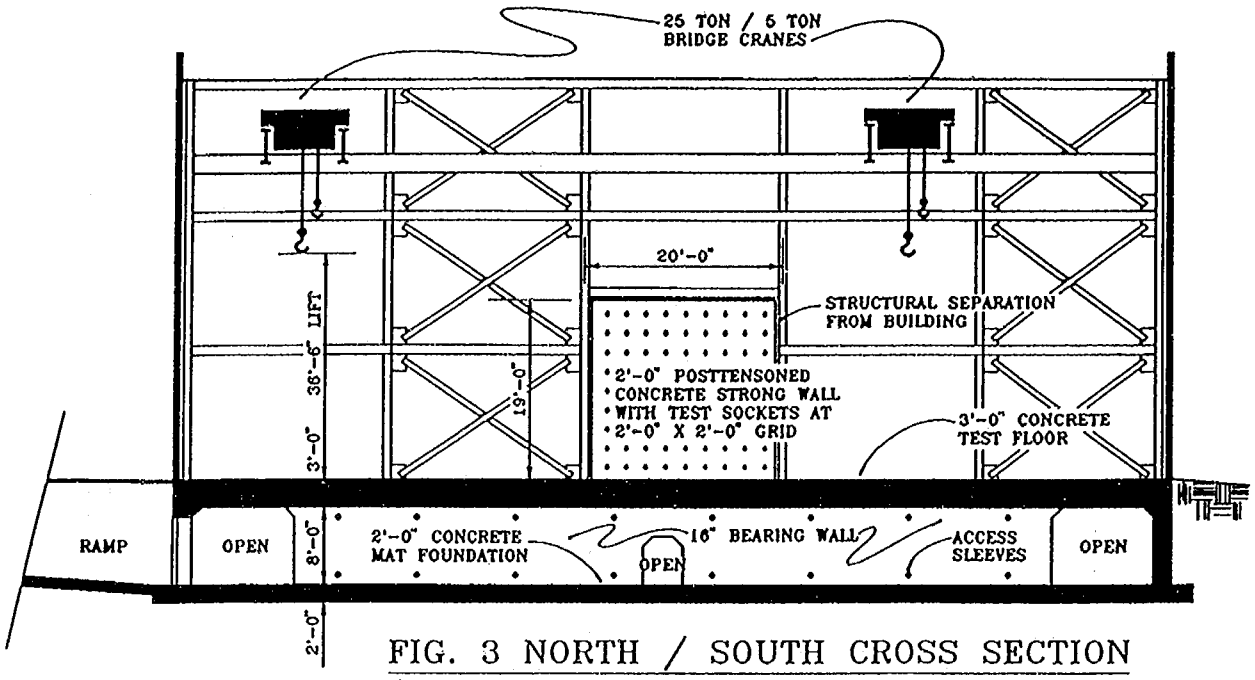

FIG. 3 NORTH / SOUTH CROSS SECTION

NO SCALE

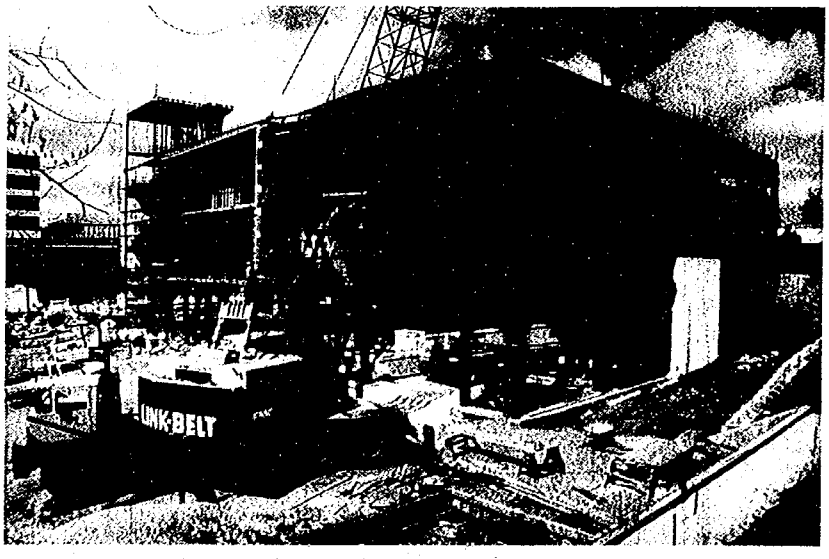

FIG. 4 OVERALL VIEW OF ENGINEERING LABORATORY CENTER UNDER CONSTRUCTION

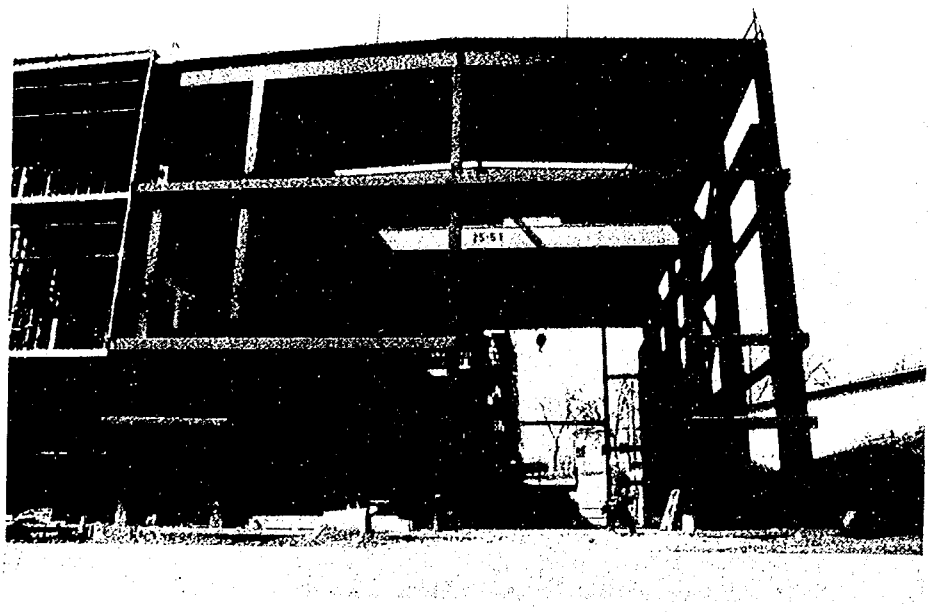

FIG. 5 FRONT VIEW OF BRIDGE LABORATORY SHOWING CRANES

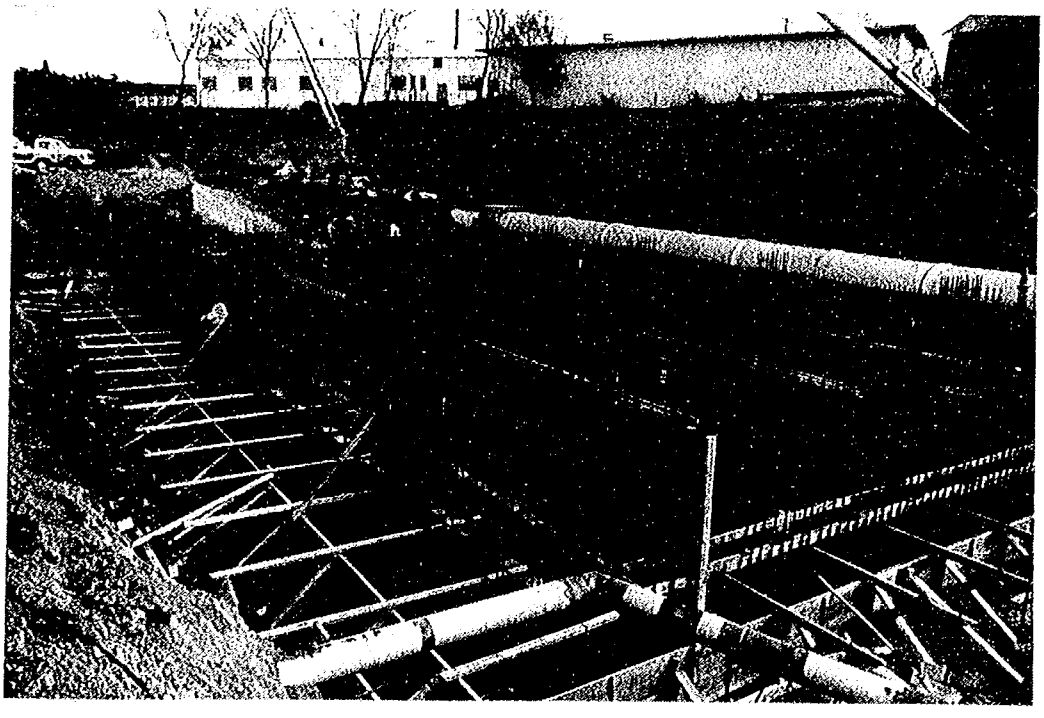

FIG. 6 MAT FOUNDATION FOR BRIDGE LABORATORY

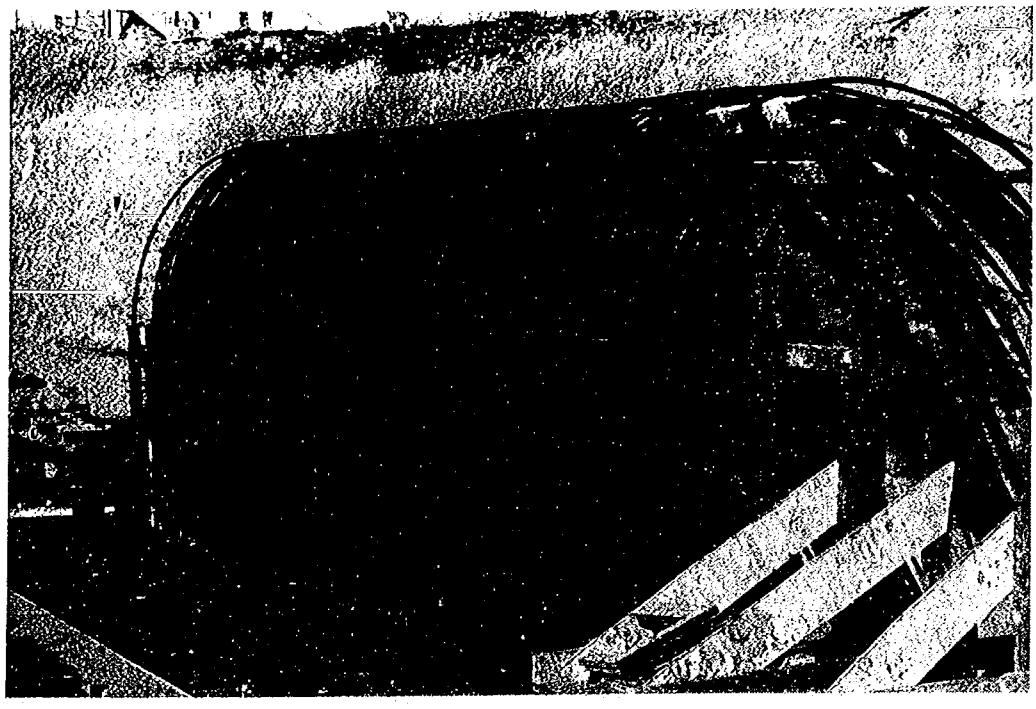

FIG. 7 PRESTRESSING STRANDS FOR STRONG WALL AND SOCKET SLEEVES FOR MAIN TEST FLOOR

Planning and Design of Multi-Span Continuous Bridges

U.Kagawa[1], T.Meta[2], S.Nakamura[3], H.Kato[4]

ABSTRACT:There is 4.4 Km bridge section in the Trans Tokyo Bay Highway (TTBH) whose total length is about 15 km. In order to improve both the seismic resistance and road surface smoothness, TTB planned continuous bridges in which the maximum number of the continuous spans goes up to eleven. In this paper the design of those continuous bridges is discussed.

1. Introduction

The Trans-Tokyo Bay Highway Bridge (TTBH) is a 15.1 Km toll highway connecting Kawasaki and Kisarazu which are situated at both sides of the Tokyo Bay, as shown in Fig. 1. The highway consists of two 10 Km long tunnels under the Kawasaki waters where marine traffic is heavy, a 4.5 Km bridge over the Kisarazu waters where marine traffic is sparse, and two gigantic man-made islands. The route is wide open to ships between the Ukishima and the Kisarazu island except the Kawasaki island. There is a 860m wide navigation area between the bridge piers P5-P9 where the bridge is elevated to pass 2,000GT class vessels. The size and scope of these structures are beyond the conventional ones. In addition, soft underground and possibility of large earthquake have made the construction more challenging.

TTBH will form the Tokyo metropolitan highway network connecting to main highways across the nation. This highway is expected to activate harmonious economic development and relieve traffic congestion in the metropolitan areas. Although most of the public highways have been constructed by the public corporations, a new project system 'the third sector system' was adopted for the TTBH in order to utilize financial and human resources of private companies.

---

1)Manager of the bridge design section, TTB, Tokyo, Japan
2)Assistant for the manager of the bridge design section, TTB, Tokyo, Japan
3)-4)Bridge design section, TTB, Tokyo, Japan

The highway carries dual two lane carriageways in the first stage, and other two lanes will be extended in the future. However, the decision on the extension is to be made judging by the future traffic volume. Traffic volume is estimated approximately 33,000 veh/day which is expected to reach 64,000 veh/day in 20 years after opening. Design vehicle speed is 80 Km/h.

The bridge is 4.4km long with 43 piers. The navigation area exists at water depth about 20m, where the span is extended up to 240m. The layout of the bridge is shown in Fig. 1 and Fig. 2, where the soil layers are also illustrated.

Alluvial sand and clay layers (As and Ac) exist 5m to 20m deep under the seabed. In some alluvial layers sands are soft with N value of the standard penetration tests under 10 and the grains are uniform and medium size, which might create a liquefaction problem. Below the alluvial soils there are diluvial soil layers with different ages, D1 to D4, where sands and clays exist alternately. D5 layer observed overall the highway layout is stiff with N value over 50 and earthquake shear wave velocity over 400m/s, and has been taken as the input base of seismic design waves.

2. Bridge Super-structure

The steel box girders with orthotropic decks have been adopted as super-structure because of its light dead weight and rapid construction. The maximum web height is 10.5m, and the width is 29.9m which accommodates dual two lane carriageways in the first stage, and extra two lanes in the future stage. The cross section of the super-structure is shown in Fig. 3.

The bridges are designed to have long continuous girders so as to improve both the seismic resistance by sharing seismic horizontal forces with many piers and road surface smoothness by eliminating expansion joints. Ultra-long continuous girders are planned culminating 1,630m long 10-span continuous girder, from P3 to P13, utilizing high steel flexible piers. In the shallow water where piers are concrete and relatively low and stiff, rubber bearings are to be used to absorb the elastic expansion of girders due to temperature change.

The girders are fabricated and assembled at a factory, but two different erection methods will be used at the site. In the navigation area a large block of girders is towed to the site and set on the piers by floating cranes, as shown in Fig. 4. In the shallow water area where a floating crane barge cannot be used, a girder block is carried on the barge and set by jacks during the high tide period, as shown in Fig. 5. The barge does not float but stays on the sea bed during the low tide periods.

3. Bridge Sub-structure

The piers of P1 to P12 located in the navigation area are constructed in the 15m to 25m deep water and will suffer strong horizontal forces due to ocean waves and earthquakes as well as huge vertical reactions from the super-structure, requiring massive structures and difficult construction. Open-caisson, pneumatic-caisson, steel pile well foundation, and composite steel piers shown in Fig. 6 are compared technically and economically, concluding that the last one is the best in all the aspects such as cost, period and easiness of construction.
A steel column and footing are fabricated and assembled into one piece at the fabrication yard, and transported to the site. The site is first dredged and sands are placed on it to form a foundation. Steel piers are then driven using a template. The steel pier is set by floating cranes on the piles driven beforehand, and both are then united with water concrete. Finally, concrete is cast into a column to increase the ultimate capacity and ductility with the composite action of steel and concrete.

Envilonmental protection is extremely important for the shallow water area from the shoreline to 5km nearshore where seaweeds and sea shells are bred. Numerical predictions on wave propagation, water velocity and seabed sand movements are extensively carried out to clarify the effect to the sea environments due to the construction of structures.
Steel pile well foundation and reinforced concrete column with 6m by 4m cross section has been adopted for the shallow water area, as seen in Fig. 8. The construction procedure is as follows. After the template is set, steel piles with 800mm diameter are driven and the gaps in between piles are sealed with cement mortal. The inside circular area is then dried up to build a concrete footing and column. The piles are then cut off at the seabed and removed.

4. Realization of Multi-span Continuous Bridge

In Japan the influence of the earthquake to the design of bridges is very important. In the Specifications for Highway Bridges in Japan, here after "SHBJ", the magnitude to be taken for the static earthquake load is specified to be from 0.24G to 0.3G depending on the structure's natural frequency. The load due to the temperature changes should be also taken into the consideration. The specified changes are at least + and - 30° centigrade from the basic temperature of 20°C.

If a load combination of the earthquake and temperature changes is considered in the design, generally the size of the sub-structure is enlarged. Therefore, some limitations must exist for the realization of the multi- span continuous bridge. On the other hand, the probability in which such load combination occurs must be very rare in reality. In addition to that, a multi-span continuous bridge usually develops larger ultimate strength than a series of simply supported bridges. In the revised "SHBJ '90" ,it is permitted not to consider the load combination of the earthquake and temperature changes. Therefore, the design of multi- span continuous bridges has been enabled.

There are several methods for the realization of the multi-span continuous bridge as seen in Fig. 8.

Method-1) Centralization of horizontal force
Method-2) Decentralization of horizontal force
Method-3) Damper system
Method-4) Rubber bearing

Because the horizontal force is centralized to a single pier in the Method-1, the size of the sub-structure is enlarged. As the result some limitations must exist from the economical considerations. The Method-2 is suitable for a bridge which is supported by flexible steel piers or tall piers. TTB's 10-span continuous bridge in the navigation area is designed by this method. The damper in the Method-3 does not show any resistance for such slow movement as occurs in the temperature changes, but it does for such quick movement as occurs in the earthquake. However, the damper itself can not support the vertical reaction so that some other bearings should be provided. In the Method-4 the expansion of the super-structure is absorbed by the shearing deformation of the rubber. Recent developments of the rubber bearings are attracting the designer's attention. TTB's continuous bridges in the shallow water area are realized by this method.

5. 10-span Continuous Bridge in the Navigation Area

The TTB's original design for the navigation area before '90 was a 4-span continuous bridge. According to the "Revised SHBJ" re-designed bridge for the navigation area has 10-span continuity from P3 to P13. A comparison among following three cases is investigated in the design.

Case-1) 7 hinged supports
The supports from P4 to P10 are hinged, and P11, P12 are movable.

Case-2) 8 hinged supports
The supports from P4 to P11 are hinged, and P12 is only movable.

Case-3) 9 hinged supports
The supports from P4 to P12 are all hinged.

In the structural analysis the super-structure and the sub-structure are united into one body. Sectional forces obtained at the top of footings are used for the stability analysis of each pier foundation. The required size of the foundation and the number of the steel piles for the original design and above 3 cases are tabulated in table 1. In general, the method using multi hinged supports in a continuous bridge gives better structural and economical results, because the horizontal force under the earthquake can be decentralized.

On the other hand, in such method the temperature changes affect predominantly on the end piers. As seen in the table 1, comparing the original design to the Case-1 or Case-2, the numbers of piles at each pier are normalized and the total number from P4 to P12 is decreased. However, in the Case-3 due to the temperature changes a large size of the end pier is required and the total number of the piles is increased. Therefore, the Case-2 is the most economical and has the best structural balance.

The bending moment and axial force along the bridge axis under the condition of dead load, live load and temperature (+35°) load are shown in Fig. 9. The maximum axial force (about 5,500t) is obtained at the neighbours of the center span. The stress caused by this axial force is only 10 % of the allowable stress. The bending moment due to the temperature load causes at most about 5% of the stress due to dead and live load. From these the validity of adopting the multi-span continuity is clearly proved. The deflections due to the live load are tabulated in table 2. They are all less than the allowable deflection specified in the "SHBJ".

Adopting the multi-span continuity it is anticipated the horizontal displacements at the top of the piers are increased due to the temperature load. The obtained displacements are tabulated in table 3. The maximum displacement is + or -430mm on the top of P13, where the both bridges from the navigation area and the shallow water area are supported. The displacemet is the cumulative of the movements of not only in the bridge from P3 to P13 but also in the one from P13 to P24 which is also a 11-span continuous bridge of 910m long. Although the relative displacement due to the expansion of the bridges is fairly large, it is not far beyond the one of the existing bridges. It must be possible to design some systems which cope with the displacement.

The calculated reactions acting on the bearings are tabulated in table 4. The maximum vertical reaction is 5,030t on P7. Negative values of the reaction are not found on any supports. The maximum horizontal reaction is about 1,840t at the hinged support on P11 whose height is the lowest among all the piers.

In order to clarify the influence of the error in the estimation of the stiffness between the analysis and the real structure, a series of the sensitivity checks using a united model of super- and sub- structures is carried out for the following three cases.

Check-1)

The spring constant of the ground reaction is changed to 5 times and 1/5 times of the original value.

Check-2)

The stiffness of the pier is changed to +20% up and -20% down of the original value.

Check-3)

The sectional area of the super-structure is changed to +20% up and -20% down of the original value.

It is found the changes of the spring constant and of the sectional area are not influential to the analysis from the results of the Check-1 and Check-3. Even if the spring constant is decreased to 1/5 times, the newly obtained sectional forces change at most 5% compared with the original ones. The change of the stiffness gives significant influence in the result of the Check-2 . However, even in such case the percentage of the change is at most 13%.

In these checkings the constants are changed equally for all piers. Followings are also carried out for the Check-1. The spring constant is changed 2 times and 1/2 times individually at every pier. For the worst case, the change is about 10% increase of the original forces. Through these investigations the possibility of 10-span continuous bridge is assured.

6. Multi-span Continuous Bridges in the Shallow Water Area

The multi-span continuous bridges in the shallow water area are realized by the use of rubber bearings. A normal rubber bearing consists of multiple layers of rubber sheets and steel plates which are bound into one piece. The steel plate prevents the rubber from swelling out to the side under the work of the vertical reaction. In other words, the rigidity in the vertical direction is stiffened. Ring bearing (RB) which is one kind of the layered rubber bearings is illustrated in Fig. 10 (a). As seen in the figure there are cuttings of a ring shape on the steel plate. The binding between the rubber sheet and the steel plate is strengthened by the rubber filled in the cutting. Fig. 10 (b) shows features of Lead rubber bearing (LRB) which is one of the layered rubber bearings but in which a bar made of lead is installed in the center of the plane. The lead works to damp kinematical energy by the characteristics of hysteresis. High damping rubber bearing (HDR) is shown in Fig. 10 (c). HDR is also one of the layered rubber bearings but the rubber preserves such characteristics as the high damping. RB has been often used for the actual and large scale bridges. LRB and HDR have been mainly used for the architectural structures. Some of them are also used for the bridges recently.

The number of continuous spans of each bridge in the shallow water area isdetermined by the investigation of the following 3 cases which are also illustrated in Fig. 11.

Case-1)
Total 30 spans are equally divided into 3 bridges. (11+10+9 spans)

Case-2)
Total 30 spans are divided into 2 bridges. (21+9 spans)
Where, the 21-spans bridge is in a shape of straight and the 9-spans bridge is in a shape of curved.

Case-3)
Total 30 spans are continued into 1 bridge. (30 spans)

The simplified model for the structural analysis is illustrated in Fig. 11, in which the depth of the water is assumed to be uniformly 6 m. Since the horizontal spring constants of the bearings are relatively smaller than the ones of the sub-structures, reasonable results can be obtained even from the simplified model. The results of the above 3 cases are tabulated in the table 5. The vertical reactions working on each bearing are in the range from 1,500ton to 1,700ton.
Applying the 3 types of RB, LRB, and HDR individually, the design of the bearings for the Case-1 is tried out. The maximum shape of the bearings for each type is almost in the same size. For example the width of the bearings in the 11-span bridge is about 1,600mm and the total thickness of the rubber is about 190mm. The horizontal displacement at the end of the bridge due to the temperature changes of + or - 35°C is about 190mm. The displacement is only 250mm even due to the earthquake. The aimed period of

the natural frequency in the bridge design is about 2 seconds in order to avoid resonance with the ground.
The same type of analysis as for the Case-1 is also carried out for the Case-2. The maximum width of the bearings in the 21-span bridge becomes only 50mm wider than the one in the 11-span bridge of Case-1. But the thickness is increased by 70%. In general, the size of the bearings depends on the magnitude of the bearing stress whose allowance is specified to be less than 80kgf/cm2 in "The guide line of the bearings in Japan". The thickness is determined from two considerations. One is the shear strain which is specified to be less than 70% in the normal condition and less than 150% in the earthquake. The other is the ratio of the deformation due to the rotation by the deflection and the one due to the compression by the vertical reaction. The ratio is specified to be less than 1.0, namely in any case tensile strain in the rubber never occurs by the rotation which is caused by the deflection.
The horizontal displacement at the bridge end is quite large. It becomes up to 370mm by the temperature changes. However, the displacement in the earthquake is less than that value. The natural frequency varies from 2.01s to 2.58s depending on the type of the bearings. This is the result from the differences of the thickness and the number of the layers consisted of the rubber sheets or steel plates.
Only the RB is applied in the design for the Case-3. The required maximum width is 1,900mm and the thickness is 631mm. Since such size exceeds the capacity of the production, the Case-3 is not realistic

The obtained results at each pier of the 11-span bridge using HDR are tabulated in table 6. The end piers, P13 and P24 are assumed to be movable. Since the horizontal displacement due to the temperature changes is larger in the neighbours of the end span than in the ones of the center span, the size of the bearings near the end span becomes larger than the one near the center span. In the static analysis the displacement due to the earthquake occurs uniformly at every pier. Therefore, the critical design values for the bearings near the end span are determined by the shearing strain in the normal condition. On the other hand, the values near the center span are determined by the shearing strain in the earthquake. The magnitude of the bearing stress and the ratio of the rotation and the compression are almost equal to the specified allowable values.
From the above investigation the followings are derived as the results. The 30-span bridge in the Case-3 is not realistic. The 21-span bridge in the Case-2 is technically possible but the detailed checks for the expansion joints, bearings, and etc. are necessary. On the other hand, the 11-span bridge in the Case-1 can be sufficiently put into the practice by the application of the existing technics.

7. Dynamic Analysis

The bridges are also checked by dynamic analyses with two kinds of earthquake magnitude. It would be irrational if structures are designed to resist the huge earthquakes with rare possibility and the medium size earthquakes by the same design philosophy. Two design earthquake levels (L1 and L2) have been therefore adopted for seismic design. L1 earthquakes would occur at least once during the design life of 100 years, while L2 earthquakes would be the largest one which have occurred and will occur at the Tokyo Bay in the future. Structures should not suffer heavy damages nor disturb the traffic in the highway by the L1 earthquake waves. On the other hand, structures might be allowed to have some damages but must not collapse and sustain ultimate strength by the L2 earthquake waves. Fig. 12 shows design acceleration response spectrum of L1 and L2 with damping ratio h of 5%. It should be reminded that these spectra are used as input forces on the base stratum, therefore they may be amplified through soil layers until waves reach the structures.

8. Conclusions

TTB adopted multi-span continuous bridges aiming to improve both the seismic resistance by sharing seismic horizontal forces with many piers and road surface smoothness by eliminating expansion joints.
Ultra-long 10-span continuous bridge whose length is 1,630m is planed for the navigation area. The flexibility of the piers produced by the steel material and the tall height enabled the realization of the continuous bridge. The most appropriate combination of the support conditions have been selected in order to obtain the balanced and economical structure.
Three continuous bridges whose length are 910m, 800m, and 714m respectively are planed for the shallow water area. The piers have high rigidity because they are all made of concrete and the height is low. The rubber bearings enabled to realize the continuity in this case.

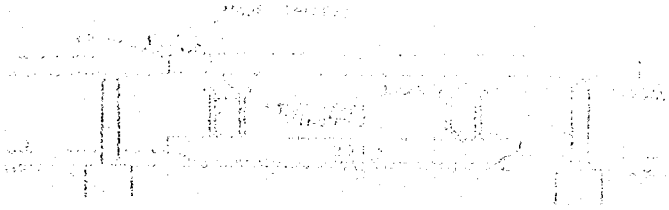

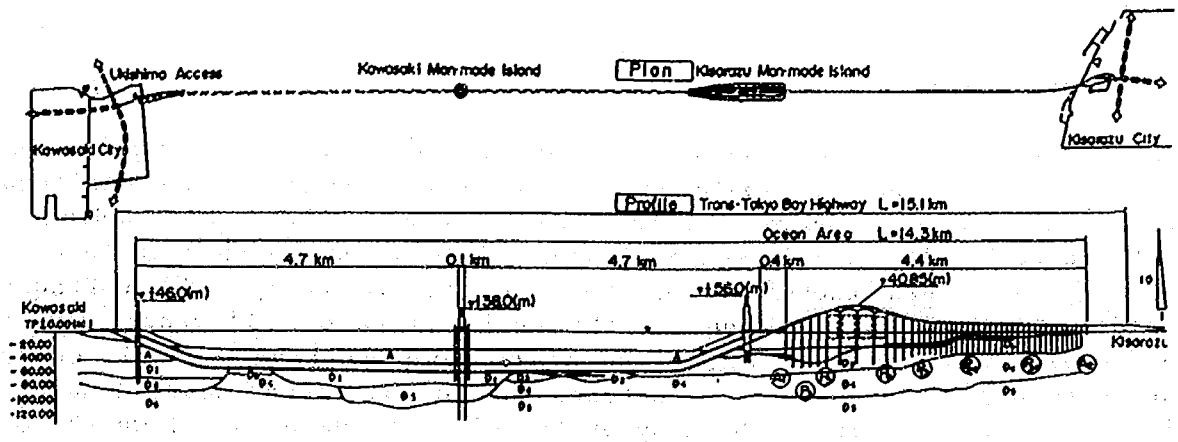

Fig. 1 Trans - Tokyo Bay Highway

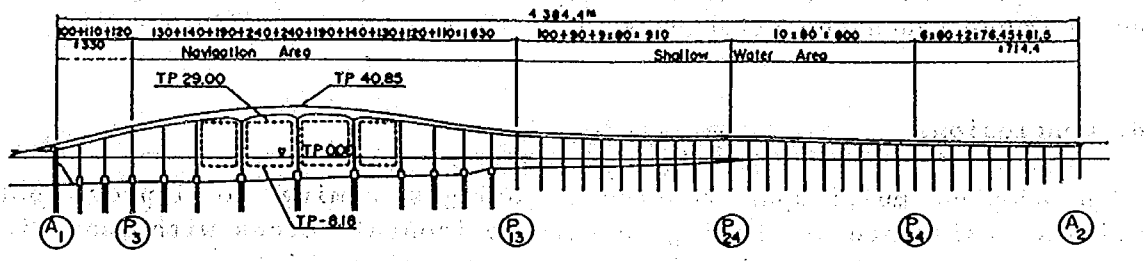

Fig. 2 Layout of the Bridge

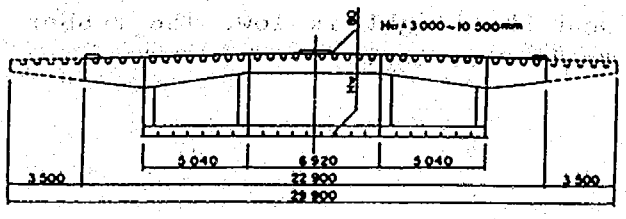

Fig. 3 Bridge Cross Section

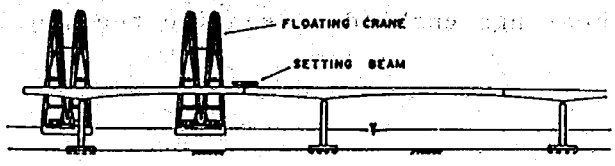

Fig. 4 Erection of Super-Structures (Navigation Area)

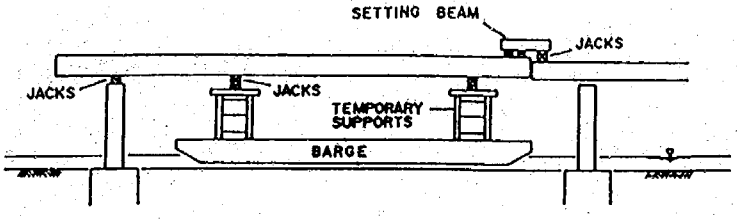

Fig. 5 Erection of Super-Structures (Shallow Water Area)

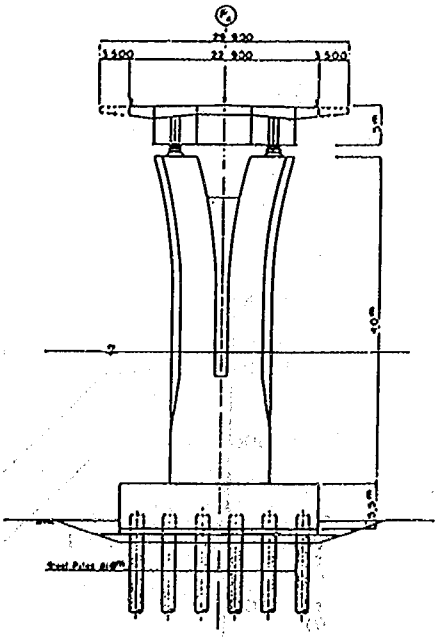

Fig 6 Composite Steel Pier

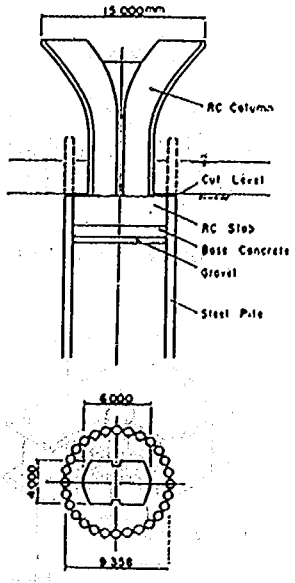

Fig. 7 Steel Pile Well Foundation

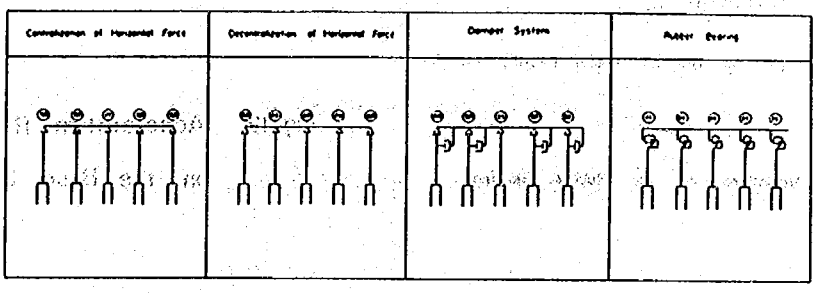

Fig 8 Method of the Multi-span Continuous Bridge

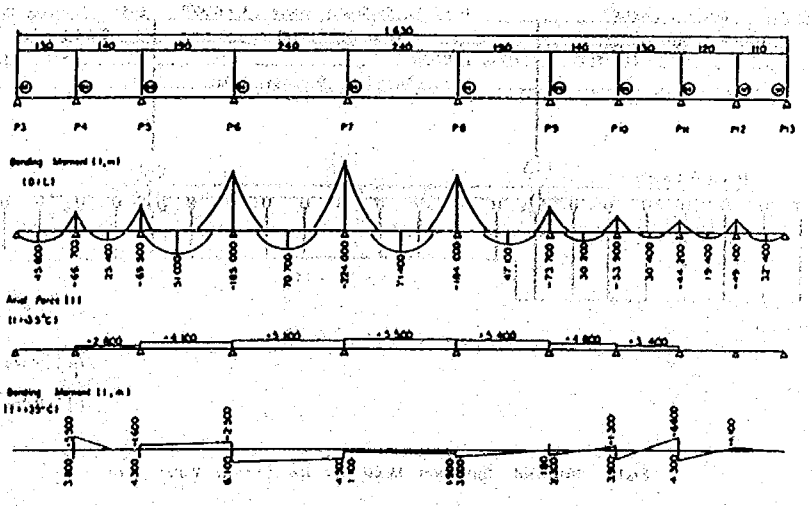

Fig 9 Sectional Forces of the Continuous Bridge for Navigation Area

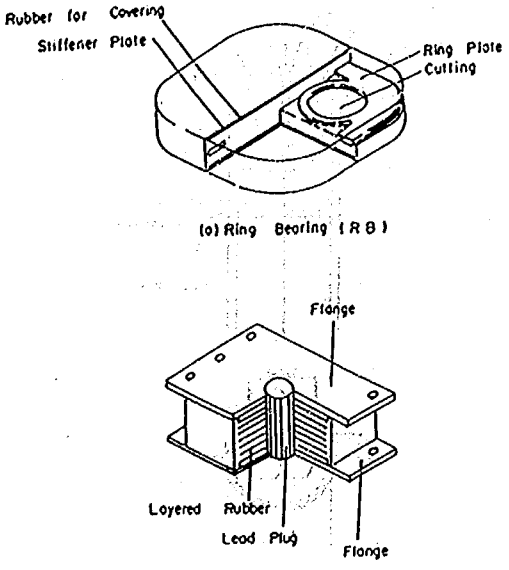

Fig. 10 Variations of the Rubber Bearing

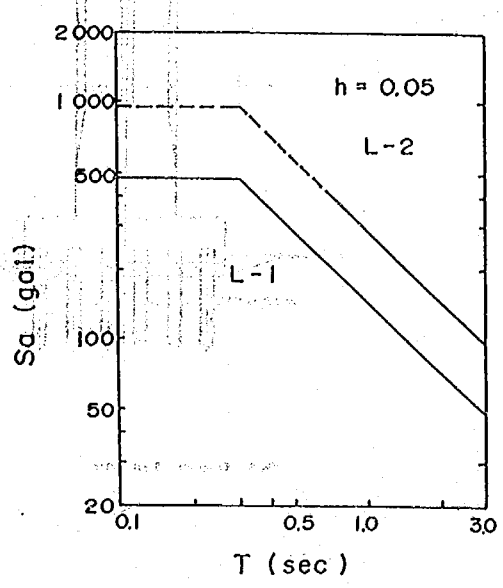

Fig. 12 Acceleration Response Spectra on the Base Stratum.

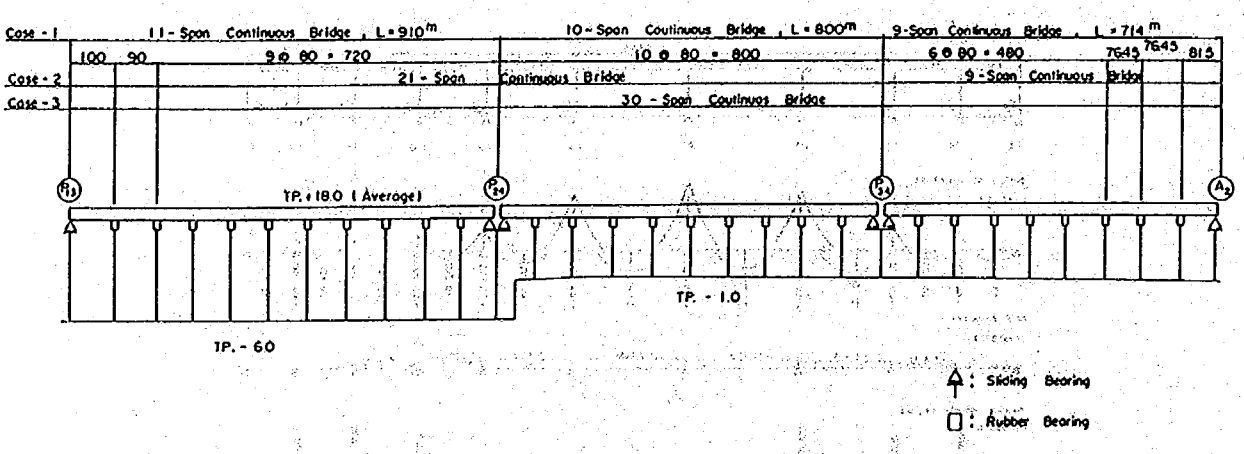

Fig. 11 Simplified Structural Model for the Shallow Water Area

Toble.1 Comporison of the Support Conditions for the Navigation Area

Ⓐ Original Design
Ⓑ 7 - Hinge
Ⓒ 8 - Hinge
Ⓓ 9 - Hinge

① Pile Arrangement
② Support Condition
③ Number of Piles
④ Total Piles

		P3	P4	P5	P6	P7	P8	P9	P10	P11	P12	P13	④
Ⓐ	①		24.0 / 30.0	28.0 / 22.0	32.0 / 32.0	28.0 / 32.0	32.0 / 32.0	28.0 / 22.0	20.0 / 24.0	20.0 / 24.0	24.0 / 28.0		398
	②	M	H	M,M	H	H	H	M,M	H	H	H	M	
	③	—	42	35	64	66	64	35	30	30	42	—	
Ⓑ	①		28.0 / 28.0	24.0 / 28.0	28.0 / 28.0	28.0 / 28.0	28.0 / 28.0	24.0 / 28.0	28.0 / 28.0	20.0 / 20.0	20.0 / 20.0		379
	②	M	H	H	H	H	H	H	H	M	M	M	
	③	—	49	42	49	49	49	42	49	25	25	—	
Ⓒ	①		24.0 / 28.0	24.0 / 24.0	28.0 / 28.0	28.0 / 28.0	28.0 / 28.0	24.0 / 24.0	24.0 / 24.0	24.0 / 28.0	20.0 / 20.0		364
	②	M	H	H	H	H	H	H	H	H	M	M	
	③	—	42	36	49	49	49	36	36	42	25	—	
Ⓓ	①		28.0 / 28.0	24.0 / 24.0	28.0 / 28.0	28.0 / 28.0	28.0 / 28.0	24.0 / 24.0	24.0 / 24.0	24.0 / 24.0	28.0 / 32.0		396
	②	M	H	H	H	H	H	H	H	H	H	M	
	③	—	49	36	49	49	49	36	36	36	56	—	

Table 2 Live Load Deflection

Unit : cm

	$P_4 \sim P_5$	$P_5 \sim P_6$	$P_6 \sim P_7$	$P_7 \sim P_8$	$P_8 \sim P_9$	$P_9 \sim P_{10}$	$P_{10} \sim P_{11}$	$P_{11} \sim P_{12}$	$P_{12} \sim P_{13}$
δ	169	155	275	406	407	275	158	140	139	188
δ_a	266	280	380	480	480	386	280	250	240	220
δ/l	1/770	1/900	1/690	1/590	1/590	1/690	1/890	1/830	1/810	1/650

δ : Live Load Def. $\quad \delta_a$: Allowable Def. $\quad l$: Span

Table 3 Horizontal Displacement

Unit : cm

	P_{11}	
	P_{12} Side	P_{13} Side
Temperature	±230	±200
	±430	
Earthquake	160	190

Table 4 Support Reaction

Unit : ton

Pier		P_4	P_5	P_6	P_7	P_8	P_9	P_{10}	P_{11}	P_{12}	P_{13}
Support Condition		Bar	R	R	R	R	R	R	R	Bar	Bar
Vertical Reaction	Rd	650	2020	2810	3440	3390	3420	2090	1770	1530	1720	540
	R1+I	380	760	820	1090	1140	1090	830	740	700	680	350
	Rt	1030	2780	2830	4530	4630	4510	2920	2510	2230	2400	890
Horizontal Reaction along Bridge Axis	Rhe	—	950	720	750	630	830	670	1040	1760	—	—
	Rht	—	1390	920	750	390	340	380	830	1840	—	—

Rd : Dead Load Reaction
Rt : Rd+R1+I
Rht : Horizontal Reaction due to Temperature
R1+I : Live Load Reaction with Impact
Rhe : Horizontal Reaction due to Earthquake

Table 5 Design of the Rubber Bearings for the Shallow Water Area

			Case-1									Case-2						Case-3
			HDR			LRB			RB			HDR		LRB		RB		RB
Continuous Span			11	10	9	11	10	9	11	10	9	21	9	21	9	21	9	30
Size of the Bearing Width × Length × Thickness of the Rubber	Maximum Size	mm	1560	1470	1470	1800	1500	1450	1550	1450	1450	1650	1470	1650	1450	1650	1450	1900
			×	×	×	×	×	×	×	×	×	×	×	×	×	×	×	×
			1560	1470	1470	1800	1500	1450	1550	1450	1450	1650	1470	1650	1450	1650	1450	1900
			×	×	×	×	×	×	×	×	×	×	×	×	×	×	×	×
			195	190	188	240	252	203	234	200	200	420	188	435	203	424	200	631
	Minimum Size	mm	1300	1300	1300	1400	1400	1400	1350	1350	1350	1370	1300	1450	1400	1400	1350	1350
			×	×	×	×	×	×	×	×	×	×	×	×	×	×	×	×
			1470	1470	1470	1400	1400	1400	1350	1350	1350	1470	1470	1450	1400	1400	1350	1350
			×	×	×	×	×	×	×	×	×	×	×	×	×	×	×	×
			148	156	152	240	240	216	140	176	180	240	152	238	216	152	180	182
Maximum Horizontal Displacement	Normal Cond. (Bridge End)	mm	196	168	151	195	168	151	196	168	151	364	151	363	151	360	151	524
	Earthquake	mm	266	253	247	250	255	242	255	250	250	397	247	249	242	283	250	265
Period of Natural Frequency		sec	2.11	2.04	2.01	2.01	2.03	1.98	2.03	2.01	2.01	2.58	2.01	2.01	1.98	2.14	2.01	2.15

HDR : High Damping Rubber Bearing
LRB : Lead Rubber Bearing
RB : Ring Bearing

Table 6 Result of the Design of the Bearings (P_{13}～P_{24})

Item		Marks	Unit	P_{13}	P_{14}	P_{15}	P_{16}	P_{17}	P_{18}	P_{19}	P_{20}	P_{21}	P_{22}	P_{23}	P_{24}
Dimension	Outside Shape	$a_1 \times b_1$	mm		1560×1560	1300×1470	←	←	←	←	←	←	1300×1470	1470×1470	
	Effective Area	$a \times b$	"		1540×1540	1280×1450	←	←	←	←	←	←	1280×1450	1450×1450	
	Height*	H	"		312	259	←	←	←	←	←	←	259	307	
	Rubber Thickness	Σte	"		39×5=195	37×4=148	←	←	←	←	←	←	37×4=148	38×5=190	
Horizontal Shear Spring (Earthquake)	①**	Ks	tf/cm		20.60	21.31	←	←	←	←	←	←	21.31	18.71	
	②	Kp	"		105	←	←	←	←	←	←	←	←	105	
	③	Kn	"		17.28	17.71	←	←	←	←	←	←	17.71	15.88	
Girder Displacement	Normal	Δl	mm	195.5	153.5	115.7	82.1	48.5	14.9	-18.7	-52.3	-85.9	-119.5	-153.1	-186.7
	Earthquake	Δl e	"	265.7	←	←	←	←	←	←	←	←	←	←	265.7
Support Displacement	Normal	ΔS	"		122.9	91.9	62.0	34.0	9.5	12.1	37.1	65.4	95.4	125.5	
	Earthquake	ΔSe	"		222.0	220.9	←	←	←	←	←	←	220.9	225.5	
④	⑤	σ	kgf/cm²		77.47	116.2	72.6	72.6	71.3	70.5	70.9	74.7	116.2	115.5	
	Shearing Strain Normal	γh	—		0.630	0.691	0.419	0.230	0.064	0.082	0.251	0.442	0.845	0.860	
	Earthquake	γeh	—		1.138	1.492							1.492	1.187	
	⑥/⑦	$\delta / \delta y$	—		0.980	0.982	0.958	0.958				0.958	0.983	0.991	
⑧	Normal	Rh	tf		321	249	210	152	56	69	160	216	253	290	
	Earthquake	Reh	tf		459	471	←	←	←	←	←	←	471	422	

* Including Flange Thickness
** Per 2 Bearings
① Bearing**
⑤ Bearing Stress (Normal)
Critical Values
② Sub-structure
⑥ Rotation due to Deflection
③ Combined
⑦ Deformation due to Compression
④ Design Value
⑧ Decentralized Horizontal Force

(11) Session 11

SESSION 11: BRIDGE MAINTENANCE 3:25pm～4:25pm
(Co-Chairmen: M. Fujiwara, J. Mander)

(30) C. H. McGogeney and J. D. Cooper* : Magnetic Perturbation for Cable Inspection of Suspension Bridges
(3:25pm～3:40pm)

(31) T. Shiozaki and K. Takizawa* : Maintenance and Repair of Bridges in Tokyo
(3:40pm～3:55pm)

(32) G. L. Hoffman: Emphasis Areas in PennDOT'S Bridge Inspection and Repair Program
(3:55pm～4:10pm)

DISCUSSION
(4:10pm～4:25pm)

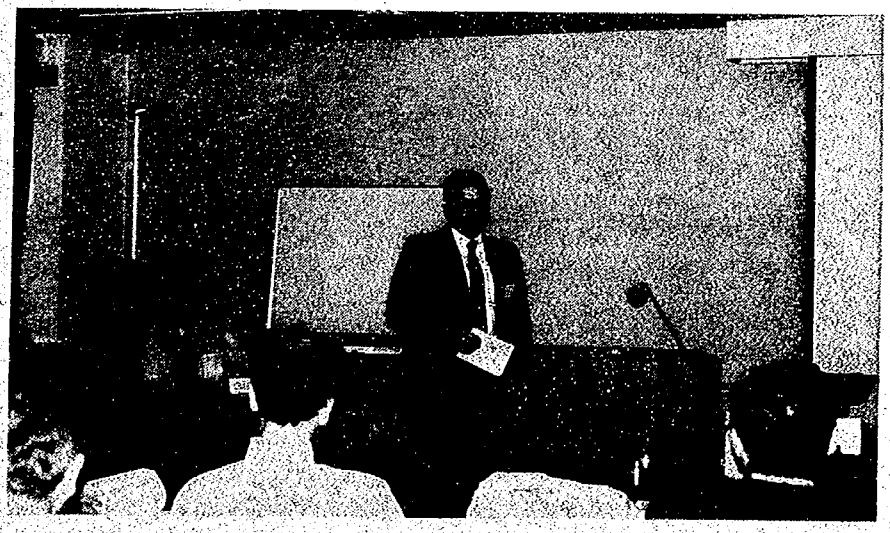

MAGNETIC PERTURBATION FOR CABLE INSPECTION OF SUSPENSION BRIDGES

Charles H. McGogney, P. E.*
James D. Cooper, P. E.**

INTRODUCTION

Of the many problems that exist among the nation's highway bridges, one of particular concern is the inspection and maintenance of main and suspender cables of suspension bridges. In a sincere effort to protect the steel elements comprising main cables and suspenders against adverse environmental conditions, bridge engineers and designers have developed unique protective systems. However, deterioration of the steel wires and rods does occur mainly due to fatigue and/or corrosion and this creates a high potential for structural collapse. This is an unacceptable risk in this time of advanced nondestructive inspection technology.

BACKGROUND

The Federal Highway Administration (FHWA) has recognized this problem and the need for a nondestructive inspection system that will provide the bridge inspector with a better tool to do routine cable inspection. As far back as 1980, FHWA sponsored research to develop a nondestructive inspection system to detect fractures and/or loss of section in the reinforcing steel of concrete beams. This development known as the Magnetic Field Disturbance (MFD) system proved successful in several field inspections and is now being considered for further development.[1,2]

In 1987 based on the experience gained with the MFD system and after a thorough search and evaluation of the most practical nondestructive inspection methods available, FHWA chose to pursue the magnetic flux leakage method for nondestructive inspection of main cables of suspension bridges.[3] The magnetic flux leakage technology is well known, however, for its field implementation, the applied magnetic field must be

*Mr. McGogney is Research Metallurgist, Structures Division, FHWA, Mclean, VA.
**Mr. Cooper is Deputy Chief, Structures Division, FHWA, McLean, VA.

carefully controlled and the signature characteristic understood. To help explain the theory, attention is drawn to figures 1a, b, and c. A spherical volume (flaw/defect) with a magnetic permeability μ' is embedded in a ferromagnetic material (steel) with a permeability μ and a magnetic field (H_o) applied along the X direction as shown in figure 1a. Figure 1b shows the arrangement for magnetizing a cable when the electromagnet and sensor are scanned as a unit over the region containing a flaw resulting in a magnetic perturbation produced by the flaw. The magnetic field component in the Y direction (Hy) in figure 1b is sensed and a continuous plot produces the record or signature. Solution of the magnetic field equation produces very useful relationships. For example for the maximum peak-to-peak-amplitude,

$$Hy = \frac{KHa^3}{d^3}$$

where:

K = constant, $\approx$ 3/2 H_o applied magnetic field
H = applied magnetic field
a = flaw radius
d = depth from the scan path to the flaw center

Characteristic features that are useful in relating nondestructive evaluation data to flaw size, depth, location, etc., are listed in figure 1c.

LABORATORY EQUIPMENT

The rudimentary laboratory prototype known as the Magnetic Perturbation for Cables (MPC) inspection system weighs approximately 2800 pounds and is 17 feet long. It consists of an electromagnet, with 12 magnetic flux sensors connected in pairs to form six data channels that move as a unit along the cable under inspection. The output of the sensors is recorded and displayed to assess flaws in the steel elements. After several

modifications to the system, the working prototype MPC is an integrated electromechanical system that consists of 1) a magnetic sensor assembly attached to a moving electromagnet, 2) electrical and hydraulic motors and actuators, 3) an electronic control and data acquisition system directed by a remotely located host computer, and 4) a self-propelled frame housing for the inspection components, figure 2.

The system is designed to be placed directly upon a bridge cable and is capable of moving itself longitudinally and circumferentially about the cable at approximately 1-inch per second acquiring magnetic perturbation data, at precise 0.1-inch intervals, pertaining to the presence of corrosion damage, broken wires or rods, and other anomalies.

FIELD DEMONSTRATIONS

To date the MPC has been successfully tested on main cables of five highway suspension bridges.[3,4,5,6,7] Two of the bridges were of cable-stayed design, while the others were typical suspension bridges. A typical analog recording of data over approximately 17-feet (5.2m) of cable are shown in figure 3. These data were taken from the Pasco-Kennewick Bridge, over the Columbia River in the State of Washington on 6-inch (150mm) diameter stay-cables. The three reference signals are from 0.25-inch (6.35mm) long wires permanently embedded in a stainless steel half cylinder covering the region on channel 3 and are readily recognizable. These reference signals are repeated at specific intervals. Figure 4 is a computer reconstruction of figure 3 data after digital subtraction. The negative polarity signal which occurs at regular intervals of approximately 40-inches (100cm) is prominent on all channels and is attributed to the spiral wire wrap. There is a strong signal occurring at approximately 125-inches (312cm) location on track 2 which masks the signal from the helical wire wrap. This strong significant signal is due to a hose clamp with magnetic screw.

MPC LABORATORY TESTS

During the period of time the MPC field inspections were being performed, two, separate in time, laboratory tests on stay-cable specimens were performed at the University of Texas, Ferguson Structural Engineering Laboratory (FSEL), Austin, Texas. Each of these specimens was subject to fatigue loading and ultimate strength tests. Loud noises were heard during the static loading and the load dropped off indicating strand fractures.[8,9] Capitalizing on these opportunities to prove the MPC's capability to detect "actual" fractures in stay-cable construction, the MPC, on each of these two occasions, was transported to the FSEL. Each specimen is comprised of 55 0.60-inch (15.2mm) diameter seven wire strands, with an overall diameter of 7.62-inches (194mm) by 17-feet (5.2m) length. To accommodate this short length, the MPC was setup on bunkers and each specimen was placed under the scanning magnet/sensor head and rotated through 360 degrees. At each of 24 intervals essentially at 1.0-inch (25mm) increments, scans were made and readings taken. Results of the first test revealed that the MPC system detected fractures in single wires 0.2-inch (5.1mm) in diameter in the outer seven-wire strands.[10] In the second laboratory test on essentially the same type of specimen, the MPC detected an inner strand fracture (seven of seven wires that had failed)--thus proving the MPC system capability to detect both inner and outer wire/strand failures.[11]

CONCLUSIONS

The MPC system has proven to be a viable means of performing cursory scans of main cables of suspension bridges to detect and locate wire and rod fractures as well as other anomalies such as grout coverage and helical wire wrap and its lay length.

In laboratory tests of two stay-cable specimens, the MPC proved to be effective in detecting and locating wire and strand fractures after fatigue and tensile tests prior to excavation, thus verifying the fracture occurrence and expediting the investigation.

Based on the performance of the MPC under this broad investigation the following observations are concluded:

- The entire prototype MPC system, as configured, must be redesigned to reduce the overall weight and length resulting in a system more portable and easier to install on cables in the field.

- The capability of the system must be expanded to provide inspection of cable areas under clamps, hangers and anchorages.

- The data acquisition program can be improved by automated continuous scanning without operator intervention and provide data review during data acquisition.

- The correlation and other signal processing techniques must be explored in order to enhance signal detectability and interpretation.

REFERENCES

1. F. N. Kusenberger and J. R. Barton, "Detection of Flaws in Reinforcing Steel in Prestressed Concrete Bridge Members." Report FHWA/RD-81/087, FHWA U.S. Department of Transportation, 1981.

2. F. N. Kusenberger and R. S. Birkelbach, "Detection of Flaws in Reinforcing Steel in Concrete Bridge Members," Report FHWA/RD-83/081, FHWA U.S. Department of Transportation, 1983.

3. John R. Barton, Cecil M. Teller, and Sidney A. Suhler, "Design, Develop and Fabricate a Prototype Nondestructive Inspection and Monitoring System for Structural Cables and Strands of Suspension Bridges," Vol. 1: Final Report. Report No. FHWA/RD-89-158 (May, 1989).

4. Cecil M. Teller, Sidney A. Suhler and George A. Matzkanin, "Nondestructive Inspection of Stay-Cables on the Pasco-Kennewick Bridge," TRI Report 89310:CMT, February 20, 1990.

5. Cecil M. Teller and George A. Matzkanin, "Nondestructive Inspection of the Waldo-Hancock Suspension Bridge Cables Using the MPC System," TRI Report 90326-D69, October 1990.

6. Cecil M. Teller and George A. Matzkanin, "Nondestructive Inspection of the Wurtz Street Suspension Bridge Cables Using the MPC System," TRI Report 90327-D69, October 1990.

7. Cecil M. Teller and George A. Matzkanin, "Nondestructive Inspection of the Ft. Steuben Suspension Bridge Cables Using the MPC System," TRI Report 90328-D69, October 1990.

8. William R. Burkett and Karl H. Frank, "Fatigue and Static Tests of 55-Strand Stay-Cable Specimen for the Baytown Bridge," Phil M. Ferguson Structural Engineering Laboratory, The University of Texas at Austin, August 1989.

9. Karl H. Frank, "Fatigue Test of Second 55-Strand Stay-Cable Specimen for the Baytown Bridge," Phil M. Ferguson Structural Engineering Laboratory, The University of Texas at Austin, March 1990.

10. Cecil M. Teller, Sidney A. Suhler and George A. Matzkanin, "Nondestructive Inspection of Fatigue Damage in a Stay-Cable Specimen Using the MPC System," TRI Report 89296:CMT, November 7, 1989.

11. Cecil M. Teller, Sidney A. Suhler and George A. Matzkanin, "Nondestructive Inspection of Fatigue Damage in Second Stay-Cable Specimen Using the MPC System," TRI Report 90323F:CMT-D64,October 10, 1990.

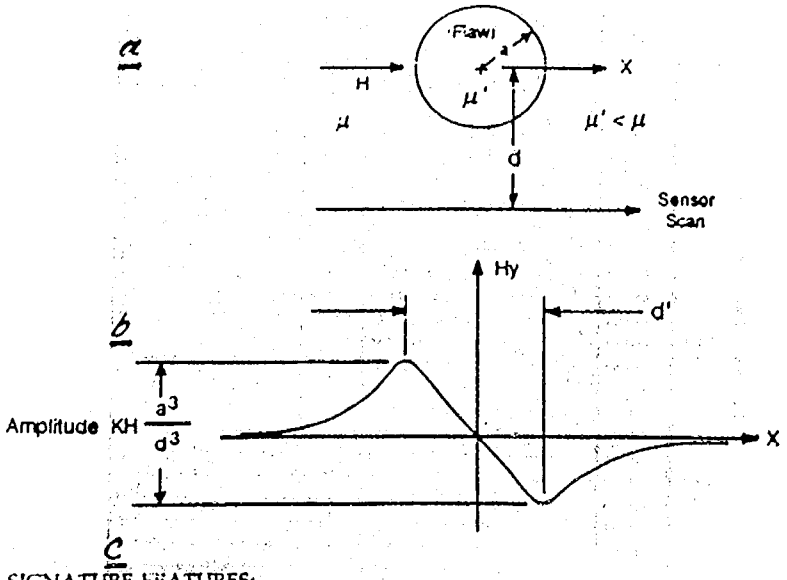

SIGNATURE FEATURES:

1. Bipolar and symmetric
2. Polarity as shown for fracture gap or corrosion pit; polarity reversed for soft spot in steel of "ferrule" splice
3. Peak separation d' equals depth to flaw d (independent of size)
4. Amplitude indicates flaw volume (dependent on depth)
5. Maximum amplitude obtained when scan path is directly over flaw
6. Amplitude decreases with flaw depth d (decrease: $1/d^3$)
7. Signal amplitude increases continuously as the magnetic field (H) is increased

Figure 1. Sketch of Spherical Void or Hole in an Infinite Magnetized Ferromagnetic Matrix and the Resulting Magnetic Field Perturbation in the Y Direction

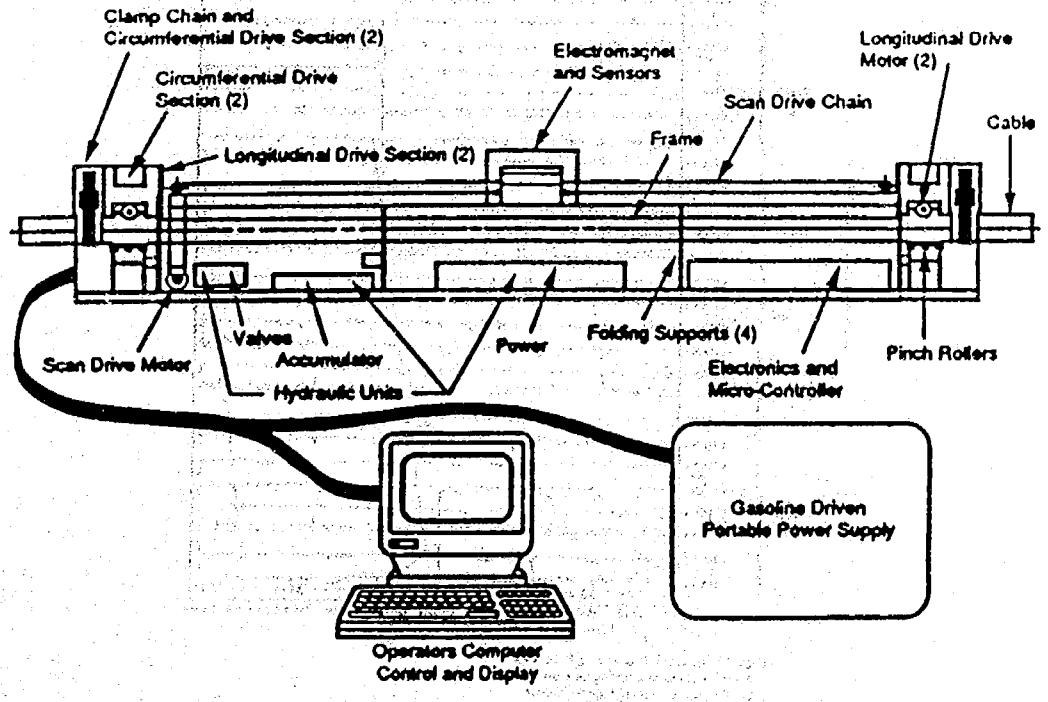

Figure 2. Schematic illustration of mechanical system.

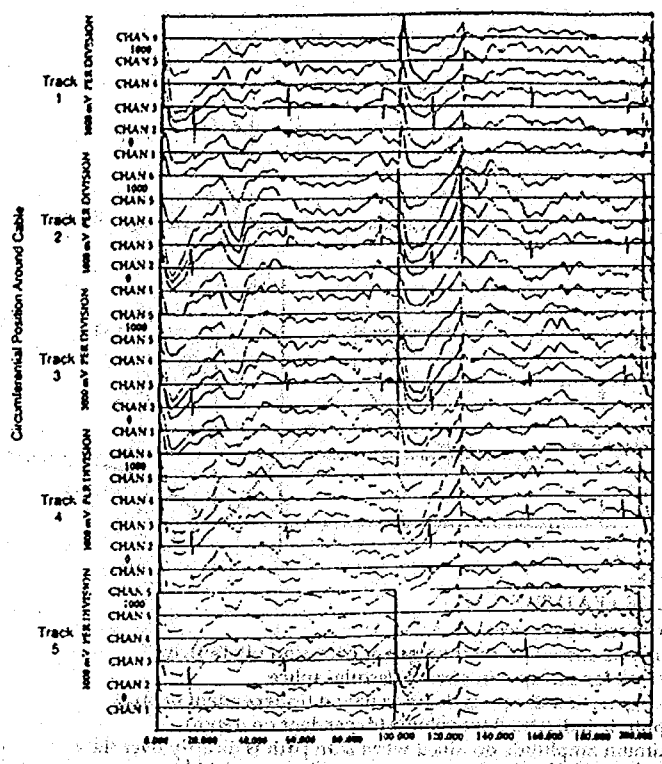

Figure 3.—Unprocessed magnetic signals observed from cable #3-N-18 on the Pasco-Kennewick Bridge.

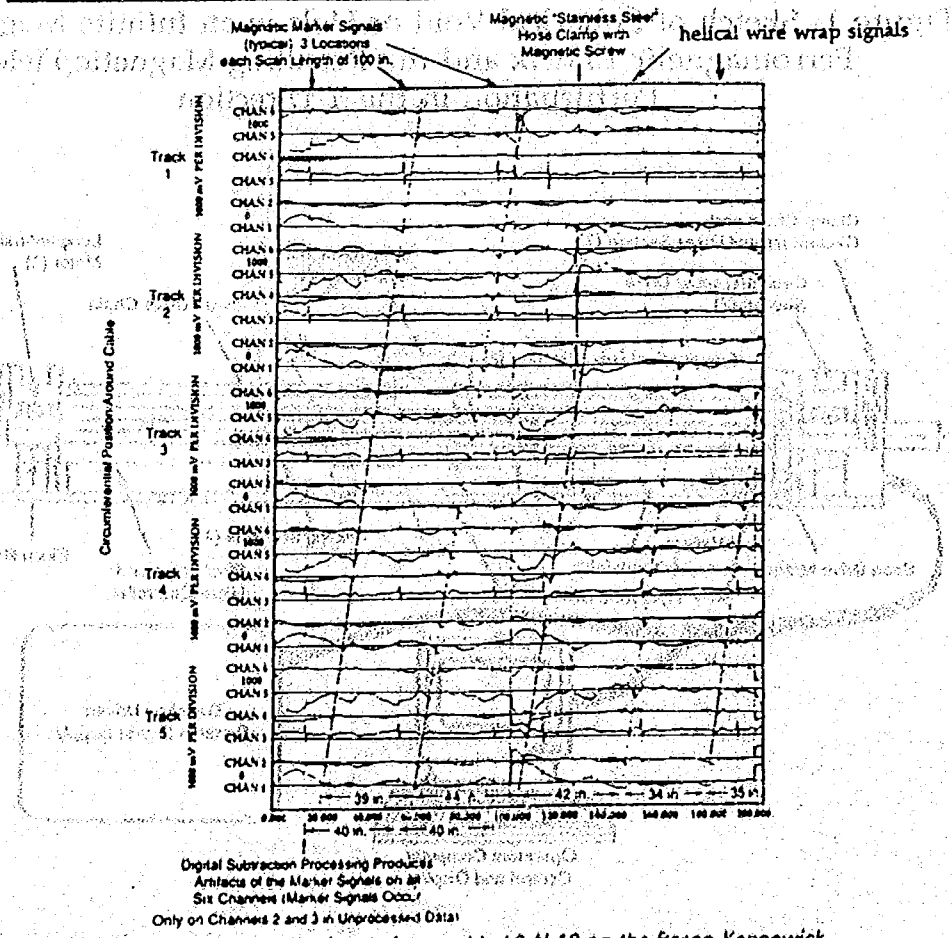

Figure 4.—Processed magnetic signals from cable #3-N-18 on the Pasco-Kennewick Bridge.

MAINTENANCE AND REPAIR OF BRIDGES IN TOKYO

Takeyoshi SHIOZAKI

Director
Division of Road and Street Administration
Bureau of Construction
Tokyo Metropolitan Government

Kazuo TAKIZAWA

Chief
Division of Road and street Administration
Bureau of Construction
Tokyo Metropolitan Government

1. Introduction

Tokyo is a big city of which population is approximately 12 million. It plays central role in all phases such as politics, economics and culture as a nucleus of Tokyo Metropolitan area.

Index of centralization in Tokyo is indicated. Its population is about 10% of all over Japan, about 56% of big companies in number, about 7% of cars, about 21% of universities and colleges are centralized in Tokyo. From these numbers, you see how things are centralized in Tokyo.

In Tokyo, such a big city, roads and bridges are very important as basic urban facilities to daily living of people in Tokyo.

There are rivers of which width is over 100 meter such as Tamagawa-river, Sumidagawa-river, Arakawa-river and Edogawa-river and bridges are constructed to connect each regions. Several roads are concentrated at those bridges, and some bridges always have traffic jams. Load given to the bridges has been increasing due to increase of automobiles' weight. And, there are still many old bridges. Bridges in Tokyo are used under very severe condition, and now maintenance is very important. So, we report current condition of bridges in Tokyo, inspection system, method of maintenance and repair, and preservation project of bridges' view.

2. Condition means of Bridges Managed by Tokyo

T.M.G(means Tokyo Metropolitan Government) manages about 1,200 bridges at present and total length is approximately 58 kilometer. The bridges are classified as Figure 1 according to year of erection. From the graph, we can see that year of erection is briefly devided in 3 peaks.

The first peak was from 1927 to 1936 when many bridges were constructed by reconstruction work after the big earthquake in 1923 which burned most of the bridges and caused destructive damages. Therefore, those bridges constructed during this time have past about 60 years after construction.

The second peak was brought by reconstruction work since 1945 after Warld War II. Reconstruction had been started from a wide stretch of burnt ruins, and many bridges were constructed.

The third peak was during the high economic growth period around the Tokyo Olympic Games in 1964 as a momentum. Bridges constructed in that period have economic and functional construction, but on the other hand,

due to development of welding technology and use of high strength steel, many swing bridges and light bridges were constructed.

Taking a bridge which is 13 meter wide and with 4 lanes as an example, as shown in Table-1, traffic volume from 9:00 to 21:00 is about 60,000, and we can see how the bridge is used under very severe condition. Besides that, number of super-heavy vehicles such as trailer is increasing and that accelerates lowering of strength by fatigue and damages of bridges. So, we must say inspection and maintenance of bridges are now very important.

As Tokyo has earthquakes often and is highly developed, and has low lands with poor ground, bridge falling prevention systems are installed in order to prevent falling of bridges. Moreover, inspection and study of new antiearthquake measures are promoted.

3. Maintenance Technology

3.1 Inspection System of Briges

Maintenance of bridges starts from inspection to obtain result of it. And, part of these works is systematized using artificial intelligence.

(1) Inspection of bridges

a. Purpose of inspection

Transition of load designed by Bureau of Construction in T.M.G is as Table-2. But, bridges are actually used under severer condition than they have been designed at the time of erection due to weight increase of vehicles and heavy traffics etc. Under these conditions, bridges in Tokyo have the following subjects.

- Early discovery of abnormality or damages, and proper treatment
- Security of good condition by removal and prevention of causes for damages
- Security of smooth and safety traffic
- Prevention of injuries to the third parties
- Incorrect use of bridges (Inspection of illegal occupancy and control)

To handle the above subjects, we are trying to grasp correcter condition of bridges by daily checks, regular checks and checks for abnormality, and we give proper maintenance if they need it.

(i) Daily checks

Engineers are given to all bridges everyday by their eyes while patrolling roads.

(ii) Regular checks

Engineers are given to all bridges every 5 years, cars and boat are used to check scaffolds and bridges.

(iii) Checks for abnormality

In case of disaster due to an earthquake, typhoon or localized torrential downpour, or to bridges which might be affected, they are given in the same manner as regular checks.

b. Flow chart of inspection

Flow chart of inspection is indicated in Figure 2.

(i) Detail inspection

For abnormality or condition change of bridges, inspection tools are used to check degree of damage and its range to grasp cause of damage and evaluate durability and safety of bridges.

(ii) Displacement observation

In case it is needed to grasp condition of damages, this inspection is given continuously to a certain bridge materials by eyes and simple inspection tools.

c. Judgement of inspection

Standard of inspection is given in Table-3 according to kinds of inspection.

Judgement by regular inspections is a base of bridge project of T.M.G. Each judgement is for entire constructions. If it become E rank, engineers must do something treatment immediately and much attention is paied for judgement.

(2) General soundness judgement expression

Inspection result according to each structural member is converted to points to calculate durability of a bridge. Load resistance is also calculated by data of traffic volume and design live load. Soundness is judged by substituting these to the general soundness judgement expression (Figure 3), and is indicated on a display. (Figure 4) From A to E is according to Table-3.

(3) Inspection of earthquake-proof

Damages caused by earthquakes spoils function as a road and lots of time and labor are needed for reconstruction. So, its influence is serious. So, inspection of earthquake-proof for existing bridges is very important as a prevention method of earthquake disaster.

Earthquake-resistance inspections given by T.M.G were '79 inspection given in 1979 and '86 inspection given in 1986.

'79 inspection (Table-4)

(i) Change condition of shoe part of superstructure and whether there is bridge-falling prevention equipment

(ii) Inspection of thickness of saturated sandy soil of ground and bearing power

(iii) Strength of bridge pier body, bearing power of foundation piles, and earthquake-resistance of foundation form.

(iv) Grasp of change condition of substructure

'86 inspection (Table-5)

(i) Earthquake-resistance according to superstructure and whether there is bridge-falling prevention equipment or not

(ii) Earthquake-resistance according to substructure and whethere there is liquefaction of a ground

(iii) Inspection of durability of reinforced concrete bridge piers to keep a bridge against horizontal power in case of an earthquake

(iv) Change condition of substructure part and grasp of its strength

From the results of 2 inspections, we do not think that damage such as bridge-falling occurs for installation of bridge-falling prevention equipment and reconstruction of old bridges. However, it is required to promote repair and reinforcement project of main beam.

Earthquake which is the most concerned at present is a direct earthquake of which scale is smaller than the Great Earthquake of 1923 (September 1, magnitude 7.9), but damage at substructure is alarmed due to liquefaction of ground. Therefore, T.M.G has started inspection of antiearthquake measures for bridges from 1990 which is planned to be continued for 3 to 5 years (Table-6 Schedule of antiearthquake measures inspection for existing bridges) using the latest antiearthquake engineering.

(i) Collection of data such as examples of antiearthquake measures
(ii) Pigeonhole structural data and soil data, and make data base for each datum
(iii) Study of estimated earthquakes, magnitude of earthquakes and service level of bridges in case of earthquake
(iv) Study of antiearthquake procedure, antiearthquake reinforcement procedure and emergency measures

Expansion of urbanization is drastic in Tokyo, and social environment is also changing a lot to aging society. Once, an earthquake happens, damage to urban facilities will be very serious. It is important to secure safety of roads as a life-line of a city, and to secure safety of bridges is also necessary. Therefore, we are planning to continue inspection which has been done from 1990, and put measures into practice as soon as we can.

<Bridge control information system (EXPERT SYSTEM)>

About bridges controlled by T.M.G, daily inspection, periodical inspection and temporary inspection will be applied in accordance with various inspection manuals related to bridge maintenance and control. From the state of flaws and defects found by these inspections, the soundness ranking will be judged by this system, and the ranking will support selection of bridges which will require detail survey and dynamic observation.

Further, when detail survey is required as the result of judgement, possible causes are estimated from the inspection results and available data, and effective survey items will be set.

Then, depending on flaws and defects found by survey, and according to the type of structural materials and the state of damage, effective remedy measures will be selected by support from this system. (Figure-5,6)

3.2 Maintenance Project of Bridges

Maintenance of bridges is done to keep bridges in good condition at any times. Major maintenance work of bridges are "repainting", "pavement", "repair of expansion joint", "cleaning of drainage system" and "brief repair of bridge hand rail", etc.

Characteristics of bridge maintenance in Tokyo are as follows. There are many bridges and we have to secure good driving and safety for enormous amount of traffic. This time, we would describe present condition about "repainting" and "pavement" which are the core of maintenance of bridges.

(1) Repainting work

At present, about 60% of bridges which T.M.G controls are steel bridges. One of the main causes of aging of steel bridges is corrosion of steel material. Factors which generate corrosion are moisture in the air, sulfite gas ejected from factories, exhaust gas from vehicles and salt grains ($cacl_2$). According to exposure inspection, amount of corrosion in 10 years is from about 0.1 millimeter to 0.3 millimeter. Supposing that thickness of ordinary steel beam is from 9.0 millimeter to 10.0 millimeter, if the bridge is no coated in urban environment, 1/3 of a section of thickness is lost in 30 years. Even if repainting is done when rust is about 30%, 1/3 of section loss is generated in 60 years and serious influence is given to structure of the body. Also, repaining work with 30% of rust costs two times of the same work done at a stage when rust is 15%.

Therefore, we consider it is the most suitable to repaint for bridges every 8 years during that time rust generation ratio becomes smaller than

15% as an average repainting cycle of steel bridges in Tokyo, and it done accordingly.

For selection of paints for repainting, they are classified to 10 kinds considering old painting system and painting environment. As first, it is devided to general outer surface and special part, and each is classified to 4 kinds and 6 kinds. The details are as Table-7.

As a subject for future, we think it is needed to adopt new paints in order to keep color for long time, study coating concrete surfaces of concrete bridges or concrete materials not only steel bridges to prevent deterioration and to keep nice view.

(2) Pavement of bridge surface

Pavement of bridge surface is needed to secure good transmission of load of vehicles to slab, protection of slab and good driving.

Due to big volume of traffic and big vehicles, pavement has to be changed every 6 to 8 years at grade separation bridges of which pavement is severely damaged.

With reinforced concrete slab, most of the damage is caused by rain water percolated inside. So, we execute security of smooth driving and making of water-protection layer.

There are crack, difference in level, rut groove, pot hole etc. in damage of pavement. To secure good driving, depth of rut groove is to be 25 mm or less (Note 1, Standard of road construction design: Bureau of Construction T.M.G) according to standard. Volume of rut groove in a year is about 2.6 millimeter, and desirable repair cycle is thought as 10 years. Improved asphalt mixture is used for material of pavement, and thickness of pavement is 7 to 8 centimeter. Water-protection layer is installed when pavement is changed.

As a subject for future, it is necessary to develop method to judge condition of a road synthetically just as general roads instead of judging repair cycle not only by volume of rut groove.

(Note 1) Rut groove: It is a phenomenon that a part of asphalt pavement where vehicle pass becomes hollow and its both ends go up.

(Note 2) Improved asphalt: It is improved petroleum asphalt for pavement. There are asphalt with rubber in which improvement of durability is put stress and asphalt with resin for improved flow resistance.

3.3 Repair Project

For damage of change of condition discovered by inspection of a bridge, its position and scale are inspected in detail, cause is clarified, proper repair or reinforcement is given to secure safe traffic. Characters for method of repair and reinforcement are mentioned below.

(1) Reinforcement of slab

There are many cases that developing cracks are generated on a slab, this is because of big traffic volume, increase of vehicle's load, lack of main beam's rigidity, and lack of thickness of a slab and iron bar.

As cause can be judged by position and direction of cracks, detailed inspection is executed to select method for measures.

a. Adhesive work of steel plate

Steel plates are stuck under the slab which does not have enough reinforcing iron bars with resin (Figure-7) to prevent increase of cracks, deterioration of concrete and corrosion of reinforcing bars.

According to reinforcement position of steel plates, there are wide steel adhesive and narrow steel adhesive. There are (1) Pressure adhesive method and (2) Injection method. In general, injection method is mostly used.

b. Adding work of new sub beams

By installing stringers between existing main beams (Figure-8) and injecting resin to a gap between a slab, generating stress of concrete slab is reduced and prevent increase of cracks on a slab. After adhesion, tensile force is generated to a slab of stringer. Stringers are welded to existing cross beams in the field, but it is necessary to study workability and stress generated to stringer. It has effects in reducing load to existing main beams, and improving load-resistance of a slab. It is necessary to study balance of rigidity between newly equipped beams and existing beams and influence given to a slab in the stage of designing. This work is often done with adhesion of steel plates. As this work can be done under the beams, traffic restriction is not needed.

c. Renewal work of slab

For concrete slab which deterioration has become very serious, renewal is studied. It is necessary to observe that composition balance of the entire bridge does not become unstable for selection of method. It is also needed to adjust environment of the area and traffic handling in full when renewal of slab and its method are decided.

In general, I-shape steel grid slab, steel slab or precasting concrete slab are used.

(2) Prevention work of bridge-falling

As prevention method of bridge-falling due to an earthquake, to prevent falling of super structure from substructure, either (i) security of width of shoe seat, or (ii) installation of restriction device of shoe movement or (iii) connection of beams is executed.

(3) Change work of expansion joint

It is a work to change expansion joint which is damaged by big volume of traffic, increase of vehicle load and shock due to uneven road surface.

Work condition, structure of a bridge and traffic condition are considered for selection of expansion material.

(4) Reinforcement work of substructure

Reinforcement work of substructure is done to prevent displacement and deformation of substructure and to stop them to be worse. Foot protection work for prevention of scour on bridge piers and ground improvement work as a measure of displacement of abutment in poor ground area are generally executed. Method of work is decided after soil property where a bridge is erected and topography are studied in detail.

3.4 Reconstruction Work of Bridges

According to the result of soundness inspection, reconstruction work is done to obsolete bridges of which load resistance of main beam is not enough or seriously damage in substructure is too much to be repaired.

In management of bridges in Tokyo where has enormous and various traffic, it is a basic policy not to restrict traffic such as road close or weight restriction.

So, for reconstruction of obsolete bridges, the following methods are normally used.

(i) Work is done while the existing bridge is devided in bridge length direction.

(ii) Temporary bridge is equipped along the existing bridge, and work is done.

(iii) A new bridge is erected near the exisiting bridge.

Method (i) is applied to wide bridges which can bear traffic load even if it is devided in bridge axis direction. Temporary bridge for passing of people is equipped by bridge square or borrowing private land, and this bridge deals foot passengers and attachments of the existing bridge such as gas pipes, electric and telephone wires. Then, sidewalk of the existing bridge is reinforced to make it a roadway in order to secure width of a roadway. While traffic of vehicle is dealt, section of a bridge is devided into 2 or 3 depending on condition of each bridge to execute construction work of the new bridge. This time, bridge square is very useful for installation of temporary bridge for pedestrian or as workings.

The picture 1 shows a bridge under renewal by deviding works.

Method of (ii) let vehicles and pedestrians go through a temporary brdige. Attachment of the existing bridge also are dealt by the temporary bridge. This method is applied to through type bridges or ones with small width or of which devision is difficult according to structure. This method is difficult to be used either unless enough bridge square in which a temporary bridge can be installed or land can be borrowed.

The picture 2 shows the installation of a temporary bridge.

Method (iii) is applied in case by-pass road is constructed and an exisisting bridge goes out of use. It is hardly used in urban area where many houses are there, and is used in the suburbs or in mountain areas often.

4. Improvement Project of Famous Bridges

There are about 7,600 bridges in Tokyo which are managed by national government, T.M.G. and municipal governments, and there are many bridges with historic value, characteristic bridges in structure and bridges with nice views including bridges on Sumidagawa-river which is a friendly river of the Seine in Paris among those bridges.

It is very difficult for those bridges to keep their superior view by damages due to aging.

T.M.G. considers view of the city not only economics and function for repair and reinforcement of bridges. And, improvement project of well-known bridges is executed in order to make 'bridges' a symbol of the area and to reproduce attractive and beautiful bridges.

Bridges which are well-known in history or view, and are worth notice from a view point of technology are called famous bridges with our wish to see a city well and rediscover bridges.

To realize the above, improvement is done with the following 3 basic policies.

(i) Take good consideration about relation between bridges and history or culture of the area, and reproduce and improve bridges as precious gifts from predecessors to offspring.

(ii) With bridges which have value in histrical technology of civil engineering and beautiful bridges, they are reproduced and improved based on concept of design which has been carried.

(iii) Bridges are improved to make them more attractive in urbun view or natural surrounding environment, accepted and pleased by many people.

Among approximately 1,200 bridges which T.M.G. manages, 110 of "Famous bridges in Tokyo" are selected, and they are improved on repair or reinforcement of those bridges according to the plan.

5. Conclusion

Overcrowding in Tokyo which is one of the largest cities in the world does not seem to stop, improvement of urban facilities is behind. Especially, increase of vehicle traffic is drastic, and congestion of roads is the order of the day.

For management of bridges, we have a basic principle to execute inspection, maintenance and repair work, reconstruction work without doing traffic restriction.

So, we are trying to develop scientific inspection system to give preventive management and construction method with which we do not have to stop traffic.

However, they are still in trial and there are parts which are not clearly established. And, they are our subjects for future.

We think it is needed to promote bridge structures which can be easily managed, and to get enough budget for management of existing bridges and also to develop scientific technology for management.

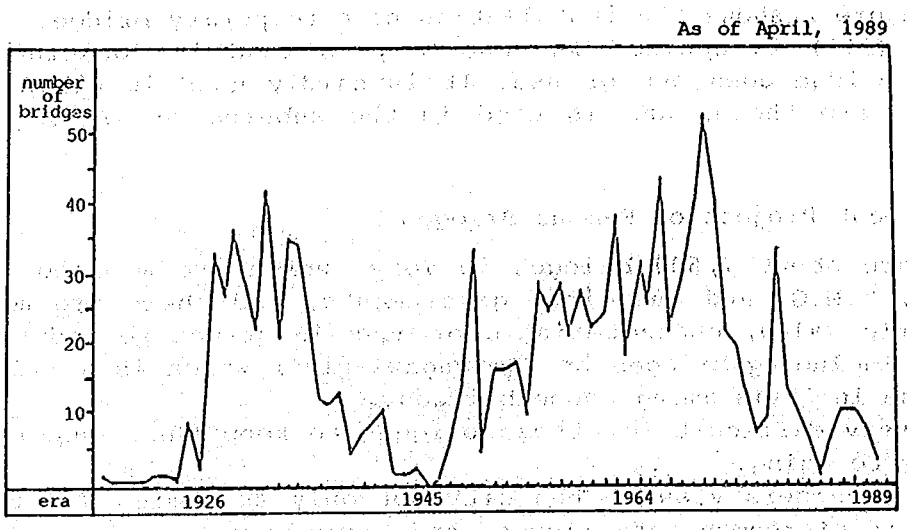

Figure-1 Number of bridges by the year of erection

Table-1 Traffic volume according to kind of vehicles

November 20th, 1987 A.M. 9:00 to P.M. 9:00

Direction	Up direction			Down direction			Total
Kind of vehicle / Name of point	Big vehicles	Ordinary vehicles	Subtotal	Big vehicles	Ordinary vehicles	Subtotal	
Komone in No. 7 Ring Road	6,799	23,725	30,524	6,802	22,522	29,324	59,848

Table-2 Changes of Design Live Load

	Design Live Load	
August 1886 Structural standards for National Highway and Prefectural Road	National Highway and Prefectural Road Uniform load 454 kg/m^3	
December 1919 Road Standards and Street standards	Street National Highway Prefectural Road	11.250 kg 7.875 kg 6.375 kg
June 1926 Detailed Regulation proposed on Road standards	Street National Highway Prefectural Road	First Class Bridge 12t Second Class Bridge 8t Third Class Bridge 6t
February 1939 Proposed Design Specification for Steel Road standards	National Highway Prefectural Road	First Class Bridge 13t Second Class Bridge 9t
May 1956 Design Specification for Steel Road Bridges standards	First and Second Class National Highway Principal Prefectural Road Prefectural Road Municipal Road	First Class Bridge 20t Second Class Bridge 14t
March 1972 Specification for Road Bridges standards	National Highway Prefectural Road Municipal Road Prefectural Road Municipal Road	First Class Bridge 20t Second Class Bridge 14t
April 1973 Design Codes for Bridges on Special Route, Elevated Roads and others	Tokyo Bay shore road National expressway and Others	43t

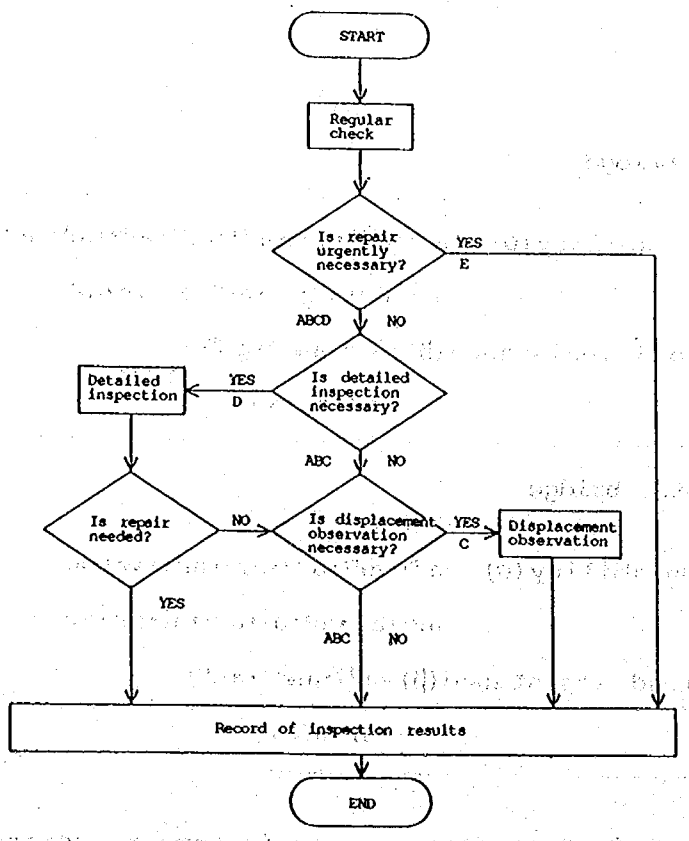

Figure-2 Flow chart of bridge inspection

Table-3

(1) Daily check

Result of daily checks is judged according to the standards mentioned below.

Judgement standards for daily checks

Division of judgement		Condition	Measures
I	Good	Damage is not seen.	-
II	Take notice	There is damage.	Record
III	Dangerous	Damage is severe.	Emergency repair

(2) Regular inspection

Result of regular inspections is judged according to standards mentioned below.

Judgement standards of regular inspections

Division of judgement		Condition	Measures
A	Good	Damage is not seen.	-
B	More or less good	Damage is slight.	Record
C	Take notice	There is damage.	Movement observation
D	Caution	Damage is big.	Detail inspection
E	Dangerous	Damage is drastic. Or it has possibility to influence the third party	Emergency repair

(3) Inspection for abnormality

Result of inspection for abnormality is judged according to judgement standards mentioned below.

Judgement standards for inspections in case of abnormal condition

Division of judgement		Condition	Measures
I	Good	There is no damage or it is slight.	-
II	Take notice	There is damage.	Displacement observation
III	Dangerous	Damage is severe.	Emergency measures

Steel bridge

$$\text{Durability}(\alpha) = a_1^{b_1} \cdot a_2^{b_2} \cdot a_3^{b_3} \cdot a_4^{b_4} \cdot a_5^{b_5} \cdot a_6^{b_6} \cdot a_7^{b_7} \cdot a_8^{b_8}$$

$$= a_1^{30} \cdot a_2^{5} \cdot a_3^{5} \cdot a_4 \cdot a_5^{30} \cdot a_6 \cdot a_7^{4} \cdot a_8^{4}$$

$$\text{Load resistance}(\beta) = a_9^{b_9} \cdot a_{10}^{b_{10}} \cdot a_{11}^{b_{11}}$$

$$= a_9^{2} \cdot a_{10} \cdot a_{11}$$

Concrete bridge

$$\text{Durability}(\alpha) = a_1^{b_1} \cdot a_2^{b_2} \cdot a_3^{b_3} \cdot a_5^{b_5} \cdot a_6^{b_6} \cdot a_7^{b_7} \cdot a_8^{b_8}$$

$$= a_1^{30} \cdot a_2^{3} \cdot a_3^{3} \cdot a_4 \cdot a_5^{10} \cdot a_6 \cdot a_7^{3} \cdot a_8^{3}$$

$$\text{Load resistance}(\beta) = a_9^{b_9} \cdot a_{10}^{b_{10}} \cdot a_{11}^{b_{11}}$$

$$= a_9^{2} \cdot a_{10} \cdot a_{11}$$

Figure-3 General soundness judgement expression

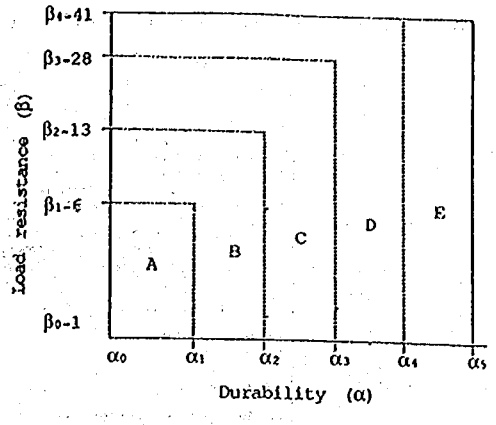

Border value for judgement of toughness

Type of bridges	α_0	α_1	α_2	α_3	α_4	α_5
Steel bridge	1	2×10^{22}	2×10^{22}	4×10^{33}	5×10^{44}	8×10^{55}
Concrete bridge	1	2×10^{7}	1×10^{14}	9×10^{20}	9×10^{27}	9×10^{34}

Figure-4 General soundness judgement diagram

Table-4 Inspection table for earthquake-proof of bridges (1979)

Check points		Check items			Expenses
Primary inspection	Super-structure	Change condition of shoe part	Damage of shoe (Yes, No) Draw of anchor bolt (Yes, No) Damage of seat (Yes, No) Abnormal displacement (Yes, No.)		
		Earthquake-resistance device on shoe part	Straight bridge	Movement restriction device (Yes, No) Isolation distance of seat (Enough, Not enough) Beam connection device (Yes, No)	
			Skew bridge, Curved bridge	Movement restriction device (Yes, No) Isolation distance of seat (Enough, Not enough) Beam connection device (Yes, No)	
	Substruc-ture	Earthquake-resistance of ground	Saturated sandy ground (Yes, No) Very poor ground (Yes, No)		
		Type of foundation	Pile-bent foundation (Yes, No) Independent caisson foundation (Yes, No) Plain concrete (Yes, No) RC Rahmen bod (Yes, No) Brick body (Yes, No) Stone body (Yes, No)		
		Change displacement of substructure	Scour (Yes, No) Displacement of foundation (Yes, No) Abnormality of body (Yes, No)		
	Total				

Check points		Judgement of safety level			Expenses
Secondary inspection	Ground	Thickness of saturated sandy soil	Good (Thickness is 1.0 m or less) Medium (Thickness is over 1.0 m and less than 10.0 m) Bad (Thickness is 10.0 m or over)		
		Holding force of earth	Good (A range) Medium (B range) Bad (C range)		
	Substruc-ture	Strength of body of bridge piers	Good (A range) Medium (B range) Bad (C range)		
		Bearing power of foundation piles	Bearing pile	Good (Safety ratio is 2 or more) Medium (Safety ratio is over 1.5 and under 2) Bad (Safety ratio is 1.5 or less)	
			Friction pile	Good (Safety ratio is 3 or more) Medium (Safety ratio is over 2 and under 3) Bad (Safety ratio is 2 or less)	
		Earthquake-resistance according to type of foundation	Pile-bent foundation, Independent caisson foundation, RC Rahmen, Plain concrete, Brick body, Stone body		
		Change of substructure	Scour, displacement of foundation, abnormality of body		
	Total				

Note from the primary inspection		Total expenses of antiearthquake measures
Note from the secondary inspection		

Table-5 Inspection table of bridges (1986)

Inspected by				Date of inspection		Reference number		
Kind of road		Name of route		Traffic volume		Name of a bridge		
Place except DID	DID (In, Out)	Bus service route	(Yes, No)	Length of a bridge		Width of a bridge		
Inspection items								
Inspection of bridges	(A) Superstructure	1) Applied indication method		4.0 Detailed rules of 1926, standard of 1939 2.0 Standard of 1956 or 1964 1.0 Standard of 1971, standard of 1980				
		2) Superstructure type		3.0 Cantilever bridge or simple beam bridge with more than 2 spans 1.5 Simple beam with 1 span (15 m or more) or continuous beam of more than 2 1.0 Deck bridge, half through arch, Rahmen, one-block continuous beam, cable stayed bridge, suspension bridge				
		3) Line form of a plane		1.2 Skew bridge, curved bridge 1.0 Straight line				
		4) Superstructure material		1.2 RC·PC 1.0 Steel				
		5) Grade		1.2 6% or more 1.0 Less than 6%				
		6) Bridge-falling preventive structure		2.0 No 1.0 1 kind				
		P_A = 1)x2)x3)x4)x5)x6)		P_A =				
	(B) Deformation of substructure	7) Structure type of substructure		2.0 Single-row pile-bent 1.0 Others				
		8) Height of bridge piers		2.0 10 m or more 1.5 More than 5 m and less than 10 m 1.0 Less than 5 m				
		9) Ground		5.0 Very poor ground in Class 4 ground 2.5 Class 4 2.0 Class 3 1.2 Class 2 1.0 Class 1				
		10) Influence of liquefaction		2.0 There is 1.0 There is not				
		11) Bearing ground		1.2 Uneven 1.0 Even				
		12) Scour		1.5 There is 1.0 There is not				
		P_B = 7)x8)x9)x10)x11)x12)		P_B =				
	(C) Strength of step part of main reinforcing bar	13) Shear span ratio (h/D)		2.0 $1<h/D<4$ 1.0 $h/D \geq 4$ 0.5 $h/D \leq 1$				
		14) Bending, stretch and crack of step part		2.0 produced 1.0 possibly 0.5 not produced				
		15) Safety ratio for yield strength of step part	15)^1 S_{Pa}	3.0 1 or less 2.0 1.1~1.3 0.5 1.5 or more				
			15)^2 S_{Pm}	3.0 1.1 or less 2.0 1.1~1.3 1.0 1.3~1.5 0.5 1.5 or more				
		16) Shearing stress		3.0 45 or more 2.0 30~45 1.0 15~30 0.5 15 or less (Unit: tf/m^2)				
		P_C = 13)x14)x15)^{1}x15)^{2}x16)		P_C = (However, if P_C<1.0, P_C=1)				
	(D) Strength and deformation of substructure	17) Abnormality in fixed shoe and around shoe		5.0 There is a serious defect 2.0 There is a slight defect 1.0 No				
		18) Abnormality in body		5.0 There is a serious defect 2.0 There is a slight defect 1.0 No				
		19) Structural material of substructure		2.0 Plain concrete according to detailed rule of 1926, or road indication of 1939 (Except gravity abutment) 1.0 RC·PC·Steel, plain concrete or plain gravity abutment based on road laws after 1956				
		20) Construction method of foundation		2.0 Wood pile, brick caisson, stone caisson, box frame construction method, unknown 1.5 Precast RC pile, pedestal pile, 2-pier caisson 1.0 One manufactured after 1971's guidance, positioning pile, PC pile, steel pile, spread foundation, general caisson				
		21) Structural type of substructure		1.5 RC Rahmen 1.0 Others				
		22) Abnormality of foundation		2.0 Yes 1.0 No				
		P_D = 17)x18)x19)x20)x21)x22)		P_D =				
Evaluation point				$X = P_A \times P_B$ = $Y = P_C \times P_D$ =				
Note								

Table-6 Inspection schedule of earthquake-proof measures for existing bridges

Inspection items, contents / Fiscal year		1990	1991	1992	1993	1994
(Anticearthquake inspection of bridges) Judgement of earthquake resistance of bridges	Preparation of judgement resume for earthquake resistance (Plan I is for basic inspection) (Plan II is for inspections considering liquefaction measures and natural period of bridges) Inspection of bridges of which foundation structure is unknown	Preparation of general plan Collection of data Preparation of Original Plan I Simulation 10 bridges	Preparation of Original Plan II Simulation 10 bridges Inquiry of substructure of bridges	Preparation of actual plan I Trial 20 bridges Inquiry of substructure of bridges Trial 10 bridges	Completion of actual plan	Start of inspection Preparation of long-term plan of anticearthquake measures
Selection of anticearthquake repair method	Preparation of anticearthquake repair method resume		Collection of data Preparation of the original plan I	Simulation 10 bridges	Preparation of the original plan II Trial 20 bridges	Completion of making an actual plan
(Measures in case of earthquake) Inspection and judgement of damages	Inspection and judgement of damage	Collection of data Preparation of the original plan I	Simulation 10 bridges	Preparation of the original plan II	Trial 20 bridges	Completion of making an actual plan
Selection of emergency repair method in case of earthquake	Preparation of manual for selection method for emergency repair in case of an earthquake	Collection of data	Preparation of the original plan I	Simulation 10 bridges	Preparation of the original plan II Trial 20 bridges	Completion of making an actual plan
Selection of repair method of bridges after an earthquake	Preparation of manual for selection method for repair after an earthquake	Collection of data	Preparation of the original plan I	Simulation 10 bridges	Preparation of the original plan II Trial 20 bridges	Completion of making an actual plan

(Note) Depending on the 5th Tokyo Metropolis Earthquake Disaster Prevention Plan (from 1993~), contents of inspections, schedule and cost might be changed.

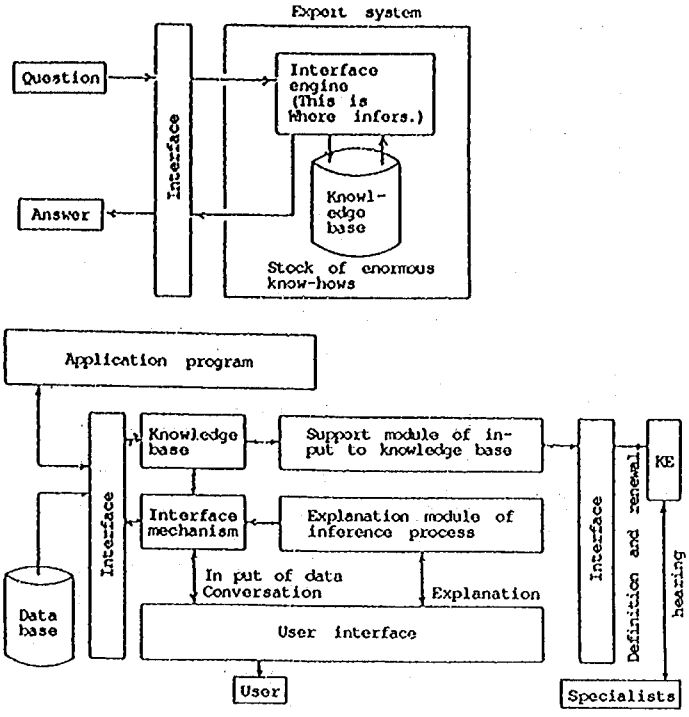

Figure-5 Composition of "EXPERT SYSTEM"

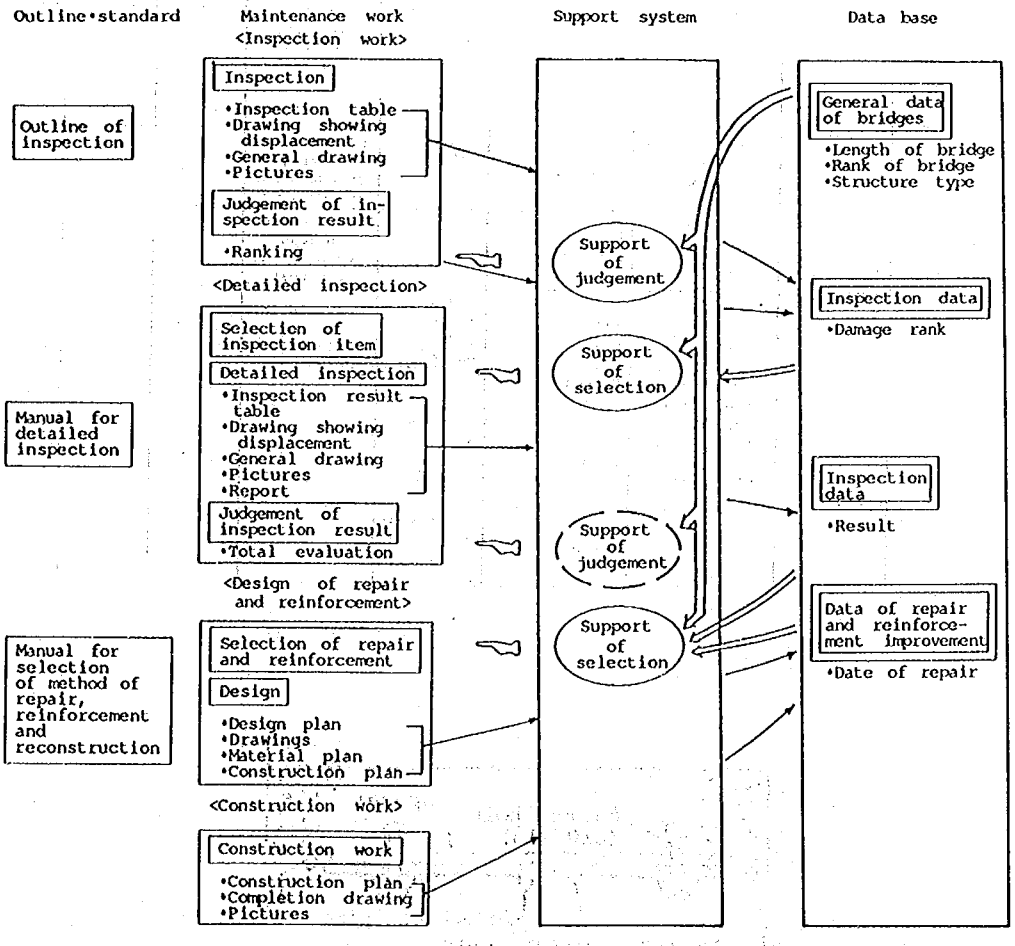

Figure-6 Outline and actual work in maintenance work of bridges, support systems by "EXPERT SYSTEM" and relation with "DATABASE SYSTEM"

Table-7 Table for Selection of repainting

Kind of applied surface preparation	Old painting system	Repainting type	Applicable environment	Painting process			Amount used (kg/m^2)	Method of painting	Target thickness of coating (μ)	Interval for coating (day)
					Name of paint	Standard				
Class 2	I-A	A	Applicable to general environment	First undercoat[a]	Lead anti-corrosion paint	JISK-5623-5 Class 1	0.140	Brush	35	2-10
				Second undercoat	"	" "	0.140	"	35	2-10
				Middle coat	Synthetic resin blend paint	JISK-5516 Class 2	0.120	"	30	1-10
				Top coat	"	" "	0.110	"	25	
Class 3 Class 4		B	Applied to comparatively corrosive environment	First undercoat[a]	Lead anti-corrosion paint	JISK-5623-5 Class 1	0.140	"	35	3-10
				Second undercoat	"	" "	0.140	"	35	3-10
				Second middle coat	Phenol MIO paint	Construction Bureau Standard	0.250	"	45	3-10
				Second middle coat	Chloric rubber paint	Construction Bureau Standard	0.170	"	35	1-10
				Top coat	"	"	0.150	"	30	

Note 1: First undercoat with [a] cannot be applied to Class 3 or Class 4 surface preparation.

Kind of applied surface preparation	Old painting system	Repainting type	Applicable environment	Painting process			Amount used (kg/m^2)	Method of painting	Target thickness of coating (μ)	Interval for coating (day)
					Name of paint	Standard				
Class 2	I-B II A-1	C	Applied to comparatively corrosive environment	First undercoat[a]	Epoxy resin undercoat paint	Construction bureau standard	0.200	Brush	50	2-10
				Second undercoat	"	"	0.200	"	50	2-10
				Middle coat	Chloric rubber paint	Construction Bureau Standard for middle coat	0.170	"	35	1-10
				Top coat	"	Construction Bureau Standard for top coat	0.150	"	30	
Class 3	II A-2	D	Points where high weather-resistance is required in the above environment	First undercoat[a]	Epoxy resin undercoat paint	Construction Bureau Standard	0.180	"	45	2-10
Class 4				Second undercoat	"	"	0.180	"	45	
				Middle coat	Polyurethane resin middle coat paint	"	0.140	"	30	1-15
				Top coat	Polyurethane resin top coat paint	"	0.120	"		

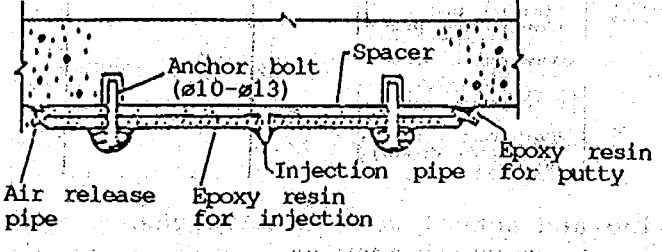

Figure-7 Reinforcement by injection method

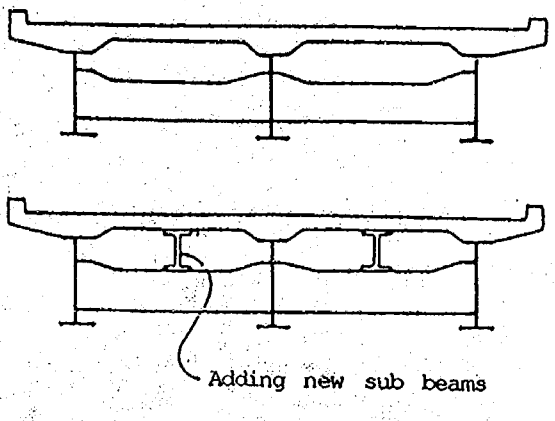

Figure-8 Reinforcement by adding new sub beams

Kind of bridge-falling prevention works

(1) Movement restriction device of movable shoe (directly equipped to a movable shoe)

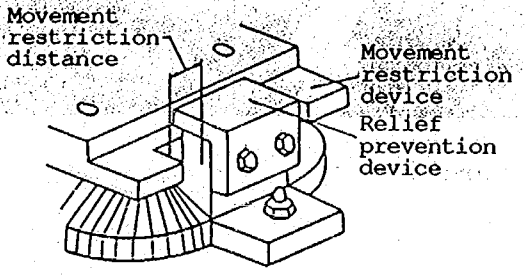

(2) Length of beam from the end of the beam to top end of lower structure

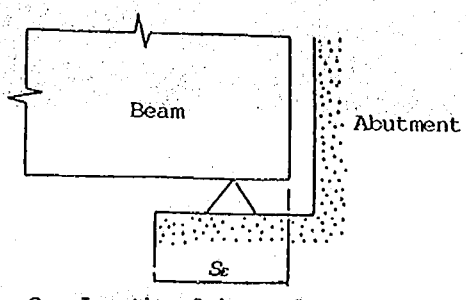

Sc : Length of beam from the end of the beam to top end of sub-structure

(3) Bridge-falling prevention device

Structure with mutually connected 2 with each beams

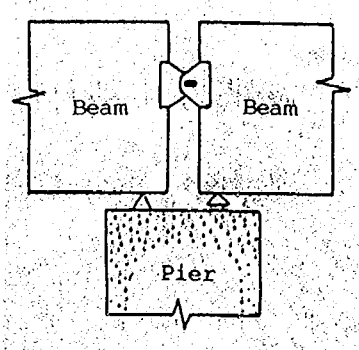

Figure-9 Bridge-falling prevention I

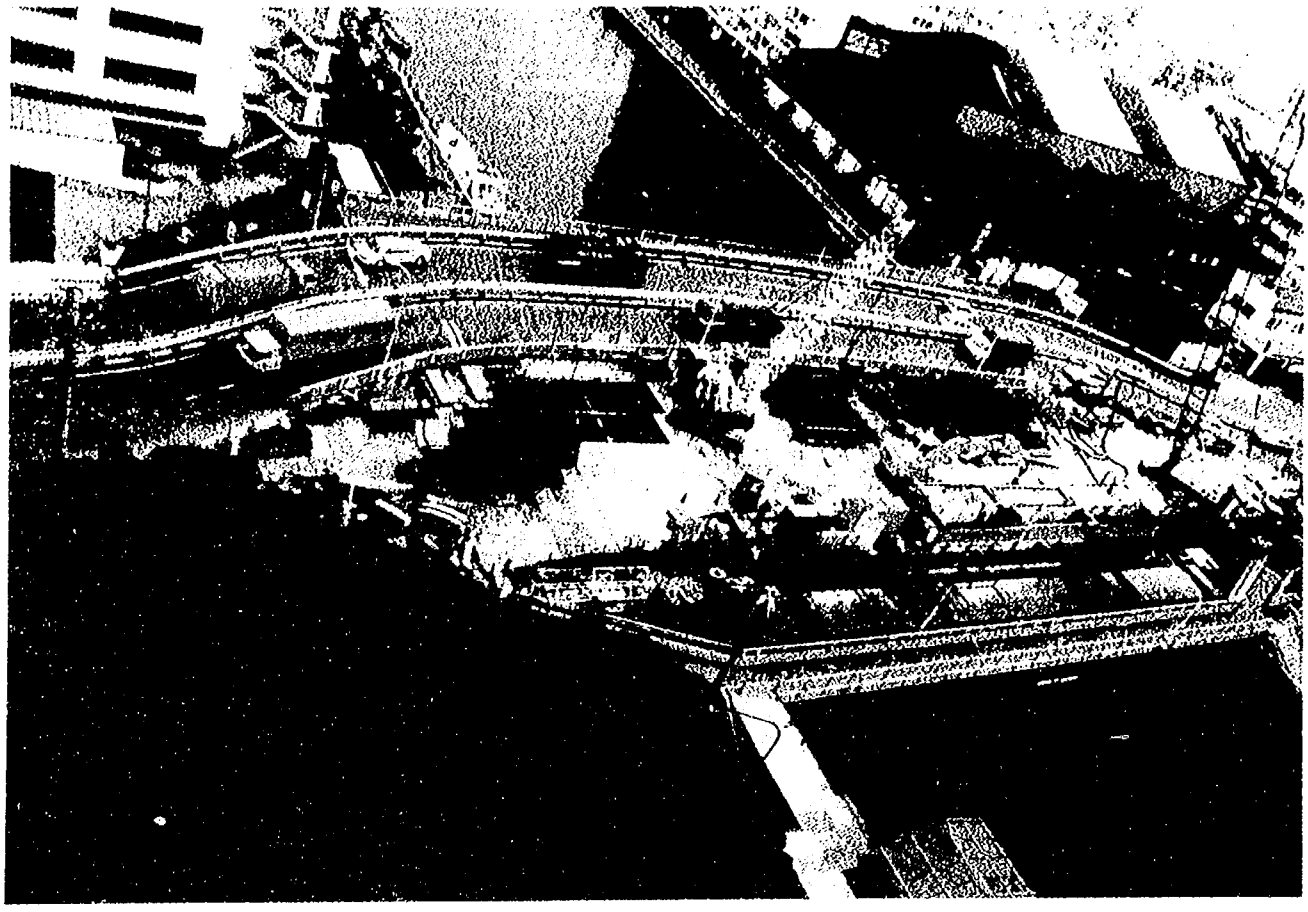

Picture 1

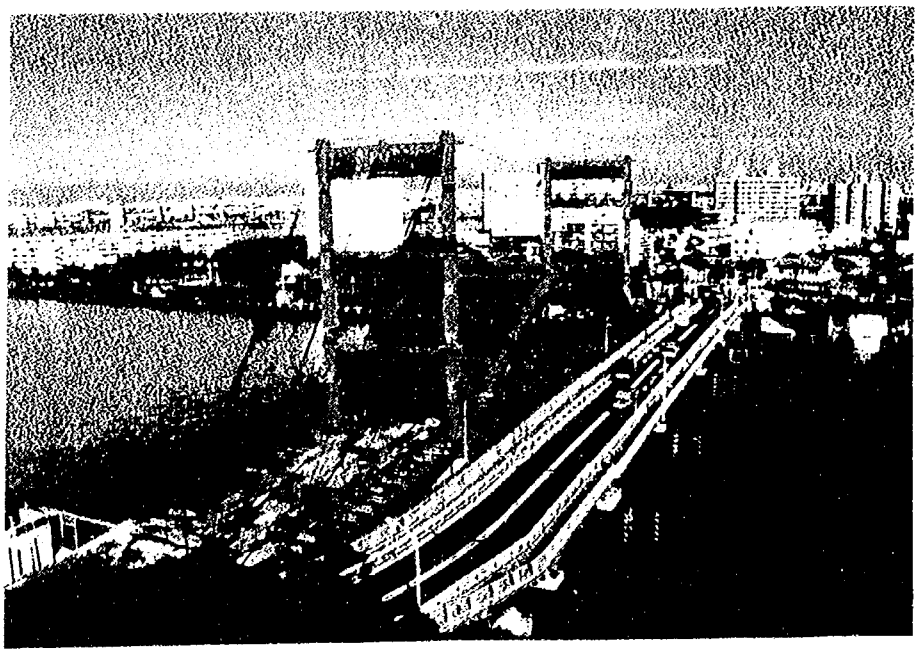

Picture 2

"Emphasis Areas in PennDOT's Bridge Inspection and Repair Program"

by Gary L. Hoffman, P.E.
Director, Bureau of Bridge
and Roadway Technology
Pennsylvania Department of Transportation

Index pg.

I. Background
- A. Why Bridge Inspection 1
- B. Pennsylvania Bridge Statistics 2
- C. Inspection Program Organization/Resources ..2
- D. Posting and Closing Policy/Procedures 3
- E. Administrative Support and Leadership 4

II. Inspection Emphasis Areas
- A. Training & Certification 5
- B. Quality Control and Quality Assurance 5
- C. FHWA Review and Oversight 6
- D. NBIS "Catch-Up" and Local Gov. Effort 6
- E. Fatigue and Fracture Criticality Program ...7
- F. Underwater Inspection Program 7
- G. Scour Analysis 7
- H. Non-destructive Testing 8
- I. Load Testing 8

III. Repair Emphasis Areas
- A. Critical Maintenance Repair Items 9
- B. Pin/Hanger Retrofits 9
- C. Fracture Repairs 10
- D. Expansion Dams & Joint Elimination 11
- E. Scour Repair & Protection 11
- F. Maintenance Precast Culvert Replacement ...11 Program
- G. Emergency Contracting Procedures for ..... 12 Repairs

IV. Summary
- A. BMS Description 12
- B. BPRIS Description 12
- C. Collapse Board of Inquiry 13
- D. Safety Utmost Concern 13

I. BACKGROUND

The Pennsylvania Department of Transportation has developed, implemented, and maintained a Bridge Management System (BMS) and Bridge Safety Inspection Program that are recognized nationally and touted as models for other states by the FHWA. The description of this program and how it was attained is the topic of this paper. The Department has had an aggressive, proactive posture towards bridge safety inspection and bridge management since 1983, and it is this attitude that has resulted in today's leadership position. In 1983, then Secretary of Transportation in Pennsylvania, Thomas D. Larson, P.E., commissioned a multidisciplinary task force to evaluate the Department's bridge safety inspection program and to determine the feasibility of developing a formal bridge management system. The task force identified some inadequacies with the bridge safety inspection program, notably the lack of enforcement on locally owned bridges, and determined that a BMS was not only feasible but absolutely necessary. At about the same time the Department was reorganizing and recognizing the importance of having zealots to bring new technology into practice, created the unique Bureau of Bridge and Roadway Technology (BART). BART was assigned the functions of bridge safety inspection and developing and maintaining a BMS along with developing and maintaining a Roadway Management System, product evaluation and field experimentation program. It was primarily the creation of this new bureau that afforded significant attention to the bridge safety inspection program and provided a "third party" view of the Department's bridge network separate from the bridge design and bridge maintenance organizations. A sense of ownership of bridge safety inspection and BMS was provided and zealots were created.

Why Bridge Safety Inspection?

Unquestionably, the primary reason for bridge inspection is and always must be to insure the safety of the motoring public. The depth or degree of any safety inspection, by definition, is that level of detailed inspection and analysis that will insure the public safety at least until the next scheduled inspection. Ancillary reasons for safety inspections are: the determination of bridge needs for prediction and programming, the evaluation of bridge conditions for network performance level monitoring and the determination of need for posting or closing, the compliance with Federal and State laws, and the reduction of tort liability exposure.

The National Bridge Safety Inspection Standards (NBIS) was initiated by the unfortunate collapse of the Silver Bridge in the State of West Virginia in 1967 from which many fatalities were recorded. Subsequently, the 1968 Federal Highway Act dedicated specific funds for bridge safety inspection, bridge replacement, and rehabilitation activities. This program has continued to expand in types of activities.

Pennsylvania's Bridge Statistics

There are approximately 54,800 highway bridges in Pennsylvania. Of these 22,800 bridges are more than 20 feet in length and are required by Federal Regulation to be inspected for structural condition and safety at least once every two years.

The Pennsylvania Department of Transportation is directly responsible for inspecting 16,100 state owned bridges that are greater than 20 feet in length and also for ensuring the timely inspection of 6,700 local bridges that are greater than 20 feet in length. The Department also inspects 9,500 state bridges with span lengths between 8 and 20 feet. Federal Funds are available to inspect all highway bridges that are greater than 20 feet in length (at a Federal participation rate of 80%). The Department's Bureau of Bridge and Roadway Technology (BART) is responsible for managing the statewide inspection of both state and local bridges.

Our Statewide Bridge Inspection Program yields the following additional statistics concerning Pennsylvania's bridges. Of the 22,800 bridges greater than 20 feet in length, about 9,000 are considered to be structurally deficient or functionally obsolete. Of these, 4,210 bridges are weight restricted and an additional 314 bridges are closed to traffic. The estimated cost to rehabilitate or replace these bridges is $5.9 billion.

Pennsylvania's bridges consist of the following general structure types: reinforced concrete (38%), structural steel (37%), prestressed concrete (21%), and other materials (4%). In addition, more than 8,000 bridges are over 50 years old.

Inspection Program Organization/Resources

The Regulations on National Bridge Inspection Standards require that each Highway Department include a Bridge Inspection Organization capable of performing inspections, preparing reports and determining ratings in accordance with the provisions of the AASHTO Manual and the Standards.

Normally, this inspection function rests with those responsible for Maintenance or Design within the Highway Department. However, in Pennsylvania, the organization set-up is somewhat unique.

The Transportation Department is highly decentralized with the Central Office providing direction in terms of policies and procedures and assuring uniformity among the eleven engineering districts through quality assurance checks; the regional districts perform the hands-on inspections.

The Central Office function falls under the Bureau of Bridge and Roadway Technolgy whose mission is to develop and maintain the Bridge and Roadway Management Systems, Coordinate Technology transfer, electronic data processing and value engineering. Within the Bureau, the Bridge Management Systems Division discharges the Central Office function on Bridge Management and Bridge Inspection.

The hands-on inspections at the regional level are performed by district inspection teams who come under the District Bridge Engineer working under the Assistant District Engineer for Design.

There are currently 26 two-man inspection teams performing inspections. Their efforts are supplemented by consultants who perform approximately 15% of the work.

The organization chart of a typical regional inspection unit is shown. Note that the function of coordinating with local governments and with the Department's maintenance organization on bridge matters also falls within this unit.

Posting And Closing Policy/Procedure

Every effort is made to minimize both additional postings and economic impact, while not compromising public safety. Additionally, potential adverse public reactions to any new postings are carefully considered and addressed.

If the governing bridge members are inspectible and corrosion losses can be measured, provided they are not fracture critical, the operating rating is generally used to determine the level of posting. Engineering judgement is exercised when posting bridges with critical members. The stress level chosen between inventory and operating is determined after analysis of factors such as:

a. Frequency of Inspection.
b. Magnitude and frequency of truck traffic.
c. ADT and percentage of truck traffic.
d. Location and Alignment.

e. Condition, frequency and depth of inspection.
f. Structure type/detail, fatigue consideration.
g. Essentially for public use.
h. Possible violations of load limit.

Before restrictive posting is recommended, special capacity analysis techniques such as load factor, 3D finite element Structural Analysis are tried whenever possible. In some cases, bridge members are instrumented to determine load carrying capacity.

The lowest posting allowed is 3 tons, which permits passage of cars over the bridge. When the bridge is unable to carry this load, it is closed to traffic.

Administrative Support And Leadership

One of the most important items in any organizations ability to implement and maintain an effective bridge management and inspection program is the interest and support of its leadership. Earlier comments in this paper attest to the aggressive attitude of former Secretary, Thomas D. Larson, P.E., toward the bridge network. Likewise, one of the first things that the present Secretary of Transportation, Howard Yerusalim, P.E., did when he took office was to commission a Task Force to identify actions needed to improve bridge safety in Pennsylvania. Although routine inspection procedures provide some degree of assurance, the leadership must not consider them to be adequate and must remain aggressive when it comes to bridge safety. Among the aggressive steps that the state has taken under the present Secretary's leadership to ensure safety are:

1. Development and implementation of guidelines for inspection of bridges with fracture critical members.
2. Detailed analysis of remaining life at fatigue sensitive locations of bridges with fracture critical members.
3. Hands-on inspection backed by Non-destructive testing, if deemed necessary, at critical locations.
4. Auxiliary support systems for 21 two-girder pin/hanger bridges.
5. An aggressive posting policy that ensures that bridges are properly analyzed and posted, if necessary.
6. An aggressive underwater inspection program that exceeds national requirements. In addition, follow-up inspections are made at vulnerable bridges following heavy rains.

7. Identification of bridge substructures in scour prone areas and detailed scour analysis at each of these locations.
8. Bridges are immediately closed when safety of the motoring public is in jeopardy. In such instances, problems are quickly reviewed; emergency contract procedures are quickly instituted; and the problems are rectified soon as possible, so that there is minimal disruption to traffic.

II. INSPECTION EMPHASIS AREAS

Training and Certification

The Bureau of Bridge and Roadway Technology through consultant contracts provides bridge inspection training to all Department Bridge Inspectors, consultant bridge inspectors and to other outside agencies as well. Training consists a 75 hour, comprehensive basic bridge inspection course and refresher courses that are required at two year intervals in order for inspectors to maintain certification.

Specialized training courses are also offered for fracture and fatigue of steel bridges, underwater inspection, culvert inspection and other specialty inspections. A testing and certification process ensures that Pennsylvania's bridge inspections are conducted by fully trained, competent and responsible bridge inspectors.

Over the last 10 years, the Department has presented 15 Basic and 14 Refresher Training Courses to over 1300 bridge inspectors.

Quality Control and Quality Assurance

A Bridge Management System is only as good as the data it contains. The Quality Assurance Program ensures that inspections are accurate, complete and uniform throughout the state. Independent inspection reviews are conducted by an outside engineering consultant on a select number of state and local bridges. Over 345 quality assurance reviews are conducted each year. These complement quality control reviews performed by District Management Personnel.

The Quality Control and Quality Assurance Program bring to surface areas that need more clarity in terms of rating. These issues are then addressed at the Bridge Inspection training sessions. Special letters are also issued from time to time from Central Office which ensure uniformity of inspection, analysis and reporting procedures.

FHWA Review and Oversight

Each year representatives from the Federal Highway Administration visit three or four engineering districts to review the inspections program for compliance. For this review, FHWA assesses the qualification of the inspection personnel, inspection procedures, documentation, reporting and load posting. Special emphasis is placed on inspection of fracture critical members and review of the underwater inspection. The quality control program in each district is thoroughly reviewed, and visits are made to local agencies to ensure that not only the state owned bridges are in compliance but also that local bridge inspections are performed, as required. These visits also ensure that there is adequate follow-up by the state to the problems raised at the local level.

NBIS "Catch-Up" And Local Government Effort

When BART was created in 1983, there were about 4300 bridges that were overdue for inspection and 1200 bridges that were not load posted but should have been posted according to the criteria used by the Federal Highway Administration. The majority of these delinquent bridges existed on the local bridge network owned and maintained by counties, townships, and cities (about 2600 Statewide).

Two basic problems existed that fostered this delinquency at the local level. First, most local government officials were not aware of the criteria and importance of bridge safety inspection. Second, the Pennsylvania Department of Transportation had no legal authority to enforce bridge safety inspection programs at the local level even though the FHWA held the state transportation department accountable for all bridges open to public traffic - regardless of ownership.

A number of positive actions were taken to correct these deficiencies and to ensure that they did not occur again in the future. A communication link was established between a local government coordinator and all the local governments in each of the eleven engineering districts in the Department. Pamphlets and video teleconferencing were used to educate and encourage local government officials toward inspection compliance. After all the delinquent bridges were identified through the bridge management system, engineering consulting contracts were established in each engineering district to get all state and local bridges over 20 feet in span length into strict inspection and posting compliance within two years. A mechanism whereby the local government could choose among three inspection options (locals inspect themselves, locals hire their own

consultant, locals default inspection to PennDOT consultants) was established to ensure continued compliance. Finally, the Pennsylvania legislature enacted Act 44 of 1988, which gave the Department the authority to inspect potentially delinquent locally owned bridges and to backcharge the local government owner for the cost involved with the inspection and administrative oversight.

Fatigue and Fracture Criticality Program

Over six percent of the State's bridges have members which are fracture critical. By definition, these are members in tension whose failure could cause collapse of the bridge. Department efforts are being augmented by contracts with consultants which zoom in on the critical details of these structures to detect problems in their early stages to avoid catastrophes. More then 300 bridges with fracture critical members have been analyzed at a cost of about 1.7 million dollars. In addition, about one-half million dollars have been spent on hands-on inspection of fatigue prone details at critical locations identified through the analysis. PennDOT initiated its fracture critical program even before it became a federal requirement.

Underwater Inspection Program

For bridges carrying highways over water, inspections do not stop at the water line. Special underwater inspections by hard hat/scuba divers are required to inspect bridges with underwater members which cannot be visually evaluated during periods of low water flow or examined by feel for condition, integrity and safe load capacity due to excessive water depth or turbidity. Firms specializing in such inspections are contracted to perform this work since we generally do not have this in-house capability, except in one district.

Statewide open-ended contracts administered by the Central Office ensure that inspections are performed on a regular basis and after high water events. Corrective measures are taken when dangerous conditions are noted by divers. When necessary, cores are taken to evaluate the condition of substructure elements, especially timber piles.

Identify And Prioritize Scour Critical Bridges

In order to determine the scour criticality of bridges over waterways, a comprehensive methodology was initially developed to screen all bridges over waterways and determine those that would be most vulnerable to scouring action.

This methodology considers actual physical bridge conditions as well as the importance of the bridge to serve traffic needs.

Factors used to evaluate bridges for scour susceptibility include: waterway adequacy, channel condition, foundation type and depth, characteristics of the stream bed history of flood events at the site. Pilot projects are underway to evaluate seven bridge sites taking into account hydraulic, geotechnical and structural parameters. Scour depths are calculated for the 500 year flood event. In-depth detailed analyses of the type mentioned above will first be carried out on priortized bridges. These are bridges on networks that carry a large portion of traffic and bridges whose failure would cause substantial detouring of traffic.

Non-Destructive Testing

Liquid penetrate and magnetic particle tests are routinely performed to clearly identify the location of suspected tight cracks. Ultrasonic methods are used to determine thinness of components. Also, straight beam and angle beam procedures are used to check the integrity of pins and hangers of two-girder pin/hanger bridges.

Load Testing

Several alternatives are available to the engineer for quantifying a bridge's structural integrity. These methods include analysis, visual inspection, load testing, or a combination thereof. An actual load test of a bridge provides more information on actual live load response behavior than an analysis based on assumption. Hence, whenever possible, load testing should be included in the evaluation process.

Through research performed by Dr. George Goble of the University of Colorado, a simple load capacity test has been developed. The test has an electronic data acquisition system that can quickly and easily measure live load strains in a bridge's structural members. Next, elastic structural analysis techniques are used to develop a representative computer model of the bridge that simulates the experimentally measured behavior. Permit or posting loads are then applied to the computer model of the bridge, and live load stress levels are predicted. Thus, the actual behavior of the structure is taken into account for evaluation and posting decisions.

The strain transducers are reusable; and the system collects, digitizes, and stores strain-data from twenty different locations on the loaded structure.

III. Repair Emphasis Areas

Critical Maintenance Repair Items

The Department's Bridge Management System (BMS) includes a Bridge Maintenance Subsystem that allows bridge inspectors to identify and store needed bridge maintenance activities on a bridge by bridge basis.

Maintenance repair items are identified during routine inspections. Critical repair items are immediately targeted for repair or correction. If repairs can not be made immediately, the use of the bridge may be restricted to ensure public safety. Some examples of critical maintenance items include: severe scour or undermined substructure foundation, fractured primary structural member due to either fatigue or vehicle damage, or missing bridge load posting or warning signs.

Other non-critical repair activities are identified and stored in the system along with an indication of their relative priority. The system then prioritizes all bridges according to identified bridge maintenance needs. These prioritized lists serve as the basis for developing annual maintenance improvement programs.

After bridge maintenance activities have been completed, they are removed from the maintenance needs screen in BMS and transferred to a maintenance history screen where they are stored for future reference.

Pin/Hanger Retrofits

In October 1988, inspectors found problems on an Interstate 80 bridge. Its fracture-critical pin hanger connections which were held together by retainer rods and pin caps showed distress. One retainer rod had failed, and a pin cap had disappeared.

The bridge was closed immediately and emergency procedures were involved to replace the failed rod an cap. Also, methods were explored to provide a higher level of redundancy to these types of bridges. The choices were narrowed down on most bridges to the following:

1. Eliminate the pin-hanger connection and provide flange and web splices to obtain continuity at the pin-hanger location (used on three bridges).
2. Provide an auxiliary support or cantilever type system under the floor beams to avoid changing the bridge profile. (used on seven bridges, also see sketch).
3. Provide an auxiliary support on "catcher" type system under the girders; this of course, would affect the bridge profile (used on 10 bridges, also see sketch).

FRACTURE REPAIRS

The high number of old steel structures, high numbers of significant loading cycles and a corrosive environment in an industrialized State like Pennsylvania mandate the need for a fatigue and fracture inspection program as described earlier in the paper. When cracks are uncovered during inspection, they are immediately analyzed, and the integrity of the structure is assessed. Sometimes this assessment dictates an emergency closure of the structure; but, at all times, some fracture repair techniques are used to relocate or redistribute stresses in the cracked member or detail. Some standard fracture repair techniques include: drilling holes at the end of the cracks, bolting plates or structural angles over the cracks with high strength bolts, and strengthening of the web gaps.

A few recent examples of emergency closures due to uncovered cracks and the subsequent repair schemes warrant discussion. The Black Moshannon River Bridge on Interstate 80 was closed in 1988 when one of the two main girders was found to have a major crack close to the end of the end span. The crack extended entirely through the top flange and part way down into the web in an area that was designed to be in compression. An analysis of the field conditions revealed that the bridge back wall had shifted enough to "lock-up" the end expansion dam which was welded to the steel superstructure of the bridge. This caused the beam to act as a fixed end and created a tension zone in the top flange. An emergency work order was executed to remove deck concrete, to make the expansion dam operational, and to bolt plates to the web and flanges over the cracked section.

A second recent closure incident due to cracking occurred in January 1990 when bridge safety inspectors witnessed cracks progressing 12 to 18 inches in welds on the Vanport Bridge across the Ohio River. This cracking was occurring in the bottom two corner welds of a rectangular box beam that formed the bottom chord of this through truss structure. A thorough inspection of the entire structure revealed that the weld breaks were occurring at every location where a vertical and two diagonal truss members connected to the bottom chord. It was determined that, at these locations, the gusset plate formed a corrosion cell, and pack rust expansion stresses cracked the welds. The development of the corrosion was exacerbated by pigeon droppings, the caustic environment in the Pittsburgh area, and lack of maintenance flushing and clearing in this nearly inaccessible portion of the box beam. This example reinforced PennDOT's relatively recent efforts to design simple bridges so they are inspectable and maintainable and to undertake a systematic and rigorous bridge flushing and cleaning program. The repair of the Vanport Bridge included cleaning of the box beam bottom chord, retrofitting with bolted structural angles and bottom plate, and closure of all the port holes in the box beam to keep out pigeons and deicing chemicals.

Expansion Dams and Joint Eliminations

One of the most frequently occurring and potentially one of the most damaging maintenance problems is non-functioning expansion dams. Through the 1970's and 1980's, many types of expansion dams with various combinations of preformed neoprene seals and metal armoring were manufactured and installed on the Department's bridges. These generic types included: modular expansion systems, metal reinforced expansion systems, strip seals and armored expansion systems. Past and on-going monitoring of these expansion dams showed that many of them cannot withstand the high traffic impact loadings and are failing-primarily in their anchorage systems. A recent task force has recommended that only two types of systems be used in future designs-the conventional sliding steel plate "tooth dam" with a trough beneath it to catch and redirect water and the single strip seal design which has a positive anchorage in the steel armoring. The Department has recently proposed a special program to repair steel and prestressed concrete beam ends and to replace faulty expansion dams. This program involves 2726 structures at an estimated total cost of $115m.

Scour Repair and Protection

The Department's efforts in identifying scour prone structures and in performing on-going underwater inspections of these scour prone elements has led to the revelation of numerous and some significant scour holes. The Department maintains a list of scour hole repair needs which is prioritized based on criticality. Treatment schedules and costs are also maintained on this statewide list. Some of the typical scour hole repair techniques include large rip-rap, tremied concrete and collars, grout bags and stream flow deflectors.

Maintenance of Small Bridges/Culverts

Each of the 67 county maintenance organizations in Pennsylvania has at least one and sometimes two or three crews dedicated full-time to bridge structure maintenance. The primary function of these crews is to perform routine maintenance activities like cleaning and repairing expansion dams and bearings, repointing masonry substructures, etc. However, over the past few years these crews have been making a significant impact by replacing some of the smaller (under 30 foot span length) posted structures with precast concrete box culverts. The precast elements are fabricated in-house over the winter months when the crew's field construction activities have diminished. In fiscal year 1989-90, 106 bridges have been replaced and eliminated from posting restrictions by this technique using Department force and 66 by contractors.

A few criteria have been imposed on this operation. The bridge replacement cannot take longer than 6 to 8 weeks so a crew's available time is not spent on just a few bridges in a season-thus neglecting routine maintenance operations. Satisfactory quality control procedures on both the precasting and construction phases must be in place to attain a similar level of quality as required of contractors.

Emergency Contracting Procedures for Responses

Emergency contracting procedures are in place which authorizes the district engineer to take prompt and immediate action to correct or mitigate any emergency situation on a highway or bridge. These procedures may be implemented when the approving authority determines that the normal procedure may delay the repair to a point where the Commonwealth, its property, or the health and welfare of its employees, visitors or citizens would be endangered.

IV. Summary

BMS Description

The Department's Bridge Management System (BMS) is a powerful management tool that not only records and stores data for Pennsylvania's bridges but also enables Department managers to make key decisions concerning bridge inspection, design, maintenance, rehabilitation and replacement. BMS includes 17 on-Line data screens and up to 397 data elements for every bridge. The system also has the ability to produce a wide range of reports including standard monthly statistics reports, menu driven reports and customized, user-generated reports.

In addition to storing and recording bridge inspection information, BMS has the capability to automatically generate improvement costs, by bridge, for maintenance, rehabilitation and replacement needs. BMS also has the ability to prioritize bridges for capital improvements as well as maintenance improvements. A unique feature of BMS is its modeling capability which enables the user to predict future bridge needs by programmatically degrading bridge condition and load carrying capacity over time.

BMS has been in production since December 1986, and improvements and enhancements have occurred almost continuously. Future enhancements include refinement of the modeling capabilities, development of a bridge rating and routing subsystem, development of a benefit/cost optimization subsystem and additional integration with other systems.

BPRIS Description

The Bridge Problem/Resolution Information System (BPRIS) was developed for the purpose of sharing bridge and roadway problem information and problem resolutions on a statewide and nationwide is in a systematic and expeditious manner.

BPRIS is intended to track critical information concerning bridge and roadway design, construction, inspection and maintenance problems and their ultimate resolutions. By utilizing computer communications, vital information can be shared almost instantaneously through the Department's computer network. This same information is then stored for future updates, problem resolution and future reference. The system also has search and reporting capabilities.

A portion of the system has also been utilized to automate the Department's "Incidents Affecting Highway Traffic" reporting form. Automation of this form has significantly enhanced the distribution of "serious incident" information to all interested and affected parties.

BPRIS has proven to be an effective tool in monitoring and tracking bridge and roadway problems and incidents.

Collapse Board of Inquiry

A publication is updated annually to serve as a handy reference for guidelines and action to be taken in the event of a bridge collapse or failure of a tunnel's structural components. The publication includes names of District and Central Office personnel nominated by the Districts and the Chief Engineer. Home telephone numbers are also included to facilitate contact during emergencies.

The responsibility of these personnel is to collect facts, report findings and highlight issues to improve bridge and tunnel safety practices that arise from a collapse of failure incident.

The Board of Inquiry has the authority to contract with experts when needed.

Safety Utmost Concern

In the final analysis, all these previously discussed actions and initiatives are driven by the Department's priority objective of providing a safe and reliable bridge network. That is why $7 million are spent annually for bridge inspection, $250m for bridge replacement and rehabilitation, and $25m for bridge maintenance. If there is <u>any</u> doubt about the safety of a structure, the Department has determined that it is wise to temporarily close the structure and take public pressure for traffic flow disruption than to risk even one life in a catastrophic collapse.

(12) Session 12

SESSION 12: CLOSING SESSION
(Co-Chairmen: M. Fujiwara, James D. Cooper)

4:25pm~4:40pm

Settlement of Resolution

Remarks: James D. Cooper (Chairman for the U.S. side)

Closing Remarks: Minoru Fujiwara (Chairman for the Japan side)

(13) 討　議　録

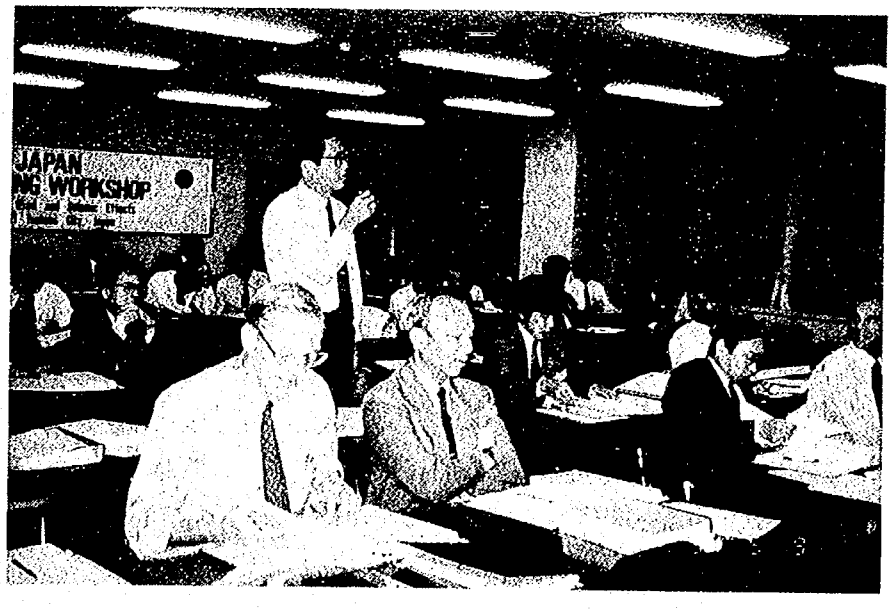

Session 2 Seismic Design(1)

Q. Goldschmidt

使用した杭はなにか。

A. Nanjo

直径150cmの場所打ち杭である。

Q. Gates

模型実験と実橋の減衰の相関はいかがか。

A. Kawashima

減衰の評価手法はよいと考える。ただし、実橋の加振実験が必要であろう。

Q. Kawashima

ＬＲＢ以外のダンパーは応用が可能か。

A. Ghaffar

まだ研究を終えていない。

Q. Maragakis

基礎形式はどうなっているのか。

A. Ghaffar

固定としており、杭などは使用していない。

Session 4 Seismic Design(3)

Q. Kawashima

Mr.Gatesに質問があります。ロマプリーエータ地震から得た教訓は何ですか。特に、耐震補強された構造物について。あなたは、レストレイナーがうまく働いたと言っていますが、耐震補強され、被害の無かった構造物についてロマプリエータ地震から学んだ教訓は何でしょうか。

A. Gates

何かを聞き逃したようで、何か答えるのでしょうか。

Q. Kawashima

1971年以来、カリフォルニアでは耐震補強をされていますね。ロマプリエータ地震程度の加速度では、何事もなかったと言われましたが、ロマプリエータ地震から学んだ将来の設計に役立つ、あるいはレストレーナーなどを用いた既存橋の耐震補強に役立つ教訓は何でしょうか。

A. Gates

最初に申しておきたいのは、あなたが考えられているより橋は強いということです。サイプレス高架橋は、最低のもので、ユニークな構造で一目瞭然の欠点がありました。その他の橋ではレストレーナーが、部分的に壊れたものもありますが、全体としてはうまく働いていました。1978年以来建設してきた新しい橋では、ひび割れさえもなく、ほとんど無被害でした。質問がよくわからないのですが、これで

よろしいでしょうか。

Q．Kawashima

私がお聞きしたいのは、カルトランスで採用されている耐震補強が、今後も有効であるかどうかです。

A．Gates

耐震補強、それが、私たちの現在の結論です。Dr.Saidiが個人的にも言っているように、最初の段階としては、私たちが設置しているようなレストレーナーがそれです。それはうまく働いています。古い時代に低い設計荷重で設計していた橋梁は、耐力不足です。しかし、新しい弾性解析を行っている現在の橋梁は、現実的な荷重を計算しようとしているもので、地震に対して適切な応答特性を有し、ほとんど被害はありませんでした。

C．Margakis

少しつけ加えたいのですが、これらの耐震補強がうまく働いたという一般的な証拠としては、数量的なものが必要です。レストレーナーのモデル化から荷重がどのくらい実際に作用したかについて、Mr.Gatesが言ったようにいくつかは作動し、いくつかは壊れたという点を参考にして、ネバダ大学で研究を進めています。この結果をもとに設計基準を改善していくこともできると考えています。

Q．Okahara

Mr.Goldschmidtに質問があります。普通のパイルに比べて、スピンフィンパイルの主な特徴は何ですか。

A．Goldschmidt

スピンフィンパイルの直径は、普通のパイプパイルと同じです。フィンは、大体4インチで、パイルの直径は、合計で8インチです。

Q．Kawashima

これは質問ではなくMr.Goldschmidtにお願いしたいことです。アメリカからの論文の多くは、構造物の応答あるいは上部構造、柱の被害に関するものです。あなたは、カリフォルニアで基礎をどのように設計するかを話し、それは私にはたいへん興味深いものでした。私は、1971年サンフェルナンド地震以後の基礎の設計に関する主な変更、あるいは改善について興味があるのですが。私は、基礎の設計に関する論文をあまり見たことがありません。もし、そのような情報をお持ちで、教えて頂ければありがたいのですが。

A．Goldschmidt

私は、基礎の設計には関与していません。私が、設計技術者を通して理解しているものとしては、アッパー・レインフォースメントに関する考慮があります。それ以外には、パイルの細目に関する変更でしょうか。Mr.Gatesが補足してくれると思います。

C．Gates

設計の主な変更点は次のようなものでしょうか。サンフェルナンド以前は、ＵＢＣのように低減された値、日本でお使いの地震力レベルによく似ていますが、0.25から0.15Ｇといった値により計算される地震力を用いて、ワーキングレベルの例えば125%という過剰耐力に対する安全率２を考慮して基礎の設

計が行われていました。例えば45tfのパイルは90tfの終局耐力を持っており、私たちは45tfに対して設計を行っていました。サンフェルナンド以降は、合理的な設計法が開発され、基礎は柱の塑性耐力を上回るように設計されています。例えば前に述べた45tfのパイルでは、柱の塑性耐力に対して90tfの終局耐力が用いられます。それが基礎に対する主な変更点です。Mr. Goldshmidtのグループは、終局耐力を我々に教えてくれます。したがって、彼らは、変更点を知らないわけで、われわれ構造技術者が変更を行った訳です。

Session 5 Wind Resistant Design(1)

Q. Cooper

特に論文に対する質問ではないが二次元模型試験と三次元全橋模型試験の使い分けに対するコメントが欲しい。

A. Jones

二次元では、模型を精度良く出来、現象を明確に把握できるが、モードの影響は三次元でなければ把握できないなど一長一短はあるが、いずれにしても両者をバランス良く使い分け総合的に問題を解決する必要がある。

A. Yokoyama

（補足として）日本では架設時の耐風性の検討に三次元弾性模型を用いた風洞試験を行う場合が多い。

Q.

制御装置としてアクティブタイプを採用したのは何故か。

A.

風洞実験結果より、架設時の作業班に支障となると思われる50gal以上の振動を抑制することを目標としたが、低いレベルの振動を抑えるためにはアクティブタイプの方が効果的であり、また設置期間も架設時のであるため信頼性も問題ないと考えこれを採用した。

Q.

渦励震には気流の乱れが影響すると思われるが、乱流中の試験は行ったか。

A.

今回報告したものについては乱流中実験は実施していない。二年前に報告したものには乱流中実験の結果もあるので参照願いたい。

Session 7 Design Method(1)

Q. Gates

我々は、柱状体基礎の杭の載荷試験に大変興味を持っている。実杭の載荷試験、およびその結果の詳細な内容について説明をお願いしたい。

A．Okahara

我々は多くの杭の鉛直および水平載荷試験データを持っている。しかし、柱状体基礎のデータはまだ少ない。論文6ページに示したデータは、大口径杭、鋼管杭、地中連続壁で、大変位に達しているものを選んで掲載している。必要であれば他のデータを提供することは可能である。

Q．Gates

我々のコンピュータプログラムで同じデータを用いて数値解析、特に大口径杭で大変位に達しているものについて行いたいので提供をお願いしたい。

A．Okahara

了解

Q．Clark

地震荷重のような動的な載荷試験データは用いていないのか。

A．Okahara

ここで用いた載荷試験はすべて静的に実施されたものであり、地震動の動的な影響については考慮されていない。

Q．Okahara

支承の移動について説明されたが、地盤沈下にともなう鉛直方向の移動について質問したい。日本では、軟弱地盤に基礎を構築する例が多い。このため、将来の地盤および基礎の沈下量の予測が必要な場合がある。

軟弱地盤に基礎を構築する場合に、支承の設計はどのようにするのか。

A．Roader

ここで説明した支承は鉛直方向に対して剛な支承である。したがって、このような沈下が生じた場合、上部工も一緒に沈下することになる。これを防ぐためには柔な支承を用いることが必要となるが、所要の支承の剛性を簡易に評価する手法が必要である。

Q．Okahara

なにか特別な装置を支承に設けていますか。

A．Roader

浮き上がりが生ずる場合には特別な装置を設ける場合がある。

Session 8 Design Method(2)

Q．Okahara

Maragakis教授に質問したい。私は橋の余寿命の予想に大変興味があるが、これについてもう少し詳細な情報を知りたい。

A．Maragakis

詳細については、Sander教授に問い合わせていただきたい。

Q．Cooper

Dr.Kulickiに質問したい。荷重抵抗係数設計法（LRFD）がすべての州に一様に受け入れられるのにどの位時間がかかると予想されているか。

A．Dr.Kulicki

橋梁のLRFDは1974年にできて、現在半分の州で使われており、他の州は許容応力度設計法である。LRFDに少しずつは移行している。しかし早く移行させる方法がある。それは命令や法律である。我々の示方書は法律ではない。AASHTOは1993年までにできるだけ早く移行するように決定しており、Guide Specificationを用意している。FHWAも早く移行するよう支持している。

Q．Kawashima

Dr.Kulickiに質問したい。AASHTOとは何か。そこに何人いるのか。各機関から何人代表が出ているのか。ワーキンググループはいくつあるのか。現在の示方書を修正する目標はいつなのか教えて欲しい。

A．Dr.Kukicki

AASHTOは、全米州政府道路運輸協会（The American Association of State Highway and Transportation Officials）のことであり、幾つかの委員会や組織を持っている。委員会の下に、橋梁構造小委員会がある。各州（50州）は一人、通常橋梁技術者の代表を持っている。この小委員会は橋梁示方書などいくつかの文書（document）を出し、管理している。ここには大学やコンサルタント、建設会社の研究員も含まれている。これらの文書は、投票によって26～7の過半数が得られれば出版されることになる。しかし各州はこれにしたがう必要はなく、独自で基準をつくることができる。次の示方書は短期間で修正する予定で、いくつかの州で作業している。

Q．Kawashima

大学の先生はいつもLFDが良いと言っているが、“正直なところ”設計者として、LFDと許容応力度設計法（ASD）のどちらが良いと思うか。

A．Dr.Kulicki

私はいつも確率的であるLRFDの方が必要性があると答えることにしている。上部構造に対するLFDとASDはスパン15mでほとんど等しい答が得られる。つまり、この15mの橋においては、LFDによる設計でも橋の材料は減らない。アメリカでこの問題について話すときは、LFDで設計されて許可された橋について、同時にASDで行ったものを公表している。私は個人的にLFD，LRFDは実際におこる挙動と密接につながっているがW.SD（A.SDのこと）は実際の挙動と関係がないと主張している。

Session 9 Bridge Construction(1)

Q．Yokoyama

Dr.Clarkに質問したい。なぜ鋼橋でなくてコンクリート橋を建設したのか。

A．Dr.Clark

コンクリートの方が強くて、経済的である。そして、バランスの問題である。バランスしている方が

動きやすい。

Q. Okahara

Dr. Clarkに質問したい。なぜ、さや管(Sleeve Pile)を使ったのか。

A. Dr. Clark

杭が水路の斜面になるからである。それによって杭を地盤の動きから自由にしている。

Q. Okahara

Sleeve Pileに水平抵抗を期待しているのか。

A. Dr. Clark

Sleeve Pileを同じレベルにしているので、土からの抵抗も同じレベルで期待している。

Q. Okahara

Sleeve Pileとの境界が弱点になると思うが、境界部に裏込め土を入れているから、弱点にはならない。

Session 11 Bridge Maintenance

Q. Hoffman

アメリカでは、鉛系のペイントは環境上使用できないが、日本ではどうか。

A. Takizawa

東京都では鉛系ペイントはあまり使用されていないが山間部の橋梁では現在も用いている。

Q. Hoffman

塗り替えの周期は。

A. Takizawa

約5年である。

5. 視察旅行記

視察旅行記

5月10日から5月11日まで、2日間の橋梁ワークショップ・スタディーツアーが行われた。行程は、表－1に示す通り、阪神高速道路公団の東神戸大橋、関西国際空港株式会社の関西国際空港、本州四国連絡橋公団の明石海峡大橋の3現場を視察するものでする。参加者は、クーパー夫人を含めた米国側出席者14人と日本側随行者として藤原構造橋梁部長、岡原基礎研究室長、木村基礎研究室研究員、長谷川耐震研究室主任研究員の合計18名であった。

5月10日（金）8:15、天気晴れ、研究会館のおじさん、おばさんに見送られながら、土研のマイクロバスで予定通り出発した。8:45、荒川沖駅に到着。藤原構造橋梁部長、岡原基礎研究室長と落ち合った後、ひたち106号で上野駅に向かった。ＪＲに初めて乗車し、外を見ながら日本人随行者にあれこれ聞く参加者、昨日までの会議の疲れからか、眠ってしまう参加者など、各自、自由な時間を過ごした。9:19、上野駅に到着。東京の北の玄関口、上野駅の人混みに揉まれながら、山手線に乗り換えた。東京駅到着後、10:44発のひかり223号に乗車し、一路、新大阪に向かった。乗車した新幹線には、食堂車が連結されていなかったが、米国側参加者の一部は、テイクアウト形式のカフェテリアまで昼食用のサンドイッチなどを買うため、車内探検に出かけた。待望の富士山を見ることができず、残念であったが、浜名湖大橋を見つけて写真を撮っている参加者もいた。

13:48、新大阪駅に到着。阪神高速道路公団本社工務部の前川調査役、南荘係長、浜田氏に迎えられ、東海道線の新快速で芦屋駅に向かった。芦屋駅では阪神高速道路公団東神戸工事事務所の北沢副所長に迎えられ、貸し切りバスで東神戸大橋の建設現場へ向かった。現場では、まず東神戸大橋の設計、施工に関する英語ビデオを見せて頂いた。ビデオは、施工方法、耐風・耐震設計などについて分かりやすく説明されたもので、

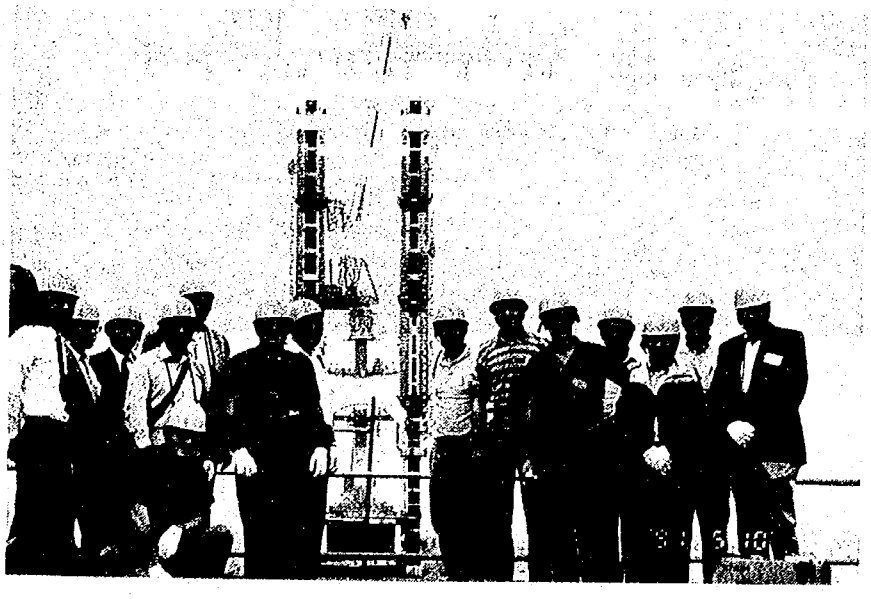

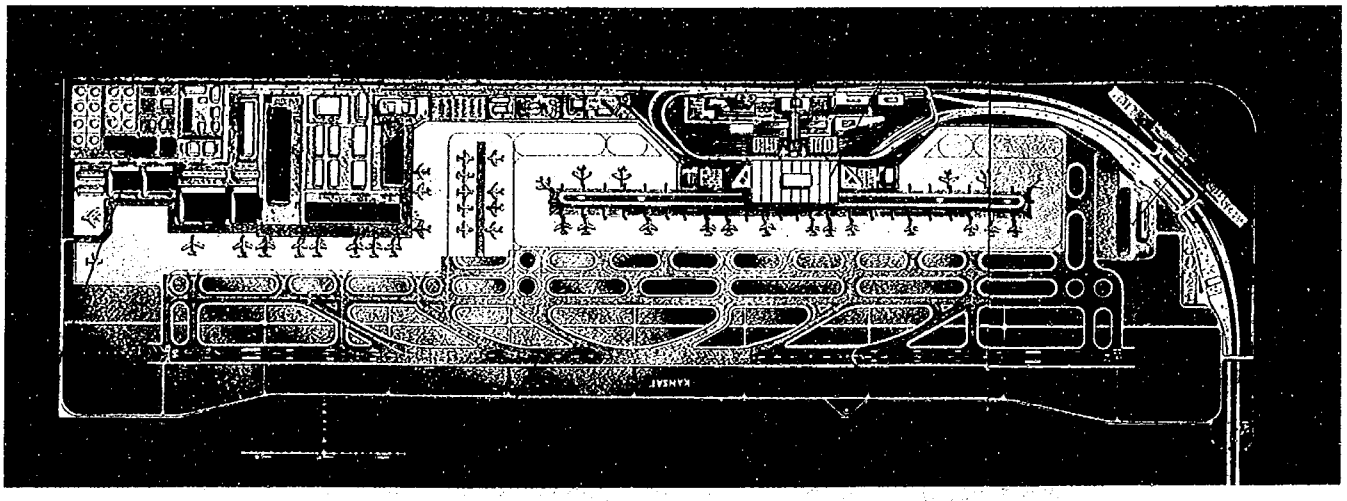

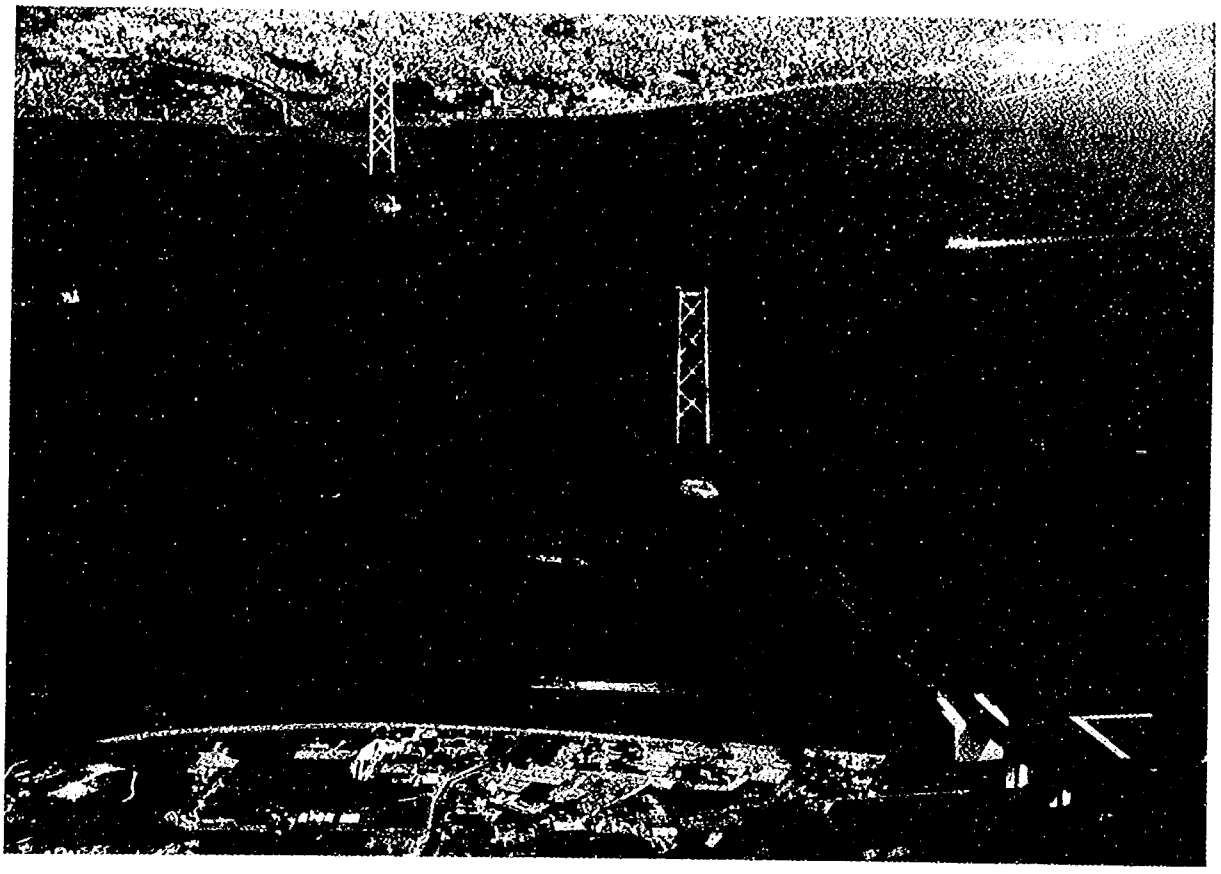

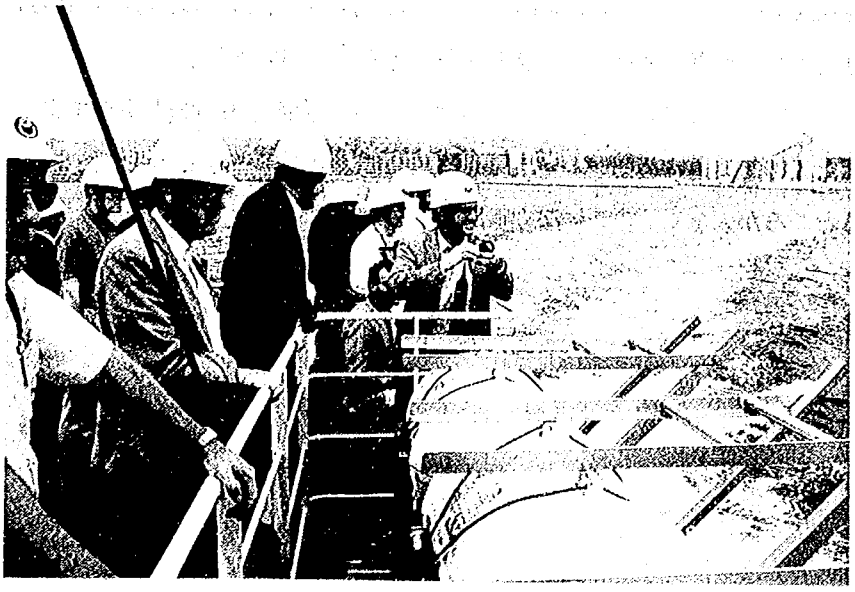

米国側参加者には大変、参考になったようであった。その後、西側のタワーからけた上、さらにタワー頂上まで登り、ＴＭＤなどを見学した。見学後、見学者名簿に毛筆を使って、各自サインし、「Congratulation! You touched the top of this bridge.」と書かれたキーホールダーを記念品として頂いた。また、東神戸大橋のポスターを頂いた参加者もいた。現場を後にし、大阪市内の宿泊所、後楽園ホテルに向かった。

ホテルでは18:00から、阪神高速道路公団による歓迎レセプションが行なわれた。阪神高速道路公団側からは、松橋常任参与をはじめとして20人を越える方に歓迎して頂いた。大阪第二建設部の沖野部長の司会により、松橋常任参与のご挨拶で始まり、南荘係長のクラリネット演奏、Dr.DouglasによるChanter演奏など、2時間、楽しい時間を過ごすことができた。レセプション終了後、米国側参加者だけで近くの心斎橋通りに出かけたようであった。

5月11日、8:30、ホテルロビーに集合し、関西国際空港株式会社工務第二部の高橋常議役、小林設計第一課長に迎えられ、貸し切りバスで岸和田に向かった。途中、阪神高速道路公団の梅町橋梁，天保山大橋，港大橋等ユニークな橋梁を見ることができ、米国側参加者は盛んに写真を撮っていた。岸和田から船に乗り換え、空港建設現場へと向かった。船の中では、関西国際空港建設に関する英語ビデオを見せて頂いた。まず、管理用のプラットフォームの屋上から現場を見渡し、その後、埋め立て及び連絡橋の現場を見学した。参加者の熱心な質問等により予定時間を越えてしまった。関西国際空港を後にし、船で大阪湾を横断し、新垂水漁港に到着した。本州四国連絡橋公団垂水工事事務所の古屋第一工事長、那須第三工事長代理に出迎えられ、舞子ビラで昼食を御馳走になった。昼食後、舞子ビラの庭から明石海峡大橋建設現場を見渡した。

その後、１Ａの現場に向かい、現場で計測されている水圧、ひずみ等を測定した結果をパソコンと大型テレビを使用して、ヴィジュアルに示すことのできるシステムを用いて説明を受けた。概要説明の後、転落防止用の安全帯を着用し、掘削状況を見学した。１Ａの施工は連壁逆巻き工法で行なわれており、厚さ2.2$_m$、深さ75.5$_m$の地中連続壁を直径85$_m$の円形状に構築し、その内部を深さ64.5$_m$までを掘削するという、中央支間1,990$_m$の長大橋ならではの大規模基礎であり、参加者一同圧倒された。１Ａの見学後、２Ｐの現場を船から見学した。明石海峡大橋の現場を後にし、新神戸駅にバスで向かい、15:15発ひかり116号に乗車した。18:32東京駅に予定通り到着し、無事、スタディーツアーを終えることができた。

今回のスタディーツアーは2日間という短いものであったが、大変、有意義なものであった。これも現場見学でお世話になった阪神高速道路公団、本州四国連絡橋公団、関西国際空港株式会社をはじめとする各関係者のご配慮によるところが大きく、ここに深く感謝させて頂きます。

あとがき

あ と が き

今回のワークショップは２日間の短期間ではあったが、橋梁の耐風・耐震工学を中心に補修・補強まで幅の広い論文発表と討議が行われた。日米間での橋梁に係る重要な課題に対して最新の情報が交換され、今後の検討の方向が示されたのは誠に意義が大きい。会議参加者からも中身の濃いワークショップだったとの声が聞かれた。

なお、今回のワークショップの開催にあたっては、土木研究所構造橋梁部、地震防災部を中心に準備会を設けた。役割分担は以下のとおりである。

事　務　局（橋梁計画官，基礎研究室）

全体スケジュールの作成，対外連絡文書作成，各機関・出席者との連絡

論　文　班（橋梁研究室）

プログラムの作成，論文のコピー・ファイル作成，議事録とりまとめ

会議運営班（構造研究室）

会場準備，写真撮影，OHP・スライド準備，会議運営，コーヒー・昼食の準備

視察旅行班（耐震研究室）

旅行計画，関係機関との調整，随行，宿泊（東京）

レセプション班（振動研究室）

空港出迎え，宿舎送迎，宿泊（つくば），レセプション

最後に、視察旅行に際しては、阪神高速道路公団，関西国際空港株式会社，本州四国連絡橋公団の方々にお世話いただいた。記して感謝の意を表します。

付 属 資 料

（1）　ＵＪＮＲ耐風耐震構造専門部会
第23回合同部会におけるワークショップ報告(英文)

RESOLUTION OF THE SEVENTH U.S.-JAPAN BRIDGE ENGINEERING WORKSHOP
ANALYSIS, DESIGN, PERFORMANCE AND STRENGTHENING

TSUKUBA, JAPAN
May 8 and 9, 1991

The following resolutions are proposed by the organizers of the 7th U.S.-Japan Bridge Engineering Workshop to the Task Committee J of UJNR:

1. The seventh U.S.-Japan Bridge Engineering Workshop provided valuable exchange of technical information which was beneficial to bridge engineering communities of both countries. 81 participants representing government, academia, industry and private practice presented 32 papers in 10 technical sessions. Main themes included : 1) Seismic Design; 2) Wind Resistant Design; 3) Bridge Construction; 4) Design Methods; and 5) Bridge Maintenance. In view of the importance of cooperative programs on the subject of wind and seismic effects on bridges and on performance, strengthening, structural monitoring, safety, non-destructive evaluation and design innovation of these transportation structures, the continuation of technical cooperation and interaction is considered essential.

2. The Workshop recognizes the importance of continued exchange of personnel, technical information, research data and bridge response data from significant earthquakes and strong winds, and the use of available unique research facilities in both countries and encourages cooperative efforts in mutually agreeable areas of bridge research.

3. The primary purpose of the Workshop is to exchange technical information on a timely basis that is usable by bridge engineering profession. The specific objectives of this Workshop are :

   3.1 To ensure a first-hand exchange of information resulting from the unique problems each country is faced with; for example, the development and implementation of limit state or load and resistant factor design methods.

   3.2 To stimulate collaborative research work in the important area of bridge engineering for better design, construction, performance, rehabilitations and strengthening of bridge structures in both countries.

   3.3 To facilitate the exchange of technical information and ideas and to promote the broadening of viewpoints for those involved.

4. The Workshop identifies the following technical topics for continued cooperative research programs :

4.1 Dynamic control and seismic isolation of bridge structures including : active, passive and hybrid control, damping augmentation, experimental studies and application to long-span cable-supported bridges.

4.2 System identification techniques for wind and seismic engineering including : data interpretation studies, development of mathematical models, identification of non-linear systems, reduced-order models, computational algorithms and optimum sensor locations.

4.3 Non-destructive evaluation techniques including damage detection by sensor monitoring, expert systems, inspection techniques, structural monitoring, condition assessment for safety, performance evaluation and repair procedures.

4.4 Experimental and analytical studies on the effects of dynamic soil characteristics, including bridge-soil interactions, on the behavior of bridge structures.

4.5 Retrofitting and strengthening methodologies for bridge structures.

4.6 Development of design criteria based on limit-state concepts.

5. The Workshop identifies the following technical topic for future cooperative technical programs :

5.1 Use and performance of structural materials including new materials.

6. It is anticipated that the interaction among the delegates from the United States and Japan during the round-table discussions and the technical study tour will lead to an enhanced exchange of data and innovative ideas, and will also lead to the establishment of cooperative research efforts, both theoretical and experimental, on bridge engineering. Because of the importance, benefits and potential of these Workshops, it is recommended to conduct the 8th bridge engineering workshop in Chicago, Illinois, just prior to the 24th UJNR joint meeting in the United States, in May 1992. A study-tour will be planned to visit research laboratories and bridge-construction sites.

（2）　ＵＪＮＲ耐風耐震構造専門部会
第23回合同部会におけるＪ部会部会報告(英文)

Report of Task Committee on
(J) WIND AND EARTHQUAKE ENGINEERING FOR TRANSPORTATION SYSTEMS

Date: May 14, 1991

Place: Public Works Research Institute
Tsukuba , JAPAN

Attendees: Japan Side - M. Fujiwara (Chairman) (PWRI)
M. Okahara (PWRI)
T. Fujitani (MRI)
K. Nishikawa (PWRI)
Y. Ninomiya (PWRI)
K. Hasegawa (PWRI)

U.S. Side - J.D. Cooper (Chairman) (FHWA)
W.E. Roper (Corps of Eng.)

MISSION STATEMENT

1. Objectives

The objectives of this Task Committee are to plan, promote, and foster research on the behavior of highway bridges when subjected to wind and seismic forces and to disseminate research results and provide specifications and guidelines based on the task committee's finding. Surface transportation systems for movement of goods and people play a vital part of commerce and intercourse between people. Highway bridges are especially influenced by the forces of wind and earthquakes because of their open exposure to those forces.

2. Scope-of-Work

The scope of the work is applicable mostly to highway bridges without any limitation on their size and function such as existing bridge and new bridge designs; whole system of bridges; and/or to single components of a bridge.

The mission is performed through:

Conducting workshops, exchanging researchers, developing methods for design evaluations and test procedures; developing inspection techniques, rehabilitation and maintenance specifications and policies, and performing cooperative research programs and other relevant cooperative administrative activities.

3. Accomplishments (past 2 years)

Japanese side hosted an ad hoc T/C(J) Retrofit Subcommittee meeting in December 17 to 22, 1990 to discuss and review practical seismic retrofit applications in both countries. Nineteen technical presentations were made by 5 U.S. researchers and 30 Japanese researchers. Technical topics included the

history of developing retrofit techniques for bridges; damage assessment from the Loma Prieta earthquake; discussion on condition assessment and prioritization of bridges for seismic retrofit; seismic strengthening methods; and research in progress. Site visits were made to view retrofit technology applied to bridges on Tokyo metropolitan expressways.

- United States and Japanese post earthquake investigative teams collaborated to investigate the damage to transportation systems with emphasis on highway bridges caused by the Loma Prieta Earthquake of October 17, 1989. Technical information was exchanged at the 22nd and 23rd Joint Panel Meetings.

- Conducted coordinated research studies on seismic performance of bridge piers and columns. Details of this work involved determining the performance of reinforced concrete piers and columns subjected to dynamic cyclic loading, performing model tests on the failure of reinforced concrete piers, testing full and large-scale concrete columns and for the behavior of concrete filled steel tubes.

- Held the seventh bridge workshop in Tsukuba, Japan in 1991, which was followed by site visits of Higashi Kobe bridge, Kansai international airport, and Akashi Kaikyo bridge. Held the sixth bridge workshop in Lake Tahoe Nevada U.S. in 1990, dealing with the determination and evaluation of the performance and strengthening of bridge structures, structural monitoring, repairs, safety and nondestructive evaluation. Special attention was given to the seismic and wind loadings of modern cable-stayed bridges, vibration suppression, base isolation, dynamic control techniques, construction techniques of long span bridges, maintenance of existing bridges and limit state design.

- Both sides presented technical papers at the 22nd and 23rd UJNR Joint Meeting and participated in technical study tours to buildings, bridges, factories construction sites, and instrumented structures.

4. Future Plans

- Conduct the 8th bridge workshop just prior to the 24th Joint Panel meeting in the Chicago Illinois area of the United States.

- United States side plans to host a follow-up ad hoc T/C(J) Retrofit Subcommittee meeting to study practical seismic retrofit measures.

- Continue to investigate and exchange technical information on improved seismic retrofit and strengthening procedures for highway bridges based on experimental, analytical, and field studies. This exchange should include information on maintenance of existing bridges.

- Continue experimental research study on the seismic performance of bridge piers and columns, and support emphasis on base isolation of bridges in cooperation with T/C (G).

- Develop a coordinated research study on seismic, aeroelastic, and aerodynamic response of cable-supported bridges with emphasis on cable inspection, vibration control and corrosion protection.

- Conduct a coordinated research study to compare the seismic design criteria for bridges in Japan and the U.S. and discuss the method and analysis for bridge column design. Information on application of limit state design method should be exchanged.

- Continue a coordinated research study on seismic response control, system identification techniques, and nondestructive evaluation of bridge structures.

- Encourage a coodinated research study on use and performance of structural materials including new materials.

5. Information Exchange

- Exchanged technical reports, research program documentation, construction logs, design plans, and assorted photographs and videos, including technical data appropriate for investigating the Philippine earthquake of 1990.

- Mr. Keiichi Tamura who studied at Stanford University, Mr. Kinji Hasegawa who studied at University of California and Mr. Shigeki Unjoh who studied at University of Southern California, returned to PWRI.

- Mr. Mohsen Sultan, California Department of Transportation is on a one year exchange with PWRI in Tsukuba.

6. Impact

- The free exchange of literature, instrumentation technology, and earthquake response data has led to the advancement in design technology, and development of preliminary retrofit guidelines, and to the calibration and verification of specifications.

- Greater uniformity was achieved in wind engineering test procedures and modeling resulting in more efficient solutions to the aerodynamic bridge problem.

- The workshop and study tours in the two countries have facilitated technology transfer, as an example, in the area of cable protection and vibration suppression of cable-stayed bridges.

- A set of priorities for needed research from a more international viewpoint has reduced the conduct of duplicative research efforts.

7. Barriers

There are no major technical barriers to achieve the Task Committee mission. However, financial barriers, especially funding needed to participate in workshops and panel meetings and for conducting actual bridge tests and large scale model tests, continue to limit the effectiveness of the work in this Task Committee's work.

（3）　ＵＪＮＲ耐風耐震構造専門部会
第23回合同部会におけるＪ部会部会報告(和文)

（Ｊ）交通システムの耐風耐震技術に関する作業部会報告

開催日：　１９９１年5月１４日

場　所：　建設省土木研究所、つくば市

出席者：　日本側　篠原　稔　（作業部会長）　（土木研究所）
岡原美知夫　（土木研究所）
藤谷徳之助　（気象研究所）
西川　和広　（土木研究所）
二宮　嘉朗　（土木研究所）
長谷川金二　（土木研究所）

米国側　J.D.Cooper　（作業部会長）　（FHWA）
W.E.Roper　（U.S. Corps）

〔活動要約〕

1．作業部会の目的

交通システムは、人々の交流及び物資の輸送等において重要な役割を有する。この交通システムの中で、特に道路橋はその建設条件から地震や風の影響を受け易い。こうした点を考慮し、本作業部会では、地震や風に対する道路橋の挙動に関する調査研究を計画、推進し、発展させるとともに、それらの調査研究の成果に基づいて、道路橋の耐震、耐風に関するガイドラインや指針を作成することを目的とする。

2．作業範囲

本作業部会では、道路橋の諸元と機能の多様性にかかわらず、あらゆる道路橋を主要な対象とし、既設橋の維持管理および新設橋の設計施工に関する事項の調査研究を行うものとする。本作業部会では、これらの調査研究を進めるために、橋梁の設計における数値計算や試験および橋梁の点検・補修補強・維持管理等に関してワークショップ・人事交流・共同研究などを実施するものとする。

3．活動状況（過去２年間）

・　日本側はアドホックＪ作業部会補修補強小委員会のワークショップを１９９０年１２月１７日から２２日に開催し、耐震補強についての議論を行った。米側５名、日本側３０名の研究者によって１９の発表が行われた。議題は橋梁の補修補強技術の開発の歴史、ロマプリエータ地震の被害評価、橋梁の耐震補強についての条件評価および優先度評価についての議論、耐震補強法、現在進行中の研究等である。首都高速道路の橋梁に適用された補強技術に関する視察旅行が行われた。

・　１９８９年１０月１７日のロマ・プリエータ地震では交通システムの被害、特に被害を受けた道路橋について、米国と日本の地震被害調査団が協力して調査を行った。また、日米双方の調査結果についての情報交換を第２２回および第２３回ＵＪＮＲ合同部会において行った。

・　橋脚および柱の耐震性能に関して、動的繰返し荷重に対する鉄筋コンクリート橋脚や柱の耐荷性能、鉄筋コンクリート橋脚の破壊に関する模型実験、実物大および大型鉄筋コンクリート柱供試体の実験およびコンクリート充填鋼管柱の耐荷性能についての共同研究を実施した。

・　１９９０年に米国のネバダ州レークタホ市で第６回橋梁ワークショップを開催し、また１９９１年に日本のつくば市で第７回橋梁ワークショップを開催し、東神戸大橋、関西新空港、および明石海峡大橋の視察旅行を行った。これらのワークショップでは、橋梁の性能評価、構造物の監視システム、補修補強方法、安全性評価および非破壊診断技術について討議された。特に、最近の斜張橋の地震・耐風応答に係わる振動制御技術、免震技術、動的制御技術、長大橋の建設技術、既存橋梁の補修および限界状態設計法について大きな関心が寄せられた。

・　日米両サイドは、第２２回及び第２３回ＵＪＮＲ合同部会において数多くの報告を行うとともに、建築物、橋梁、製作工場、建設現場および計測現場等へのスタディツアーを行った。

4．将来計画

・　第２４回ＵＪＮＲ合同部会に先だって、米国イリノイ州シカゴで第８回橋梁ワークショップを開

催する予定である。
・　米国側は、実用的な耐震補強法の研究のためにアドホックＪ作業部会補修補強小委員会の開催を計画している。
・　実験・数値解析および現場研究に基づく、改善された道路橋耐震補強についての調査や情報交換を継続する。情報交換には既設道路橋の維持管理についての情報を含む。

・　Ｇ作業部会と共同で橋脚および柱の耐震性能に関する実験的研究を継続するとともに免震技術に関する研究を行う。
・　吊橋や斜張橋の耐震性能、空力弾性学特性および空気力学特性、ケーブルの検査技術および振動や腐食の防止対策についての共同研究を推進する。
・　日米双方における橋梁の耐震設計基準の比較のための共同研究を推進し、柱の設計法および解析について議論を行い、限界状態設計法の適用についての情報交換を行う。
・　橋梁の地震応答制御、システム同定技術および非破壊診断技術に関しての共同研究を推進する。
・　新素材を含めた構造材料の利用と性能に関する共同研究を推進する。

5．情報交換
・　１９９０年フィリピン地震調査データを含む、技術報告、研究プログラム、建設計画、設計計画およびこれらに関する写真やビデオを交換した。
・　米国スタンフォード大学で研究に従事していた建設省土木研究所の田村敬一主任研究員、カリフォルニア大学で研究に従事していた建設省土木研究所の長谷川金二研究員、および南カリフォルニア大学で研究に従事していた建設省土木研究所の運上茂樹研究員が帰国した。
・　ＣＡＬＴＲＡＮＳのモーセン・サルタン研究員は１９９１年４月から１年間の予定でつくば市の建設省土木研究所で調査研究に従事している。

6．主要成果
・　文献、測定、技術および地震応答測定データの交換により、設計基準や補修指針の改善が図られた。
・　耐風に関する調査研究における試験方法やモデルの統一を図り、これにより耐風技術に関する諸問題に対する有効な方策を見出した。
・　日米双方における橋梁ワークショップやスタディツアーの実施により、斜張橋のケーブルの防食対策および振動防止対策をはじめとする多くの項目の技術交換ができた。
・　国際的な観点からその実施が必要とされる研究の優先性を明らかにすることにより、日米双方で同種の研究を行うことを省くことができた。

7．問題点
本作業部会における調査研究を進めるにあたっては、現在のところ特段の問題点は見あたらない。ただし、合同部会やワークショップへの参加、実橋を対象とした試験や大型モデル供試体を用いた実験の遂行にあたって、これらの予算の不足が続いており、本作業部会の活動が制限される状況にある。

第７回日米橋梁ワークショップ論文集

ISSN 0386－5878
土木研究所資料第3086号
平成４年３月(１９９２)

構造橋梁部長　藤原　稔

要旨　1991年５月８日，９日の２日間にわたって，建設省土木研究所において第７回日米橋梁ワークショップが開催された。本資料は，同ワークショップに提出された論文および会議プログラム，討議内容，ワークショップ後に行われた視察旅行の内容をとりまとめたものである。

キーワード：橋梁工学，日米技術協力，耐風工学，耐震工学

郵便はがき

41円切手をはって下さい

305-□□

茨城県つくば市大字旭一番地

建設省土木研究所

構造橋梁部橋梁研究室　御中

No. 74

No. 74

配布先氏名

配布先住所

土木研究所資料第3086号　　部

上記のとおり受領しました。

所　属（住所）

氏　名　　印